Double-strand break repair during meiosis in Arabidopsis thaliana

Miguel Hernandez Sanchez-Rebato

UNIVERSITÉ CLERMONT AUVERGNE.

ECOLE DOCTORALE SCIENCES DE LA VIE, SANTE, AGRONOMIE ET ENVIRONNEMENT.

THÈSE

POUR L'OBTENTION DU GRADE DE

DOCTEUR D'UNIVERSITÉ.

Spécialité: Biologie Santé.

Presentée et soutenue le 29/06/2022 par

MIGUEL HERNÁNDEZ SÁNCHEZ-REBATO

et dirigée par

CHARLES WHITE & MARÍA GALLEGO.

DOUBLE-STRAND BREAK REPAIR DURING MEIOSIS IN *ARABIDOPSIS THALIANA.*

President du Jury:	Mathilde Grelon, Institut Jean-Pierre Bouigin, INRA.
Rapporteurs:	Valerie Borde, Institut Curie, CNRS.
	Mónica Pradillo, Facultad de Biología, UCM.
Examinateurs:	Antoine Molaro, iGRED, INSERM.
	Rodrigo Bermejo, Centro de Investigaciones Biológicas, CSIC.

AVRIL 2022, CLERMONT-FERRAND.

Equipe "Recombinaison et maintenance de l'intégrite du génome",
Institut Génétique, Reproduction et Développement,
iGReD - CNRS UMR6293 - INSERM U1103 – Université Clermont Auvergne.
Faculté de Médicine. 28, place Henri Dunant,
63001 Clermont-Ferrand.

Abstract

Meiosis, the specialized cell division of gametogenesis, ensures the halving of chromosome number essential for sexual reproduction in eukaryote organisms. At the outset of meiosis, programmed induction of DNA double-strand breaks (DSBs) initiates an intricate and highly regulated process for their repair via homologous recombination (HR), leading to the formation of crossovers - reciprocal exchanges of extensive chromosomal segments.

The first steps of DSB repair involve the processing of the DSBs and the formation of recombinase-DNA nucleofilaments which, with the help of multiple cofactors, catalyse the search for and invasion of an homologous template. In somatic tissues, RAD51 is the recombinase in charge of this. During meiosis however, RAD51 plays a supporting role to the meiotic-specific recombinase, DMC1, which catalyses these first steps of meiotic HR. In accordance with this, some of the RAD51 cofactors instrumental in somatic repair, such as RAD54 and the RAD51 paralogues RAD51B, RAD51D and XRCC2, are dispensable during meiosis. Given that in absence of DMC1, RAD51 is able to catalyse homology search and strand exchange in *Arabidopsis thaliana*, proficiently repairing meiotic DSBs, we wondered whether this lack of role in wild-type meiosis could simply be a consequence of the non-catalytic role of RAD51. Indeed, this was the case for RAD54, which we show is essential for meiotic DSB repair and RAD51 nucleofilament function in the absence of DMC1. Intriguingly, this is not so for RAD51B, RAD51D and XRCC2, which remain dispensable in the absence of DMC1, hinting at different needs for RAD51-mediated DSB repair in somatic and meiotic cells and leaving the door open for further exploration.

In *Arabidopsis thaliana*, meiotic DSBs largely outnumber crossovers (≈ 20:1). Approximately 95% of DSB are thus repaired either through sister-chromatid donors or by non-crossover pathways. The molecular detection of non-crossover repair products has proven challenging, presumably due to the short length of the resulting gene conversion tracts and their dispersed localization across the genome. Furthermore, some of the mechanistic features of both crossover and non-crossover recombination described in other model organisms, as well as factors that modulate their localization and regulation, remain poorly understood in the model plant. To overcome current technical limitations, we propose the introduction of targeted DSBs at early meiosis using CRISPR/Cas9 systems. By doing so, we would generate an initiation point for HR events at desired locations that would facilitate the detection and mechanistic analysis of repair products. The introduction of DSBs in varied genetic and epigenetic contexts

and in multiple genetic backgrounds would permit the direct comparisons under controlled conditions to study how they affect DSB repair during meiosis. We designed multiple CRISPR/Cas9 constructs that were able to cleave their target sites at moderate efficiencies and, for some, to induce increases of the recombination rate of intervals spanning these sites. In the context of this study however, we did not succeed in detecting CRISPR/Cas9-induced DSB repair outcomes at single-molecule level via next-generation sequencing of meiotic products.

Nucleotide analogues are commonly used for the cytological and molecular detection of DNA synthesis and notably DNA replication. Given that DNA synthesis is inherent to all meiotic recombination pathways, we tested whether the use of one of these analogues (EdU) would permit the labelling of meiotic DSB repair events during meiosis in *Arabidopsis thaliana*. To do so, we designed and validated a protocol that permitted the cytological identification and characterisation of SPO11-dependent meiotic DSB repair-associated DNA synthesis tracts, which offers a new standard tool for the study of meiotic recombination in Arabidopsis. Following cytological confirmation of these EdU-labelled tracts, we carried out a ChIP-like approach for their molecular characterization - pulling-down, sequencing and mapping these tracts - which revealed enrichments over multiple features related to meiotic recombination. Nonetheless, the replication of these enrichments in *spo11* negative controls poses doubts about their origin that we are actively working to solve and extend.

Keywords: Meiosis, *Arabidopsis thaliana*, DNA repair, double-strand breaks, homologous recombination, CRISPR/Cas, DNA synthesis.

Résumé

La méiose, la division cellulaire spécialisée de la gamétogenèse, assure la réduction de moitié du nombre de chromosomes essentiels à la reproduction sexuée chez les organismes eucaryotes. Au début de la méiose, une induction programmée de cassures double-brin de l'ADN (CDB) initie un processus complexe et hautement régulé pour leur réparation par recombinaison homologue (RH) conduisant à la formation de crossovers - échanges réciproques de segments chromosomiques étendus.

Les premières étapes de la réparation des CDB impliquent le traitement des CDB et la formation de nucléofilaments ADN-recombinase qui, avec l'aide de multiples cofacteurs, catalysent la recherche et l'invasion d'une matrice homologue. Dans les tissus somatiques, ce rôle est porté par RAD51. Pendant la méiose cependant, RAD51 joue un rôle de soutien d'une recombinase spécifique à la méiose, DMC1, qui catalyse ces premières étapes de la RH. Conformément à cela, certains des cofacteurs de RAD51, instrumentaux dans la réparation somatique, comme RAD54 et les paralogues de RAD51, RAD51B, RAD51D et XRCC2, sont dispensables pendant la méiose. Étant donné qu'en l'absence de DMC1, RAD51 est capable de catalyser la recherche d'homologie et l'échange de brins, réparant ainsi efficacement les CDB méiotiques, nous nous sommes demandé si leur absence de rôle dans la méiose serait simplement une conséquence du rôle non catalytique de RAD51. En effet, c'était le cas pour RAD54, dont nous montrons qu'elle devient essentielle pour la réparation méiotique des CDB et la formation des nucléofilaments RAD51/ADN en absence de DMC1. Curieusement, ce n'est pas le cas pour RAD51B, RAD51D et XRCC2, qui restent dispensables en l'absence de DMC1, ce qui laisse supposer que la réparation des DSB médiée par RAD51 a des besoins différents dans les cellules somatiques et méiotiques et laisse la porte ouverte à de nouvelles explorations.

Chez *Arabidopsis thaliana*, les CDB méiotiques sont largement plus nombreux que les *crossovers* (≈ 20:1). Environ 95% des CDB sont ainsi réparés soit utilisant les chromatides sœurs, soit par des voies *non-crossovers*. Cependant, la détection moléculaire des produits de réparation *non-crossovers* s'est avérée difficile, probablement en raison de la courte longueur de segments de conversion génétique et de leur localisation éparse le long du génome. En plus, certaines des caractéristiques mécanistiques de la réparation *crossovers* et *non-crossovers* décrits chez d'autres organismes modèles, ainsi que les facteurs qui modulent leur localisation et leur régulation, restent mal comprises chez la plante modèle. Pour surmonter les limitations techniques actuelles, nous proposons l'introduction de CDBs ciblés au début de la

méiose en utilisant les systèmes CRISPR/Cas9. Ce faisant, nous générerions un point d'initiation pour les événements HR aux endroits souhaités, ce qui faciliterait la détection et l'analyse mécanistique des produits de réparation. L'introduction de CDBs dans des contextes génétiques et épigénétiques variés et dans des milieux génétiques multiples permettrait d'étudier comment elles affectent la réparation des CDBs pendant la méiose. Nous avons construit de multiples constructions CRISPR/Cas9 qui ont été capables de cliver leurs sites cibles à des efficacités modérées et pour certaines d'entre elles, d'induire des augmentations du taux de recombinaison des intervalles recouvrant ces sites. Cependant, nous n'avons pas pu détecter les résultats de la réparation des CDBs induits par CRISPR/Cas9 au niveau de la molécule unique via le séquençage de nouvelle génération des produits méiotiques.

Les analogues de nucléotides sont couramment utilisés pour la détection cytologique et moléculaire de la synthèse de l'ADN et notamment de la réplication de l'ADN. Étant donné que la synthèse de l'ADN est inhérente à toutes les voies de recombinaison méiotique, nous avons testé si l'utilisation de l'un de ces analogues (EdU) permettrait le marquage des événements méiotiques de réparation des DSB au cours de la méiose chez *Arabidopsis thaliana*. Pour ce faire, nous avons conçu et validé un protocole permettant l'identification cytologique et la caractérisation des segments de synthèse d'ADN associés à la réparation des DSB méiotiques dépendants de SPO11, ce qui offre un nouvel outil standard pour l'étude de la recombinaison méiotique chez Arabidopsis. Après la confirmation cytologique de ces tracts marqués à l'EdU, nous avons effectué une approche de type ChIP pour leur caractérisation moléculaire - *pulling-down*, séquençage et cartographie de ces segments d'ADN- qui a révélé des enrichissements sur de multiples caractéristiques liées à la recombinaison méiotique. Néanmoins, la réplication de ces enrichissements dans les contrôles négatifs *spo11* pose des doutes sur leur origine que nous travaillons activement à résoudre et à étendre.

Mots-clés : Méiose, *Arabidopsis thaliana*, réparation de l'ADN, cassures double-brin, recombinaison homologue, CRISPR/Cas, synthèse de l'ADN.

Acknowledgments / Agradecimientos

First and foremost, I would like to thank my supervisors, Charles and María, for the opportunity to start and complete this PhD in the first place. For their dedication to provide all the necessary advice and guidance on all the work done, while leaving me enough room to explore and pursue own research interests, which I specially appreciate and believe it is the ideal situation for the development a young scientist. For all the formation, not only in DNA repair, meiosis, genetics or biology in general, but in the different professional aspects around being a scientist, which I think will be of great help to continue my career. But, above all, I would like to thank you for the attention throughout these years, in particular these last two. I really appreciate your effort to make sure that things were going well, offering your help in everything that was within your reach.

I would like to thank Mónica and Juan Luis, my supervisors in Madrid during my time in the lab there. They have been doing an amazing job for years teaching, training and developing bachelor and master students in their laboratory, many of whom have succeeded to pursue their subsequent career goals, while maintaining excellent research in the field. And, by finishing this work, I become just another one of them, I suppose. I'm grateful that you spent the time and effort not only to train me, but to transmit me your passion for science and research and to help me to get this opportunity, even after I left the lab.

I would also like to thank different people that have somehow helped me in my career and/or this work in particular. Pablo, Bianca, and Nadia, which were in the lab when I started and taught me many things while having a great time there. Pachón, with whom I not only shared some time in the lab but who has accompanied from the distance along these years of PhD. Fivos, who gave me an opportunity for a short but very formative tour outside this field. Olivier and Sébastien, part of the projects here presented and who offered me advice and a helping hand whenever I needed it. Jeremy, Nathalie, Michel, Heïdi and Floriane, who have helped me in the lab and made these years easier in one way or another, as well as Alida, who made essential contributions to one of the projects here presented. And finally to anyone who has contributed by any means, research or non-research-wise.

Cómo no, agradecer a mi padre y a mi madre. No creo que vaya a escribir nada aquí que no sepáis, o eso espero. Pero sí quería dejar por escrito que, aunque se os haga dura la lectura si os ponéis a ello, esto es tanto o más vuestra tesis que la mía. Tanto como todos los pasos anteriores al doctorado. Llegar es mucho más fácil cuando tienes a dos personas preocupándose y currando para que las condiciones sean ideales, en esto igual que en cualquier otra cosa durante 28 años. A Irene también. Seguro que te he dicho mucho menos que a papá y mamá lo importante que eres para mí, pero así es.

A Zoe. Sé que no han sido fáciles estos cuatro años de tesis a distancia, especialmente los dos últimos, así que solo puedo darte las gracias. Primero simplemente porque sin la generosidad de haberme apoyado desde el primer momento que te propuse irme tres o cuatro años, con lo que ello supone, probablemente me lo hubiera pensado mucho más. A lo mejor no estaría escribiendo esto ahora. Luego por aguantarme y seguir ahí, en momentos mejores y peores, sobre todo estos meses finales. Dentro de poco te tocará a ti ponerte a escribir tu tesis, espero estar yo a la altura.

Por último, dar las gracias al resto de mi familia. No somos muchos, así que tocáis a una buena parte cada uno. A mis amigos y amigas también, sin los que todo sería demasiado aburrido.

Funding

- MEICOM: EU H2020 Program, Marie Sklodowska-Curie actions: Innovative Training Network (H2020-MSCA-ITN-2017-765212).

- ANR: RecInChromatin (PRCI ANR-16-CE91-0010).

Publications

- Hernandez Sanchez-Rebato M, Boutta AM, Gallego ME, White CL, Da Ines O (2021) RAD54 is essential for RAD51-mediated repair of meiotic DSB in Arabidopsis. PloS Genet 17(5): e1008918. https://doi.org/10.1371/journal.pgen.1008918

Table of Contents

Table of figures

Table of tables

Para mi abuela Margarita,

CHAPTER I. General introduction

1. Introduction to DNA damage & repair

Deoxyribonucleic acid (DNA) is the molecule that encodes genetic information and functions as the primary unit of inheritance in most living organisms. DNA molecules are an heteropolymer of four deoxyribonucleotides, comprising one out of four different nitrogen bases: cytosine (C), guanine (G), adenine (A) and thymidine (T); covalently linked together in a chain by the deoxyribose sugar-phosphate backbone. In eukaryotic organisms, DNA molecules are typically in the form a double helix structure of two polynucleotide DNA chains coiled one around each other. Genetic information is physically codified by the sequence of nucleotides of DNA molecules but its interpretation also relies in how this sequence is modified, transcribed, translated and how all these processes are regulated by the cell machinery and the environment in which the cell exists. Thus, physical, chemical and enzymatic modifications of DNA molecules may introduce changes in the DNA sequence and/or in how it is interpreted and consequently in the structure and function of the cell and of the organism. The study of how DNA is modified and repaired has been a major research field since its structure was determined in the 1950's [1].

The sources of DNA damage can be grouped into two broad categories according to their endogenous and exogenous origins. Endogenous DNA damage mainly arises from errors during DNA replication, interactions of DNA with reactive byproducts of cellular metabolism and spontaneous modification. Exogenous damage involves environmental physiochemical agents that modify DNA, such as ionizing and UV radiation and chemical mutagens such as crosslinking agents or alkylating agents.

The chemical nature of the modifications is diverse and will determine the way they are signalled and repaired. Lesions range from reversible modifications that can be easily repaired in an error-free manner to modifications that may end up causing permanent loss of part of the genetic material or its reorganization, leading to cell malfunction, cell death and a wide spectrum of pathologies in living beings. Nevertheless, DNA modifications are also one of the main drivers of evolution as they may produce hereditable mutations in an organism that are potentially beneficial in terms of fitness. In the study of DNA damage and its repair, the use of the classic model organisms has been predominant, as in many other fields. From the 1970s/80s, *Arabidopsis thaliana* has become the model organism for higher plants.

1.1. *Arabidopsis thaliana* as a model for plant genetic studies

Arabidopsis thaliana (L.) Heynh is a vascular flowering plant that belongs to the family of the Brassicaceae. First described and named *Pilosella siliquosa* by Johannes Thal in Germany in 1577 [2], its present name was given by Gustav Heynhold in 1842 [3]. It is a small plant, typically 20-25 centimetres tall with an annual (rarely biannual) life cycle, although this can be as fast as 6-8 weeks in some accessions and environmental conditions. At the base of the plant, leaves form a rosette from which multiple stems arise and branch generating corymb inflorescences at the tip. These inflorescences are composed of hermaphrodite flowers of around 3mm with six stamens surrounding a single pistil. Its fruits, in the form of siliques, can hold between 30 and 60 seeds. Native to Europe, Asia and Africa, it has been introduced and naturalized worldwide given its facility to germinate and grow in diverse soils and conditions. Genetically diploid, its genome is divided into 5 pairs of chromosomes in somatic tissues (2n = 10) [4–7].

Friedrich Laibach described the chromosome number of *A. thaliana* in 1907 [8], effectively starting its use as a subject for plant genetics and cytogenetics. During the 1940s and 50s, Laibach and his students begin irradiating Arabidopsis with X-rays, isolating and studying the first induced mutants, published in 1945 by Erna Reinholz [9]. An active research community started building up in the 1960s, when the first international Arabidopsis conference was held up in Göttingen, Germany, in 1965, as well as the first seed stock centre of ecotypes and induced mutants funded by Gerhard Röbbelen. Research on Arabidopsis grew rapidly during the 1980s and 90s with the expansion of molecular techniques and a series of technical advances that, in addition to its particular biological characteristics, end up instating *Arabidopsis thaliana* a model organism for plant research.

We may divide the features that make this plant a model organism in:

I) Physiological and morphological features: Its small size and fast life cycle allows growing large number of plants in reduced space, obtaining flowers in 3-4 weeks and seeds ready to germinate in 6-8 weeks depending on the growing conditions, making possible up to 6-8 generations a year in the laboratory. A seed output of up to tens of thousands per plant guarantees enough material for subsequent experiments as well as for different kinds of screenings for rare events. Seed number and size is convenient for storage in collections and distribution between laboratories. Barely outcrosser, its self-fertilizing nature permits the effortless maintenance of pure lines through generations.

II) Ecological features: Arabidopsis can germinate in a great variety of substrates, from a simple piece of humid paper to a liquid medium, an agar plate or plain soil. This

feature allows cheap germination of large numbers of seeds and application of different treatments and studies at all stages of plant development. Growing conditions in the laboratory are well established, they are compatible with different formats of growing chambers and greenhouses and easily reproducible.

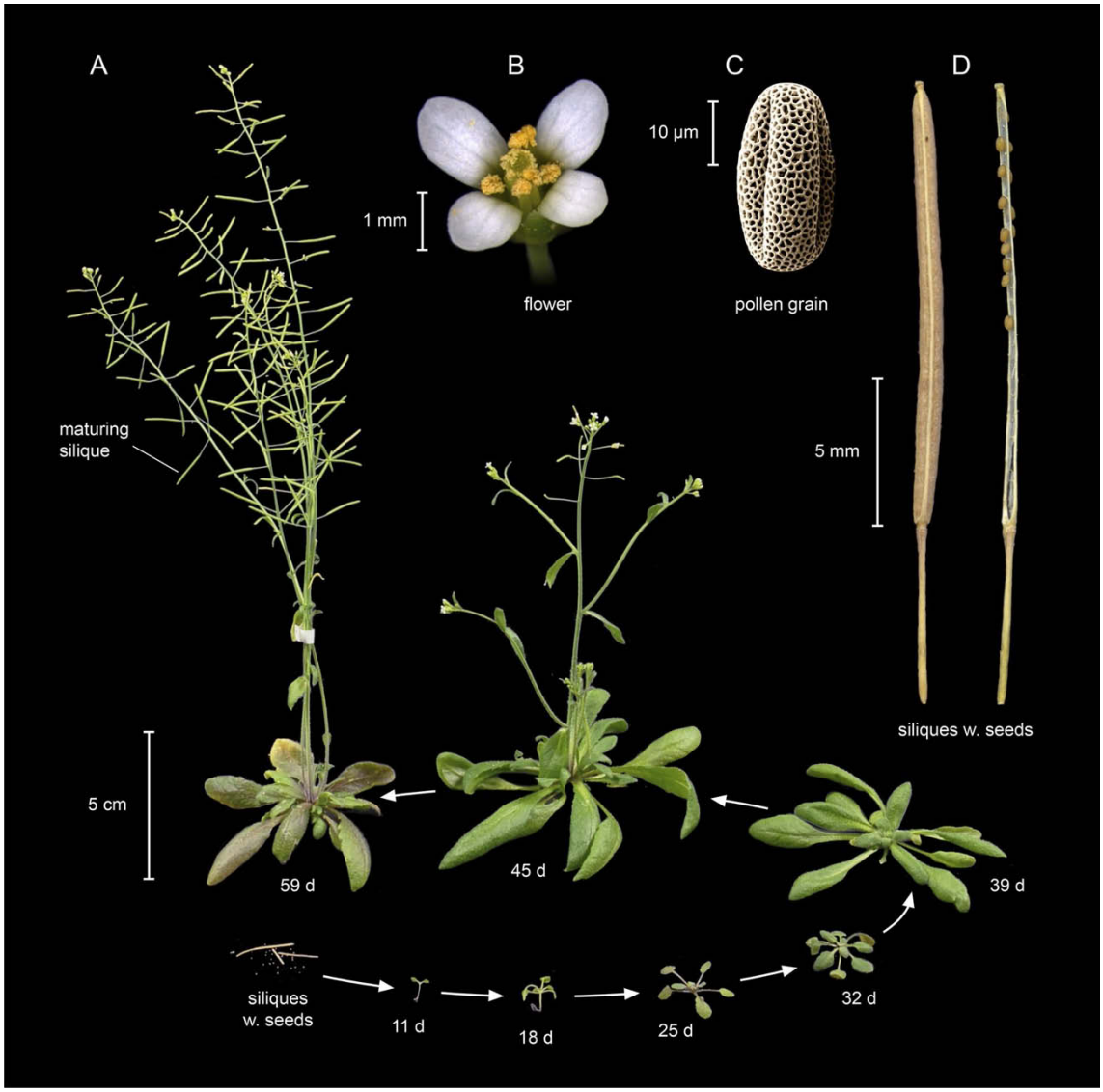

Figure 1. ***Arabidopsis thaliana*** **life cycle.**

Original from Krämer (2015). (**A**) Different stages of the life cycle of Arabidopsis thaliana of the accession Columbia (Col) from seeds to mature plant. Detail of *A. thaliana* (**B**) flower, (**C**) pollen grain and (**D**) dried siliques, both closed (left) and open (right) with a few remaining seeds.

III) Genetic features: A small genome among higher plants (between 131 and 134Mb according to the latest reports [10,11]), diploid and almost fully annotated makes *Arabidopsis thaliana* a good platform for genetic studies. Its biological and taxonomical

closeness to more genetically complex higher plants allows frequent transfer of knowledge with, for example, economically important crop species. The small size of the genome complicated cytological analysis for many years but the improvement of microscopy and informatic processing of images in the last few decades overcame this problem and nowadays combining molecular and cytological genetics is a standard practice. The possibility to efficiently outcross Arabidopsis plants manually, not only with specimens of the same accession or species, but with other species from the Arabidopsis genus, offers many opportunities to combine phenotypes, genotypes and study the effects of hybridization or introgression. Furthermore, the existence of natural polyploid accessions and their diploid counterparts as well as the tolerance for neo-polyploidization has established *Arabidopsis thaliana* as a model for polyploidy and evolutionary studies.

IV) Technological advances: As mentioned above, the first X-ray-induced mutants of Arabidopsis were isolated and analysed in the 1940s and 50s. However, it was the emergence of T-DNA and chemical mutagenesis techniques which, together with the improvement of mutation screening approaches, the construction of genetic and physical maps and the sequencing of the genome have made Arabidopsis a powerful modern biological model organism. It is thus now possible to carry out large-scale studies using standard collections of plants carrying mapped and sequenced mutant alleles. The development of efficient and reproducible transformation strategies, both in somatic and germ cells, made possible not only insertional mutagenesis but the generation of reporter lines, the introduction of cloned genes of interest and later on the application of precise genetic modification technologies.

1.2. Nature of DNA lesions and pathways involved in their repair

Ultraviolet light induces lesions on adjacent pyrimidines by generating cyclobutane pyrimidine dimers (CPDs) and (6-4) pyrimidine-pyrimidones (6-4 PPs). These lesions may be directly reversed by a mechanism called photoreactivation. The main actors of this pathway are light-activated enzymes called photolyases. In *Arabidopsis thaliana* three classes of photolyases have been described: I) class II CPD photolyases (PHR1/UVR2, PHR2); II) 6-4 PP-specific photolyases (UVR3); and III) Cryptochrome-Drosophila, Arabidopsis, Synechocystis, Human (CRY-DASH) photolyases (CRY3) [12–14]. These enzymes mediate an electron transfer than results in the breaking of the pyrimidine dimer bonds [15,16].

Deamination, oxidation or alkylation of DNA bases, abasic sites and single strand breaks (SSBs) generated by different agents that do not alter significantly the structure

of the DNA helix (non-bulky lesions) are primarily repaired via base excision repair (BER). This pathway involves a series of steps that can be summarize as: 1) lesion recognition and damaged base removal, performed by a series of substrate specific DNA glycosylases that cleave the N-glycosidic bond; 2) cleavage of the sugar-phosphate backbone at the abasic site, either by the apurinic/apyrimidinic (AP) lyase activity of some DNA glycosylases or by AP endonucleases; 3) clean-up of the resulting DNA ends to generate conventional 3' OH and 5' phosphate DNA ends suitable for gap-filling and ligation of the ends by AP endonucleases and a 3' DNA phosphatase respectively; and 4) gap filling through DNA synthesis and ligation, carried out by a different set of DNA polymerases and ligases depending if only one nucleotide is inserted (short patch BER) or more than one (long patch BER) [15,17].

UV-induced CPDs, 6-4 PPs and other bulky lesions that distort the DNA helix are primarily repaired via the nucleotide excision repair (NER) pathway. This is a multi-step pathway consisting in: 1) damage recognition, which further divides the NER pathway into two sub-pathways: global genome NER (GG-NER) and transcription-coupled NER (TC-NER). While GG-NER recognizes lesions in the whole genome and is not dependent on transcription, TC-NER only acts in the transcribed strand of active genes. GG-NER is dependent on DNA damage sensors, such as DDB and XPC-Rad23B complexes, that scan the genome for helix distortions and recruit downstream actors. On the other hand, TC-NER is initiated by stalled RNA polymerases, with the help of cofactors such as CSA and CSB. Once the damage is recognized and signalled, both sub-pathways converge into similar downstream processing; 2) formation of a stable pre-incision complex around the damage site, the transcription factor II H (TFIIH) complex, composed of ten subunits. TFIIH partially unwinds the DNA duplex and recruits RPA, XPG and XPA, the latter in turn recruiting the XPF-ERCC1 heterodimer, main actors in step 3) excision of the damage nucleotide. Incisions by XPF to the 5' side of the lesion and XPG at the 3' side, release a 24-32 base pair single-strand oligonucleotide containing the damage site. The upstream cut is performed first, generating a 3'-OH end which primes DNA synthesis to fill the gap before the downstream end is cut. Finally, 4) the completion of DNA synthesis by different polymerases and nick ligation by Ligase 1 (LIG1) finalize the repair process [15].

Single base mismatches and unpaired nucleotides can arise from errors in replication, deaminations and recombination between non-homologous sequences. These alterations are recognized and repaired by the mismatch repair (MMR) system. The repair process is initiated with the recognition of base mismatches and insertion/deletion loops by the MutS complexes. These complexes are heterodimers of the MSH proteins: MutSα and MutSβ [18,19]. In plants there is a third complex, MutSγ,

that preferentially recognizes certain base mismatches [20]. MutS complexes recruit the MutL heterodimer (MLH1-PMS2 in humans, MLH1-PMS1 in budding yeast and plants) to the site. Replication factor C (RFC) and Proliferating Cell Nuclear Antigen (PCNA) identify the newly synthesized DNA strand, locating and loading into strand breaks, inherent to the synthesis process, at the 3' end of the segment containing the mismatch. PCNA physically interacts with MutL, activating the latter to cleave at the 5' end of the segment. Exonuclease digestion from this nick followed by gap filling via DNA synthesis and ligation completes the repair [18,19].

Ionizing radiation, reactive oxygen species, chemical compounds (alkylating agents, crosslinking agents, radiomimetic compounds, DNA polymerase inhibitors and topoisomerase inhibitors) or errors during replication (collisions between transcription and replication machineries and replication over a single strand break) can lead to the simultaneous breakage of the phosphate backbone of both DNA strands yielding a double-strand break (DSB). Double-strand breaks are one of the most cytotoxic DNA lesions and their repair involves multiple DSB repair mechanisms. The discontinuity generated in the DNA helix can result in the loss of the complete fragment by the terminal end of the break if it is not repaired, which depending on the position of the break, genetic content and cell cycle status, among other factors, may potentially lead to cell cycle arrest, cell death or major genetic alterations. Moreover, erroneous repair of DSBs may lead to deletions, insertions and translocations with similar potential consequences for genome integrity. The highly deleterious nature of DSBs has thus driven the emergence and evolution of ubiquitous DSB detection, signalling and repair mechanisms throughout the living world.

2. Double-strand break repair in somatic tissues

2.1 DSB detection and signalling

The detection of double-strand breaks is the first step of the DSB-triggered DNA damage response (DDR). A key component in this is the MRX/MRN complex (Mre11, Rad50 and Xrs2 in budding yeast; MRE11, RAD50 and NBS1 in vertebrates and Arabidopsis). MRX/MRN detects and binds DNA ends, both clean (potentially religatable) and blocked (non-religatable) DNA ends, in the latter case releasing the blockage by cleaving the DNA 15-25bp upstream from the end [21,22]. MRX/MRN has the ability to bridge DNA ends, contributing to the tethering of the two ends of the break together [21,23,24]. This complex also plays a prominent role in activating Tel1/ATM. Tel1

(budding yeast)/ATM (human, Arabidopsis), a member of the PI3K-like protein kinases (PIKKs) family, is the main actor in DNA damage signalling altogether with Mec1 (budding yeast)/ATR (human, Arabidopsis), member of the same protein family [25]. At least three possible mechanisms of Tel1/ATM activation by MRX/MRN have been described: I) both in budding yeast and humans an interaction of the C terminus of Xrs2/NBS1 with Tel1/ATM mediates the recruitment of the latter to DSBs and promotes the activation of Tel1/ATM [26,27]; II) in absence of Xrs2/NBS1, the MRE11/RAD50 subcomplex is able to interact and promote the activation ATM in budding yeast and human cells [28,29]; III) in human cells the MRN complex association holds open the DNA helix and inhibition of this activity affects ATM activation [30]. These interactions collectively contribute to release the inhibited Tel1/ATM dimer into active monomers, to recruit it to the DSB and to induce its autophosphorylation [31]. Once Tel1/ATM is active, positive feedback loops between it and MRX/MRN has been described both in humans, via ATM phosphorylation of RAD17 [32] and via MDC1, primary "reader" of γH2AX [33]; and in budding yeast, promoting the retention of MRX to the DSB site [34,35].

The activation of Mec1/ATR, the other main DDR sensor, is not dependent on the MRX/MRN complex. Mec1/ATR is activated by persistent single-stranded DNA coated with RPA [36], so its function is broader than ATM's acting in a wide range of replication and damage stress situations [37]. When a DSB occurs, resection of one of the DNA strands at the DSB ends generates ssDNA segments where RPA binds (detailed further on). RPA-coated ssDNA interacts with Mec1/ATR via Ddc2/ATRIP [36,38], which facilitates its recruitment, and its kinase function activation depends on different proteins like Dpb11, Ddc1 and Dna2 [39–41] in budding yeast; TOPB1 and ETAA1 in humans [37,42].

Once Tel1/ATM and Mec1/ATR are activated and recruited to DSB sites they phosphorylate a large number of targets coordinating chromatin remodelling, DSB repair, cell cycle regulation and gene expression associated to genotoxic stress [43–45]. A key target for downstream events in DSB repair is H2A/H2AX. The phosphorylated variant of this histone by the DDR PIKKs, named γH2AX, plays a key role in the recruitment and accumulation of DNA repair proteins at DSB sites [46,47].

In Arabidopsis, homologues of MRN genes have been described [48–50], as well as *ATM* [51] and *ATR* [52]. RPA subunits (RPA1/2/3) are encoded by multiple genes, in contrast to budding yeast and human, that have sub-functionalized and play different although partially overlapping roles in the DNA damage response [53,54]. While disruption of MRN genes in animal models leads to embryonic stem cell lethality [55–57], MRN

mutants in Arabidopsis are viable, which offered a great opportunity for understanding the different roles of the complex. Null mutants of *MRE11* and *RAD50* genes show developmental deficiencies, hypersensitivity to DNA damaging agents, defects in telomeric maintenance and chromosomal instability, increasing the frequency of anaphase bridges [49,58–61]. NBS1 physical interaction with MRE11 as well as developmental defects and sensitivity to DNA damage agents in the null mutant have been described [50]. ATM and ATR roles in Arabidopsis, as in other organisms, are functionally differentiated, although partially overlapping in activating DNA damage response. Both *atm* and *atr* mutants are sensitive to multiple DNA damaging agents [62–65]. Induced H2AX phosphorylation via ATM/ATR is absent after γ-irradiation in *mre11* and *rad50* mutants, confirming the role or the MRN complex in activating ATM/ATR following DNA damage as in other organisms. However, DNA damage response is already spontaneously activated in these mutants, as they show γH2AX foci and arrested cells in non-irradiated plants. This spontaneous activation is dependent on ATR and not ATM, which may suggest a conservation of the MRN-mediated activation of ATM but not ATR in response to DNA damage observed in other organisms [66]. Analysis of the expression of genes involved in DNA repair, recombination and checkpoint activation in response to DNA damage induction also points to different effector functions of ATM and ATR, with ATM playing a prominent role [67,68]. The phosphoproteomic landscape of ATM/ATR in Arabidopsis has further confirmed their main function as effector kinases that phosphorylate a wide array of targets after irradiation [69]. An ATM/ATR-mediated response to telomeric damage has also been elucidated, again presenting functional distinctions between the two [70,71].

2.2. DSB processing and repair pathway choice

After DSB recognition and triggering of the DNA damage response, the way the DSB ends are processed will likely play an important role in the way the break is repaired. Two major pathways drive somatic DSB repair: non-homologous end joining (NHEJ) and homologous recombination (HR). Homologous recombination, generally considered an error-free pathway compared to the more mutagenic NHEJ, requires resection of the 5' ends of the break to generate 3' overhangs that with the help of recombination proteins can perform the search for a homologous DNA template for repair. For this reason, it is favoured during S and G2 phases in which a sister chromatid is present while NHEJ, independent of a template, is thought to be prominent at other cell cycles stages [72,73]. The choice between the two pathways is subject to complex multifactorial regulation, but the way the DSB ends are processed is key to direct the repair in one sense or another.

Xrs2/NBS1, member of the MRX/MRN complex, interacts with phosphorylated Sae2/CtIP, an essential cofactor for DNA end resection initiation that is recruited to the DSB site [74,75]. A second member of MRN, MRE11, is the catalytic subunit for the first steps of DNA strand resection. MRE11 has both 3'-5' exonuclease and endonuclease activity. MRE11 introduces a nick upstream the 5' end at both sides of the DSB to then use its 3'-5' exonuclease activity to digest that same strand from the nick towards the DSB [76,77]. This process results in short 3' single-stranded overhangs (~100nt) [73] that are coated by RPA. RAD50-ATP-dependent regulation of MRN complex conformation is thought to act as a "switch" that modulates the two different nuclease activities of MRE11 [78]. Extensive 5'-3' resection beyond MRE11 nicks is performed by EXO1 [79,80]. EXO1 has 5'-3' dsDNA exonuclease activity and *in vitro* it has preference for dsDNA substrate with 3' overhangs [81]. DNA2, an enzyme with both DNA helicase and ssDNA endonuclease activity, is also instrumental for extensive resection combined with the helicase Sgs1 in budding yeast and two orthologues in human: BLM and WRN helicases [82–84]. Different mechanisms have been proposed for resection termination, such as RPA dissociation, RAD51-RPA switching or EXO1 degradation (see review [73]).

It is now understood that resection is a key switch in the choice of HR versus NHEJ pathways for the repair of a given DSB. The heterodimeric KU70-80 complex (KU), hub of the NHEJ machinery, binds DNA ends soon after DSB formation at all cell cycles stages [85,86]. In budding yeast, KU-dependent blockage of resection is predominant in G1, when MRX-Sae2 are not activated by CDK1 [87]. In human, CDK-mediated phosphorylation of BRCA1 promotes a BRCA1-CtIP interaction that modulates resection initiation, although the mechanism is still unclear [73,88]. When they are active, the first step of nick plus 3'-5' exonuclease activity perform by active MRX/MRN-Sae2/CtIP complex is thought to release the KU barrier from the ends [89,90]. KU70 phosphorylation has also been shown to promote the dissociation of the KU complex from DNA ends during S phase [91]. Rad9/53BP1 is another modulator of end processing and pathway choice. In humans, 53BP1 promotes NHEJ by recruiting RIF1, which inhibits BRCA1 [92]. In addition, 53BP1-RIF1 acts after resection initiation by recruiting the shieldin complex, which binds ssDNA and protects it from extensive resection by recruiting CST-Polα, that is able to fill resected 3' ends [93]. In budding yeast, Rad9 accumulation inhibits Dna2-Sgs1 resection and hyperactivation of its downstream kinase Rad53 inhibits Exo1 by phosphorylating it [94]. The regulation of pathway choice is complex and fluid and it comprises a series of promoting and inhibiting factors at different levels that accumulate to tilt the balance towards one repair outcome.

In addition to the MRN complex, Arabidopsis orthologues of genes involved in DSB end processing such as *SAE2/CtIP* (*COM1*), *DNA2* (*JSH1*), *SGS1/BLM* (*RECQ4a* and *RECQ4b*) and the putative functional homologue of human *WRN* (*RECQ2*) show defects in DNA repair when the plants are subject to DNA damage [95–99]. A putative *EXO1* functional orthologue has been described in rice but has not yet been studied in Arabidopsis [100,101]. The conservation of their particular roles in the context of DSB end resection is probable, but remains poorly understood given the limitations in biochemical assays and the pleiotropic roles of these proteins at different steps of the DSB repair process. Mutant plants of *JSH1* display an increase of both spontaneous and induced homologous recombination using direct and inverted repeats as the reporter substrate [96]. *recq4a* and *recq4b* mutants have opposite phenotypes when analysing somatic recombination. While *recq4a* plants present and increase in both intramolecular and intermolecular recombination, presumably associated to its function as a D-loop dissolvase; in *recq4b* plants there is a decrease with respect to the control, suggesting a possible separation of function after the duplication [97]. Biochemical studies of RECQ2 also have shown a D-loop disrupting activity, but its possible role in resection remains unknown [98].

2.3. DSB repair pathways

Non-homologous end joining

The term non-homologous end joining (NHEJ) covers a number of DSB repair mechanisms characterized by the ligation of the two ends of the DSB without the need of a homologous DNA template. It however may be guided by the use of short microhomologies. In prokaryotes it appears to have a minor role as it has been lost in many families and its mechanism is minimalistic compared to eukaryote NHEJ [102]. Generally classified as mutagenic due to the absence of a requirement for a homologous repair template, NHEJ is not necessarily an inherently error-prone mechanism, being able to faithfully re-ligate DNA ends without inducing mutations. Nevertheless, the presence of blocked or incompatible DNA ends that need to be processed, or intrastrand microhomology-directed repair, may lead to the presence of deletions and/or insertions. Moreover, incorrect ligation of two DSBs may lead to chromosomal translocations or fusions [103].

The first step of NHEJ involves KU complex binding to the DSB ends. KU is a heterodimer of the proteins KU70 and KU80, encoded by the *XRCC6* and *XRCC5* genes in vertebrates, with DNA binding affinity for blunt ends and short 5' or 3' overhangs.

The KU complex acts as a scaffold for downstream NHEJ proteins to localize to the break and catalyse the repair [104]. In human, KU recruits DNA-PKcs to the DSB, a component of the PIKK family like ATM and ATR, to form the DNA-PK complex [105]. KU is also able to promote the binding of DNA ligase IV (LIG4) and its stimulatory cofactor XRCC4 to the DSB ends [106]. In budding yeast, which lacks DNA-PKcs, the MRX complex is responsible for recruiting Dnl4 and Lif1, orthologues of DNA ligase IV and XRCC4 respectively [107]. When the DSB ends are blunt, the KU-XRCC4-LIG4 complex is able to form a bridge between both sides and ligate them without further processing with the help on XLF/Nej1. When DSBs are not compatible for direct re-ligation, the NHEJ machinery has to process them prior to ligation. Different polymerases as Polμ and Polλ in human, Pol4 in budding yeast, promote the ligation of incompatible ends by adding some nucleotides in a template independent manner, sometimes generating short homologies, or filling-in 3' overhangs. Artemis, a nuclease with 5'-3' exonuclease activity plus endonuclease activity upon activation by DNA-PKcs, is thought to play a role at processing certain types of incompatible ends by performing short resection and digesting DNA flaps to facilitate ligation after microhomology recognition [108–110].

XRCC6 (*KU70*), *XRCC5* (*KU80*), DNA ligase IV (*LIG4*), *XRCC4* and *POLλ* homologue genes have been described in Arabidopsis, but not of genes encoding DNA-PKcs, Artemis and XLF [111–113]. KU70/80 complex formation is conserved as are its ATPase, helicase and DNA end binding activities. It is expressed in all plant tissues and their transcription is increased after DNA damage induction [111,114]. Both *ku70* and *ku80* mutants are sensitive to several DNA damage agents and *ku80* mutants display reduced end joining efficiency in a plasmid DNA assay [115–118]. LIG4 interaction with XRCC4 is conserved and their expression is also inducible by γ-irradiation. *lig4* mutants are sensitive to MMS and X-rays [119]. *POLλ* expression is up-regulated upon UV-B exposure, MMC treatment or high salinity and its knockout confers sensitivity to these DNA damage-inducing treatments. *polλ* plants also show DSB repair deficiencies as observed by comet assay [120,121]. These data together point to a conserved function of the NHEJ core mechanism and function in the model plant.

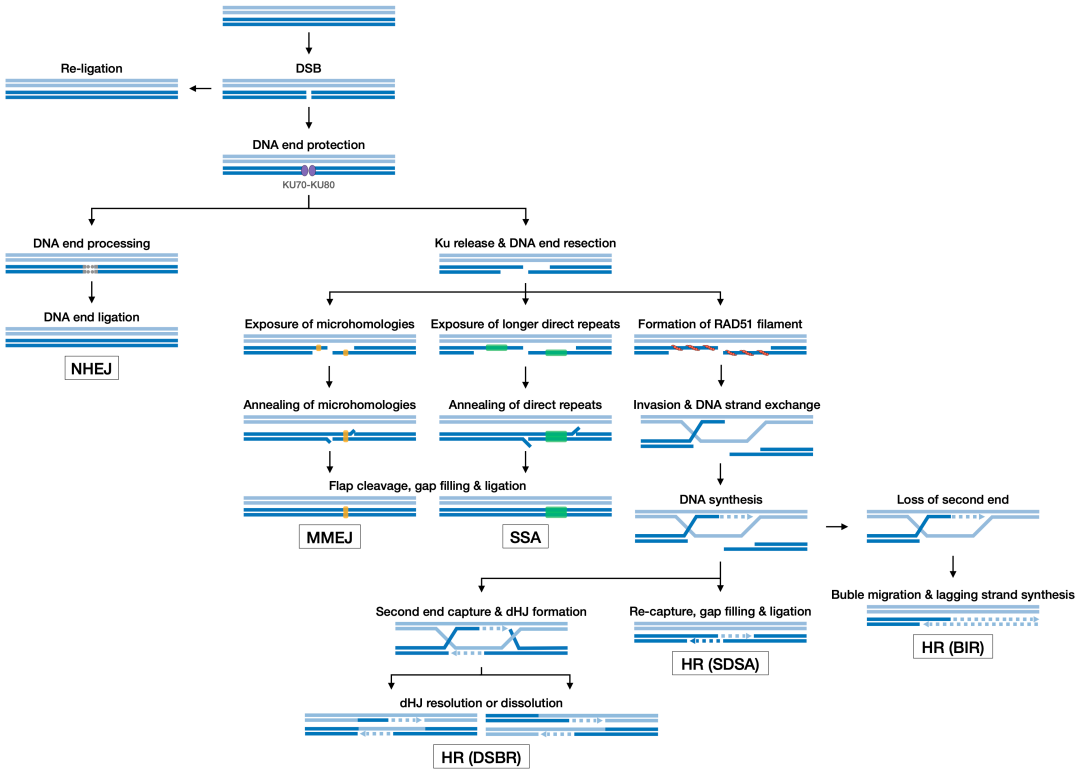

Figure 2. Model for double-strand break repair pathways in somatic tissues.

Following the formation of a double-strand break (**DSB**), the DSB ends may be religated if they have compatible overhangs and do not require further processing. Blunt ends have high affinity for KU70-KU80 binding (**DNA end protection**) which, if not removed from the DSB ends, channels the repair towards canonical non-homologous end joining (**NHEJ**). This however may be disrupted by the MRX/MRN complex, whose endonucleolytic and exonucleolytic activity is able to both release KU70-KU80 from the DSB ends and initiate the resection of these ends, generating 3'-ssDNA overhangs (**KU release and DNA end resection**) that may be extended by other exonucleases. These 3'-ssDNA resected ends are substrates for homology search and DNA base pairing. If short homologies are exposed, they may be annealed (**Annealing of microhomologies**) and resolved via cleaving of the non-homologous tails, gap filling via DNA synthesis and ligation of the DNA ends (**Flap cleavage, gap filling and ligation**) following the microhomology-mediated end joining pathway (**MMEJ**). Longer intrastrand homologies may be annealed and resolved in a similar fashion via the single-strand annealing pathway (**SSA**) with different factors involved. Loading of RAD51 and formation of the RAD51-ssDNA nucleofilament (**Formation of RAD51 filament**) channels the repair toward homologous recombination pathways via RAD51-mediated homology search and strand exchange (**Invasion and DNA strand exchange**). In somatic tissues, the sister chromatid is the preferred template over the homologous chromosome. Following strand exchange, the invading strand may be extended via DNA synthesis stabilising the D-loop intermediate (**DNA synthesis**). At this step, the invading strand may be dissociated from the D-loop and recaptured back to its original chromatid, using the extended end to bridge the DSB gap, anneal with the other side of the DSB and resolve via gap filling and ligation (**Re-capture, gap filling and ligation**) in what is known as the synthesis-dependent strand annealing (**SDSA**) pathway. If the second end is captured into the D-loop, the resulting double Holiday junction or dHJ (**Second end capture & dHJ formation**) may be then resolved via topological dissolution or nucleolytic resolution of the dHJ (**dHJ resolution or dissolution**). All SDSA, dHJ dissolution and part of the dHJ nucleolytic resolution outcomes will result in gene conversion products not associated to a crossover between the implicated chromatids. Nucleolytic resolution of the dHJ intermediate results in gene conversion associated (CO) or not (NCO) with a reciprocal exchange of the terminal segments of the implicated chromatids, depending of the cleavage planes of the two HJs. In the event in which the second end of the broken chromatid is not present as in the case of deprotected telomeres or in collapsed replication forks (**Loss of second end**), the D-loop may turn into a migrating bubble able to regenerate the lost segment of the chromatid via a replication-like mechanism (**Bubble migration & lagging strand synthesis**) known as break-induced replication or **BIR**.

Microhomology-mediated end joining

Microhomology-mediated end joining (MMEJ), also referred to as alternative non-homologous end joining (alt-NHEJ) or simply alternative end joining (a-EJ), is a repair pathway that shares features with both NHEJ and homologous recombination (HR). Its physiological function is not completely clear although some reports class it as a backup pathway for NHEJ. Unlike other end-joining mechanisms, it requires short resection carried by MRX/MRN and it usually uses longer homologies (less than 5bp for NHEJ versus 2 to 20bp for MMEJ) but it is not dependent on recombinase-catalysed strand invasion as for HR. Its mechanism is considered inherently mutagenic as the involvement of non-allelic short homologies will by definition result in DNA sequence deletions, inversions or translocations.

MMEJ shares the initial phase of resection carried out by MRX/MRN-Sae2/CtIP but it does not depend on the extensive resection by EXO1 and DNA2 in human cell lines [122]. In contrast, Exo1 has been proven necessary for MMEJ repair in budding yeast [123]. PARP1 binding to the DSB ends, in competition with the KU complex, has been associated with MRN recruitment in human and with the promotion of MMEJ via interactions with downstream members of the pathway [124,125]. PARP1 however is absent in yeast. Exposed microhomologies generated by the resection machinery then anneal in a recombinase-independent manner by a mechanism than is not yet understood. RPA coating of the ssDNA overhangs generated by the resection machinery antagonizes MMEJ by preventing this annealing, directing the repair towards HR [126,127]. Intrastrand annealing of microhomologies generates ssDNA flaps that are recognized and clipped by the structure-specific endonuclease activity of the Rad1-Rad10 complex in budding yeast, XPF-ERCC1 in human [128,129]. Resulting 3'-OH ends are extended by multiple polymerases in budding yeast, POLθ in human, to stabilize the annealed segment and fill the gap [130,131]. Multiple cycles of annealing-clipping-synthesis-separation can lead to insertion of patches from different templates before ligation, increasing the mutagenic potential of MMEJ pathway [132–134]. Finally, Ligase 1 (LIG1) or the Ligase 3 (LIG3)-XRCC1 complex in human and Dnl4 in budding yeast mediate the ligation of both DSB ends to complete the repair process [135].

Arabidopsis orthologues for *XPF*, *ERCC1* and *POLθ* (*TEBICHI*) have been described and the corresponding mutants present the expected sensitivity to DSB-inducing agents [136–138]. Defects on intrachromosomal recombination between tandem direct repeats have also been described in mutant plants of the three genes. In knockouts of *XPF* and *ERCC1*, which in other organisms catalyse flap removal prior to ligation, these defects are not detected when flap clipping is not necessary for

recombination [138–140]. Further evidence of a functional MMEJ machinery has been suggested in studies of telomere maintenance in *ku70/80* mutants, as MMEJ backup function when NHEJ is not active might explain telomeric elongation in these mutants as well as an increase in the implication of microhomology in telomere fusion that is lost when also mutating *MRE11* [115,116,141,142]. Moreover, *xpf* and *ercc1* mutations in absence of telomerase lead to the loss of telomeres and genomic instability [143]. Strong inhibition of T-DNA integration in mutants of *POLθ*, usually associated to microhomologies, and frequent patchwork around the insertion sites, might also be explained by a faulty MMEJ pathway [144,145]. *LIG1* and *XRCC1* orthologues have also been identified, but not *LIG3*. Both *lig1* and *xrcc1* mutants display defects in DSB repair [146,147].

Kinetic analysis of DSB repair after γ-irradiation confirmed an important physiological role of MMEJ in Arabidopsis during the first minutes after DNA damage induction, not merely as a backup for NHEJ or other pathways. These epistasis analyses also suggested the existence of not two, but three different end joining repair pathways in Arabidopsis: KU-dependent classical NHEJ, XPF-dependent MMEJ and an alternative end joining pathway that might act independently of the other two mediated by XRCC1. The three pathways are proposed to act in a temporally hierarchical manner with different windows during the minutes post-irradiation [148].

Single strand annealing

Single-strand annealing (SSA) is a pathway believed to be of particular importance in the repair of DSBs occurring between tandem direct repeat sequences. Sometimes included within the homologous recombination category, as it also depends on extensive resection and the annealing of medium-long homologies, this annealing does not involve strand invasion catalysed by recombinases. Although it does share the recombinase-free annealing of exposed DNA sequence homologies with MMEJ, some mechanistic features differentiate the two pathways [149].

SSA relies on the same components of DSB end resection machinery detailed above, including factors mediating the first steps of end processing such as MRX/MRN and those that catalyse extensive resection such as EXO1, WRN and DNA2 both in human and budding yeast cells [150–154]. Consistently, factors known to inhibit end resection favouring NHEJ such as Rad9/53BP1, RIF1 or RNF168 also inhibit SSA [151,155–158]. After end resection, the homologous sequences that flank the DSB anneal and the non-homologous 3'-ssDNA flaps are cleaved to permit gap filling by DNA polymerases and nick ligation. RAD52 has been proposed as a mediator of the annealing

both in mammals and yeast cells while the cleavage of DNA flaps is performed by the Rad1-Rad10/XPF-ERCC1 complex [153,159–162]. The MMR system appears to be implicated at different stages of the process as heteroduplex rejection mediated by different components of the MMR machinery together with Sgs1 has been observed in budding yeast SSA reporter systems [163,164]. Additionally, the Msh2-Msh3 dimer has been proposed to promote Rad1-Rad10 flap removal [159,164]. The polymerases and ligases implicated however are not certain [149]. Absence of factors involved in RAD51-mediated HR pathways such as RAD51 itself, RAD54 or BRCA2 increases SSA frequency, likely because long resected ss-DNA overhangs are a common intermediate of both pathways [153,165,166].

In Arabidopsis the presence of the SSA pathway has been mostly studied using a tandem direct repeat transgenic tester locus, the recombination of which reconstructs a reporter gene [167]. Nonetheless, contrasting results have been reported with respect to other organisms. Strikingly, MRE11 and COM1 (AtSae2/CtIP) were found not to be essential for SSA and overexpression of *RAD52* results in a significant decrease of SSA frequency [168,169]. ERCC1 however was instrumental for the repair via SSA using *in vivo* plasmid assays, arguing in favour of the conservation of its role in the SSA pathway [139]. MSH2 and RECQ4a (AtSgs1/BLM) also appear to have conserved roles in Arabidopsis SSA pathway [170,171]. Disruption of the nuclease MUS81, which has been reported to function in an interhomologue SSA pathway resulting in gross chromosomal rearrangements in fission yeast, impacts the frequency of SSA repair in Arabidopsis as well [171,172]. The absence of HR genes such as *RAD51*, *XRCC3*, *RAD51C* or *RAD54* does not seem to favour SSA, as it does in human or budding yeast cells, given that no increase of its relative frequency was detected [168]. Surprisingly, mutants of the *RAD51* paralogues *XRCC2*, *RAD51B* and *RAD51D* suffer a severe reduction of the SSA frequency and this was confirmed to be RAD51-independent, suggesting a direct role of these genes in the SSA pathway [173]. Whether these discrepancies reflect a divergence in the factors implicated in the Arabidopsis SSA pathway or the particularities of the exogenous reporter system used in many of the studies (or both) remain to be tested.

Homologous recombination

Homologous recombination (HR) comprises a series of double-strand break repair mechanisms that share their early steps, all being dependent on DNA damage response PIKKs signalling plus extensive resection of the DSB ends. Use of a homologous DNA molecule as a template results in the exchange, reciprocal or not, of sequence between the donor and recipient molecules implicated in the repair process. HR mechanisms are

highly conserved, both functionally and mechanistically, among prokaryote and eukaryote organisms. In somatic tissues HR preferentially uses the sister chromatid as the primary template for repair, and thus it is most active during S/G2 phases of the cell cycle. Homologous recombination can be divided into at least three differentiated pathways: synthesis-dependent strand annealing (SDSA), double-strand break repair (DSBR), break-induced replication (BIR). All have four general steps: 1) DSB detection and end processing; 2) presynaptic filament assembly; 3) homology search and strand exchange; and 4) DNA synthesis and resolution of intermediates.

MRX/MRN early processing followed by long-range resection mediated by EXO1 and DNA2 results in long 3'-ssDNA overhangs coated by RPA. At this point, assembly of the RAD51 presynaptic filament on these overhangs is critical for successful repair via HR. RAD51, homologue of the bacterial recombinase RecA [174,175], binds ssDNA replacing RPA and forms a helical nucleofilament along the 3' overhang in an ATP-dependent manner [176]. In budding yeast, RPA replacement is mediated by Rad52, which destabilizes the ssDNA-RPA interaction and physically interacts with RAD51 to promote its loading [176]. Rad52 protein is conserved in humans but this function is thought to be carried out by the BRCA2-DSS1 complex [177]. In addition to *RAD51*, a series of ancient genome duplications have generated *RAD51* paralogue genes that encode proteins which interact with RAD51. In budding yeast there are six paralogues: *DMC1*, *RAD55*, *RAD57*, *SHU1*, *CSM2* and *PSY3* [175,178–180]; whereas vertebrates have seven: *DMC1*, *RAD51B*, *RAD51C*, *RAD51D*, *XRCC2*, *XRCC3* and *SWSAP1* [181–186]. DMC1 functions as a meiotic specific recombinase (treated in detail further below). Budding yeast Shu complex (Shu1, Shu2, Csm2 and Psy3) and the Rad55-Rad57 heterodimer promote Rad51 filament assembly [187,188]. Rad55-57 opposes as well the filament disruption activity of the Srs2 helicase by promoting its reassembly [189]. Human RAD51 paralogues are members of at least three different complexes (BCDX2, CX3 and Shu complex) that regulate RAD51 filament formation and function, but their individual molecular functions are not completely understood [186,190,191]. The dsDNA-specific ATPase RAD54 also promotes the stabilization of the RAD51 nucleofilament [192].

Once the RAD51 presynaptic filament/complex is assembled together with its cofactors it is able to invade the donor DNA molecule to initiate the search for homology. Single-molecule studies with RecA and RAD51 filaments suggests that homology search involves transient opening of the donor DNA duplex and short microhomology sampling (synaptic complex) that is stabilised by further homology leading to extended strand exchange and formation of the more stable three-stranded postsynaptic filament [193–197]. RAD54 is an essential protein during this process, playing

different roles both in the template scanning for homology and in the stabilization and extension of the synaptic complex [198]. Additional factors needed to complete successful homology search in human are RAD51AP1, PALB2 and the HOP2-MND1 and BRCA1-BARD1 complexes [199–202]. The invading strand then needs to be intertwined with the complementary strand of the template to generate a dsDNA segment suitable for DNA synthesis. This intertwined invasion structure, named displacement loop or D-loop, is also promoted by RAD54 motor activity [203]. The activity of different helicases, such as Srs2/FBH1 [204,205], Mph1/FANCM [206,207], and the Sgs1/BLM-Top3/TOPOIIIα-RMI1 [208] complex can disrupt the D-loop at this step, which may be important to avoid ectopic recombination and/or multiple invasions of the same filament. If not rejected, the D-loop can be elongated from the 3' end of the invading strand by polymerases, but the RAD51 filament has to be disassembled first. Srs2/FBH1 and RAD54 are implicated in the disassembly [209–211]. PCNA and RFC complex can be recruited after RAD51 removal, promoting the activity of Polδ, principally responsible for this DNA synthesis [212,213]. From this common intermediate, three of the HR pathways diverge in its resolution:

In SDSA, the extended D-loop is unwound by the same helicases that were able to disrupt it in the previous step, leaving an elongated 3'-ssDNA end that is again coated by RPA and recaptured to the DSB site. The newly-synthetized extended overhang can then anneal with the opposite end of the DSB in a process mediated by Rad52 in budding yeast [214]. The gaps can then be filled by DNA synthesis and the nicks ligated, but the mediators of this events remain elusive.

In DSBR, the second resected end of the DSB is captured and annealed to the displaced strand of the D-loop. DNA synthesis primed by the invading 3'-ended strands of the broken DNA molecule, followed by nick ligation, generates a canonical double Holiday junction (dHJ) [215–218]. The presence of nicked (unligated) double Holiday junctions as a substrate for resolution has also been proposed [219,220]. Extension and direction of DNA synthesis together with adjacent DNA unwinding will determine the length of the double junction as well as its migration from the DSB site in a process called branch migration. Different resolution scenarios arise from this point. One involves the complex formed by Sgs1-Top3-Rmi1 in budding yeast, BLM-TOPOIIIα-RMI1/RMI2 in humans. Convergent migration of the two Holiday junctions mediated by Sg1/BLM followed by decatenation by the topoisomerase Top3/TOPOIIIα yields two DNA duplexes without a crossing-over between the two chromatids that initiated the recombination process (non-crossover) [221–223]. A second scenario involves the action of structure-specific endonucleases that resolve the dHJ structure by nicking at the junctions. In somatic tissues, three resolvases are involved in nicking the dHJ: Yen1/GEN1, Mus81-Mms4/EME1-2 and SLX1-SLX4 [219,224–228]. The symmetrical/non-

symmetrical orientation of the cleavage of the two junctions will determine if the products are two repaired DNA molecules with a reciprocal interchange of their flanking segments (crossover) or only with smaller interchanged segments resulting from the synthesis and ligation processes that configured the dHJ structure (non-crossover).

The homologous recombination core machinery is also conserved in plants, in which the two main somatic pathways (SDSA and DSBR) have been described. Mutant plants of the Arabidopsis orthologue of *RAD51*, although normal in vegetative development (as many other DNA damage repair genes), was proven sensitive to DNA damage agents and display a severe reduction of somatic homologous recombination when tested using reporter systems [168,229–231]. *RAD51* expression is induced when the plants are exposed to DNA damage agents and the RAD51 protein can be localized in the chromosomes at DNA damage sites [232–234]. The DNA damage sensitivity and defective somatic HR phenotypes observed in absence of RAD51 are phenocopied by plants expressing a catalytically inert RAD51-GFP fusion protein, corroborating the importance of its strand exchange activity for DSB repair via HR and confirming it as the conserved recombinase in somatic tissues [234]. Orthologues of genes that encode for mediators of RAD51 filament formation and/or modulators of its activity such as *BRCA2*, *RAD54* and the *RAD51* paralogues *RAD51B*, *RAD51C*, *RAD51D*, *XRCC2* and *XRCC3* have been described in Arabidopsis and all of them show sensitivity to DNA damage agents and defects in somatic HR [235–239]. The molecular function of many of them, although in many cases still not certain, is discussed in more detail further below in section 3.5. "*Presynaptic filament modulators*".

In addition to *RECQ4a/b*, the Arabidopsis genome does encode the other two main helicases involved in HR: *SRS2* and *FANCM*. Arabidopsis RECQ4a is the Arabidopsis BLM orthologue and, together with TOP3α and RMI1/2 forms the conserved SRT (RTR in this case) complex, although possible roles independent of the complex are also suggested by the observation that *top3α* mutants present a much more severe phenotype (early lethality) than mutants of the other two components [97,240,241]. Mutants of the three genes (hypomorphic for *TOP3α*) show sensitivity to multiple DNA damage agents and hyperrecombination when tested using reporter systems for inter-molecule HR events, as observed in mammal and yeast cells [97,241–243]. SRS2 has conserved helicase activity and ability to unwind multiple branched DNA structures including HJs *in vitro,* as well as ssDNA annealing activity, but no functional characterization *in vivo* has yet been published [244]. FANCM has been described as a suppressor of spontaneous and cisplatin-induced HR and a promotor of bleomycin and I-SceI-induced HR [245,246]. This apparent discrepancy might be explained by the nature of the DNA lesion which could impact the repair pathways engaged: cisplatin-induced

HR events predominantly originate from the repair of DNA cross-links during replication, also the probable source of spontaneous HR events, while I-SceI cleavage and bleomycin are expected to directly generate DNA breaks [245,247,248].

Regarding HR resolvases, Arabidopsis orthologues for *MUS81*, *MMS4/EME1-2* and *YEN1/GEN1* (*SEND1*) have been reported [249–252]. Both Arabidopsis MUS81 and SEND1 are able to cleave HJs *in vitro* [250,252]. *mus81* plants are sensitive to DNA damage agents and show mild cell division and genome stability defects, while *send1* plants show no significant phenotypes [249,251]. SEND1 is essential however in the absence of MUS81, with *mus81 send1* double mutants presenting very severe developmental defects and genome instability with respect to the single mutants. The two nucleases do thus act in somatic tissues, with SEND1 apparently playing a secondary role and only becoming essential when MUS81 is absent [251]. This secondary role of SEND1 complicates its study and little more information is available as yet. Simultaneous depletion of MUS81 and RECQ4a is lethal in Arabidopsis, similarly to other eukaryotes as budding yeast or Drosophila, and this lethality is suppressed by the absence of RAD51-dependent recombination in *rad51c* mutants, further confirming the conservation of the two HR resolution pathways: HR intermediate dissolution by the SRT (RTR) complex and resolution via nucleases and the main factors implicated [171,249,253,254].

BIR is a resolution pathway specific to certain situations in which only one end of the DSB can be used to complete the repair process through the initiation of a replication-like bubble on the donor chromatid by the invading DNA end. This contrasts to SDSA, which requires second end to re-capture the extended invading end for completion and for DSBR, where the second end must invade the template molecule to form the dHJ. Replication fork collapse when the fork passes through an unrepaired single strand break and telomeric recombination are the main situations in which BIR is believe to play an important role for DSB repair [255,256]. A mix of replicative machinery and BIR-specific factors are recruited generating a replication-like bubble from the D-loop that slides along the template DNA molecule with the help of the helicase Pif1 [257–260]. In the current model of BIR, leading strand synthesis from the invading 3' overhang along the sliding bubble generates a long fragment of ssDNA that is later used as a template for lagging strand synthesis to reconstitute the dsDNA molecule from the DSB breakpoint [261]. There is little evidence of BIR in Arabidopsis, although its activation as a telomere maintenance mechanism in absence of telomerase has been proposed. While sudden loss of telomeric repeats in presence of telomerase is corrected by addition of new repeats, in telomerase mutants the telomere loss phenotype is worsened by the depletion of RAD51 catalytic activity, found to colocalize with telomeric repeat probes,

suggesting a role of RAD51-mediated strand invasion of the sister chromatid in telomere maintenance in an HR pathway that the authors propose to rely on BIR mechanism. This mechanism might be supported by the action of the RTEL1 helicase [262].

Double-strand break repair via either end joining or homologous recombination mechanisms is an essential process to deal with the spontaneous appearance of these lesions in the genome, in order to preserve genome integrity. Spontaneous DNA damage is however not the only source of DSBs. Physiological introduction of double-strand breaks to induce recombination is a conserved feature among eukaryotes in particular situations or cell/organism processes and has also been observed in some viruses. Bacteriophage integrases cleave both donor (phage) and template (host) DNA molecules to facilitate the integration of the phage DNA via recombination into the host genome [263]. Eukaryotes' type II topoisomerases are enzymes that bind to a DNA duplex and induce topological changes by generating transient DSBs. They have a key role in essential cell processes such as replication, transcription or resolving detrimental supercoiled DNA structures. The shuffling potential of DSB repair via recombination to generate genetic variation has also been positively selected in mammals' adaptive immune system. Generation of new antigen-binding immunoglobulins and T-cell receptors is achieved by DSB induction and recombination in the antigen receptor V, D and J genes arrays in lymphoid cells (V(D)J recombination). In mature B-cells, class switch recombination (CSR) generates isotypes of immunoglobulins that bind the same antigen but with different effector function by inducing DSBs and recombining the genes encoding for their heavy chain [264].

A physiological and programmed induction of double-strand breaks is also a conserved feature among eukaryotes with sexual reproduction, occurring at the beginning of meiosis and repaired using homologous recombination as the primary pathway in a highly regulated manner.

3. Meiotic double-strand break repair

Sexual reproduction is the prevailing method of reproduction among eukaryotic organisms. Direct evidence of either obligate or facultative sexual reproduction or indirect evidence by the presence of genes involved in plasmogamy (gamete fusion) and/or karyogamy (nuclear fusion) has been gathered in evolutionary distant groups of the Eukarya domain, suggesting its presence back to LECA (Last Eukaryotic Common Ancestor) [265,266]. Syngamy, the predominant type of sexual reproduction in eukaryotes,

requires the production of two cells that carry half the genetic information of their parentals, called gametes, which will fuse and regenerate a new individual with the same genetic content as the parents. Meiosis is the chromosomal foundation of this process.

Meiosis is a specialized cell division of the germ cells consisting of one round of DNA replication followed by two rounds of chromosome segregation (or division) as opposed to mitosis, in which only one step of chromosome segregation happens. The second meiotic division resembles the mitotic division, where sister chromatids of each chromosome migrate to opposite spindle poles. The first meiotic division is however reductional, achieved by monopolar attachment of the sister chromatids to the spindle that leads to the migration of the two chromosomes of each homologous pair (in diploid organisms) to opposite poles reducing the chromosome number of the daughter nuclei to half. Meiosis produces four gametes with half the chromosome number of the parental germ cell.

In the course of the first meiotic division, an induced and highly regulated process of DNA damage and repair is essential, in most cases, for proper chromosome alignment and segregation. The primary DNA repair mechanisms involved lead to extensive genetic recombination, shuffling parental and maternal genomes and generating new allelic combinations. Meiotic recombination is thus one of the main drivers of natural evolution in sexually reproducing organisms and its modulation a key element in the toolbox for artificial evolution and the generation of new varieties of human interest in the plant field. This, in addition to the importance of fertility in the disciplines of human and animal health, has put the spotlight on the study of the mechanistic insights of DNA damage induction, repair and their regulation happening during meiosis.

3.1. Stages of meiosis

The two meiotic divisions conserve the four main stages of the mitotic division, described primarily by cytological studies analysing the structure and condensation of the chromatin and the position of the chromosomes in relation to each other. These stages are prophase, metaphase, anaphase and telophase, commonly named I or II to refer to the first or the second meiotic division. Prophase I is however further subdivided into five extra stages as, in contrast to mitosis, meiotic prophase I is particularly long and the chromosomes undergo a series of changes associated to meiotic recombination and synapsis. The five meiotic prophase I stages are leptotene, zygotene, pachytene, diplotene and diakinesis.

The first description of *Arabidopsis thaliana* meiosis was published in 1965 by Steinitz-Sears [4] but it was not until the late 1990s with the evolution of cytogenetic techniques and microscopy that a detailed characterization in the model plant was published [267,268]. Arabidopsis is a monoecious species with bisexual flowers, meaning that they produce both male and female gametes, pollen and ovule respectively. Somatic cell differentiation into germ cell precursors, pollen mother cells (PMC) and megaspore mother cells (MMC), as well as their meiotic entry is independent in the two cell lineages, resulting in asynchronicity between the male and female meiotic division stages. In addition, the number of PMCs is far superior to the MMCs (250 to 50 per flower bud, approximately) [269,270]. These two factors have resulted in the use of male meiosis as the standard for *Arabidopsis thaliana* meiotic characterization and so it is in the present work.

The meiotic divisions are preceded by a round of genome replication followed by a G2 phase. During pre-meiotic S-phase, meiosis-specific subunits of the cohesin ring, such as REC8 (SYN1 in Arabidopsis), are loaded in substitution of their mitotic counterparts [271]. The cohesin ring plays an important role during meiosis as it maintains sister chromatid cohesion all the way though prophase I and its specific depletion from the chromosome arms in metaphase is essential for the migration of homologous chromosomes at metaphase I and the sister chromatids at metaphase II.

Prophase I

As the nucleus moves from G2 into meiotic prophase I, the chromatin still has a diffuse appearance and the telomeres start to cluster in a limited area of the nuclear periphery, arrangement known as chromosomal bouquet, which is thought to play a role in the initial steps of chromosome pairing and homologous recombination [272,273].

The first stage of prophase I, leptotene, is characterized by the initiation of the condensation of the chromatin, that changes its look from the more diffuse appearance in G2 to observable fibres in chromosome spreading preparations (Figure 3B). During the course of this stage, the meiotic axial element is polymerized, a proteinaceous structure that anchors chromatin loops. In Arabidopsis the structural components of the axial elements are ASY1, ASY3, ASY4 and the cohesin ring [274–276]. The axial element not only plays an important structural role, but it regulates meiotic recombination at different levels along prophase as the recombination machinery is recruited to the vicinity of this structure. As the axial elements polymerize, DSBs are induced and this initiates meiotic recombination. Coupled to DSB induction, chromosome movements

inside the nucleus propitiate the coalignment of homologous chromosomes, named chromosome pairing [277,278]

Paired homologous chromosomes with their chromatin organized along the axial elements start polymerizing a proteinaceous scaffold composed of transverse filaments in between the axial elements that physically links them. In Arabidopsis these transverse filaments are formed by the protein ZYP1. The tripartite structure formed by the two axial elements (from here on referred as lateral elements) and the newly synthetized central element is called synaptonemal complex (SC) [279–281]. This event defines the transition from leptotene to zygotene (Figure 3C). The occurrence of these events is not synchronous in the whole genome. During zygotene, some regions of the genome are still subject to the induction of DSBs or chromosome pairing while in others synapsis is completed and DSBs start to be resolved [282]. However, early intermediates of recombination are prominent over the course of zygotene as observed by the dynamics of the recombinases RAD51 and DMC1 [283,284]. The chromosomes keep condensing and the polymerization of the synaptonemal complex linking homologous chromosomes together gives them the appearance of thick fibres with respect to the regions that are not synapsed yet.

Completion of synapsis in the whole genome, generally determined by the detection of ZYP1 and the significant fainting of ASY1 fluorescent signal by immunolocalization, defines the boundary between zygotene and pachytene (Figure 3D). Chromosomes are noticeably shorter due to chromatin condensation and individual pairs of synapsed homologous chromosomes can be tracked from end to end. There is a significant decrease of early intermediates of recombination (RAD51 or DMC1) and proteins implicated in the resolution of late intermediates can be localized, such as MLH1, suggesting the completion of the meiotic recombination during this stage [283–285].

Chromatin condensation continues and the synaptonemal complex starts depolymerizing from the chromosomes, transitioning from pachytene to diplotene (Figure 3E). Diplotene chromosomes have still a fibrous appearance and the degradation of the SC remove the physical linkage between their axes. However, they remain attached by chiasmata. A portion of the DSBs repaired via homologous recombination gives rise to crossovers between homologous chromosomes. These interhomologue crossovers, in the context of a meiotic chromosome with the sister chromatids held together by cohesins, result in the physical linkage of the two homologous chromosomes. The cytological visualization of this physical link is called a chiasma. In Arabidopsis and most species, at least one chiasma per pair of homologous chromosomes is needed to ensure proper reductional segregation in metaphase I.

Nevertheless, achiasmatic meiosis with proper reductional segregation is observed in some organisms [286–288]. Homologous chromosomes held together by chiasmata are named bivalents.

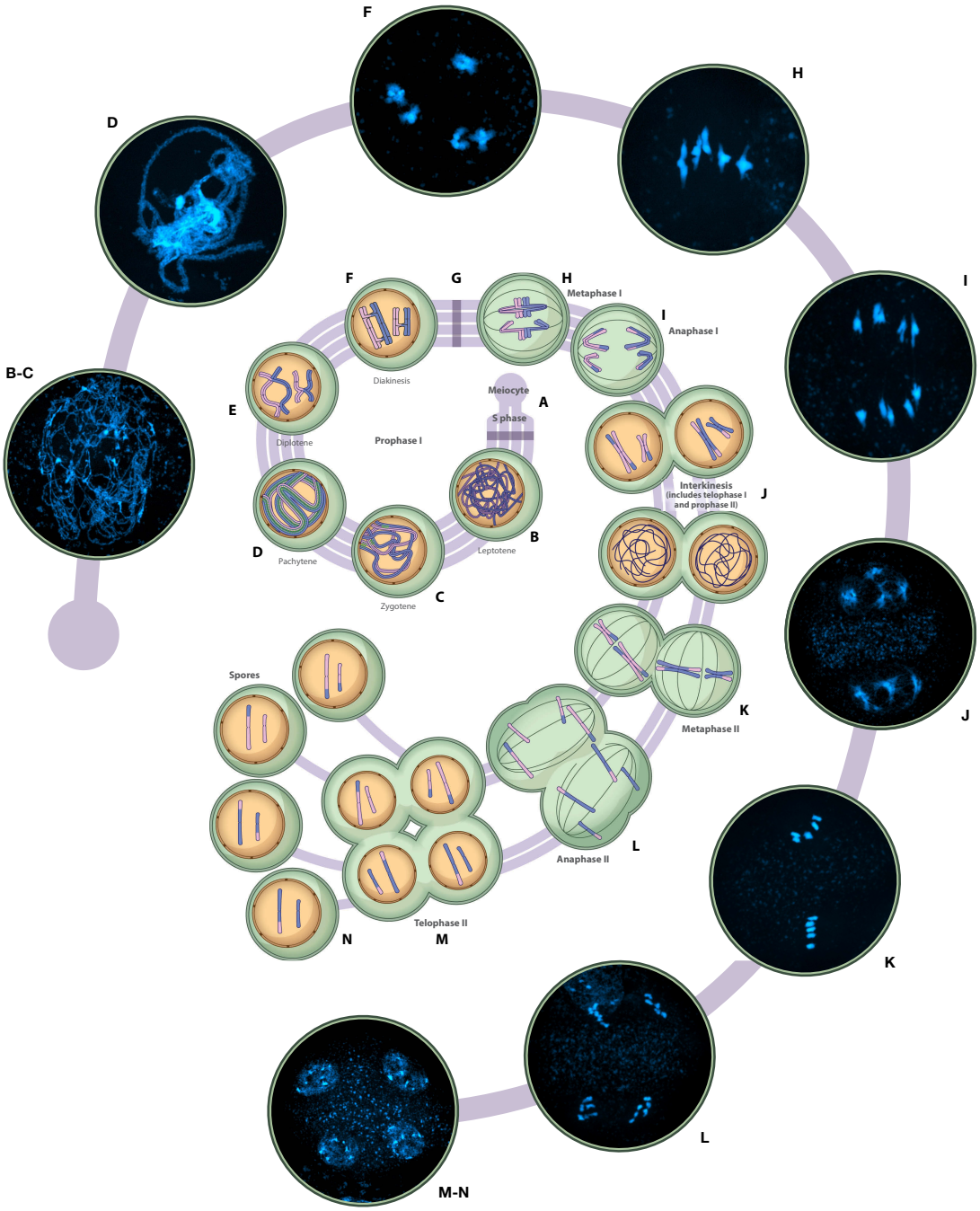

Figure 3. Meiosis in *Arabidopsis thaliana*.

Adapted from Mercier *et al.* (2015). Internal pictograms depict the different stages and events of the meiotic divisions matched with microscopy pictures of *A. thaliana* meiocytes by the letters.

Complete depolymerization of the synaptonemal complex and further condensation of the chromosomes, changing the fibre-like structure into more compact entities, lead to diakinesis (Figure 3F). In species with big chromosomes, chiasma structures are easily distinguishable and countable at this step, but not in Arabidopsis, in which the size and the state of the chromatin makes this difficult. The nuclear envelope begins to disorganize and will disappear before metaphase I [289]. Spindle microtubules and kinetochores start interacting to achieve to align the chromosomes in the soon-to-be metaphase I plate with the sister kinetochores aligned to the same spindle pole [290,291].

Metaphase I

When chromosomes achieve maximum condensation, the nuclear envelope is lost and the bivalents are aligned in the metaphase plate with the kinetochores of the two chromosomes of each pair pulled towards opposite poles of the spindle, the cells reach the stage of metaphase I (Figure 3H). Arabidopsis chiasmata numbers can be inferred on metaphase I chromosomes by observation of chromosome morphology, analysis of FISH signals of the 5S and 45S rDNA gene arrays and the shape of each bivalent [292,293]. Bivalents remain together until the Anaphase-Promoting Complex (APC/C) releases Separase from its inhibitor, Securin (AESP and PANS1 in Arabidopsis, respectively) [294,295]. Separase then cleaves the cohesin rings freeing sister chromatid arms, resolving chiasmata and releasing the tension between the two chromosomes of each bivalent allowing migration towards opposite spindle poles. Centromere cohesion is still necessary to avoid premature sister chromatid disengagement and segregation errors, and this is protected in Arabidopsis by a not yet fully described mechanism mediated by PP2A and Shugosin [296,297].

Anaphase I

Cohesin cleavage triggers anaphase I (Figure 3I). Homologous chromosomes migrate to opposite spindle poles driven by the shortening of the microtubules attached by the kinetochores achieving reductional segregation. Organelles are redistributed inside the cell, moving towards the space between the two sets of chromosomes.

Telophase I

The two sets of chromosomes arrive at the spindle poles and there a is rapid decondensation of the chromatin (Figure 3J). Organelles form a clear barrier between

the two sets of chromosomes and the nuclear envelope start reorganizing around both of them in a shared cytoplasm. This configuration with two haploid nuclei is called dyad.

Prophase II

During prophase II chromosomes recondense again into individualized entities, the nuclear envelopes are disorganized and two new spindles are formed. Microtubules attach to the kinetochores, in this case aligning sister kinetochores to opposite poles of the spindle. This stage is much faster than prophase I and neither induction of DSBs nor meiotic recombination processes are involved.

Metaphase II

Maximum chromatin condensation during the second meiotic division is reached again in metaphase II (Figure 3K). Chromosomes align into two metaphase plates with sister chromatids kinetochores facing opposite poles of the spindle. Cleavage of the centromeric cohesins permit sister chromatid migration towards the two poles [298].

Anaphase II

Once cohesion is released, microtubule shortening drives the migration of sister chromatids (Figure 3L). This second division is equational, not reductional, maintaining the chromosome number with respect to the haploid dyad. Organelles again are redistributed to form a barrier in between the two sets of single chromatid chromosomes at both sides of the dyad.

Telophase II

Chromosomes reach the spindle poles and start decondensing (Figure 3M). The four sets of chromosomes are clearly separated by an organelle barrier in the shape of a cross. The nuclear envelopes start to organize around the chromosome sets and so do the cell membranes and the cell walls as, in contrast to the first meiotic division, there is cytokinesis after the second division [299]. The final products of the meiosis of one PMC are four haploid microspores that when still attached together are called tetrad. The tetrad will be fragmented into four individual microspores (Figure 3N), each one undergoing two mitotic divisions and an specific program of cell differentiation to end up generating four pollen grains [300].

3.2. Double-strand break formation

Meiotic recombination is initiated at the onset of meiosis by the induction of double-strand breaks distributed throughout the genome. Different proteins collaborate to generate DSBs but it is SPO11 that catalyses the breakage of the DNA. SPO11 is a highly conserved protein that has evolved from the A subunit of the type IIB topoisomerase Topo VI. Topo VI acts as an A_2B_2 heterotetrametric complex where the A subunits perform the DNA cleavage and the B subunits have ATP binding and hydrolysis activities supporting strand passage and break ligation [301,302]. SPO11 was long thought to work as a A_2 dimer, but recent reports in Arabidopsis and mouse have identified MTOPVIB/TOPOVIBL, the B subunit of the SPO11 complex [303,304]. Encoded by a single gene in many species, *SPO11* has been duplicated in plants, with Arabidopsis having three *SPO11* paralogues: *SPO11-1*, *SPO11-2* and *SPO11-3* [305,306]. Analyses of single mutants of these genes and their combinations have shown that SPO11-3 has somatic functions and is not involved in meiotic recombination. Both SPO11-1 and SPO11-2, on the other hand, are required for DSB formation in meiosis, likely in the form of an A_1A_2 heterodimer [303,307–309].

While the presence and function of SPO11 is conserved across most eukaryotes, the proteins that collaborate with it to form the DSB machinery are variable. In *S. cerevisiae,* Spo11 and nine other proteins have been shown to be needed for DSB formation. These are classed into three sub-groups: the core complex (Spo11, Ski8, Rec102, Rec104), the MRX complex (Mre11, Rad50, Xrs2) and the RMM proteins (Rec114, Mei4, Mer2) [310]. Core complex proteins Rec102 and Rec104 would function as the B subunits of a Topo VI-like heterotetramer with Ski8 playing an essential although unclear role in the formation of the complex [311–313]. MRX function in DSB formation has only been reported in budding yeast and *C. elegans* [314]. The specific DSB promoting activity of MRX is unknown, but it has been proposed that its early recruitment might ensure the coordination between DSB formation and DSB resection [315,316]. RMM proteins localize to the chromosomes prior to DSB formation and biochemical studies link them in two complexes [317]. As with the core and MRX complex proteins in those organisms, absence of any of the RMM proteins impairs DSB formation. Their molecular role is unclear, although it has been proposed that they might localize the DSB machinery to the chromosome axis [310,318,319]. In mouse, the most studied model for mammal meiosis, the core complex is formed by SPO11 and TOPOVIBL [304,320] and the homologues of budding yeast RMM (REC114, MEI4, IHO1) conserve their interactions and their chromosome axis localization [321–323]. A fifth protein, MEI1, is also instrumental in mouse DSB formation and although its function is not clear, it mediates the

association of MEI4 with the axis [324,325]. The mouse MRN complex, however, is not needed for DSB formation [326].

Besides SPO11-1 and SPO11-2, five other proteins have been shown to be involved in DSB formation in Arabidopsis: MTOPVIB, PRD1, PRD2, PRD3 and DFO [303,327–329]. MTOPVIB interaction with SPO11-1 and SPO11-2 has been proven necessary to promote the interaction between the two paralogues, suggesting a core complex formed by these three proteins [303]. PRD1, which shows homology to mouse MEI1, interacts with most of the DSB proteins, possibly acting as a platform for the DSB machinery [282]. PRD2 and PRD3 have been postulated to be homologues of MEI4 and MER2 [282,328]. The third component of the RMM complex, REC114, is also present in Arabidopsis (PHS1), although it is not needed for DSB formation. Furthermore, PRD3 interaction with the other two homologues of the RMM complex proteins has not been detected. These two observations suggest that the RMM complex structure may not be conserved in Arabidopsis [282]. PHS1 and PRD2 do however interact with a plant specific DSB protein, DFO, but the absence of meiotic defects in *phs1* mutants argues against a divergent RMM complex formed by these three proteins [282]. Association of several of the DSB machinery proteins with the chromosome axis has been detected, although neither MTOPVIB nor SPO11-1 focus numbers are affected in single mutants of the axis proteins ASY1 and ASY3. PRD3 foci numbers are, however, hinting at differences in the hierarchy of these associations [282,328]. The MRN complex, as in mammals, is not required for DSB formation [50,60,330]. Neither is the homologue of budding yeast Ski8, identified in Arabidopsis but not required for meiotic recombination or progression [331]. This high variability in SPO11 cofactors is not only observed between eukaryote kingdoms, but also between species belonging to the same kingdom. In Plantae, as an example, proteins that are not involved in DSB formation in the dicot Arabidopsis, such as SDS or PHS1, has been shown to be essential in monocots like rice and maize respectively [282,328,332,333].

When the DSB machinery is assembled and loaded onto the chromosomes, DSBs are introduced by SPO11. Detailed biochemical analysis of cleavage sites and their subproducts indicate that SPO11 covalently binds DNA and cuts both strands, leaving 2 nucleotides 5' overhangs. After the cleavage, SPO11 remains covalently attached to both sides of the DSB, blocking the ends until the first steps of end processing release short oligonucleotides with SPO11 bound to their termini [334,335]. Two prominent size populations of SPO11-oligos are detected: around 8-12nt and 25-35nt. In addition, recent high-resolution analyses in budding yeast and mouse have unveiled a faint ladder of 10nt periodical oligos ranging from 33nt to more than 100nt. Less frequent in mouse, they add up to 20% of detected SPO11 cuts in budding yeast. These longer Spo11-

oligos correspond to close double cuts, called concerted cuts. The periodicity, corresponding to multiples of the helical pitch of the DNA (around 10.5nt), is evidence of constrained SPO11 interaction with only one face of the double helix and the cleavage in DNA bending motifs [336,337].

3.3. Double-strand break regulation

Notwithstanding its importance for balanced chromosome segregation and the generation of genetic variation in gametogenesis, the induction of DNA damage during meiosis is potentially highly deleterious. Unrepaired, partially or mis-repaired DSBs generate structures such as acentric and dicentric chromosomes that cannot be resolved without persistent damage. Therefore, regulatory mechanisms have evolved in eukaryote organisms to control the time window for meiotic DSB induction, the number of DSBs and their distribution at both local and genome-wide scales.

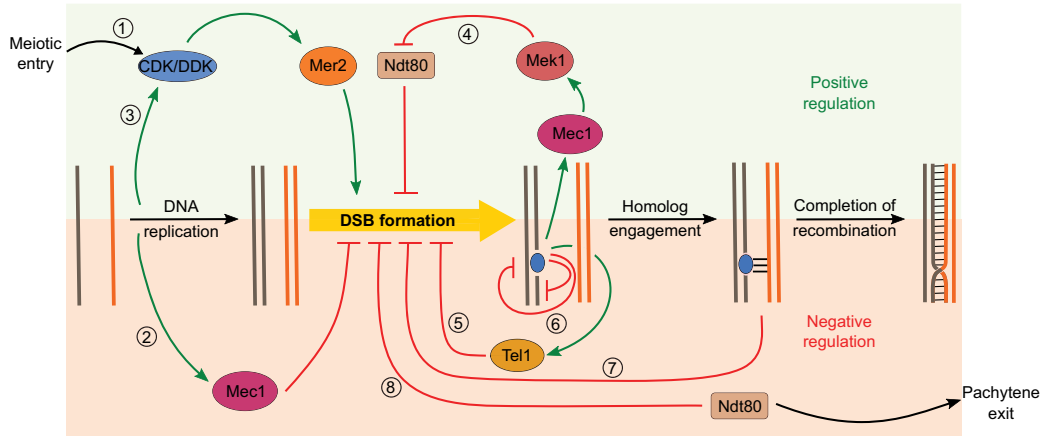

Figure 4. Regulatory mechanisms control DSB formation in meiosis.

Adapted from Yadav & Bouuaert (2021). Depiction of the multiple regulatory circuits controlling DSB formation that have been described in different organisms, although primarily budding yeast. DSB formation is tied to cell cycle control through **(1)** CDK/DDK-mediated phosphorylation of Mer2, promoting DSB formation. It is as well connected to pre-meiotic replication though **(2)** Mec1-mediated inhibition of DSB formation in case of replication stress and **(3)** replication-dependent promotion of Mer2 phosphorylation, thereby DSB formation. **(4)** Recombination defects activate a positive feedback loop for DSB formation via induction of a Mec1/Mek1-mediated inhibition of Ndt80, which extends prophase I, extending as well the DSB-competent window. **(5)** Activation of the DNA damage kinase Tel1/ATM inhibits further DSB formation, hence generating a negative feedback loop for it. **(6)** DSB interference limits the formation of adjacent DSBs in *cis* and in *trans* via Tel1/ATM activation. **(7)** Homolog engagement shuts the window for DSB formation though the SC-dependent removal of DSB proteins as well as **(8)** pachytene exit triggered by the activation of Ndt80.

Temporal regulation

Double-strand breaks are especially problematic during replication as they are a major cause of fork collapse. Coupling completion of pre-meiotic DNA replication and DSB induction is thus essential to ensure proper initiation of meiosis. Such coordination between replication and DSB induction has been observed in multiple organisms, such as budding and fission yeasts, mouse, human and barley [338–341]. In budding yeast, blocking replication prevents DSB formation and delaying the replication of a chromosome segment specifically delays break formation in that segment [338]. The cell cycle kinases CDK-S and DDK, recruited to the replisome, independently promote DSB formation by sequentially phosphorylating Mer2 in the wake of the replication fork. These modifications are important for the chromatin association of other members of the DSB machinery, like Rec114 and Mei4, and the interaction between Mer2 and Xrs2 [342–344]. Replication stress activates a Mec1/DDK-mediated replication checkpoint than delays the induction of DSBs by inhibiting Mer2 phosphorylation, downregulating Spo11 transcription and blocking chromosomal loading of Rec114 and Mre11 [345].

In mouse and human, the relative abundance of DSBs correlates with replication timing, with preference for early- compared to late-replicating regions. This correlation is also observed when analysing recombination intermediates and recombination products, with small distortions in the earliest replicating regions related to hotspot erosion and intersister DSB repair [340]. Local modifications of replication origin efficiencies in fission yeast lead to changes in Rad51 distribution, used as a marker for DSBs, and recombination rates [339]. In barley, DSB formation using γH2AX as cytological marker appears to happen first in euchromatin-rich distal portions of the chromosomes than in interstitial/proximal regions. Analyses of replication timing using pulses of detectable nucleoside analogues showed that replication was completed first in these same portions, so a S-phase-linked regulation of DSB formation was proposed [341].

The modulation of the DSB permissive period is also an important mechanism to ensure that all breaks are repaired by the end of prophase and, in species with DSB-dependent chromosome pairing and synapsis, that all chromosomes associate and are able to form at least one crossover in later stages. *spo11* hypomorphic mutants of budding yeast, in which fewer numbers of DSB are generated, fire a Mec1-dependent checkpoint that activates Mek1, which inhibits Ndt80, delaying pachytene exit and extending the DSB permissive window. Homeostatic control of DSB numbers is thus achieved via counteraction of the defects in DSB formation by extending the period in which DSBs can be formed via this positive loop [346,347]. This Mec1/Ndt80-mediated

mechanism has been described also in mutants with defective crossover formation to ensure the presence of the obligatory crossover before chromosome segregation [348]. Single *ndt80* mutants, in which Spo11 function is not impaired, accumulate higher numbers of DSB than wild-type cells as the DSB permissive period is also extended [348,349]. *C. elegans* mutants with crossover formation defects, either in the whole genome or just lacking crossovers in one chromosome, retain proteins involved in DSB formation on the chromosomes, suggesting also the existence of mechanisms that allows the extension of the DSB permissive window to ensure the obligatory crossover [350].

Homologue engagement has been proven to play an important role in regulating the end of the DSB permissive window in different species. A second layer of regulation of this, independent of Ndt80 and dependent on homologue engagement, was discovered in budding yeast ZMM mutants with severe crossover formation defects [348]. Recent analysis of karyotypically abnormal strains carrying homoeologous chromosomes, monosomies or trisomies in which the abnormal chromosomes do not form synaptonemal complex have shown that the implicated chromosomes specifically hold DSB proteins for longer periods and accumulate more DSBs. Synapsis-defective, crossover-proficient mutants also accumulate extra DSBs in a genome wide manner. The proposed mechanism involves chromosome axis remodelling by Pch2, that promotes Hop1 relocalization dissociating it from Red1 and removing Rec114 and Mer2 from the axis [351]. This hypothesis is supported by the observation that certain telomere adjacent regions that retain Hop1 throughout pachytene continue to receive DSBs [352,353]. A similar mechanism has been proposed in mouse. Both unsynapsed regions in mutants with defective synapsis and the unsynapsed portion of the sex bivalent in male mice accumulate DSBs as prophase progresses [354]. Cytological analysis of the dynamics of IHO1 (Mer2) indicate that it is removed from the axis when chromosomes synapse and this removal is partially dependent of TRIP13 (Pch2), whose remodelling function of the chromosomal axis proteins in mouse has also been described [355,356].

Spatial regulation

Meiotic double-strand breaks are not randomly distributed along the chromosomes. There are regions both at local and chromosomal scale that are cleaved more frequently at population level as observed by the enrichment of DSB markers in those regions when mapped. This non-random distribution is the result of a combination of mechanisms and factors that shape the DSB landscape. Genome-wide single-nucleotide-resolution maps of the DSB landscape have been built in different species during the last decade thanks to the combination of the immunoprecipitation of DSB

proteins (SPO11) or early recombination proteins (DMC1, RAD51), with next generation sequencing of the chromatin fragments pulled down with them [357–361].

Double-strand break distribution profiles have revealed DSB-enriched regions at the local level, named hotspots. Comparative analysis of these hotspots with the rest of the genome have permitted the characterization of factors that promote DSB formation in those locations. Hotspot density and width are variable among species but there are features that define the hotspots conserved across some of them. Budding yeast, Arabidopsis and maize hotspots frequently occur in nucleosome depleted regions, which might suggest that local chromatin accessibility of the DSB machinery is a major factor that promotes DSB formation in these species [357,360,361]. Budding yeast and Arabidopsis hotspot sequence is AT-enriched, feature that has been linked with lower nucleosome deposition [357,361]. Gene regulatory regions often associated with "open" chromatin at local level, like gene promoters, show enrichment of DSBs not only in Arabidopsis and budding yeast, but also higher recombination rates in some vertebrates that lack PRDM9 (birds) or without functional PRDM9 (dogs) [357,361–363]. High SPO11-oligo density has been reported in some nucleosome-depleted transposon families in Arabidopsis, whereas others, such as retrotransposons, are coldspots [360]. These features, although overrepresented among hotspots, do not predict location or DSB density *per se,* but they probably are either prerequisites or promotors of DSB formation. Analysis of DSB hotspots of mouse and human (and other vertebrates later) led to the discovery of a DNA sequence motif, present in the vast majority of them, recognized by the zinc-finger motif of the methyltransferase PRDM9 [364]. PRDM9 deposits two methylation marks at the sites it binds: H3K4me3 and H3K36me3 [365,366]. Interestingly, budding yeast hotspots are also H3K4me3-enriched regions, especially in gene promoters [357,367]. Mouse gene promoters are H3K4me3-rich but most PRDM9 hotspots are situated in genic and intergenic regions. However, *prdm9* mutant mice, despite being sterile, show a shift of DSB-dense spots towards H3K4me3-rich regions including promoters, similarly to dogs with naturally dysfunctional PRDM9 and budding yeast [357,362,368]. Likewise, it has been proposed that PRDM9 remodels the nucleosome vicinity of the hotspot when it binds, generating a nucleosome depleted region in the centre [369,370]. These observations thus suggest the possibility of a common basis for the DSB hotspot designation machinery that is supported by the discovery of analogous mechanisms that link hotspot chromatin with DSB and recombination proteins in the context of the tethered loop-axis complex model for DSB formation and repair.

Table 1. Meiotic recombination features in model species.

Original from Zelkowski et al. (2019)

Species	Genome size	Chromosome no.	Average DSB no.	Average CO no.	Most common DSB location	Most common CO location	DNA sequence motifs	Recombination sites are associated with			Refs
								H3K4me3	Nucleosome depletion	Reduced DNA methylation	
Saccharomyces cerevisiae (budding yeast)	12.1 Mb	16	175	90	Gene promoters	Gene promoters	None	Yes	Yes	n/a[a]	[16,48,80]
Schizosaccharomyces pombe (fission yeast)	13.8 Mb	3	60	36	All genome regions	All genome regions	None	No	No	n/a[a]	[7,18]
Drosophila melanogaster[b]	123 Mb	4	23	5.5	n/a	Genes	Many diverse motifs	Not known	Yes	Not known	[8,45]
Arabidopsis thaliana	135 Mb	5	300 (male)	10 (male) 6 (female)	Gene promoters and terminators	Genes	DSB CO CO CO	No (DSBs) Yes (COs)	Yes	Yes	[20,44,46]
Zea mays (maize)	2.4 Gb	10	500	18	All genome regions	Genes	DSB CO	No (DSBs) Yes (COs)	Yes	Yes	[19,43]
Mus musculus (laboratory mouse)	2.8 Gb	20	250	23 (male) 27 (female)	Intergenic	Intergenic	Different PRDM9 alleles bind different DNA motifs, e.g.,	Yes	Yes	Yes	[17,35]
Homo sapiens (human)	3.3 Gb	23	150 (male) 350 (female)	50 (male) 70 (female)	Intergenic	Intergenic	Different PRDM9 alleles bind different DNA motifs, e.g.,	Yes	Yes	No (at local scale)	[15,31,32,49]

[a]There is no significant level of cytosine methylation in budding and fission yeasts.

[b]*Drosophila* males and chromosome 4 in females are not known to undergo recombination. DSB patterns have not been studied in this species.

DSBs form preferentially in chromatin loops, not in the DNA anchored to the chromosome axis [371–373], but cytological and molecular characterization of the DSB complexes and early recombination proteins places them in close association with the axis [310,373,374]. The tethered loop-axis complex reconciles these two observations to resolve the apparent discrepancy. In this model, DSB sites in the chromatin loops are recruited to the proximity of the chromosome axis where they remain tethered, allowing interactions with different protein complexes that catalyse DSB formation, end processing and promote interhomologue repair [371,375]. The actual mechanism by which DSB hotspots at the loops were physically recruited to the axis was then unknown. The missing piece was found to be Spp1 in budding yeast. Spp1 is a H3K4me3 "reader". It has a PHD finger motif that binds H3K4me3 marks and it physically interacts with Mer2 [376–378]. The current working model involves DSB machinery recruitment to the axis prior to DSB formation followed by the recruitment of H3K4me3-rich hotspots via Mer2-Spp1 interaction favouring DSBs in nucleosome depleted regions around them [376,377]. Even so, budding yeast H3K4me3 levels are a poor predictor of DSB frequency at a global level as, despite this mark is enriched at hotspots, it is detected as well in many other genomic locations, which reflects that hotspot designation is a multifactorial process [379]. In mouse, the CXXC1 protein has a PHD finger motif that binds H3K4me3 and can interact with IHO1 (Mer2). Mutant mice show repair defects in meiosis, but it is not clear if they are results of defective DSB formation/distribution or in later steps of the repair process [380,381]. ZCWPW1 has also been postulated as a "reader" involved in localizing recombination into hotspots. ZCWPW1 has higher affinity for H3K4me3/H3K36me4 double marks and it is specifically recruited to PRDM9 binding sites. Mutant cells present severe repair defects and are arrested in a pachytene-like stage. However, they do not show altered DSB positioning [382,383]. A molecular mechanism than links the DSB machinery and PRDM9 hotspots is yet to be discovered in mammals, but these observations suggest than that the hotspot recognition mediated by PRDM9-deposited histone marks is important, at least, for later stages of the DSB repair process.

Mapped crossovers in Arabidopsis show enrichment of the H3K4me3 mark, but surprisingly, DSB hotspots not only are not enriched but they have depleted H3K4me3 density [361,384]. It can be hypothesized that the positive selection for these H3K4me3 regions might not happen at the DSB formation level, but at later stages in the context of a tethered-loop axis model by mechanisms that resemble mouse CXXC1 and ZCWPW1 action, but more evidence is required. Recent mapping of the axis component REC8 in the model plant has shown the expected negative correlation between REC8 enrichment and both DSB levels and crossover frequencies. This corresponds to

expectation from a tethered loop-axis model in which DSBs are situated in the chromatin loops as in budding yeast, and not in the axis-anchored chromatin [385]. However, no evidence for hotspot recruitment by a histone mark "reader" mechanism has been found.

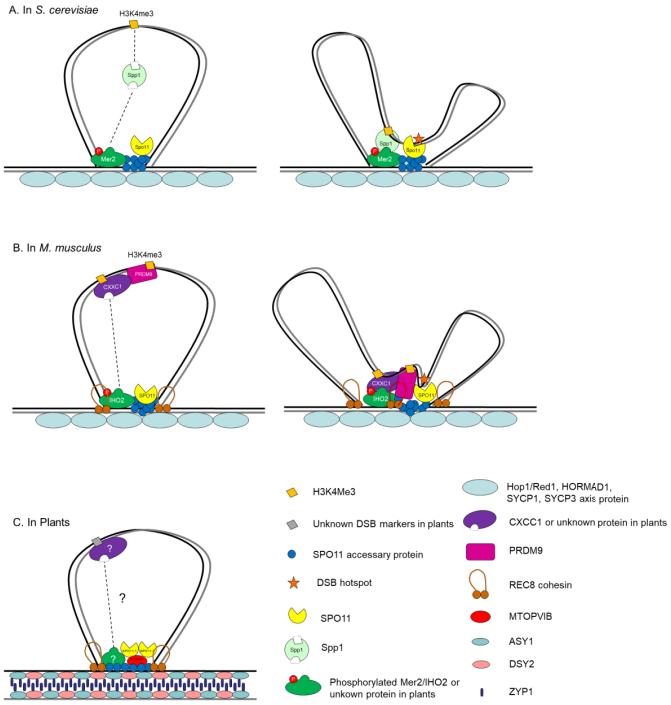

Figure 5. Tethered loop-axis complex models in budding yeast, mouse and plants.
Original from Jing *et al.* (2019).

An extra layer of DSB regulation at the local level is established via the phenomenon of DSB interference. In budding yeast, Tel1-mediated inhibition of new DSBs in adjacent sequences has been observed both in the same DNA molecule (*cis* interference), the sister chromatid and the homologous chromosome (*trans* interference). Double cut analysis in hotspots separated by variable distances indicated that Tel-1 mediated DSB interference in yeast may extend out to around 100kb, but it is prominent at close range (<10kb), impeding concurrent double cuts in the same molecule in a domain that might be defined by the chromatin loop given the width [386]. This effect is supported by observations of SPO11-oligo density maps in two of the strongest natural hotspots and their vicinity. With the loss of Tel1, weaker hotspots surrounding these two become stronger [387]. Statistical analysis of recombination events at one DSB site showed a *trans*-inhibition of DSB formation at the same locus on the

other three chromatids (the sister and the two homologous chromosome chromatids) mediated by Tel1 and Mec1. This *trans*-interference might be important to avoid harmful double recombination products or the lack of an intact homologous template to repair with [388].

In addition to DSB regulation at a local level, higher order regulation has been described in multiple organisms. Large megabase-scale regions are found to be enriched or depleted in DSB density relative to the whole genome, although the factors mediating these patterns remain poorly understood [357,361,389]. In budding yeast, centromere and telomere-proximal regions show a reduction in mean Spo11 oligo density [357]. Interstitial regions of the chromosomes also show alternations of large domains of low and high Spo11 oligo density that can be observed in other species such as mouse or Arabidopsis [357,361,389]. Depletion of Tel1/ATM leads to significant large-scale alterations of the DSB pattern. DSB-poor regions in mouse seem more sensitive to the absence of ATM-mediated regulation experiencing a significantly stronger enrichment that DSB-hot regions [389]. In budding yeast, telomere and centromere-proximal regions suppressed for DSBs in wild-type experience such suppression at early prophase I in *tel1* mutants but end up accumulating DSBs as prophase I advances reaching similar levels as the rest of the genome, hence losing the suppression effect. Interstitial regions show variable responses with no evident pattern [387].

Regulation of DSB distribution at genome wide level has been proposed as well in some organisms. Species with significant differences in size between chromosomes and with a relatively low number of total DSBs with respect to the number of chromosomes might have an important risk of frequently undergoing meiosis with unbroken short chromosomes if DSB distribution among chromosomes is random, consequently posing a threat of segregation defects. Simulations in budding yeast have quantified and confirmed this risk [353]. Different observations have shown a negative correlation between chromosome size and DSB density and DSB-protein binding, which might suggest that there are mechanisms that compensate the size differences to limit the threat [348,353,357,373,390]. Detailed analysis of the dynamics of DSB proteins along meiosis in budding yeast have unveiled multilayered mechanisms that boost DSB formation in short chromosomes, offering mechanistic evidence for this phenomenon [353].

Regulation of DSB numbers

Numbers of double-strand break hotspots exceed numbers of double-strand breaks per meiosis in all species analysed. Furthermore, while potentially every site of the genome is susceptible to receive a double-strand break, no site appears to be cut in every single

meiosis. It is thus probable that at single cell level, DSB designation involves a mix of stochastic and pro-DSB factors that ends up with the cleavage of a number of locations out of the pool of available sites in that particular cell. However, the total number of DSBs per cell is relatively similar between cells of the same individual and individuals of the same species, suggesting the existence of homeostatic regulatory mechanisms control the DSB numbers within a certain range. The number of DSBs varies substantially between species, both in absolute numbers and relative to different genomic features. Arabidopsis and other plants such as wheat or maize stand out among model species as organisms that generate a particularly high number of DSBs per chromosome and per crossover independently of genome size, which differs substantially between Arabidopsis and the two cereals. The reason behind this observation is not known. It may be hypothesized that this feature reflects an adaptation to cope with a more inefficient crossover formation process than other species, needing higher numbers of DSBs to produce each crossover, or to have a more diverse pool of crossover precursors. In the line of the first hypothesis, Arabidopsis *spo11* hypomorphs with an estimated number of DSBs reduced by 5-to-10-fold the average number of crossovers have substantial fertility defects (probably associated to crossover formation defects) suggesting that the high excess of DSBs with respect to crossovers observed in wild-type plants is not facultative but essential for proper meiotic completion, although a more detailed characterization of those strains remain to be done [391].

Limitation of meiotic DSB numbers by a conserved mechanism involving ATM signalling that sets a negative feedback of DSB formation throughout the whole genome has been proposed in multiple organisms. Mouse *atm* knockdown mutants have >10-fold higher SPO11-oligo levels in the testis [392]. Drosophila *tefu* (*ATM* orthologue) mutants show a 1.5 to 3-fold increase of γH2AV signals, used as marker of DSB levels [393]. Budding yeast *tel1* mutants have a >2-fold increase of Spo11-oligo complexes as well as higher DSB frequencies at some artificial and natural hotspots [387,388,394]. However, at least two studies have reported a decrease of DSB frequency in *tel1* [345,395]. This discrepancy might arise from the use of DSB repair-defective mutants for electrophoresis-based assays in budding yeast and therefore the result from SPO11-oligo quantification might be more reliable [396]. Arabidopsis *atm* mutants display an increase of both RAD51 and DMC1 foci in meiosis (markers for DSB numbers), and an increase of SPO11-oligo complexes measured by an *in vitro* assay with meiotic protein extracts [397].

3.4. DSB processing and pathway choice

In mitotic cells, the first steps of DSB processing are essential in the direction of repair towards end joining or homologous recombination pathways in a cell cycle dependent manner. The use of NHEJ for double-strand repair is prevalent in these cells, evidenced by the hypersensitivity to induced DNA damage of NHEJ mutants. However, meiotic progression does not seem affected in these mutants, indicating that NHEJ does not play an essential role in the repair of meiotic SPO11-induced double-strand breaks [116,119,141,398–400]. The mechanisms by which meiotic cells apparently block NHEJ repair have not been clearly established, but cell cycle-related regulation and DSB end resection, which predominates in SPO11-induced breaks, might play a role similarly to somatic cells (see section 2.2. *DSB processing and repair pathway choice*). In mouse, a downregulation of KU70 has been described at early prophase I and radiation-induced DSBs at this stage does not activate NHEJ-mediated repair but they are repaired via HR [401–403]. In *C. elegans*, absence of KU80 partially corrects the meiotic DSB repair and crossover formation defects of mutants of the MRN complex and this effect is not seen in the absence of LIG4, a downstream effector of the NHEJ pathway. It is therefore suggested that KU binds DSB ends after SPO11-oligo release and initial resection by the MRN complex would remove KU in a COM1 (Sae2/CtIP) dependent way to continue with extensive resection and generate long 3' overhangs [404–406]. Similar results have been observed in budding yeast *rad50 ku70* double mutants [407]. In Drosophila, absence of MEI-218 (a component of MCM helicase complex) partially mitigates the DSB repair defects of *spn-b* (Xrcc3) or *spn-d* (Rad51C) mutants. This amelioration is dependent on LIG4, suggesting that it functions via activation of LIG4-mediated NHEJ. Likewise, these phenotypes suggest a possible function of the MCM complex and RAD51-dependent recombination at inhibiting NHEJ during Drosophila meiosis [408,409].

Meiotic roles for NHEJ in certain conditions or genomic locations have also been proposed. While irradiation-induced DNA damage in mouse meiotic cells is repaired via RAD51- and DMC1-dependent recombination at early prophase (like SPO11-induced DSBs), when these recombinases are removed at mid-pachytene there is an activation of NHEJ repair mediated by 53BP1, KU70 and XRCC4. RAD51-dependent DMC1-independent homologous recombination then takes over NHEJ 24 hours post-irradiation. These observations suggest a "switch" from meiotic repair to somatic-like repair with quick NHEJ action, followed by slower HR activation that might be important to repair unresolved or spontaneous DSBs at late prophase [403]. A similar behaviour was observed in a SCID mouse model with hypomorphic DNA-PKcs, another component of the NHEJ repair pathway [402]. Activation of NHEJ as a backup mechanism

for unrepaired breaks has also been suggested in Drosophila: LIG4-mediated NHEJ backup using a retained SPO11-oligo as primer for fill-in synthesis followed by end ligation would be activated when an homologous template cannot be found [410]. In Arabidopsis there is no evidence of NHEJ function in meiosis in the whole genome however, NHEJ-mediated repair has been observed in the highly repetitive 45S rDNA arrays. 45s rDNA regions, recruited to the nucleolus during prophase and transcriptionally active, receive less than average numbers of DSBs and these DSBs are not repaired via HR but using LIG4-mediated NHEJ. This mechanism might be important to impede deletions arising from mispairing and illegitimate recombination between repeated sequences [411].

In spite of these hints of possible roles of NHEJ during meiosis, as stated before, the vast majority of the breaks are repaired via homologous recombination mechanisms. DSB end resection is needed to generate the proper substrates for recombinase loading and strand invasion for HR. Meiotic resection machinery components and their functions are very similar to somatic DSB resection (see section 2.2. *DSB processing and repair pathway choice*). The main particularity of meiotic DSBs is the covalent binding of SPO11 to the DSB ends after cleavage. SPO11 must be removed from the end to permit subsequent events in the repair process in a situation. The way in which this is achieved resembles the release of KU blockage of DSB in somatic tissues. The MRX/MRN complex plus Sae2/CtIP possess endonucleolytic activity and it introduces nicks upstream the 5'-end at both sides of the DSB. MRE11, thanks to its exonucleolytic (3'->5') activity, digests those strands from the nick towards the break, thus releasing SPO11 bound to a short oligo. Extensive resection is then achieved in somatic tissues by the combined action of EXO1 and DNA2-Sgs1/BLM-WRN.

Detailed molecular characterization of the products of resection in budding yeast and mouse have unveiled differences in the role of these nucleases in the resection of DSB ends. *exo1* mutants in budding yeast show a significant decrease in resection length, from an average of 822nt from the hotspot centre (200-2000nt range) in wild-type, to 373nt (<1100nt range) in the mutant. It is hypothesized that the value observed in *exo1* might correspond to the mean length of the MRE11 nick plus 3->5' initial resection and that Exo1 is responsible for extensive resection beyond that point [412]. *exo1* mutant mice, on the other hand, show only a mild reduction of the mean resection tract length (1,117 to 973nt), which might point to the involvement of additional resection actors, such as DNA2-BLM/WRN, redundant with EXO1 as in somatic cells [370]. Conserved roles for ATM in resection have been identified in both species, both in the initial step (unresected DSBs accumulate in *atm* mutants) and in the extensive resection step (*atm* mutants show shorter average tracts). Another

conserved feature between budding yeast and mouse is hyperresection in *dmc1* mutants, likely indicating that DMC1 nucleoprotein filament polymerization limits the access of the DSB resection machinery to the break ends [370,412].

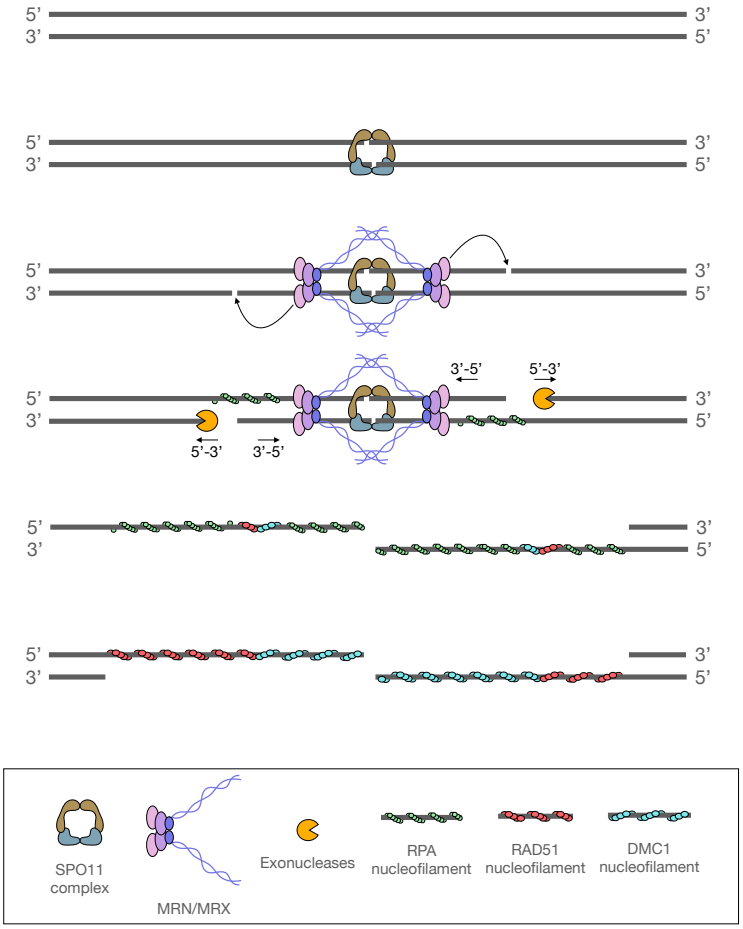

Figure 6. Early steps of double-strand break formation and end resection.

Once the SPO11 complex is bound to the DNA with the help of the multiple DSB proteins that coordinates DSB localization and timing in the context of the tethered loop-axis model, it cleaves the DNA generating a DSB with 2-nucleotide 5'-overhangs and remains covalently bound to the DSB ends. The MRX/MRN complex is recruited and one of its components, MRE11, generates nicks upstream of both exposed 5'-ends thanks to its endonuclease activity to then, given its 3'-5' exonuclease activity, digest those strands from the nicks towards the DSB. These initial events of end resection release the SPO11 complex bound to a short DNA oligo. The resulting 3'-ssDNA overhangs are then substrate for further resection by 5'-3' exonucleases such as EXO1 or DNA2-BLM/Sgs1, and the loading of RPA, which coats and protects the exposed ssDNA from degradation and the formation of detrimental secondary structures. The recombinases RAD51 and DMC1 load onto the RPA-coated ss-DNA, replacing RPA and forming presynaptic filaments suitable for homology search and strand exchange.

Arabidopsis *mre11*, *rad50* and *com1* mutants are infertile and show extensive SPO11-dependent fragmentation and chromosome entanglements in meiotic metaphase

I [60,95,330]. From these observations, together with the somatic characterization, it is inferred that their function in meiotic DSB processing is conserved and also that most of the SPO11-induced DSBs are repaired via resection-dependent HR. The role of NBS1 in Arabidopsis meiotic resection is not clear. The mutant allele characterised expresses a truncated protein that retains the MRE11 and the putative ATM interaction domains and closely resembles the behaviour of mouse and human hypomorphic alleles, including unaffected DSB repair in male meiosis [413–416]. Further studies with null *nbs1* mutants are required to disclose its role during meiosis.

The resected 3'-ssDNA overhangs are coated by the heterotrimeric complex RPA protecting them from nucleolytic degradation. RPA1, 2 and 3 subunits are encoded by single genes in budding yeast or mouse, but they have been duplicated in plants. Thus, different RPA complexes with combinations or the paralogues of all three subunits can be formed and they have sub-functionalized. Partial sterility has been described for *rpa1a* mutants which, when combined with an *rpa1c* mutation, display complete sterility. It is thus possible than during Arabidopsis meiosis multiple RPA complex are functional, but the roles of the individual subunits and the genetic interactions between them remain to be elucidated [53,54,417].

3.5. RAD51, DMC1 and the meiotic presynaptic filament

RAD51 and DMC1

RPA-coated 3'-ssDNA overhangs are substrate for presynaptic filament assembly in meiotic and in somatic cells, but the nature of this filament confers fundamental differences on its homology search and strand exchange activities. Two RecA-family proteins are essential for meiotic recombination in most eukaryotic organisms: RAD51 and DMC1. These two recombinases arose from a gene duplication event early in the evolutionary history of the eukaryotes. RAD51 is expressed in both somatic and meiotic cells, however DMC1 is expressed almost specifically in the meiotic cells [418]. They share 45-55% percent amino acid sequence identity across species and many of their structural and biochemical properties [419,420]. Both proteins have ATPase activity and are able to form helical nucleoprotein filaments on exposed ssDNA in an ATP-dependent manner. Once the nucleoprotein filament is formed, they are able to catalyse homology search, invasion of a homologous template and strand exchange [421,422]. Nevertheless, detailed biochemical characterization has revealed differences between the two proteins that might give a clue on their functional diversification. *In vitro* assays with the human proteins suggested that while both RAD51 and DMC1 require ATP binding for

nucleofilament formation and ATP hydrolysis for nucleofilament disassembly. However, attenuation of ATP hydrolysis enhances the homologous DNA pairing and strand exchange activity of RAD51 but not of DMC1 nucleoprotein filaments [423]. The divergence of the inherent biochemical activities of the two proteins might reflect (or result in) different needs for cofactors that stimulate their activity. For example, differences of mechanism and intensity of stimulation of *in vitro* strand exchange by divalent calcium ions have been described for purified budding yeast, human and Arabidopsis RAD51 and DMC1 [421,424–426]. Structural studies of presynaptic filaments have revealed that they are organized as base triplets and that strand exchange occurs in 3nt steps, presumably reflecting this triplet organization. This feature is conserved across prokaryote and eukaryote members of the RecA family [193,427]. *In vitro* biochemical comparison of bacterial RecA with human RAD51/DMC1 and budding yeast DMC1 presynaptic filaments strand exchange activities shows all three of them can step over mismatches but only human and budding yeast's DMC1 can stabilize triplets with mismatches if they are flanked by at least another homologous triplet [427,428]. While RAD51-mediated somatic recombination primarily uses a recently synthesized sister chromatid as a template in which sequence polymorphisms are not abundant, meiotic recombination uses the homologous chromosome as primary template, inherited from a different parent and therefore subject to a greater density of naturally occurring DNA sequence polymorphism accumulated through generations. The tolerance for mismatches in a triplet by DMC1 might thus reflect an evolutionary selected feature with respect to RAD51, permitting it to better support meiotic recombination. However, the importance of stabilizing a single unpaired triplet within a paired intermediate of tens or hundreds of paired triplets is not certain and both RecA and RAD51 can tolerate a limited number of mismatches between homologous loci, thus establishing the extent of the *in vivo* impact of this biochemical difference will require further study [428–430].

Presynaptic filament assembly

The stoichiometry of RAD51 and DMC1 proteins in the meiotic presynaptic filaments has been discussed since early cytological observations in budding yeast showed that foci of the two proteins do colocalize [431]. Recent observations with super-resolution microscopy techniques in budding yeast and mouse have resolved that they do not completely colocalize but they have distinct spatial localization and both RAD51 and DMC1 bind to the two ends of the DSB at least the majority of breaks (around 80%) with DMC1 further away from the axis than RAD51 [432–434]. These observations have been supported with biochemical data. *In vitro* analysis of branch migration

directionality using fission yeast Rad51 and Dmc1, proposed to be the same as the direction of filament elongation, indicated that while Rad51 filaments elongate in the 3'-5' direction, Dmc1 filaments do so 5'-3' [435,436]. Single molecule experiments with the two budding yeast proteins have demonstrated that both have the ability to form spatially distinct homotypic filaments side-by-side on the same ssDNA molecule and that Dmc1 has a preference for 5'-3' filament formation, stimulated by patches of Rad51 [437,438]. *In vivo* mapping of RAD51 and DMC1 binding sites at mouse DSB hotspots also shows distinct spatial localizations, with DMC1 closer to the DSB than RAD51 [433]. Together these observations suggest a meiotic presynaptic filament with both RAD51 and DMC1, not intermixed but in a side-by-side homotypic configuration in which DMC1 is closer to the 3' end and RAD51 upstream. From biochemical data it can be hypothesized an early RAD51 patch might drive RAD51 filament polymerization in a 3'-5' direction and nucleate DMC1 filament polymerization from that point in a 5'-3' direction towards the end of the ssDNA overhang. The initial position of the RAD51 patch would determine the length of both filaments, which might explain the differences in observed focus sizes and the partially overlapping distributions of the mapped proteins at mice hotspots. Although an earlier analysis of the localization of RAD51 and DMC1 foci by fluorescence microscopy in Arabidopsis led to proposition of a different model in which RAD51 would bind one end of the break and DMC1 the other [283], it appears very likely that the situation in Arabidopsis is equivalent to that in yeast and mouse.

The configuration of the presynaptic filament with DMC1 situated at the 3' end implies, in functional terms, that either RAD51 and DMC1 work together in their homology search and strand exchange activities or that DMC1 has the leading role. Functional and biochemical studies in budding yeast, Arabidopsis and rice pointed towards the second hypothesis by analysing separation-of-function mutant variants of RAD51 which were able to form nucleofilaments but not to catalyse the interaction with the template dsDNA molecule [234,439–442]. Although these *rad51-II3A* and RAD51-GFP mutants have the expected somatic DNA repair and recombination defects, meiotic recombination is not affected. Arabidopsis meiocytes show a WT-like phenotype with five bivalents, unaffected crossover formation and complete repair of DSBs. Budding yeast shows unchanged genetic distances in several chromosomal intervals and no differences in interhomologue or intersister meiotic joint molecule (JM) formation at a hotspot. Double mutants with *dmc1* in Arabidopsis and triple with *dmc1* and *hed1* in yeast (contexts in which wild-type RAD51 is able to repair meiotic DSBs) display severe fragmentation in the plant and a complete block of JM formation in yeast. These

results in both species confirm that meiotic recombination is catalysed by DMC1 with RAD51 playing an essential supporting role.

In vivo, filament assembly requires the help of a variable number of cofactors. Budding yeast Rad52 is necessary for Rad51 focus formation and colocalizes with it at sites of DNA damage [443,444]. *In vitro*, Rad52 physically interacts with Rad51 and RPA, and promotes the loading of Rad51 into RPA-coated ssDNA, although the detailed mechanism remains unclear [445,446]. Rad52 however does not directly promote Dmc1 nucleofilament formation on RPA-coated ssDNA, but this support is thought to be carried out by Mei5-Sae3, whose promoting role for Dmc1 filament formation has been verified *in vitro* and *in vivo* [447–449]. Although Rad52 does not interact with Dmc1, *rad52* mutants are defective in meiotic DSB repair, suggesting that its role in supporting Rad51 loading is needed for a functional presynaptic filament in meiosis [446,450]. Mei5-Sae3 interacts with Rad51 although it does not promote Rad51 filament formation, but this interaction might mediate Dmc1 loading at meiotic DSB overhangs where Rad51 is already present [446,451]. The role of RAD52 in promoting RAD51 filament formation is not conserved in other eukaryotes as mammals [452]. Mei5-Sae3 orthologues are accessory factors to both Rad51 and Dmc1 in fission yeast (Swi5-Sfr1), whereas in mammals (SWI5-SFR1) they function with RAD51 but not DMC1, and in plants no orthologues have yet been described [453–455].

Rad52's supporting role for nucleofilament assembly is thought to involve BRCA2 in mammals and plants, rather than the corresponding RAD52 orthologue. *brca2* knockouts are embryonic-lethal in mouse but hypomorphic mutants show meiotic DSB repair defects and reduced numbers of RAD51 and DMC1 foci. Furthermore, mouse cell lines expressing a truncated BRCA2 protein have impaired RAD51 focus formation [456–458]. RNAi lines and double knockout mutants of the two *BRCA2* genes of Arabidopsis display severe meiotic DNA repair defects and the double knockout loses RAD51 and DMC1 signals on meiotic chromosomes [238,459]. Human and Arabidopsis BRCA2 physically interact with RAD51 and DMC1 and the human protein promotes nucleofilament assembly and strand exchange *in vitro* [459–463], [464]. Unlike Rad52, BRCA2 does not physically interact with RPA, but forms a complex with DSS1 that mediates this interaction, enhancing the BRCA2-mediated RAD51 filament assembly into RPA-coated ssDNA *in vitro* [465]. The BRCA2-DSS1-RAD51 interaction has been detected in Arabidopsis, as well as the BRCA2-DSS1-DMC1 interaction, but the role of DSS1 in meiosis is not clear in either plants or vertebrates [460]. Finally, recent reports in mouse have unveiled an analogous meiosis-specific mechanism mediated by two proteins, MEILB2 and BRME1, that bridges BRCA2 and RPA-coated ssDNA, facilitating the BRCA2-mediated localization of RAD51 and DMC1 to the DSB sites [466,467].

Presynaptic filament modulators

The assembled presynaptic filament is ready to catalyse template invasion, homology search and strand exchange, but these activities are also supported by a number of cofactors that either promote or repress them by stabilizing, remodelling or disassembling the filament as well as antagonizing proteins that might dismantle it. The molecular functions of many of these cofactors are not completely clear as they might play different roles during the process and different activities might lead to the same promoting phenotype *in vitro* or *in vivo*. For example, the importance of the role of Rad52 in promoting Rad51 filament assembly has been challenged recently after observations that lead to a hypothesis in which this function is facultative and the main activity would be protecting the Rad51 filament against disassembly from the helicase Srs2, together with increasing its stability [468,469].

Hop2 and Mnd1 form a heterodimer that stabilizes presynaptic filaments and is conserved in different eukaryotes, although its expression pattern and activity varies. In budding yeast, Hop2-Mnd1 is expressed only in meiosis and single mutants of the two proteins have severe meiotic DSB repair defects [470,471]. It interacts with Dmc1 but not Rad51 and specifically stimulates strand exchange of Dmc1 filaments by promoting dsDNA capture during the homology search [472–474]. It also binds Dmc1-Rad51 mixed filaments *in vitro* but does not spread appreciably into the Rad51 section of the filament, suggesting that a meiotic presynaptic filament not only is spatially differentiated by the side by side loading of Rad51 and Dmc1, but also by differential loading of cofactors [474]. Mouse and human HOP2-MND1 are implicated as well in meiotic DSB repair and the single mutants present severe defects. However, they have been found to interact with both RAD51 and DMC1 and promote *in vitro* D-loop formation by nucleofilaments of the two proteins by stabilizing the filament and facilitating dsDNA capture [475–478]. A mitotic role for this complex has been suggested given observations of a RAD51-promoting role in telomeric recombination in ALT cells or the presence of HOP2 mutations in some human pathologies [479–481]. Interestingly, mammalian HOP2 presents some of the distinctive features and activities of a recombinase *in vitro*, able to promote strand invasion by itself, and *mnd1* mutant mice, with apparently inactive RAD51 and DMC1, show high levels of synapsis and repaired DSBs in a fraction of cells, suggesting a possible role of HOP2 as a catalyser of recombination independent of RAD51 and DMC1 [482].

Arabidopsis HOP2 and MND1 interact with RAD51 and DMC1 and single knockout mutants of the two respective genes present severe meiotic DSB repair defects [483,484]. Plants carrying hypomorphic alleles of *HOP2* lack interhomologue crossovers

although they are able to repair DSBs (no notable meiotic chromosome fragmentation) [328,485]. The truncated HOP2 protein encoded by an analogous allele in rice stimulates DMC1 filament D-loop formation significantly less than the wild-type protein. While neither DMC1 nor RAD51 focus formation is affected in *hop2* plants, numbers of DMC1 (not RAD51) foci are increased in *mnd1* mutants, which suggests that HOP2 and MND1 may have individual functions in addition to acting as a complex [484,485]. The lack of crossovers in repair-proficient hypomorphic *hop2* mutants suggests that the Arabidopsis HOP2-MND1 complex, besides its stimulation of strand invasion activity, has a role in modulating interhomologue bias in meiotic recombination. A recent preprint has analysed the phenotype of haploid *hop2* meioses in Arabidopsis. While haploid cells with intact HOP2 protein show efficient DSB repair, presumably using the sister chromatid as template, the *hop2* mutants present chromosome entanglements and bridges at anaphase I, suggesting a role for HOP2 in suppressing illegitimate recombination. This work also shows increased presence of mitotic anaphase bridges after irradiation of these plants, pointing to a possible mitotic role of HOP2 in Arabidopsis [486]. Finally, it is noteworthy that although *HOP2* and *MND1* are present in many eukaryotic organisms, they are absent in species like *Sordaria macrospora*, *Drosophila melanogaster* and *Caenorhabditis elegans* that also lack *DMC1*, suggesting a coevolution of these genes and underlining the meiotic role of HOP2-MND1 in supporting DMC1-mediated strand invasion.

RAD51 paralogues are important modulators of the presynaptic filament also in meiosis. Budding yeast has five paralogous genes of *RAD51* (in addition to *DMC1*), whose products are part of two different complexes: the Rad55-Rad57 heterodimer and Shu1, Csm2 and Psy3 as part of the Shu complex altogether with Shu2. *rad55* and *rad57* single mutants show defective DNA repair and a loss of Rad51 foci in meiosis and in vegetative cells [487–490]. *In vitro* assays indicate that Rad55-Rad57 promote Rad51 nucleofilament assembly on RPA-coated ssDNA, otherwise inhibited by the presence of RPA, suggesting a role for this complex in supporting replacement of RPA by Rad51 [189,491]. Rad55-57 also functions as an antagonist of Srs2, counteracting its disruption of Rad51 nucleofilaments by promoting their rapid reassembly [189,492]. These *in vitro* observations are supported by genetic assays in which the hypersensitivity of *rad55* and *rad57* mutants to DNA damage agents is partially suppressed by deletion of *SRS2* [492]. In addition, Rad55 has been found to interact with Csm2, member of the Shu complex, and this interaction is required for the association of the Shu complex with Rad51 and Rad52. Disruption of this interaction impairs the Rad51 filament-stimulating function of the Shu complex and the cells show similar phenotypic traits to the *csm2* null mutant [493]. Shu complex mutants are also sensitive to DNA damage, but to a lesser extent than

rad55 or *rad57* [494]. All Shu complex mutants have reduced spore viability and interhomologue recombination in meiosis. In the *csm2* mutant, however, intersister recombination suffers a 10-fold increase, inverting the positive bias towards interhomologue repair versus sister chromatid repair in a hotspot. Meiotic Rad51 foci are greatly reduced but Dmc1 foci only shows a slight reduction in these mutants. Concordantly, *shu1* and *psy3* mutants abolish Rad51 binding to a meiotic DSB hotspot but not Dmc1 binding [495]. Both Rad55-Rad57 and the Shu complex thus have key roles in meiotic DNA repair through Rad51 nucleofilament stabilization and protection from disassembly, at least.

Vertebrates have six *RAD51* paralogues in addition to *DMC1*: *RAD51B*, *RAD51C*, *RAD51D*, *XRCC2*, *XRCC3* and *SWSAP1*. At least three different complexes involving their respective proteins have been described: CX3 (RAD51C and XRCC3), BCDX2 (RAD51B, RAD51C, RAD51D and XRCC2) and the Shu complex (SWSAP1 and SWS1). The embryonic lethality in mice of knockouts of the five canonical *Rad51* paralogues (*Rad51B/C/D* and *Xrcc2/3*) has made meiotic characterization of these mutants a challenging task [496]. The more divergent *SWAP1* mutants are however viable and initiate meiosis, shedding some light on its possible meiotic role [497]. *In vitro* biochemical studies have also been challenging given the difficulties in purifying these proteins from mammalian cells, but RAD51-independent D-loop formation activity has been described with purified CX3 and XRCC2-RAD51B complexes cloned and expressed in different vectors [498,499]. In the case of CX3, however, negative results regarding its ability to catalyse D-loop formation have been also published [500].

Cell cultures have been the source of most of the information gathered on the functions of these proteins. Mouse embryonic fibroblasts (MEFs) couldn't be derived from *rad51c* and *rad51d* knockout embryos, but *xrcc2* MEFs do propagate and exhibit sensitivity to DNA damaging agents, reduced RAD51 focus formation and reduced gene conversion and sister chromatid exchanges originating from RAD51-mediated crossover events in somatic cells [501–503]. Depletion of *trp53* in mice embryos carrying knockout alleles of *Rad51B*, *Rad51C*, *Rad51D* and *Xrcc2* extended their development and allowed the propagation of double mutant MEFs of *trp53* with *rad51c*, *rad51d* and *xrcc2* [496,502–507]. These MEF lines present DNA repair defects consistent with impaired RAD51 formation or activity: sensitivity to DNA damaging agents, reduced RAD51 foci, reduced sister chromatid exchanges and generalized genome instability. The tolerance conferred by *p53* mutation to knockouts of the *RAD51* paralogues has also permitted the use of Chinese hamster ovary (CHO) and chicken (DT40) cell lines with mutant *p53* to study the phenotypes of *RAD51* paralogues mutants. CHO *xrcc2* and *xrcc3* mutant cells show increased sensitivity to DNA damage and *xrcc3* cells absence of

RAD51 foci [496,508–510]. DT40 mutant cells for each of the five canonical paralogues exhibit genomic instability, sensitivity to DNA damaging agents, reduction in MMC-induced sister chromatid exchanges and decreased IR-induced RAD51 foci [511,512]. The use of RNA interference to silence genes using siRNAs permitted the study of depleted RAD51 paralogues in transformed human cell lines. All siRNA knockdowns of the five canonical paralogues show decreased viability using HT1080 and HEK-293 cells [513]. siRNA MCF7 and U2OS cell lines for the five genes display decreased I-SceI-induced homologous recombination. siRNA knockdowns of *RAD51D* and *RAD51C* have reduced RAD51 foci after γ-irradiation, but not for *XRCC3* [514]. A recent work has finally achieved knockout human cell lines for the five genes [191]. Cre-mediated excision of the paralogous genes (except *RAD51b*) is lethal in conditional mutants in a non-transformed MCF10A line. Transformed U2OS and HEK293 cells have reduced viability. For the cell lines studied, all five knockout mutants have reduced I-SceI-induced homologous recombination, severe reduction of RAD51 foci and sensitivity to DNA damage. *rad51b* mutants show a milder phenotype and significantly different phenotype than the other four in all experiments of this publication.

Mice carrying an hypomorphic allele of *Rad51C* were found to be viable, permitting the study of the role of RAD51C in meiosis [515]. Male and female mice were infertile but with sexually dimorphic defects. Spermatocytes showed reduce RAD51 foci, defects in synapsis, presence of univalents in metaphase I and some chromosome fragmentation in metaphase II, while female infertility was apparently associated to premature sister chromatid segregation during the first division. RAD51C immunolocalization in wild-type mice showed a surprising pattern resembling the late prophase dynamics and localization of resolvases rather than the patterns observed in proteins implicated in presynaptic filaments. In this same context an interaction with XRCC3 was detected with ChIP, pointing to a possible late function of the CX3 complex in meiotic recombination at the level of dHJ resolution [516]. A mutation of *XRCC2* in humans have been associated with infertility and reproduced in mice with similar fertility defects [517]. All these observations together suggest an essential role of the five canonical paralogues in promoting RAD51 filament stability and/or strand exchange activity a possible role of members of both CX3 and BCDX2 in mammals' meiosis. Their meiotic functions however remain to be detailed.

SWS1 was identified in fission yeast and human as an orthologue of budding yeast *SHU2*, member of the Shu complex [518]. Using an affinity purification approach, SWSAP1 was isolated as a partner protein and its genetic and biochemical characterization has led to its inclusion in the family of RAD51 paralogues [519]. Downregulation of either *SWS1* or *SWSAP1* in somatic cells causes reduction of gene

conversion efficiency, sensitivity to DNA damage, decreased RAD51 foci and diminished cell viability, but these phenotypes are weaker than those of mutants of the canonical paralogues or *rad51*. SWSAP1 was found to physically interact with RAD51 and most RAD51 paralogues *in vivo* and *in vitro*. The milder phenotype observed in cell culture was confirmed when viable, infertile mutant mice were generated [497]. Mice mutant for both genes show significant reductions of RAD51 and DMC1 foci, synapsis defects and impaired DSB repair. Spermatocytes that escape the pachytene checkpoint show decreased MSH4, marker of DNA-strand exchange intermediates, and MLH1, marker of crossovers. Nevertheless, the reduction of MLH1 foci is only of about 20% and thus most bivalents are able to form at least one crossover despite the low number of RAD51 and DMC1 signals. Oocytes also show reduced MLH1 foci and univalents.

Plants have the five canonical RAD51 paralogues in addition to DMC1. Physical interactions among them suggest a conserved CX3 complex that also interacts with RAD51 but the conservation of the BCDX2 complex is not clear, as no interaction of XRCC2 with any of the other paralogues has been described [520–523]. Mutants if all five Arabidopsis paralogues are sensitive to treatment with MMC and other DNA damaging agents, although there are conflicting results concerning γ-irradiation sensitivity [235,236,521,522,524,525]. Both lack of γ-irradiation sensitivity in *rad51b*, *rad51c* and *xrcc2* mutants [236] and sensitivity to γ-irradiation in *rad51b* [521,522] have been reported. In addition, the triple mutant for these three genes displays greater sensitivity to DNA damage than any of the singles or doubles, suggesting complex functions with partially overlapping roles of these proteins in Arabidopsis somatic DNA repair [239]. All paralogues mutants show decreased spontaneous and induced homologous recombination using reporter constructs with direct repeats, that are primarily repaired using SSA, and inverted repeats, primarily repaired via RAD51-dependent SDSA or DSBR [168,173,524–526]. RAD51 focus formation is not affected in *rad51b*, *rad51d* and *xrcc2* after induced DNA damage, so the role of these proteins does not appear to be in RAD51 filament assembly but in promoting its function [526]. Interestingly, *rad51b*, *rad51d* and *xrcc2* plants show reduced RAD51-independent recombination (SSA) of a tandem direct repeat recombination substrate in Arabidopsis. Hence either they also play a role in RAD51-independent recombination or alterations of their RAD51-related function have an impact on other repair pathways [173]. Furthermore, this study showed differing impacts on SSA in the three *xrcc2, rad51b* and *rad51d* single mutants and this was confirmed by the non-epistasic phenotypes of *xrcc2 rad51b* and *xrcc2 rad51b rad51d* plants [173]. Both *rad51c* and *xrcc3* mutants have severe DSB repair defects in meiosis with loss of RAD51 foci, impaired synapsis, chromosome entanglements and fragmentation in metaphase I [235,522,524,527]. Mutants of *RAD51B*, *RAD51D* and *XRCC2* do not present

meiotic defects, although subtle implications have been suggested after observations of increased recombination rate in some chromosomal intervals of Arabidopsis in *rad51b* and *xrcc2* mutants and in wheat when XRCC2 is silenced [236,526,528]. These observations in Arabidopsis point towards an essential meiotic role of the CX3 complex in RAD51 filament assembly or stability and a possibly more subtle role of the other three paralogues in modulating the activity of either the RAD51 or the DMC1 filaments. This meiotic behaviour does not appear to be conserved among plants. Mutants of the *RAD51B* orthologue in the moss *Physcomitrella patens* not only show somatic DNA repair defects but they are infertile with severe fragmentation and entanglements in metaphase I [529]. Rice *xrccc3* and *rad51c* mutants have similar meiotic phenotypes to their Arabidopsis counterparts, but *rad51d* rice also display meiotic DSB repair defects with severe fragmentation in metaphase I that lead to infertility [530–533]. A possible telomeric role for RAD51D have been proposed in rice, as *rad51d* somatic cells have elongated telomeres with respect to wild-type cells and immunolocalization of RAD51D in meiosis show absence of signals in the chromosome arms and very localized foci in the telomeres [531,533]. RAD51C, on the other hand, has an early meiotic genome-wide localization in what resembles more the expected pattern for a protein that acts at RAD51 or DMC1 filaments [530]. Despite a similar fragmentation phenotype in metaphase I, immunolocalization of other meiotic proteins also displayed differences that points to a role of RAD51D independent of RAD51C and XRCC3 in rice. Markers of DSB end resection (COM1) and chromosome axes (REC8) are absent in *xrcc3* and *rad51c* mutants respectively but present (and in increased numbers for COM1) in *rad51d* mutants [532,533].

Rad54 and Rdh54/Tid1 are members of the SWI/SNF2 family of helicase-like chromatin remodelers. *in vitro* biochemical characterization of the budding yeast proteins show considerable functional similarities: both are dsDNA-dependent ATPases with ATP-dependent dsDNA translocation activity [534–536]; they are able to physically interact with Rad51 and Dmc1 [535,537,538], stimulate D-loop formation by Rad51 and Dmc1 filaments [534,535,538], disassemble Rad51:dsDNA filaments [539,540] and catalyse chromatin remodelling by redistributing nucleosomes [541,542]. Genetic studies have revealed partially overlapping functions in budding yeast. Rad54 and Rdh54 localize to DNA damage sites in mitotic cells [543]. Haploid and diploid *rad54* mutant strains are severely sensitive to DNA damage but *rdh54* only present mild sensitivity after longer exposures to the damaging agent, more so in diploids with respect to haploids [544]. Intra-chromosomal and intersister mitotic recombination is defective in *rad54* mutants but not in *rdh54*. However, reduction in inter-chromosomal recombination have been reported for diploid *rdh54* mutants [544]. Both *rad54* and *rdh54* mutants show partial reductions in spore

viability. Double *rad54 rdh54* mutants have significantly stronger sensitivity to DNA damage agents than any of the double mutants and complete loss of spore viability [544,545]. In addition, in mitotic recombination assays in which *rdh54* single mutants appear to have no differences with the wild-type strain, the *rad54 rdh54* double mutants show a reduction of inter-chromosomal recombination with respect to the single *rad54* [545]. Together these data point to partially overlapping roles of the two proteins in promoting recombination, with an inclination towards the use of the sister chromatid as template in events involving Rad54 and the homologous chromosome in the case if Rdh54. This would explain the more severe defects in somatic DNA repair, that preferentially uses the sister chromatid as a template, in *rad54* than in *rdh54* mutants as well as the worsened phenotype of *rdh54* mutants in diploid strains, in which there is a homologous chromosome to be used as a template, with respect to haploids, in which there is not.

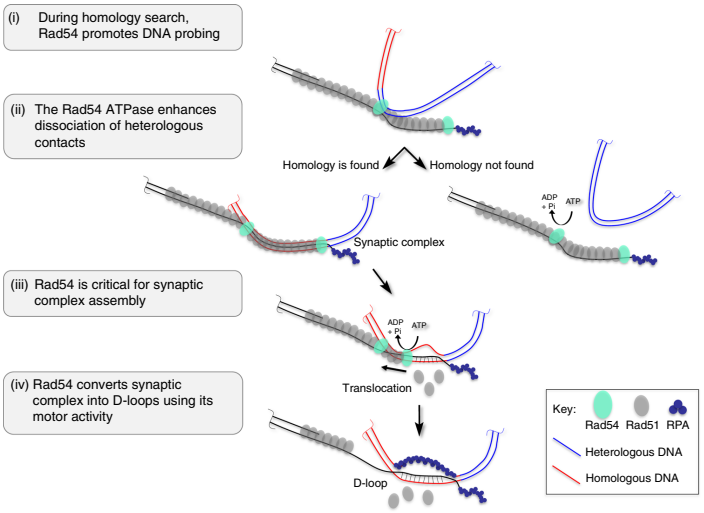

Figure 7. Rad51 and Rad54 cooperative model for homology search and D-loop formation in budding yeast.

Original from Tavares et al. (2019). (i) During homology search, Rad54 promotes DNA probing. The invading DNA (light red) uses Rad54 to bridge the Rad51 filament to dsDNA during the homology search. Rad54 ATPase activity is not required but may enhance probing. (ii) Persistent associations with heterologous DNA (blue, right arrow) may be prevented or dissociated by Rad54 in an ATPase- dependent fashion. Rad54 ATPase exerts quality control to promote homologous pairing. (iii) Rad54 is required for synaptic complex formation without strict requirement for ATPase activity, and (iv) converts such complexes into D-loops dependent on ATP hydrolysis. Rad51 left on the ssDNA outside of the heteroduplex region after removal during heteroduplex formation may able to repolymerize back into the synaptic region. Note that this is a cartoon representation not meant to model the true scale and structure of the Rad51 filament or Rad54 protein arrangement in the depicted intermediates.

The diverse and sometimes apparently contrasting biochemical activities attributed to Rad54 and Rdh54 *in vitro* have complicated the integration of *in vitro*

and *in vivo* observations to build and test model mechanisms by which these proteins promote homologous recombination. Nevertheless, recent publications using single molecule techniques have reported detailed information about the activities of Rad54 within the Rad51 presynaptic filament and the donor template at different levels of the homology search and strand exchange processes. These underline the critical role of Rad54 in homology search by promoting donor dsDNA opening and homology scan via its dsDNA translocation plus chromatin remodelling activities, as well as in the synaptic complex-to-D-loop transition via disassembling the Rad51 filament, helping to harmonize its different biochemical activities into working models that integrate them [198,546,547].

The meiotic behaviour of RAD54 accords with its role as an essential partner for RAD51 filament function. As described above, a series of *in vitro* and *in vivo* observations in different organisms have led to a meiotic presynaptic complex model in which both RAD51 and DMC1 are loaded in spatially distinct domains, but the strand invasion is catalysed by DMC1 with RAD51 playing an essential structural role in filament function while not itself catalysing invasion (as it does in somatic cells). This dependence of meiotic recombination on DMC1 and the use of the homologous chromosome as template, rare in somatic cells, have led to proposal of existence of mechanisms that inhibit the catalytic function of RAD51 in meiosis. In budding yeast, two mechanisms have been proposed to downregulate meiotic Rad51 activity by interfering with its interaction with Rad54. Hed1, a budding yeast meiotic-specific protein, was found to physically interact with Rad51 and to form foci that localize to DSB sites in a Rad51-dependent manner. Removal of Hed1 in a *dmc1* mutant context improves meiotic DSB repair and sporulation and this improvement is lost upon removal of Rad51. Furthermore, ectopic expression of Hed1 in vegetative cells inhibits Rad51-mediated recombination. These observations led to the proposition of a mechanism of Rad51 downregulation in meiosis, mediated by its interaction with Hed1 [548]. Later reports have demonstrated that Hed1 downregulates Rad51 by blocking its association with Rad54. Hed1 and Rad54 kinetically compete for Rad51 (and not Dmc1) filament binding and Hed1 loading to the filament blocks Rad54 binding [549–551]. Hed1 was found to be phosphorylated by the meiotic-specific kinase Mek1 in a Spo11-dependent manner. Hed1 phosphorylation, although not essential, was found to enhance Rad51 downregulation, likely due to increased Hed1 protein stability [552]. This mechanism provides a link between DSB formation and downregulation of Rad51 function in meiosis.

Rad54 is also a target of Mek1 kinase activity. Rad54 phosphorylation by Mek1 attenuates Rad51-Rad54 interaction and reduces D-loop formation by Rad51 filaments

in vitro. *In vivo*, Rad54 phosphorylation inhibits meiotic intersister repair in *dmc1* mutants and acts synergistically with Hed1 to suppress Rad51 activity in meiosis [553]. Hence Mek1 activation and its kinase activity appear to coordinate Rad51 downregulation by parallel mechanisms that block its interaction with Rad54. Neither *hed1* mutant strains nor strains expressing a non-phosphorylatable Rad54, nor a strain combining both present significant sporulation or spore viability. The combination of both does decrease interhomologue crossovers and thus the interhomologue/intersister ratio, by joint molecule analysis [554]. Confirming that these mechanisms have functional importance *in vivo*, this result also points to the existence of additional regulatory mechanisms for downregulation of Rad51 in favour of Dmc1 and the interhomologue bias.

Human and mouse also have two genes, *RAD54* and *RAD54B*, whose respective proteins exhibit similar biochemical characteristics to their yeast orthologues *in vitro*: dsDNA-dependent ATPase activity, ATP-dependent dsDNA translocase activity, stimulation of D-loop formation by RAD51 filaments and chromatin remodelling [555–558]. The two proteins localize to the chromosomes upon induction of DNA damage in somatic cells [559,560]. However, while budding yeast *rad54* mutants show significant sensitivity to DNA damaging agents, the single *rad54* and *rad54b* mutants display milder phenotypes in mammals and it is the disruption of both which generates important DNA damage sensitivity and impaired homologous recombination in cultured cells [557,561] and mutant mice [557]. Despite their similarities with their budding yeast orthologues and their apparent role in somatic DNA repair, no fertility defect has been described in *rad54*, *rad54b* or *rad54 rad54b* double mutants [557,561,562]. Nevertheless, *rad54* and *rad54b* mutant mice do show alterations in early germ cell development, increased chromosomal aberrations during meiosis and germ cells are significantly more sensitive to irradiation than those of wild-type mice [562,563]. *rad54* mutants have abnormal RAD51 focus distribution at late prophase I, but not *rad54b* mutants, although the double mutants do display a mild increase with respect to the *rad54* single [557]. RAD54B has been found to physically interact with DMC1 and promote D-loop formation by DMC1 filaments *in vitro* [564,565]. Further characterization is needed to determine the precise roles the two proteins play in meiotic recombination, but the budding yeast roles do not seem to be conserved.

In Arabidopsis, an orthologue of *RAD54* has been described, but so far no *RDH54*/*RAD54B* orthologue has been found [237,566]. Arabidopsis RAD54 physically interacts with RAD51, but no further biochemical characterization of its activities regarding RAD51 filament function has been performed [237]. Arabidopsis RAD54 is not only homologous in sequence to budding yeast RAD54, but it complements DNA repair

deficiencies of yeast *rad54* mutants, suggesting some conservation of function. However, it does not complement budding yeast *rad54* mutants deficiencies in a homologous recombination DNA integration assay, nor intrachromosomal recombination defects at HIS4 locus [567]. *rad54* mutant plants are viable and display sensitivity to different DNA damaging agents [237]. Analysis of somatic homologous recombination using reporter systems for inter-chromosomal and intra-chromosomal (inverted repeats) showed defects for both spontaneous recombination and at induced DSBs, but not at direct repeats, nor for induced single strand breaks [134,237,246]. Analysis of distance and pairing between homologous loci in somatic cells revealed that DSB induction promotes approaching of the two loci and this effect is lost in *rad54* mutants [568]. RAD54 foci form upon DNA damage induction in Arabidopsis and these colocalize with γH2AX and RAD51 foci. A reduction in foci observed in *sog1* and *atm* mutants confirms partial dependence on DDR signalling and absence of RAD54 foci in *rad51* mutants that DNA damage-induced RAD54 localization is dependent on RAD51 filament formation. Mean size of RAD51 foci increase in *rad54* mutants, presumably as a consequence of a role of RAD54 in RAD51 filament disassembly, as described in other organisms [569]. Finally, rad54 plants are fully fertile, but a characterization of meiosis in these plants has not yet been published [237].

3.6. Resolution of meiotic recombination

Upon successful homology search and synaptic complex formation, in which the invading ssDNA-nucleofilament and the two strands of the donor duplex form a three-stranded intermediate, the removal of the RAD51/DMC1 nucleoprotein filament together with the intertwining of the invading strand with one of the donor strands into hybrid dsDNA (hDNA) generates the D-loop, central intermediate of homologous recombination. The invading 3'-OH in the D-loop can then prime DNA synthesis extending the hDNA and driving the migration of the D-loop in that direction. Multiple resolution scenarios arise from this intermediate structure and these can be grouped into two classes based on whether or not the repair is associated with the reciprocal exchange of flanking DNA sequence: crossover (CO) and non-crossover (NCO) respectively. It is important to stress that there are not unique pathways towards these two repair products and that they can be generated via different processing of intermediates by multiple proteins and protein complexes. These are briefly described below, following a discussion of partner choice in meiosis, first determinant of the landscape of recombination resolution products.

Template choice: sister chromatid vs. homologous chromosome

The frequent use of the chromatids of the homologous chromosome as a template for DSB repair via homologous recombination is a major hallmark of meiotic cells. This contrasts to somatic/vegetative cells, in which the sister chromatid is the primary template when present (S/G2). This feature is critical in many organisms, in which proper disjunction of homologous chromosomes during the first meiotic division is dependent on chiasmata, interhomologue connections that result from reciprocal recombination events (CO) in the context of meiotic chromosome structure, which prevents their structural resolution until chromosome arm cohesins are dismantled during metaphase I. Many organisms not only rely on interhomologue recombination for the normal progress of meiosis at the late point of recombination resolution but at earlier intermediate steps as well, as early as DSB formation and homology search, needed for chromosome pairing and synaptonemal complex assembly. These events, when defective, may cause major disruptions in the course of meiosis or even triggering of checkpoints than arrest the division. In addition, meiotic interhomologue recombination generates an inheritable shuffling of paternal and maternal alleles that traduces into genetic diversity at population level, less so in the case of somatic recombination given the more prevalent use of the sister chromatid and the non-inheritance of events happening outside the germline in multicellular eukaryotes. Therefore, the use of the homologous chromosome might have been more strongly positively selected. The preferential use of the homologous chromosome as recombination template in meiosis is often referred as "homologue bias".

The identification of cytologically distinguishable structures - chiasmata - generated by interhomologue crossovers, and their importance for genetics, has driven the study of meiotic recombination [570,571]. Intersister events, on the other hand, have no detectable genetic impact in general and they are much more difficult to detect and study. Indirect evidence of intersister recombination during meiosis arises from observations of proficient DSB repair in mutants that lack interhomologue recombination. Regarding crossovers in particular, the concordance of crossover numbers scored by immunolocalization of proteins involved in late crossover resolution with crossover numbers scored by counting chiasmata analysing diakinesis/metaphase I bivalent structures lead to hypothesize that intersister crossovers are not frequent. Nevertheless, among model organisms, interhomolog crossovers represent from around 50% down to less than 5% of the total DSBs, so these observations are limited to that fraction (some examples in Table 1). Direct evidence of intersister recombination in meiosis has been obtained using circular chromosomes, recombination reporter systems

inserted at meiotic DSB hotspots and cytological techniques to differentially stain sister chromatids.

Circularized chromosomes have been used traditionally to detect intersister crossovers as these generate a dicentric circular chromosome that should be either lost or broken during meiosis. Using this approach, intersister crossovers have been detected in Drosophila, maize and budding yeast [572–575]. Budding yeast estimations of intersister and interhomologue crossovers performed by the analysis of a diploid strain carrying one linear and one circularized chromosome III established that intersister crossovers occur at a much lower frequency than interhomologue CO (0.15 vs 1.7 per meiosis) [574].

Southern blots and 2D electrophoresis further permitted the study of recombination intermediates in detail in budding yeast. Using DSB hotspots, multiple publications have inferred the interhomologue:intersister (IH:IS) ratio by developing reporter systems that can discriminate between the two populations of joint molecules (JMs) using different probes and restriction sites in the two homologues [218,554,576–579]. Intersister JMs account for between 12 and 30% of the total JMs in those studies.

Differential staining of sister chromatids achieved by the programmed incorporation of cytologically detectable nucleotide analogues during replication have been the standard method to detect sister chromatid exchanges (equivalent to intersister crossovers) for decades. Although primarily used in somatic cells, it has also been used in meiocytes, where the interpretation of the exchanges may be more challenging as both interhomologue and intersister events coexist. Direct detection of meiotic intersister crossovers using this technique has been reported for multiple species comprising several orthoptera species [580–583], mammals (mouse, Armenian hamster [584,585]) or nematodes (*C. elegans* [586]). In accordance with other reports using different techniques, the publications in which intersister crossovers were quantified show low frequencies of these events with respect to interhomologue crossovers.

Recent high resolution mapping of recombination events during meiosis via next generation sequencing of tetrads offered a new tool to understand the mechanisms regulating partner choice during meiosis [587]. Using the HIS4 DSB hotspot in budding yeast, Ahuja *et al.* found that a high proportion of recombination products contain mosaic hybrid tracts that would be generated by multiple rounds of strand invasion, extension and displacement. Among this population of mosaic products, about 1/3 involves initial invasion of the sister chromatid. This observation led the authors to propose that meiotic DSB ends would have similar likelihoods of invading the sister and the homologous chromatids and the bias towards interhomologue resolution would reflect a preferential disassembly of intersister early intermediates of recombination

instead of preferential initial invasion of the homologous chromosome. This proposal provides mechanistic evidence for the phenomenon of homologue bias, challenging previous hypotheses in which downregulation of intersister recombination would happen at the level of homology search and strand exchange (discussed in chapter 3.5. "*Presynaptic filament modulators*").

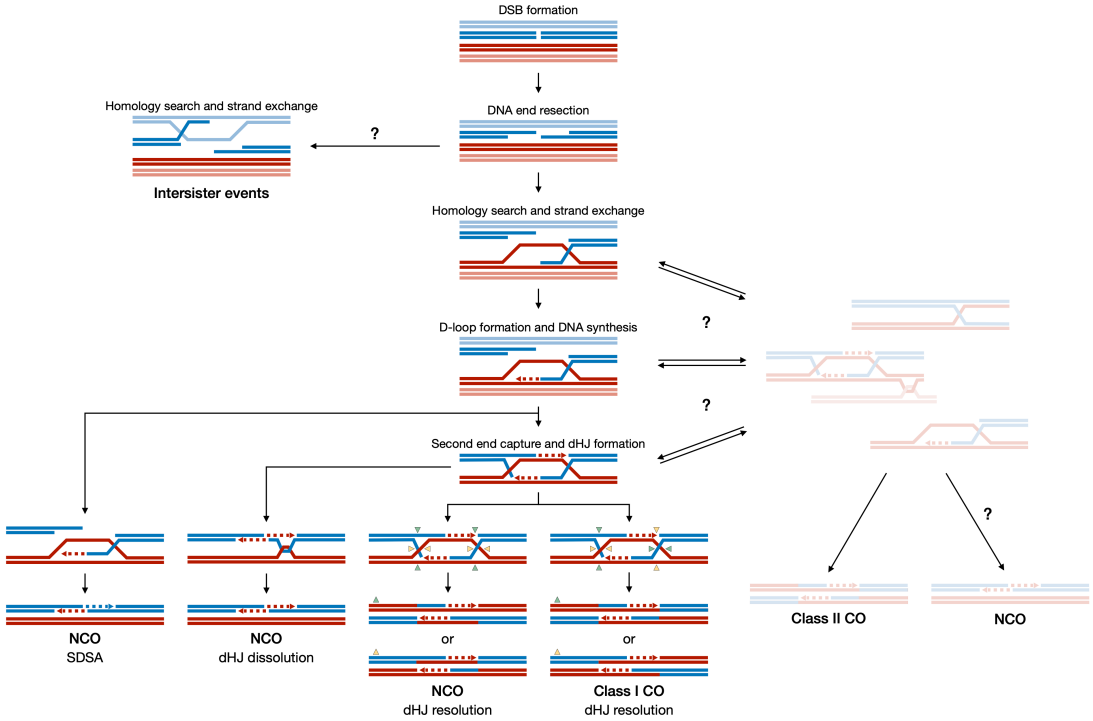

Figure 8. Model for double-strand break repair in meiosis.

Following **double-strand break formation**, the **DSB ends are resected** and the recombinases DMC1 and RAD51 are loaded onto the RPA coated 3'-ssDNA resected ends forming the presynaptic filaments. The presynaptic filaments invade the homologous chromosome catalysing **homology search and strand exchange**. Although in Arabidopsis there is currently no concrete evidence of the invasion and the resolution of recombination intermediates with the **sister chromatid**, it has been reported in other organisms. Once homology is found, the early invasion intermediate is stabilised into the **D-loop suitable for extension of the invading end via DNA synthesis**. This extended D-loop may then be processed into: I) the extended invading end is dissociated by helicases and recaptured back to its chromatid of origin, favouring from the extended segment to bridge the two ends of the break, anneal, fill and ligate to complete repair producing a NCO gene conversion event **(SDSA)**; or II) the second end of the DSB is captured into the extended D-loop, generating a **double Holiday junction (dHJ)**. The dHJ may as well be resolved via multiple pathways: I) through the STR/RTR-mediated topological dissolution of the dHJ, producing a NCO gene conversion event **(dHJ dissolution)**; II) through the MLH1-MLH3-mediated resolution introducing nicks in the same cleavage plane, producing a NCO gene conversion event **(NCO - dHJ resolution)**; or III) through the MLH1-MLH3-mediated resolution introducing nicks in different cleavage planes, producing a class I CO event with its associated gene conversion **(Class I CO - dHJ resolution)**. MLH1-MLH3-mediated resolution is biased towards the production of Class I CO events in meiosis. A second class of CO **(Class II CO)** arise from the resolution of a poorly understood set of recombination intermediates via the action of structure-specific nucleases. The formation of NCO events via this pathway has also been suggested in organisms such as budding yeast.

Crossover pathways

In accordance with the DSBR recombination model, following D-loop extension via DNA synthesis and stabilization of the single-end invasion (SEI) intermediate, the second end of the DSB may anneal with the displaced strand of the template dsDNA molecule, an event termed as second end capture. DNA synthesis primed by both ends then fills the gaps generated by resection and nick ligation forms a four-stranded intermediate known as the double Holiday junction (dHJ) [216,588–590]. As mentioned before, unligated – nicked - dHJs have also been proposed as substrates for resolution [220]. A set of proteins of varied molecular functions, named ZMM proteins, play essential roles as mediators of this process, facilitating the resolution of recombination intermediates towards crossovers via what is commonly referred to as the class I crossover pathway. In budding yeast, most of the intermediates stabilized by ZMM proteins are designated to be crossovers, however in other species the number of ZMM-bound intermediates outnumbers the final number of crossovers (around 20-fold for Arabidopsis).

Arabidopsis encodes orthologues for all of the described yeast ZMM proteins: ZYP1a and ZYP1b (Zip1), MER3 (Mer3), SHOC1 (Zip2), PTD (Spo16), ZIP4 (Zip4), HEI10 (Zip3), MSH4 (Msh4) and MSH5 (Msh5). This is so in other species in which class I pathway is the primary source of meiotic crossovers such as mouse or human, but not in *S. macrospora*, *C. elengans* and *D. melanogaster*, for which not all orthologues are present or have been identified [591]. Arabidopsis mutants for all ZMM genes except *ZYP1* present severe fertility defects, incomplete synapsis and a reduction of crossovers of up to 75-85%. They are however proficient for meiotic DSB repair as seen by the absence of chromosome fragmentation. Multiple combinations of mutations of these genes do not further reduce the number of crossovers below around 85% of the wild-type average and situate them in the same epistasis group responsible for the 75-80% of crossovers generated through the class I pathway in Arabidopsis [592–600]. Double knockouts of either *MSH4* or *SHOC1* with the structure-specific nuclease *MUS81*, component of the class II crossover pathway (to be detailed below), reduce the crossover number below 90% of the wild-type average, suggesting that not all of the residual crossovers are class II but there are yet to be described mechanisms able to generate crossovers in Arabidopsis meiosis [596,601]. Absence of the budding yeast ZMM proteins results in reduced formation of single end invasion strand exchange intermediates (SEI) and dHJs and reduced crossover formation both at hotspot and genome-wide levels [602–605]. As with Arabidopsis, a fraction of the remaining crossovers are dependent on the action of structure-specific nucleases [591,606,607]. The observation of impaired SEI formation in yeast *zmm* mutants suggests that ZMM proteins bind as early as the

invasion step and promote the stabilization of the D-loop and subsequent processing of intermediates promoting resolution via crossover [588,591].

Although grouped together because their absence generates similar defects of crossover formation, ZMMs have diverse molecular functions and form different complexes, mainly described in budding yeast. Mer3 is a helicase that *in vitro* is able to unwind D-loops, HJs and stimulate strand exchange activity by extending D-loops, although its helicase activity is thought to be responsible of only part of its function [591,608–611]. Zip2, Zip4 and Spo16 form a complex in budding yeast [612]. Zip4 is thought to act as a hub coordinating several meiotic processes, interacting with the axis and other ZMMs [612]. Zip2 and Spo16 share homology with XPF/ERCC1-family proteins. Although they do not show structure-specific endonuclease activity *in vitro*, the Zip2 XPF domain is needed for its pro-crossover activity and it preferentially binds branched DNA structures [599,612,613]. Physical interaction has been detected between the Arabidopsis Zip2-Spo16 orthologues SHOC1-PTD [596]. Zip3/HEI10 are functional E3 SUMOylation/ubiquitination ligases [591,600,614–616]. No direct Zip3/HEI10 substrates have yet been described, but they are thought to regulate recombination by inducing post-translational modifications on different substrates that promote crossover formation [591,617]. A recent publication describing the SUMO landscape during meiosis has underlined the prevalence and importance of this post-translational modification in events happening at prophase I, recombination included [618]. *C. elegans*, which lacks a Zip3/HEI10 orthologue, does have at least four E3 ligases that promote accumulation of pro-crossover factors [619,620]. Msh4 and Msh5 form an heterodimer (MutSγ) reminiscent of the MutS complex involved in mismatch repair, although it does not have mismatch repair activity [591,621–623]. It has been proposed that it binds and stabilizes dHJs, protecting them from dissolution by helicases, as well as a role in recruiting the MutLγ heterodimer (Mlh1-Mlh3) to promote resolution of dHJs [591,617,623–625]. In summary, ZMM proteins appear to stimulate crossover formation from early recombination intermediates to resolution by performing differentiated tasks at multiple steps of the process.

Zip1/ZYP1 is a special case among ZMM proteins. It is a structural component of the synaptonemal complex, forming the transverse filaments [626,627]. Although functionally and structurally conserved across different organisms, it has a high divergence at sequence level [591]. There is one orthologous gene of budding yeast *ZIP1* in mammals (*SYCP1*) but two in Arabidopsis (*ZYP1A* and *ZYP1B*) in a close inverted tandem disposition that has complicated their functional characterization [279,628]. Budding yeast *zip1* mutants have a milder phenotype than other *zmm* mutants in terms of reduction of SEI and dHJ formation [602]. It is important for the loading of other ZMMs

at recombination sites and for the elongation of the synaptonemal complex [629–631]. Analysis of *sycp1* mutants in mouse show a severe reduction of late crossovers markers, consistent with its role as a ZMM [628]. The first functional description of the Arabidopsis orthologues using RNAi lines showed absence of synapsis and a very mild reduction of crossovers [279]. Nonetheless, recent publications with the analysis of knockout mutants for the two Arabidopsis genes have described a surprising phenotype [280,281]. Immunolocalization of the proteins confirms the structural role in the synaptonemal complex forming transverse filaments but, despite the mutants are asynaptic, they do present chromosome pairing. Surprisingly, *zyp1a/b* mutants not only do not have a reduction of crossovers, but a slight increase. Nevertheless, these plants do present metaphase I univalents more frequently than the wild-type, postulating ZYP1a/b as a mediator of crossover assurance. In addition, reduced inter-crossover distance in these mutants suggests a role in regulating crossover interference, phenomenon by which the generation of one crossover decreases the probability of second one in adjacent regions that may span long chromosomal domains. Crossover interference is a major determinant of class I crossover positioning along the chromosomes, but the underlying mechanisms remain poorly understood [632]. A budding yeast *zip1* separation-of-function mutant evidenced that Zip1 promotes crossover formation independently of synaptonemal complex formation and that in absence of synaptonemal complex interhomologue crossovers are generated [631]. It may thus be hypothesized that, analogously, the pro-crossover activity of ZYP1 in Arabidopsis might be dispensable, independently of its structural function in the synaptonemal complex [281].

In order to yield a class I crossover, dHJs need to undergo nucleolytic processing of the junctions. The MutLγ heterodimer formed by MLH1 and MLH3, is key to this step. MutLγ is related to the MMR machinery but its main function in meiosis is not mismatch repair. Mutations of either *MLH1* or *MLH3* result in absence of class I crossovers [285,606,633]. Arabidopsis mutants of *MLH3* show a reduction of around 60% of crossovers that derive in the presence of univalents in metaphase I and both *mlh1* and *mlh3* mutants display partial infertility [285,634]. Budding yeast MutLγ has nicking endonuclease activity and preferentially binds HJs *in vitro*, although it is not a structure-specific nuclease [635–637]. MutLγ has been linked with different co-factors to promote dHJ resolution. Both in yeast and mouse the exonuclease EXO1 interacts with MutLγ and promotes the crossover resolvase activity of the dimer independently of its exonuclease activity [636,638–640]. *In vitro*, EXO1 stimulates the nuclease activity of MutLγ, as well as MutSγ, RFC and PCNA [639,640]. In addition, in budding yeast, interaction of Exo1 with Cdc5 regulates the timing of crossover formation. Upon successful homologue synapsis and formation of recombination intermediates, Cdc5 expression is induced by

Ndt80 and its interaction with Exo1 is essential for MutLγ-dependent crossovers, thereby preventing potential deleterious effects of premature crossover formation [641]. Given their protein-protein interaction and *in vitro* stimulation MutSγ, which binds earlier during prophase I, is thought to promote the recruitment and activity of MutLγ [624,640,642]. RFC and PCNA might mediate the cutting orientation of MutLγ, as they do during MutLα-dependent MMR [639,643]. This orientation is particularly important as the symmetricity in the cleave planes of the two junctions of the dHJ determines the nature of the product of recombination. Asymmetrical nicks in the two Holiday junctions will generate a crossover between the two implicated chromatids while a symmetrical configuration of the nicks will generate non-crossover products, both bearing a tract of gene conversion. Nevertheless, *mlh1/mlh3* mutants in yeast present a reduction of crossovers but not of non-crossovers and immunolocalization of either MLH1 or MLH3 in different species, mouse and Arabidopsis included, show numbers of foci of these two proteins that correspond to the numbers of class I crossovers inferred by analysis of diakinesis/metaphase I bivalent structures or by molecular detection of COs via sequencing of meiotic products [285,633,644,645]. While MutLγ could potentially resolve dHJs in either symmetrical or asymmetrical configuration, these observations indicate a biased resolution towards crossover products in practice. This bias must implicate a coordination between the resolution of the two Holiday junctions and presumably the differential loading of the implicated factors to promote asymmetrical cleavage, but the underlying mechanisms are poorly understood.

A second class of crossovers (class II CO) arises from the resolution of joint molecules of probably multiple origins and natures. This class is not dependent on ZMM proteins and MutLγ-mediated resolution but involves structure-specific nucleases (SSNs). It is characterized by the absence of crossover interference, hence the presence a class II crossover does not inhibit the occurrence of a second crossover in adjacent regions as is the case for class I CO [646,647]. At least three different SSNs has been linked with crossover formation during meiosis: the dimers Mus81-Mms4/EME1-2, Slx1-Slx4/BTBD12 and Yen1/GEN1. These endonucleases recognize and cleave ssDNA flaps and diverse branched structures, including HJs. Only Yen1/GEN1 displays a RuvC-like religatable symmetrical cleavage of the Holiday junction [219,648]. Nonetheless, Yen1/GEN1 is dispensable for meiotic recombination and it only becomes essential when Mus81-Mms4 is absent in budding yeast. Yen1 is inhibited during budding yeast prophase I via CDK-mediated phosphorylation and it becomes active in later stages following Cdc14-mediated dephosphorylation, presumably as a safeguard for unresolved JMs. Therefore, although *mus81/mms4 yen1* double mutants show almost normal levels of recombination, they fail during chromosome segregation due to unresolved JMs [649–

[653]. In Yen1 phosphorylation-refractory mutants, in which it becomes constitutively active throughout prophase I, Yen1 resolves JMs prematurely and form crossovers independently of MutLγ. Yen1-mediated resolution during prophase I rescues mutants with defects in JM processing, but impairs crossover patterning and results in a mild decrease of spore viability with respect to wild-type strains [652]. Two putative orthologues of Yen1 has been proposed in Arabidopsis with cannonical HJ resolvase activity *in vitro*: GEN1 and SEND1 [654]. *In vivo* genetic interactions with other members of the DNA repair machinery points to SEND1 as the functional Yen1 orthologue, but no apparent role in meiotic recombination was observed [251]. Nor has a meiotic function for Yen1 orthologues been described in other organisms [651].

Mus81-Mms4/EME1-2, on the other hand, accounts for a fraction of crossovers in wild-type meiosis of multiple species. Mus81 is not a bona fide HJ resolvase (like bacterial RuvC or Yen1/GEN1), but is able to cleave HJs in an asymmetrical configuration that produces unligatable ends. It can process a great variety of joint molecules, it has low activity on intact HJs with continuous strands and it is strongly stimulated by the presence of a discontinuity or a nick adjacent to the branch point of the junction [219,252]. Mus81 belongs to the XPF-family of endonucleases and, like other members of this family, it forms an heterodimer with a non-nucleolytic partner: Mms4 in budding yeast, EME1 and EME2 in mammals or EME1a and EME1b in Arabidopsis [252,655,656]. The CO-yielding meiotic substrate for Mus81-Mms4/EME1-2 is not known but models invoke sequential D-loop nicking as well as a more general role in processing aberrant JMs and other branched DNA structures [646,651,657,658]. Mus81-dependent crossovers account for around 5 to 25% of total crossovers in most of the species in which they are present, although there are exceptions [590]. Notably, in fission yeast (which lacks MutLγ and Yen1), Mus81-Eme1 is the resolvase for the only crossover pathway described to date and its absence nearly abolishes crossover formation and fertility [646,659–661]. On the other hand, although Drosophila does have MUS81-MMS4, no role in meiotic recombination has been attributed to it [662]. Arabidopsis *mus81* mutants showed a mild reduction of crossovers using two genetic intervals (9 and 12%) but no effect was observed when scoring chiasmata at genome wide level [663,664]. A reduction of the average chiasma frequency however was detected in the *mus81/msh4* and *mus81/shoc1* mutants with respect to the single *zmm* mutants (0.85 vs. 1.25), this drop representing less than 5% of the wild-type average number of COs [596,664]. A similar situation was observed in mice, in which *mus81* mutants do not show a decrease in crossovers with respect to the wild-type but when combined with a *mlh3* mutation the residual chiasmata of *mlh3* mutants suffer a reduction adding up to about 5% of the wild-type average [665]. Both in Arabidopsis and mouse the absence of Mus81 causes only

a very slight reduction in fertility [663–665]. In budding yeast, Mus81-Mms4-dependent crossovers represent a 20-25% of the total and their absence has a stronger impact in fertility [606,607,649]. *mus81* and *mms4* mutants complete prophase I without triggering checkpoints and, despite their role in JM resolution, almost normal levels of recombination are detected, presumably due to overlapping in substrates with other pathways and safeguard mechanisms (Sgs1-mediated dissolution or Yen1-dependent resolution) [606,607,649,651]. They however show defects in chromosome segregation attributed to unresolved JMs that may explain the fertility defects [649]. As for class I crossovers, class II crossovers are timely regulated by Ndt80-Cdc5 via Cdc5-mediated phosphorylation of Mms4, conditioning as well Mus81-Mms4-mediated crossover formation to successful homologue synapsis and recombination intermediates formation [649].

Slx1-Slx4/BTBD12 is the third structure-specific nuclease with an attributed role in class II crossover formation. Slx1 belongs to the GIY-YIG family of endonucleases. It has a weak nuclease activity which is strongly stimulated upon binding to the scaffold protein Slx4/BTBD12. Similarly to Mus81-Mms4/EME1-2, Slx1-Slx4/BTBD12 is able to cleave HJs asymmetrically as well as other branched DNA structures, although it does not have the ability of resolving HJs as a RuvC-like resolvase. In budding yeast, neither *slx1* nor *slx4* mutants display a significant reduction in sporulation or spore viability and they undergo meiosis without detectable defects in homologous recombination by JM analysis [649,651]. No HJ resolvase activity was detected when the complex was purified from meiotic cells with respect to proliferating mitotic cells, in which resolvase activity was detected, suggesting that Slx1-Slx4 might be downregulated during budding yeast meiosis [649]. Its absence, in combination with that of *mus81* or *yen1*,does not worsen the meiotic phenotype of either of the two strains, but when combined with sgs1 the cells accumulate unresolved JMs and meiotic chromosomes are unable to properly segregate, pointing to an activity in the resolution of a subset of JMs in certain conditions [651]. No meiotic role has been attributed to SLX1 in mouse, where *slx1* and *slx1 mus81* mutants do not show significant defects in fertility [666]. BTBD12 (SLX4) however was found to localize to meiotic chromosomes and *btbd12* mutant mice have impaired meiotic DSB repair and reduced fertility associated to increase apoptosis during prophase I. Crossovers form at normal levels but MLH1 foci are increased, attributed to a compensation of class I for the loss of class II crossovers, postulating BTBD12 as a factor in mouse class II crossover pathway [667]. Likewise, meiotic DSB defects have been described in budding yeast *slx4* mutants independently of Slx1 in genome-wide recombination analyses [668]. Slx4/BTBD12 is known to interact not only with Slx1 but with other nucleases involved in DNA repair in multiple

organisms, budding yeast and mouse included, so a meiotic Slx1-independent role cannot be excluded [669]. In *C. elegans*, as an example, mutants of the Slx4 orthologue HIM-18 show reduced crossover frequency and segregation errors [670]. HIM-18 was found to interact not only with SLX-1 but with MUS-81 and XPF-1 and all of them participate in meiotic crossover resolution pathways [670–672]. No orthologues of neither Slx1 nor Slx4 have been described in Arabidopsis to date.

Non-crossover pathways

Interhomologue crossovers represent a minor fraction of the meiotic recombination products in many eukaryotes. In Arabidopsis only about 5% of the total estimated DSBs are repaired via crossover with the homologous chromosome and this proportion is estimated to be around 10% in mice. In other species, such as budding or fission yeast, the repair of approximately 50% of the DSBs yield crossover events. The absence of meiotic phenotypes in mutants of end joining pathways and their unchanged numbers of cytological foci of early recombination markers (RAD51 & DMC1) suggest that the remaining (around 95% in Arabidopsis) DSBs are repaired via homologous recombination mechanisms, either with a sister chromatid template or as non-crossovers with the homologous chromosome. The direct detection of these events in Arabidopsis has been, and still is, a challenge. They do not generate cytologically detectable structures that help to identify them, the electrophoresis and southern blot techniques to detect and measure proportions of recombination intermediates at DSB hotspots have not been implemented in the model plant and the absence of polymorphisms in one case (intersister events) or the short exchange tracts in the other (interhomologue non-crossovers) have impeded in some cases and difficulted in others their detection using hybrid strains. Nevertheless, while impaired crossover formation results in intact univalents at metaphase I, defects in both crossover and non-crossover formation generally result in fragmentation, chromosome entanglements and/or chromosomal bridges. The study of these phenotypes has permitted the characterization of some of the pathways leading to non-crossover products during Arabidopsis meiosis.

The two main recombination mechanisms leading to non-crossover outcomes are SDSA and dHJ dissolution. A third possibility results from the nucleolytic resolution of dHJs in a configuration that yields non-crossovers depending on the cleavage planes, but the crossover bias observed in MutLγ-mediated resolution of intermediates and the limited fraction of SSNs-dependent events of many species raise questions about their biological importance during meiosis. SDSA, as detailed in previous chapters, involves disassembly of an extended D-loop and the reannealing of the two ends of the DSB

thanks to the homology tract gained during this extension. If the D-loop is stabilized and the second end captured, a second non-crossover resolution scenario emerges from JM dissolution via convergent branch migration followed by the topological resolution of the junction. These two mechanisms involve the components of the STR/BTR complex: Sg1/BLM, Top3/TOPOIIIα and Rmi1/RMI1-2.

Sgs1/BLM is an helicase homologue to the bacterial RecQ. *In vitro* studies using recombinant human BLM have shown that it has D-loop dissociation activity, it binds HJs and promotes branch migration [673–675]. It forms a complex with the topoisomerase Top3/TOPOIIIα and Rmi1 in yeast, RMI1 and RMI2 in humans, that is able to process dHJs by a mechanism that involves convergent branch migration mediated by the helicase activity of Sgs1/BLM and decatenation of the junctions by the topoisomerase activity of Top3/ TOPOIIIα with the necessary support of Rmi1/RMI1-2, resulting in the dissolution of the structure without a crossover between the implicated DNA molecules [223,676–682]. *In vivo*, mutants of Sgs1/BLM in budding yeast and mouse have a partial reduction of fertility and show a modest increase in crossovers that in budding yeast is abolished when combined with a *mus81* mutation and in mouse is not accompanied by an increase in class I crossover markers, suggesting that the increase would be via the class II pathway [683,684]. The analysis of recombination intermediates in budding yeast have permitted the description of the important role of this complex as a modulator of pathway choice during meiosis. The STR complex dissolves nascent and extended D-loops permitting in both the release of the invading end for re-invasion of a different template and, in the case of extended D-loops, for re-annealing with the other end of the break to repair via SDSA yielding non-crossover events [685,686]. Later on in the recombination process, it is able to dissolve aberrant or "off-pathway" JMs that cannot be resolved via ZMM-MutLγ and that otherwise would be resolved by SSNs. In absence of Sgs1 there is an accumulation not only of total JMs but of multi-chromatid JMs and their resolution relay primarily on Mus81-Mms4 but also partially on Slx1-Slx4 and Yen1. Removal of the meiotic SSNs in a *sgs1* mutant context results in a drastic reduction of both crossovers and non-crossovers and meiotic catastrophe at the segregation step [576,577,650,651,683]. Interestingly, that reduction of crossovers corresponds to the loss of MutLγ-dependent crossovers, which suggests that the activity of SRT in preventing the accumulation of aberrant JMs (or processing those JMs) might facilitate as well the generation of intermediates that can be resolved via the class I crossover pathway [651,685]. The SRT complex thus prevents the accumulation of aberrant JMs by disassembling D-loops in a first instance and by actively dissolving those JMs later on promoting non-crossover events via SDSA or topological resolution of JMs. It could also promote class I crossover by both disassembling nascent D-loops - releasing the

invading ends for re-invasion - and by processing aberrant JMs - generating a substrate that can be resolved by MutLγ. As for other proteins involved in meiotic recombination resolution, it is regulated by cell-cycle kinases: CDK-mediated phosphorylation of Sgs1 stimulates its activity during prophase I up to pachytene exit, when Ndt80-Cdc5-mediated hyperphosphorylation reduces its activity. This regulation would facilitate the processing of JMs and the resolution via non-crossover up to the pachytene exit point in which the resolution nucleases become activated overcoming the task of resolving the remaining JMs and generating crossovers [687].

Arabidopsis encodes two orthologues of Sgs1/BLM (RECQ4a and RECQ4b), one of Top3/TOPOIIIα (TOP3α) and two of Rmi1 (RMI1 and RMI2). A complex of RECQ4a-TOP3α-RMI1-RMI2 has been detected *in vivo* by tandem affinity purification [240]. Mutants of *RECQ4a* show a partial reduction of fertility and the presence of chromosomal bridges in 25% of the cells while in the case of *RECQ4b* there is no reduction of fertility [688]. The single mutants do not display increased crossover frequency but the double *recq4a recq4b* have a drastic increase both at a series of genetic intervals and genome wide while maintaining similar levels of class I crossover markers and reduced crossover interference, hence attributed to the class II crossover pathway. The increase of crossovers is maintained when combined with *zmm* mutants, partially rescuing crossover frequency and fertility [240,689]. This increase is notably higher than that observed in budding yeast and mouse, probably attributable to the relatively high excess of DSBs repaired via NCO in Arabidopsis, potential substrates for class II crossovers in absence of RECQ4a/b. MUS81 becomes essential for somatic development in this context and the triple mutants are lethal [240]. It thus seems plausible that the function of the SRT complex in preventing the formation of aberrant JMs or/and dissolving them resulting in non-crossover events during meiosis is conserved in the model plant

Interestingly, *top3α* hypomorph (the null is lethal) and *rmi1* mutants display defects in meiotic DNA repair not observed in *recq4a recq4b*. Bivalents appear entangled at metaphase I, resulting in severe fragmentation when they migrate during anaphase I [241,690]. Plants homozygous for *top3α* mutant allele that expresses a truncated protein lacking C-terminal zinc-finger motifs were found to be viable with unaffected development and fertility despite the presence of univalents at meiotic metaphase I. An increase in class II crossovers was detected in different genetic intervals in these plants (not accompanied by an increase in class I crossover markers and still detected in double mutants with *zmm* mutant alleles) and its combination with *mus81* results in defective meiotic repair with entanglements and anaphase I fragmentation [240]. These zinc finger domains were later described as being important for the role of TOP3α in processing

HJs, but not for other roles of TOP3α providing thus a potential explanation for the moderate phenotype of the truncated protein allele, which might behave as a separation of function allele with respect to the null or hypomorphic alleles [240,241,691]. This observation, together with the absence of the defective repair phenotype in mutants of *RECQ4a/b* observed in mutants of *TOP3α* and *RMI1*, suggests RECQ4a/b-independent roles for the two proteins. Budding yeast *top3* and *rmi1* mutants also have stronger spore formation defects than *sgs1* mutants and these are worsened in Arabidopsis and budding yeast when combined *top3/top3α* and *sgs1/recq4a-b* mutations [240,241,686,690]. Detailed analysis of JMs and nuclear divisions in budding yeast revealed that Top3 and Rmi1 act together independently of Sgs1 in the resolution of recombination-dependent chromosome entanglements to allow segregation in anaphase I and to suppress ectopic recombination [685,686]. The conservation of this function might explain the described differences in the phenotypes of mutants of the SRT complex during Arabidopsis meiosis.

A second helicase, Mph1/FANCM, has been shown to favour meiotic non-crossover formation at the expense of crossovers (and maybe intersister events) in Arabidopsis and other organisms. Both budding yeast Mph1 and human FANCM have D-loop dissolution activity *in vitro* and Mph1 was shown to channel recombination intermediates towards non-crossover resolution in budding yeast mitotic cells independently of Sgs1 and Srs2 [692,693]. In a screen for mutations that restore fertility of *zip4* Arabidopsis mutants, the absence of FANCM was found to rescue the crossover formation defects of *zip4* (and other ZMM mutants). An excess of crossovers was later detected in multiple genetic intervals, attributed to the class II pathway as class I crossover markers showed no differences with the wild-type and *fancm mus81* mutants have chromosome entanglements in metaphase I and fragmentation in anaphase I analogously to other mutants that derive JM resolution to the class II pathway [694,695]. A similar phenotype was observed in mutants the two DNA-binding cofactors of FANCM, MHF1 and MHF2, but not of other members of the Fanconi Anemia pathway [696,697]. Similar results were observed in the closely related *Brassica rapa* and *Brassica napus* [698]. Nevertheless, while the increase in crossover frequency is observed in inbred but not in hybrid Arabidopsis plants, *Brassica napus* allohaploids, in which recombination happens between homeologous chromosomes, do show it [695,698]. Fission yeast *fml1* mutants (Mph1/FANCM orthologue), also display increases in crossover frequency, while Fml1 overexpression partially rescues the sterility of a *mus81* mutant, from which the authors propose a Fml1-dependent non-crossover pathway via D-loop disassembly and SDSA resolution [699]. A recent study in budding yeast has revealed that Mph1 prevents precocious strand exchange before the pairing homologous

chromosomes, after which it is inactivated in a Zip1-dependent manner [700]. By doing so it favours homologue bias during meiosis by avoiding the stabilization of recombination intermediates at time points at which the homologous chromosomes are not yet (or not-fully) paired and strand exchanges occurs preferentially with the sister chromatid. In absence of Mph1, a higher proportion of DSBs thus generate intersister JMs with interhomologue crossovers remaining unchanged while interhomologue non-crossovers are reduced at a hotspot. The authors propose than in the presence of a higher number of intersister JMs, thereby less interhomologue intermediates, a homeostatic mechanism would favour crossover outcomes over non-crossover to ensure wild-type crossover levels. Mph1/FANCM would thus not act as the mediator of a non-crossover pathway than when disrupted diverts those (or part of those) intermediates into crossovers but rather the alterations of crossover/non-crossover distribution in the mutants would be a consequence of a compensatory mechanism. The same authors propose two hypothesis to translate these observations into species in which *fancm* mutants suffer an increase in crossovers such as Arabidopsis: I) there might be an analogous homeostatic mechanism favouring crossover formation in *fancm* mutants, not just at the expense of reducing non-crossovers to maintain wild-type levels of crossovers but actually overcompensating resulting in an augmentation of crossovers; II) it might be possible than precocious strand exchange in *mph1/fancm* mutants bypasses crossover homeostasis mechanisms. However, this hypotheses remain to be tested in Arabidopsis.

A third factor has been associated in Arabidopsis with the limitation of meiotic crossovers, probably favouring non-crossover events: FIGL1 and its cofactor FLIP. These two proteins physically interact and show similar phenotypes when the genes that encode them are disrupted. These phenotypes include an increase of crossover frequency at genetic intervals, partial rescue of crossover formation defects of *zmm* mutants, wild-type numbers of class I crossover markers and genetic interaction with *mus81* resulting in fragmentation at anaphase I. [284,701] Therefore, the extra crossovers detected in the absence of FIGL1 or FLIP1 are attributed to the class II pathway. Altered numbers of RAD51 and DMC1 foci are reported in *figl1* and *flip1*, although the two publications show opposite dynamics using the same *figl1* allele [284,701]. Both *figl1 sds* and *flip sds* double mutants rescue the loss of DMC1 foci observed in *sds* single mutants, suggesting a role in regulating the loading and dynamics of DMC1, although it is not yet understood how absence of SDS leads to loss of DMC1 filament formation [284,701]. Absence of FIGL1 in a *brca2a brca2b* mutant context, in which RAD51 and DMC1 foci are not detected and meiotic DSB repair is defective, also restores the formation of foci of both recombinases and partially rescues DNA repair defects, crossover formation and fertility [702]. The authors thus propose that FIGL1-FLIP

regulates the dynamics of RAD51 and DMC1, preventing the accumulation of aberrant JMs. In their absence, those aberrant JMs would be repaired by SSNs yielding class II crossovers. Little is known however about the role of FIGL-FLIP orthologues during meiosis in other organisms. FIGNL1, the human and mouse orthologue of FIGL1, was found to interact physically with RAD51 and it is recruited to DNA damage sites in a γH2AX-dependent, RAD51-independent manner in cell cultures [703]. Purified FIGNL1 promotes the disassembly of RAD51 nucleofilaments *in vitro* and this activity is inhibited by SWAPS1 both *in vitro* and *in vivo*. Concordantly, *swaps1* mutants show reduced RAD51 and DMC1 focus formation in meiosis [704]. It is thus hypothesized that the FIGNL1-mediated RAD51 nucleofilament-disassembling activity might be, as for other translocases, important to avoid aberrant strand exchange intermediates, which are known substrates for SSNs processing during meiosis. Their accumulation thus might explain an increase in class II crossovers resulting from nucleolytic resolution by SSNs.

Combinations of mutants of the three pathways or mechanisms that limit crossovers described in Arabidopsis (RECQ4a/b, FANCM and FIGL1) show additive increments of crossover frequency with respect to the singles (except for *fancm* in hybrids), suggesting that they act independently of each other [695,701]. However, disruption of all three does not give further increases, possibly pointing to an upper limit of crossover formation during Arabidopsis meiosis. These multiple knockouts do however have significant fertility defects, probably due to unresolved JMs or a deleterious effect of such high crossover density [695].

3.7. Regulation of meiotic recombination

Meiotic recombination is a tightly regulated process. Recombination results from the repair of DNA DSBs and results in transfer of information from a donor DNA molecule, accompanied or not by the reciprocal exchange of flanking DNA sequences. It thus comes as no surprise that the first layer of regulation of meiotic recombination involves control of double-strand break numbers and distribution. As discussed above however, not all DSBs become crossovers and thus crossover patterns do not necessarily reproduce the underlying DSB patterns. The choice of donor DNA molecule and of NCO versus CO mechanism for the repair of a given DSB thus determines the translation of the underlying DSB pattern into the CO distribution. Given the importance of meiotic crossovers as a natural evolutionary force and for animal and plant breeding, the study of the crossover landscapes at genome, chromosomal and local scales has been a major focus of the genetics community for many years. This is also

true for non-crossover products of meiotic recombination, which are however considerably more difficult to detect and therefore less information has been collected regarding their regulation. Given their common mechanistic origins, they are however necessarily affected by crossover regulation mechanisms and alterations in the crossover landscape will inevitably modify the landscape of non-crossovers.

3.7.1 Genome wide regulation

Crossover homeostasis

Crossover homeostasis is a phenomenon that refers to the conservation (or the non-proportional change) of the numbers of crossovers in contexts in which the number of DSBs is altered either by excess or by deficiency, although it was first described and mostly studied in the latter case. Budding yeast *spo11* hypomorphic mutant strains form less DSBs than the wild-type but genetic distances measured in multiple intervals across different chromosomes did not show a corresponding reduction of crossovers, with some showing no reduction at all even in the most extreme case in which the drop of DSBs was scored at 80%. This maintenance of crossover rates was achieved at the expense of decreasing numbers of non-crossovers [705]. *SPO11*/spo11 mice display a decrease of SPO11 proteins levels that translates into a reduction of about 15-30% in numbers of foci of early recombination markers (RAD51 and DMC1) and a drop of γH2AX relative intensity in early prophase I, both concordant with a reduction of DSBs. Nonetheless, these reductions were compensated as prophase I advances and class I crossover markers (MLH1) remained at wild-type levels [706]. In a more extreme situation in *C. elegans*, in which an inducible DSB by transposon excision was monitored, crossovers were extremely favoured with respect to non-crossovers in *spo11* mutants with no DSBs when compared to wild-type worms, suggesting the action of compensatory mechanisms as well [707]. Arabidopsis *spo11* hypomorphic lines with drops of about 30-40% in DSBs numbers as scored by γH2AX and RAD51 localization have reductions of less than 15-20% in chiasmata and MLH1 foci as well as pollen viability, indicating presence of (maybe weaker) crossover homeostasis. A similar behaviour has been proposed in maize inbred lines that differ in numbers of RAD51 foci and show a linear correlation of this with average chiasma numbers [708].

Inter-specific differences has also been observed in the opposite sense. Mice with extra copies of the SPO11 gene show increased SPO11 and γH2AX levels as well as RAD51 and DMC1 foci in early prophase I but, similarly to the hypomorphic strains, these increases tend to be compensated as prophase I advances and no increase of MLH1

foci was observed in pachytene [706]. It is worth noting that MLH1 is marker of class I crossovers but not class II and that these were not scored. As class I crossovers are subject to the limiting action of crossover interference but class II are not, it might be speculated that the second class could have more "freedom" to be increased as it is seen in other species in certain mutants with altered JM metabolism described above, but this has not been tested directly in these mice to our knowledge. This effect has however been described in budding yeast, in which absence of Tel1 leads to increased DSB numbers, accompanied by an increase in crossovers. In this context, ZMM-dependent crossovers appear to represent a smaller share of the total crossovers than in the wild-type and crossover interference is reduced, suggesting a prominent role of class II crossovers in this increase. The crossover to non-crossover ratio does also suffer a mild reduction when compared to the wild-type, despite the absolute increase in crossovers. Thus, mechanisms that buffer a proportional augmentation of crossovers with DSB numbers by directing intermediates towards interhomologue NCO and/or intersister events should not be excluded [709]. *atm* mutant mice arrest meiosis at the pachytene checkpoint but when combined with *SPO11/spo11* heterozygosity they are able to progress while maintaining a 4.5-7.8-fold increase of DSB numbers. In this context, a significant increase of MLH1 foci was observed in contrast with the result observed when introducing extra SPO11 copies [392,710]. Given the key role of Tel1/ATM in DSB signalling and the DNA damage response, these mutants might well not only increase DSB numbers, but also cause general alterations of the DSB repair machinery that might explain contrasting results with DSB increases through other means.

In Arabidopsis, loss of the FAS1 subunit of the CAF-1 chaperone was described to introduce an excess of DSBs at early prophase, scored by localization of γH2AX, RAD51 and DMC1. The numbers of recombination intermediates (MSH4), class I (MLH1) and class II crossovers (MUS81) remained unaltered in these plants, as did mean chiasmata frequencies in metaphase I. Gene conversion frequency measured at one locus using a transgenic reporter system was significantly increased, which together with the increase in numbers of early recombination marker foci (RAD51 and DMC1) and unchanged mean chiasmata frequency, might suggest the existence of an homeostatic mechanism impeding the formation of extra crossovers in this situation and the repair of those extra DSBs via non-crossover homologous recombination pathways [711].

Heterochiasmy

Sex differences in meiotic recombination are widespread across multiple taxa. Some species directly show no meiotic recombination in one of the sexes, such as Drosophila males or females of some lepidopterans. Among the species in which both sexes recombine but show sexual dimorphism, the more common scenario is higher crossover rates in female than males, although the opposite case has been described in multiple species such as domestic sheep or some metatherian mammals [712,713]. Humans and mice, in which this phenomenon has been studied in more detail, fall among the species with higher recombination rates in females, with around 1.6-fold and 1.2-fold more respectively [714,715]. Interestingly, the differences are not limited to the total number of crossovers but also to their distribution or the local determinants of recombination frequency and outcome. Human males, as an example, recombine significantly more near the telomeres than females, a trend that is also observed in other animals [712]. At the local level, significant sexual dimorphism has been described for the correlation of GC content and meiotic recombination in multiple species [713]. At the step of recombination initiation, male and female humans and mice show few sex-specific DSB hotspots but a clearly sex-biased use of them [714,716]. Differences in the promotion/suppression of crossovers in particular chromosomal regions as well as in the local enrichment of genomic and epigenetic features have also been described in humans [714]. In the plant kingdom, angiosperms with sexual dimorphism in recombination rates have been described, but without a clear trend in favour of one sex [712]. Arabidopsis in particular shows a clear dimorphism with a 1.7-fold longer genetic map in male versus female meioses [717,718]. Crossovers are also distributed differently, with significantly higher rates at subtelomeric regions in male meiosis accounting for most of the variation [695,718]. Arabidopsis female crossover densities were found to correlate negatively with GC content and gene density and positively with transposable elements density but none of these features correlates with male crossovers [718]. Surprisingly, in hyper-recombinant mutants such as *recq4a/b figl1*, the differences are not only compensated but female meioses show higher crossover rates both genome wide and in the subtelomeric regions, which have an almost 60-fold increase of recombination rate [695].

Loss of sexual dimorphism in recombination rate has also been reported in *zyp1* mutants [281]. Synaptonemal complex length is another meiotic feature that shows sexual dimorphism in multiple species and it is known to positively correlate with recombination rates [719–723]. This is notably the case in Arabidopsis, with male synaptonemal complexes being significantly longer when measured by ZYP1

immunolocalization [724]. The authors of this study propose that crossover interference propagates not only along the axes, as previously established, but along the tripartite synaptonemal complex. Therefore, in absence of an essential component of the central element, as in Arabidopsis *zyp1* mutants, interference is abolished and with it the dimorphism in recombination rates [281,725]. A crossover interference hypothesis to explain sexual dimorphism in recombination rates would also fit with the result in *recq4a/b figl1* double mutants in which the extra crossovers are thought to be interference-insensitive (class II), but this idea remains to be tested.

Environmental factors

The interaction of environmental factors and meiotic recombination has been a subject of study ever since the construction of the first genetic maps in Drosophila, soon followed by the description of the effect of temperature on them [726,727]. Among the different variable environmental factors to which plants are subject, temperature changes have become of major interest in the last decades as concern for climate change is on the rise and fertility defects derived from alternations of meiotic recombination pose an important threat to crops. As for many other genetic studies, Arabidopsis has been used as model plant despite its low agronomical interest with the aim of gathering data that could be later translated into these species.

Recombination rates have been found to be positively correlated with temperature in the range of 18-28°C in lab grown *Arabidopsis thaliana* and in wild populations of the closely related *Arabidopsis arenosa* subjected to seasonal changes [728–731]. In the case of *Arabidopsis thaliana*, these increases were not to be associated with augmented DSB numbers but rather with changes in crossover regulation [730]. At 28°C, an increase of MLH1 has been reported by at least two independent groups with respect to 18-20°C that together with the observation of unaltered crossover interference and the conservation of the increase in recombination in *mus81* mutants, suggests that these extra crossovers at 28°C would happen via the class I pathway [729,730]. An increase of recombination has also been reported as temperature decreases from 18°C to 8°C, drawing a U-shaped profile in the recombination rate-to-temperature relation of Arabidopsis with a valley in 18°C without changes in crossover interference, shape that was also observed in the *A. arenosa* wild populations [730,731]. This increase was associated with unchanged MLH1 foci but increased HEI10 foci as well as an increase in synaptonemal complex length with respect to plants at 18°C, in contrast with the results at 28°C in which synaptonemal complex length was reduced. The authors propose that the increases in crossover rates as temperatures drop from 18 to 8°C would

also come from augmentation of class I crossovers, but the differences observed between the effects at 8°C and 28°C suggest distinct mechanistic origins of the increase between the two conditions [729]. Temperatures over 30°C have been associated in Arabidopsis with multiple meiotic and recombination alterations comprising partial asynapsis, presence of univalents, chromosomal bridges and fragmentation in the first and second meiotic divisions, defective cytoskeleton and aberrant cytokinesis ultimately leading to severe drops in fertility [732,733].

In crop species, the relation between recombination rate and temperature is not that clear but what appears to be conserved is that temperatures above approximately 30°C generate very important drops in seed production, not only in Arabidopsis but also in barley, rice, wheat or sorghum [341,734–736]. Barley grown at 30°C presented defective synapsis and moderate drops in chiasmata numbers, accompanied by a change in their distribution to more interstitial positions of the chromosomes [341]. Another report using markers to build genetic maps found an increase in the genetic map of male barley meiocytes that was not observed in female cells when comparing plants at 30°C with plants at 25°C and 15°C. Comparing plants grown at 15°C and 25°C, the second group showed longer bivalent length measured by intervals delimited by fluorescent markers at pachytene and a change in the distribution of MLH3 foci that shifted towards more distal portions of the chromosomes [737]. In both reports, growth at 30°C reduces seed production to less than 10% of that under in standard conditions. The analysis of wild subpopulations of barley have revealed a correlation between recombination rate and temperature but, in contrast with Arabidopsis, it has a reverse U-shape with optimal temperatures being the peak and not the valley of the distribution, suggesting interesting differences in the evolutionary regulation and the adaptation responses of these two species. In addition, these subpopulations show an even stronger correlation with other environmental factors, such as isothermality and solar radiation in the shape of an reverse U-shape as well and a positive linear correlation with precipitation which underlines the importance not only of temperature but of multiple environmental factors in the regulation of recombination [738].

3.7.2. Regulation at chromosome level

Crossover assurance

Chiasma formation is essential for proper bivalent aligning on the metaphase I plate and successful chromosome disjunction in anaphase I in most species. Achiasmatic meiosis is rare, although there are organisms that have developed mechanisms that

permit achiasmatic meiotic chromosome disjunction, such as Drosophila and some other arthropods, tardigrades, annelids, plathelminths or molluscs [739]. Nevertheless, aside from achiasmatic organisms, the lack of at least one crossover between homologous chromosomes, commonly referred as obligatory crossover, often leads to important fertility defects associated to the loss of those chromosomes. Paradoxically, several organisms present a wide size range among their chromosomes and the number of crossovers is so low that, if they were randomly spatially distributed along the whole genome, the small chromosomes would frequently receive no crossover and thus fail to properly segregate. Early cytogenetic studies in grasshopper species with great disparities in chromosome length (*Stenobothrus parallelus and Locusta migratoria)* showed that short chromosomes have a disproportionate number of chiasmata with respect to their size [740,741]. Darlington and Dark thus proposed that this phenomenon might be an adaptation to secure the formation of at least one chiasma in all bivalents and Mather added that the first chiasma would be formed irrespectively of the length of the chromosome while the formation of the second and subsequent chiasmata would occur at a mean distance from the previous one dependent on interference and constant throughout the chromosomes. Crossover assurance has later been observed in multiple organisms and although the molecular basis remains uncertain, a series of mechanisms have been proposed to contribute to it as an extra layer to ensure the formation of this obligatory crossover on top of the general mechanisms that promote interhomologue crossover formation, many of them addressed earlier in this text.

Mapping of DSBs in budding yeast and mouse have revealed that short chromosomes often have a greater DSB density in these organisms [373,389]. As DSBs are crossover precursors, a higher DSB density in smaller chromosomes might be a compensatory mechanism to ensure the formation of the obligatory crossover. This enrichment is especially evident in the pseudoautosomal region of mouse sex chromosomes in which about two orders of magnitude higher SPO11-oligo density than the genome average was detected. Moreover an inverse correlation between chromosome size and DSB density can be observed genome wide [389]. The study of mechanisms that might promote this differential enrichment in budding yeast have described a targeted boost of DSB formation towards small chromosomes mediated by the preferential binding of the axis components Hop1 and Red1 as well as DSB proteins such as Rec114 and Mer2. It is not certain how this boost is achieved, but the observation that when segments of those small chromosomes are translocated into larger chromosomes they maintain the boost suggests that there are inherent genetic features of budding yeast small chromosomes that promotes the enrichment of DSBs. In addition, small chromosomes seem to retain DSB proteins longer during prophase I, which might also

promote the formation of higher numbers of DSBs in them [353,742]. In *C. elegans*, with only one crossover per chromosome, defects in DSB or crossover formation appear to extend the DSB permissive window as observed by the persistence of DSB-1 and DSB-2, markers for this window, in a feedback loop mediated by CHK-2 [350,743,744].

Additional downstream mechanisms in the meiotic recombination process that ensure the formation of the obligatory crossovers can be inferred from the presence of univalents in mutants in which DSB formation is not impaired and that maintain a considerable number of crossovers. In Arabidopsis, mutants of the kinesin *PSS1* have no overall decrease in crossovers, but univalents can be frequently observed [745]. A similar phenotype has been observed in mutants of the SC transverse filament *ZYP1* or "anti-recombinases" such as *TOP3α*, *FIGL1* or *FLIP* in which, despite a genome wide increase in crossovers, a proportion of meiotic cells show a pair of univalents at metaphase I, revealing that crossover assurance is impaired in these mutants. The underlying cause is not however known [240,280,281,284]. In mouse, the increased crossover density observed in smaller autosomes and the PAR region cannot be numerically explained only by the aforementioned relation of chromosome size and DSB density, pointing as well to mechanisms downstream DSB formation to promote crossover formation differentially in small chromosomes with respect to larger ones. When crossovers are normalized with SPO11-oligo density per chromosome, a negative correlation is still observed between normalized crossover density and chromosome size with the smaller chromosome (chr19) and the PAR region of the sex chromosomes still standing out for their "disproportionate" crossover density [389].

Crossover interference

The building of the first genetic map in Drosophila in 1913 after previous genetic observations of crossing over between sex-linked factors, which set the idea of a physical linear arrangement of these factors in the chromosomes, together with the enunciation of the chiasmatype theory some years before bolstered the chromosome view of inheritance [570,726,746,747]. Based on his data and previous observations, Sturtevant remarked that the occurrence of one crossover in an interval delimited by two of the linked factors makes a second crossover less likely to occur in an adjacent interval [726]. Later, he and Muller confirmed that this phenomenon was restricted to factors that were linked in the same chromosome, as it was not observed when positioned in two different chromosomes, and named it interference [748,749]. Interference was discovered to negatively correlate with genetic distance after observed double crossovers were found to approximate to the expected values if randomly positioned as the intervals studied

were longer [748,750]. Muller also proposed a measure for interference expressed as the ratio of observed double crossovers in adjacent intervals (coincidence) divided by the expected double crossovers, later referred to as the coefficient of coincidence (CoC) and used to express interference as I = 1 - CoC [751,752]. Hence I equals 1 when there is no interference (observed and expected double crossovers match) and 0 when there is complete interference with intermediate values expressing different degrees of this phenomenon. Values over 1 would express negative interference, situation in which a crossover would actually increase the likelihood of a second crossover in an adjacent interval. From those years on crossover interference has been described in numerous organisms across the Eukarya domain.

Different mechanistic models have been proposed to describe the interference phenomenon since its discovery, all of them concurring in that the crossover designation and interference processes operate on an array of "precursor" interactions that correspond to DSB-mediated interhomologue interactions [632,753]. Some of them, such as the polymerization model and the beam-film model, imply that every crossover designation event would trigger an interference signal that propagates along the chromosomes inhibiting crossover formation and whose intensity decreases with distance from the designated crossover site [632,753]. In the polymerization model, the propagation of interference is modelled as a polymerization reaction of a (yet to discover) polymer that would eject recombination intermediates in nearby regions [754]. In the beam-film model, interference is modelled as a beam-film system subjected to tensile stress in which flaws in the film (crossover precursors) could trigger the crack of the film at that position (crossover designation) generating a local relief and a redistribution of the tensile stress that propagates from that site on (interference signal) [755]. On the other hand, the telomere-initiated model advocates for an interference signal that would propagate from the telomeres towards the middle of the chromosomes by "counting" a (nearly) fixed number of precursors before designating a second event, which fits with an observed pattern of crossover distribution with a reduction of crossover in the centre of chromosomes relative to their peripheries irrespectively of centromere position conserved in multiple species [632,753,756,757]. In any of these cases, the interference signal is thought to diffuse along the physical length of the chromosomes (measured as chromosome axis length) rather than the genomic distance (measured as DNA bases) by molecular mechanisms that remain a mystery [632,753,758]. It is also yet unknown why from the two classes of crossovers conserved among most eukaryote organisms, only class I crossovers are subject to interference.

Centromeres and telomeres

In many organisms crossovers are not evenly distributed along the chromosomes but there are large chromosomal domains in which they are differentially enriched, depleted or even suppressed, with important inter-specific differences. Crossover suppression in the centromeres and centromere-proximal segments however is a feature conserved among many eukaryotes [752]. Centromeres are a region of the chromosomes defined in eukaryotes by the presence of the histone variant CENPA/CENH3 that directs the assembly of the kinetochore to which the spindle microtubules are attached to permit chromosome alignment and segregation in cell division [759]. Meiotic crossovers in centromeres have been associated with segregation errors and thus with fertility defects. Although the cause is not completely certain, two principal models have been proposed: I) centromere-proximal crossovers may disrupt sister chromatid cohesion causing premature separation of sister chromatids; or II) as proximal cohesion is not released at anaphase I to permit the co-segregation of both sister chromatids of each chromosome, crossovers in those regions would cause entanglements or/and fragmentation, resulting in segregation errors [752]. Despite the conserved identity (CENPA/CENH3 presence) and function, eukaryotic centromeres are physically very variable, ranging from point centromeres of less than 150bp to megabase-long arrays of tandem repeats [759]. This highly repetitive nature of the centromeres have difficulted for years the determination of their sequence and their epigenetic landscape, limiting the mapping of recombination and meiotic recombination proteins as well as the characterization of potential genetic and epigenetic features that play a role in this suppression.

Centromeric and pericentromeric regions typically consists on compact heterochromatin, which might restrict the access of the recombination machinery to the DNA. In Arabidopsis, disruption of CG and non-CG/H3K9me2 methylation has been associated with an increase in DSBs in pericentromeric regions [361,760]. However, while loss of CG-methylation does not increase crossover frequency in these regions despite the increase in DSBs (and in some reports it actually reduces it), loss of non-CG/H4K9me2 does so [760–765]. These observations suggest that multiple heterochromatin-associated epigenetic modifications might act as different layers of regulation that suppress crossovers close to the centromeres. Recent mapping of Arabidopsis centromeres have confirmed the suppression of crossovers not only in previously known centromere-adjacent regions but in the actual centromeres, revealing as well that DSB formation is also suppressed and thereby meiotic recombination in general from the initiation step [11]. In multiple crop species such as wheat, barley, tomato or maize,

pericentromeric heterochromatic is extended up to more than half of the chromosome in some cases and with it the suppression of crossovers and the linkage drag of genes situated in those regions [766–769]. Mapping of DMC1 DNA binding in wheat have shown that although enriched in crossover-rich distal portions, peaks of DMC1 are detected all along the chromosomes. Thus meiotic recombination is not completely suppressed in these long pericentromeric heterochromatin regions, as it happens in centromeres, but mechanisms downstream initiation might suppress the formation of crossovers [770]. Similar centromeric and centromere-proximal suppression linked to heterochromatin has been detected in other species such as Drosophila. Nevertheless the observation that adjacent euchromatin regions also have low crossover frequency that steeply increases with distance from the centromere together with the discovery that in some mutants the heterochromatin-mediated suppression is maintained but this distance effect is lost and that the insertion of a 2Mb block of heterochromatin far from the centromere does not similarly affect adjacent regions have led to propose that centromere suppression might be multi-causal and not only linked to the nature of the chromatin in those regions [771].

Telomeres are also regions with a particular behaviour in meiosis but with a more variable effect in crossover density and distribution than centromeres in between species. Telomeres are tethered to the nuclear envelope during prophase I and through the nuclear envelope to the cell cytoskeleton. This connection mediates chromosomal movements and is thought to be an important part in many of the events happening during prophase I [273,772]. In several organisms, including Arabidopsis, telomeres cluster early in prophase I in a structure called the bouquet, that is hypothesized to mediate the initial steps of homologue recognition and pairing [272,273]. There are species such as *C. elegans* or Drosophila, in which the bouquet has not been detected and others, such as budding yeast, Sordaria or mouse, in which it appears when homologous chromosomes are almost already co-aligned [753]. Telomere flanking regions are typically euchromatic and show elevated crossover frequencies in many eukaryotes, including budding yeast, mouse or human [773–775]. This is also so for, notably, cereal species in which crossovers are suppressed over a large part of the chromosomes and accumulate mostly in distal regions with a clear gradient of reducing crossover frequency from the telomeres towards proximal segments [766–769]. Interestingly, a temporal-spatial bias that mirrors the distal bias in crossover distribution has been described in wheat for axis morphogenesis, synapsis and initiation of recombination and these regions are found to be enriched in the axis component ASY1 and in DMC1 [770,776]. Arabidopsis crossovers are more evenly distributed along the chromosomes but do show an enrichment in subtelomeric regions, particularly in some chromosome arms. In mutants with both

with lower (*asy1*) and higher (*recq4a/b figl1*) crossover frequency, the distal bias of crossover distribution becomes more pronounced, suggesting that these regions might maintain a higher recombinogenic potential [695,777].

3.7.3. Regulation at local level

DNA sequence determinants

The mapping of crossover sites in multiple species has permitted the analysis and comparison of the DNA sequence motifs of these sites. In mammals, the great majority of DSB hotspots correspond to PRDM9 sites and consequently crossover hotspots [364,778]. The PRDM9 zinc-finger motif is under strong positive selection and thus it is hypervariable in the species in which it has been studied [779,780]. More than 170 alleles of PRDM9 have been described in mouse and at least 69 in humans with important differences in their distribution in between human populations [781]. Human PRDM9 DNA binding site is not an unique sequence, but a degenerate 13-mer motif and the variability among the DNA binding zinc-finger motifs of PRDM9 is reflected in differential preferences for these sites [782].

Besides mammals, DSB and crossover hotspots are not defined by a particular motif, although local biases in base composition have been described for crossover sites. GC richness has been found to positively correlate with crossover frequency in multiple organisms such as budding yeast, birds and maize [783–785]. The reason behind this correlation is not certain, although it has been proposed that GC-rich regions might be more susceptible to local modifications of histones that promote the loading of the recombination machinery. Also, the repair of mismatches (inherently generated in the recombination process leading to crossover) is biased towards GC rather than AT, which might result in GC-enrichment within recombination hotspots with time [786–789]. On the other hand, Arabidopsis recombination frequency positively correlates genome wide with AT-richness whereas Poly(A/T) and CTT-repeat motifs are the most represented at crossover sites at local level [384,790,791]. This discrepancy is surprising, given that the local chromatin landscape of crossover sites is similar to organisms that show GC-enrichment (see next chapter) and that the sequence composition is known to affect some of this features (methylation level or nucleosome occupancy i.e.) but the underlying explanations are not certain.

The presence of sequence polymorphisms/mismatches is another factor that modulates the crossover landscape. Whereas in mitotic cells (in which recombination is performed preferentially with the sister chromatid), the occurrence of polymorphisms

is restricted to the accumulation of mutations in their lineage, meiotic cells have to deal as well with inherited polymorphisms between the two homologous chromosomes. Sequence polymorphisms may range in size from single base mismatches to large-scale structural variants which will directly (and presumably negatively) impact the extent of the effect on recombination generated by their presence at multiple levels of the process: from complete absence of an homologous template to minor modifications on the stability of recombination intermediates, in example. However opposite trends have been described when the effect of polymorphisms on recombination frequency has been looked at different scales and species which might reflect a complex relation between the two factors.

At the local level, recombination frequency is inversely correlated with DNA mismatch density, as seen in budding yeast mitotic and meiotic cells, which show that the presence of only one mismatch in intervals of hundreds of base pairs already has a significant detrimental effect on recombination frequency [792–794]. This effect is counteracted by the disruption of the mismatch repair system (Msh2 i.e.) and is principally attributed to heteroduplex rejection [793–795]. However from a certain threshold of sequence divergence (around 10% in some reports), the mismatch-associated decrease in recombination is seen irrespective of the presence of a functional mismatch repair machinery [793,794]. A similar negative correlation of mismatch density and recombination frequency that is partially rescued by the disruption of MSH2 has been described for Arabidopsis and in mouse mitotic cells [796,797]. In Arabidopsis, this negative correlation has also been detected in meiosis at crossover hotspots by comparing crossover rates at intervals with different mismatch density using hybrid strains [798]. Nevertheless absence of MSH2 does not generate an increase in recombination frequency at meiotic polymorphic hotspots (~1-3% mismatch density) in Arabidopsis, nor in mouse hybrid strains [798,799].

At a wider chromosomal scale, when analysing the effect of megabase-long intervals in Arabidopsis, juxtaposition of polymorphic heterozygous and non-polymorphic homozygous intervals resulted in an increase of crossovers in the heterozygous interval at the expense of flanking homozygous intervals, suggesting in this case a positive relation between polymorphism and crossover frequency. The total number of chiasmata remained unaltered and the effect appeared to be chromosome-independent, interference-dependent and was lost in absence of MSH2, confirming the role of the mismatch machinery [800,801].

At the genome-wide level, different reports have also described a positive relationship between meiotic recombination and interhomologue polymorphism.

Measurements of historical recombination via linkage disequilibrium show positive correlation with sequence diversity in multiple species, including Drosophila, human, maize and *Medicago truncatula* and both via linkage disequilibrium and directly mapping crossovers in Arabidopsis [800–806]. Surprisingly, while absence of Msh2 in budding yeast leads to increased crossovers and crossover landscape remodelling towards more sequence divergent regions, no change in crossover was observed in Arabidopsis and the remodelling had the opposite sense (towards less divergent regions). The authors proposed that this might reflect differences in genome architecture or regulation of meiotic recombination and that these might explain differences observed at hotspot level [801,807,808].

Local chromatin landscape and epigenetic factors

Crossover hotspots in eukaryotes, as a subset of the total DSBs, have similar chromatin and epigenetic characteristics at the local level and these correspond in broad terms to hallmarks of open chromatin (see chapter 3.3. "*Spatial regulation*"). Crossover sites in budding yeast, mammals and plants correspond to nucleosome-depleted regions, suggested to be more accessible to the recombination machinery [357,369,384,766,809]. Hence a reasonable assumption supported by reports is that recombination processes involves chromatin remodelers that are known to actively slide and modify nucleosomes to further expose DNA [810,811]. Crossover sites are also associated with local enrichment of H3K4me3, known to mediate the localization of DSBs either by "de novo" PRDM9 deposition (human, mouse) or by recognition of regions with previous enrichment in H3K4me3 (budding yeast) [367,775]. Interestingly in Arabidopsis and maize H3K4me3 local enrichment have been described for crossovers but not for DSBs suggesting that it might have a role in downstream events, rather than in DSB formation [361,384,766,785]. Arabidopsis crossover hotspots at transcription start sites also show enrichment of the histone variant H2A.Z [384]. Mutants of the SWR1 nucleosome remodelling complex, required for H2A.Z deposition, show a slight reduction of crossovers as well as of early recombination markers (RAD51 and DMC1) [384,812]. H2A.Z has been associated with DSB formation in fission yeast and with meiotic telomere-driven chromosomal movements in budding yeast, its absence resulting in both cases in a reduction of spore formation and spore viability [813–815].

In Arabidopsis, a negative impact of DNA methylation on crossover formation has been described both locally at crossover sites and genome wide [760,765,801]. Targeted RNA-directed DNA methylation of euchromatic crossover hotspots is able to significantly reduce crossover rate and it is associated not only with the expected

increase in DNA methylation but with an increase in nucleosome density and H3K9me2, supporting the importance of local chromatin accessibility for meiotic recombination and the associations between different chromatin modifications to regulate it [765]. At higher scales, DNA methylation negatively correlates with crossover rate when the genome is divided into percentiles according to DNA methylation levels but this relationship is complex and differs depending on type of methylation and probably on chromosomal domain (see section 3.7.2. "*Centromeres and telomeres*") .

CHAPTER II. RAD54 is essential for RAD51-mediated repair of meiotic DSB in Arabidopsis

Initial hypothesis

Previous biochemical, molecular and cytological data in Arabidopsis, yeast and mouse suggests that DMC1 is responsible of catalysing the strand exchange reaction of the presynaptic filaments with RAD51 playing an essential supporting role in the repair of most, if not all, meiotic double-strand breaks. In the absence of DMC1, RAD51 proficiently repairs the meiotic double-strand breaks, however it does so without producing interhomologue crossovers.

Notwithstanding its key role in RAD51-dependent recombination in somatic cells, the fertility of *rad54* mutant plants has been interpreted to show that RAD54 does not function in meiosis. We hypothesised that this apparent lack of meiotic role of RAD54 could simply be a consequence of RAD51's non-catalytic role in supporting DMC1 function in meiosis. If this is so and given that RAD51 does catalyse meiotic recombination in the absence of DMC1, RAD54 should be required to repair SPO11-induced DSB in *dmc1* mutant meiosis. We also applied this argument to the RAD51 paralogues RAD51B, RAD51D and XRCC2, key cofactors of RAD51 nucleofilament formation and/or activity in somatic cells but not required in meiosis.

Objectives

I) To confirm the activity of RAD54 as a cofactor in RAD51-catalysed somatic homologous recombination and the deficit in this activity in the plants carrying the mutant alleles analysed.

II) To characterise the progression of meiotic division, the repair of meiotic DSBs and the formation of interhomologue crossovers in absence of RAD54 and in absence of both DMC1 and RAD54.

III) To analyse RAD51 filament formation in absence of RAD54 and in absence of both DMC1 and RAD54

IV) To characterise the progression of the meiotic division, the repair of meiotic DSBs and the formation of interhomologue crossovers in *rad51b*, *rad51d* and *xrcc2* mutants combined with the absence of DMC1.

Methods, results and discussion

PLOS GENETICS

RESEARCH ARTICLE

RAD54 is essential for RAD51-mediated repair of meiotic DSB in Arabidopsis

Miguel Hernandez Sanchez-Rebato, Alida M. Bouatta, Maria E. Gallego, Charles I. White*, Olivier Da Ines*

Institut Génétique Reproduction et Développement (iGReD), Université Clermont Auvergne, UMR 6293 CNRS, U1103 INSERM, Clermont-Ferrand, France

* charles.white@uca.fr (CIW); Olivier.da_ines@uca.fr (ODI)

Citation: Hernandez Sanchez-Rebato M, Bouatta AM, Gallego ME, White CI, Da Ines O (2021) RAD54 is essential for RAD51-mediated repair of meiotic DSB in Arabidopsis. PLoS Genet 17(5): e1008919. https://doi.org/10.1371/journal.pgen.1008919

Editor: Mathilde Grelon, INRA, FRANCE

Received: June 4, 2020

Accepted: May 3, 2021

Published: May 18, 2021

Data Availability Statement: All relevant data are within the manuscript and its Supporting Information files.

Funding: This work was supported by the CNRS, INSERM, Université Clermont Auvergne, a grant from the French government through the IDEX-ISITE-CAP20-25 initiative (16-IDEX-0001-CAP20-25 to O.D.I) and the European Union (H2020-MSCA-ITN-2017:765212-MEICOM to C.I.W). The doctoral fellowship of MH is financed by the European H2020-MSCA-ITN-2017:765212-

Abstract

An essential component of the homologous recombination machinery in eukaryotes, the RAD54 protein is a member of the SWI2/SNF2 family of helicases with dsDNA-dependent ATPase, DNA translocase, DNA supercoiling and chromatin remodelling activities. It is a motor protein that translocates along dsDNA and performs multiple functions in homologous recombination. In particular, RAD54 is an essential cofactor for regulating RAD51 activity. It stabilizes the RAD51 nucleofilament, remodels nucleosomes, and stimulates the homology search and strand invasion activities of RAD51. Accordingly, deletion of RAD54 has dramatic consequences on DNA damage repair in mitotic cells. In contrast, its role in meiotic recombination is less clear. RAD54 is essential for meiotic recombination in Drosophila and *C. elegans*, but plays minor roles in yeast and mammals. We present here characterization of the roles of RAD54 in meiotic recombination in the model plant *Arabidopsis thaliana*. Absence of RAD54 has no detectable effect on meiotic recombination in otherwise wild-type plants but RAD54 becomes essential for meiotic DSB repair in absence of DMC1. In Arabidopsis, *dmc1* mutants have an achiasmate meiosis, in which RAD51 repairs meiotic DSBs. Lack of RAD54 leads to meiotic chromosomal fragmentation in absence of DMC1. The action of RAD54 in meiotic RAD51 activity is thus mainly downstream of the role of RAD51 in supporting the activity of DMC1. Equivalent analyses show no effect on meiosis of combining *dmc1* with the mutants of the RAD51-mediators RAD51B, RAD51D and XRCC2. RAD54 is thus required for repair of meiotic DSBs by RAD51 and the absence of meiotic phenotype in *rad54* plants is a consequence of RAD51 playing a RAD54-independent supporting role to DMC1 in meiotic recombination.

Author summary

Homologous recombination is a universal pathway which repairs broken DNA molecules through the use of homologous DNA templates. It is both essential for maintenance of genome stability and for the generation of genetic diversity through sexual reproduction. A central step of the homologous recombination process is the search for and invasion of a homologous, intact DNA sequence that will be used as template. This key step is

MEICOM contract. The funders had no role in study design, data collection and analysis, decision to publish, or preparation of the manuscript.

Competing interests: The authors have declared that no competing interests exist.

catalysed by the RAD51 recombinase in somatic cells and RAD51 and DMC1 in meiotic cells, assisted by a number of associated factors. Among these, the chromatin-remodelling protein RAD54 is a required cofactor for RAD51 in mitotic cells. Understanding of its role during meiotic recombination however remains elusive. We show here that RAD54 is required for repair of meiotic double strand breaks by RAD51 in the plant *Arabidopsis thaliana*, and this function is downstream of the meiotic role of RAD51 in supporting the activity of DMC1. These results provide new insights into the regulation of the central step of homologous recombination in plants and very probably also other multicellular eukaryotes.

Introduction

Homologous recombination (HR) is an universally conserved DNA repair mechanism essential for maintaining genomic integrity and ensuring genetic diversity [1,2]. In somatic cells, HR is used to repair DNA breaks caused by environmental and endogenous factors and is critical in the recovery of stalled and collapsed replication forks. In meiotic cells of the majority of studied eukaryotes, HR is essential for accurate chromosome segregation during the first meiotic division, also generating genetic diversity among meiotic products [3,4].

Homologous recombination is a DNA repair pathway that involves the use of a homologous template for restoration of the original sequence. It is initiated by DNA double-strand breaks (DSBs) and subsequent resection of the 5'-ended strands of the DSB, generating long 3' single-stranded DNA (ssDNA) overhangs [5]. The ssDNA overhangs are further coated by replication protein A (RPA), protecting them from nucleases and removing secondary structures [6,7]. In a subsequent step, RPA is displaced by the recombinase RAD51 in somatic cells, or RAD51 and DMC1 in meiotic cells, forming a right-handed helical nucleofilament on the exposed single-stranded DNA (ssDNA) flanking the DSB [8,9]. This helical nucleofilament performs the homology search and catalyses the invasion of a homologous DNA template sequence by the 3′-ended DNA strands, which are then extended through DNA synthesis. The resulting joint recombination intermediate can be processed through several different pathways eventually leading to separation of the recombining DNA molecules and restoration of chromosome integrity [1,2].

The nucleoprotein filament is the active protein machinery for DNA homology search and strand exchange during HR. In somatic cells, the nucleoprotein filament is formed by the RAD51 recombinase. The *in vivo* assembly and disassembly of the RAD51 nucleoprotein filament is a highly dynamic process, regulated via the coordinated actions of various positive and negative factors, and notably, the RAD51 mediators [10,11]. These proteins, involved in the regulation of the formation, stability and activity of the RAD51 nucleofilament, include the RAD51 paralogues and the SHU complex that are known to be essential RAD51 positive regulators (for reviews see [10–13]. The RAD51 paralogues are important for homologous recombination and DNA repair in somatic cells [11,14]. In contrast, clear understanding of their roles during meiosis remains elusive. Budding yeast has two RAD51 paralogues, Rad55 and Rad57, which form a heterodimer, and are essential for meiotic recombination [15–17] and 4 Shu proteins (Psy3, Csm2, Shu1 and Shu3) forming the Shu/PCSS complex that is also required for Rad51 filament assembly and meiotic recombination [18]. Vertebrates, like *Arabidopsis thaliana*, have five RAD51 paralogues (in addition to DMC1): RAD51B, RAD51C, RAD51D, XRCC2 and XRCC3 which form different complexes [10–13]. Vertebrate mutants for any of the RAD51 paralogues are embryonic lethal and this has hampered the study of

their meiotic phenotypes. Nevertheless, a number of studies have demonstrated that RAD51C and XRCC3 are essential for meiotic recombination both in vertebrates and plants [19–29]. In contrast, the possible meiotic roles of RAD51B, RAD51D and XRCC2 are less clearly understood. These three genes are highly expressed in meiotic tissues in animals [30–32] and plants [33–35]. In humans, mutation in XRCC2 has been linked to meiotic arrest, azoospermia and infertility [36] and absence of RAD51B or RAD51D lead to meiotic defects in the moss *Physcomitrella patens* and rice, respectively [37–39]. The Arabidopsis *xrcc2* mutant and, to a lesser extent *rad51b*, have been associated with increased meiotic recombination rates, but all three mutants are fully fertile and present no detectable meiotic defects [26,40–42]. Vertebrate genomes also encode two Shu-related proteins, SWS1-SWSAP1, which form a complex dispensable for mouse viability but essential for meiotic progression [43]. To date, Shu proteins have not been identified in plants.

RAD51 nucleofilament activity is further supported by the highly conserved RAD54 protein, which belongs to the SWI2/SNF2 DNA helicase family. It is a dsDNA-dependent ATPase that uses energy from ATP hydrolysis to translocate along dsDNA. It is thus a motor protein and performs multiple functions in homologous recombination. In particular, RAD54 is an essential cofactor stimulating RAD51 activity. It has been shown to stabilize the RAD51 nucleofilament, remodel nucleosomes, stimulate homology search and strand invasion activity of RAD51, dissociate bound RAD51 after completion of strand exchange and even to catalyse branch migration [44–46]. Accordingly, deletion of RAD54 has dramatic consequences on DNA damage repair in mitotic cells (For reviews see [44–46]).

The role of RAD54 in meiotic recombination is less clear. In Drosophila and C. *elegans*, which exclusively rely on RAD51 (not DMC1), RAD54 is essential for meiotic recombination [47–49]. Yet, in most eukaryotes, meiotic HR is mediated by RAD51 and the meiosis-specific DMC1 [8,50]. Interestingly however, while RAD51 is essential for homology search and strand invasion in mitotic cells, it only plays an accessory role for DMC1 in meiosis [51,52]. Thus, DMC1 is the active meiotic recombinase but requires the support of RAD51 to function [51,52]. Accordingly, data from budding yeast have demonstrated that Rad51 activity is down-regulated during meiosis to favour Dmc1 catalysing DNA strand-exchange using the homologous chromosome as a template [51,53–56].

In yeast, down-regulation of Rad51 activity is mediated by the coordinated phosphorylation of Hed1 and the Rad51-cofactor Rad54 by the meiosis-specific kinase Mek1 [53–59]. Hed1 is a meiosis-specific protein that binds to Rad51, impeding access of Rad54 and thereby restricting activity of Rad51 nucleofilaments in meiosis [54,57,58,60]. Phosphorylation of Rad54 by Mek1 also reduces its affinity for Rad51 [53,61]. Thus, both pathways downregulate Rad51 through inhibition of Rad51-Rad54 complex formation and this in turns favour Dmc1-dependent inter-homologue recombination. In accordance with this down-regulation, Rad54 is also not essential for Dmc1 activity and plays a relatively minor role in meiotic recombination in budding yeast [62–68]. This is however due to the presence of a second, Dmc1-specific Rad54 homologue, Rdh54/Tid1 [64,66–68]. Biochemical and genetic experiments have demonstrated that Rdh54 preferentially acts with Dmc1 to promote inter-homologue recombination whereas Rad54 preferentially stimulates Rad51-mediated strand invasion for sister chromatid repair of excess DSBs [62,63,66,69,70].

In mouse, two RAD54 homologues, RAD54 and RAD54B, have been identified. Both are required for somatic recombination but neither is essential for meiotic recombination as single and double mutant mice are fertile, although RAD54 may be needed for normal distribution of RAD51 on meiotic chromosomes [71,72]. To date in plants, only one RAD54 orthologue has been characterized (Arabidopsis locus AT3G19210). As in yeast and mammals, Arabidopsis RAD54 is essential for RAD51-mediated recombination in somatic cells. Absence of

RAD54 leads to DNA damage hypersensitivity, strong reduction in homologous recombination efficiency and defects in pairing of homologous loci following DSB formation [73–78]. However, beyond the fact that Arabidopsis *rad54* plants are fertile, a role for RAD54 in Arabidopsis meiotic recombination has not been assessed. Given its essential role in RAD51-nucleofilament activity and its expression in meiocytes [34,35] we hypothesized that RAD54 may also play an important role in meiotic recombination in plants.

Here, we present a detailed analysis of RAD54 function in meiotic recombination in Arabidopsis. Our data show that absence of RAD54 has no detectable effect on meiotic recombination in otherwise wild-type plants, but that RAD54 becomes essential for meiotic DSB repair in absence of DMC1. In Arabidopsis *dmc1* mutants, RAD51 repairs meiotic DSBs but does not produce chiasmata and absence of RAD54 in *dmc1* mutants leads to massive chromosome fragmentation (a "*rad51*-like" phenotype). RAD51 immunolocalization confirms that meiotic RAD51 nucleofilaments are formed (but non-productive) in *dmc1 rad54* double mutants. Strikingly, similar analyses show no effect on meiosis of combining *dmc1* with the mutants of the RAD51-mediators RAD51B, RAD51D and XRCC2.

Our data demonstrate that RAD54 is required for RAD51-dependent repair of meiotic DSBs in Arabidopsis in the absence of DMC1. We propose that the absence of a detectable meiotic phenotype in *rad54* plants is a consequence of RAD51's RAD54-independent, non-catalytic supporting role to DMC1 in meiotic recombination. We cannot exclude the possibility that RAD51-RAD54-dependent recombination plays a minor role in WT meiosis (for instance as a back-up of DMC1), but note that should this be the case, it does so without producing detectable modification of meiotic progression or outcomes. Our findings have several interesting implications for the regulation of the strand invasion step during meiotic recombination in Arabidopsis, which are further discussed.

Results

RAD54 is essential for somatic DNA repair

RAD54 is instrumental for homologous recombination in both mitotic and meiotic cells in many organisms (see above). In plants, previous analyses have also demonstrated a role of RAD54 in RAD51-mediated DSB repair in somatic cells, while the observation that *rad54-1* Arabidopsis mutant plants are fertile showed that the RAD54 protein does not play an essential role in Arabidopsis meiosis [73–78]. However, the existence of more subtle evidence for meiotic roles of RAD54 has not yet been assessed in plants. In addition to using the previously characterised *rad54-1* allele, we have characterised a second RAD54 T-DNA insertion allele (SALK_124992), which we have named *rad54-2* (Fig 1A). The exact genomic structure of the T-DNA insertion in the *rad54-2* allele was verified by PCR and sequencing (Fig 1A) and homozygous mutant lines were analysed by RT-PCR to confirm the absence of the respective transcripts (Fig 1B). In *rad54-2*, the T-DNA is inserted in exon 4 of the *RAD54* gene. This insertion is flanked by T-DNA LB sequences in opposite orientations and is associated with a deletion of 11 bp of the *RAD54* exon 4 sequence (Fig 1A). No transcript was detected with primers spanning the T-DNA insertion site, confirming the absence of full-length transcript (Fig 1B), although as commonly observed in the insertions, a transcript could be detected in *rad54-2* upstream and downstream of the T-DNA insertion. Sequence analysis showed that an in-frame stop codon is present in the upstream T-DNA left border, 24 bp after the chromosome-T-DNA junction (Figs 1A and S1). Thus, a protein of the first 285 amino acids (out of 910) of RAD54 fused to 8 amino acids translated from the first 24 nt of the T-DNA LB could potentially be expressed from the *rad54-2* allele. If present, this protein would lack all of the described essential domains for RAD54 activity (S1 Fig).

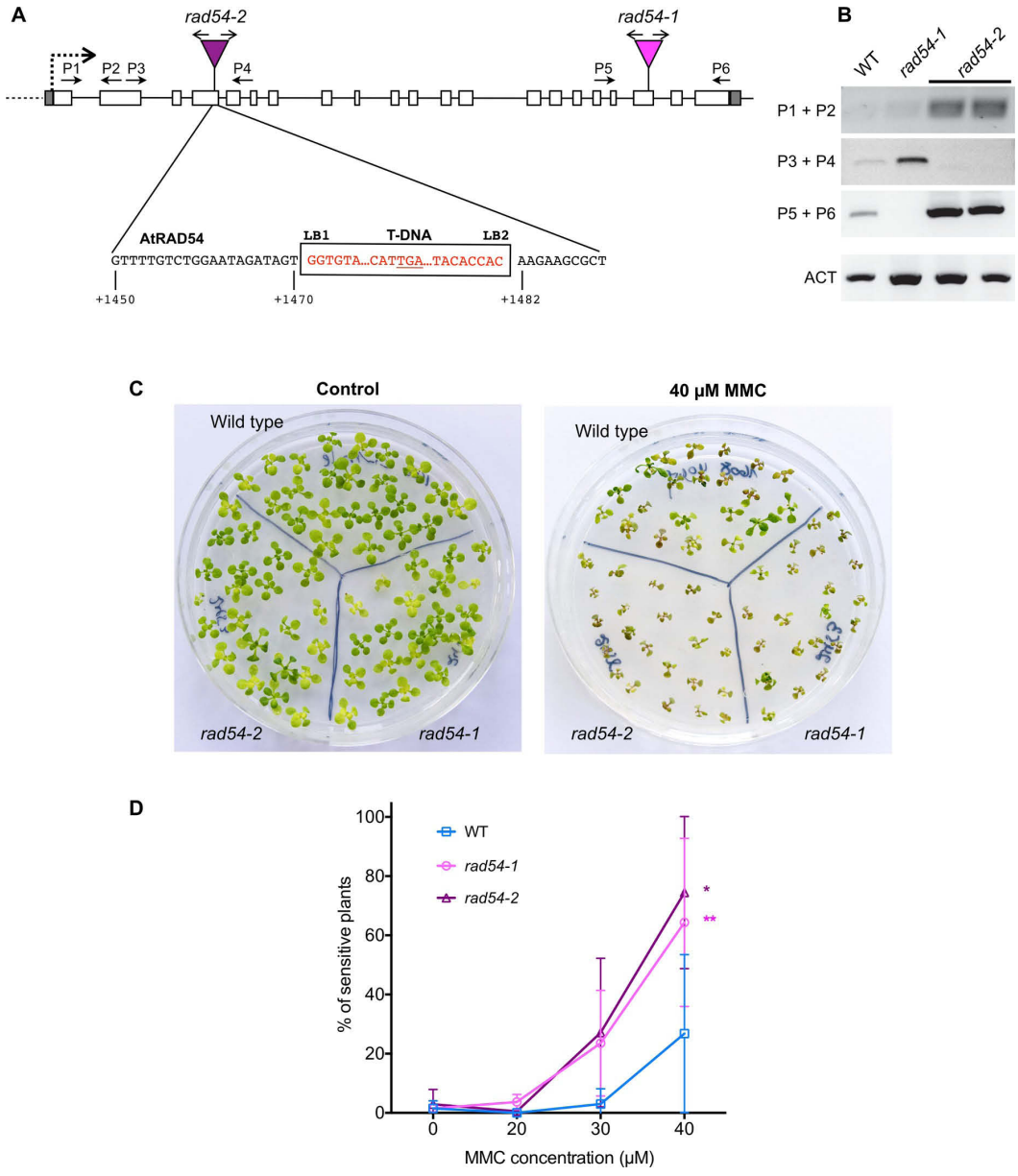

Fig 1. Characterisation of *rad54-2* T-DNA insertion mutant and sensitivity to MMC. (A) Structure of *AtRAD54* (At3g19210) and the *rad54-1* and *rad54-2* T-DNA insertion mutant alleles. Boxes show exons (unfilled) and 5' and 3'UTRs (grey fill). The positions of the T-DNA insertions in the two alleles (inverted triangles) is indicated, with arrows above showing orientation of the left borders, and the sequences of the *rad54-2* T-DNA/chromosome junctions below. The *rad54-2* T-DNA insertion is flanked by two left borders (LB1, LB2) and accompanied by a 11 bp deletion in exon 4. An in-frame TGA STOP codon in *rad54-2* is underlined. Numbering under the sequences is relative to the *RAD54* start codon. (B) RT-PCR analyses of transcripts of *rad54-1* and *rad54-2*. Amplification of the actin transcript (ACT) was used as a control for RT-PCR. Positions and orientations of the PCR primers are shown on the diagrams. (C-D) Sensitivity of *rad54-1* and *rad54-2* plants to MMC. (C) Two-week-old seedlings grown without, or with 40 µM MMC are shown. (D) Sensitivity of the seedlings was scored after 2 weeks (see Materials and Methods) and the percentages of sensitive plants (plants with 3 true leaves or less) are shown. Symbols are mean ± SD of at least 3 independent experiments with ≥ 25 seedlings per genotype per experiment. (*$p<0.05$ and **$p<0.005$; paired two-tailed t-test).

https://doi.org/10.1371/journal.pgen.1008919.g001

The *rad54-1* and *rad54-2* plants were used to confirm the role of RAD54 in DSB repair and homologous recombination in somatic cells by testing the sensitivity of the mutants to the DNA damaging agent Mitomycin C (MMC; Figs 1C and 1D and S2). MMC is known to form DNA interstrand cross-link adducts, which produce DNA strand breaks *in vivo*. The importance of homologous recombination in the repair of DNA cross-links has led to the use of MMC hypersensitivity as a test for HR capacity in a number of organisms. In Arabidopsis, this is seen in the MMC hypersensitivity of many homologous recombination-deficient mutants [26,28,52,76,79]. As previously shown, *rad54-1* plants display clear hypersensitivity to MMC [76] (Figs 1C and 1D and S2). MMC hypersensitivity is also seen in *rad54-2* plants, particularly visible at 40 μM MMC (p-value > 0.05, paired two-tailed t-tests; Figs 1C and 1D and S2) and confirming the importance of RAD54 in homologous recombination in somatic cells.

Absence of RAD54 does not affect meiotic progression

Meiotic defects are usually reflected in reduced fertility and thus in a reduction in seed number in Arabidopsis [80]. We thus monitored number of seeds per silique in our two *rad54* mutant lines and found, as expected, no fertility defects in either *rad54-1* or *rad54-2* (S3 Fig and S1 Data). The mean seed number per silique was 56 seeds per silique for both *rad54-1* (n = 40 siliques) and *rad54-2* (n = 80), while wild-type siliques contained on average 58 seeds per silique (n = 40 for RAD54-1 and n = 60 for RAD54-2) (S3 Fig and S1 Data). These small differences are not statistically significant ($p > 0.05$; unpaired, two-tailed Mann-Whitney test). In agreement with previous results [76], this confirms that RAD54 is not instrumental for meiosis in plants, notwithstanding its importance in somatic recombination. This conclusion was further supported through cytogenetic analyses of 4',6-diamidino-2-phenylindole (DAPI) stained chromosomes through male meiosis. Wild-type Arabidopsis meiosis has been well described and the major stages are shown in Fig 2. During prophase I, meiotic chromosomes condense, pair, recombine and undergo synapsis. Full synapsis of homologues is seen at pachytene (Fig 2A). Chromosomes further condense and five bivalents (two homologous chromosomes attached by sister chromatid cohesion and chiasmata) are visible at metaphase I (Fig 2B). Each chromosome then separates from its homologue, leading to the formation of two groups of five chromosomes easily visualised at metaphase II (Fig 2C). Meiosis II proceeds and gives rise to 4 balanced haploid nuclei (Fig 2D). In *rad54* mutants, meiotic stages appear indistinguishable from the wild-type, resulting in the expected 4 haploid meiotic products (Fig 2E–2L). Thus, meiotic progression is not affected by absence of RAD54.

Absence of RAD54 does not affect crossover recombination rate and interference

We next sought to analyse more closely the impact of RAD54 on meiotic recombination by measuring meiotic CO rates in genetic intervals marked by transgenes encoding fluorescent marker proteins expressed in pollen (FTLs; [81,82]). Combined with mutation of the *QUARTET1* gene (*qrt*) which prevents separation of the four pollen grains [83], these FTL lines permit direct measurement of recombination between the linked fluorescent markers by scoring tetrad pollen fluorescence [81,82]. We determined CO rates in two adjacent intervals on chromosomes 1 (I1b and I1c) and 2 (I2f and I2g) in wild-type and *rad54-2* mutant plants. In wild-type plants, I1b (1.8 Mb) spans 10.3 cM and I1c (4.1 Mb) 22.2 cM (Fig 3 and S1 Table). No difference in recombination frequency was observed for either interval in *rad54-2* mutants with 9 cM and 22.7 cM for I1b and I1c, respectively (Fig 3 and S1 Table). Analyses of two additional intervals, I2f (0.7 Mb) and I2g (0.4 Mb), on chromosome 2 confirmed this result, with no

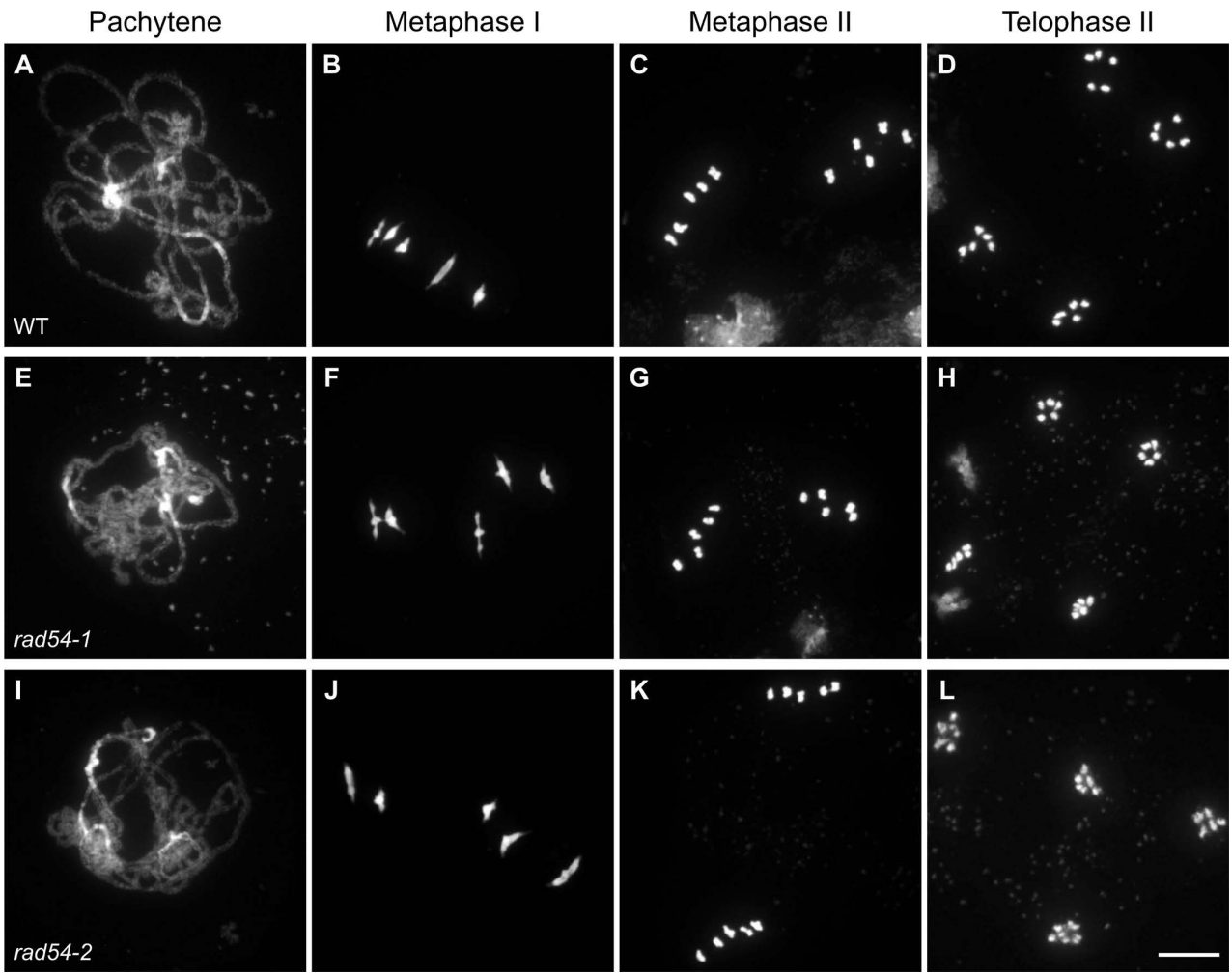

Fig 2. Both *rad54-1* and *rad54-2* mutants have WT meiosis. Chromosome spreads of male meiocytes in wild type (A-D), *rad54-1* (E-H) and *rad54-2* (I-L). Pachytene (A,E,I); Metaphase I (B,F,J); Metaphase II (C,G,K); Telophase II (D,H,L). Chromosomes were spread and stained with DAPI. (Scale bar = 10 μm).

https://doi.org/10.1371/journal.pgen.1008919.g002

significant difference in recombination frequency observed between the wild-type and *rad54-2* mutants (6.8 cM to 6.9 cM for I2f and 4.3 cM to 4.9 cM for I2g; Fig 3 and S1 Table). We obtained similar results for *rad54-1* mutant plants with 6.5 cM and 4.7 cM in I2f and I2g, respectively (S4 Fig and S1 Table). In accordance with these results, we found a similar interference ratio (IR) in wild-type plants and *rad54* mutants for both intervals (IR I1bc: 0.35 in wild-type and 0.36 in *rad54-2*; IR I2fg: 0.09 in wild-type, 0.1 in *rad54-1* and 0.1 in *rad54-2*; $p > 0.05$, z-test; S1 Table).

Thus, absence of RAD54 does not affect meiotic CO rates in at least 4 different intervals on 2 chromosomes. These results were further confirmed genome-wide through counting chiasmata in metaphase I of wild-type, *rad54-1* and *rad54-2* male meiocytes, which show means of 9.6 (SD = 1.3; n = 19), 9.6 (SD = 1.5; n = 25) and 9.1 (SD = 1; n = 19) chiasmata per meiosis, respectively ($p > 0.05$, unpaired two-tailed t-tests).

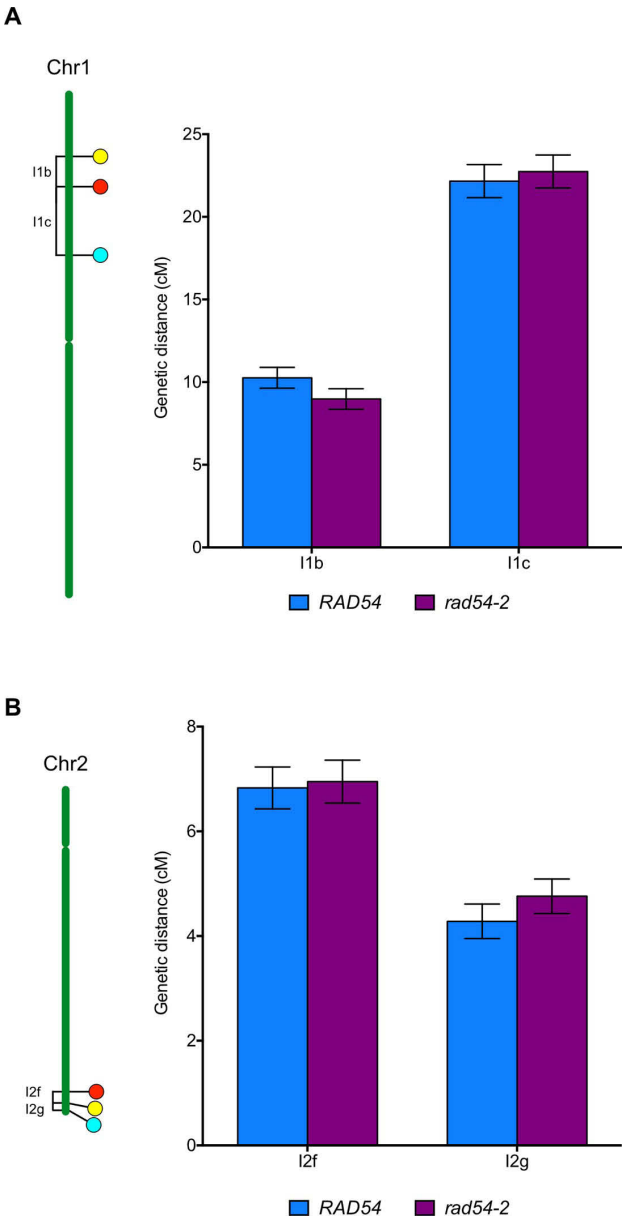

Fig 3. Crossing-over is not affected in *rad54-2* mutant meiosis. Genetic distances (in centiMorgans, cM) measured from fluorescent tetrad analyses in marked intervals on (A) chromosome 1 (I1b and I1c) and (B) chromosome 2 (I2f and I2g). Bars indicate mean ± SD. On all intervals, WT and *rad54* do not significantly differ ($p>0.05$; Z-test).

https://doi.org/10.1371/journal.pgen.1008919.g003

RAD54 is essential for RAD51-dependent repair of meiotic DSB in absence of DMC1

These data confirm that RAD54 is not required for meiotic recombination in Arabidopsis, an *a priori* surprising conclusion given the importance of RAD54 in homologous recombination

(see Introduction). Data from budding yeast have shown that RAD54 is not essential for meiotic recombination in presence of DMC1 and the DMC1-specific RAD54 homologue Rdh54 (Tid1) [53,63,66–68]. Instead, interaction of RAD54 with RAD51 is constrained during meiotic recombination in yeast and this represents a key point in the mechanisms leading to downregulation of RAD51 activity in meiosis [53,60]. The RAD51-RAD54 pathway however becomes essential for sister chromatid repair in absence of DMC1 [62,63]. We thus hypothesized that RAD54 may be essential for RAD51-mediated repair of meiotic DSB in Arabidopsis. To test this hypothesis, we analysed meiosis in the absence of DMC1. Meiosis in Arabidopsis *dmc1* mutants has been well described [84,85] and the major stages are summarized in Fig 4. Absence of DMC1 leads to asynapsis and lack of inter-homologue CO. However intact univalents are observed in metaphase I owing to DSB repair by RAD51, most probably using sister chromatid donors (Fig 4E–4H).

In striking contrast, analyses of *dmc1 rad54* double mutants show an absence of synapsis (Fig 4) and massive chromosome fragmentation (Fig 4I–4P), a meiotic phenotype analogous to that seen in *rad51* mutants (Fig 4Q–4T). Absence of synapsis in *dmc1 rad54* double mutants was confirmed by immunolocalization of the synaptonemal complex (SC) axial element protein ASY1 and the SC transverse filament protein ZYP1 (S5 Fig). Thus, in the absence of DMC1, RAD51-dependent meiotic HR repair indeed depends upon the presence of RAD54 (Fig 4I–4P). This effect is confirmed by the significant reduction of fertility caused by the absence of RAD54 in *dmc1* mutant plants (S6 Fig and S1 Data). Thus, beyond supporting DMC1, either RAD51 does not play an (or plays only a minor) active role in meiotic recombination in WT plants, or its role is able to be compensated for by DMC1 without producing detectable modification of meiotic progression or outcomes.

To confirm this RAD54 requirement of RAD51-dependent recombination in meiosis, we crossed the *rad54* mutants with the Arabidopsis *sds* mutants. SDS is a meiosis-specific cyclin-like protein that is instrumental for normal DMC1 focus formation/stabilization, meiotic DSB repair with the homologous chromosome and CO formation [86–90]. Mutant plants lacking SDS have thus a *dmc1-like* phenotype, with absence of detectable DMC1 foci and presence of intact univalents, pointing to RAD51 repairing meiotic DSBs in *sds* mutants (as is the case in *dmc1* meiosis). As expected, our analysis of *sds rad54* meiosis does show increased numbers of meiosis showing chromosome fragmentation (S7 Fig), however the effect is noticeably less pronounced than that seen in *dmc1 rad54* meiosis. The reduced penetrance of the *sds rad54* meiotic phenotype relative to that of *dmc1 rad54* points to a (residual?) capacity of DMC1 to catalyse DSB repair in *rad54 sds* mutants, or that the RAD54-dependency of RAD51 in meiosis is partially alleviated in absence of SDS.

Absence of RAD54 does not affect RAD51 focus formation during meiosis

RAD54 is an essential cofactor for regulating RAD51 activity and has been implicated in both early and late steps of the HR pathway (see Introduction). Our data show that RAD54 is required for repair of meiotic DSB by RAD51 in Arabidopsis. Furthermore, that RAD54 is not required in the presence of DMC1 suggests that the RAD54-dependent meiotic role of RAD51 intervenes downstream of that of the RAD51 nucleofilament in supporting DMC1 activity. This being so, it would follow that meiotic RAD51-nucleofilament formation would be RAD54-independent. We thus quantified meiotic RAD51 focus formation as a proxy for RAD51 nucleofilament formation in these plants. We performed co-immunolocalization of RAD51 and the axis protein, ASY1, in wild-type, *rad54*, *dmc1*, and *dmc1 rad54* meiocytes and counted the number of RAD51 foci throughout early prophase I (Fig 5). In wild-type meiocytes, we observed a mean of 91 ± 29 RAD51 foci (± SD, n = 35). Similar numbers of RAD51

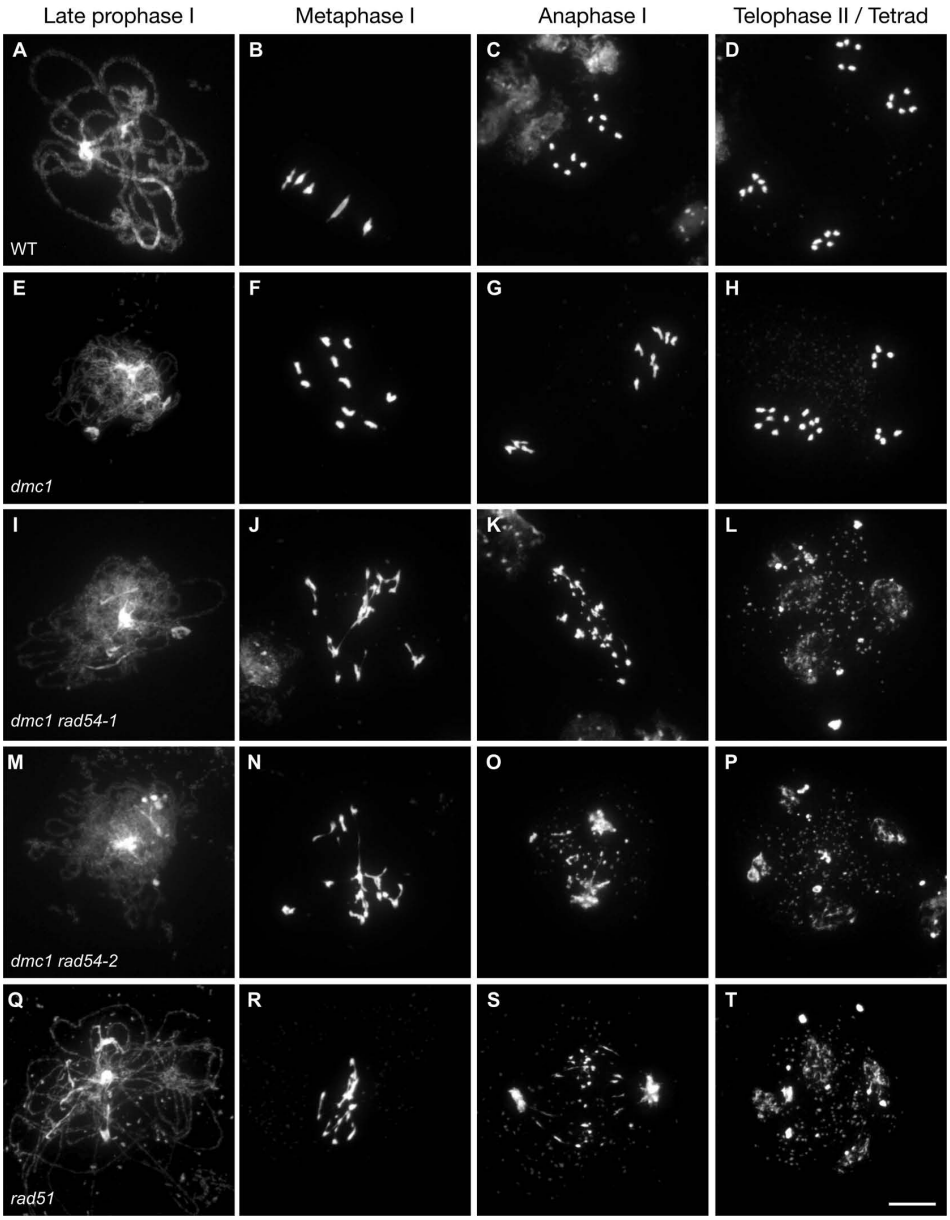

Fig 4. Absence of RAD54 leads to chromosome fragmentation in *dmc1* meiosis. Male meiosis is shown in (A-D) wild-type, (E-H) *dmc1*, (I-L) *dmc1 rad54-1*, (M-P) *dmc1 rad54*-2, and *rad51* (Q-T). Chromosome spreads at late prophase I (A,E, I,M,Q), Metaphase I (B,F,J,N,R), Anaphase I (C,G,K,O,S) and Telophase II/Tetrad (D,H,L,P,T). Chromosomes were spread and stained with DAPI. (Scale bar = 10 μm).

https://doi.org/10.1371/journal.pgen.1008919.g004

foci were observed in *rad54* (89 ± 18, n = 22) and *dmc1* (97 ± 26, n = 50) single mutant plants and importantly, the numbers of RAD51 foci were also unchanged in *dmc1 rad54* double mutants (94 ± 16, n = 56) (Fig 5).

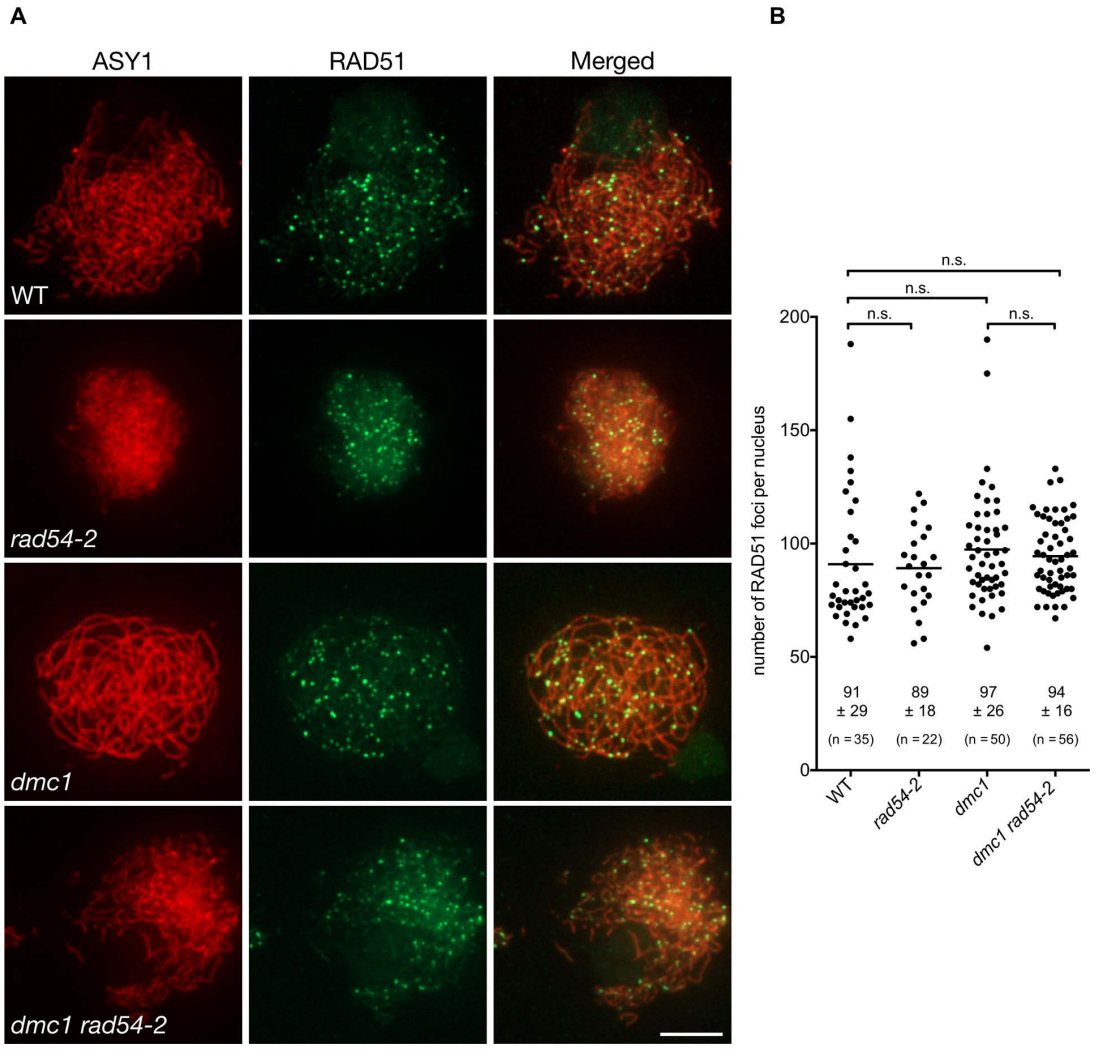

Fig 5. Absence of RAD54 does not affect numbers of meiotic RAD51 foci. (A) Co-immunolocalization of RAD51 (green) and the chromosome axis protein ASY1 (red) on leptotene/zygotene meiotic chromosome spreads. (Scale Bars: 5 μm). (B) Quantification of RAD51 foci per positive cell through early prophase I in wild-type, *rad54*, *dmc1*, and *dmc1 rad54-2* mutants. Means ± SD are indicated. n.s.: not significantly different (p-value > 0.05, Kruskal-Wallis test).

https://doi.org/10.1371/journal.pgen.1008919.g005

To test for a possible role for RAD51-mediated recombination late in prophase, we performed co-immunolocalization of ZYP1 and RAD51 in pachytene cells of *rad54* single mutants (S8 Fig). Similar numbers of RAD51 foci were observed in wild-type (16.8 ± 11, n = 60) and *rad54-2* mutant plants (13.1 ± 8, n = 40) (S8 Fig and S1 Data). Thus, absence of RAD54 does not detectably affect numbers of meiotic RAD51 foci in late prophase I. Given the role of RAD54 in disassembling RAD51-ssDNA nucleofilaments [74,75,91,92], it might have been expected to find more RAD51 foci in the *dmc1 rad54* meioses. However, with the absence of synapsis and significant chromosomal fragmentation that occurs in this mutant, it isn't possible to draw meaningful conclusions concerning RAD51 focus numbers beyond leptotene-early zygotene in these plants. Notwithstanding, this does not affect the conclusion that

apparently normal numbers of RAD51 nucleofilaments are formed in *dmc1 rad54* double mutants, but that these are not productive for recombination. Hence, these results fully concord with the conclusion (above) that RAD54 acts downstream of meiotic RAD51 nucleofilament formation. In accordance with RAD54's known role in supporting the activity of the mitotic RAD51 nucleofilament, this meiotic role is presumably in facilitating RAD51-dependent invasion of the donor DNA duplex [93].

RAD51-dependent repair of meiotic DSB does not require RAD51 paralogues RAD51B, RAD51D and XRCC2

RAD51 nucleofilament activity is also extensively regulated by the RAD51 paralogues (see Introduction). In Arabidopsis, RAD51C and XRCC3 are essential for meiotic recombination, with absence of either leading to massive chromosome fragmentation [24–26,28,29]. In contrast, the roles of RAD51B, RAD51D and XRCC2 in meiosis are less clear and their absence does not lead to any obvious visible meiotic defects [26,41,42]. They are however expressed in meiotic tissues [33–35] and we have previously reported an increased meiotic recombination rate in Arabidopsis *xrcc2* (and to a lesser extent *rad51b*) mutants in two genetic intervals [41], suggesting potential roles for these paralogues during meiosis.

It thus appears possible, in analogy to RAD54 (above), that the absence of visible meiotic phenotype in *rad51b*, *rad51d* or *xrcc2* mutants could simply be a consequence of RAD51 strand-invasion activity not being required for meiotic recombination in the presence of DMC1. We thus sought to test the impact of RAD51 paralogues in RAD51-dependent meiotic DSB repair by analysing meiotic progression in their absence in a *dmc1* mutant background (Fig 6). As described above, *dmc1* mutants are characterized by strong synaptic defects and lack of CO (Fig 6A–6C). However, meiotic DSB are still repaired as seen in the presence of intact achiasmate univalents at metaphase I (Fig 6B), that segregate randomly at anaphase I (Fig 6C). These analyses did not show any detectable effects of the absence of RAD51B, RAD51D or XRCC2 in the *dmc1* mutant background (Fig 6D–6L). In contrast, the expected chromosome fragmentation is observed in *xrcc3* mutant meiosis [28] and this is not affected by the additional absence of DMC1 (Fig 6M–6O). Thus, despite being expressed in meiotic cells and playing key roles in RAD51 activity in somatic cells, RAD51B, RAD51D and XRCC2 are not required for RAD51-dependent meiotic DSB repair in Arabidopsis.

Discussion

Here, we provide evidence that Arabidopsis RAD54 is essential for meiotic double-strand break repair mediated by RAD51. This requirement for RAD54 is not observed in the presence of DMC1 as most (all?) meiotic DSBs are repaired by DMC1, with RAD51 playing a supporting role to DMC1 in this process [51,52,61]. In the absence of DMC1 however, RAD51 catalyses the repair of meiotic DSB, leading to segregation of intact univalent chromosomes at meiotic anaphase I. Thus, absence of Arabidopsis RAD54 has no detectable effect on meiotic recombination in otherwise wild-type plants, but becomes essential for RAD51-dependent meiotic DSB repair in the absence of DMC1 (as seen in *dmc1* and *sds* mutants).

That this effect is not simply a reflection of a "mitotic" RAD51-dependent recombination context in *dmc1* meiosis is seen in the results of equivalent analyses with three RAD51 paralogue proteins, XRCC2, RAD51B and RAD51D, essential positive regulators of homologous recombination in somatic cells (reviewed in [11–13]). Mutants of these key RAD51-mediator proteins have no detectable meiotic phenotypes, beyond a mild meiotic hyper-rec phenotype reported for *xrcc2* and *rad51b* plants [26,41,42]. We report here that, in striking contrast to RAD54, the RAD51 paralogues RAD51B, RAD51D and XRCC2 are not required for

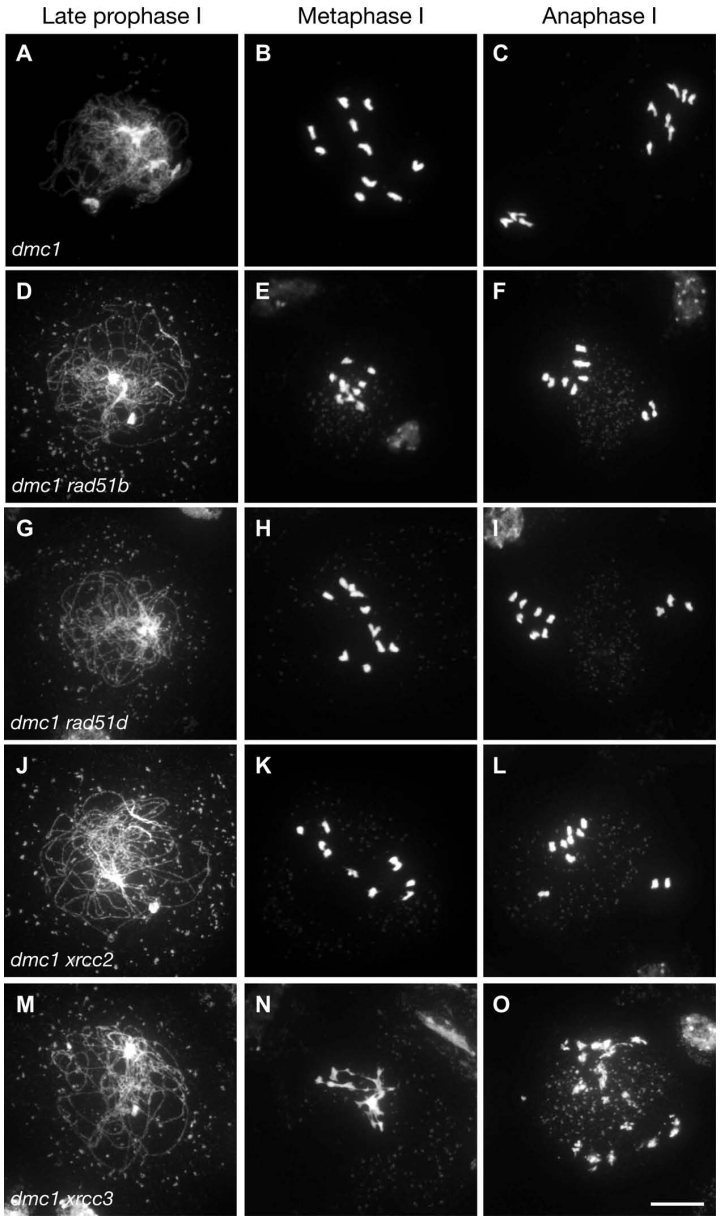

Fig 6. Absence of RAD51B, RAD51D or XRCC2 does not affect *dmc1* meiosis. Male meiosis is shown in (A-C) *dmc1*, (D-F) *dmc1 rad51b*, (G-I) *dmc1 rad51d*, (J-L) *dmc1 xrcc2*, and *dmc1 xrcc3* (M-O). Chromosome spreads at (A,D, G,J,M) late prophase I, (B,E,H,K,N) Metaphase I, (C,F,I,L,O) Anaphase I. Chromosomes were spread and stained with DAPI. (Scale bar = 10 μm).

https://doi.org/10.1371/journal.pgen.1008919.g006

RAD51-dependent meiotic DSB repair in Arabidopsis, despite being expressed in meiotic cells and playing key roles in somatic RAD51 activity.

RAD54 is a required cofactor for RAD51 activity and is thus instrumental for both mitotic and meiotic recombination in organisms lacking the meiosis-specific recombinase DMC1

[47–49]. The role of RAD54 in meiosis is however less clear in organisms expressing DMC1. Studies in budding and fission yeast have shown that Rad54 plays a relatively minor role in meiotic recombination [62–68]. This is however due to the presence of a second RAD54 homologue, Rdh54/Tid1. While both *rad54* and *rdh54* mutants form viable spores (albeit at reduced frequency), the *rad54 rdh54* double mutant rarely produces spores and is severely defective in meiotic recombination [64,66–68]. These data reveal overlapping roles of Rad54 and Rdh54/Tid1 in meiotic recombination. In addition, Rdh54 preferentially acts with Dmc1 to promote inter-homologue recombination, whereas Rad54 preferentially stimulates Rad51--mediated strand invasion for sister chromatid repair [62,63,66,70]. It is thus suggested that Rad54 is involved with Rad51 in sister chromatid repair of residual meiotic DSBs and this is in accordance with the recent demonstration of Rad51 being essential only to support Dmc1 and to repair residual DSBs after IH recombination is complete [51,69,94,95].

In multicellular eukaryotes, evidence for a role of RAD54 homologues in meiosis however remains to be demonstrated. Mammals have two known RAD54 family members, RAD54 and RAD54B, neither of which appear to have important functions in meiosis, as mice lacking RAD54, RAD54B or both exhibit no, or only minor meiotic recombination defects [71,72]. Our data demonstrate that RAD54 is essential for RAD51-mediated repair of meiotic DSBs in *dmc1* Arabidopsis. SDS is a meiosis-specific cyclin-like protein essential for normal DMC1 activity. In particular, absence of SDS leads to defects in DMC1 focus formation/stabilization, meiotic DSB repair with the homologous chromosome and CO formation [86–90]. Analysis of *sds rad54* double mutants reveals chromosome fragmentation defects in these mutants, however these are considerably less frequent that those seen in the absence of DMC1 (*dmc1* mutant). We conclude that the expected impact of absence of RAD54 is seen in *sds* meiosis, but that the phenotype is considerably less penetrant than that seen in the absence of DMC1 protein. These results thus confirm the role of RAD54 in meiotic DSB repair. To our knowledge this is the first evidence of a clear meiotic role of RAD54 in a DMC1-expressing multicellular eukaryote. In Arabidopsis *dmc1* mutants, DSBs are repaired without formation of inter-homologue CO and this concords with the suggestion that RAD51 repairs meiotic DSB using the sister chromatid template [84,85,96]. Although this essential role is only observed in the absence of DMC1, we cannot exclude that the RAD51/RAD54 DSB repair pathway is also active (albeit weakly) in wild-type plants, possibly to repair excess DSBs as has been shown in yeast [62,63]. Whether this pathway also exists in wild-type plants, remains however to be demonstrated.

Another conclusion inferred from our data is that Arabidopsis RAD54 is not necessary for DMC1 activity, either alone or as a RAD51 cofactor. That absence of RAD54 has no detectable effect on meiotic recombination in the presence of DMC1 tells us that RAD51's function as an essential accessory factor for DMC1 is RAD54-independent. This conclusion concords with the reported absence of interaction between Arabidopsis RAD54 and DMC1 [76]. Yet, the DMC1 nucleofilament must perform homology search and strand invasion and this requires ATP-dependent DNA translocases (reviewed in [44,46,97]). We thus hypothesize that there exists a second, as yet unknown, DMC1-specific RAD54 homologue in plants. RAD54 is a SWI2/SNF2-remodelling factor that belongs to the SF2 helicase family, a number of which are encoded by the Arabidopsis genome [76,78,98], but to date only RAD54 (this work) has been found to play a role in meiosis.

Control of Rad51/Rad54 complex formation is used to downregulate Rad51 activity during meiosis in budding yeast, presumably to favour interhomolog recombination driven by Dmc1 [8,51,55,56,61]. This downregulation is largely achieved through preventing Rad51/Rad54 complex formation via two pathways involving two meiosis-specific proteins: the RAD51--binding protein Hed1 and the Mek1 kinase (which phosphorylates both RAD54 and Hed1)

[53–55,57,58,60]. Briefly, Mek1-mediated phosphorylation of RAD54 weakens RAD51-RAD54 interaction [53,55] and binding of Hed1 to RAD51 also prevents association of RAD54 [54,55,57,58,60]. Interestingly, no apparent Hed1 or Mek1 orthologues have been identified in higher eukaryotes and in particular in plants. Several reports suggest that RAD51 is also down-regulated in Arabidopsis meiosis [52,84,85,96,99,100], but the evidence for this remains indirect. Thus, whether RAD51 strand exchange activity is down-regulated during meiosis in higher organisms and if so, how this is achieved, is not clear. The absence of meiotic phenotype of Arabidopsis *rad54* mutants, together with the demonstration of the RAD54-dependence of meiotic RAD51 activity (in the absence of DMC1), supports the idea of a hypothetical RAD54-dependent control of RAD51 activity through modulation of the RAD54/RAD51 interaction. It also, however, invites speculation concerning whether it is necessary to invoke such a downregulation to explain numbers of CO vs non-CO recombination events in plants, and very likely in vertebrates. Previous work has shown that DMC1 is capable of catalysing repair of all meiotic DSB in Arabidopsis in strand-invasion mutants of RAD51 [52,99], or as shown here, by blocking RAD51 activity through the absence of RAD54. In both of these contexts, no evidence of alteration of numbers nor distribution of meiotic recombination has been found.

In conclusion, we present here an essential role for RAD54 in supporting meiotic RAD51-mediated DSB repair in the absence of DMC1 in Arabidopsis. In striking contrast, testing of three other key RAD51 mediator mutants (*rad51b*, *rad51d*, *xrcc2*) did not reveal any detectable impact on *dmc1* meiosis, notwithstanding the fact that they are, like RAD54, needed for RAD51-dependent recombination in somatic cells. This RAD54-dependent, RAD51-mediated meiotic DSB repair is thus not the reflection of a simple "mitotic-like" RAD51 DSB repair in meiocytes lacking DMC1, but points to RAD54 mainly acting downstream of the role of the RAD51 nucleofilament in supporting meiotic DMC1-mediated recombination. It will be of particular interest to further study in which context this pathway is activated in wild-type meiosis and also whether a similar pathway exists in other organisms outside the fungal taxa. Although further studies are needed to confirm whether (and how) RAD51 strand-invasion activity is downregulated during meiosis in plants, we speculate that this could be achieved through prevention of RAD54/RAD51 interaction, and/or via helicases dissociating precocious strand-invasion between sister chromatids, as has recently been shown in budding yeast [101].

Materials and methods

Plant material and growth conditions

All *Arabidopsis thaliana* plants used in this study were in the Columbia background. Seeds of the *rad54-2* (SALK_124992) [102] T-DNA insertion mutant were obtained through the Nottingham Arabidopsis Stock Centre and characterised in this study. For other mutants, we used the following alleles: *rad54-1* [76], *dmc1-2* [85], *rad51-1* [103], *rad51b-1 [26]*, *rad51d-3* [41] and *xrcc2-1* [26]. Fluorescent-Tagged lines (FTLs) were: I1bc (FTL567-YFP/FTL1262-DsRed2/FTL992-AmCyan/*qrt1-2*), and I2fg (FTL800-DsRed2/FTL3411-YFP/FTL3263-AmCyan/*qrt1-2*) [81].

Seeds were stratified in water at 4˚C for 2 days and grown on soil in a growth chamber. For *in vitro* culture, seeds were surface sterilised for 5 min with 75% Ethanol, 0.05% SDS, rinsed with 95% Ethanol for 5 min and air-dried. Sterilised seeds were then sown on half-strength Murashige and Skoog (MS) medium, stratified at 4˚C for 2 days and placed in a growth cabinet. All plants were grown under 16h light /8 h dark cycles at 23˚C and 60% relative humidity.

Molecular characterization of *rad54-2* T-DNA insertion mutants

The *rad54-2* (SALK_124992) mutant was genotyped using primers P1 and P2 to detect the wild-type loci and primers P1, P2, and Lba1 (SALK T-DNA Left Border specific primer) were used to detect the T-DNA insertion allele. The junctions of the T-DNA insertion in the *RAD54* locus (AT3G19210) were amplified by PCR and verified by DNA sequencing.

For semi-quantitative RT–PCR, total RNA was extracted from young buds of wild-type, *rad54-1* and *rad54-2* plants using RNeasy Plant mini Kit (QIAGEN), following the manufacturer's instructions. 2 μg RNA were treated with RQ1 RNase-free DNase (Promega) followed by reverse transcription using M-MLV Reverse Transcriptase (Promega) according to the manufacturer's instructions. PCR amplifications were eventually performed in homozygous lines showing the absence of full-length *RAD54* transcripts (Fig 1).

Mitomycin C sensitivity assays

For the MMC sensitivity assay, seeds were surface-sterilised and sown onto solid medium (half strength Murashige and Skoog salts, 1% sucrose, 0.8% agar) supplemented with 0, 20, 30 or 40μM Mitomycin C (SIGMA). Seeds were stratified in the dark for 2 days at 4˚C, transferred to a growth cabinet and grown for two weeks. Sensitivity was then analysed in two-week-old seedlings by counting the number of true leaves as previously described [28]. Plants with more than three true leaves were considered as resistant. In each case, the number of leaves was counted on at least 25 seedlings in three to five independent experiments.

Recombination measurement using Fluorescent-Tagged Lines (FTL) tetrad analysis

We used Fluorescent Tagged Lines to estimate male meiotic recombination rates at two pairs of genetic intervals: I1bc on chromosome 1 and I2fg on chromosome 2. For each experiment, heterozygous plants for the linked fluorescent markers were generated and siblings from the same segregating progeny were used to compare the recombination frequency between different genotypes. Slides and fluorescent tetrad analysis were performed as described by Berchowitz and Copenhaver [81]. Tetrads were counted and attributed to specific classes (A to L). Genetic distances of each interval were calculated using Perkins equation as follows: $X = 100 [(1/2\text{Tetratype} + 3\text{Non-Parental Ditype})/n]$ in cM.

The Interference Ratio (IR) was calculated as described previously [81]. Briefly, for two adjacent intervals I1 and I2, two populations of tetrads are considered: those with at least one CO in I2 and those without any CO in I2. Genetic distance of I1 is then calculated for these two populations using the Perkins equation, i.e. $X1$ (I1 with CO in I2) and $X2$ (I1 without a CO in I2). The Interference Ratio is thus defined as $IR = X1/X2$. An IR ratio <1 reveals the presence of interference while an IR ratio close to 1 reveals absence of interference. The Stahl Lab Online Tools was used for statistical analyses of the data.

Arabidopsis male meiotic chromosome spreads

Meiotic chromosome spreads were prepared according to [104]. Whole inflorescences were fixed in ice-cold ethanol/glacial acetic acid (3:1) and stored at -20˚C until further use. Immature flower buds of appropriate size were selected under a binocular microscope and incubated for 75–90 min on a slide in 100μl of enzyme mixture (0.3% w/v cellulase (Sigma), 0.3% w/v pectolyase (Sigma) and 0.3% cytohelicase (Sigma)) in a moist chamber at 37˚C. Each bud was then softened for 1 minute in 20 μl 60% acetic acid on a microscope slide at 45˚C, fixed with

ice-cold ethanol/glacial acetic acid (3:1) and air dried. Slide were mounted in Vectashield mounting medium with DAPI (1.5 μg.ml^{-1}; Vector Laboratories Inc.).

Immunolocalization of meiotic proteins in pollen mother cells (PMCs)

Spreads of PMCs for immunolocalization of RAD51, ASY1 and ZYP1 were performed as described previously [105]. Primary antibodies used for immunostaining were: anti-ASY1 raised in guinea Pig (1:500) [106] anti-RAD51 raised in rat (1:500) [107], and anti-ZYP1 raised in rabbit (1:500) [108]. Secondary antibody: anti-rat Alexa fluor 488; anti-rat Alexa fluor 594, anti-guinea pig Cy3, and anti-rabbit Alexa fluor 488 were used at 1:100 dilution.

Microscopy

All observations were made with a motorised Zeiss AxioImager.Z1 epifluorescence microscope (Carl Zeiss AG, Germany) driven by the ZEN Pro software (Carl Zeiss AG, Germany). Photographs were taken with an AxioC.am Mrm camera (Carl Zeiss AG, Germany) and Zeiss filter sets adapted for the fluorochromes used. Image stacks were captured in three dimensions (x, y, z) and further processed and adjusted for brightness and contrast on ZEN Pro and ImageJ/FIJI software. RAD51 foci were counted on collapsed z-stack projections by using counting tool of the ZEN Pro software.

Supporting information

S1 Fig. Sequence of RAD54/T-DNA junction in *rad54-2* allele and corresponding putative predicted protein. (A) pairwise alignment between AtRAD54 coding sequence (cds) and sequence from T-DNA left border amplification at the T-DNA insertion site in the *rad54-2* allele. An in-frame TGA stop codon is highlighted in cyan. T-DNA insertion derived nucleotides deletion is highlighted in grey. **(B)** Pairwise alignment of the Arabidopsis RAD54 protein and the putative predicted protein from the *rad54-2* allele. Alignment was generated using clustalOmega. Numbers indicate amino acid positions. Under the sequences, asterisks, colons and full stops indicate identical, conserved and semi-conserved residues, respectively. The seven conserved ATPase motifs are indicated with black boxes and red roman numerals. These motifs define the two RecA-like domains (parts defined by green and blue lines, respectively), which constitute the "core" translocation motor domains. If translated, the truncated protein from the *rad54-2* allele would lack these two recA-like domains.
(TIFF)

S2 Fig. Sensitivity of *rad54-1* and *rad54-2* plants to MMC. Shown are representative photographs of two-week-old seedlings grown without or with the indicated concentrations of MMC.
(TIFF)

S3 Fig. Fertility of *rad54-1* and *rad54-2* mutants. (A) pictures of wild-type and *rad54* mutant siliques. **(B)** Number of seeds per silique in Wild-type, *rad54-1* and *rad54-2* mutants. Each point represents the number of seeds in one silique. Bars indicate mean ± SD. n.s.: not significantly different. $P > 0.05$ (unpaired, two-tailed Mann-Whitney test).
(TIFF)

S4 Fig. Genetic recombination in wild-type, *rad54-1* and *rad54-2* mutants measured using I2fg fluorescent-tagged lines. Genetic distances (in centiMorgans, cM) calculated from tetrad analysis of the I2f and I2g intervals on chromosome 2. Bars indicate mean ± SD. For both

intervals, WT and *rad54* plants do not significantly differ ($p<0.05$; Z-test).
(TIFF)

S5 Fig. Absence of synapsis in *dmc1 rad54* mutant plants. Immunolocalization in wild-type, *rad54-2* and *dmc1 rad54-2* meiocytes shows that synaptonemal complex transverse filament protein, ZYP1, is not correctly loaded along chromosome axes in *dmc1 rad54-2* indicating lack of synapsis. DAPI (blue), ASY1 (red), ZYP1 (green) and merged images are shown. (Scale Bar: 5 μm).
(TIFF)

S6 Fig. Fertility of *dmc1 rad54-1* and *dmc1 rad54-2* mutant plants. Number of seeds per silique in Wild-type, *dmc1*, *dmc1 rad54-1* and *dmc1 rad54-2* mutants. Each spot represents the number of seeds in one silique. Bars indicate mean ± SD. ****: significantly different. $P < 0.0001$ (unpaired, two-tailed Mann-Whitney test).
(TIFF)

S7 Fig. Absence of RAD54 leads to partial chromosome fragmentation in *sds* meiosis. (A) Male meiosis is shown in wild-type, *sds rad54-1*, and *sds rad54-2*. Chromosomes were spread and stained with DAPI. (Scale bar = 10 μm). **(B)** Quantification of male meiocytes showing intact chromosomes or fragmentation. Each bar represents one plant.
(TIFF)

S8 Fig. RAD51 foci in wild type and *rad54* mutant pachytene cells. (A) Dual immunolocalization of ZYP1 (green) and RAD51 (red) in wild-type and *rad54-2* pachytene cells. (Scale Bar: 5 μm). **(B)** Quantification of RAD51 foci per positive pachytene cell in wild-type and *rad54-2* mutants. Means ± SD are indicated. n.s.: not significantly different (p-value > 0.05, unpaired, two-tailed Mann-Whitney test).
(TIFF)

S1 Table. FTLs raw data and Interference ratio calculation. Tetrad count for all tetrad categories for I1bc and I2fg intervals. Tetrad categories (a to l) were classified as described previously by Berchowitz and Copenhaver (2008).
(XLSX)

S1 Data. Raw data for fertility and RAD51 foci countings. This are numerical data that supports the findings of this study.
(XLSX)

Acknowledgments

We thank Gregory Copenhaver and Ian Henderson for FTL lines, Chris Franklin and Peter Schlögelhofer for providing the ASY1 and RAD51 antibodies, respectively and Mathilde Grelon and Rajeev Kumar for sharing ZYP1 antibody and *sds* mutant seeds. We thank members of the recombination group for their help and discussions.

Author Contributions

Conceptualization: Maria E. Gallego, Charles I. White, Olivier Da Ines.

Formal analysis: Miguel Hernandez Sanchez-Rebato, Alida M. Bouatta, Charles I. White, Olivier Da Ines.

Funding acquisition: Maria E. Gallego, Charles I. White, Olivier Da Ines.

Investigation: Miguel Hernandez Sanchez-Rebato, Alida M. Bouatta, Olivier Da Ines.

Supervision: Maria E. Gallego, Charles I. White, Olivier Da Ines.

Writing – original draft: Charles I. White, Olivier Da Ines.

Writing – review & editing: Maria E. Gallego, Charles I. White, Olivier Da Ines.

References

1. Heyer WD, Ehmsen KT, Liu J. Regulation of homologous recombination in eukaryotes. Annu Rev Genet. 2010; 44:113–39. https://doi.org/10.1146/annurev-genet-051710-150955 PMID: 20690856.
2. Ranjha L, Howard SM, Cejka P. Main steps in DNA double-strand break repair: an introduction to homologous recombination and related processes. Chromosoma. 2018; 127(2):187–214. https://doi.org/10.1007/s00412-017-0658-1 PMID: 29327130.
3. Mercier R, Mezard C, Jenczewski E, Macaisne N, Grelon M. The molecular biology of meiosis in plants. Annu Rev Plant Biol. 2015; 66:297–327. https://doi.org/10.1146/annurev-arplant-050213-035923 PMID: 25494464.
4. Hunter N. Meiotic Recombination: The Essence of Heredity. Cold Spring Harb Perspect Biol. 2015; 7 (12). https://doi.org/10.1101/cshperspect.a016618 PMID: 26511629.
5. Symington LS. Mechanism and regulation of DNA end resection in eukaryotes. Crit Rev Biochem Mol Biol. 2016; 51(3):195–212. https://doi.org/10.3109/10409238.2016.1172552 PMID: 27098756.
6. Chen H, Lisby M, Symington LS. RPA coordinates DNA end resection and prevents formation of DNA hairpins. Mol Cell. 2013; 50(4):589–600. https://doi.org/10.1016/j.molcel.2013.04.032 PMID: 23706822.
7. Chen R, Wold MS. Replication protein A: single-stranded DNA's first responder: dynamic DNA-interactions allow replication protein A to direct single-strand DNA intermediates into different pathways for synthesis or repair. Bioessays. 2014; 36(12):1156–61. https://doi.org/10.1002/bies.201400107 PMID: 25171654.
8. Brown MS, Bishop DK. DNA strand exchange and RecA homologs in meiosis. Cold Spring Harb Perspect Biol. 2014; 7(1):a016659. https://doi.org/10.1101/cshperspect.a016659 PMID: 25475089.
9. Crickard JB, Greene EC. Biochemical attributes of mitotic and meiotic presynaptic complexes. DNA Repair (Amst). 2018; 71:148–57. https://doi.org/10.1016/j.dnarep.2018.08.018 PMID: 30195641.
10. Kowalczykowski SC. An Overview of the Molecular Mechanisms of Recombinational DNA Repair. Cold Spring Harb Perspect Biol. 2015; 7(11). https://doi.org/10.1101/cshperspect.a016410 PMID: 26525148.
11. Zelensky A, Kanaar R, Wyman C. Mediators of homologous DNA pairing. Cold Spring Harb Perspect Biol. 2014; 6(12):a016451. https://doi.org/10.1101/cshperspect.a016451 PMID: 25301930.
12. Suwaki N, Klare K, Tarsounas M. RAD51 paralogs: roles in DNA damage signalling, recombinational repair and tumorigenesis. Semin Cell Dev Biol. 2011; 22(8):898–905. https://doi.org/10.1016/j.semcdb.2011.07.019 PMID: 21821141.
13. Pradillo M, Varas J, Oliver C, Santos JL. On the role of AtDMC1, AtRAD51 and its paralogs during Arabidopsis meiosis. Front Plant Sci. 2014; 5:23. https://doi.org/10.3389/fpls.2014.00023 PMID: 24596572.
14. Liu J, Renault L, Veaute X, Fabre F, Stahlberg H, Heyer WD. Rad51 paralogues Rad55-Rad57 balance the antirecombinase Srs2 in Rad51 filament formation. Nature. 2011; 479(7372):245–8. https://doi.org/10.1038/nature10522 PMID: 22020281.
15. Gasior SL, Olivares H, Ear U, Hari DM, Weichselbaum R, Bishop DK. Assembly of RecA-like recombinases: distinct roles for mediator proteins in mitosis and meiosis. Proc Natl Acad Sci U S A. 2001; 98 (15):8411–8. https://doi.org/10.1073/pnas.121046198 PMID: 11459983.
16. Gasior SL, Wong AK, Kora Y, Shinohara A, Bishop DK. Rad52 associates with RPA and functions with rad55 and rad57 to assemble meiotic recombination complexes. Genes Dev. 1998; 12(14):2208–21. https://doi.org/10.1101/gad.12.14.2208 PMID: 9679065.
17. Schwacha A, Kleckner N. Interhomolog bias during meiotic recombination: meiotic functions promote a highly differentiated interhomolog-only pathway. Cell. 1997; 90(6):1123–35. https://doi.org/10.1016/s0092-8674(00)80378-5 PMID: 9323140.
18. Sasanuma H, Tawaramoto MS, Lao JP, Hosaka H, Sanda E, Suzuki M, et al. A new protein complex promoting the assembly of Rad51 filaments. Nat Commun. 2013; 4:1676. https://doi.org/10.1038/ncomms2678 PMID: 23575680.
19. Serra H, Da Ines O, Degroote F, Gallego ME, White CI. Roles of XRCC2, RAD51B and RAD51D in RAD51-independent SSA recombination. PLoS Genet. 2013; 9(11):e1003971. https://doi.org/10.1371/journal.pgen.1003971 PMID: 24278037.

20. Kuznetsov S, Pellegrini M, Shuda K, Fernandez-Capetillo O, Liu Y, Martin BK, et al. RAD51C deficiency in mice results in early prophase I arrest in males and sister chromatid separation at metaphase II in females. J Cell Biol. 2007; 176(5):581–92. https://doi.org/10.1083/jcb.200608130 PMID: 17312021.

21. Liu Y, Tarsounas M, O'Regan P, West SC. Role of RAD51C and XRCC3 in genetic recombination and DNA repair. J Biol Chem. 2007; 282(3):1973–9. https://doi.org/10.1074/jbc.M609066200 PMID: 17114795.

22. Zhang B, Wang M, Tang D, Li Y, Xu M, Gu M, et al. XRCC3 is essential for proper double-strand break repair and homologous recombination in rice meiosis. J Exp Bot. 2015; 66(19):5713–25. https://doi.org/10.1093/jxb/erv253 PMID: 26034131.

23. Tang D, Miao C, Li Y, Wang H, Liu X, Yu H, et al. OsRAD51C is essential for double-strand break repair in rice meiosis. Front Plant Sci. 2014; 5:167. https://doi.org/10.3389/fpls.2014.00167 PMID: 24847337.

24. Su H, Cheng Z, Huang J, Lin J, Copenhaver GP, Ma H, et al. Arabidopsis RAD51, RAD51C and XRCC3 proteins form a complex and facilitate RAD51 localization on chromosomes for meiotic recombination. PLoS Genet. 2017; 13(5):e1006827. https://doi.org/10.1371/journal.pgen.1006827 PMID: 28562599.

25. Abe K, Osakabe K, Nakayama S, Endo M, Tagiri A, Todoriki S, et al. Arabidopsis RAD51C gene is important for homologous recombination in meiosis and mitosis. Plant Physiol. 2005; 139(2):896–908. https://doi.org/10.1104/pp.105.065243 PMID: 16169964.

26. Bleuyard JY, Gallego ME, Savigny F, White CI. Differing requirements for the Arabidopsis Rad51 paralogs in meiosis and DNA repair. Plant J. 2005; 41(4):533–45. https://doi.org/10.1111/j.1365-313X.2004.02318.x PMID: 15686518.

27. Bleuyard JY, Gallego ME, White CI. The atspo11-1 mutation rescues atxrcc3 meiotic chromosome fragmentation. Plant Mol Biol. 2004; 56(2):217–24. https://doi.org/10.1007/s11103-004-2812-4 PMID: 15604739.

28. Bleuyard JY, White CI. The Arabidopsis homologue of Xrcc3 plays an essential role in meiosis. EMBO J. 2004; 23(2):439–49. https://doi.org/10.1038/sj.emboj.7600055 PMID: 14726957.

29. Li W, Yang X, Lin Z, Timofejeva L, Xiao R, Makaroff CA, et al. The AtRAD51C gene is required for normal meiotic chromosome synapsis and double-stranded break repair in Arabidopsis. Plant Physiol. 2005; 138(2):965–76. https://doi.org/10.1104/pp.104.058347 PMID: 15923332.

30. Cartwright R, Dunn AM, Simpson PJ, Tambini CE, Thacker J. Isolation of novel human and mouse genes of the recA/RAD51 recombination-repair gene family. Nucleic Acids Res. 1998; 26(7):1653–9. https://doi.org/10.1093/nar/26.7.1653 PMID: 9512535.

31. Cartwright R, Tambini CE, Simpson PJ, Thacker J. The XRCC2 DNA repair gene from human and mouse encodes a novel member of the recA/RAD51 family. Nucleic Acids Res. 1998; 26(13):3084–9. https://doi.org/10.1093/nar/26.13.3084 PMID: 9628903.

32. Tarsounas M, Munoz P, Claas A, Smiraldo PG, Pittman DL, Blasco MA, et al. Telomere maintenance requires the RAD51D recombination/repair protein. Cell. 2004; 117(3):337–47. https://doi.org/10.1016/s0092-8674(04)00337-x PMID: 15109494.

33. Chen C, Farmer AD, Langley RJ, Mudge J, Crow JA, May GD, et al. Meiosis-specific gene discovery in plants: RNA-Seq applied to isolated Arabidopsis male meiocytes. BMC Plant Biol. 2010; 10:280. https://doi.org/10.1186/1471-2229-10-280 PMID: 21167045.

34. Walker J, Gao H, Zhang J, Aldridge B, Vickers M, Higgins JD, et al. Sexual-lineage-specific DNA methylation regulates meiosis in Arabidopsis. Nat Genet. 2018; 50(1):130–7. https://doi.org/10.1038/s41588-017-0008-5 PMID: 29255257.

35. Yang H, Lu P, Wang Y, Ma H. The transcriptome landscape of Arabidopsis male meiocytes from high-throughput sequencing: the complexity and evolution of the meiotic process. Plant J. 2011; 65(4):503–16. https://doi.org/10.1111/j.1365-313X.2010.04439.x PMID: 21208307.

36. Yang Y, Guo J, Dai L, Zhu Y, Hu H, Tan L, et al. XRCC2 mutation causes meiotic arrest, azoospermia and infertility. J Med Genet. 2018; 55(9):628–36. https://doi.org/10.1136/jmedgenet-2017-105145 PMID: 30042186.

37. Byun MY, Kim WT. Suppression of OsRAD51D results in defects in reproductive development in rice (Oryza sativa L.). Plant J. 2014; 79(2):256–69. https://doi.org/10.1111/tpj.12558 PMID: 24840804.

38. Charlot F, Chelysheva L, Kamisugi Y, Vrielynck N, Guyon A, Epert A, et al. RAD51B plays an essential role during somatic and meiotic recombination in Physcomitrella. Nucleic Acids Res. 2014; 42(19):11965–78. https://doi.org/10.1093/nar/gku890 PMID: 25260587.

39. Zhang F, Shen Y, Miao C, Cao Y, Shi W, Du G, et al. OsRAD51D promotes homologous pairing and recombination by preventing non-homologous interactions in rice meiosis. New Phytol. 2020. https://doi.org/10.1111/nph.16595 PMID: 32275774.

40. Osakabe K, Abe K, Yamanouchi H, Takyuu T, Yoshioka T, Ito Y, et al. Arabidopsis Rad51B is important for double-strand DNA breaks repair in somatic cells. Plant Mol Biol. 2005; 57(6):819–33. https://doi.org/10.1007/s11103-005-2187-1 PMID: 15952068.

41. Da Ines O, Degroote F, Amiard S, Goubely C, Gallego ME, White CI. Effects of XRCC2 and RAD51B mutations on somatic and meiotic recombination in Arabidopsis thaliana. Plant J. 2013; 74(6):959–70. https://doi.org/10.1111/tpj.12182 PMID: 23521529.

42. Wang Y, Xiao R, Wang H, Cheng Z, Li W, Zhu G, et al. The Arabidopsis RAD51 paralogs RAD51B, RAD51D and XRCC2 play partially redundant roles in somatic DNA repair and gene regulation. New Phytol. 2014; 201(1):292–304. https://doi.org/10.1111/nph.12498 PMID: 24102485.

43. Abreu CM, Prakash R, Romanienko PJ, Roig I, Keeney S, Jasin M. Shu complex SWS1-SWSAP1 promotes early steps in mouse meiotic recombination. Nat Commun. 2018; 9(1):3961. https://doi.org/10.1038/s41467-018-06384-x PMID: 30305635.

44. Ceballos SJ, Heyer WD. Functions of the Snf2/Swi2 family Rad54 motor protein in homologous recombination. Biochim Biophys Acta. 2011; 1809(9):509–23. https://doi.org/10.1016/j.bbagrm.2011.06.006 PMID: 21704205.

45. Crickard JB, Greene EC. Helicase Mechanisms During Homologous Recombination in Saccharomyces cerevisiae. Annu Rev Biophys. 2019. https://doi.org/10.1146/annurev-biophys-052118-115418 PMID: 30857400.

46. Mazin AV, Mazina OM, Bugreev DV, Rossi MJ. Rad54, the motor of homologous recombination. DNA Repair (Amst). 2010; 9(3):286–302. https://doi.org/10.1016/j.dnarep.2009.12.006 PMID: 20089461.

47. Ghabrial A, Ray RP, Schupbach T. okra and spindle-B encode components of the RAD52 DNA repair pathway and affect meiosis and patterning in Drosophila oogenesis. Genes Dev. 1998; 12(17):2711–23. https://doi.org/10.1101/gad.12.17.2711 PMID: 9732269.

48. Kooistra R, Vreeken K, Zonneveld JB, de Jong A, Eeken JC, Osgood CJ, et al. The Drosophila melanogaster RAD54 homolog, DmRAD54, is involved in the repair of radiation damage and recombination. Mol Cell Biol. 1997; 17(10):6097–104. https://doi.org/10.1128/mcb.17.10.6097 PMID: 9315669.

49. Mets DG, Meyer BJ. Condensins regulate meiotic DNA break distribution, thus crossover frequency, by controlling chromosome structure. Cell. 2009; 139(1):73–86. https://doi.org/10.1016/j.cell.2009.07.035 PMID: 19781752.

50. Bishop DK, Park D, Xu L, Kleckner N. DMC1: a meiosis-specific yeast homolog of E. coli recA required for recombination, synaptonemal complex formation, and cell cycle progression. Cell. 1992; 69(3):439–56. https://doi.org/10.1016/0092-8674(92)90446-j PMID: 1581960.

51. Cloud V, Chan YL, Grubb J, Budke B, Bishop DK. Rad51 is an accessory factor for Dmc1-mediated joint molecule formation during meiosis. Science. 2012; 337(6099):1222–5. https://doi.org/10.1126/science.1219379 PMID: 22955832.

52. Da Ines O, Degroote F, Goubely C, Amiard S, Gallego ME, White CI. Meiotic recombination in Arabidopsis is catalysed by DMC1, with RAD51 playing a supporting role. PLoS Genet. 2013; 9(9):e1003787. https://doi.org/10.1371/journal.pgen.1003787 PMID: 24086145.

53. Niu H, Wan L, Busygina V, Kwon Y, Allen JA, Li X, et al. Regulation of meiotic recombination via Mek1-mediated Rad54 phosphorylation. Mol Cell. 2009; 36(3):393–404. https://doi.org/10.1016/j.molcel.2009.09.029 PMID: 19917248.

54. Tsubouchi H, Roeder GS. Budding yeast Hed1 down-regulates the mitotic recombination machinery when meiotic recombination is impaired. Genes Dev. 2006; 20(13):1766–75. https://doi.org/10.1101/gad.1422506 PMID: 16818607.

55. Callender TL, Laureau R, Wan L, Chen X, Sandhu R, Laljee S, et al. Mek1 Down Regulates Rad51 Activity during Yeast Meiosis by Phosphorylation of Hed1. PLoS Genet. 2016; 12(8):e1006226. https://doi.org/10.1371/journal.pgen.1006226 PMID: 27483004.

56. Lao JP, Cloud V, Huang CC, Grubb J, Thacker D, Lee CY, et al. Meiotic crossover control by concerted action of Rad51-Dmc1 in homolog template bias and robust homeostatic regulation. PLoS Genet. 2013; 9(12):e1003978. https://doi.org/10.1371/journal.pgen.1003978 PMID: 24367271.

57. Busygina V, Saro D, Williams G, Leung WK, Say AF, Sehorn MG, et al. Novel attributes of Hed1 affect dynamics and activity of the Rad51 presynaptic filament during meiotic recombination. J Biol Chem. 2012; 287(2):1566–75. https://doi.org/10.1074/jbc.M111.297309 PMID: 22115747.

58. Busygina V, Sehorn MG, Shi IY, Tsubouchi H, Roeder GS, Sung P. Hed1 regulates Rad51-mediated recombination via a novel mechanism. Genes Dev. 2008; 22(6):786–95. https://doi.org/10.1101/gad.1638708 PMID: 18347097.

59. Hong S, Sung Y, Yu M, Lee M, Kleckner N, Kim KP. The logic and mechanism of homologous recombination partner choice. Mol Cell. 2013; 51(4):440–53. https://doi.org/10.1016/j.molcel.2013.08.008 PMID: 23973374.

60. Crickard JB, Kaniecki K, Kwon Y, Sung P, Lisby M, Greene EC. Regulation of Hed1 and Rad54 binding during maturation of the meiosis-specific presynaptic complex. EMBO J. 2018; 37(7). https://doi.org/10.15252/embj.201798728 PMID: 29444896.

61. Liu Y, Gaines WA, Callender T, Busygina V, Oke A, Sung P, et al. Down-regulation of Rad51 activity during meiosis in yeast prevents competition with Dmc1 for repair of double-strand breaks. PLoS Genet. 2014; 10(1):e1004005. https://doi.org/10.1371/journal.pgen.1004005 PMID: 24465215.

62. Arbel A, Zenvirth D, Simchen G. Sister chromatid-based DNA repair is mediated by RAD54, not by DMC1 or TID1. EMBO J. 1999; 18(9):2648–58. https://doi.org/10.1093/emboj/18.9.2648 PMID: 10228176.

63. Bishop DK, Nikolski Y, Oshiro J, Chon J, Shinohara M, Chen X. High copy number suppression of the meiotic arrest caused by a dmc1 mutation: REC114 imposes an early recombination block and RAD54 promotes a DMC1-independent DSB repair pathway. Genes Cells. 1999; 4(8):425–44. https://doi.org/10.1046/j.1365-2443.1999.00273.x PMID: 10526232.

64. Catlett MG, Forsburg SL. Schizosaccharomyces pombe Rdh54 (TID1) acts with Rhp54 (RAD54) to repair meiotic double-strand breaks. Mol Biol Cell. 2003; 14(11):4707–20. https://doi.org/10.1091/mbc.e03-05-0288 PMID: 14551247.

65. Schmuckli-Maurer J, Heyer WD. Meiotic recombination in RAD54 mutants of Saccharomyces cerevisiae. Chromosoma. 2000; 109(1–2):86–93. https://doi.org/10.1007/s004120050415 PMID: 10855498.

66. Shinohara M, Gasior SL, Bishop DK, Shinohara A. Tid1/Rdh54 promotes colocalization of rad51 and dmc1 during meiotic recombination. Proc Natl Acad Sci U S A. 2000; 97(20):10814–9. https://doi.org/10.1073/pnas.97.20.10814 PMID: 11005857.

67. Shinohara M, Sakai K, Shinohara A, Bishop DK. Crossover interference in Saccharomyces cerevisiae requires a TID1/RDH54- and DMC1-dependent pathway. Genetics. 2003; 163(4):1273–86. PMID: 12702674.

68. Shinohara M, Shita-Yamaguchi E, Buerstedde JM, Shinagawa H, Ogawa H, Shinohara A. Characterization of the roles of the Saccharomyces cerevisiae RAD54 gene and a homologue of RAD54, RDH54/TID1, in mitosis and meiosis. Genetics. 1997; 147(4):1545–56. PMID: 9409820.

69. Subramanian VV, MacQueen AJ, Vader G, Shinohara M, Sanchez A, Borde V, et al. Chromosome Synapsis Alleviates Mek1-Dependent Suppression of Meiotic DNA Repair. PLoS Biol. 2016; 14(2): e1002369. https://doi.org/10.1371/journal.pbio.1002369 PMID: 26870961.

70. Nimonkar AV, Dombrowski CC, Siino JS, Stasiak AZ, Stasiak A, Kowalczykowski SC. Saccharomyces cerevisiae Dmc1 and Rad51 proteins preferentially function with Tid1 and Rad54 proteins, respectively, to promote DNA strand invasion during genetic recombination. J Biol Chem. 2012; 287 (34):28727–37. https://doi.org/10.1074/jbc.M112.373290 PMID: 22761450.

71. Essers J, Hendriks RW, Swagemakers SM, Troelstra C, de Wit J, Bootsma D, et al. Disruption of mouse RAD54 reduces ionizing radiation resistance and homologous recombination. Cell. 1997; 89 (2):195–204. https://doi.org/10.1016/s0092-8674(00)80199-3 PMID: 9108475.

72. Wesoly J, Agarwal S, Sigurdsson S, Bussen W, Van Komen S, Qin J, et al. Differential contributions of mammalian Rad54 paralogs to recombination, DNA damage repair, and meiosis. Mol Cell Biol. 2006; 26(3):976–89. https://doi.org/10.1128/MCB.26.3.976-989.2006 PMID: 16428451.

73. Klutstein M, Shaked H, Sherman A, Avivi-Ragolsky N, Shema E, Zenvirth D, et al. Functional conservation of the yeast and Arabidopsis RAD54-like genes. Genetics. 2008; 178(4):2389–97. https://doi.org/10.1534/genetics.108.086777 PMID: 18430956.

74. Hirakawa T, Hasegawa J, White CI, Matsunaga S. RAD54 forms DNA repair foci in response to DNA damage in living plant cells. Plant J. 2017; 90(2):372–82. https://doi.org/10.1111/tpj.13499 PMID: 28155243.

75. Hirakawa T, Katagiri Y, Ando T, Matsunaga S. DNA double-strand breaks alter the spatial arrangement of homologous loci in plant cells. Sci Rep. 2015; 5:11058. https://doi.org/10.1038/srep11058 PMID: 26046331.

76. Osakabe K, Abe K, Yoshioka T, Osakabe Y, Todoriki S, Ichikawa H, et al. Isolation and characterization of the RAD54 gene from Arabidopsis thaliana. Plant J. 2006; 48(6):827–42. https://doi.org/10.1111/j.1365-313X.2006.02927.x PMID: 17227544.

77. Roth N, Klimesch J, Dukowic-Schulze S, Pacher M, Mannuss A, Puchta H. The requirement for recombination factors differs considerably between different pathways of homologous double-strand break repair in somatic plant cells. Plant J. 2012; 72(5):781–90. https://doi.org/10.1111/j.1365-313X.2012.05119.x PMID: 22860689.

78. Shaked H, Avivi-Ragolsky N, Levy AA. Involvement of the Arabidopsis SWI2/SNF2 chromatin remodeling gene family in DNA damage response and recombination. Genetics. 2006; 173(2):985–94. https://doi.org/10.1534/genetics.105.051664 PMID: 16547115.

79. Mannuss A, Dukowic-Schulze S, Suer S, Hartung F, Pacher M, Puchta H. RAD5A, RECQ4A, and MUS81 have specific functions in homologous recombination and define different pathways of DNA repair in Arabidopsis thaliana. Plant Cell. 2010; 22(10):3318–30. https://doi.org/10.1105/tpc.110.078568 PMID: 20971895.

80. Crismani W, Mercier R. Identifying meiotic mutants in Arabidopsis thaliana. Methods Mol Biol. 2013; 990:227–34. https://doi.org/10.1007/978-1-62703-333-6_22 PMID: 23559218.

81. Berchowitz LE, Copenhaver GP. Fluorescent Arabidopsis tetrads: a visual assay for quickly developing large crossover and crossover interference data sets. Nat Protoc. 2008; 3(1):41–50. https://doi.org/10.1038/nprot.2007.491 PMID: 18193020.

82. Francis KE, Lam SY, Harrison BD, Bey AL, Berchowitz LE, Copenhaver GP. Pollen tetrad-based visual assay for meiotic recombination in Arabidopsis. Proc Natl Acad Sci U S A. 2007; 104(10):3913–8. https://doi.org/10.1073/pnas.0608936104 PMID: 17360452.

83. Francis KE, Lam SY, Copenhaver GP. Separation of Arabidopsis pollen tetrads is regulated by QUARTET1, a pectin methylesterase gene. Plant Physiol. 2006; 142(3):1004–13. https://doi.org/10.1104/pp.106.085274 PMID: 16980565.

84. Couteau F, Belzile F, Horlow C, Grandjean O, Vezon D, Doutriaux MP. Random chromosome segregation without meiotic arrest in both male and female meiocytes of a dmc1 mutant of Arabidopsis. Plant Cell. 1999; 11(9):1623–34. https://doi.org/10.1105/tpc.11.9.1623 PMID: 10488231.

85. Pradillo M, Lopez E, Linacero R, Romero C, Cunado N, Sanchez-Moran E, et al. Together yes, but not coupled: new insights into the roles of RAD51 and DMC1 in plant meiotic recombination. Plant J. 2012; 69(6):921–33. https://doi.org/10.1111/j.1365-313X.2011.04845.x PMID: 22066484.

86. Crismani W, Portemer V, Froger N, Chelysheva L, Horlow C, Vrielynck N, et al. MCM8 is required for a pathway of meiotic double-strand break repair independent of DMC1 in Arabidopsis thaliana. PLoS Genet. 2013; 9(1):e1003165. https://doi.org/10.1371/journal.pgen.1003165 PMID: 23300481.

87. Azumi Y, Liu D, Zhao D, Li W, Wang G, Hu Y, et al. Homolog interaction during meiotic prophase I in Arabidopsis requires the SOLO DANCERS gene encoding a novel cyclin-like protein. EMBO J. 2002; 21(12):3081–95. https://doi.org/10.1093/emboj/cdf285 PMID: 12065421.

88. De Muyt A, Pereira L, Vezon D, Chelysheva L, Gendrot G, Chambon A, et al. A high throughput genetic screen identifies new early meiotic recombination functions in Arabidopsis thaliana. PLoS Genet. 2009; 5(9):e1000654. https://doi.org/10.1371/journal.pgen.1000654 PMID: 19763177.

89. Fernandes JB, Duhamel M, Seguela-Arnaud M, Froger N, Girard C, Choinard S, et al. FIGL1 and its novel partner FLIP form a conserved complex that regulates homologous recombination. PLoS Genet. 2018; 14(4):e1007317. https://doi.org/10.1371/journal.pgen.1007317 PMID: 29608566.

90. Girard C, Chelysheva L, Choinard S, Froger N, Macaisne N, Lemhemdi A, et al. AAA-ATPase FIDGETIN-LIKE 1 and Helicase FANCM Antagonize Meiotic Crossovers by Distinct Mechanisms. PLoS Genet. 2015; 11(7):e1005369. https://doi.org/10.1371/journal.pgen.1005369 PMID: 26161528.

91. Agarwal S, van Cappellen WA, Guenole A, Eppink B, Linsen SE, Meijering E, et al. ATP-dependent and independent functions of Rad54 in genome maintenance. J Cell Biol. 2011; 192(5):735–50. https://doi.org/10.1083/jcb.201011025 PMID: 21357745.

92. Solinger JA, Kiianitsa K, Heyer WD. Rad54, a Swi2/Snf2-like recombinational repair protein, disassembles Rad51:dsDNA filaments. Mol Cell. 2002; 10(5):1175–88. https://doi.org/10.1016/s1097-2765(02)00743-8 PMID: 12453424.

93. Zhang Z, Fan HY, Goldman JA, Kingston RE. Homology-driven chromatin remodeling by human RAD54. Nat Struct Mol Biol. 2007; 14(5):397–405. https://doi.org/10.1038/nsmb1223 PMID: 17417655.

94. Argunhan B, Leung WK, Afshar N, Terentyev Y, Subramanian VV, Murayama Y, et al. Fundamental cell cycle kinases collaborate to ensure timely destruction of the synaptonemal complex during meiosis. EMBO J. 2017; 36(17):2488–509. https://doi.org/10.15252/embj.201695895 PMID: 28694245.

95. Prugar E, Burnett C, Chen X, Hollingsworth NM. Coordination of Double Strand Break Repair and Meiotic Progression in Yeast by a Mek1-Ndt80 Negative Feedback Loop. Genetics. 2017; 206(1):497–512. https://doi.org/10.1534/genetics.117.199703 PMID: 28249986.

96. Uanschou C, Ronceret A, Von Harder M, De Muyt A, Vezon D, Pereira L, et al. Sufficient amounts of functional HOP2/MND1 complex promote interhomolog DNA repair but are dispensable for intersister DNA repair during meiosis in Arabidopsis. Plant Cell. 2013; 25(12):4924–40. https://doi.org/10.1105/tpc.113.118521 PMID: 24363313.

97. Daley JM, Gaines WA, Kwon Y, Sung P. Regulation of DNA pairing in homologous recombination. Cold Spring Harb Perspect Biol. 2014; 6(11):a017954. https://doi.org/10.1101/cshperspect.a017954 PMID: 25190078.

98. Knizewski L, Ginalski K, Jerzmanowski A. Snf2 proteins in plants: gene silencing and beyond. Trends Plant Sci. 2008; 13(10):557–65. https://doi.org/10.1016/j.tplants.2008.08.004 PMID: 18786849.

99. Singh G, Da Ines O, Gallego ME, White CI. Analysis of the impact of the absence of RAD51 strand exchange activity in Arabidopsis meiosis. PLoS One. 2017; 12(8):e0183006. https://doi.org/10.1371/journal.pone.0183006 PMID: 28797117.

100. Vignard J, Siwiec T, Chelysheva L, Vrielynck N, Gonord F, Armstrong SJ, et al. The interplay of RecA-related proteins and the MND1-HOP2 complex during meiosis in Arabidopsis thaliana. PLoS Genet. 2007; 3(10):1894–906. https://doi.org/10.1371/journal.pgen.0030176 PMID: 17937504.

101. Sandhu R, Monge Neria F, Monge Neria J, Chen X, Hollingsworth NM, Borner GV. DNA Helicase Mph1(FANCM) Ensures Meiotic Recombination between Parental Chromosomes by Dissociating Precocious Displacement Loops. Dev Cell. 2020; 53(4):458–72 e5. https://doi.org/10.1016/j.devcel.2020.04.010 PMID: 32386601.

102. Alonso JM, Stepanova AN, Leisse TJ, Kim CJ, Chen H, Shinn P, et al. Genome-wide insertional mutagenesis of Arabidopsis thaliana. Science. 2003; 301(5633):653–7. https://doi.org/10.1126/science.1086391 PMID: 12893945.

103. Li W, Chen C, Markmann-Mulisch U, Timofejeva L, Schmelzer E, Ma H, et al. The Arabidopsis AtRAD51 gene is dispensable for vegetative development but required for meiosis. Proc Natl Acad Sci U S A. 2004; 101(29):10596–601. https://doi.org/10.1073/pnas.0404110101 PMID: 15249667.

104. Ross KJ, Fransz P, Jones GH. A light microscopic atlas of meiosis in Arabidopsis thaliana. Chromosome Res. 1996; 4(7):507–16. https://doi.org/10.1007/BF02261778 PMID: 8939362.

105. Armstrong SJ, Caryl AP, Jones GH, Franklin FC. Asy1, a protein required for meiotic chromosome synapsis, localizes to axis-associated chromatin in Arabidopsis and Brassica. J Cell Sci. 2002; 115(Pt 18):3645–55. https://doi.org/10.1242/jcs.00048 PMID: 12186950.

106. Higgins JD, Armstrong SJ, Franklin FC, Jones GH. The Arabidopsis MutS homolog AtMSH4 functions at an early step in recombination: evidence for two classes of recombination in Arabidopsis. Genes Dev. 2004; 18(20):2557–70. https://doi.org/10.1101/gad.317504 PMID: 15489296.

107. Kurzbauer MT, Uanschou C, Chen D, Schlogelhofer P. The recombinases DMC1 and RAD51 are functionally and spatially separated during meiosis in Arabidopsis. Plant Cell. 2012; 24(5):2058–70. https://doi.org/10.1105/tpc.112.098459 PMID: 22589466.

108. Higgins JD, Sanchez-Moran E, Armstrong SJ, Jones GH, Franklin FC. The Arabidopsis synaptonemal complex protein ZYP1 is required for chromosome synapsis and normal fidelity of crossing over. Genes Dev. 2005; 19(20):2488–500. https://doi.org/10.1101/gad.354705 PMID: 16230536.

A

```
AtRAD54  cds 561  TGTCCAGTTCATGTTCGATTGTGTTTCAGGATTACATGGTTCGGCAAATATAAATGGTTGCATTCTGGCT
rad54-2      561  TGTCCAGTTCATGTTCGATTGTGTTTCAGGATTACATGGTTCGGCAAATATAAATGGTTGCATTCTGGCT

AtRAD54  cds 631  GATGACATGGGTTTAGGGAAGACATTACAGTCCATTACTTTACTATACACACTTCTTTGTCAAGGATTTG
rad54-2      631  GATGACATGGGTTTAGGGAAGACATTACAGTCCATTACTTTACTATACACACTTCTTTGTCAAGGATTTG

AtRAD54  cds 701  ATGGGACGCCTATGGTTAAAAAGGCCATTATTGTTACACCAACGAGTCTTGTCAGTAACTGGGAAGCTGA
rad54-2      701  ATGGGACGCCTATGGTTAAAAAGGCCATTATTGTTACACCAACGAGTCTTGTCAGTAACTGGGAAGCTGA

AtRAD54  cds 771  AATTAAGAAATGGGTTGGAGACAGGATTCAGCTTATAGCCCTCTGTGAGAGCACCAGAGATGATGTTTTG
rad54-2      771  AATTAAGAAATGGGTTGGAGACAGGATTCAGCTTATAGCCCTCTGTGAGAGCACCAGAGATGATGTTTTG

AtRAD54  cds 841  TCTGGAATAGATAGTTTCACTCGACCAAGAAGCGCTTTGCAGGTACTTATCATTTCTTACGAGACATTCC
rad54-2      841  TCTGGAATAGATAGTGGTGTAAACTTAATAACACATTGATATTGTGGTGTAAACAAATTGAC--------

AtRAD54  cds 911  GAATGCACTCATCCAAGTTCTGCCAGAGTGAATCCTGTGATCTTCTAATATGCGATGAGGCTCATAGGTT
rad54-2      902  ----------------------------------------------------------------------

AtRAD54  cds 981  GAAAAATGACCAGACACTTACAAACAGGGCTTTGGCTTCATTGACATGCAAACGTCGAGTTTTGTTGTCT
rad54-2      902  ----------------------------------------------------------------------

AtRAD54  cds 1051 GGAACTCCCATGCAGAATGACTTGGAAGAGTTTTTTGCCATGGTCAACTTCACAAATCCAGGGAGTTTAG
rad54-2      902  ----------------------------------------------------------------------

AtRAD54  cds 1121 GTGATGCTGCACACTTTCGCCATTATTATGAGGCACCTATTATATGTGGAAGAGAACCTACAGCCACTGA
rad54-2      902  ----------------------------------------------------------------------
```

B

```
AtRAD54      MEEEDEEILSSSDCDDSSDSYKDDSQDSEGENDNPECEDLAVVSLSSDADRKSKNVKDLL   60
rad54-2      MEEEDEEILSSSDCDDSSDSYKDDSQDSEGENDNPECEDLAVVSLSSDADRKSKNVKDLL   60
             ************************************************************

AtRAD54      RGNLVVQRQPLLPRVLSVSDGAAVCRKPFKPPCSHGYDSTGQLSRRLSARKRFVPWGSST   120
rad54-2      RGNLVVQRQPLLPRVLSVSDGAAVCRKPFKPPCSHGYDSTGQLSRRLSARKRFVPWGSST   120
             ************************************************************

AtRAD54      PVVVALPTKLEASTNIERDEEEEVVCLPPDIEPLVLWQSEEDGMSNVTTIMVHSVLVKFL   180
rad54-2      PVVVALPTKLEASTNIERDEEEEVVCLPPDIEPLVLWQSEEDGMSNVTTIMVHSVLVKFL   180
             ************************************************************

AtRAD54      RPHQREGVQFMFDCVSGLHGSANINGCILADDMGLGKTLQSITLLYTLLCQGFDGTPMVK   240
rad54-2      RPHQREGVQFMFDCVSGLHGSANINGCILADDMGLGKTLQSITLLYTLLCQGFDGTPMVK   240
             ************************************************************
                                                I

AtRAD54      KAIIVTPTSLVSNWEAEIKKWVGDRIQLIALCESTRDDVLSGIDSFTRPRSALQVLIISY   300
rad54-2      KAIIVTPTSLVSNWEAEIKKWVGDRIQLIALCESTRDDVLSGIDSGVNLITH*-------   292
             *********************************************** .. :
                Ia

AtRAD54      ETFRMHSSKFCQSESCDLLICDEAHRLKNDQTLTNRALASLTCKRRVLLSGTPMQNDLEE   360
rad54-2      ------------------------------------------------------------   292
                                    II                        III

AtRAD54      FFAMVNFTNPGSLGDAAHFRHYYEAPIICGREPTATEEEKNLAADRSAELSSKVNQFILR   420
rad54-2      ------------------------------------------------------------   292

AtRAD54      RTNALLSNHLPPKIIEVVCCKMTTLQSTLYNHFISSKNLKRALADNAKQTKVLAYITALK   480
rad54-2      ------------------------------------------------------------   292

AtRAD54      KLCNHPKLIYDTIKSGNPGTVGFENCLEFFPAEMFSGRSGAWTGGDGAWVELSGKMHVLS   540
rad54-2      ------------------------------------------------------------   292

AtRAD54      RLLANLRRKTDDRIVLVSNYTQTLDLFAQLCRERRYPFLRLDGSTTISKRQKLVNRLNDP   600
rad54-2      ------------------------------------------------------------   292
                                    IV

AtRAD54      TKDEFAFLLSSKAGGCGLNLIGANRLVLFDPDWNPANDKQAAARVWRDGQKKRVYVYRFL   660
rad54-2      ------------------------------------------------------------   292
                                V                           VI

AtRAD54      STGTIEEKVYQRQMSKEGLQKVIQHEQTDNSTRQGNLLSTEDLRDLFSFHGDVRSEIHEK   720
rad54-2      ------------------------------------------------------------   292

AtRAD54      MSCSRCQNDASGTENIEEGNENNVDDNACQIDQEDIGGFAKDAGCFNLLKNSERQVGTPL   780
rad54-2      ------------------------------------------------------------   292

AtRAD54      EEDLGSWGHHFTSKSVPDAILQASAGDEVTFVFTNQVDGKLVPIESNVSPKTVESEEHNR   840
rad54-2      ------------------------------------------------------------   292

AtRAD54      NQPVNKRAFNKPQQRPREPLQPLSLNETTKRVKLSTYKRLHGNSNIDDAQIKMSLQRPNL   900
rad54-2      ------------------------------------------------------------   292

AtRAD54      VSVNHDDDFV      910
rad54-2      ----------      292
```

S1 Fig. Sequence of RAD54/T-DNA junction in rad54-2 allele and corresponding putative predicted protein.
(A) pairwise alignment between AtRAD54 coding sequence (cds) and sequence from T-DNA left border amplification at the T-DNA insertion site in the *rad54-2* allele. An in-frame TGA stop codon is highlighted in cyan. T-DNA insertion derived nucleotides deletion is highlighted in grey. **(B)** Pairwise alignment of the Arabidopsis RAD54 protein and the putative predicted protein from the *rad54-2* allele. Alignment was generated using clustalOmega. Numbers indicate amino acid positions. Under the sequences, asterisks, colons and full stops indicate identical, conserved and semi-conserved residues, respectively. The seven conserved ATPase motifs are indicated with black boxes and red roman numerals. These motifs define the two RecA-like domains (parts defined by green and blue lines, respectively), which constitute the "core" translocation motor domains. If translated, the truncated protein from the *rad54-2* allele would lack these two recA-like domains.

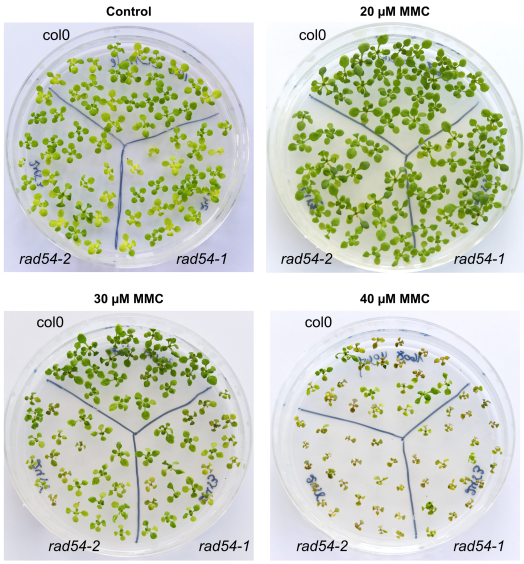

S2 Fig. Sensitivity of *rad54-1* and *rad54-2* plants to MMC.
Shown are representative photographs of two-week-old seedlings grown without or with the indicated concentrations of MMC.

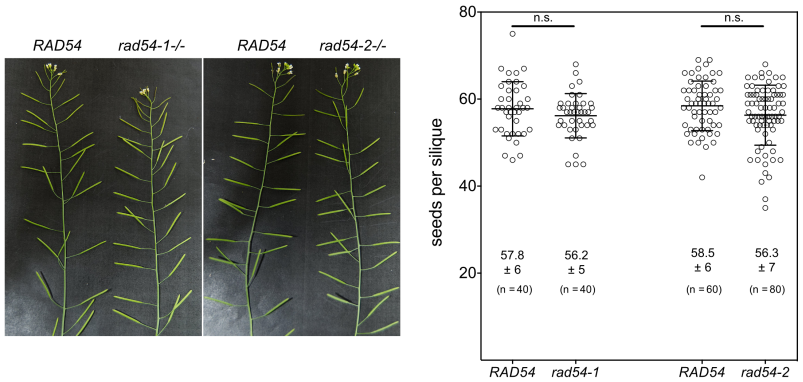

S3 Fig. Fertility of *rad54-1* and *rad54-2* mutants.
(A) pictures of wild-type and *rad54* mutant siliques. (B) Number of seeds per silique in Wild-type, *rad54-1* and *rad54-2* mutants. Each point represents the number of seeds in one silique. Bars indicate mean ± SD. n.s.: not significantly different. $P > 0.05$ (unpaired, two-tailed Mann-Whitney test).

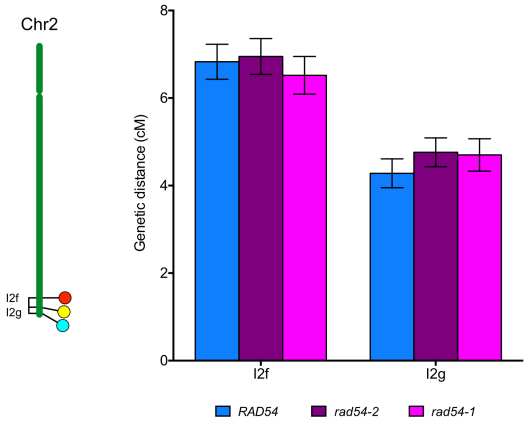

S4 Fig. Genetic recombination in wild-type, *rad54-1* and *rad54-2* mutants measured using I2fg fluorescent-tagged lines.
Genetic distances (in centiMorgans, cM) calculated from tetrad analysis of the I2f and I2g intervals on chromosome 2. Bars indicate mean ± SD. For both intervals, WT and *rad54* plants do not significantly differ ($p<0.05$; Z-test).

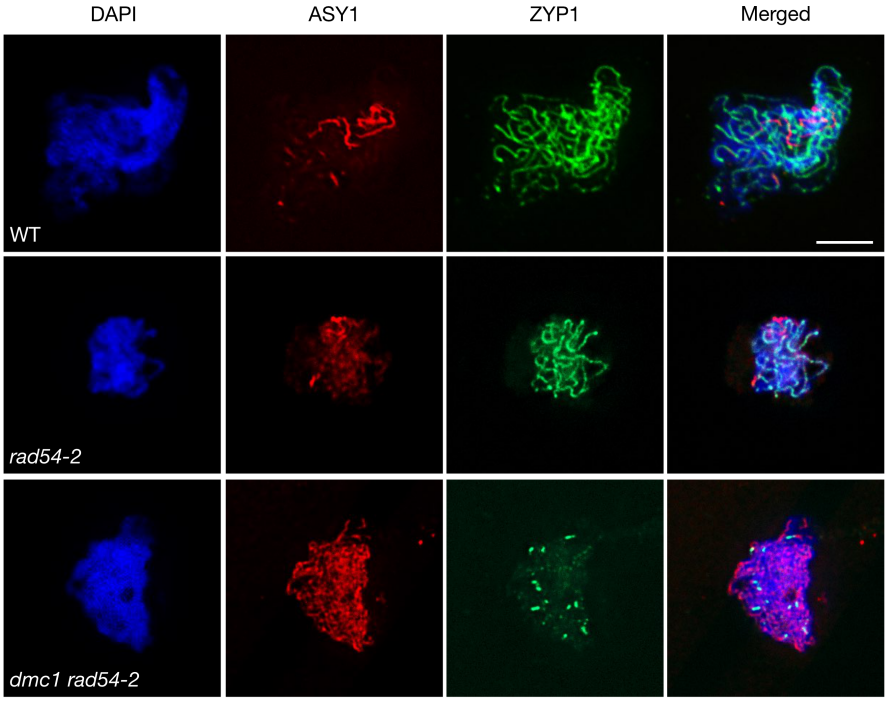

S5 Fig. Absence of synapsis in *dmc1 rad54* mutant plants.
Immunolocalization in wild-type, *rad54-2* and *dmc1 rad54-2* meiocytes shows that synaptonemal complex transverse filament protein, ZYP1, is not correctly loaded along chromosome axes in *dmc1 rad54-2* indicating lack of synapsis. DAPI (blue), ASY1 (red), ZYP1 (green) and merged images are shown. (Scale Bar: 5 μm).

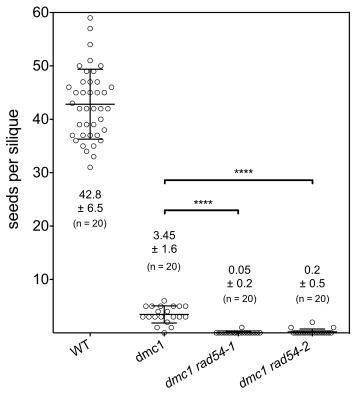

S6 Fig. Fertility of *dmc1 rad54-1* and *dmc1 rad54-2* mutant plants.
Number of seeds per silique in Wild-type, *dmc1*, *dmc1 rad54-1* and *dmc1 rad54-2* mutants. Each spot represents the number of seeds in one silique. Bars indicate mean ± SD. ****: significantly different. $P < 0.0001$ (unpaired, two-tailed Mann-Whitney test).

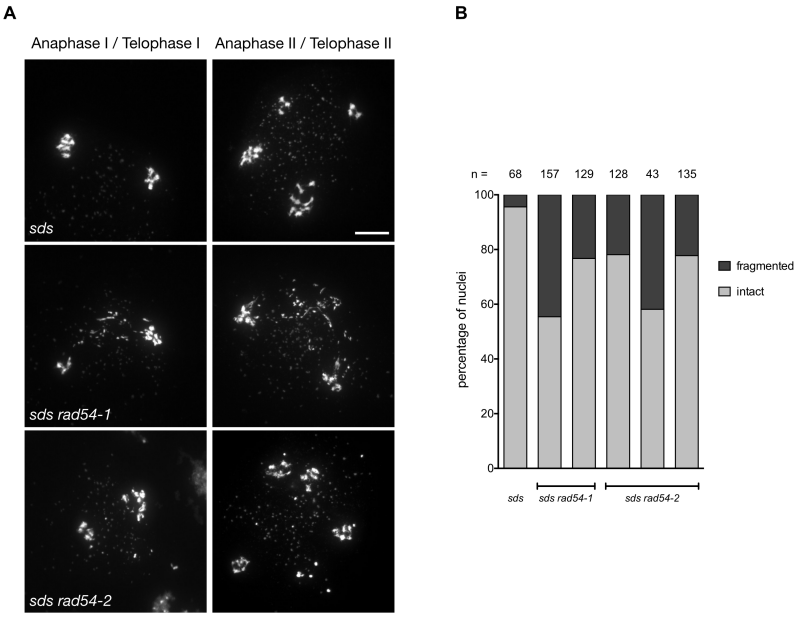

S7 Fig. Absence of RAD54 leads to partial chromosome fragmentation in *sds* meiosis.
(A) Male meiosis is shown in wild-type, *sds rad54-1*, and *sds rad54-2*. Chromosomes were spread and stained with DAPI. (Scale bar = 10 μm). **(B)** Quantification of male meiocytes showing intact chromosomes or fragmentation. Each bar represents one plant.

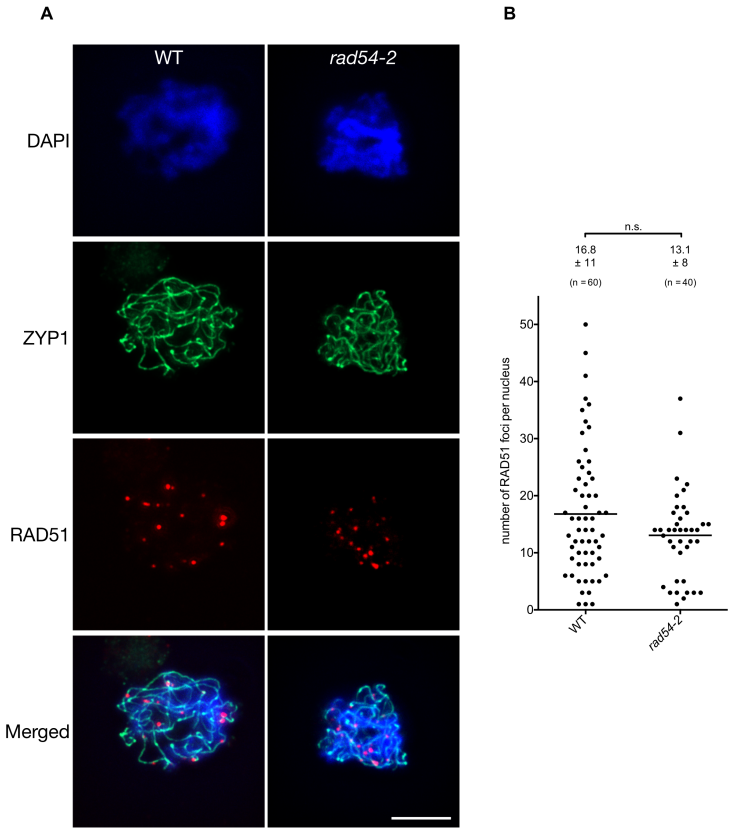

S8 Fig. RAD51 foci in wild type and *rad54* mutant pachytene cells.
(A) Dual immunolocalization of ZYP1 (green) and RAD51 (red) in wild-type and *rad54-2* pachytene cells. (Scale Bar: 5 µm). **(B)** Quantification of RAD51 foci per positive pachytene cell in wild-type and *rad54-2* mutants. Means ± SD are indicated. n.s.: not significantly different (p-value > 0.05, unpaired, two-tailed Mann-Whitney test).a

FTLs raw data and Interference ratio calculation.

I2f I2g	Total	a	b	c	d	e	f	g	h	i	j	k	l
Wild-type	**1801**	1403	244	151	2	0	0	0	0	1	0	0	0
rad54-1	**1542**	1198	199	143	0	1	0	1	0	0	0	0	0
rad54-2	**2006**	1544	270	188	0	2	0	1	1	0	0	0	0

I1b I1c	Total	a	b	c	d	e	f	g	h	i	j	k	l
Wild-type	**1311**	577	206	464	13	16	9	13	2	11	0	0	0
rad54-2	**1381**	625	186	514	16	5	11	10	2	9	0	2	1

Interference ratio (IR) calculation (according to Berchowitz and Copenhaver, Nature protocol, 2008)

X1 = Genetic distance for I1 with adjacent CO in I2 = (1/2(D+E+F+G+K)+3(J+L)) / (C+D+E+F+G+I+J+K+L)
X2 = Genetic distance for I1 without adjacent CO in I2 = ((1/2B)+3(H)) / (A+B+H)
IR = X1/X2

	IR I2fg		
	X1	X2	IR
WT	0.006	0.074	0.088
rad54-1	0.007	0.071	0.097
rad54-2	0.008	0.076	0.103

	IR I1bc		
	X1	X2	IR
WT	0.048	0.139	0.349
rad54-2	0.044	0.122	0.361

S1 Table. FTLs raw data and Interference ratio calculation.
Tetrad count for all tetrad categories for I1bc and I2fg intervals. Tetrad categories (a to l) were classified as described previously by Berchowitz and Copenhaver (2008).

		seeds / silique																					
		S1	S2	S3	S4	S5	S6	S7	S8	S9	S10	S11	S12	S13	S14	S15	S16	S17	S18	S19	S20	Mean	pooled Mean	SD
RAD54-1	plant 1	67	52	53	53	51	50	57	63	64												57		
	plant 2	46	52	57	55	58	60	52	57	62	62	58	47	58	59	57						56	58	6.2
	plant 3	67	56	60	58	75	52	47	66	63	58	53	58	64	60	66						60		
rad54-1	plant 1	54	45	59	59	53	54	45	59	57	58											54		
	plant 2	68	59	54	55	47	57	57	66	51	55	54	57	55	57	51						56	56	5.1
	plant 3	58	58	61	64	57	55	45	63	58	57	58	61	53	54	59						57		
RAD54-2	plant 1	62	69	62	68	66	66	69	56	65	55	60	59	64	64	62						63		
	plant 2	51	52	58	55	63	59	57	60	52	50	61	50	50	63	57						56		
	plant 3	59	66	60	59	61	54	61	42	59	58	53	65	53	54	52						57	58	5.7
	plant 4	67	57	53	57	62	52	66	53	59	54	62	60	57	58	49						58		
rad54-2	plant 1	45	61	46	59	52	60	62	62	65	61	48	61	58	56	56						57		
	plant 2	59	60	65	61	58	55	54	61	35	37	46	53	53	58	63						55		
	plant 3	46	68	59	58	54	42	50	65	56	54	55	54	56	55	49						55	56	6.9
	plant 4	56	55	59	56	55	55	41	47	55	43	48	46	56	59	54						52		
	plant 5	61	60	63	61	61	62	60	56	66	64	62	63	56	60	63	57	65	57	65	66	61		

		seeds / silique												
		S1	S2	S3	S4	S5	S6	S7	S8	S9	S10	Mean	pooled Mean	SD
WT	plant 1	38	45	50	45	46	49	36	50	37	39	44		
	plant 2	43	42	54	42	45	45	35	49	46	33	43	43	6.6
	plant 3	37	47	31	37	40	42	36	47	45	47	41		
	plant 4	59	35	57	42	39	39	51	42	34	37	44		
dmc1	plant 1	0	1	3	5	3	4	4	1	2	6	3	3	1.6
	plant 2	3	5	5	5	5	3	5	3	3	3	4		
dmc1 rad54-1	plant 1	0	0	0	0	0	0	0	1	0	0	0.1	0.05	0.2
	plant 2	0	0	0	0	0	0	0	0	0	0	0.0		
dmc1 rad54-2	plant 1	0	1	0	0	0	0	0	0	0	0	0.1	0.20	0.5
	plant 2	0	0	0	0	0	1	2	0	0	0	0.3		

RAD51 foci per nucleus			
WT	*rad54-2*	*dmc1*	*dmc1 rad54-2*
74	78	80	76
69	91	106	84
89	118	91	80
68	95	119	79
82	103	127	101
72	58	71	86
103	94	107	95
91	71	90	115
75	81	125	111
73	115	89	116
97	65	102	72
79	90	99	85
119	80	77	80
67	94	78	79
72	74	87	93
73	100	95	77
78	109	108	109
72	77	101	72
76	56	85	92
77	86	68	96
75	107	119	113
155	122	121	80
138		114	93
132		113	127
188		72	81
114		175	98
101		133	128
127		83	72
58		84	100
79		81	96
74		54	95
82		97	112
64		96	78
65		104	104
123		91	86
		85	102
		97	106
		113	89
		190	86
		84	112
		107	88
		86	117
		94	111
		77	87
		106	103
		80	82
		82	115
		75	88
		69	115
		82	85
			72
			78
			109
			133
			67
			81
Mean	**91**	**89.27**	**97**	**94**
SD	**29.3**	**18.7**	**24.6**	**16.3**

RAD51 foci in pachytene	
WT	*rad54-2*
31	31
35	3
17	5
25	11
20	37
26	12
16	12
1	14
5	17
1	3
8	12
8	14
33	5
14	11
10	14
11	23
6	15
20	14
36	2
16	22
45	14
14	10
10	14
28	14
10	18
50	21
41	15
13	12
1	1
9	18
12	13
9	3
23	15
11	3
5	4
37	17
8	20
17	14
16	16
12	3
20	
5	
13	
22	
21	
5	
18	
12	
12	
3	
14	
32	
6	
6	
17	
24	
26	
3	
16	
23	
Mean	**16.8**	**13.1**
SD	**11.3**	**7.7**

S1 Data. Raw data for fertility and RAD51 foci countings.
This are numerical data that supports the findings of this study.

Conclusions

Revisiting the initial hypothesis and the objectives proposed at the beginning of this project, we may conclude that:

I) Characterisation of *rad54* mutants confirms that Arabidopsis meiosis is not affected by the absence of RAD54. Mutants of RAD54 with impaired somatic DSB repair show normal meiotic progression, recombination rate and crossover interference.

II) In the absence of DMC1, RAD54-dependent, RAD51-mediated DSB repair becomes essential during meiosis. This concords with current understanding that RAD51 plays a non-catalytic, supporting role for DMC1-mediated strand exchange activity during wild-type meiosis. When DMC1 is not present, RAD51 must catalyse strand-exchange and to do so requires the presence of RAD54.

III) RAD54 is not required for meiotic RAD51 nucleofilament formation and this is not affected by the presence or absence of DMC1. This indicates that RAD54 meiotic activity is rather at the level of assisting RAD51 nucleofilament function than RAD51 nucleofilament formation.

IV) The somatic roles of the RAD51 paralogues RAD51B, RAD51D and XRCC2 assisting RAD51-mediated DSB repair are not conserved during Arabidopsis meiosis.

Our initial hypothesis – the apparent lack of meiotic role of RAD54 could simply be a consequence of RAD51's non-catalytic role in supporting DMC1 function in meiosis – has been thus validated, helping to deepen the understanding of RAD51 and DMC1 roles during meiosis in Arabidopsis and providing a parsimonious explanation for the apparent absence of function of RAD54 in wild-type meiosis.

Interestingly, this is not so for RAD51B, RAD51D and XRCC2. Thus, while RAD51 is the recombinase in charge of catalysing homology search and strand exchange in somatic cells and meiotic cells lacking DMC1, the needs for cofactors assisting these processes are different. Given that the function of RAD51B, RAD51D and XRCC2 promoting RAD51 nucleofilament activity seems instrumental for somatic HR in Arabidopsis and in eukaryotes in general, we believe that this result poses an interesting challenge in the understanding of RAD51 nucleofilament function.

Future work

This surprising contrast between the results concerning RAD54 and those with the RAD51 paralogues during somatic and RAD51-mediated meiotic DSB repair opens the door for future research on the topic.

In this regard, it might interesting to delve into the *in vitro* biochemical characterization of DMC1 and RAD51 presynaptic filament formation, function and the action of their modulators using purified Arabidopsis proteins.

In vivo, we believe that current technical limitations in the molecular analysis of meiotic recombination outcomes restrict these kind of studies to the detection of strong impairments of meiotic DSB repair. As mentioned in the introduction and as addressed in more detail in the next chapters, the difficulties detecting non-crossover products of recombination as well as any event involving the sister chromatid (if there are) in Arabidopsis are a limiting factor to detect subtle consequences of the impairment of a repair pathway if it is not a crossover formation pathway (less than 5% of DSBs) or if it cannot be compensated by other pathways (thus we see DNA fragmentation or chromosomal bridges). The use of precisely localised and frequently broken DSB hotspots in other organisms, whether engineered or endogenous, has facilitated the detailed mechanistic analyses via the exploration of meiotic recombination intermediates with southern blots and 2D gels and more modern NGS-based approaches using gene conversion tracts in the products to reconstruct meiotic recombination events. We believe than a successful application of technologies such as CRISPR/Cas to induce events at precise locations or the development of techniques that permit to detect and identify recombination events irrespective of their location and polymorphic marker density, which has been another limiting factor apparently to score NCO events in Arabidopsis, might set new standards for mutant studies when their effects are more subtle, potentially uncovering roles or functions yet to be described.

CHAPTER III. Targeted introduction of double-strand breaks at early meiosis in Arabidopsis using CRISPR/Cas9

The targeting of DSBs and use of meiotic DSB hotspots for molecular studies of the mechanisms and regulation of meiotic recombination remains a challenge in *Arabidopsis thaliana* and other plant species. If available, fine-scale targeting of the initiation points of meiotic recombination events would offer:

I) a pre-determined window including a detailed overview of the genetic and epigenetic landscape of the site for observation and analysis of events of interest;

II) the discrete initiation point of these events would facilitate the analysis of downstream recombination intermediates and/or products, as well as offer the potential to control the directionality of HR events by inducing the cleavage site in one of the two homologous chromosomes;

III) a tool for reproducible analysis and comparison of meiotic recombination in individuals with different genetic backgrounds, local landscapes or subjected to treatments or conditions.

The recently published mapping of SPO11-oligonucleotides in Arabidopsis revealed thousands of endogenous meiotic DSB hotspots, distributed throughout the genome [361]. However, no common DNA sequence motif (such as the PRDM9 motif in most vertebrates) or any other signature that may serve to centre to some extent the initiation of recombination events was identified within them. Arabidopsis DSB hotspots are rather wide regions of enrichment of DSBs with respect to other organisms (≈900bp mean versus ≈150bp in mouse or ≈250bp in budding yeast) [357,361,389]. To our knowledge, no extensive study mapping individual recombination events to the reported DSB hotspots has been published in Arabidopsis, as has been done in mouse for example [775]. A reverse approach has been explored, mapping SPO11-oligo density along known Arabidopsis crossover hotspots. Surprisingly, although recombination rate and SPO11-oligo density positively correlate at chromosomal scale, no positive correlation is found at finer scales in these locations [361,798]. In order to interpret this apparently contradictory result, it is important to recall that the crossover marks the site of the resolution of a recombination event and the proximity of the initiation and resolution sites may be influenced by a number of factors. These include variability in resection-track length and symmetry with respect to the DSB site, occurrence of multiple rounds of end invasion and dissolution, migration of Holliday junctions and presence and density of interhomologue polymorphisms. Notwithstanding these considerations, the non-

correlation between DSB density and recombination rate at crossover hotspot does suggest a great variability in DSB positioning and thus complicates the analysis of meiotic recombination outcomes and their mechanistic details based on the use of endogenous DSB hotspots.

An interesting alternative to the study of endogenous DSB hotspots has been the targeted introduction of DNA breaks at desired locations. Among the systems used to induce meiotic DSBs, those introduced by nucleases such as HO, I-SceI or VDE have been proven to be able to be repaired via the canonical meiotic recombination pathways followed by SPO11-catalysed DSBs [816–820]. These nucleases are however site-specific, meaning that they target a defined recognition sequence which, in species such as Arabidopsis, would involve the integration of these sequences via T-DNA transformation. This approach has thus two main drawbacks: I) the limitation of studying the repair of a transgene T-DNA sequence, not an Arabidopsis endogenous genomic sequence; and II) the random nature of T-DNA integration, hindering the control over the genomic, genetic and epigenetic context of the site.

The emergence of CRISPR/Cas as a versatile, efficient and easy-to-engineer tool to target and cleave any endogenous sequence adjacent to a PAM motif of the Cas version of choice opens the door for the induction of localised DSBs during meiosis for this type of studies [821,822]. Among the different CRISPR/Cas systems, those including Cas9 are able to induce blunt ended DSBs, presumably a proper substrate for repair via meiotic recombination pathways.

Initial hypothesis

Considering the potential of the CRISPR/Cas9 technology to induce DSBs at high efficiency and at desired genomic locations with single-base level control of the cleavage site, we hypothesised that CRISPR/Cas9-induced DSBs at early meiosis in Arabidopsis will be repaired via the canonical meiotic recombination pathways, including the formation of interhomologue crossovers. As discussed above, the successful application of such tool permitting the targeting of meiotic recombination would be of great importance for the application and study of meiotic recombination in the model plant.

Objectives

I) To design CRISPR/Cas9 constructs that are expressed at early meiosis in Arabidopsis targeting multiple genomic locations.

II) To test the cleavage capabilities of these constructs in Arabidopsis somatic tissue by analysing the mutational profile of the target sites.

III) To test for the formation of CRISPR/Cas9-induced interhomologue crossovers using a fluorescent pollen marker system to measure the genetic distances of chromosomal intervals spanning the different target sites.

IV) To detect products of CRISPR/Cas9-induced meiotic recombination at single molecule level via next-generation sequencing and analysis of gene conversion tracts in hybrid plants.

Methods

Plant material and growing conditions

The *Arabidopsis thaliana* ecotypes and strains used in this work (which did not require selection of transformants, Table 2) were sown on soil substrate (Klasmann-Deilmann GmbH TS 3® Geeste, Germany), stratified for 2-4 days at 4°C and subsequently grown in a climate chamber at 23°C and 60% relative humidity under a daily cycle of 16 hours of light (110-140µmol m^{-2} s^{-1}) and 8 hours of darkness. Transgenic seeds obtained via *Agrobacterium tumefaciens*-mediated transformation that required the application of chemical treatments for the selection of positive transformants were sterilized for 5 minutes with 75% ethanol/0.05% SDS, rinsed for 5 minutes with 75% ethanol and air-dried. Sterilized seeds were sown on plates with 0.8% agar 1/2-diluted Murashige and Skoog (MS) medium supplemented with the appropriate concentration of the selective agent (Table 6), stratified for 2-4 days at 4°C and placed in growth chambers under the same growing conditions as the plants shown on soil. When the positive transformants could be visually identified they were transferred from plate to soil and placed again in the growth chamber. These conditions were applied as well for the experimental work of Chapter IV.

Table 2. Arabidopsis thaliana strains.

Strain name	Ecotype	Genotype	Catalogue code	Origin
Col-0	Columbia (Col-0)	WT		
Ler-0	Landsberg (Ler-0)	WT		
rad54-1	Columbia (Col-0)	RAD54 -/-	SALK_088057	[237]
rad54-2	Columbia (Col-0)	RAD54 -/-	SALKseq_124992	[823]
dmc1-2	Columbia (Col-0)	DMC1 +/-	SAIL_170_F08	[824]
rad51-1	Columbia (Col-0)	RAD51 +/-	GABI-KAT 134A01	[825]
rad51b-1	Columbia (Col-0)	RAD51B -/-	SALK-024755	[236]
rad51d-3	Columbia (Col-0)	RAD51D -/-	SAIL_564_A06	[233]
xrcc2-1	Columbia (Col-0)	XRCC2 -/-	SALK-029106	[236]
xrcc3	Columbia (Col-0)	XRCC3 +/-	SALK_045564	[235]
sds-2	Columbia (Col-0)	SDS +/-	SAIL-129-F09	[328]
spo11-1-2 *	Columbia (Col-0)	SPO11 +/-	TAIR Accession polymorphism:4515087631	[307]

FTL I1bc	Columbia (Col-0)	FTL567-YFP/ FTL1262-DsRed2/FTL992-AmCyan/ QRT1 +/-		[826]
FTL I2fg	Columbia (Col-0)	FTL800-DsRed2/FTL3411-YFP/FTL3263-AmCyan/ QRT1 +/-		[826]
FTL CEN3	Columbia (Col-0)	FTL3332-YFP/FTL2536-DsRed2/QRT1 +/-		[826]

*Strain corresponding to Chapter IV.

Molecular genotyping of Arabidopsis plants

Arabidopsis leaf fragments were placed into 2ml Eppendorf tubes with 40µl ice-cold DNA extraction buffer (100mM Tris-HCl pH9.5, 250mM KCl, 10mM EDTA) and macerated, either manually using blunted micropipette tips or in batches with a 5mm diameter stainless steel grinding bead per tube and shaking the tubes in a TissueLyser II® (Qiagen) two times 30s at $30s^{-1}$. The macerated solution was incubated for 10 minutes at 96°C and 5 minutes at 4°C in a thermocycler, put back on ice and 40µl of dilution buffer (3% w/v BSA in water) was added. The tubes were centrifuged for one minute at maximum speed in a microcentrifuge to pellet the remaining leaf tissue fragments and use the extracted genomic DNA in solution for polymerase chain reaction (PCR).

In the case of T-DNA mutant lines, oligo combinations to differentially amplify the wild-type allele and the T-DNA insertion allele were used to genotype individual plants. For CRISPR-Cas9-transformed lines, oligos annealing inside the T-DNA were used to identify plants carrying the insertion (Table 3). The PCR mix (Table 4) was prepared with the appropriate oligonucleotides to prime the amplification of the desired fragment and loaded in a thermocycler for 35 cycles (Table 5). To visualize the PCR products, 10µl of the reaction mix were loaded in a 0.8% w/v agarose gel in 0.5x TBE buffer with 0.2µg/ml ethidium bromide along with an Invitrogen 1kb+ ladder, ran for 30 minutes and photographed with a Syngene U:GENIUS^3 gel documentation system. These method was followed as well for the molecular genotyping of Chapter IV plant material.

Table 3. PCR primers.

Name	Target	Orientation	Sequence (5'-3')	Annealing temperature
***rad54-1* #1**	RAD54	Forward	GCTTCAAAAAGTTATTCAGCA	55°C
***rad54-1* #2**	RAD54	Reverse	TTGTGGTCTCGTTGAGAGATA	55°C
***rad54-2* #1**	RAD54	Forward	GCTTGTCAAATTTCTTCGCC	55°C
***rad54-2* #2**	RAD54	Reverse	ATGTCAATGAAGCCAAAGCC	55°C
***dmc1-2* #1**	DMC1	Forward	GACTCATTGTTGCTTGATCCC	55°C
***dmc1-2* #2**	DMC1	Reverse	TCCACTCGGAATAAAGCAATG	55°C
***rad51-1* #1**	RAD51	Forward	TGCCGTATGCTCAACAGGAGGT	55°C
***rad51-1* #2**	RAD51	Reverse	GAACGCTATTGTGATCTCATGTG TGTTACA	55°C
***rad51b-1* #1**	RAD51B	Forward	GAGTTAGTTGGTCCTCCTGG	56°C
***rad51b-1* #2**	RAD51B	Reverse	AAATTCAGCAAGCGATCTGG	56°C
***rad51d-3* #1**	RAD51D	Forward	TGGCTTTCTTTGTGGGTTTCT	58°C
***rad51d-3* #2**	RAD51D	Reverse	CAATGGTTAACAGTTGTGCGG	58°C
***xrcc2-1* #1**	XRCC2	Forward	TAGTCCAATGTAACTTTCGCAG	56°C
***xrcc2-1* #2**	XRCC2	Reverse	GTCACGAGACAATGACAATACC	56°C
***xrcc3* #1**	XRCC3	Forward	ATGCAAAATGGGAAAATTAAGC CG	58°C
***xrcc3* #2**	XRCC3	Reverse	CTACGCTTGAACCGCACAAATC	58°C
***sds-2* #1**	SDS	Forward	CTGCTCCCTGATTACAAGCAG	55°C
***sds-2* #2**	SDS	Reverse	CTTAACGCATTCAGGCAACTC	55°C
spo11-1-2* #1	SPO11	Forward	GGATCGGGCCTAAAAGCCAACG	56°C
spo11-1-2* #2	SPO11	Reverse	CTTTGAATGCTGATGGATGCATG TAGTAG	56°C
SALK LB1	SALK T-DNA	Forward	TGGTTCACGTAGTGGGCCATCG	55°C
SAIL LB2	SAIL T-DNA	Forward	GCTTCCTATTATATCTTCCCAAA TTACCAATACA	55°C
GABI LB	GABI T-DNA	Reverse	ATATTGACCATCATACTCATTGC	55°C
Cas9 T-DNA #1	Cas9 T-DNA	Forward	GAATTCAGCGAGAGCCTGAC	55°C
Cas9 T-DNA #1	Cas9 T-DNA	Reverse	ACATTGTTGGAGCCGAAATC	55°C
sgRNA T-DNA #1	sgRNA T-DNA	Forward	GAAGAACTCGTCAAGAAGG	55°C
sgRNA T-DNA #1	sgRNA T-DNA	Reverse	ATGACGCACAATCCCACTATCC	55°C
I1bc site 2 NGS #1	I1bc site 2	Forward	TCGTCGGCAGCGTCAGATGTGT ATAAGAGACAGCTTTGATGTAA GGTTAAGAGTTTAAGATTC	58°C
I1bc site 2 NGS #2	I1bc site 2	Reverse	GTCTCGTGGGCTCGGAGATGTG TATAAGAGACAGACCATTGTTTT GGTTTTTATGATAATTG	58°C

I1bc site 2 NGS #3	I1bc site 2	Reverse	GTCTCGTGGGCTCGGAGATGTG TATAAGAGACAGACAAATATTAA CCAATCATGTCACTAAG	58°C
CEN3 site 1 NGS #1	CEN3 site 1	Forward	TCGTCGGCAGCGTCAGATGTGT ATAAGAGACAGACCCATTTTAGA GAGTGGTTTG	58°C
CEN3 site 1 NGS #2	CEN3 site 1	Reverse	GTCTCGTGGGCTCGGAGATGTG TATAAGAGACAGCCGGTCTGAA AATGGTGATTAT	58°C
Nextera® dual index oligos	P5 & P7 tags	Nextera® XT Index Kit v2 (FC-131-1096)		
NEBNext® dual index oligos	P5 & P7 tags	NEBNext® Ultra™ II FS DNA Library Prep Kit for Illumina® (NEB #7805S/L)		

*Primers corresponding to Chapter IV.

Table 4. Genotyping PCR reaction.

Components	Volume (µl)
Genomic DNA	1
5x GoTaq® buffer	4
$MgCl_2$ (concentration)	1.6
dNTPs mix (10mM)	0.4
Forward primer (10µM)	1
Reverse primer (10µM)	1
GoTaq® DNA polymerase	0.1
Ultra-pure distilled water	10.9

Table 5. Genotyping PCR program.

Steps	Temperature	Time	
Initial denaturation	95°C	2min	
Denaturation	95°C	30s	x35
Annealing	50-60°C	30s	
Extension	72°C	60-90s	
Final extension	72°C	5min	
Storage	4°C	∞	

CRISPR-Cas9 design and cloning

In this work we have used human codon-optimised *Streptococcus pyogenes* Cas9 [827], obtained from Addgene (Boston, USA). pRAD51::Cas9 or pDMC1::Cas9 expression vectors suitable for Arabidopsis transformation were built as follows. The SpCas9 gene, originally encoded within an *att*L-containing entry clone suitable for Gateway® cloning, was transferred via Gateway® LR recombination reaction into *att*R-containing destination vectors to generate expression constructs driven by the promoter of the *Arabidopsis thaliana* RAD51 and DMC1 genes plus and estradiol-inducible promoters [234,828]. The Gateway® LR recombination reactions were carried out as specified by the Invitrogen Gateway® LR clonase™ II kit (Table 8) and incubated at room temperature for one hour after which one microliter of the LR reaction was used to transform 50µl of chemically competent DH5α™ cells following the manufacturer's protocol (Invitrogen). The next day, individual colonies were picked and inoculated into liquid culture to perform plasmid isolation and purification as previously described. The plasmid constructs were verified by restriction enzyme-based plasmid fingerprinting.

The crRNAs for the different target sites were designed to fulfil the following criteria: I) 20 nucleotide sequences complementary to an *Arabidopsis thaliana* Col-0 genomic sequence target; II) adjacent to a NGG triplet downstream (3') the complementary gDNA strand to the homologous sequence (Cas9 PAM); III) unique in the genome to prevent off-site cleavage; and IV) including DNA sequence polymorphisms in the corresponding Ler-0 genomic sequence to impede Cas9 cleavage in the Ler-0 chromosome in Col-0/Ler-0 hybrid plants. For this purpose, a set of potential Cas9 sites over the Arabidopsis Columbia genome meeting these criteria was generated by an in-house bioinformatics script (R. Pogorelcnik and C. White, unpublished). After the sites were chosen, we ordered syntheses (Integrated DNA technologies, https://eu.idtdna.com) of linear dsDNA molecules encoding the different sgRNAs (crRNA + tracrRNA) under the *Arabidopsis thaliana* U6-29 promoter flanked by *att*B sequences for Gateway cloning into a pDONR™ vector. These were used in Gateway® BP recombination reactions as detailed in the Invitrogen Gateway® BP clonase™ II kit protocol (Table 7), incubated for one hour at room temperature and the product was transformed into chemically competent DH5α™ cells, positive clones were selected and the plasmids were isolated and purified. These sgRNA constructs were transferred to via Gateway® LR recombination reactions into an *att*R-containing destination vector (Table 6) to generate the binary expression vectors compatible with Arabidopsis transformation as described above for the Cas9 expression vectors.

Table 6. Plasmids.

Plasmid name	Backbone	Nature	Selective agent in bacteria	Selective agent in plant
pDMC1 destination vector	pMDC32 [828]	*att*R-containing Gateway® destination vector	Kanamycin (concentration)	Hygromycin (concentration)
pRAD51 destination vector	pMDC32 [828]	*att*R-containing Gateway® destination vector	Kanamycin (concentration)	Hygromycin (concentration)
Cas9	pDONR221	*att*L-containing Gateway® entry clone	Kanamycin (concentration) Ccdb	
pDONR™/ Zeo	pDONR™/Zeo	*att*L-containing Gateway® entry clone	Zeocin (concentration) Ccdb	
pCW555 destination vector	pMDC100 [828]	*att*R-containing Gateway® destination vector	Kanamycin (concentration)	Kanamycin (concentration)

Table 7. Gateaway BP reaction.

Components	Volume (µl)
***att*B-linear product (40-100fmol)**	1-10
pDONR™ vector (150ng/µl)	2
5x BP clonase™ reaction buffer	4
TE buffer pH 8	to 20

Table 8. Gateaway LR reaction.

Components	Volume (µl)
Entry clone (100-300ng)	1-10
Destination vector (300ng)	2
5x LR clonase™ reaction buffer	4
TE buffer pH 8	to 20

Agrobacterium-mediated transformation of Arabidopsis

The desired expression vectors carrying Cas9 and sgRNAs were transferred into Arabidopsis plants via Agrobacterium-mediated transformation. 40µl aliquots of electrocompetent C58C1 *Agrobacterium tumefaciens* were thawed and transferred into electroporation cuvettes on ice, 100ng of plasmid DNA was added and after gentle mixing, the cuvettes were given a pulse of 1.8kV in the Bio-Rad *E. coli* Pulse™ electroporation device. 1ml of S.O.C. medium was added, the cells incubated for 3 hours at 28°C shaking at 200rpm and plated onto LB agar with the appropriate antibiotic to specifically select for the expression vector (Table 6) plus rifampicin (to maintain the VIR expressing minichromosome of Agrobacterium. The plates were incubated for two days at 28°C and individual colonies were picked to inoculate 5ml LB liquid cultures. These were incubated overnight at 28°C shaking at 200rpm and used to prime 200ml liquid cultures that were incubated in the same conditions up to logarithmic grow phase (OD_{550} of 0.6 to 1). The bacteria were then pelleted for 15 minutes at 3220g and resuspended in the same volume of 5% w/v sucrose , 0.5% v/v Silwet L-77™. The to-be transformed plants were prepared by removing open flowers and siliques. The inflorescences were then dipped into the Agrobacterium cultures for a few seconds and the plants returned to the climate chamber inside mini greenhouses for a few days, after which the covers were removed and they were left to grow, produce seeds and dry out. The dry seeds were recovered, sown and cultivated as specified in "*Plant material and growing conditions*" to select for positive transformants.

Measurement of meiotic crossover rate using fluorescent tagged lines (FTLs)

When the plants started to bloom, an open flower was plucked using forceps and tapped to release pollen into a drop of Vectashield® on a glass microscope slide, followed by the quick placement of a coverslip to avoid excessive dissemination of the pollen

grains. This operation was repeated for the different plants and multiple times per plant if the pollen obtained from one flower was not enough. Pictures of pollen fields were taken using a Zeiss Axio Imager Z1 microscope with a 10x objective and Zeiss ZEN 2 software (blue edition) in three filtered channels for red (Zeiss #43 HE filter), yellow (Zeiss #46 filter) and cyan (Zeiss #47 HE filter) fluorescence. To score the four classes of fluorescent pollen (red, yellow, red & yellow and non-coloured) the pictures were analysed with the image analysis software IMARIS® v.7.6 for semi-automatic segmentation of pollen grains using the *Spots* tool and the differentiation and counting of the four classes adding filters of intensity for the two fluorescent channels. The recombination rate was then calculated in Microsoft Excel® as the number of recombinant pollen grains (red-only + yellow-only) divided by the total number of pollen grains (red-only + yellow-only + red & yellow + non-coloured) multiplied by 100. As the proportion of red to yellow loci and each of the two recombinant and parental classes to the other is expected to remain 1:1 in spite of crossover events happening within the interval, yellow:non-yellow and red:non-red chi-squared tests were done to verify the absence of detection/expression artefacts which would potentially affect the reliability of the recombination rate measurements.

Analysis of homologous recombination products and mutations via NGS

For the analysis of recombination and mutation of the target site in meiotic cells, we isolated, extracted genomic DNA from and prepared sequencing libraries from pollen of Col-0 x Ler-0 F1 plants. Open flowers of individual plants were collected and immersed in ice-cold 10% sucrose solution each 2-3 days during their flowering period and stored at -20°C. To extract and isolate pollen grains, the tubes containing the collected flowers were thawed at room temperature, vortexed at maximum speed and hand shaken until the solution was cloudy and yellowish with pollen grains in suspension, but avoiding disruption of floral tissues. The solution with pollen in suspension was transferred to a new tube by pipetting, filtering it through a nylon mesh with 150µm pores to remove tissue fragments isolating pollen grains, and centrifuged for 15 minutes at 3220g. The supernatant was discarded and the pollen pellet was resuspended in 500µl of lysis buffer and transferred to an eppendorf tube. From this point on the pollen genomic DNA extraction was performed as described by Choi *et al.* [829].

For the analysis of somatic tissues, Col-0 F2 plants were grown in 1/2 MS agar plates for 15 days after which pools of 10 plantlets were prepared for each combination

of promoter plus target site. Genomic DNA was extracted from these pools using the Wizard® Genomic DNA purification kit.

To amplify the CRISPR-Cas9 target sites, oligos that anneal both to Columbia and Landsberg chromosomes (non-polymorphic template) were designed to amplify fragments of 300-500bp spanning the target site. These oligos include 5' tails with P5 and P7 Illumina tags and were used for a first PCR (Table 9 and Table 10) followed by a spin column-based DNA purification. The purified product of the first PCR was then subject of a second PCR (Table 11 and Table 12) to introduce Illumina adapters and indexes to prepare the Illumina sequencing library using the Nextera® XT Index Kit v2 oligo set. The product of the second PCR was purified and checked by electrophoresis for the expected size and the concentration using an Agilent 2200 TapeStation®. Concentration were adjusted and samples pooled in a single isomix for sequencing on an Illumina MiSeq™ platform (paired-end 2x250bp) by the team of Dr. Yannick Bidet at the Centre Jean Perrin (Clermont-Ferrand).

Table 9. Pollen library 1st PCR reaction.

Components	Volume (µl)
Genomic DNA	2
2x KAPA HiFi HotStart ReadyMix	12.5
Forward primer (10µM)	0.75
Reverse primer (10µM)	0.75
Ultra-pure distilled water	9

Table 10. Pollen library 1st PCR program.

Steps	Temperature	Time	
Initial denaturation	95°C	3min	
Denaturation	98°C	20s	x25
Annealing	58°C	15s	
Extension	72°C	30s	
Final extension	72°C	5min	
Storage	4°C	∞	

Table 11. Pollen library 2nd PCR reaction.

Components	Volume (µl)
Template DNA (1st PCR product)	5
2x KAPA HiFi HotStart ReadyMix	25
Forward primer (10µM)	1.5
Reverse primer (10µM)	1.5
Ultra-pure distilled water	17

Table 12. Pollen library 2nd PCR program.

Steps	Temperature	Time	
Initial denaturation	95°C	3min	
Denaturation	98°C	20s	x10
Annealing	60°C	15s	
Extension	72°C	30s	
Final extension	72°C	5min	
Storage	4°C	∞	

Three custom Python/Shell informatics scripts were written (Charles White) to analyse the NGS data and identify mutations at the target sites and recombinant products.

To analyse mutations at the target site, a script was used to extract the SNP/indel data plotted in Figure 13, Figure 16 and Figure 17, and whose main steps may be summarise in:

I) To merge the fastq files corresponding to P1 and P2 paired-end reads.

II) To identify reads bearing the Col-0 allele via text search-based identification of a polymorphic site between Col-0 and Ler-0 plus a size range, both features inputted by the user in the script call.

III) To check for the presence of an intact sequence corresponding to the CRISPR/Cas9 target site in all reads individually. If this sequence is either absent or modified, that read is called as bearing a mutation at the target site.

IV) To output the different metrics corresponding to the total of reads processed, the reads identified as Col-0 and the reads bearing a mutation at the target site as well as different ratios for further processing and plotting using GraphPad Prism (version 8.4.3).

To analyse products of recombination at the target site, another script was written to extract the recombination data plotted in Figure 16 and Figure 17, following these steps:

I) To merge the fastq files corresponding to P1 and P2 paired-end reads.

II) A series of polymorphic sites between Col-0 and Ler-0 within the sequenced fragment were used for the analysis of conversions between the two haplotypes. For each position, the Col-0 allele and the Ler-0 allele are inputted in the script call.

III) To identify parental and recombinant reads, these polymorphic positions are called in each read individually via a text-search based algorithm. A sequence in which all polymorphic sites correspond to the Col-0 allele is called as Col-0 parental sequence, and similarly for Ler-0 parental sequences. If the read bears Col-0 alleles for some polymorphic sites and Ler-0 alleles for others, that read is called as a recombinant sequence.

IV) To output the different metrics corresponding to the total of reads processed, the reads identified as Col-0 and Ler-0 parentals and the recombinant reads as well as different ratios for further processing and plotting using GraphPad Prism (version 8.4.3).

For the analysis of recombination showed in Figure 18, a different workflow built by Charles White and Miguel Hernández was followed:

I) To merge the fastq files corresponding to P1 and P2 paired-end reads.

II) To map these merged reads to the Arabidopsis genome (TAIR10) using Minimap2.

III) To pool the alignment files of the individual plants sequence per genotype (combination of promoter + target site and controls). This was done to simplify the analysis with respect to the previous one in which the different plants were treated individually and to increase the number of sequences analysed and compared per genotype.

IV) To extract the bases of each polymorphic (SNP) site between Col-0 and Ler-0 for each individual mapped read, in this case using the TAIR10 coordinates of these sites and employing the tool Sam2tsv.

V) To call for each of the sites in each sequence either Col-0 or Ler-0 if the base extracted corresponded to the Col-0 allele or the Ler-0 for that particular polymorphic site.

VI) To input this data into a custom R script which calls the different classes of parental and recombinant reads possible, these being:

- if all polymorphic sites bear the Col-0 allele, the read is call Col-0 parental.

- if all polymorphic sites bear the Ler-0 allele, the read is call Ler-0 parental.

- if part of the polymorphic sites bear either Col-0 or Ler-0 alleles (Col-0 or Ler-0 haplotype) and there is a shift the other haplotype, the read is call crossover product (CO).

- if the terminal polymorphic sites are both either Col-0 or Ler-0 but within the internal sites there are alleles called from the other haplotype, whether it is one or more than one, the read is call non-crossover product (NCO). If the terminal sites are called as Col-0 but the sequence bears internal Ler-0 alleles, hence it is inferred a Col-0 chromosomes bearing a patch of gene conversion from Ler-0, the read is called NCO C->L. In the opposite case, it is called NCO L->C. The scheme of these classes is shown in Figure 18d.

IV) To output the different metrics corresponding to the total of reads processed, the reads identified as Col-0 and Ler-0 parentals, CO, NCO C->L and NCO L->C as well as different ratios for further processing and plotting using GraphPad Prism (version 8.4.3).

Results

CRISPR/Cas9 constructs to target DSBs during meiosis

We cloned the human codon-optimised *Streptococcus pyogenes* Cas9 (SpCas9) gene into expression vectors encoding either the *Arabidopsis thaliana DMC1* promoter (pDMC1) or *RAD51* promoter (pRAD51) to drive its expression *in planta* (Figure 9a & Figure 9b). The CRISPR RNAs were ordered for synthesis as DNA molecules encoding the complete sgRNAs (tracrRNA fused individually to each of the crRNAs), preceded by a *Arabidopsis thaliana* U6 promoter (pU6) and followed by a poly(A) terminator for expression *in planta*. Each pU6::sgRNA cassette was cloned into expression vectors as well (Figure 9c & Figure 9d).

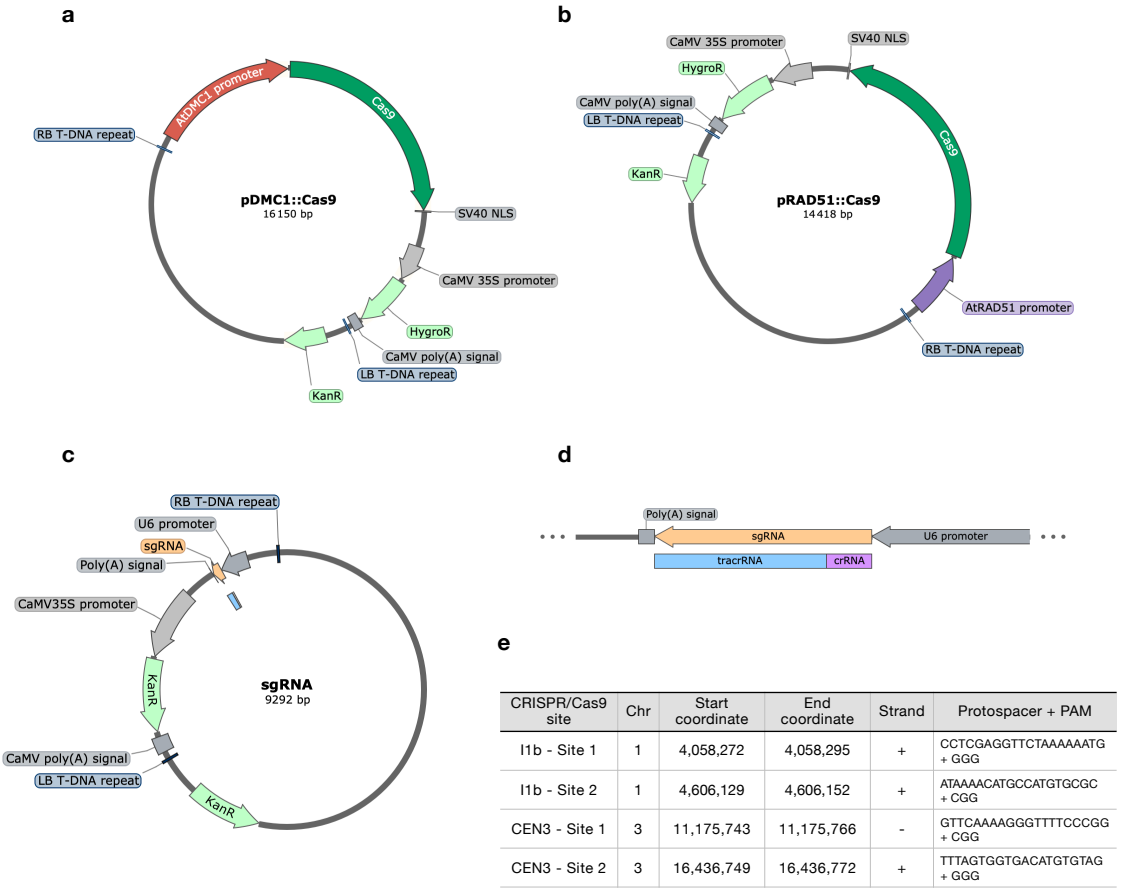

CRISPR/Cas9 site	Chr	Start coordinate	End coordinate	Strand	Protospacer + PAM
I1b - Site 1	1	4,058,272	4,058,295	+	CCTCGAGGTTCTAAAAAATG + GGG
I1b - Site 2	1	4,606,129	4,606,152	+	ATAAAACATGCCATGTGCGC + CGG
CEN3 - Site 1	3	11,175,743	11,175,766	-	GTTCAAAAGGGTTTTCCCGG + CGG
CEN3 - Site 2	3	16,436,749	16,436,772	+	TTTAGTGGTGACATGTGTAG + GGG

Figure 9. CRISPR/Cas9 construct and target design.

Schematic depictions of the plasmids used to transfer the T-DNA from bacteria to plants encoding the cassettes for antibiotic selection plus **(a)** pDMC1::Cas9, **(b)** pRAD51::Cas9 and **(c)** AtU6::sgRNA. **(d)** Detail of the sgRNA architecture within the T-DNA. **(e)** Relation of the four target sites and their respective sgRNAs .

All combinations of SpCas9 under DMC1 or RAD51 promoters and the four sgRNAs expression vectors (next section for target site design) were co-transformed via floral dip directly into the fluorescent tagged lines (FTLs), selected and genotyped for both constructs. T1 transformants were grown and crossed with Col-0 plants for the analysis of recombination rate in F1 plants. T2 seeds were collected as well and used for I) mutation analysis in plate-grown plantlets; and II) cross with Ler-0 for the NGS analysis of recombination in Col-0 x Ler-0 hybrids.

Design of target sites

To target SpCas9 activity into desired locations, the crRNAs were designed so that: I) they target unique positions in the genome; II) they are outside protein-coding genes to avoid indirect effects in the biology of the plant by disrupting a gene; and III) they include mapped DNA sequence polymorphisms within the target sequence between Col-0 (Col) and Ler-0 (Ler), such that they should be active on the Col chromosome and not the Ler chromosome in Col/Ler hybrid plants. This latter point was included to have information of the directionality of potential meiotic recombination events between homologous chromosomes in Col x Ler hybrids. Exploiting the FTL fluorescent pollen marker lines originally developed by the Copenhaver lab [764,826], we chose four different targets within two different marked genetic intervals that permit to score the recombination rate of the interval identifying an counting the different parental and recombinant classes of the gametes (pollen).

The I1b interval spans 1.85 Mb of the middle of an arm of chromosome 1. It is a relatively gene-rich region (310.8 genes/Mb) with respect to the chromosome 1 average (246.8 genes/Mb). I1b has a reported genetic distance of 8.16 cM with a mean recombination rate of 4.41 cM/Mb in male meiosis, similar to the chromosome 1 average obtained in the same study (4.88 cM/Mb) [764]. Two gRNAs were synthesized and cloned targeting genomic locations within this interval, which will l be referred as I1b – Site 1 and I1b – Site 2 (Figure 9e and Figure 10).

The CEN3 interval covers 5.405Mb of chromosome 3, spanning its centromere and pericentromeric regions. It is a gene-poor region (75.1 genes/Mb) with respect to the chromosome 3 average (240.7 genes/Mb) and the I1b interval. It has a reported genetic distance of 11.04 cM with a mean recombination rate of 2.05 cM/Mb in male meiosis, which is considerably lower than the chromosome 3 average (4.76 cM/Mb) [764], presumably due largely to the presence of the centromeric crossover-depleted region accounting for around half the physical length of the interval. However, the adjacent regions, still within the CEN3 interval, are the most recombinogenic by average of the

chromosome 3 (Figure 10). The two gRNAs targeting genomic locations within this interval are situated in this high recombinogenic regions and will be referred hereon as: CEN3 – Site 1 and CEN3 – Site 2 (Figure 9e and Figure 10).

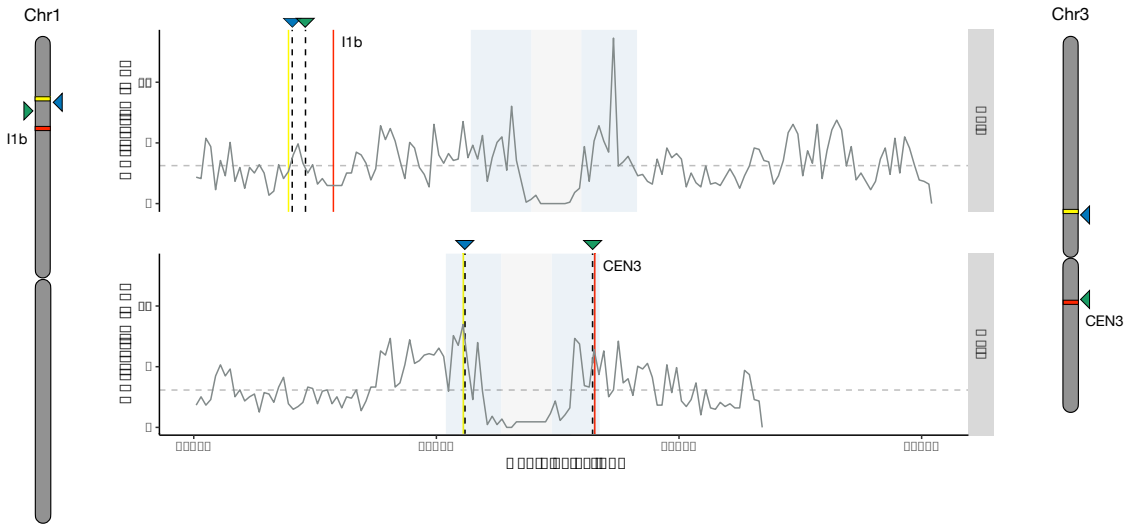

Figure 10. Location of the target sites with respect to the physical maps of the chromosomes and the recombination rate profile along them.

Pictograms of Arabidopsis chromosome 1 (left) and 3 (right) showing the loci encoding the the YFP (yellow) and DsRed2 (red) fluorescent markers delimiting the I1b and CEN3 intervals, plus the two target sites designed for each interval (green and blue triangles). Recombination rate profiles of chromosomes 1 and 3 (middle) along the physical length of their respective chromosomes, with positions of the YFP (yellow) and dsRed2 (red) fluorescent marker loci delimiting the I1b and CEN3 intervals and of the two target sites for each interval (green and blue triangles). Both the pictograms and the maps keep the relative scale of the two chromosomes. Recombination rate profiles were generated with the data provided by Rowan *et al.* (2019) following the protocol described in the publication.

For further characterization, we gathered bibliographical data to contextualize the targeted sites with respect to the local landscape of the top contributing features explaining the variation of recombination rate in Arabidopsis [830]: chromatin accessibility (ATAC) [831], gene and transposable element content, DNA methylation (mCG and mCHH) [831] and REC8 density [385]. We included SPO11-oligo density [361] and histone H3K4me3 density [832] which, while showing a weak contribution to variation in recombination rate, strongly correlate with DSB hotspot positions [361,830]. Thus, the surroundings of the I1b target sites are gene-rich compared to those of the CEN3 targets, with regions of more accessible chromatin and peaks of H3K4me3 (a mark associated with open chromatin). Unsurprisingly, the local landscape of CEN3 target sites is particularly enriched in transposable elements and cytosine methylation, both characteristic features of pericentromeric regions. When looking at the targeted sites in more detail, I1b – Site 1 is situated at a H3K4me3-enriched region, just adjacent to a

high accessible chromatin region (given the ATAC peak) and at a REC8-depleted region, three features known to positively correlate both with DSB hotspots and crossovers (Figure 11a). I1b – Site 2, on the other side, is located at a flat region for these features (Figure 11b). CEN3 – Site 1 is in close vicinity of a reported SPO11 hotspot (SPO11 oligo-enriched region), that is REC8-depleted and DNA-hypomethylated as well, although it stands just outside in a more methylated segment (Figure 12a). CEN3 – Site 2 is located in a less gene-depleted segment than CEN3 – Site1, also less DNA methylated and in a local peak of chromatin accessibility (Figure 12b).

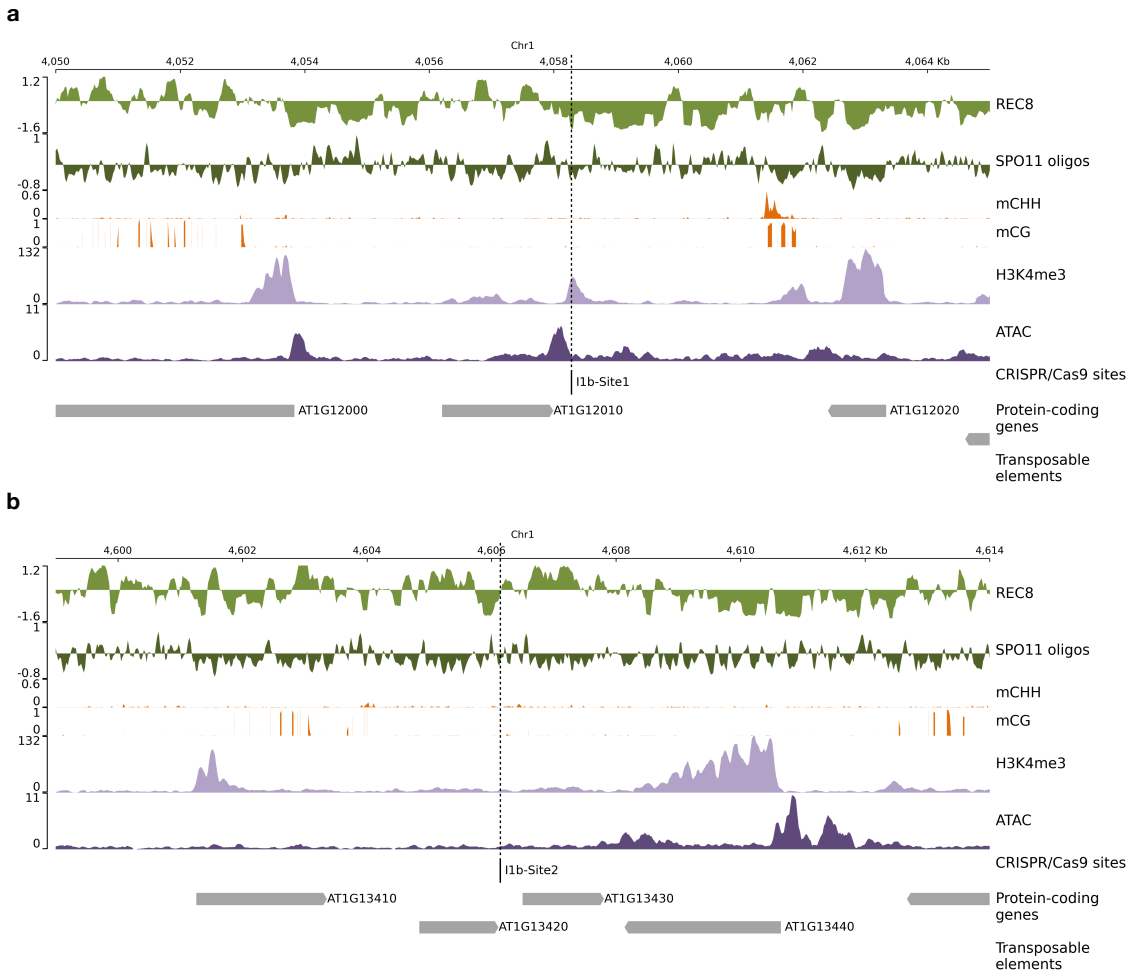

Figure 11. Local landscape of genetic, epigenetic and of meiotic-specific features for the two target sites within the I1b interval.

Density profiles of multiple features known to be correlated with DSB or crossover hotspots, SPO11-oligos and the meiotic cohesin REC8 plus genes and transposable elements located in the vicinity of the target sites. Chromosomal coordinates of the segment depicted are shown on top. Each density profile is plotted with its own scale (left). The data was gathered from multiple publications cited in the text.

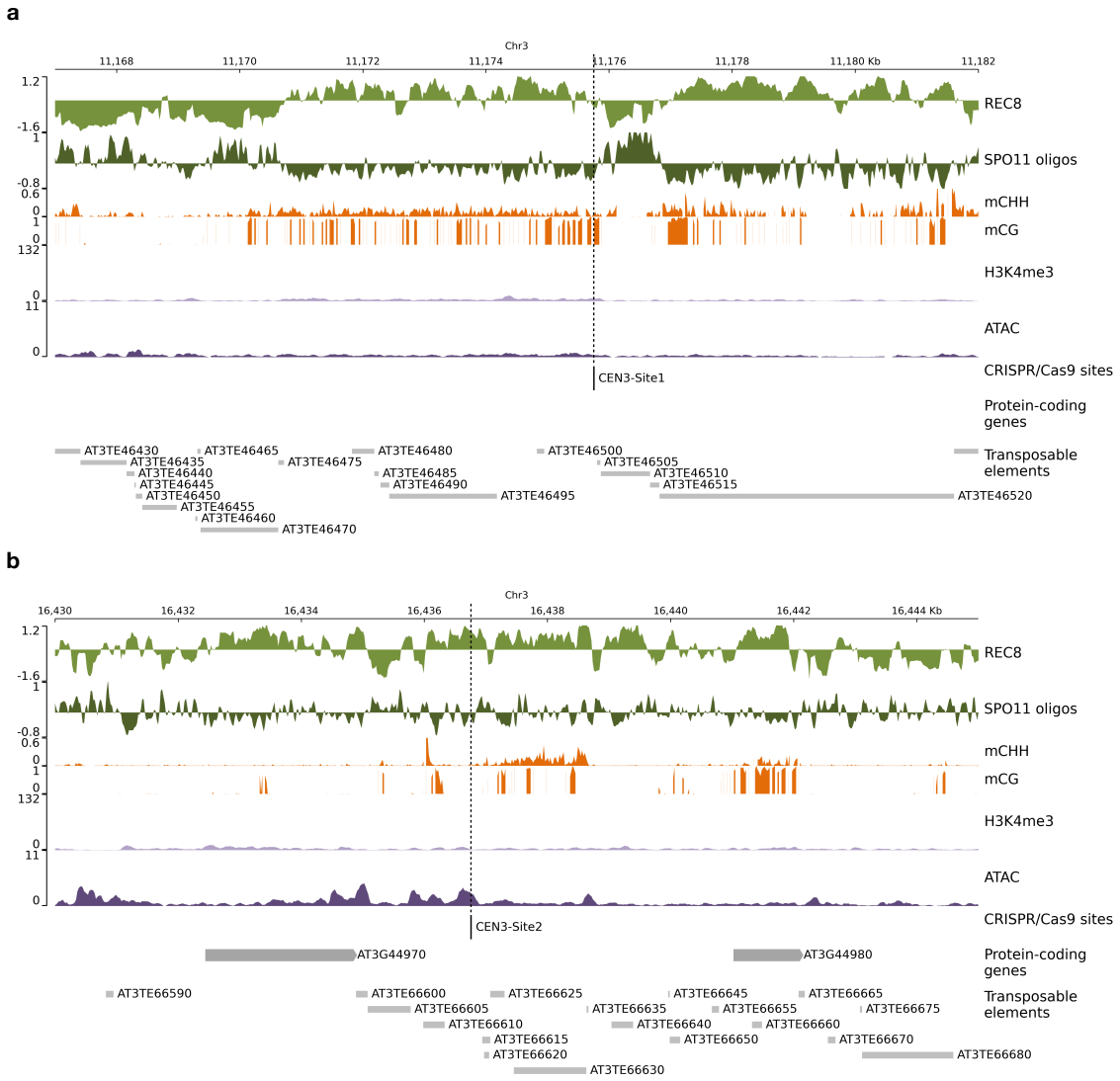

Figure 12. Local landscape of genetic, epigenetic and of meiotic-specific features for the two target sites within the CEN3 interval.

Density profiles of multiple features known to be correlated with DSB or crossover hotspots, SPO11-oligos and the meiotic cohesin REC8 plus genes and transposable elements located in the vicinity of the target sites. Chromosomal coordinates of the segment depicted are shown on top. Each density profile is plotted with its own scale (left). The data was gathered from multiple publications cited in the text.

CRISPR/Cas9 is able to cleave and induce deletions in somatic tissue

To assess the expression and cutting capability of the CRISPR/Cas9 system in the plants, we decided to grow in plates plantlets carrying either pDMC1::Cas9 or pRAD51:Cas plus one of the CEN3 target sites. We also included a third construct consisting of Cas9 driven by an estradiol-inducible promoter. Thus, we could grow plants in plates supplemented with estradiol for a strong constitutive expression of Cas9. Genomic DNA was extracted from pools of 10 plantlets of 15 days old for each combination of promoter plus target site, controls without both Cas9 and gRNAs and with Cas9 and no gRNA for that target site. In the case of the constructs with the estradiol promoter, plantlets from plates with and without estradiol in the media were collected. Illumina libraries amplifying the target sites were prepared, sequenced and the data was analysed with a custom script to detect mutations at the target sites. Mutation rates were defined as reads harbouring a mutation at the target site divided by the total reads and expressed as percentages (see methods for details).

Mutation rates at the target sites were generally low both in control and several samples (less than 0.5%) corresponding to 1bp substitutions when visually inspected. This basal level is likely originated by PCR and/or sequencing errors. We could however identify samples with a considerably higher mutation rate. Notably, in 4 out of the 5 samples corresponding to the estradiol promoter (when supplemented with estradiol), 2 to 5% of the sequences carried a mutation at the target site (Figure 13c and Figure 13d). An increased mutation rate of similar magnitude could be also detected in one of the samples carrying pDMC1:Cas9 construct and the CEN3 – Site 1 gRNA (Figure 13a). When individual sequences are mapped to the target sites, the mutations detected in the samples with increased mutation rate are mainly deletions ranging from few base pairs to around 100bp and 1bp insertions centred at the Cas9 cutting site (3-4bp upstream the PAM sequence). A few complex events involving both deletions and insertions or multiple deletions at different locations could be observed as well (Figure 13e and Figure 13f).

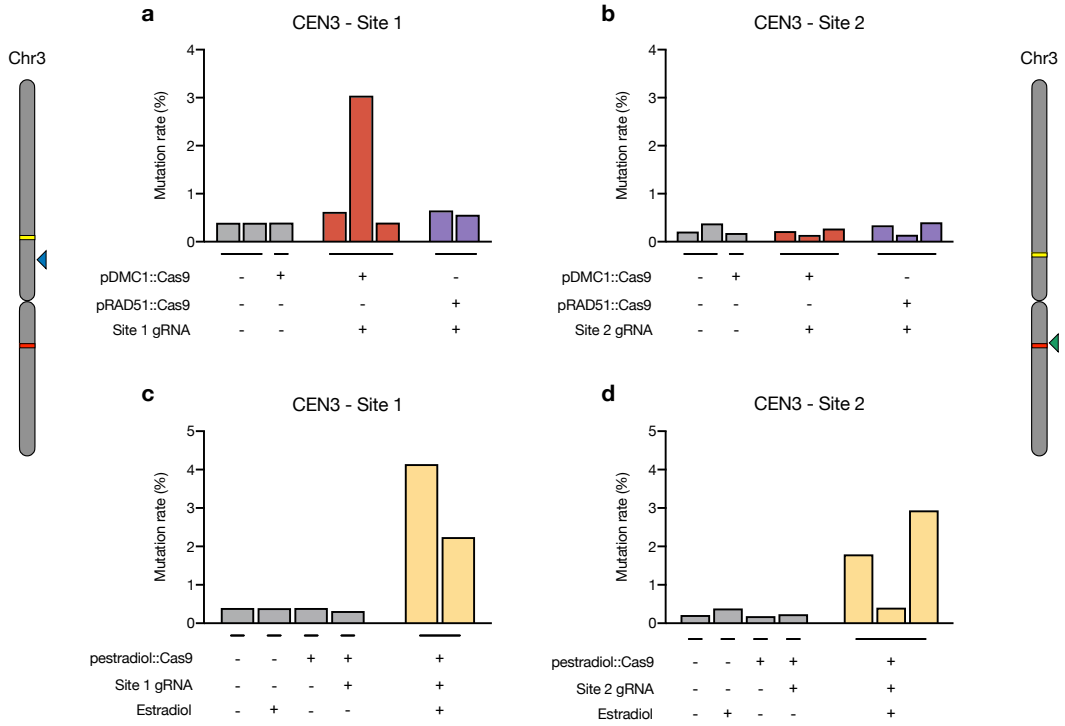

Figure 13. CRISPR/Cas9 is able to cleave and generate mutations at the target sites in somatic tissues at moderate efficiencies.

Bar plots portraying the mutation rates of 15-day plantlet pools at the CEN3 target sites. Upper plots correspond to the pools of plants carrying pDMC1::Cas9 and pRAD51::Cas9 constructs for **(a)** CEN3 – Site 1 and **(b)** CEN3 – Site 2. Lower plots correspond to the pools of plants carrying pestradiol::Cas9 constructs for **(c)** CEN3 – Site 1 and **(d)** CEN3 – Site 2. Each bar represent one plantlet pool with the corresponding genotype detailed below. The pictograms to the sides show the relative position of CEN3 – Site 1 (left) and CEN3 – Site 2 (right) within chromosome 3 of Arabidopsis. Next page: Mutational profile of the CEN3 – Site 1 for a plantlet pool carrying **(e)** pestradiol::Cas9 plus the gRNA for CEN3 – Site 1 and **(f)** pDMC1::Cas9 plus the gRNA for CEN3 – Site 1. Red bars represent individual sequences within which deletions and substitutions are depicted as clear gaps and insertions as red triangles. The target site is indicated below with the protospacer in yellow and the PAM motif in grey plus the relative coordinates upstream and downstream the site.

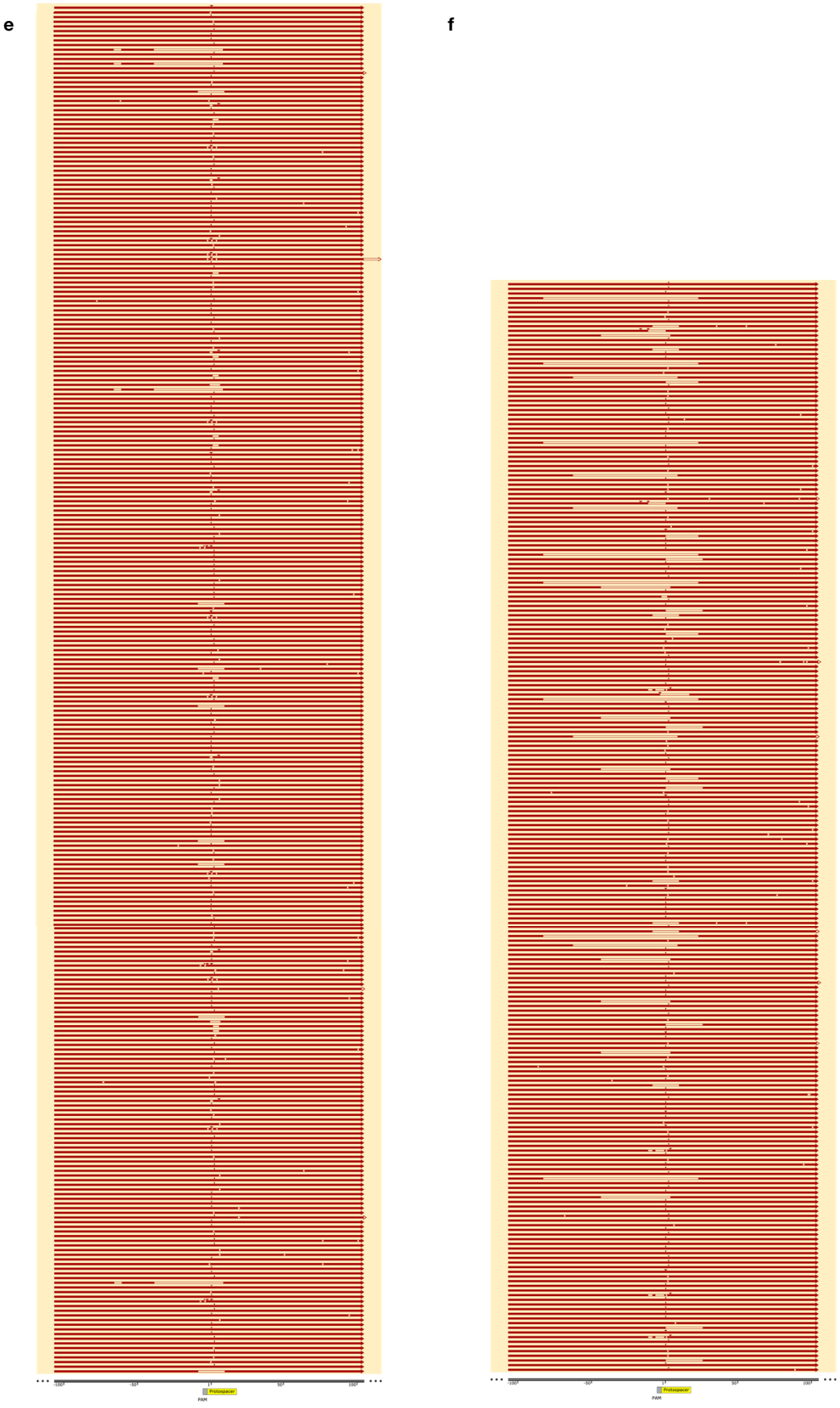
e
f
-100
-50
1
50
100
Protospacer
PAM

Increases of recombination rate are detected in plants carrying CRISPR/Cas9 despite the high variability

I1b or CEN3 primary transformants (T1) carrying the different pDMC1/pRAD51::Cas9 plus gRNAs combinations were crossed with Col-0 plants to obtain F1 plants carrying the CRISPR/Cas9 components and cis-heterozygotes for the FTL maker genes. Individuals that either did not carry Cas9 or had Cas9 but no gRNAs were used as negative controls. F1 plants were grown until flowering, pollen was collected in a drop of mounting fluid on a microscope slide, photographed and numbers of pollen of the different classes of parentals and recombinants scored using IMARIS. Per plant recombination rates were calculated by dividing the number of recombinant pollen grains by the total number of pollen grains scored and expressed as genetic distance of the interval in centimorgans (see methods for details).

Control plants (expressing neither Cas9 nor gRNA) showed the expected genetic distances of 9.07 ± 0.47 cM and 13.97 ± 0.20 cM (mean ± SEM) in the I1b and CEN3 intervals, respectively. No statistically significant increases of mean recombination rate were detected in pooled data from lines carrying pDMC1::Cas9 (unpaired t-test; $p > 0.05$; Figure 14a & Figure 14b). However, among pDMC1::Cas9 lines targeting I1b – Site 2 we could observe a widened distribution of genetic distances in the interval, with individual plants showing a considerable increase of recombination rate (Figure 14a). The data plotted in Figure 14a and Figure 14b for each of the target sites correspond to individual F1 plants coming from the crossing of different primary transformants (T1). Figure 14c and Figure 14d show the same data but in this case separated by T1 transformant line. pDMC1::Cas9 I1b – Site 2 lines show an important inter-line and intra-line variability. Thus, the widened distribution of recombination rate in these lines comes from differences between the primary transformants (T1) from which they derive - ranging from a mean recombination rate similar to the negative control (7.89 ± 0.42 cM; mean ± SEM) to almost its double (13.57 ± 0.76 cM; mean ± SEM) (Figure 14c; Site 2, first vs second line). A third line showed an intra-line variability with an even greater range, from a minimum I1b genetic distance of 6.95 cM to a maximum of 18.40 cM (Figure 14c; Site 2, third line).

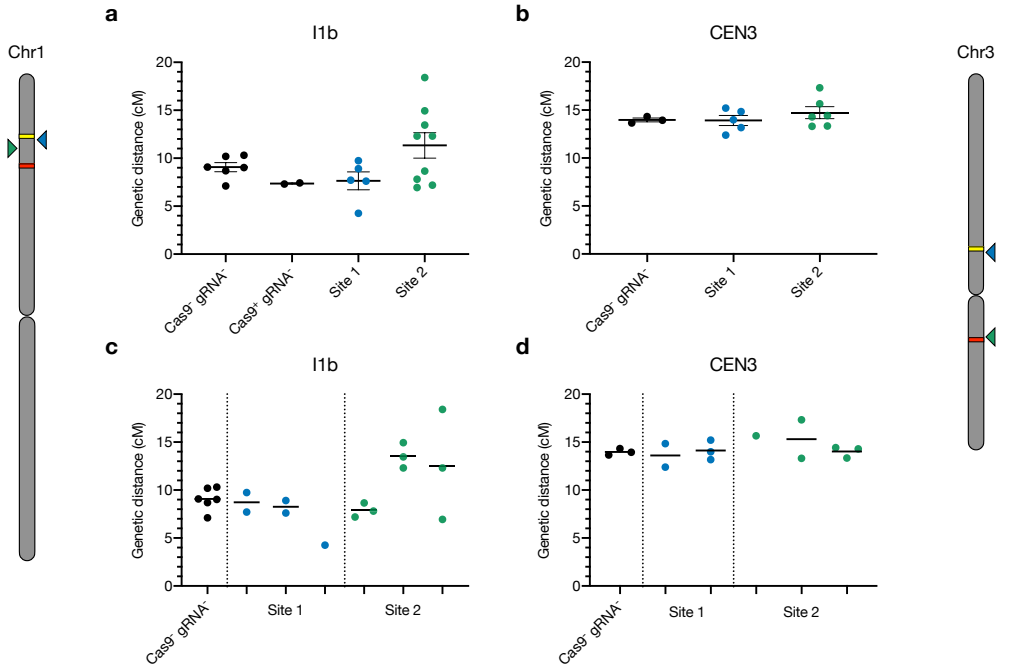

Figure 14. Increases of recombination are detected in plants carrying pDMC1::Cas9 constructs for some target sites with high overall variability.

Scatter plots of the FTL-based analysis of recombination rate expressed as genetic distance of the interval in centimorgans (cM). Each dot represent the genetic distance of the interval in an individual plant. The mean and the SEM are represented for each genotype detailed below with a line and error bars above and below it. **(a)** Genetic distances obtained for plants carrying neither pDMC1::Cas9 nor gRNA (black), pDMC1::Cas9 (black), pDMC1::Cas9 plus the I1b – Site 1 gRNA (blue) and pDMC1::Cas9 plus the I1b – Site 2 gRNA (green). **(b)** Genetic distances obtained for plants carrying neither pDMC1::Cas9 nor gRNA (black), pDMC1::Cas9 plus the CEN3 – Site 1 gRNA (blue) and pDMC1::Cas9 plus the CEN3 – Site 2 gRNA (green). Plots **(c)** and **(d)** display the same data of (a) and (b) respectively but the plants are divided into T1 transformant lines for a more detailed analysis of variability. The pictograms show the relative position of the target sites within chromosome 1 (left) and 3 (right) of Arabidopsis.

Regarding the lines carrying Cas9 under the control of the RAD51 promoter, no statistically significant increases in recombination rates were found between any of the targeted sites with the negative control (unpaired t-test; $p > 0.05$; Figure 15a & Figure 15b). However, similarly to pDMC1::Cas9 lines and in this case for more than one target site, individual increases in recombination rate with high intra- and inter-line variability were observed in these plants. Thus, subsets of pRAD51::Cas9 plants targeting both CEN3 – Site 1 and Site 2 do show increased recombination rate with respect to the negative control (Figure 15b). When separated into different groups based on the parental T1 transformant, intra-line variability is especially high for both CEN3 target sites, with none standing out as highly recombinogenic, but most showing individual plants with increases of the genetic distance spanning from 2 to 6 cM (Figure 15d). Albeit no significant increases of recombination were observed for the I1b target sites when pooled (Figure 15a), one of the lines when separated by T1 parental does

appear to have a slight increase with respect to the control (11.49 ± 1.18 vs 9.07 ± 0.47 cM; mean ± SEM; Figure 15c)

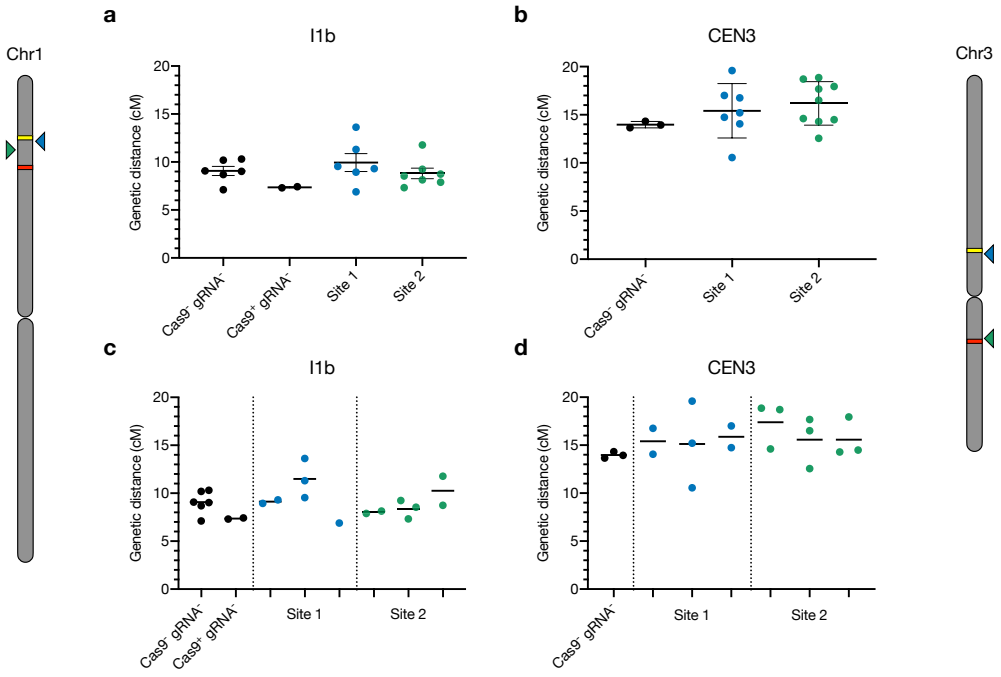

Figure 15. Increases of recombination are detected in plants carrying pRAD51::Cas9 constructs for some target sites with high overall variability.

Scatter plots of the FTL-based analysis of recombination rate expressed as genetic distance of the interval in centimorgans (cM). Each dot represent the genetic distance of the interval in an individual plant. The mean and the SEM are represented for each genotype detailed below with a line and error bars above and below it. **(a)** Genetic distances obtained for plants carrying neither pRAD51::Cas9 nor gRNA (black), pDMC1::Cas9 (black), pRAD51::Cas9 plus the I1b – Site 1 gRNA (blue) and pRAD51::Cas9 plus the I1b – Site 2 gRNA (green). **(b)** Genetic distances obtained for plants carrying neither pRAD51::Cas9 nor gRNA (black), pRAD51::Cas9 plus the CEN3 – Site 1 gRNA (blue) and pRAD51::Cas9 plus the CEN3 – Site 2 gRNA (green). Plots **(c)** and **(d)** display the same data of (a) and (b) respectively but the plants are divided into T1 transformant lines for a more detailed analysis of variability. The pictograms show the relative position of the target sites within chromosome 1 (left) and 3 (right) of Arabidopsis.

NGS analysis of CRISPR/Cas9 target sites do not show signatures of induced recombination

To study meiotic recombination events at DNA sequence level, we crossed T2 plants of lines expressing some of the CRISPR/Cas9 combinations with Ler-0 plants. Arabidopsis Col-0 and Ler-0 accessions, whose genomes are sequenced and published, show numerous DNA sequence polymorphisms. In F1 Col x Ler hybrids, combining this with CRISPR/Cas9 systems targeting unique genomic sites opens the possibility to analyse recombination in the immediate vicinity of the target sites. The very low likelihood of naturally-occurring recombination events in these very small intervals, with respect to megabase-scale reporter systems such as FTLs, is also to expected to significantly enhance the sensitivity of detection. Furthermore, as explained above, the target sites were chosen so that Cas9 cuts only in the Col chromosome, conferring directionality to the potential CRISPR/Cas9-initiated recombination events. This feature may be informative both to differentiate these events from naturally-occurring ones and to extend the mechanistic interpretation of the results.

Primers were designed to amplify ~300bp fragments spanning I1b – Site 2 and CEN3 – Site 1, adding Illumina universal adapters for library preparation and paired-end 250bp Illumina sequencing. Schematic representations of the target sites plus the designed oligos and the Col/Ler polymorphic sites in the amplified fragments are presented in Figure 16 and Figure 17. Genomic DNA was extracted from pollen of individual F1 plants, amplified and indexed so the sequencing data could be demultiplexed for the analysis of recombination products of individual plants. A custom Python script was written to process the Illumina reads and call Col/Ler at each polymorphic site individually, identifying parental and recombinant haplotypes. Crossovers were defined as reads in which there was an interchange from one haplotype to the other at some point within the sequence. Recombination rates were calculated as the number read harbouring a crossover divided by the total number of reads and expressed as percentages.

No increases of recombination rate were detected for plants carrying pRAD51::Cas9 plus the gRNA targeting I1b – Site 2 with respect to control plants with no gRNA (Figure 16a). We inspected the reads for mutations at the target site as well. No differences in mutation rate were observed between the two backgrounds (Figure 16b). For the analysis of a longer fragment including more polymorphic sites, a second oligo combination was designed for this same site to repeat the experiment in the same genomic DNA extractions. Similar results were obtained both for recombination and mutation rates. We detected no differences between plants carrying pRAD51::Cas9 plus

the gRNA targeting I1b – Site 2 with respect to control plants (Figure 16c & Figure 16d).

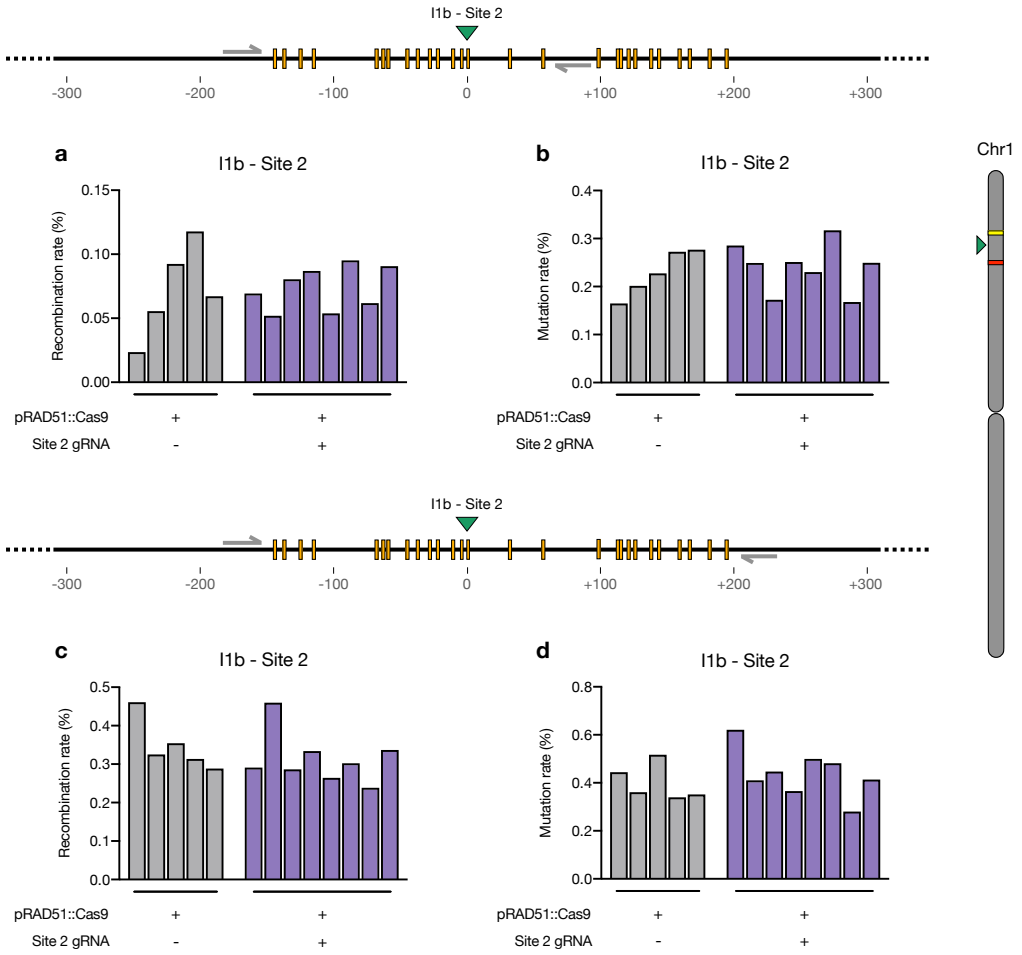

Figure 16. NGS-based analysis of recombination rate and target site mutations does not show signatures of CRISPR/Cas9 activity during meiosis at the I1b – Site 2 target site.

Bar plots of the NGS-based analysis of recombination rates and mutations at the I1b – Site 2 target site expressed as percentage of recombinant molecules and sequences bearing a mutation at the target site over the total molecules analysed. Each bar represents an individual Col x Ler F1 plant whose genotype is detailed below. Two fragments of different length were amplified and sequenced for the same plants, each one depicted above its respective plots. **(a)** and **(c)** Recombination rates of plants carrying either pRAD51::Cas9 (grey) or pRAD51::Cas9 plus the I1b – Site 2 gRNA (purple). **(b)** and **(d)** Mutation rates of plants carrying either pRAD51::Cas9 (grey) or pRAD51::Cas9 plus the I1b – Site 2 gRNA (purple). The pictograms above the bar pots show the target sites (green triangle), the polymorphic sites between Col and Ler in their vicinity (yellow boxes), the primers used for amplification (grey arrows) and the relative coordinates in base pairs upstream and downstream the site. The pictogram on the right show the relative position of the I1b – Site 2 within chromosome 1 of Arabidopsis.

For the CEN3 – Site 1, plants carrying either pDMC1::Cas9 or pRAD51::Cas9 plus the gRNA to target that site were compared with control plants carrying pDMC1::Cas9, but not gRNA. No differences in recombination rates with the controls

were observed in either case (Figure 17a). Regarding mutations at the target site, two of the plants carrying pDMC1::Cas9 plus CEN3 – Site 1 gRNA showed an increase in deletions with respect to the controls and the rest of the plants carrying Cas9 (Figure 17b). However, when parental reads were inspected, almost 100% of them corresponded to Col parentals, these two plants were not Col x Ler hybrids but the result of self-pollination of the Col parental and so non-informative for recombination analysis.

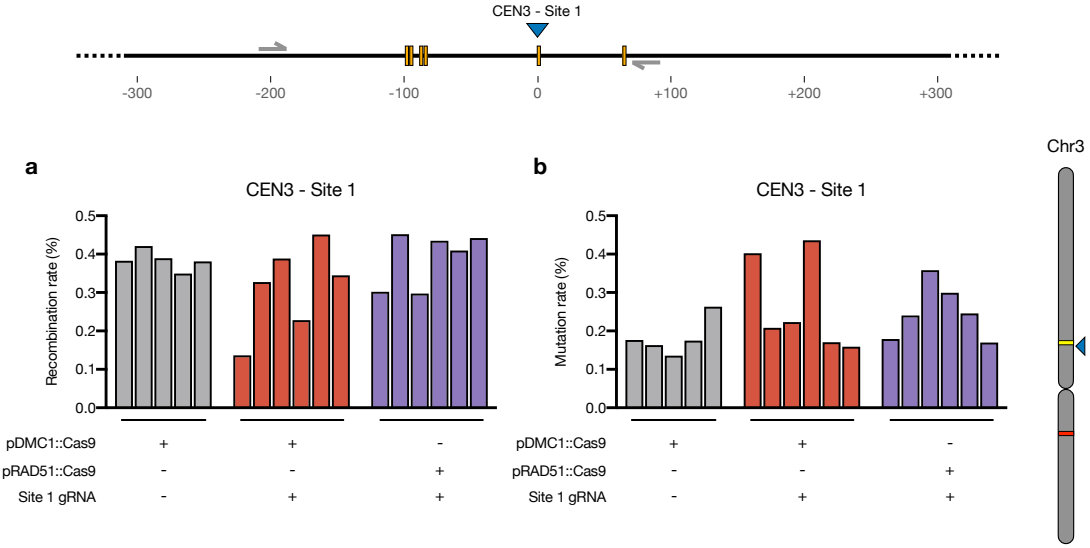

Figure 17. NGS-based analysis of recombination rate and target site mutations does not show signatures of CRISPR/Cas9 activity during meiosis at the CEN3 – Site 1 target site.

Bar plots of the NGS-based analysis of recombination rates and mutations at the CEN3 – Site 1 target site expressed as percentage of recombinant molecules and sequences bearing a mutation at the target site over the total molecules analysed. Each bar represents an individual Col x Ler F1 plant whose genotype is detailed below. **(a)** Recombination rates of plants carrying either pDMC1::Cas9 (grey), pDMC1::Cas9 plus the CEN3 – Site 1 gRNA (red) or pRAD51::Cas9 plus the CEN3 – Site 1 gRNA (purple). **(b)** Mutation rates of plants carrying either pDMC1::Cas9 (grey), pDMC1::Cas9 plus the CEN3 – Site 1 gRNA (red) or pRAD51::Cas9 plus the CEN3 – Site 1 gRNA (purple). The pictogram above the bar plots show the target site (blue triangle), the polymorphic sites between Col and Ler in its vicinity (yellow boxes), the primers used for amplification (grey arrows) and the relative coordinates in base pairs upstream and downstream the site. The pictogram on the right show the relative position of the CEN3 – Site 1 within chromosome 3 of Arabidopsis.

In order to expand the scope of the analysis, we ran the data on a second custom script (see method for details) that permit detection of interhomologue non-crossover gene conversion events in addition to crossovers. Interhomologue non-crossover (NCOs) products of meiotic recombination have been elusive in molecular studies of Arabidopsis recombination, probably due to the reduced length of conversion tracts, but they are expected to represent a higher proportion of the total recombination landscape than crossovers. While it seems apparent that meiotic CRISPR/Cas9 cleavage at target sites is not sufficiently efficient to impact crossover rates, it is also possible that it does not

(or only weakly) lead mechanistically to resolution via crossover. The analysis of NCOs is facilitated by the directionality of the potential CRISPR/Cas9-intiated events in our experimental design. Given that the target site is Col-specific, in all CRISPR-Cas9-initiated events the Col chromatid must be the one receiving the DSBs and hence the recipient of information from the Ler donor chromatid (Ler sequence patches into the Col chromosome in our case). An increase of the proportion of NCOs in which the conversion is Col -> Ler in samples carrying the CRISPR/Cas9 machinery might thus be a signature of CRISPR-Cas9-initiated recombination events.

For this analysis we pooled the F1 plants of each genotype, shown individually in Figure 16 & Figure 17. The two pDMC1::Cas9 CEN3 – Site 1 plants that were not Col x Ler hybrids but inbred Col were not included in the pool to avoid distorting the proportions. Figure 18a-c show the percentage of reads of each class classified by the script based on calling the allele of each polymorphic site individually. Reads in which all alleles belong to the same haplotype are classified as parentals (Col and Ler). Reads in which there is a shift from one haplotype to the other are classified as crossovers (CO). And reads in which the terminal polymorphic sites belong to the same haplotype but include a conversion tract to the other haplotype within the read are classified as NCOs. Among NCOs, the two sub-classes are defined as: Col chromatids that include a conversion tract of Ler alleles (NCO C->L) and Ler chromatids that include a conversion tract of Col alleles (NCO L->C) (Figure 18d).

Similarly to the previous analysis of recombination in NGS data of individual plants (Figure 16 & Figure 17), no increases of crossovers were detected for either target site in plants carrying the CRISPR/Cas9 machinery with respect to the controls. Numbers of reads bearing a putative crossover event remain very low in absolute terms, below 0.3% of all sequences for all genetic backgrounds (Figure 18a-c). Regarding NCO products, no noticeable increases of either of the two sub-classes (L->C & C->L) were detected in the plants carrying either pDMC1::Cas9 or pRAD51::Cas9 plus the gRNA for the respective target site, with respect to control plants without gRNA (Figure 18a-c). NCO also represent a very low share of the total reads, falling within the same range as COs (Figure 18a-c). When the two sub-classes of NCOs are compared, no enrichment of C->L NCO events is observed with respect of L->C NCOs in plants carrying a CRISPR/Cas9 construct plus gRNA when compared with the controls(Figure 18a-c).

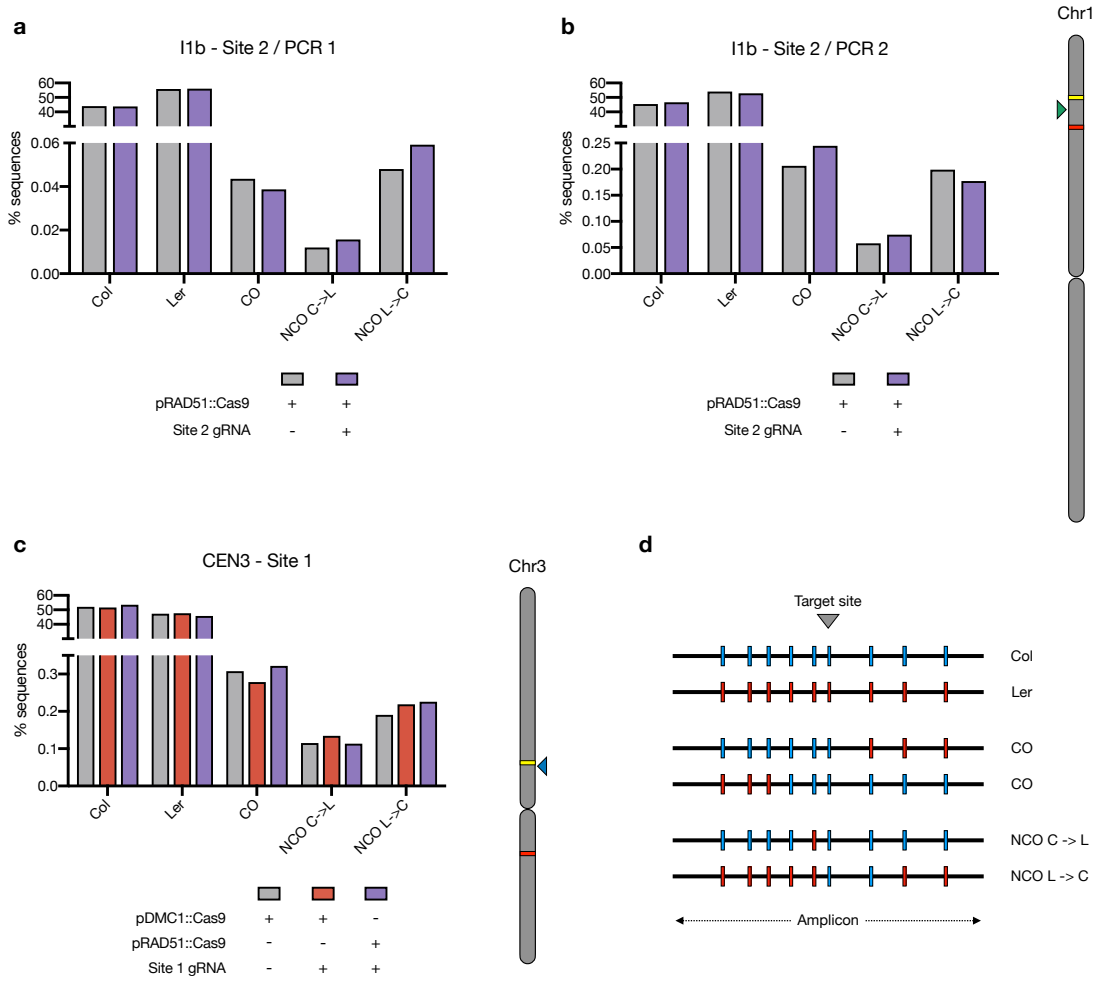

Figure 18. The proportions of parental and different classes of recombinant meiotic products are not affected in plants carrying CRISPR/Cas9 constructs.

Bar plots of the NGS-based analysis of the different classes of parental and recombinant molecules at the target sites expressed as percentage of molecules of each class over the total molecules analysed. Individual bars represent the percentage of each class for the pooled plants corresponding to the genotype detailed below. **(a)** Percentages of parental and recombinant classes of plants carrying either pRAD51::Cas9 (grey) or pRAD51::Cas9 plus the I1b – Site 2 gRNA (purple) for the upper amplicon depicted in Figure 16. **(b)** Percentages of parental and recombinant classes of plants carrying either pRAD51::Cas9 (grey) or pRAD51::Cas9 plus the I1b – Site 2 gRNA (purple) for the lower amplicon depicted in Figure 16. **(c)** Percentages of parental and recombinant classes of plants carrying either pDMC1::Cas9 (grey), pDMC1::Cas9 plus the CEN3 – Site 1 gRNA (red) or pRAD51::Cas9 plus the CEN3 – Site 1 gRNA (purple). **(d)** Schematic depiction of the method used to call the different classes of parental and recombinant molecules. The pictogram on the right of the bar plots show the relative position of the I1b – Site 2 and the CEN3 – Site 1 within chromosome 1 and 3 of Arabidopsis, respectively.

Discussion

Targeted induction of meiotic DSBs in Arabidopsis

We present here an approach to target CRISPR/Cas9-induced DSBs to specific locations at early meiosis of Arabidopsis. The human codon-optimised SpCas9 gene was placed under the control of promoters known to express in meiosis (pDMC1), meiosis and mitosis (pRAD51) or an estradiol-inducible promoter (pestradiol) that ensures strong expression when the medium is supplemented with this hormone. This latter offers control of the expression of the enzyme independently of the cell cycle stage of the cells and the response to DNA damage, two factors known to affect the state of both endogenous *RAD51* and *DMC1* promoters. These were cloned in plasmids with guide RNA expression cassettes targeting two sites in each of two marked genetic intervals, one on the left arm of chromosome I (I1bc) and the second spanning the centromeric and pericentromeric regions of chromosome III (CEN3).

CRISPR/Cas9 cleaves and induces mutations at moderate efficiencies in somatic tissues

Validation of the constructs against two target sites was carried out in somatic cells (more abundant and easier to gather than meiocytes) via next-generation sequencing as a measure of their expression and proficiency to cleave the chromosomal targets. While restricted to detection of mutagenic repair of induced DSBs, this assay does provide a more complete picture than simply testing the presence of either the transcript or the protein. We could detect target site deletions in around 2 to 5% of the sequences in most of the plant pools (4/5) carrying the pestradiol::Cas9 construct and grown in medium supplemented with estradiol for both tested targets. These sequences presented deletion profiles expected from Cas9 cleavage: mostly short deletions (few bp up to 100bp approximately) spanning the cutting site as well as 1bp insertions centred around it [833–837]. An increase was detected as well in one of the plant pools expressing pDMC1:Cas9 and the gRNA for CEN3 – Site 1 (1/6 total) with a similar profile of short deletions around the cutting site. No differences with the controls were observed in any of the 5 pools carrying pRAD51::Cas9 constructs.

Head to head comparisons of CRISPR/Cas9 cleavage (mutation) efficiencies with previous reports in plants are limited by the differences in the testing method, the material of choice (individual plants vs. pools, plant generation) and the data analysis

workflow. To this date and to our knowledge, three publications have reported the use of CRISPR/Cas9 constructs in Arabidopsis designed to cleave during meiosis:

I) maize codon-optimised SpCas9 (zCas9) under the control of three Arabidopsis meiotic-specific promoters, according to transcriptomic data [833];

II) SpCas9 under the control of the Arabidopsis *DMC1* promoter [834];

II) human codon-optimised SpCas9 (hCas9) under the control of Arabidopsis *DMC1*, *SPO11* and *CDC45* promoters [838].

The three groups had the objective of generating stable and inheritable mutations and thus they selected meiotic promoters for efficient germline modification under the hypothesis that CRISPR/Cas9 cleavage during meiosis would be repaired via error-prone pathways. They did not test for homologous recombination outcomes. The evaluation of mutation efficiencies was done via genotypic or phenotypic analysis of individual T1 plants (the descendance of the transformed plant or T0) and T2 plants that descend from a T1 plant heterozygous for a CRISPR/Cas9-induced mutation.

In the three cases, really high proportions of T1 plants carrying a mutant allele at the target site were observed for some sites (up to 100% in [833] , 69% in [834] and 100% in [838]). Surprisingly, among the two publications using cloned Arabidopsis pDMC1 promoters, there are important differences in the source of those mutations. While Xu *et al.* [834] reported the detection of inherited mutations in the T1 plants (they were heterozygote for one mutant allele), Feng *et al.* [838] T1 plants were mostly chimeric (they carry a mix of multiple mutant alleles). This means that in the first case the pDMC1::SpCas9 system was active presumably during meiosis in the T0 plant after flower dip transformation, in which the ovule is thought to be the primary target for genomic integration [839], and causing mutations that were inherited into the T1 descendance. In the second case the pDMC1::hCas9 system is active in the somatic tissues of the T1 plants generating a mosaic of independent mutations in different cells. Feng *et al.* obtained the same chimeric mutational signature using another presumptively meiotic-specific promoter, the SPO11 promoter [838].

Although we did not sequence individual T2 plants but 10-plant pools hence the numbers are risky to extrapolate, the mutation rates obtained are significantly lower than the ones obtained in these publications. We could detect some mutant alleles repeated among the sequences analysed, but none of them accounted for more than 1-1.5% of the total sequences. These numbers suggest that none of the plants of the pools carried inherited mutations, which would be expected to be ≈5% of the total sequences (10 plants, 2 alleles per plant). This is not surprising in the case of pestradiol::Cas9

constructs, which were not active in the T1 plants (not supplemented with estradiol) but only in the T2 plantlets during their early development in plates supplemented with estradiol. The pDMC1::Cas9 pool in which mutations at the target site were detected also presented a pattern more compatible to a chimera of mutant alleles generated in somatic tissues of T2 plants rather than inherited mutations surged during T1 meiosis, which suggests that our pDMC1::Cas9 construct is behaving similarly to Feng *et al.* construct.

Feng *et al.* hypothesise than differences in the fragment cloned as DMC1 promoter might be responsible of the discrepancy [838]. While Xu *et al.* amplified a 3.1kb fragment upstream the ATG motif from a Ler-0 plant to clone the promoter, Feng *et al.* used Col-0 plants and amplified 2.2kb while ours is an amplified fragment of 2.7kb from Ler-0, so it cannot be discarded that regulatory elements not carried along might add for the different behaviour. In addition to this difference, somatic expression of the endogenous copy of *DMC1* has been reported in multiple tissues, some of them belonging to early developmental stages, which might as well occur in the cloned constructs [840,841]. *DMC1* regulation in Arabidopsis has been proven complex, with factors than activate and repress its expression in a timely-regulated manner and differentially in germinal and non-germinal cells, some of them likely involving epigenetic modifications of the gene body, so its cloned promoter might lack regulatory elements of the endogenous copy [842]. It might be thus useful to study the actual temporo-spatial pattern of expression of these cloned promoters to determine how the regulation the endogenous copy translates into them.

Nevertheless, the meiotic expression of our cloned DMC1 and RAD51 promoters has been tested by using it to drive the expression of a DMC1-GFP and RAD51-GFP fusion proteins. These GFP fusion proteins could be visualised in meiotic cells and both exert a dominant negative effect in meiotic recombination, reenforcing the evidence on their expected early meiotic expression pattern [234 & unpublished data].

Despite no further analysis was done to disclose the repair pathways implicated in the mutations observed in these publications, the mutational signature is congruent to what might be expected for NHEJ and similar to what we observe, consisting on short indels centred around the cutting site. NHEJ is the primary repair pathway is plant somatic tissues. However, the absence of DSB repair defects in mutants of genes encoding for NHEJ proteins, the equivalences in numbers of foci of immunolocalized DSB proteins and HR proteins and the direct evidence of repair outcomes in other organisms suggest than NHEJ is not implicated in the repair of a significant number of SPO11-catalysed DSBs during meiosis. Letting aside the hypothesized differences of

expression and assuming that, as intended, the pDMC1::Cas9 constructs of these reports are indeed expressed and cleaving during meiosis we could permit ourselves to speculate and point out some phenomena related with the repair of those DSBs in the specific context in meiosis that might condition their outcome and generate differences between theoretically similar CRISPR/Cas systems and with respect to the endogenous machinery.

First, although both SPO11 and Cas9 generate a DSB, we do not know how they (or if they) drive their repair towards certain repair pathways. The SPO11 complex is the catalytical responsible of an intricated machinery leading to meiotic DSBs. As presented in more detailed in sections 3.2. "*Double-strand break formation*" and 3.3. "*Double-strand break regulation*" of the introduction, the SPO11 complex has been proven to participate in a network of interactions with proteins that both precede their action, likely regulating the temporo-spatial pattern of meiotic DSBs; and follow it. This includes DSB-accessory factors, members of the DSB resection machinery and meiotic chromosome axis components [282,314,316,318,319,376,377]. In addition, SPO11 is known to covalently bound DSB ends until released by the resection machinery, which has been suggested to play a role in blocking the access to the DSBs ends to end-joining pathways factors. Whether these two phenomena are essential in blocking the repair of SPO11-catalyzed DSBs via end-joining pathways and driving it towards HR or not is not clear yet. In any case, Cas9 does not either interact with the meiotic DSB and end processing machinery (in principle) or covalently bind the DSB ends. So it is an option than Cas9-catalysed DSBs might not be driven towards the known meiotic recombination pathways leaving the door open for the use end-joining, but this remains to be tested. Nevertheless, there are reports in different organisms of SPO11-independent DSBs from multiple sources that also lack these two features and that are repaired via interhomologue meiotic recombination pathways: HO [816,817] and VDE [818,819] site-specific nucleases in budding yeast, I-SceI in fission yeast [820], γ-irradiation in *C. elegans* [743,843,844] or cisplatin in Arabidopsis [845].

Another feature of SPO11-catalysed DSBs is the triggering of signalling pathways that, in budding yeast, inhibit the formation of simultaneous breaks in the same locus and adjacent regions of the sister chromatid and the homologous chromosome [386,388,846]. While this mechanism has not been reported in Arabidopsis, the main actors are conserved (Mec1/ATR & Tel1/ATM). Homologous recombination mechanisms need the presence of an intact donor strand to repair a DSB, hence simultaneous breaks in sister/homologous loci would likely prevent HR and other pathways might overtake and repair it at some point. We do not know if Cas9-catalysed DSBs trigger these same pathways, but it is unlikely that they would inhibit Cas9 cleavage as they are thought

to act via inhibitory modifications of the meiotic DSB machinery. It might be thus hypothesized than very active CRISPR/Cas systems expressed in meiosis could induce simultaneous DSBs in the same loci of multiple chromatids, preventing the use of HR pathways and ending up repair by end joining pathways, while less active versions might be able to repair via HR. It is also mechanistically possible that very active CRISPR/Cas systems could induce breaks in HR intermediates, given that extension of invading ends using an homologous template would reconstruct the target site. This might as well disrupt the completion of HR and leave unrepaired products later repaired via other pathways. These phenomena might introduce differences in the repair outcomes observed between CRISPR/Cas systems even if all expressed during meiosis and using the same enzyme.

One last feature of SPO11 regulation than might condition the repair of meiotic DSBs, if not present, is the temporal regulation. A window for SPO11-catalysed DSBs has been reported in different organisms, generally closing when getting to pachytene or pachytene-like stages and mechanistically linked to the synapsis of homologous chromosomes [348,353,355,847]. Interestingly, in mice subjected to γ-irradiation at different prophase I timepoints, a transition from a meiotic to a somatic-like DSB repair program involving NHEJ factors has been described at around mid-pachytene [403]. If this temporal regulation is conserved in Arabidopsis, it might imply when inducing DSBs using CRISPR/Cas systems that fine tuning of temporal regulation of expression might condition as well the pathway choice during meiosis, being a potential source of variability between constructs even if functional and efficient.

Individual plants carrying CRISPR/Cas9 constructs experience increases of recombination rate with high overall variability

Notwithstanding the absence of tools to track the repair of most naturally-occurring meiotic DSBs in Arabidopsis, the great majority (if not all) are believed to be repaired via homologous recombination. This is supported by direct evidence in other organisms together with indirect evidences in Arabidopsis such as the absence of meiotic phenotypes of end-joining mutants and the strong DSB-repair phenotypes of early-HR mutants. Among HR products, efficient reporter systems have been developed in Arabidopsis to measure crossover rates genome wide or in defined genomic intervals. In our experimental design to induce meiotic DSBs, as mentioned above, our target sites were placed within two FTL marked intervals that permit us to measure the recombination rate under the hypothesis that a working CRISPR/Cas9 system cleaving those sites efficiently should generate an excess of crossovers in those intervals (hence

an increase in genetic distance), as it has been reported in studies with analogous strategies in other species [848–851].

Overall, we did not obtained statistically significant increases in mean recombination rates between the lines carrying pDMC1::Cas9 or pRAD51::Cas9 plus the gRNA for any of the four target sites with respect to the controls. We did however detect increases in recombination rate in individual plants ranging from 3 to 8 cM approximately over the distribution in the control for at least three of the target sites: I1b – Site 2 in plants carrying pDMC1::Cas9 and the two CEN3 sites in plants carrying pRAD51::Cas9. More specifically, the CRISPR/Cas9 targeting resulted in a widened distribution of meiotic recombination rates between individuals, with some plants showing meiotic recombination rate increases of almost 2-fold with respect to the mean in the control.

The F2 plants analysed for each of these promoter-plus-target combinations derive from the cross of different T1 transformant plants, each with independent integrations of the CRISPR/Cas9 system T-DNAs. Thus the subset of plants with increased recombination rate for each combination might originate from either I) particular T1 lines in which the CRISPR/Cas9 system is being efficiently expressed and initiating HR events yielding crossovers while not doing it in others (inter-line variability); or II) individual plants from multiple T1 lines with increased recombination rate while others belonging to the same line maintain control-like rates (intra-line variability). To check on this, we split them into sub-pools by parental T1 line and repeated the analyses. When split by parental T1 line, it becomes noticeable for pRAD51::Cas9 plants targeting the CEN3 sites that the increases of recombination are not limited to the descendance of particular parental T1 plants, but that plants with increased and control-like recombination rates coexist in most lines. In the case of pDMC1::Cas9 I1b – Site 2, both phenomena could be observed: one of the lines seem to have a consistent increase in recombination rate in the three plants score, although probably more plants are needed for stronger confidence in the observation, while second line show a strong intra-line variability, including a plant with a 2-fold increase with respect to the control mean recombination rate.

The modulation and enhancement of meiotic recombination has been a long-sought objective in meiotic research and especially in plant breeding programs. Meiotic crossovers generate diversity by shuffling haplotypes, creating new combinations of alleles that are inherited into the descendance potentially yielding new crop varieties of agronomical interest. However, naturally occurring crossovers are not abundant in numbers in most plants, they are tightly regulated and, in multiple crops, they are

limited to relatively small portions of their chromosomes. These features impede the shuffling of alleles of genes situated in these low/no recombinant segments that transmit thought generations as haplotype blocks. The discovery and developing of CRISPR/Cas as an efficient, versatile, easy to engineer and time/cost-effective genome editing tool opened a promising door to target crossovers to these regions, breaking these linkage groups to generate new combinations and to reduce the drag of naturally-linked undesired traits. Nonetheless, to this date, the induction of targeted crossovers in plants have been proven challenging, underlining the importance of understanding the subjacent mechanisms driving DSB repair during meiosis.

The unique report to date using a CRISPR/Cas system (or any other to our knowledge) in Arabidopsis to try to induce targeted meiotic recombination events chose to tether a catalytically-dead version of Cas9 (dCas9) to MTOPVIB, member of the SPO11 complex, under the control of the own MTOPVIB endogenous promoter and terminator [852]. This approach is expected to benefit from the genome targeting potential of CRISPR/Cas while keeping the endogenous machinery to catalyse the DSB. A similar approach has been tested with positive results in budding yeast, in which SPO11 tethered to dCas9 was able to induce increases of recombination rate of between 1.2 and 6.3-fold depending on the target site and the number of gRNAs targeting the site [853]. In Arabidopsis, however, no significant increases of recombination were observed when MTOPVIB-dCas9 was engineered to target multiple positions within a crossover hotspots known as 3a [852]. Yelina *et al.* [852] performed this analysis using as input material pooled pollen from multiple plants, so a per plant evaluation of recombination rate, in which we could detect individual increases, could not be done. When they tested for per SNP gene conversion frequency, affected not only by a potential increase crossovers but by of non-crossover events as well, no increases were detected as well.

Although our principal interest was inducing targeted DSBs in meiosis with the purpose of studying their repair, it is worth to mention other approaches that have been carried out with success using CRISPR/Cas to modulate or induce homologous recombination in plants. Targeting meiosis is tempting given that DSB repair via HR is dominant, the existence of meiotic-specific promoters help preventing somatic modification of the target site that impede cleavage and the events are likely to be inherited into the descendance. But when the objective is simply the induction of targeted interhomologue crossover events that are inherited, if succeeded to do so in pre-meiotic germ cells, this will as well lead to gametes carrying this recombinant molecule. Even potentially in higher percentages if it is generated early in the germ cell lineage. Somatic interhomologue crossovers, on the other hand, are expected to be even rarer than meiotic as the use of end-joining pathways and HR using the sister chromatid

is more prevalent. Inherited interhomologue crossover events product of the repair of somatic DSBs induced by CRISPR/Cas has been reported in tomato (using SaCas9) [854], wheat (LbCas12a) [855] and Arabidopsis (SpCas9) [835]. Efficiencies are in general low but they are promising proof of concept for precise breeding approaches, some of which (like breaking haplotype blocks) does not necessarily need hundreds of different events to start with.

Another example of the use of CRISPR/Cas to modulate homologous recombination with potential application in breeding programs is the induction of inversions by designing two target sites that, when simultaneously cleaved, might be repaired generating an inversion of the inner fragment. Heterozygous inversions are problematic for meiotic pairing and synapsis and crossovers within the inverted fragment will be lost on acentric and dicentric chromosomes. CRISPR/Cas-engineered inversions in Arabidopsis have thus been shown to both: I) rescue crossover production in a recombination-dead region of closely-related F1 hybrid plants, one of which carries an inversion of that region [856,857]; and II) suppress crossovers in the region by inducing a desired inversion [858].

Single-molecule analyses of CRISPR/Cas9 target sites do not show signatures of induced meiotic recombination

In the light of the observations using reporter-based systems to analyse crossovers, we opted by moving to an NGS approach on pollen DNA from Col x Ler F1 hybrid plants. This permitted us to analyse meiotic recombination outcomes at the single-molecule level: conversion tracts, crossover and non-crossover events and their proportions. Unfortunately, these DNA sequencing analyses did not provide evidence for induction of meiotic crossovers at either of the two target sites analysed (I1b – Site 2 & CEN3 – Site 1) in plants carrying CRISPR/Cas9 plus the corresponding gRNA with respect to plants lacking the gRNA.

The contrasting results from these single molecule analyses and the measurements presented above from the pollen-marker intervals, can have multiple possible origins, whose discussion might be helpful for planning of future approaches:

I) The first is that the NGS result may simply reflect the absence or the very low efficiency of CRISPR/Cas9 cleavage in the plants analysed. High variability between transformant lines and between plants of the same line has been an issue in this work and it is a generalized issue in CRISPR/Cas studies in plants. The somatic mutations analysis showed induced mutations in 1 out of a total 11 transformant lines in which Cas9 was under the control of *RAD51* and *DMC1* promoters. In the fluorescent-pollen

reporter-based analysis of crossovers, as previously indicated, both intra-line and inter-line variability was elevated, with more than half of the plants analysed showing WT-like levels of crossovers. So it is possible that there is low cleavage efficiency in the relatively few plants used for the NGS analysis of recombinant molecules. In published studies targeting CRISPR cleavage in Arabidopsis germ cells it is frequent to find important differences in mutation rates between target sites and between transformant lines for a given target site [833–835,838,859]. Previous Arabidopsis and maize studies also report important differences between target sites and transformant lines in the induction of (pre-meiotic) crossover and non-crossover events by CRISPR/Cas. It is not rare to find transformant lines with zero or WT-like levels of these events [835,855]. This variability in cleavage efficiencies might originate from many factors that remain to be tested. They include effects on Cas/gRNA expression depending on the numbers or copies and the integration location of the T-DNAs, as well as possible impacts of the sequence and chromatin contexts of the chosen target sites. In the work presented here, an extra factor to take into account is that while our target sites were designed to cleave the Col-0 allele and not the Ler-0 allele (for information about the directionality of the HR events), the reporter-based analysis of crossovers was done in Col x Col (+FTLs) F1 plants - hence four target sites in meiosis - while the NGS analysis was done in Col x Ler F1 plants - hence two target sites in meiosis. Combined with low cutting efficiency, the two-fold difference in the number of target sites to cleave might have contributed to the differences between the results.

II) A second issue potentially affecting our NGS approach could be high levels of background crossovers. Taking CEN3 – Site 1 as example, recombination rates measured in the controls (Cas9+, gRNA-) are 0.375% or 0.375cM. Given the fragment length (302bp), converting this to cM/Mb, the standard unit of length-normalised recombination rate, this site would have a basal recombination rate of 1241.7 cM/Mb. In the case of I1b – Site 2, this would be 180.5 or 721.2 cM/Mb, depending on the fragment amplified. Two known natural crossover hotspots in Arabidopsis, named 3a and 3b, have reported recombination rates of 33.3 cM/Mb and 21.3 cM/Mb, with internal sub-intervals reaching about 80 cM/Mb [765]. The fact that our sites have orders of magnitude higher normalised-recombination rate than reported natural crossover hotspots might mean that either these sites are really strong natural hotspots or that this is a technical artefact. Artefactual crossover molecules may be generated at the library preparation PCR step via incomplete elongation and template switching. In either case, such high levels of crossovers in the controls relative to the fragment size would likely significantly impact the detection of mild increases of recombination.

III) A third possible issue related to our experimental design of the NGS approach concerns the length of the sequences. At the time of deciding what NGS method to use, we opted for 2x250bp paired-end Illumina sequencing from pollen DNA mainly because I) we needed the best sequence quality and the lowest error rate possible for scoring SNP markers; II) the choice of using pollen was based on recovering as many individual events as possible with the hope of detecting even rare HR events. Long read sequencing, although it has undergone a huge evolution in the last few years, was still far behind Illumina in this combination of sequence accuracy plus depth, however these advantages come at the expense of fragment length.

Our sequenced fragment length ranges between 277 and 416bp with the target site situated around the centre of the fragment spanned by Col/Ler polymorphic markers. A crossover is identified by the transition within one sequence from one haplotype to the other. Although crossover resolution is complex and may lead to multiple resolution scenarios, crossover analysis at one DSB hotspot in multiple organisms yields a set of crossovers whose exchange points are generally centred (symmetrically or not) around the DSB site. However, considering our very short fragment lengths, there are (at least) two phenomena that might result in the exchange point of an induced crossover, initiated at the target site, being outside the fragment sequenced: mismatch repair of heteroduplex tracks and branch migration.

Double Holiday junction nucleolytic resolution via crossover mechanistically implies the formation of hybrid DNA tracks in which the two strands are from different homologous chromosomes (hence parents). If these tracks harbour polymorphisms, they will have mismatched bases after dHJ resolution, case in which they are commonly referred as heteroduplexes. When heteroduplex tracks are generated, the mismatch repair machinery repairs mismatched bases via either restoration of parental allele frequencies, leading to a 4:4 mendelian segregation of that DNA track; or conversion, leading to a 6:2/2:6 segregation of the DNA track [215,587,860,861]. Given that we analyse individual meiotic products and we cannot reconstruct the whole HR event, the choice of either restoration or conversion will shift the detected exchange point between the two haplotypes. Studies in Arabidopsis sequencing pollen tetrads and double-haploids have permitted the detection of crossover-associated gene conversion tracks (segments segregating as 6:2/2:6 within crossover events) and estimate the mean length of these tracks to be 300-400bp [862]. These numbers are in the ballpark of our sequenced fragment sizes and over the distance of our more external polymorphic markers in any of the sites. It is thus plausible to speculate that a significant proportion of induced crossover events at the target sites could result in heteroduplex tracts covering our markers, the mismatch repair of which would co-convert them to one of the haplotypes, effectively

shifting the exchange point between the two haplotypes outside the sequenced fragment. These events would however be detected in the reporter-based assay, in which the florescent pollen marker genes are integrated megabases away from the target site.

Branch migration refers to exchange of one strand of a DNA duplex by a third one via the stepwise breakage and reformation of the hydrogen bonds between the DNA base pairs. It is mediated by helicases and other proteins with ATPase activity (such as RAD54). This essential process in DSB repair via HR is an important determinant of HR repair outcome of a given DNA break. In meiotic recombination models, branch migration happens both at the level of single-end invasion intermediates, mediating the extension step of the invading end and D-loop; and after the capture of the second end and the establishment of the dHJ, sliding the Holliday junctions [215,449,587,863]. A recent publication in budding yeast reported that hallmarks of branch migration at dHJ resolution are almost ubiquitous in the crossover events detected at one hotspot [587]. The authors divided these into events in which both HJs migrated in the same direction towards one side of the DSB, events in which there was a divergent migration of the two HJs away from the DSB and events in which one of the HJs was at the DSB location. In the first two classes, independently of heteroduplex resolution, the resulting exchange point between the two haplotypes in the resolved crossed-over molecules moves away from the DSB site. The median junction movement reported is ≈660bp and most of the final dHJs measured spanned more than 600-700bp up to some kilobases. The absence of DSB hotspots with a fine-scale location of the break in Arabidopsis has prevented this type of studies and it might be delicate to directly extrapolate the numbers from one budding yeast hotspot to the Arabidopsis genome, but branch migration is an inherent mechanistic feature of homologous recombination models. It is thus plausible to hypothesise that branch migration of the HJs could slide the exchange point of the two haplotypes in a portion of induced crossovers at the target site, making them invisible in short-read NGS analysis but detectable in the reporter-based system.

IV) A fourth factor that might lead to the absence of detected induced crossovers in our NGS approach, even if we assume efficient CRISPR/Cas cleavage, is the presence of polymorphisms between Col and Ler at and around the target sites, absent in the reporter-based system (Col x Col). At local level, polymorphisms are known to inhibit recombination, as mentioned in the section 3.7.3. "*DNA sequence determinants*" of the introduction. The inhibitory effect is not linear and few SNPs have been shown to dramatically decrease recombination rate. In Arabidopsis meiosis this inhibitory effect has been studied and confirmed in at least two crossover hotspots [864]. To this date, the presence of polymorphic sites is essential in these NGS-type approaches to identify

conversions and exchanges between haplotypes. In the bibliography we can find successful examples of the use of F1 hybrids of multiple organisms with similar experimental setups [587,799]. The response of HR to polymorphisms at a given site is likely species-dependent and it is a function of the basal level of recombination, so while a decrease of some fold in the super-recombinogenic budding yeast, as example, might still allow to accumulate events for analysis, an analogous drop in a less efficient system might drop it below technically profitable levels.

To finish, it is noteworthy to mention that the different hypothesis here presented as potential limitations and drawbacks in the NGS analysis of potential CRISPR/Cas-induced crossovers are not mutually exclusive. These factors may rather combine to complicate the detection of such events.

Our NGS approach permitted us to score NCO events if present as well. While there is no evidence on whether SPO11-independent DSBs might be repaired using the same HR pathways and in the same ratios than the ones catalysed by SPO11, the high proportion of DSB to CO events in Arabidopsis WT meiosis (≈20-30:1) might leave headroom for an excess of NCOs and/or intersister events even in absence of detectable induced COs. However, the proportions of sequences bearing a NCO event were similar in plants carrying or not the gRNA and lower than COs. In our system, DSBs catalysed by Cas9 must happen in the Col chromosome and consequently, in interhomologue HR events, its resected ends act as invading strand. Non-crossover-associated gene conversion tracts generated in repair products via SDSA or dHJ dissolution must thus happen in the Col chromosome in these Cas9-initiated HR events. This phenomenon would generate a bias towards NCO products consisting on Col sequences bearing a patch of the Ler chromosome and away from Ler chromosomes with a Col patch. When we split these two classes of NCO products however, we could not detect any bias specific to the plants in which the complete CRISPR/Cas9 machinery was present. Similarly, in Yelina *et al.* [852], no excess of NCO events could be detected at the MTOPVIB-dCas9 target sites.

The detection of NCO events in Arabidopsis has been elusive when compared to other organisms. The efforts to map NCO events genome-wide by sequencing Arabidopsis tetrads, have estimated NCO frequencies of less than 10 events per meiosis with gene conversion tracts of between 25 and 50bp in one report and less than 100bp in the other [862,865]. This surprisingly low number is backed up by the fact that in both studies the number of COs are in accordance with chiasmata countings and immunolocalization of CO markers. Estimations of numbers of DSBs/meiosis in Arabidopsis range between 200 and 300 - thus more than 95% of the breaks do not

have a known repair outcome. The picture is strikingly different in budding yeast: 66 NCO events are estimated per meiosis (1.8kb median GC length), which in addition to 90.5 estimated COs add up to the estimated 140-170 DSBs [603]. In mice, 273 NCO events are estimated per meiosis (30-40bp mean GC length) that together with the 27 estimated COs are also in accordance with almost the totality of DSBs repaired via interhomologue recombination (the authors estimate 300 DSBs, immunolocalization numbers range between 200 and 400) [775].

In the Arabidopsis studies, three main hypothesis are presented to try to explain this discrepancy between the numbers in the model plant and other organisms: I) the densities of polymorphisms in Arabidopsis F1 hybrids are not high enough to detect NCO events given the very short GC track length; II) contrarily to the other two species, there is an strong bias of mismatch repair in NCO-associated heteroduplex tracks towards restoration of the invading strand allele, making the events invisible; and/or III) there is a much frequent use of the sister chromatid for repair, and thus of events "invisible" to polymorphic marker-based analysis of recombination.

Combining a precisely located meiotic DSB, designed to cleave only one of the chromosomes and with a high SNP density around it, the work presented here was carried out with the aim of finding answers to these questions among others. While this work did not produce evidence for an excess of NCO events, this could of course have an explanation in one or more of the four issues presented above for CO detection considering our NGS experimental approach. It does however seem unlikely that we would be missing a significant number of NCO events due to low density of polymorphism, discarding the first hypothesis. However, a bias towards restoration of the invading strand allele and/or the use of the sister-chromatid donors would have hidden the events from our analysis.

The repair fate of more than 95% of Arabidopsis meiotic DSBs thus remains a mystery. Detection of NCO events, if the model plant behaves similarly to other organisms, is a long sought goal of the Arabidopsis meiotic community but, despite a considerable effort, has not yet provided compelling results. A new approach might be necessary to avoid the constraints imposed by DNA polymorphic markers-based analysis of HR events. A potential alternative approach involving the molecular detection of DNA neo-synthesis at DSB repair sites through EdU incorporation is presented in Chapter IV.

Conclusions

Revisiting the initial hypothesis and the objectives proposed at the beginning of this project, we may conclude that:

I) We designed and transformed into Arabidopsis plants CRISPR/Cas9 constructs controlled by promoters known to expressed during early meiosis that were able to induce double-strand breaks at the target sites chosen at moderate efficiencies.

II) Individual plants carrying these CRISPR/Cas9 systems underwent increases in the genetic distance of intervals spanning some of the target sites with respect to control plants, suggesting an induction of interhomologue crossovers at these sites. Nevertheless, high intra-line and inter-line variability within and between transformant lines was observed for these systems.

III) Analysis of two of the target sites via next-generation sequencing of pollen genomic DNA showed no increase of interhomologue crossovers, non-crossovers or mutations at the target site in the plants carrying CRISPR/Cas9 systems with respect to the controls.

The observed increases of the genetic distances of intervals spanning CRISPR/Cas9 target sites is thus not confirmed by the Illumina amplicon sequencing of the products. It seems probable that this can be explained by limitations of the short-length NGS sequencing might have had for the detection of these events (see discussion), but in any case this precludes any firm conclusion concerning the promising genetic results.

Future work

Based on this dissertation, we may raise some points for future works aiming address this subject:

I) Although the chosen CRISPR/Cas9 system has proven effective at inducing mutations in Arabidopsis, this technology is in constant evolution. New CRISPR/Cas systems are constantly being discovered and engineered with higher cleavage efficiencies, more diverse PAM motifs, different DSB ends, innovative delivery systems and improved algorithms to predict and design ideal gRNAs [822,866–871]. In addition and focusing on plants, multiple reports have been published with strategies to improve the efficiency of CRISPR/Cas. These include the choice of regulatory elements (promoters,

terminators, NLS) before and after the Cas gene and the CRISPR array, the introduction of genetic elements such as introns that enhance their expression, the architecture of the different elements within the T-DNA, the introduction of multiple cuts at the target site or exogenous ways to improve the efficiency such as modulating the temperature [869,872–874]. A deep dive into all these new elements and strategies to update the CRISPR/Cas system for new attempts to induce DSBs during meiosis in Arabidopsis seems vital for maximum efficiency and for its success.

II) A high variability of CRISPR/Cas9 efficiency between plants of the same transformant line and between transformant lines has been an issue in most of the experimental work and, as mentioned in the discussion, it may be in general terms when using these systems in Arabidopsis. While, to our knowledge, the causes are not clear and likely involve the sum of multiple phenomena, the development and application of assays that permit to select the most efficient transformant lines and plants for posterior analyses seems crucial to minimise this issue, in addition to using the most efficient system CRISPR/Cas system possible.

III) Regarding the NGS experimental setup, these last years have witnessed the emergence and refinement of long-read sequencing technologies, including PCR-free direct sequencing of genomic DNA. These third generation NGS approaches are highly interesting for many fields, and this is especially so in the NGS analysis of homologous recombination. Removing the limitation of short-read sequences will be of great importance for the analysis of homologous recombination events, an important proportion of which are known to involve longer tracts longer than 500bp and others known to migrate further than the reach of short-read sequencing. Avoiding amplicon library preparation PCR to add sequencing adapters also poses a major advantage, given that PCR is well known to create artefactual recombinant products via template switching or incomplete amplification that are indistinguishable from real recombinant sequences. Long-read direct sequencing technologies, such as Nanopore, had some important drawbacks when compare to short-read sequencing, notably the sequencing error rate which is particularly important when analysing recombination products by the conversion of SNPs. However, the evolution of the sequencing chemistry and the bioinformatic processing of the data is closing this gap, making them a potentially ideal sequencing method of choice for the analysis of homologous recombination at DSB hotspots.

CHAPTER IV. Analysis of meiotic DSB repair-associated DNA synthesis tracts in Arabidopsis

DNA synthesis is inherent in multiple DNA repair mechanisms and, notably, DSB repair via homologous recombination. Given the occurrence of programmed DSBs at early meiosis that are repaired using HR as the primary repair mechanism, it may be expected that if a pulse of a nucleoside analogue is synchronized with meiotic DSB repair, patches of incorporated nucleotide analogue could be localized as long as their size and brightness are enough to be visible at microscope resolution. Mid-prophase I incorporation of either H^3-thymidine or C^{14}-thymidine was already observed in the 1960s in autoradiographies of meiotic cells of the plants *Lilium longiflorum* and *Trillium erectum*, the amphibian *Triturum viridescens*, mouse or human [875–879]. Although at that time the actual molecular mechanism of homologous recombination was yet to be described (Holliday published his model in 1964 and it didn't include DNA synthesis until Meselson and Radding's update in 1975 [880,881]), Wimber and Prensky already proposed, regarding their observation in *T. viridescens,* a relation between meiotic prophase I DNA synthesis and genetic crossing-over, adding: "*we cannot rule out the possibility that the DNA synthesis seen during prophase results from actual chromatid breakage and repair*" [877]. After DNA synthesis was included as an inherent process in the HR molecular models, H^3-thymidine incorporation during pachytene has also been described in Drosophila female meiocytes associated to recombination nodules and in mouse spermatocytes associated to the synaptonemal complex, offering direct evidence of the relation between DNA synthesis and recombination [882,883].

Further characterization of the incorporation of nucleotide analogues during meiotic prophase I has later been done using 5-Bromo-2´-Deoxyuridine (BrdU) in budding yeast, in which the labelling was found to be SPO11-dependent and its presence was confirmed at recombination hotspots and in recombinant DNA molecules, characterizing as well single-molecule BrdU tracts at the hotspots and the timing of their appearance in relation to other meiotic features [884]. This work offered direct evidence of the meiotic DSB-repair associated DNA synthesis predicted by the HR models in detail, confirming some of the expected mechanistic signatures and revealing the potential of this technique in the study of meiotic recombination. Observation of a similar SPO11-dependent BrdU labelling pattern has been described in Tetrahymena but, to our knowledge, no further data has been published in other organisms [885]. Hence the interest of this study in trying this approach to localize DSB repair events at

Arabidopsis meiotic prophase I via the incorporation of nucleotide analogues that can be cytologically detected.

Studies in Arabidopsis have used the incorporation of BrdU or 5-ethynyl-2'-deoxyuridine (EdU) during pre-meiotic S-phase with the aim of analysing the timeline of meiosis. To do so, pulses of 2 hours were applied to the inflorescences after which they were rinsed with water to stop EdU/BrdU incorporation and left to incubate for a variable number of hours to then track the stages labelled with BrdU/EdU at every timepoint [845,886,887]. This experimental setup permits the incorporation of the nucleotide analogues during pre-meiotic S-phase, labelling extensive regions of the genome easily detected in chromosomal preparations at the microscope as a particularly bright fluorescent signal of either big patches in the chromosomes or directly whole genome labelling, depending on the synchronization between the pulse and the S-phase.

Despite this application of BrdU/EdU incorporation to Arabidopsis pollen mother cells prior to meiosis, there are no reports of its incorporation to DSB-repair associated DNA synthesis during meiosis. Successful incorporation and detection of these nucleotide analogues might turn out as a powerful tool for the localization and analysis of most meiotic recombination events happening during Arabidopsis meiosis, including those undetectable with the current molecular tools.

Initial hypothesis

We thus hypothesised that Arabidopsis meiotic cells undergoing prophase I in the presence of EdU would incorporate the nucleotide analogue within meiotic DSB repair-associated DNA synthesis tracts that would become detectable using cytological and molecular techniques. Such EdU-substituted tracts in the genome would be the "footprints" of meiotic recombination and have great potential for the study of meiotic DSB repair.

Objectives

I) To design, test and validate a protocol that permits the incorporation of EdU in prophase I pollen mother cells. Cytological detection of these substituted DNA tracts and their distinction from EdU incorporated during pre-meiotic replication.

II) To characterise the EdU labelling signal in the different meiotic stages as well as the numbers and patterns of EdU individual signals in late prophase I cells.

III) To design, test and validate a protocol for the molecular detection of meiotic DSB repair-associated DNA synthesis tracts including the isolation of meiotic cells, the conjugation of EdU with biotin and the precipitation and sequencing of biotinylated EdU-substituted tracts.

IV) To process and map the sequencing data of biotinylated EdU-substituted tracts in order to detect meiotic DSB repair-associated DNA synthesis hotspots and characterise them by themselves and in relation to published data of Arabidopsis meiotic features.

V) To analyse individual DSB repair-associated DNA synthesis tracts at single molecule level using Nanopore sequencing to directly sequence genomic DNA and call BrdU tracts on it.

Methods

Meiotic chromosome preparations by spreading

Meiosis was analysed following the chromosome spreading method of Ross, Fransz & Jones [267] (with minor modifications). Inflorescences were collected in 3:1 ethanol:glacial acetic acid fixative solution and left overnight at room temperature. The fixative was then substituted with fresh fixative solution and the tubes were transferred to 4°C. This step was repeated the following 2-3 days. At this point, fixed inflorescences can be stored at 4°C for further use or prepared for microscopy.

To do the preparations, a number of inflorescences were selected, deposited in a glass dissection well with 3:1 fixative solution and dissected under a stereomicroscope into individualized flower buds discarding open flowers and buds with pollen (yellow anthers). The flower buds were then washed three times in 1x citrate buffer for 2 minutes each wash. After the last wash, the buffer is removed and replaced with 500µl of digestion enzyme mix (0.3% w/v cellulase from *Trichoderma* sp. (Sigma-Aldrich), 0.3% w/v pectolyase from *Aspergillus japonicus* (Sigma) and 0.3% w/v cytohelicase from *Helix pomatia* (Duchefa Biochemie) in 1x citrate buffer). The flower buds were then incubated in the digestion mix for 2 hours at 37°C. The incubation was stopped by adding a greater volume of ice-cold 1x citrate buffer and the well was placed again under the stereomicroscope. A single flower bud (in most cases) was transferred to a slide in a small volume of solution carried in the Pasteur pipette. The flower bud was prepared by maceration with a flat needle, followed by the addition of a 10µl drop of ice-cold 60% glacial acetic acid and the incubation of the slide for one minute on a hot plate at 45°C while gently moving the drop with a flat needle. After the incubation, an extra 10µl of ice-cold 60% glacial acetic acid were added, followed by 100µl of 3:1 fixative slowly pipetted, first circling and flooding the drop and then disrupting the drop by vigorously pipetting the last microliters. The liquid was retired tilting the slide, which was then further washed with another 100µl of 3:1 fixative, drained and left to air dry at room temperature.

To visualize the chromosomes, the slides are stained with 1.5µg/ml DAPI in Vectashield® by placing a drop in a coverslip and gently depositing and squishing the slide by the side of the material on top of it. Pictures were taken using a Zeiss Axio Imager Z1 microscope with a 100x oil-immersion objective and the Zeiss ZEN 2 software (blue edition) in the channel for blue fluorescence (Zeiss #49 HE filter).

EdU labelling and cytological detection

EdU working solutions were prepared in 1x PBS buffer at 10mM. To incubate Arabidopsis inflorescences in EdU, stems with apical inflorescences were submerged in water to avoid the introduction of air bubbles (submerging only the stem segment to be cut, without wetting the inflorescences) and cut obliquely with a sharp razor blade to make the cleanest cut possible in order to avoid crushing of vascular tissues, leaving 4-5cm of stem below the inflorescence. These inflorescences were incubated for 24 hours in a 2ml eppendorf tube with 800µl of 10mM EdU under the same growing conditions than the plants. Several inflorescences may be incubated in the same tube (avoiding tight packing). After 24 hours the inflorescences are retired from the EdU solution and fixed in 3:1 fixative solution.

Chromosomal spreads were prepared as previously described and visualized under the microscope to identify those slides with cells at the desired meiotic stages. These slides were first incubated in 4T (4x SSC, 0.5% v/v Tween 20) in a Coplin jar until the coverslips detached from the slides and a second time without coverslips in fresh 4T for 30 minutes. The Click-iT™ reaction mix to label EdU with fluorochrome was meanwhile prepared as Table 13. Before the incubation with the Click-iT™ mix, the slides were washed for 5 minutes with 1x PBS. A 30µl drop of Click-iT™ mix per slide was placed in a 32x24 piece of parafilm and the slides were deposited on top of the mix on the parafilm. The slides were incubated with the mix for 30 minutes at 37°C in a dark moist chamber, washed for 5 minutes with PBS in a Coplin jar in the dark and re-stained with DAPI.

Pictures were taken using either a Zeiss Axio Imager Z1 microscope with a 100x oil-immersion objective and the Zeiss ZEN 2 software (blue edition) in filtered channels for blue (Zeiss #49 HE filter) and red (Zeiss #43 HE filter) fluorescence; or with a Zeiss LSM800 confocal microscope using the Airyscan module and selecting the presets for each specific dye. EdU foci were detected and quantified semi-automatically using the IMARIS® software *Spots* tool by adding filters of intensity for both channels to specifically segment visually detectable foci that overlapped the chromosomes.

Table 13. EdU-Alexa Fluor 555 Click-iT reaction.

Components	Volume (µl)
1x Click-iT™ EdU reaction buffer	25.8
$CuSO_4$	1.2
Alexa Fluor® 555 azide	0.075
Reaction buffer additive	3

***Modified from Invitrogen Click-iT™ Plus EdU Alexa Fluor® 555 Imaging Kit (C10638) manual**

Isolation of EdU-labelled meiotic cells and genomic DNA extraction

Inflorescences were incubated in EdU for 24 hours as previously described with the difference that after 24 hours they were not fixed but they were transferred to a glass, where the stems were rinsed with water several times to interrupt the EdU pulse. The EdU negative controls correspond to inflorescences that were incubated following the same protocol in PBS without EdU. While the first inflorescences were being dissected, the rest were left with water in the plant growth chamber and transferred to the dissection set up in the laboratory in small groups to be dissected. If the dissection was expected to last for several hours, inflorescences were set to incubate at different time points the previous day so that the 24 hour periods ended as the day advanced for improved reproducibility.

Meiotic cells were isolated and their genomic DNA extracted following a protocol developed in the laboratory on the basis of C. Chen & E. Retzel and Sims *et al.* capillary collection methods [888,889] and the Choi *et al.* genomic DNA extraction method [829]. One inflorescence at a time was placed under a stereomicroscope on humid filter paper (to avoid drying) in a Petri dish and dissected into individual flower buds. The length of the flower buds was measured to identify the buds with the desired meiotic stages (0.42 – 0.5mm) and the buds outside the desired range were discarded. This step was repeated with multiple inflorescences until the desired number of flower buds within the size range was gathered. To isolate meiotic cells, 2-3 flower buds were placed in a 20µl water drop on a slide, a coverslip was deposited on top and tapped vigorously over each flower bud to squish them and release the meiotic cells grouped in sporogenous archesporial columns (SACs) which could be visually identified. The slide was submerged into liquid nitrogen until it stopped bubbling and the frozen coverslip removed using a sharp razor blade. By doing this, the coverslip is retired without losing the material that generally

remains stick to the slide. The slide was then left to thaw for a few seconds and a drop of 20µl of water pipetted over each flower bud to rehydrate. The rehydrated SACs are carefully separated from the other flower tissues using a thin needle to minimize carry through of flower debris and gathered together to facilitate the collection of the SACs. If the water drop starts to evaporate during the process, extra 20µl were added so the SACs do not dry out. To collect the SACs, thin home-made glass capillaries were made by heating a Pasteur pipette with an alcohol burner until the glass starts to melt to, by carefully pulling the ends in opposite directions, elongate the pipette slimming it down as a result. The pipette was then cut at the thinnest section using a sharp razor blade to obtain a capillary with a thinner tip than the original Pasteur pipette. The capillaries were tested to verify than it has sufficient diameter to aspire the SACs while permitting control and visual tracking of their position, not possible (or much more difficult) with the broader original tip. As many SACs as were identified and isolated per flower bud were collected and transferred using this capillary from the slide to a "DNA LoBind®" Eppendorf tube with a small volume of water to permit pipetting inside liquid and avoid loss of material on the dry walls of the tube. This process was repeated until all of the material was dissected, keeping the tube with the collected SACs on ice. When finished, the tube was snap frozen in liquid nitrogen and stored at -20°C.

To extract genomic DNA, the stored samples were thawed at room temperature and 2 volumes of 1% w/v enzymatic digestion mix were added for a final concentration of 0.3% cellulase, 0.3% pectolyase and 0.3% cytohelicase prepared in SDS cell lysis buffer (50mM Tris-HCl pH8, 100mM NaCl, 1mM EDTA, 1% v/v SDS, 20µg/ml proteinase K). The samples were incubated with the digestion mix for 3 hours at 37°C, followed by the addition of an extra volume of fresh lysis buffer pre-warmed at 65°C and an incubation for 15 minutes at 65°C. The samples were left to cool down for 5 minutes at room temperature, after which RNAseA is added to a concentration of 0.5µg/µl and they are incubated for 15 minutes at 37°C. To purify genomic DNA, one volume of 25:24:1 phenol:chlororform:isoamyl alcohol saturated with 10mM Tris-HCl pH8 1mM EDTA was added and gently homogenized in a rotating wheel for 30 minutes at room temperature. The samples were centrifuged for 10 minutes at 15000g at room temperature and the supernatants transferred to clean DNA LoBind Eppendorf tubes®. One volume of 24:1 chloroform:isoamyl alcohol was then added, gently homogenized by hand inversion and centrifuged for 10 minutes at 15000g at room temperature. The supernatant was transferred to a clean DNA LoBind Eppendorf tube® and 0.7 volumes of isopropanol were added to precipitate DNA followed by a 10 minute incubation at room temperature and a 10 minute centrifugation at 15000g in a pre-cooled centrifuge

at 4°C. The supernatant was discarded and the DNA pellet washed carefully two times with 1ml of freshly prepared 70% ethanol doing a 5 minute 15000g centrifugation at 4°C after each wash. After the second wash, the supernatant was discarded and the tubes were centrifuged again for 30 seconds to then retire the remaining volume of ethanol with a 10µl micropipette (without disturbing the pellet). The samples were left to air dry for 5 minutes and rehydrated with ultra-pure distilled water. The tubes were gently tapped and left overnight at 4°C to resuspend the DNA pellet after which they were used for the preparation of sequencing libraries.

EdU-labelled DNA pull-down

The concentration of the genomic DNA extractions was measured in an Invitrogen Qubit™ 4 fluorometer. Extractions of the same genotype and class from different dissection days were pooled so as to have two biological replicates of each, prepared and sequenced independently. The sequencing libraries were prepared using the NEBNext® Ultra™ II FS DNA Library Prep Kit for Illumina® (NEB #7805S/L) with modifications to the kit protocol to adapt the EdU-biotin azide Click-iT™ reaction and the pull-down of biotinylated DNA. This protocol is partially based on that published by Kit Leng Lui *at al.* [890]. The DNA samples were incubated with NEBNext Ultra II FS Reaction Buffer and NEBNext Ultra II FS Enzyme Mix for 30 minutes at 37°C and 30 minutes at 65°C for DNA fragmentation and end-preparation. At this step, each sample (of 35µl volume) was split into two: 33µl that for pull-down of biotinylated fragments and 2µl that was not to be subjected to pull-down, to serve as the input control sample. Both input and pull-down tubes of each sample were brought up to 35µl and NEBNext UMI Adaptors for Illumina (NEB #E7395) were ligated for sequencing and downstream demultiplexing and deduplication of the sequencing data. After a 15 minute incubation at 20°C with the ligation mix, a cleaning step was added to purify the DNA from the different components of the previous reactions. This step was done using NEBNext Sample Purification Beads as described in the NEBNext® Ultra™ II FS DNA Library Prep Kit for Illumina® manual. The DNA was eluted from the beads with 20µl of 0.1x TE buffer and used for the Click-iT™ reaction with biotin-TEG azide (BT1085 Berry & Associates, Dexter, MI, USA) to biotinylate EdU-labelled DNA fragments (Table 14), incubating the reaction for 45 minutes at room temperature. The DNA was cleaned again with the NEBNext Sample Purification Beads and eluted in 20µl 0.1x TE buffer. At this step, the input control samples were kept on ice for later PCR and the pull-down samples were mixed with Dynabeads™ MyOne™ Streptavidin C1 (#65001 Invitrogen) to pull down the biotinylated fragments. The Dynabeads™ (10µl of 10µg/µl beads per sample) were prewashed twice with 200µl of 1x

B&W buffer (10mM Tris-HCl pH7.5, 0.5mM EDTA, 1M NaCl) + 0.05% v/v Tween 20 and resuspended in 2x B&W buffer + 0.1% v/v Tween 20 calculating 20µl per sample. Each sample was then mixed in a 1:1 proportion with Dynabeads™ to a final bead concentration of 5µg/µl. The tubes were incubated for 20 minutes at room temperature in the dark with gentle shaking to avoid precipitation of the beads and maximize the binding of the fragments. The tubes were placed in a magnetic rack to pellet the Dynabeads™ with the bound biotinylated fragments thanks to their magnetic properties and remove the supernatant in which the non-biotinylated fragments were expected to remain in solution. The Dynabeads™ were then subjected to multiple washes to remove as much non-biotinylated fragments as possible: five washes in 200µl of 1x B&W buffer + 0.05% v/v Tween 20, changing the beads from one tube to another between the fourth and fifth wash to eliminate non-biotinylated fragments potentially stuck to the walls of the tube, two washes in Tris-HCl buffer pH8 + 0.05% v/v Tween 20, one wash in Tris-HCl buffer pH8 and one wash in ultra-pure distilled water. After this last wash, the beads were resuspended in 20µl 0.1x TE buffer. The input controls and the pull-down samples attached to the Dynabeads™ were then used as substrate for PCR to amplify adaptor-ligated fragments using NEBNext Primers Mix (Table 15, Table 16) and the reaction were cleaned using NEBNext Sample Purification Beads as described in NEBNext® Ultra™ II FS DNA Library Prep Kit for Illumina® manual, resuspending the samples in 16µl of 0.1x TE buffer.

Input and pull-down libraries quality, sizing and concentration were assessed by running 1µl per sample in an Agilent 2200 TapeStation system using a D1000 ScreenTape. Input and pull-down libraries of samples incubated in EdU and input libraries of samples incubated in PBS were pooled normalizing concentrations for a 1ng/µl isomix. Pull-down libraries of samples incubated in PBS did not show PCR bands in the D1000 ScreenTape (Figure 24h, Figure 24i & Figure 24j) so the 1ng/µl concentration could not be matched. We used them to dilute other samples down to 1ng/µl, including them this way in the pool for sequencing understanding that their concentration might be below the instrument lower limit. Pooled samples were send to BGI for paired end (2x100bp) sequencing in a MGISEQ-2000 platform.

Table 14. EdU-biotin Click-iT reaction.

Components	Volume (µl)
Adapter-ligated DNA	25
Tris-HCl buffer pH8	5
$CuSO_4$ (100mM)	1
Biotin-TEG azide (100mM)	1
Sodium ascorbate (100mM)	5
Ultra-pure distilled water	14

Table 15. EdU library PCR reaction.

Components	Volume (µl)
Adapter-ligated DNA	20*
NEBNext primer mix	5
NEBNext Ultra II Q5 master mix	25

*Volume of Dynabeads for the pulled-down samples

Table 16. EdU library PCR program.

Steps	Temperature	Time	
Initial denaturation	98°C	30s	
Denaturation	98°C	10s	x18-24*
Annealing/Extension	65°C	75s	
Final extension	65°C	5min	
Storage	4°C	∞	

*18 cycles for input samples and 24 cycles for pulled-down samples

Bioinformatic processing and analysis of EdU-labelled DNA pull-down sequencing data

Multiplexed R1 and R2 raw reads (.fastq files) were first processed to extract the Unique Molecular Identifiers (UMIs) and move them from each read to the header of the read for later use. To do this, we used UMI-tools extract (version 1.1.2) with the following parameters: string barcode extraction method, barcode at the 3' of the R2 read, barcode pattern NNNNNNNNNNNXXXXXXXX, ignore '\1' and '\2' read name suffixes. By doing so, the 11nt of the UMIs (N's in the barcode pattern) were extracted and added to the header while re-pasting the 8nt indexes that identifies each library (X's in the barcode pattern) for latter demultiplexing. Demultiplexing was done using Cutadapt (version 3.5) with the following parameters: anchored adapters at the 3' end of R2 (-a ADAPTER$), 2 mismatches allowed in the indexes (-e 0.3; minimum Hamming distance between indexes equal 3), no indels. Indexes are clipped from the reads as they are demultiplexed. Individual .fastq files of R1 (100bp) and R2 (110bp) reads of all input and pull-down libraries were obtained. R2 reads were trimmed down to 100bp with Trimmomatic (version 0.38) to remove those extra 10bp that are part of the UMI-containing adapter. R1 and R2 files are then processed with Trim Galore! (version 0.6.3) Illumina universal default option to clip remaining adapters within the 100bp reads. R1 and R2 adapter-free .fastq files of the input and pull-down libraries for each sample with the UMIs at the header of each read were used as input for mapping into the genome.

Alignment, filtering and merging of aligned files was performed following a modified version of Choi *et al.* (2018) SPO11-oligos workflow (Supplemental Methods, Bioinformatics analysis of SPO11-oligonuclotide data) [361]. Reads were aligned to the TAIR10 *A. thaliana* reference sequence using Bowtie2 (version 2.3.4.1) with the following parameters: paired-end, very sensitive end-to-end. Mapped reads were split into uniquely and multiply mapped reads with Bamtools filter (version 2.4.0) using the XS tag, absent in uniquely mapped reads and present in multiply mapped reads. Multiply mapped reads were filtered to discard reads with MAPQ scores of less than 10 with Bamtools filter (version 2.4.0). Both uniquely and multiply mapped reads were deduplicated with UMI-tools deduplicate (version 1.1.2) to remove duplicated reads that share the same UMI with the following parameters: BAM is paired-end, barcodes are contained at the end of the read separated by a delimiter (--extract-umi-method), "-" delimiter (--umi-separator), identify clusters based on distance and counts, restrict

network expansion by threshold (--method). Filtered and deduplicated BAM files corresponding to uniquely and multiply mapped reads were merged with Samtools merge (version 1.9). The resulting merged .bam files of each input and pull-down libraries for every sample were the alignment files used for downstream analysis.

For each input and pull-down alignment file (.bam), a normalized bigwig coverage file was generated using Deeptools bamCoverage (version 3.3.2) with the following parameters: 1bp bin size, normalized to counts per million (CPM), mitochondria and chloroplast excluded for normalization, paired-end extension. Bigwig files consisting on the log2 of the pull-down to input signal ratio were generated using Deeptools bigwigCompare (version 3.3.2) with the following parameters: compute log2 of the signal ratio, 1bp bin size.

Peak calling and characterization

Peak calling was performed using the callpeak function from Macs2 (version 2.1.1.20160309). Each sample was ran independently with the pull-down alignment file as treatment file and the corresponding input alignment file as control file, using the following parameters: paired-end BAM, effective genome size of 119000000, no shifting model, 200bp extension size, minimum FDR (q-value) cut-off of 0.05 for peak detection and 0.1 for broad regions. The called broad peaks were used for subsequent analyses. Intersection between peaks from different samples was done using Bedtools intersect (version 2.27.1) with a minimum required overlap of 1bp. Venn diagrams of peak and region intersections were generated with Intervene venn (version 0.6.5). Peaks and regions width characterization and plotting was done using the Descriptive statistics function of GraphPad Prism (version 8.4.3) plus the unpaired t-test function for analysis of difference significance.

Density profiles and heatmaps over peaks, genomic features and chromosomes

The bigwig coverage files and log2 ratio signal profiles were visually inspected for analysis with Integrative Genomics Viewer (IGV; version 2.7.2). To profile the signal density of our samples and SPO11-oligos over the called peaks and different genomic features (genes, TEs, SPO11 hotspots…) as well as elaborating the heatmaps with the color-coded density we used different tools of the Deeptools suite (version 3.3.2). Data was prepared using Deeptools computeMatrix with the interval (.bed) files as input for regions to plot and log2 ratio pull-down/input bigwig files as input for score files. Depending on the features, the output option was set to scale-regions, in which the

regions are stretched or shrunken to a given width in base pairs and a distance upstream the start and downstream the end of the region is defined to be plotted along; or reference-point, in which the regions were centred using their midpoint and a distance upstream and downstream that midpoint is defined to be plotted. The election between the two modes and the widths and distances chosen are explicit in the different plots. A bin size 50bp was used for non-overlapping bins to average the score over the region length.

The computeMatrix outputs were used as inputs for plotting using Deeptools plotProfile and Deeptools plotHeatmap. plotProfile was ran selecting scale-regions mode or not depending on the election done in for respective computeMatrix file. The mean signal was chosen as the statistic to be plotted as the profile line together with the standard error as fills around the profile line. The option --perGroup was set to Yes to make one plot per group of regions in all cases. plotHeatmap was ran using the same computeMatrix file in parallel with plotProfile selecting heatmap and colorbar to show and setting the --perGroup option to Yes as well. Plots generated with both tools were later mounted together in Keynote.

Random shuffling of the different interval files was used recurrently as controls. Bedtools ShuffleBed (version 2.27.1) was employed for this purpose with the following parameters: the different interval files as input to be shuffled over TAIR10 sequence, random shuffling without choosing seed.

To profile the signal of our different samples and SPO11-oligos along the chromosomes, bedgraph files computing the log2 of the pull-down to input signal ratio were generated with Deeptools bigwigCompare (version 3.3.2) using 10kb bins to average the score over each bin. These bedgraph files were input into a custom R script in which:

I) for each bin defined by a start and end coordinate, the central point was calculated to be used hereon as reference point for plotting the value of that bin;

II) the log2 ratio values were smoothed by calculating a rolling mean of 1Mb moving windows using the rollapply function of the zoo package (version 1.8.9) with the following parameters: log2 ratio as input data, width of 100 (100 windows of 10kb bins for 1Mb total), using the mean as function to be applied and aligned at centre of the 100 windows. The different chromosomes were treated individually so the rolling mean was not applied for the last bins of one chromosome using the first bins of the next chromosome.

III) the smoothed log2 ratio profiles for all samples were plotted using the geom_line function of ggplot2 (version 3.3.5). The centromeric region was added with the geom_rect function of ggplot2 using the coordinates reported by Underwood *et al.* (2018) [760]. The profiles were plotted along the five chromosomes separately by using the facet_wrap function of ggplot2 with the coordinates calculated in I as x values.

Results

EdU labelling of DSB repair-associated DNA synthesis in Arabidopsis

Methods for the synchronization of vegetative and meiotic cell cultures are well established in budding yeast, facilitating pulse labelling approaches to specifically target either S-phase DNA synthesis or prophase I DNA synthesis in the whole cell population. In Arabidopsis, pre-meiotic and meiotic cells of a given flower bud are only partially synchronous and not experimentally synchronizable to date. At the inflorescence level, flower buds coexist bearing germ cells at different stages of pre-meiotic cell cycle and meiotic division. This window narrows when a single flower bud is analysed, although the pollen mother cells (PMC) of its different anthers are not completely synchronous [891,892]. The two DNA synthesis windows (S-phase and prophase I) are however temporally separated by several hours in these cells and the linear nature of meiosis with stages that are cytologically distinguishable facilitates the relative situation of a given cell subpopulation with respect to others (i.e. labelled metaphase I cells were likely at a more advance stage than labelled zygotene cells at the beginning of the pulse).

Our approach thus consisted in the incubation of Arabidopsis inflorescences with the nucleoside analogue for a long pulse that would likely cover the DSB repair-associated DNA synthesis window at prophase I entirely in the cells that undergo prophase I at the time of the pulse, although cells at pre-meiotic stages would also incorporate it at S-phase. Taking advantage of the expected different signature of S-phase labelling with respect to DSB repair-associated labelling (if conserved as in other organisms cited above) and the relative temporal situation of the subpopulations of meiotic cells at different stages we hypothesized that we could distinguish S-phase labelled cells from prophase I-labelled cells, when observed at chromosomal preparations, for the study of the second ones.

In Arabidopsis, as in other organisms, DSBs formation is thought to start at the very onset of prophase I and it continues along the first hours, as measured by the immunolocalization of DSB proteins [282]. Although there is no direct evidence of the timing of the different recombination intermediate DNA molecules, DNA labelling and the immunolocalization of meiotic proteins that act at the level of early invasion intermediates (RAD51/DMC1), JMs (MSH4, early HEI10) and resolution of recombination (MLH1, late HEI10) gives a clear picture of the advance of these events through prophase I. In pachytene, when synapsis is complete, the number MLH1 foci generally corresponds (by mean) to the number of class I crossovers measured by

chiasmata counting at metaphase I. Given that Mlh1 functions at the last step of dHJ resolution and that, in the organisms in which recombination intermediates can be tracked, non-crossover products resolution precedes crossovers, it is assumed that at pachytene stage most of the meiotic recombination events are either resolved or close to resolution, similarly to other organisms. According to the different published timelines of Arabidopsis male meiosis pre-meiotic G2 phase lasts 7-10 hours and cells advance from meiotic entry (beginning of leptotene) to the end of pachytene in 19 to 21 hours [289,845,887,893].

Given this, we decided to incubate the cells with the nucleoside analogue for of 24 hours to cover the window of DSB repair-associated DNA synthesis throughout prophase I up to the end of pachytene. By doing so, pachytene cells observed at the end of the 24 hours incubation would likely have undergone the whole prophase I up to that point in the presence of the nucleotide analogue, potentially incorporating it to every event of DNA synthesis happening during the incubation period. Pre-meiotic cells undergoing S-phase during the period would have extensive labelling and, at the end of it, would be at earlier stages given the meiotic timeline, permitting a clear differentiation together by the stage observed and the signature of S-phase labelling.

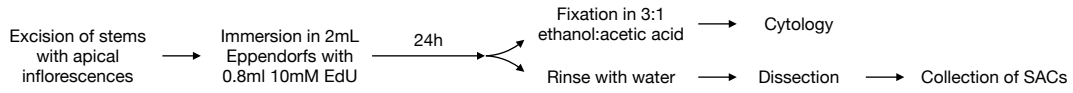

Figure 19. Experimental setup for EdU incorporation into Arabidopsis prophase I cells.

Among the different thymidine analogues than can be incorporated *in vivo* into the genome, EdU has a number of advantages and has been preferred by the Arabidopsis community in recent studies labelling DNA synthesis [442,887,894–896]. EdU offers the possibility of simplified labelling with standard fluorochromes for fluorescent microscopy and avoids the need to work with radioactivity imposed by the traditional options such as H^3-thymidine or C^{14}-thymidine. Detection of BrdU involves use of an anti-BrdU antibody conjugated with a fluorochrome, requiring cell membrane permeabilization and DNA denaturation for the antibody to access the BrdU labelled tracks in genomic DNA. EdU can be detected in intact double-strand DNA without cell membrane permeabilization. It uses small fluorochrome-azide molecules that are not conjugated to an antibody but can be covalently bond to the terminal alkyne group of EdU via a "click" copper-catalysed cycloaddition reaction. This antibody-free technique not only simplifies the protocol and offers greater reproducibility by removing the

permeabilization and denaturation steps, but offers the potential to link EdU to any molecule that can be conjugated with an azide group [897,898].

The experimental setup for EdU incorporation into Arabidopsis meiotic prophase I cells (Figure 19) was adapted from Stronghill, Azimi & Hasenkampf (2014) [887]. Arabidopsis stems with a terminal inflorescence were cut with a sharp razor blade under water to a length that permits easy accommodation into 2ml Eppendorf tubes (around 5cm; Figure 24a). Open flowers and big leaves (if present) were removed to avoid crowding the tube and minimize the risk of exhausting the solution due to excessive transpiration. Up to four or five inflorescences were incubated in a 2ml tube with 0.8ml of 10mM EdU solution. The inflorescences were left to incubate for 24 hours in the growth chamber under the same conditions as the Arabidopsis plants. After 24 hours, the inflorescences were fixed in 3:1 ethanol:glacial acetic acid. Chromosomal spreads were prepared, EdU was labelled and pictures at the microscope were taken for analysis as detailed in the methods section.

Non-replicative DNA synthesis foci are detected from pachytene to the end of meiosis

Wild-type (Col-0) early prophase I meiocytes, including cells in leptotene and zygotene, showed complete or extensive EdU labelling of their chromosomes, similarly to that previously reported for incorporation of EdU during pre-meiotic S-phase and as expected from the length of the incubation period (Figure 20, Early PI) [442,845,887,893,894]. One of the predictions that could be drawn from our experimental setup is that we would find cells with partial EdU replicative labelling corresponding to cells that were in mid/late S-phase when the incubation with EdU started. These cells would thus have incorporated EdU only in late replicating regions. According to genome-wide analyses of the Arabidopsis replication program, late replicating regions are predominantly heterochromatic, with pericentromeric and centromeric regions of the chromosomes concentrating most of the late replicating activity detected [899]. Heterochromatic regions can be cytologically identified at early prophase I as DAPI-dense regions that generally colocalize with centromeric or pericentromeric FISH probes and ribosomal gene arrays [894,900,901]. As shown in the second row of Figure 20, early PI, we did find the expected cells with partial labelling showing large patches of the bright EdU signal characteristic of S-phase labelling colocalizing with DAPI-dense regions of the chromosomes.

After detecting cells with complete replicative labelling (that underwent S-phase during the incubation period) and cells with partial replicative labelling (that were caught in late S-phase during the incubation period), it would be expected to find cells

at immediate posterior meiotic stages that would not have replicative labelling (as they would have completed S-phase before the incubation). These cells would have undergone meiotic recombination (partially or totally) in the presence of EdU, potentially incorporating it at recombination-associated DNA synthesis tracts.

The next easily recognizable prophase I stage is pachytene, in which meiotic recombination is likely at the point of resolution or completed. The pachytenes observed ($n > 50$) did not show replicative EdU labelling, but much fainter and discrete foci of a considerably smaller size than replicative EdU patches could be detected (Figure 20, Pachytene; Figure 22b). These foci are hardly visible through the microscope eyepiece in a considerable proportion of the cells (depending upon the quality of the preparation). They are however clearly visible when the images are processed. The disparities in image acquisition parameters preclude quantitative comparisons of intensity between the (very strong) EdU signals coming from S-phase labelling and the prophase I signals. Nevertheless, a qualitative comparison can made using mitochondria and chloroplasts as reference. Mitochondria and chloroplasts carry their own genomes and are visible when preparations are stained with DAPI as small circular objects surrounding the chromosomes (Figure 20, all stages). Although the replication and division dynamics of these two organelles during meiosis are not well characterized in Arabidopsis, their strong EdU labelling (Figure 20 Pachytene to TII) confirms that they replicate during G2 or/and prophase I. These organellar signals, visible from pachytene on, are also present in early prophase I cells but not immediately visible due to the very strong fluorescence of the S-phase replicative nuclear labelling (Figure 20, Early PI vs. Pachytene-to-Tetrad). The difference of the chromosomal signal between early prophase I (S-phase incorporation) and pachytene (prophase incorporation) is expected considering that DSB repair-associated DNA synthesis tracts might range from tens of DNA base pairs up to some kilobases (to be discussed later) and replicative DNA synthesis in the cells here shown is either covering the whole genome (130 megabases approximately) or at least megabase-long regions.

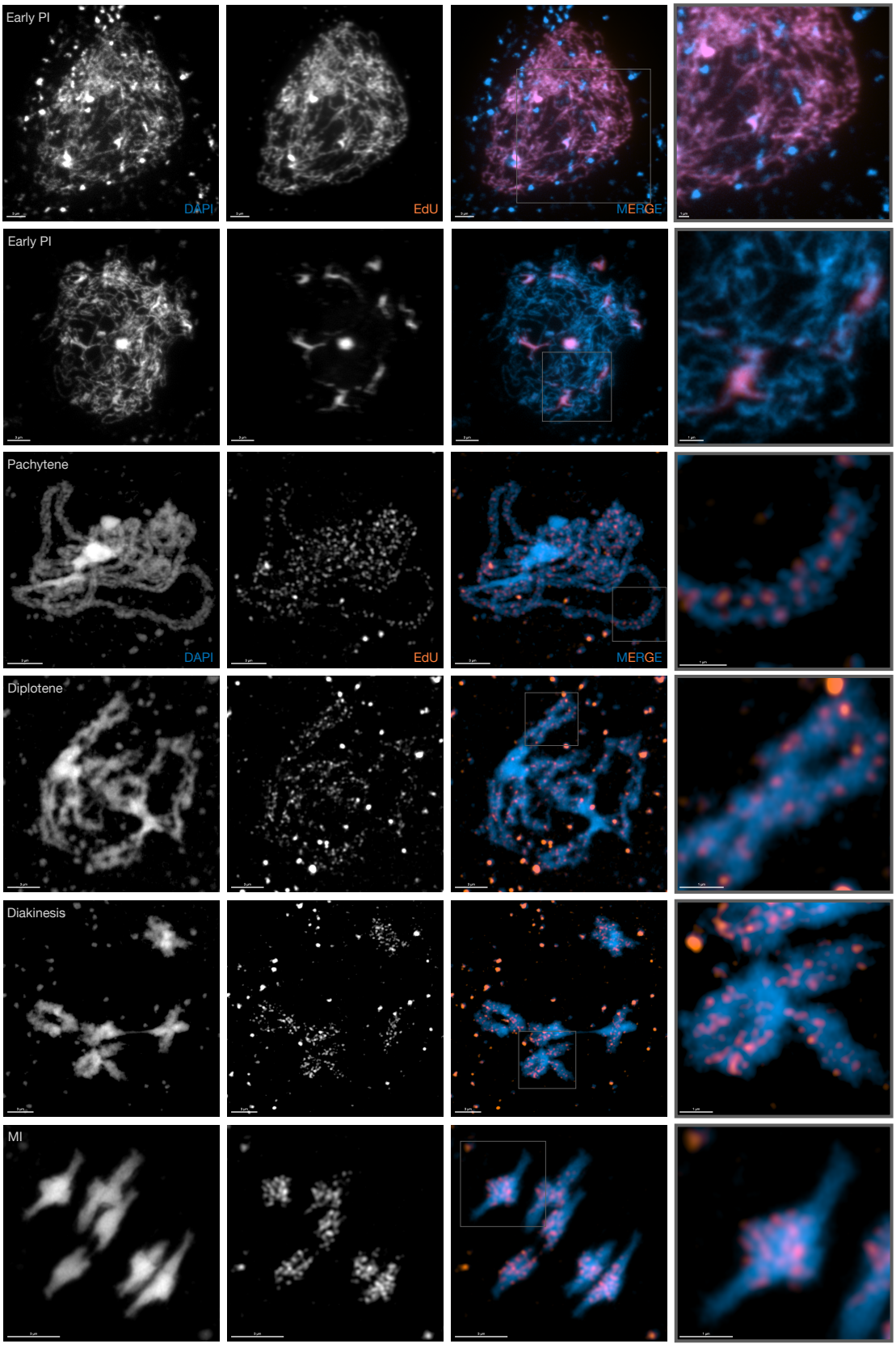
Early PI
DAPI
EdU
MERGE
Early PI
Pachytene
DAPI
EdU
MERGE
Diplotene
Diakinesis
MI

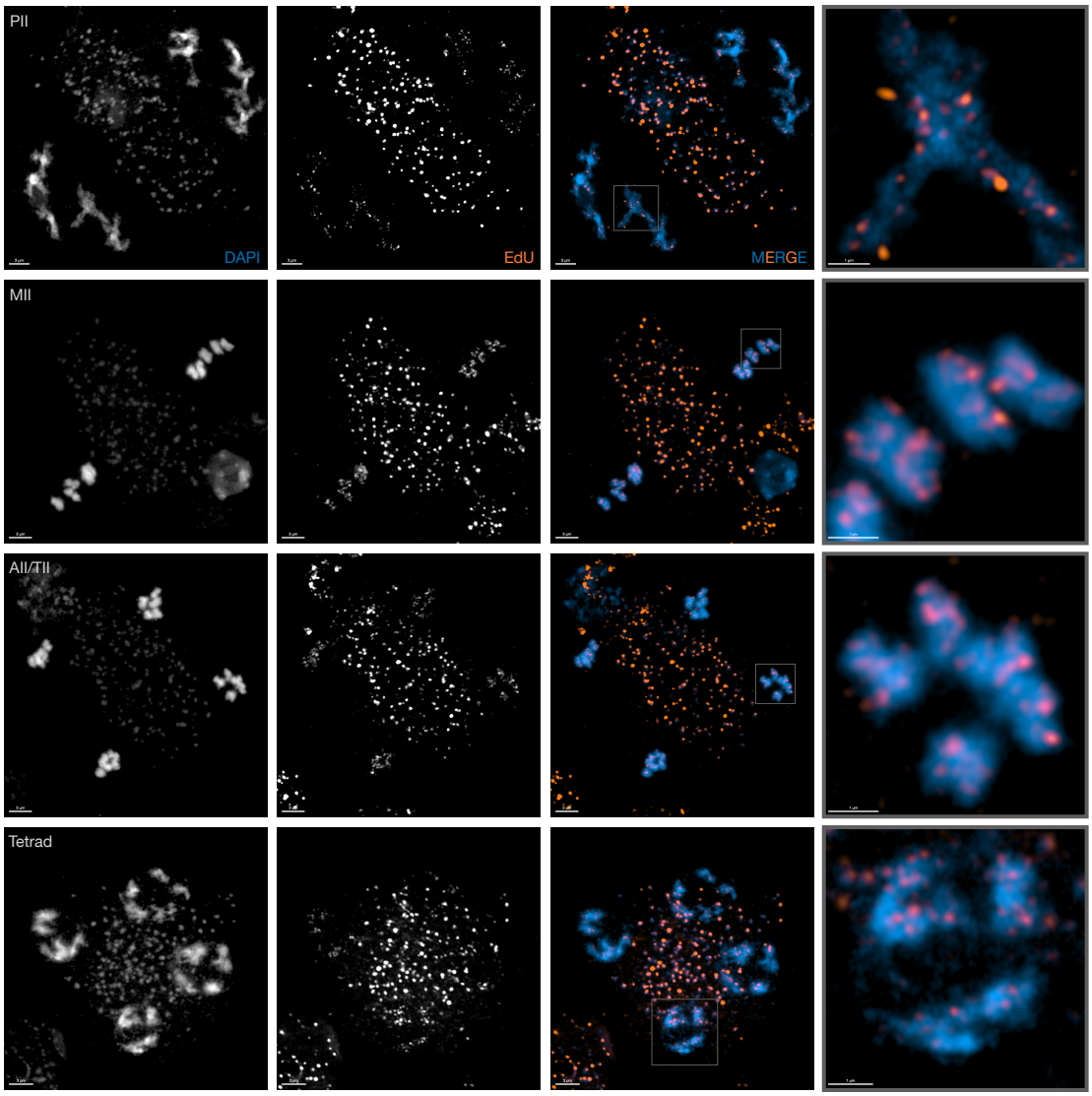

Figure 20. An EdU-labelling pattern that resembles EdU incorporation at DSB repair-associated DNA synthesis tracts is detected from pachytene up to the end of meiosis.

Representative microscope images of chromosome spreadings of WT cells at different stages of meiosis after a 24 hour EdU pulse (stage indicated in the top-left corner of the first column's images). Images of one row correspond to the same cell in which the chromosomes have been stained with DAPI (first column) and the EdU-substituted tracts labelled with AlexaFluor 555 (second column). Both signals are merged in the third column (DAPI in blue, EdU in orange). Column four are magnified sections from the cell for detailed observation of the signals on the chromosomes. The sections taken are marked by a grey window in the third column images.

Immunofluorescence studies of the distribution of early recombination proteins, genetic crossover mapping and SPO11-oligo sequencing in Arabidopsis show recombination to follow a relatively flat distribution across the genome, with the exception of centromeric and pericentromeric regions which have significantly lower densities of SPO11-oligos and crossovers than the rest of the genome [11,361,791]. The EdU foci observed in pachytene cells (Figure 20, Pachytene; Figure 22b) were well distributed throughout the chromosomes and indeed, DAPI-dense regions displayed a lower density of EdU foci than the rest of the chromosomes. It is important to remark that these heterochromatic DAPI-dense regions have tighter-packed DNA than the chromosome arms and this difference is presumably even greater in terms of the number of foci per megabase of DNA.

While Arabidopsis meiotic prophase I up to the end of pachytene takes almost 24 hours, the subsequent stages of meiosis are considerably faster, with post-pachytene meiosis completing in about 2.7 to 9 hours [289,845,887,893]. Consequently, it might be expected that if the EdU foci observed in meiotic cells at pachytene correspond to EdU incorporation at DSB repair-associated DNA synthesis tracts that formed during zygotene-pachytene, this signal would likely be observable in cells at multiple (or even all) stages up to the end of meiosis. This is indeed the case, with the foci visible from pachytene to the end of meiosis (TII/tetrad).

All along prophase I chromosomes gradually condense, evolving from a mass of hardly-distinguishable thin fibres at early leptotene, to thick synapsed fibres in pachytene and to individualized dense bivalents with a more polygonal shape in metaphase I. This condensation is accompanied by significant shortening of the chromosomes and results in changes of the visual character of the EdU signals observed. While most EdU foci at pachytene look discrete, they merge into larger signals at diplotene, even more so at diakinesis and up until the highest condensation point in metaphase I (Figure 20, Diplotene-MI). Metaphase I EdU signals cover the chromosome arms almost entirely, although regions of higher and of lower density are observed. When bivalents individualize at diakinesis, centromeric and pericentromeric regions become more easily identifiable and the relatively low density of EdU signals in these regions is notable. This phenomenon becomes even more obvious at metaphase I, in which the alignment of the chromosomes on the metaphase plate with the kinetochores of the homologous chromosomes being pulled away to opposite poles of the spindle, permits a clear differentiation between the centromeric and pericentromeric regions of the two homologous chromosomes of each pair. Finally, the EdU signals are observed throughout the second meiotic division, changing their appearance with evolving

chromosome condensation and shape in a way similar to that seen during the first meiotic division (Figure 20, PII-Tetrad).

Prophase I DNA synthesis is SPO11-dependent

If the EdU foci observed at pachytene and subsequent stages are originated from the incorporation of this thymidine analogue at DNA synthesis tracts associated to meiotic DSB repair, we would expect to lose them in cells that do not form DSBs at the beginning of meiosis. To test this hypothesis, we chose to repeat the experiment in a *spo11-1* mutant, which encodes a non-functional allele of SPO11-1, catalytic subunit of the SPO11 complex, responsible of meiotic DSBs [307].

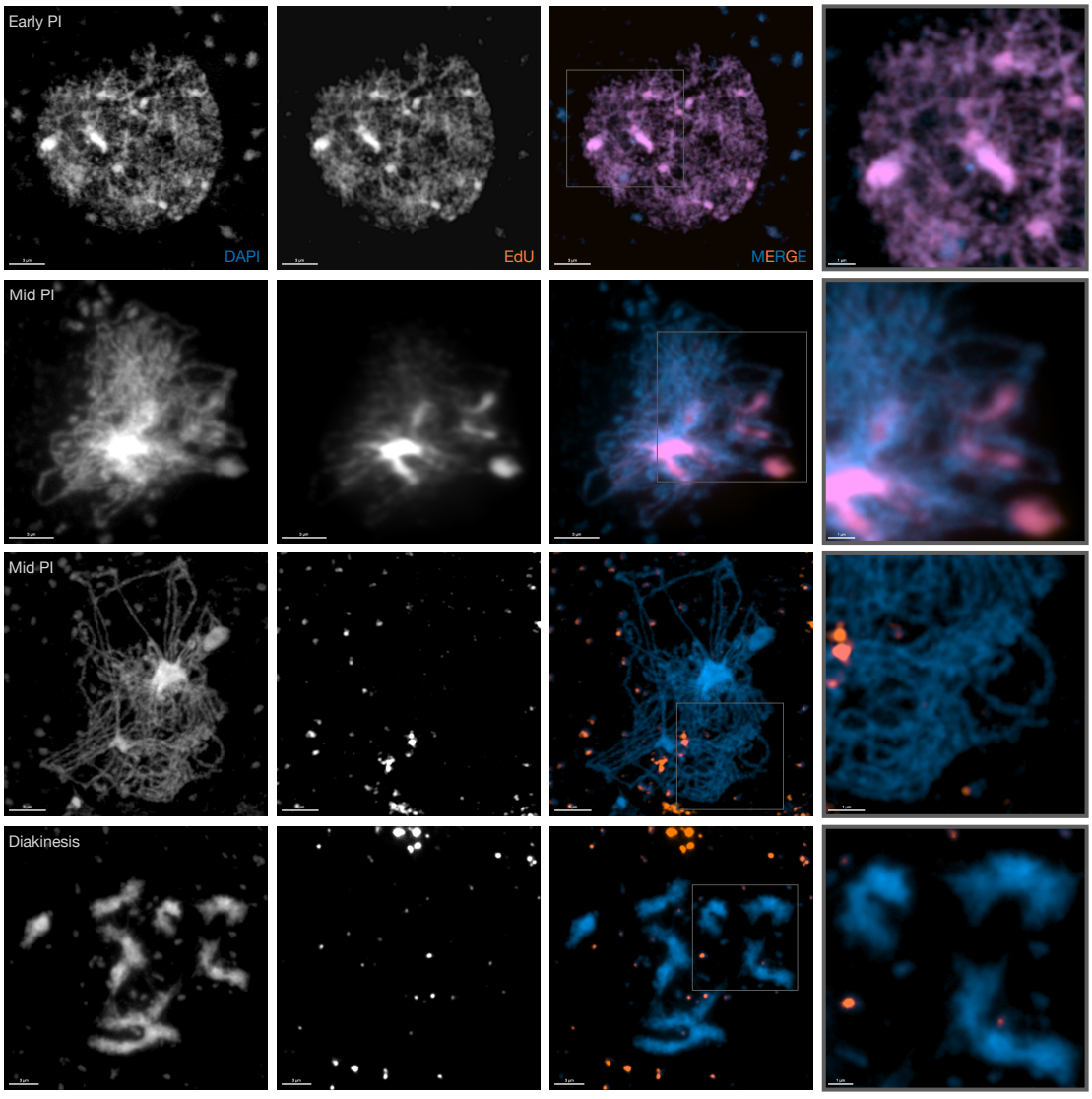

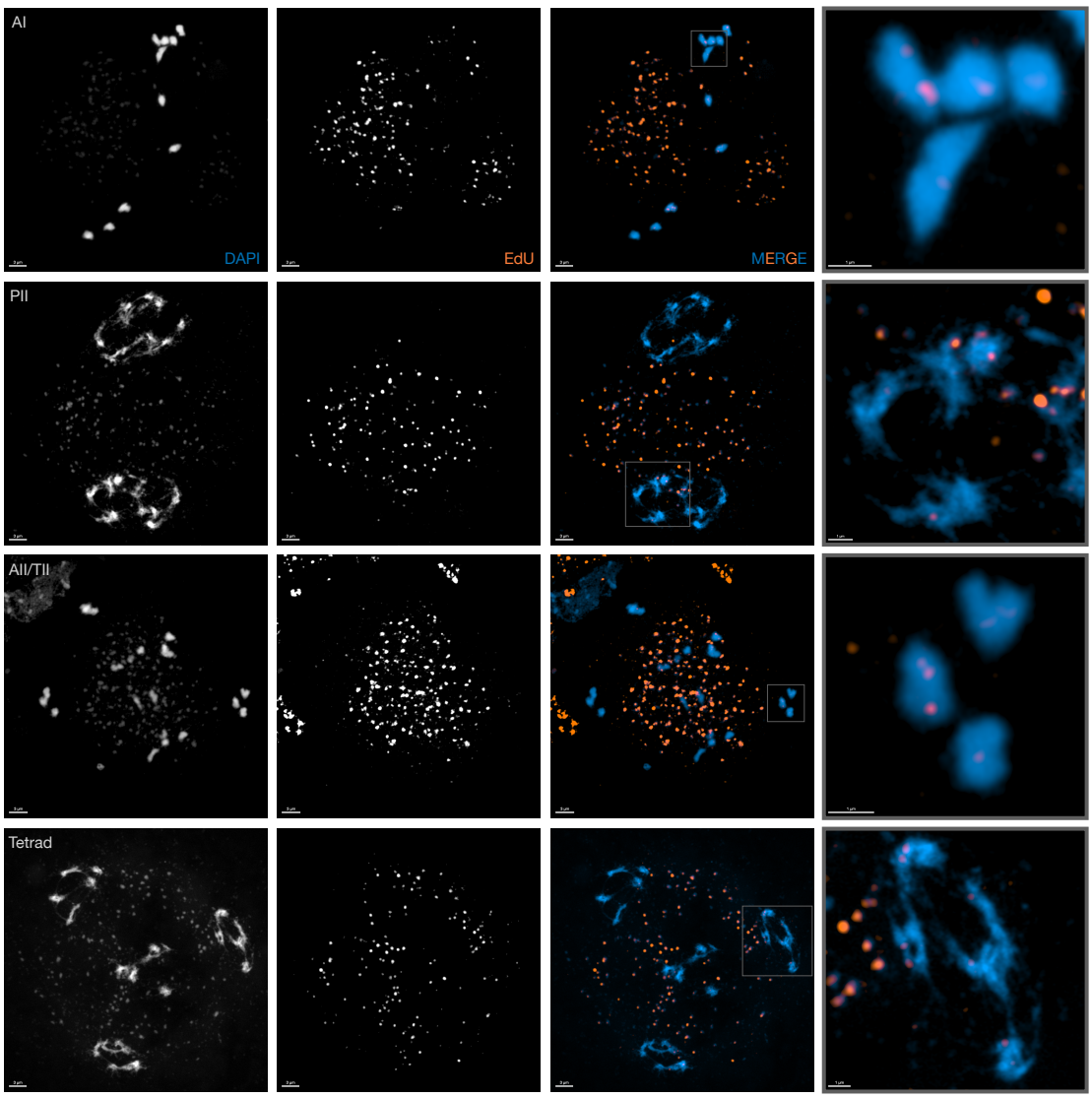

Figure 21. The EdU-labelling pattern of putative DSB repair-associated DNA synthesis tracts is SPO11-dependent.

Representative microscope images of chromosome spreadings of *spo11* cells at different stages of meiosis after a 24 hour EdU pulse (stage indicated in the top-left corner of the first column's images). Images of one row correspond to the same cell in which the chromosomes have been stained with DAPI (first column) and the EdU-substituted tracts labelled with AlexaFluor 555 (second column). Both signals are merged in the third column (DAPI in blue, EdU in orange). Column four are magnified sections from the cell for detailed observation of the signals on the chromosomes. The sections taken are marked by a grey window in the third column images.

In *spo11* early prophase I cells (Figure 21, early PI) we could observe the expected replicative EdU signal characterized by extensive strong fluorescence along the chromosomes as seen in the WT. As with the WT, we could also observe cells in more advanced prophase I stages in which the signal is incomplete, presumably due to them

having been caught at mid/late-S-phase at the start of the incubation with EdU (Figure 21, mid PI, second row).

The *spo11* mutants however show important differences from the WT in the following stages. It is worth mention that the different substages of meiotic prophase I are arbitrary divisions of a continuous process based on three main features that evolve over its course: chromatin condensation (thickening of the chromatin fibres), chromosome pairing and synapsis. In Arabidopsis, the latter two features are contingent upon the initiation and successful progress of homologous recombination. In genetic backgrounds in which DSBs are not formed, such as *spo11,* pairing and synapsis do not occur or are highly defective. *spo11* cells at leptotene can be differenced from a zygotene-like state by the condensation of the chromosomes (thickness of the fibres) and the clustering of DAPI-dense regions. It is however much more difficult to distinguish cells at the *spo11* equivalents of zygotene and pachytene. Luckily, our experimental setup together with the linear progression of meiosis offers an approximation to solve this issue. Given the same incubation time (24h), we may consider that *spo11* zygotene/pachytene-like cells that do not show replicative EdU labelling are in a more advanced state that those that show it, as they would have completed S-phase at the beginning of the pulse (Figure 21, mid PI, third row vs second row, respectively).

These zygotene/pachytene-like cells without replicative labelling did not show the EdU signal observed at WT pachytene cells consisting on numerous faint and discrete EdU foci distributed similarly all along the chromosomes but in DAPI-dense regions, in which they are less abundant (Figure 21, mid PI, third row; Figure 22c). Some EdU foci could be detected but in significantly lower numbers and of, in general, considerably lesser size and brightness when compared to WT foci. A similar signature could be observed in *spo11* cells at subsequent stages of both the first and second meiotic divisions (Figure 21, diakinesis to TII). In the stages in which chromosomes are at the peak of chromatin condensation (MI and MII), some EdU foci could be detected but in much lower abundance, not even present in all chromosomes and in much lower numbers than WT. In *spo11* cells we could observe as well the EdU signal in organelles around the chromosomes similarly to WT cells, which is helpful as an extra positive technical control of EdU incorporation.

Prophase I DNA synthesis patterns mirror meiotic recombination features

The meiotic EdU foci were counted in both WT and *spo11* cells for its characterisation and comparison with each other and with published data of

immunolocalization of different meiotic recombination proteins. To do so, pachytene images were analysed with the IMARIS software (Oxford Instruments, UK) *Spots* function. EdU foci were selected based on diameter and EdU fluorescence (mean intensity in the EdU channel) plus colocalization with chromosome fibres (mean intensity in the DAPI channel). A high-cut filter of mean intensity in the EdU channel was also applied to filter out the much brighter organelles.

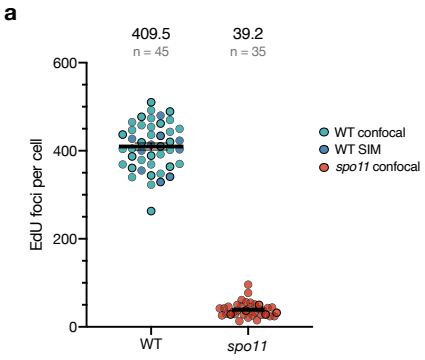

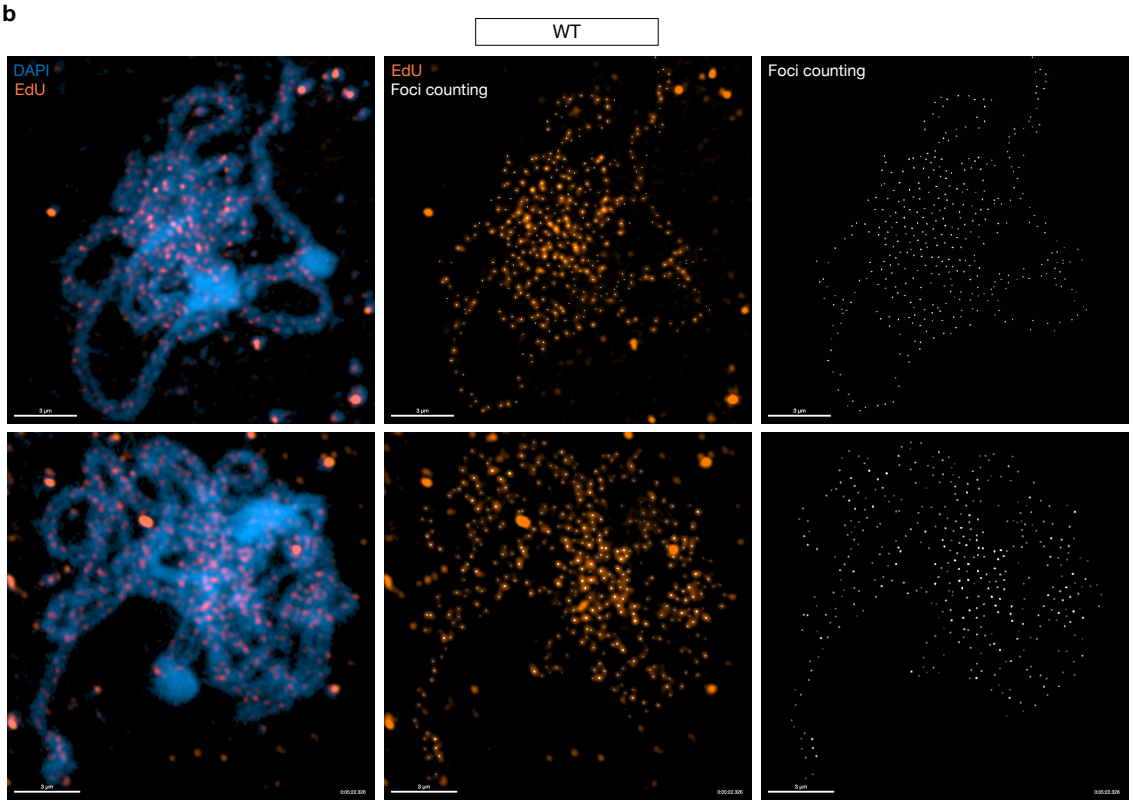

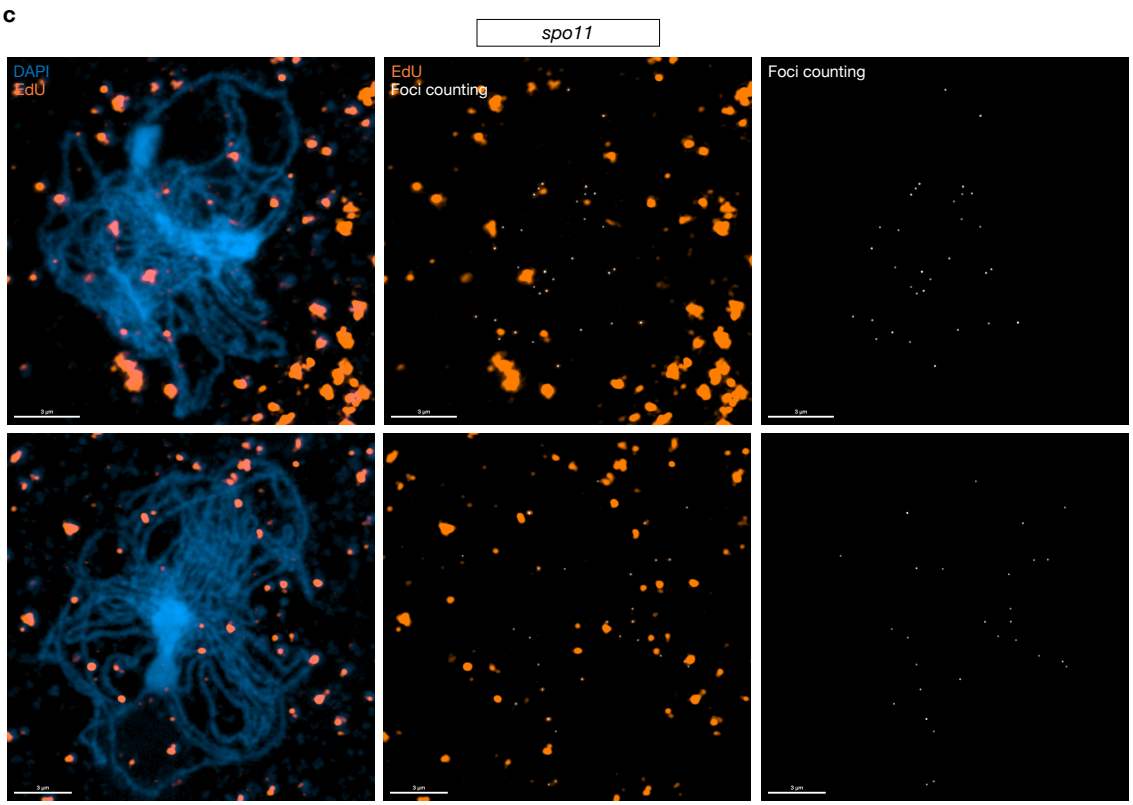

Figure 22. DSB repair-associated DNA synthesis foci at pachytene are compatible with estimations of DSBs in Arabidopsis.

(a) Numbers of EdU foci per cell located on the chromosomes in cells at pachytene in WT, pachytene-like stages in *spo11*. The mean numbers of EdU foci per genotype and the number of cells scored are specified above. WT cells imaged with a confocal microscope (green) and SIM microscope (blue) are pooled together in WT. Examples of images of cells scored in **(b)** WT and **(c)** *spo11* are shown below. Images of one row correspond to the same cell. The first column shows the merged signals of DAPI (blue) and EdU (orange). The second column correspond to the signal of EdU (orange) plus the computer-generated image of the scored EdU foci (white). The third column correspond to the computer-generated image of the scored EdU foci (white).

409.5 ± 7.96 EdU foci per cell (mean ± SEM ; n = 45 cells; Figure 22a & Figure 22b) were observed in WT pachytenes, ranging from 323 to 510 (plus one outlier with 263). 10 of these 45 images were taken with a super-resolution SIM microscope in collaboration with Veit Schubert and Andreas Houben (IPK, Gatersleben, Germany), to compare with the our images taken with a confocal (plus Airyscan) microscope and confirm that we were not missing foci. WT cells imaged with SIM had a mean 400.6 ± 14.74 EdU foci (n = 10) while WT cells imaged with the confocal microscope had a mean 412.1 ± 9.38 EdU foci (n = 35), hence no significant difference was observed between the two systems (unpaired t-test; p = 0.55).

In *spo11* plants, 39.2 ± 2.83 EdU foci per cell (mean ± SEM; n = 35 cells; Figure 22a & Figure 22c) were detected at zygotene/pachytene, ranging from 13 to 61 (plus two outliers with 77 and 96). This difference with respect to the WT (unpaired t-test;

$p < 0.0001$) confirms the SPO11-dependence of the great majority of the EdU incorporation events.

Meiotic recombination models predict different patterns of DNA synthesis tracts depending on how recombination intermediates are formed and resolved. Non-crossover events generated by either SDSA or dHJ dissolution produce DNA synthesis tracts in only one of the two chromatids implicated (and thus in one of the homologous chromosomes in interhomologue recombination). On the other hand, double Holiday junction nucleolytic resolution resulting in either crossover or non-crossover products will generate DNA synthesis tracts in both chromatids implicated, hence both chromosomes in interhomologue events. In well spread WT pachytene cells, despite synapsis keeping both homologous chromosomes together, there are segments in which they can be visually differentiated as the two DAPI signals are separated by a gap of lower DAPI intensity. Different patterns of EdU foci could thus be observed when looked at in detail.

When individual EdU foci are visually analysed with respect to the chromosomes, no obvious bias in their disposition is observed. EdU foci located at both the internal (facing the homologous chromosome) and external sides of the chromosomes were observed as well as right in middle of the chromosome (Figure 23). When EdU foci are analysed with respect to adjacent foci, different classes could be visually detected (Figure 23): single foci at one of the homologues with no focus in parallel in the other homologue; pairs of foci in parallel (at similar location) in both homologues that are spatially separated; and pairs of foci in parallel (at similar location) in both homologues whose signals are in contact to some extent. Whether the differentiation of these latter two classes is biologically relevant or results from an artifact of imaging resolution or perspective remains to be determined. A quantification of the proportions of each class remains to be done in the near future.

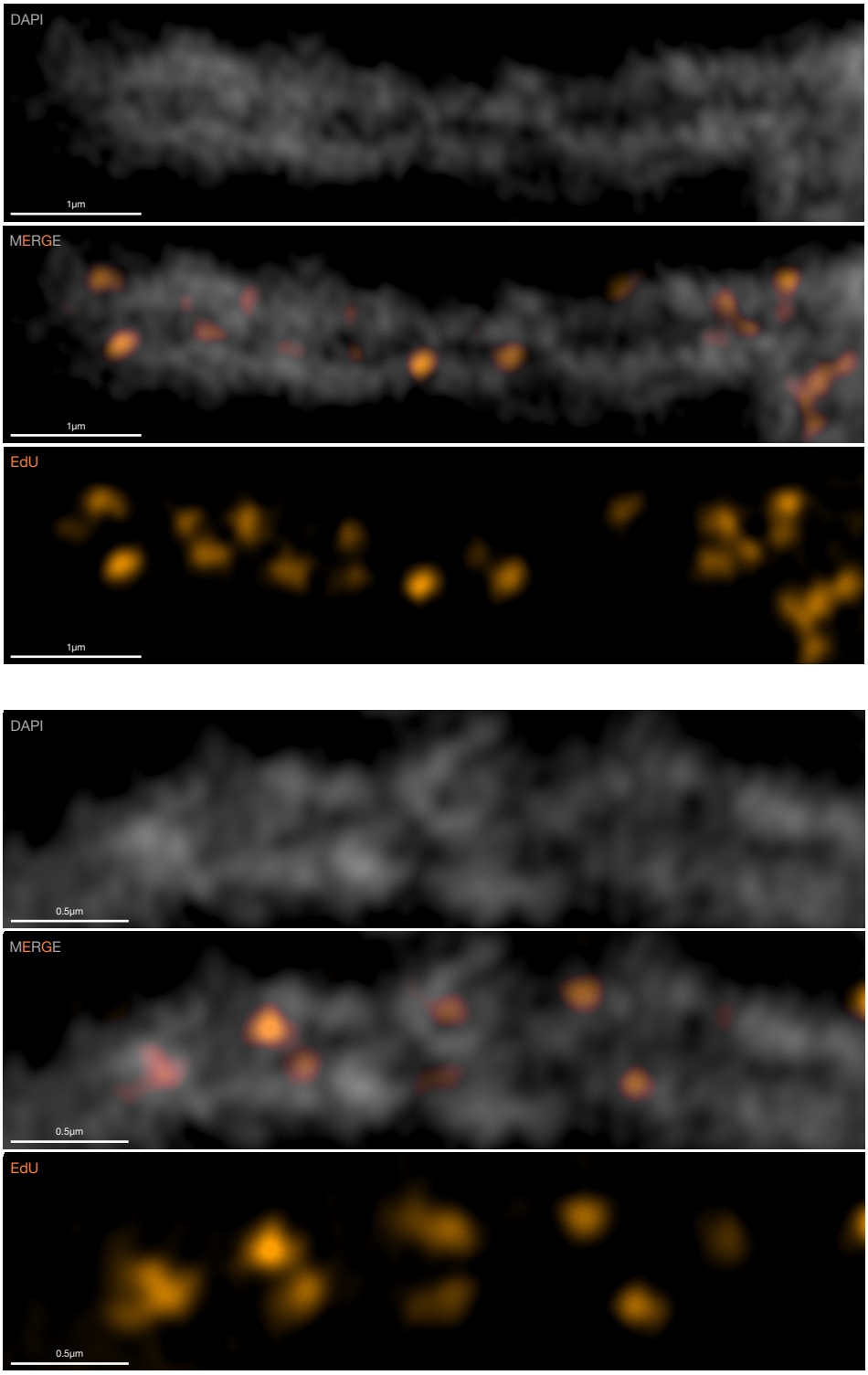

Figure 23. Different patterns of EdU foci are visually identified over the chromosomes of WT pachytene cells.

Two magnified sections of synapsed homologous chromosomes at pachytene in WT cells. For each panel, the top image correspond to the DAPI staining of the chromosomes (grey), the bottom image to the EdU signal (orange) and the middle image to the merge of the two signals.

Mapping and characterization of meiotic EdU-substituted tracts hotspots

Novel approaches using chromatin immunoprecipitation plus NGS have permitted the molecular detection of nucleotide analogues to analyse DNA replication to precisely determine replication patterns and initiation regions of DNA synthesis in the genome. In Arabidopsis, different reports have used the incorporation of BrdU and EdU to study the dynamics of S-phase as well as the detection and characterization of DNA replication origins using complementary experimental designs to gather somatic S-phase cells and detect the incorporation:

I) Cell cultures synchronized by transiently arresting cells at G0 using sucrose deprivation. S-phase cells were accumulated by adding hydroxyurea together with BrdU, known to arrest cells in S-phase by inhibiting ribonucleotide reductase hence reducing the free nucleotide pool, essential substrate for DNA replication; as well as Polδ, a central replicative polymerase [902,903]. An anti-BrdU antibody was used to immunoprecipitate BrdU-substituted DNA fragments out of size-fractioned genomic DNA to then prepare Illumina sequencing libraries [904].

II) Non-synchronized cell cultures subjected to a pulse of EdU, cell fixation and nuclei isolation. Incorporated EdU in the isolated nuclei was conjugated with Alexa Fluor 488 (AF488) via the 'Click-it' reaction. S-phase cells were identified and fractionated by flow cytometry using DNA content (DAPI intensity) and EdU incorporation (AF488 intensity), excluding cells at G1 or G2/M. An anti-AF488 antibody was used to immunoprecipitate EdU-incorporated DNA fragments from a digested genomic DNA extraction from the fractioned S-phase nuclei to then prepare Illumina sequencing libraries [899,905].

Given these precedents of successful pull-down, sequencing and mapping of BrdU/EdU-incorporated DNA fragments, we decided to try a similar approach in our material. Precise genomic mapping of meiotic EdU foci would work as a proxy to shape the genomic landscape of homologous recombination events in Arabidopsis meiosis as well as to identify and characterize homologous recombination hotspots and their associated genetic and epigenetic features. Nevertheless, a number of technical and practical limitations did not allow us to directly replicate any of the approaches described to analyse S-phase incorporation:

I) Isolation of meiotic cells from somatic tissues.

Arabidopsis meiotic cells cannot be cultured *in vitro* to this date. *In vivo* they represent only a fraction of the total cells of a flower bud as they are surrounded by multiple somatic tissues, including dividing mitotic cells. These somatic cells would

incorporate EdU while replicating their genome, "contaminating" the sample with replicative EdU tracts virtually indistinguishable at later steps of the protocol from the target DSB repair-associated EdU tracts. Meiotic cells have the same genetic content as somatic G2/M cells (4C). In addition, meiotic cells with the EdU labelling signature of interest (pachytene up to the end of meiosis) have a significantly fainter signal that the ones with replicative EdU labelling (Figure 20). It thus seemed unlikely that we could easily isolate the subpopulation of interest using flow cytometry by combining DNA content and EdU fluorescence. To solve this issue, we opted to manually dissect flower buds in order to isolate the meiotic pollen mother cells (PMC). In Arabidopsis flower buds, male meiotic cells are organized in sporogenous archesporial columns (SACs) inside the anthers, each of the six anthers of one flower bud harbouring four SACs carrying about 40 cells per SAC [891]. With different publications already describing the dissection of flower buds as a start point, we developed a simple protocol (detailed in methods) to release those SACs containing meiotic cells from the rest of the flower bud and collect them, accumulating as many as possible (Figure 24).

II) Isolation of meiotic cells at pachytene from early prophase I cells.

Not only somatic cells surrounding meiocytes may have incorporated EdU throughout their whole genome if replicated during the incubation period but, as described above, meiotic cells at early prophase I were either complete or partially labelled after the 24 hours incubation as they incorporate EdU in pre-meiotic S-phase as well. To isolate cells at pachytene or later stages from early prophase I we took profit of the semi-synchronization of meiotic division inside each flower bud. Flower buds grow as meiosis advances and multiple reports have characterized the timeline of these two phenomena together, reporting which meiotic stages are prominent at different flower bud sizes [891]. We decided to test ourselves the staging of the meiotic cells observed in flower buds of different sizes to try to find a sweet spot of bud size in which we did not find (or almost not) cells at leptotene and zygotene but only pachytenes and/or subsequent stages. As shown in Figure 20, all stages up to TII show non-S-phase EdU labelling and are thus valid to pull-down DSB repair-associated EdU tracts. Taking previous reports as a start point, we scored the stages observed in multiple flower buds of less than 0.4mm and flower buds between 0.4 and 0.5mm (from the bud-pedicel joint to the tip of the bud). In the first group (<0.4mm) we could detect exclusively G2 and early prophase I meiotic cells at (G2/leptotene and zygotene; Figure 24e). Among the flower buds between 0.4 and 0.5 mm long however, we could detect all stages with a clean separation between flower buds carrying cells at early prophase I and buds carrying cells from pachytene on (Figure 24e). Given this result, we subsequently used a microscope calibration slide with a 1mm height grid divided

into 12 squares to measure the flower buds and select only those measuring between 0.42 and 0.5mm for the isolation of meiotic cells (Figure 24b) - incubating whole inflorescences for 24 hours as described above (Figure 19) and retaining only 0.42 to 0.5mm flower buds for dissection.

III) Pull-down of EdU-incorporated DNA fragments.

While antibodies were used to immunoprecipitate BrdU (anti-BrdU) and EdU conjugated with AF488 (anti-AF488), we opted to exploit the versatility of "click" chemistry to conjugate the DNA-incorporated EdU to a biotin azide and capture the resulting biotinylated DNA fragments on streptavidin-coupled magnetic beads [890,906]. These two reactions are highly efficient and specific, and could be accommodated into a sequencing library preparation workflow (see methods). We tested the EdU-biotin azide reaction efficiency and specificity via cytological detection of biotin with avidin-TexasRed conjugate on slides from flower buds incubated with EdU. Cells with incorporated EdU could be cleanly detected when the biotin azide was present in the reaction, confirming a proper conjugation of biotin with EdU (Figure 24f). When the biotin azide was not present in the click reaction, no unspecific binding of avidin-TexasRed was detected (Figure 24g).

The next step, to test the efficiency and specificity of the capture of biotinylated DNA fragments onto streptavidin-coupled magnetic beads, was performed directly on the prepared sequencing libraries as described below.

Meiotic cells were collected for the pull-down and sequencing of EdU-incorporated fragments from WT and *spo11* plants, each under two conditions: incubated with EdU for 24 hours (EdU+) or incubated in PBS for 24 hours (EdU-). By doing so, in addition to our samples of interest (WT EdU+), we would have a "biological" negative control (*spo11* EdU+) from which no DSB repair-associated EdU tracks should be pulled-down. In addition, "technical" negative controls (WT EdU- & *spo11* EdU-) would give us information about the affinity and specificity of the capture of biotinylated EdU-incorporated fragments onto the streptavidin-coupled magnetic beads. Two biological replicates were prepared per sample corresponding to independent genomic DNA extractions. For each replicate, an input library and a pull-down library resulted from the library preparation workflow, the input being a fraction of the adapter-ligated fragments sampled prior to the capture on streptavidin-coupled magnetic beads - serving as a standard internal control for each replicate.

Adapter-ligated libraries were prepared as described in the methods section, after which both input and pull-down libraries were verified using a quantitative electrophoresis platform (Agilent TapeStation) to assess their size and quality (Figure

24h & Figure 24hi). No fragments (300bp peak) could be detected in the pull-down libraries of either WT or *spo11* EdU- samples (Figure 24i), while their respective inputs had similar profiles to those of the EdU+ fragments (Figure 24h). A chart of the pull-down/input ratio of all samples is shown in Figure 24j for a normalized quantitative evaluation of this observation. The absence of pull-down fragments (at this sensitivity) in the samples from flower buds incubated with PBS instead of EdU confirms that biotinylated EdU-incorporated fragments are specifically captured onto the streptavidin-coupled magnetic beads with little unspecific binding. Notwithstanding the absence of the pull-down band in these control samples, they were also sequenced as further controls. Input and pull-down libraries of all samples were sequenced in a MGISEQ-2000 platform to deliver 100+100bp paired end reads with the sequence depths indicated in Table 17 and Table 18 (Total reads).

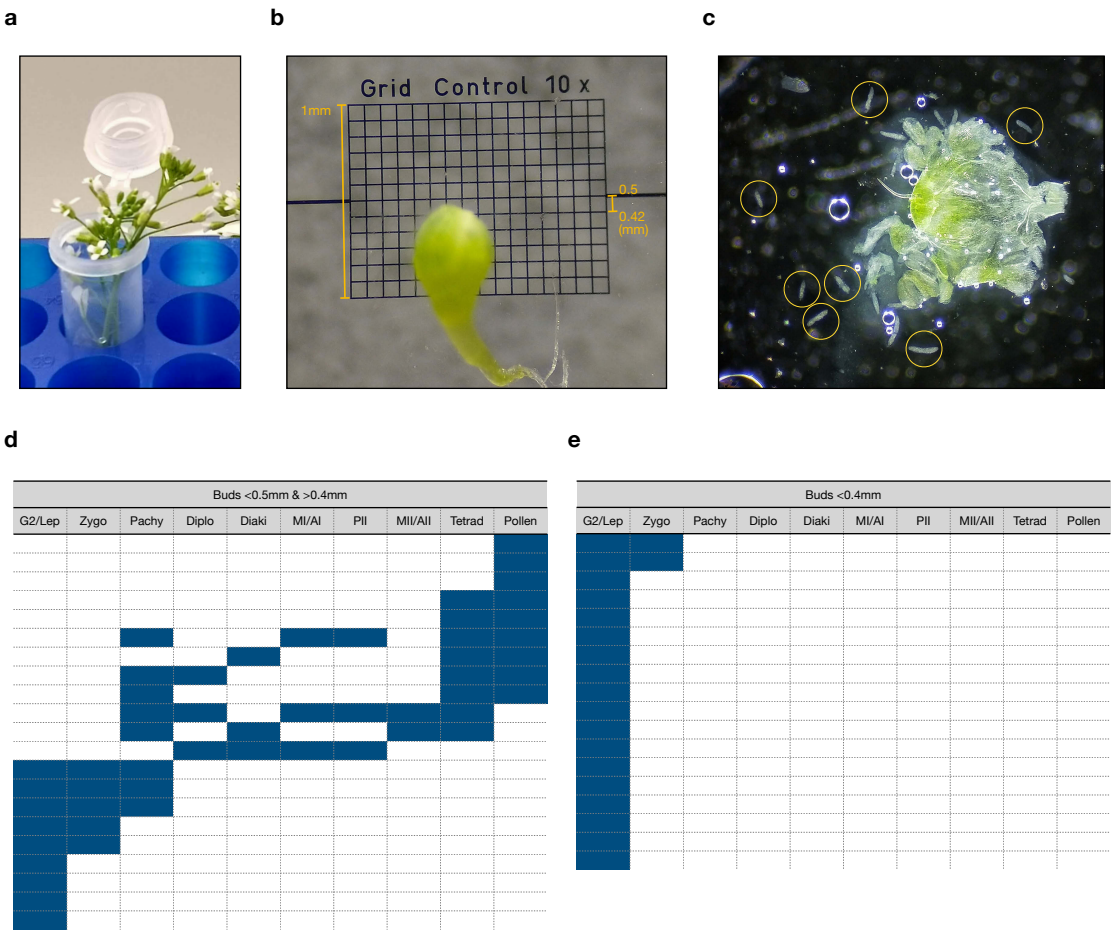

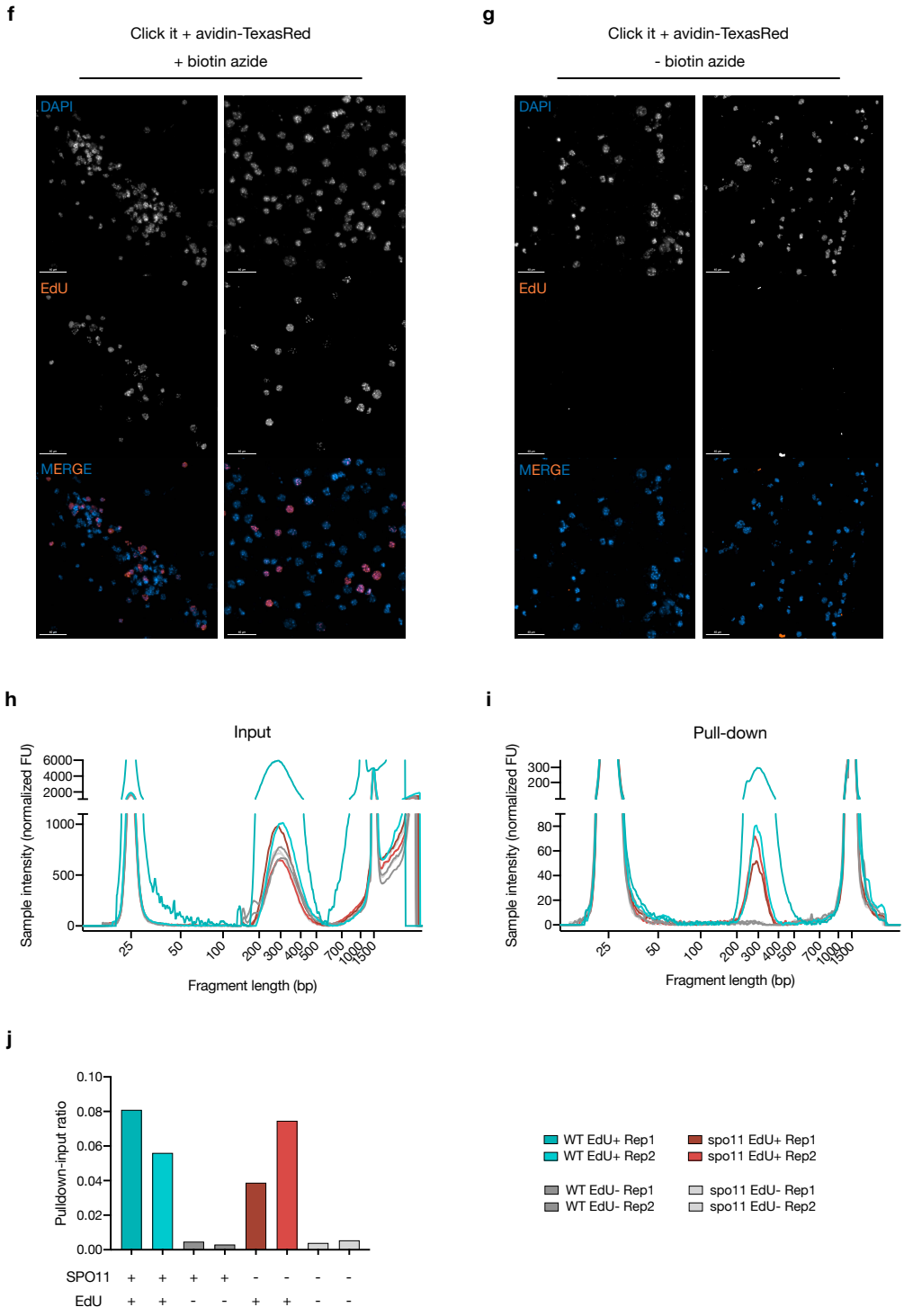

Figure 24. Experimental setup for the pull-down of DSB repair-associated DNA synthesis tracts.

(a) Incubation setup for the 24 hour EdU pulse. **(b)** Detail image of the method employed to measure the flower buds and isolate those in the desired size range. The height of the grid is indicated to its left and the target size range to the right. **(c)** Detail image of the dissection of a flower bud with columns of meiocytes (SACs) extracted for collection from the bud circled in yellow. **(d)** Stages of meiosis observed in chromosome spreadings of flower buds between 0.4 and 0.5mm. Each row is an individual flower bud, cells in blue represent the presence of the correspondent stage in that flower bud. **(e)** Stages of meiosis observed in chromosome spreadings of flower buds bellow 0.4mm. Each row is an individual flower bud, cells in blue represent the presence of the correspondent stage in that flower bud.

Continuation in next page.

(f) Control test for the conjugation of biotin azide to EdU via click-it reaction. The two columns correspond to two different microscope fields. Top row corresponds to the DAPI staining of the chromosomes (blue). Middle row corresponds to the biotinylated-EdU signal labelled via immunodetection of biotin with an avidin-TexasRed conjugate. Third row corresponds to the merge of the previous two images. The same disposition is shown in **(g)** in absence of biotin in the click-it reaction as a negative control for the signal of biotinylated-EdU detected in (f). **(h)** Electropherogram of the NGS libraries of the input samples. X-axis represent fragment size and Y-axis normalised sample intensity of the intercalant agent, used by TapeStation to estimate DNA concentration of the samples relative to a standard control sample. Peaks centred at 25bp and 1500bp correspond to the lower and upper markers of the gel as standards for fragment size. Colour coding of the samples is indicated in the bottom-right section of the panel. **(i)** Electropherogram of the NGS libraries of the pull-down samples. The details of (h) apply to (i) as well. **(j)** Pull-down-input ratio of the concentrations of adapter-ligated fragments obtained in the pull-down and input NGS libraries for each sample. Colour coding of the samples is conserved.

Figure 25. Bioinformatic data processing and analysis workflow of the NGS samples.

Each step in black include the tool employed for that particular step below in grey.

Table 17. EdU-sequencing data processing of pull-down libraries.

Sample	EdU	Total reads	Trimmed reads	Mapped reads	Uniquely aligning	Unique UMI deduplicated
WT Rep1	+	26,570,052	27,563,524	26,356,722 (95,56%)	15,505,229	2,573,492 (16.60%)
WT Rep2	+	20,774,778	20,770,008	20,611,216 (99.24%)	12,182,181	1,769,786 (14.53%)
WT Rep1	-	227,396	227.396	215,230 (94.65%)	123,074	107,655 (87.47%)
WT Rep2	-	516,284	516,284	490,147 (94.94%)	291,214	140,437 (48.22%)
spo11 Rep1	+	16,033,234	16,029,710	15,885,584 (99.10%)	9,237,810	1,942,880 (21.03%)
spo11 Rep2	+	14,081,236	14,077,496	13,945,240 (99.06%)	8,068,864	1,746,748 (21.65%)
spo11 Rep1	-	1,117,562	1,117,232	1,015,204 (90.87%)	569,238	507,359 (89.13%)
spo11 Rep2	-	372,386	372,078	351,554 (94.48%)	204,881	134,840 (65.81%)

Sample	EdU	Multiply aligning	Multiple unique fp10	Multiple unique fp10 UMI deduplicated	Merged reads
WT Rep1	+	11,058,295	3,171,587	517,200 (16.31%)	3,090,692
WT Rep2	+	8,429,035	2,428,550	347,778 (14,32%)	2,117,564
WT Rep1	-	92,156	23,074	19,121 (82.87%)	126,776
WT Rep2	-	198,933	50,009	23,088 (46.17%)	163,525
spo11 Rep1	+	6,647,774	1,827,363	372,926 (20.41%)	2,315,806
spo11 Rep2	+	5,876,376	1,586,949	333,937 (21.04%)	2,080,685
spo11 Rep1	-	445,966	100,811	86,518 (85.82%)	593,877
spo11 Rep2	-	146,673	35,759	22,662 (63.37%)	157,502

Table 18. EdU-sequencing data processing of input libraries.

Sample	EdU	Total reads	Trimmed reads	Mapped reads	Uniquely aligning	Unique UMI deduplicated
WT Rep1	+	84,381,990	84,361,878	80,668,601 (95.62%)	44,824,118	43,566,964 (97.20%)
WT Rep2	+	318,400,420	318,322,628	304,399,552 (95,63%)	169,042,689	164,078,524 (97.06%)
WT Rep1	-	210,098,984	210,098,984	114,432,101 (54.47%)	113,696,156	27,743,868 (24.40%)
WT Rep2	-	459,228,832	459,228,832	440,059,912 (95.83%)	248,668,279	240,377,893 (96.67%)
spo11 Rep1	+	489,467,872	489,333,866	450,878,855 (92.14%)	251,906,435	244,126,770 (96.91%)
spo11 Rep2	+	441,673,722	358,267,780	342,947,799 (95.72%)	189,597,187	183,428,617 (96.75%)
spo11 Rep1	-	377,725,086	377,620,408	318,687,316 (84.29%)	178,722,401	173,217,994 (96.92%)
spo11 Rep2	-	358,371,098	358,267,780	342,947,799 (95.72%)	189,597,187	183,428,623 (96.75%)

Sample	EdU	Multiply aligning	Multiple unique fp10	Multiple unique fp10 UMI deduplicated	Merged reads
WT Rep1	+	35,844,483	8,000,919	7,379,657 (92.24%)	50,946,621
WT Rep2	+	135,356,863	30,226,241	27,819,095 (92.04%)	191,897,619
WT Rep1	-	735,945	431,796	422,465 (97.84%)	28,166,333
WT Rep2	-	191,382,633	44,330,651	40,481,760 (91.32%)	280,859,653
spo11 Rep1	+	198,972,420	44,773,275	41,233,716 (92.09%)	285,360,486
spo11 Rep2	+	153,350,612	33,895,743	31,214,825 (92.09%)	214,643,442
spo11 Rep1	-	139,964,915	31,896,313	29,489,809 (92.46%)	202,707,803
spo11 Rep2	-	153,350,612	33,895,743	31,214,812 (92.09%)	214,643,435

The data was processed following Choi *et al.* [361] SPO11-oligo data processing workflow modified to adapt it to our libraries (Figure 25, detailed in methods). Indeed, although raw reads were obtained from the EdU- samples, they were significantly less in number than the EdU+ samples and their numbers became even more significantly reduced as they were processed, dropping to values which are appear uncertain for supporting analysis due to insufficient genomic coverage (Table 17, merged reads). It should be noted that this further supports the selectivity of the EdU pull-down. We therefore decided to proceed with the data analysis of the WT EdU+ samples using the *spo11* EdU+ samples as the negative controls.

Given that neither meiotic DSBs nor crossovers are uniformly distributed across genomes but tend to occur in regions (hotspots) of higher incidence, our first approach was to identify regions of enrichment of EdU incorporation. To do this, we used Macs2 to call EdU enrichment peaks independently on the two replicates of both WT and *spo11*, using their respective input libraries as negative controls. In WT samples, 392 and 217 peaks were identified in the two replicates, while 238 and 113 peaks were identified in *spo11* replicates (Figure 26a). Out of the total 609 WT peaks, 565 (92.78%) were WT-specific (did not intersect with *spo11* peaks). Only 23 (3.6%) intersected between the two WT replicates and of these only 5 (5/23 = 22%) did so without coinciding with *spo11* peaks (Figure 26b). For the *spo11* peaks, 305 were *spo11*-specific (not found in WT) and only 17 of these were found in both *spo11* replicates (17/305 = 5,6%). The majority of these (15/17 = 88.2%) were also found in the WT samples.

The low proportion of peaks shared between the replicate samples makes drawing concrete conclusions from this initial analysis difficult. The complexity of our libraries is constrained by the number of meiotic cells we were able to collect with a time-consuming manual dissection protocol (see Table 19 for numbers). While the numbers of EdU+ foci and their SPO11-dependence are strong evidence for the presence of meiotic DSB repair-associated synthesis in these meiocytes, importantly these data do not carry any implication of the presence of favoured chromosomal sites (hotspots) at which they occur. The likelihood of detecting multiple events at a given locus (hotspot) is the product of the frequency with which such events occur per meiosis and the number of meioses analysed. Thus, the lower the number of meioses, the "stronger" a hotspot must be to be detected. The low reproducibility of called peaks between replicate libraries could thus reflect the existence of a large number of low-amplitude hotspots or an insufficient complexity of our sequencing libraries, or both.

a

Sample	Number of peaks/regions	Origin
WT EdU+ Rep1	392	This study
WT EdU+ Rep2	217	This study
spo11 EdU+ Rep1	238	This study
spo11 EdU+ Rep2	113	This study

Sample	Number of peaks/regions	Origin
WT EdU+ specific peaks	565	This study
spo11 EdU+ specific peaks	308	This study
SPO11 hotspots	5,593	Choi *et al*. 2018
Crossovers	17,077	Rowan *et al*. 2019
Replication initiation regions	5,597	Wheeler *et al*. 2020

b

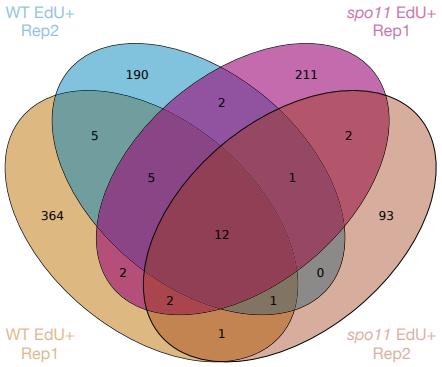

c

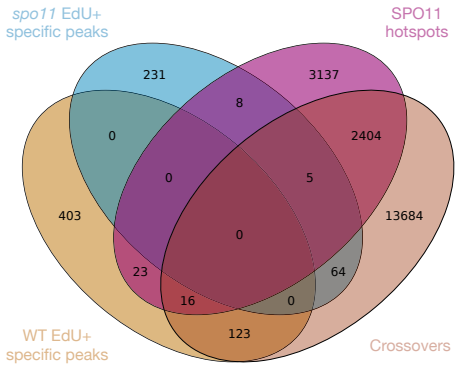

d

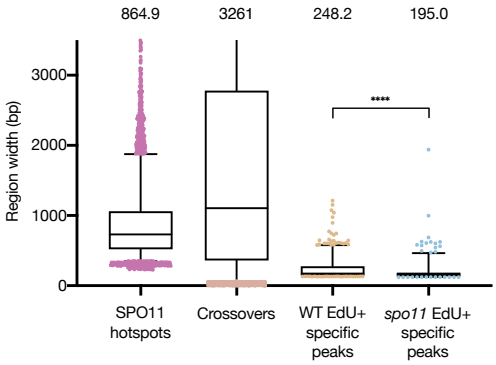

e

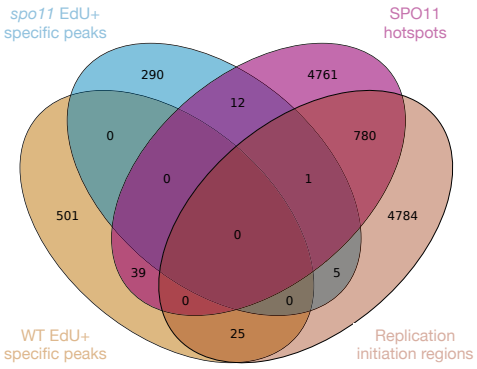

Figure 26. Peaks of EdU-substituted tracts are detected both in WT and *spo11* samples with no significant overlapping between them and with other meiotic features.

(a) Relation of samples used in the analysis with the number of peaks/regions of each sample and the origin. **(b)** Genomic coordinates-based overlapping analysis between the peaks called in the two WT and *spo11* samples. The numbers represent the number of peaks overlapping between the respective samples overlapping in the Venn diagram. **(c)** Genomic coordinates-based overlapping analysis between the merged peaks of WT and *spo11* samples and two meiotic-specific features: SPO11 hotspots and crossovers in Arabidopsis. **(d)** Size comparison of the peaks called in WT and *spo11* samples with the SPO11 hotspots and crossovers. The box represent the upper and lower quartiles of the data with a line at the median plus whiskers with the 5-95 percentiles. Data points outside these percentiles are included. The mean length is indicated above each sample. **(e)** Genomic coordinates-based overlapping analysis between the merged peaks of WT and *spo11* samples, SPO11 hotspots and replication initiation regions in Arabidopsis. *Minor differences between the numbers of peaks in the table and the Venn diagrams are consequence of the outputs of the different tools employed, but do not impact the interpretation.

To extend these analyses, we analysed the 565 WT-specific peaks in parallel and in comparison with the 308 *spo11*-specific peaks. Firstly by comparing them with published data of SPO11-oligos, crossovers and replication initiation regions [361,791,905], with the working hypothesis that if the WT-specific peaks correspond to DSB repair-associated DNA synthesis and *spo11*-specific peaks were either artefacts or replicative EdU "contamination", we should see differences in their intersection with those features. Our WT DSB repair-associated DNA synthesis peaks should correlate well with SPO11-oligo hotspots, while comparisons with crossover patterns might be less informative as Arabidopsis crossovers are the repair outcome of around 5% of the total DSBs. In the case of "contamination" from replicative EdU incorporation, replication initiation regions might be overrepresented if partially replicated cells contaminated the target subpopulation of meiocytes.

Interval files for both crossover and replication initiation regions were directly provided by the authors along with their publications [791,905]. The SPO11-oligo data was processed from the raw files provided by the authors, as described in the supplementary methods of the publication, with almost identical results to those published in the article (Table 20). A different peak calling algorithm was used to identify SPO11 hotspots (Macs2 versus PeakRanger in the publication) due to difficulties in the usage of PeakRanger, which presumably explains the minor differences in the number of regions identified and their mean width.

Of the WT-specific peaks, 6.9% (39/565) intersect with SPO11-oligo hotspots and 24.6% with crossovers (139/565) (Figure 26c). Similar results were obtained for *spo11*-specific peaks, of which 4.2% (13/308) intersect with SPO11-oligo hotspots and 22.4% with crossovers (69/308) (Figure 26c). WT-specific peaks are significantly wider than *spo11*-specific peaks (248.2 vs 195bp; $p<0.0001$) but remain narrow when compared to SPO11-oligo hotspots and specially to crossovers (Figure 26d). With respect to

replication, 4.4% (25/565) of WT-specific and 1.9% (6/308) of *spo11*-specific peaks intersect with replication initiation regions (Figure 26e).

Table 19. Numbers of estimated meiocytes isolated per sample and gDNA yield.

Background	EdU	Estimated cells	Extracted genomic DNA (ng)	Pools for library preparation
WT	+	16.840	26.67	WT EdU+ Rep1
WT	+	16.200	16.9	
WT	+	16.000	14.8	WT EdU+ Rep2
WT	+	17.120	25.02	
WT	+	15.800	21.42	
WT	-	16.480	19.5	WT EdU- Rep1
WT	-	16.080	20.02	WT EdU- Rep2
spo11	+	11.120	18.98	*spo11* EdU+ Rep1
spo11	+	15.200	28.34	
spo11	+	13.920	19.24	*spo11* EdU+ Rep2
spo11	+	16.480	23.79	
spo11	-	14.680	23.01	*spo11* EdU+ Rep2
spo11	-	12.800	17.42	
spo11	-	16.520	21.71	*spo11* EdU+ Rep2

Table 20. Reconstruction of SPO11-oligo data.

Genotype	Library barcode	Total reads	Trimmed reads	Mapped reads	Mismatch filtered	Uniquely aligning	Unique rmdup
Col	RPI1	209,124,715	140,685,106	85,708,657	76,147,821	56,093,177	26,049,437
Col	RPI3	205,166,702	172,856,279	131,601,991	123,150,472	89,791,279	12,620,592
Col	RPI8	72,517,675	60,579,240	54,115,435	51,619,430	39,985,012	10,172,066
Col	RPI1	209,124,715	207,357,279	85,500,140	78,533,531	60,262,534	27,062,342
Col	RPI3	205,166,702	202,331,636	129,083,714	123,719,523	93,187,103	13,071,112
Col	RPI8	72,517,675	72,512,386	48,038,223	46,086,537	35,801,251	9,431,603
Genotype	Library barcode	Multiply aligning	Multiple unique fp10	Multiple unique fp10 rmdup	Unique both rmdup	Called peaks	Mean peak length (bp)
Col	RPI1	20,054,644	4,574,715	1,966,294	28,015,731	5,914	823
Col	RPI3	33,359,193	7,258,667	889,638	13,510,230		
Col	RPI8	11,634,418	3,581,199	855,527	11,027,593		
Col	RPI1	18,270,997	4,701,776	2,101,615	29,163,957	5,593	865
Col	RPI3	30,532,420	7,478,312	1,107,907	14,179,019		
Col	RPI8	10,285,286	3,267,147	885,829	10,317,432		

Choi *et al.* (2018) Reconstructed for this study

Although no significant intersection was detected between WT-specific peaks and SPO11 hotspots, we decided to compare the actual SPO11-oligo density and the density of our four samples over the detected peaks in both backgrounds. This avoids restricting the analysis to called peaks and might unveil local enrichments or depletions when the intervals are stacked together even if they were not strong enough individually to be called as peaks. For this purpose, we computed the mean density profile of the two WT EdU+ replicates, the two *spo11* EdU+ replicates and the SPO11-oligos (mean log2 ratio of CPM-normalized ChIP/input) over the called peaks of the four samples normalized to 1kb plus 1kb upstream and downstream the start and the end of the intervals. Upper plots display the mean density profile of each of the samples (with the SEM shaded around it), while lower plots are heatmaps with the color-coded density over all individual intervals stacked together for each of the samples (Figure 27). As expected, both WT EdU+ and *spo11* EdU+ replicates display strong enrichment over their respective called peaks. However, no enrichments were detected in neither of the two backgrounds over the peaks of the other replicate (WT EdU+ Rep1 over WT EdU+ Rep2, in example). No specific enrichment of SPO11-oligos was detected over WT peaks as well, which show a flat profile similarly to *spo11* peaks.

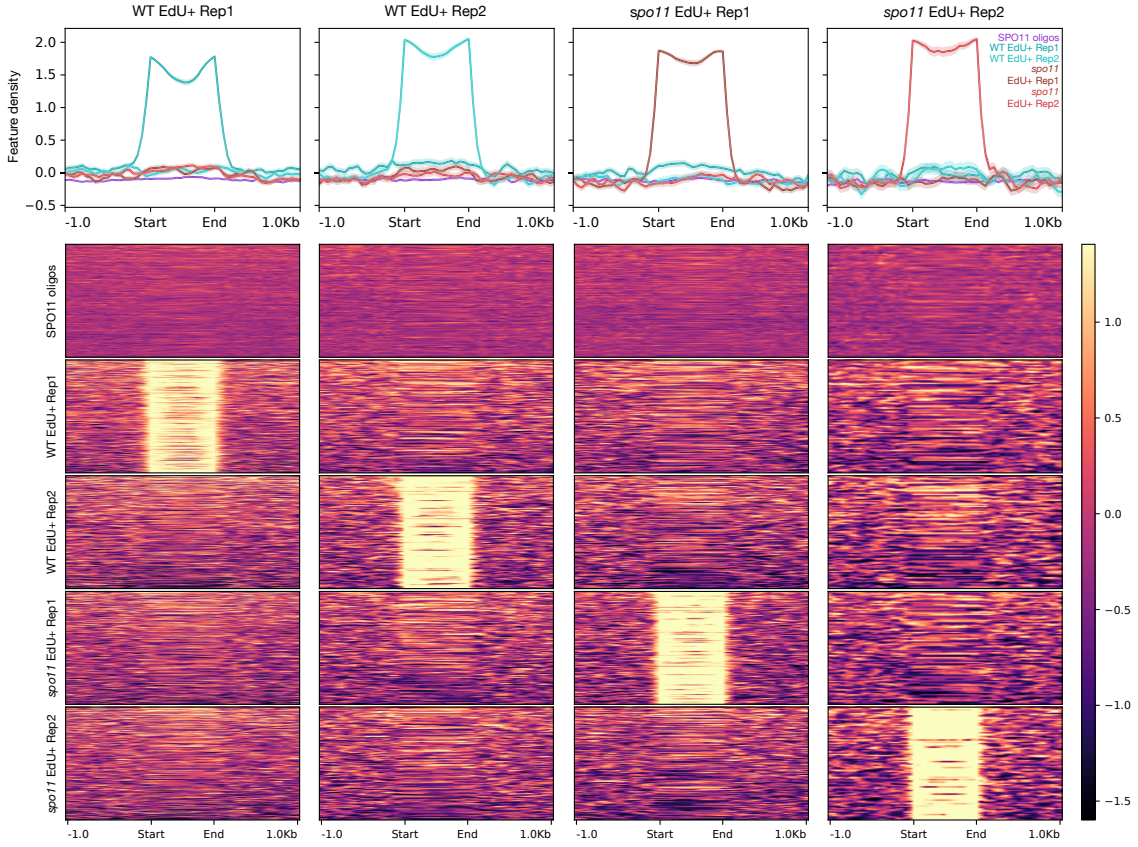

Figure 27. Detected enrichments of EdU-substituted tracks are not reproduced over the called peaks of the different replicates.

Upper plots: Read density profiles expressed as the mean log2 ratio of CPM-normalised ChIP/input of our two WT samples (WT EdU+ Rep1 & WT EdU+ Rep2) , our two *spo11* samples (*spo11* EdU+ Rep1 & *spo11* EdU+ Rep2) plus SPO11-oligos over the peaks called in our four samples. Samples colour coding is indicated in the top right corner of the last plot. Each plot corresponds to the peaks of the sample referenced above normalised to the same length (1kb), with the start and end indicated below the plot plus 1kb upstream and downstream.

Lower plots: Heatmaps with the stack of all the normalised peaks used to compute the profile of the plot right above expressed as the colour-coded log2 ratio of CPM-normalised ChIP/input. Heatmap scale is shown on the right. For each profile, a column of five heatmaps is shown below corresponding to each individual sample profiled with their names indicated to the left.

Following an analogous logic, we inverted this last analysis to, instead of trying to detect enrichments of previously-published meiotic recombination-related data over our EdU called peaks, profile the density of our WT and *spo11* libraries over hotspots and features associated with meiotic recombination in the bibliography. Local enrichments or depletions over, in this case, features known to be associated with meiotic recombination that were not significant enough to be called peaks individually might be detectable when those features are stacked together and normalized to similar length and the density of the different samples is averaged. The interval files of the different features were shuffled around the Arabidopsis genome to obtain sets of intervals with the same characteristics (number and width distribution) but randomly

positioned in the genome, which adds an extra control to crosscheck that the profile observed over the feature of interest is specific to that feature and not an artifact of a random stack of intervals.

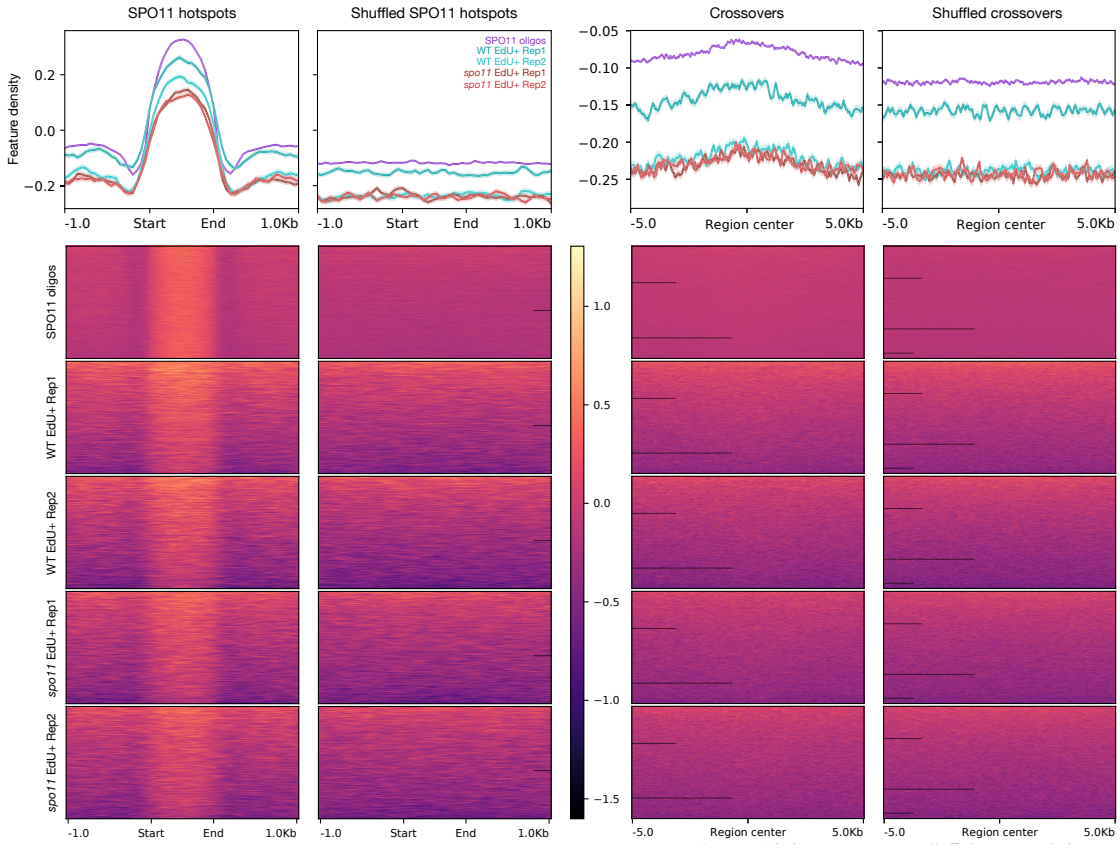

Figure 28. Both WT and *spo11* samples show enrichments over SPO11 hotspots and mapped crossovers equivalent to SPO11-oligos.

Upper plots: Read density profiles expressed as the mean log2 ratio of CPM-normalised ChIP/input of our two WT samples (WT EdU+ Rep1 & WT EdU+ Rep2) , our two *spo11* samples (*spo11* EdU+ Rep1 & *spo11* EdU+ Rep2) plus SPO11-oligos over SPO11 hotspots, crossovers and their respective sets of shuffled intervals. Samples colour coding is indicated in the top right corner of the second plot. Each plot corresponds to the intervals of the feature referenced above normalised to the same length (1kb), with the start and end indicated below the plot plus 1kb upstream and downstream in the case of SPO11 hotspots and shuffled SPO11 hotspots. Crossovers and shuffled crossovers are centred to the middle of the interval as a reference point plus 5kb upstream and downstream

Lower plots: Heatmaps with the stack of all the normalised intervals used to compute the profile of the plot right above expressed as the colour-coded log2 ratio of CPM-normalised ChIP/input. Heatmap scale is shown at the middle. For each profile, a column of five heatmaps is shown below corresponding to each individual sample profiled with their names indicated to the left.

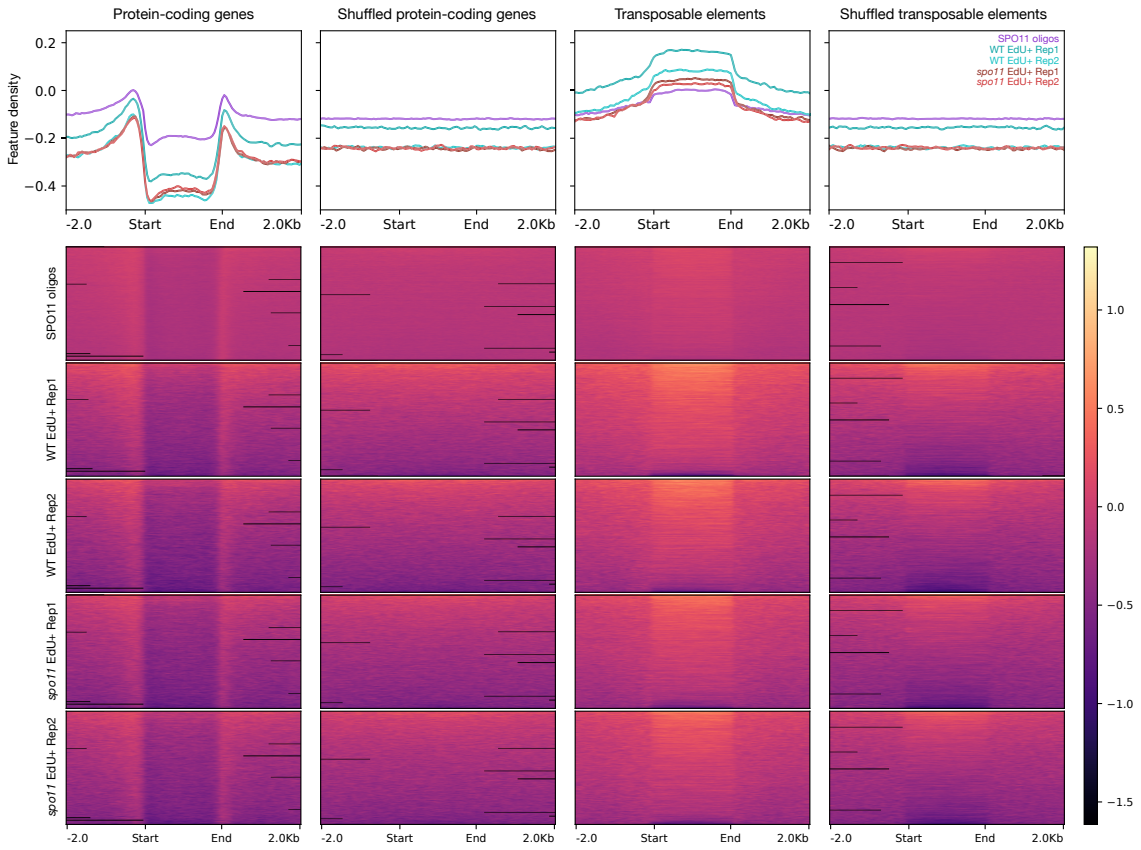

Figure 29. Both WT and *spo11* samples show equivalent profiles over protein-coding genes and transposable elements than SPO11-oligos.

Upper plots: Read density profiles expressed as the mean log2 ratio of CPM-normalised ChIP/input of our two WT samples (WT EdU+ Rep1 & WT EdU+ Rep2) , our two *spo11* samples (*spo11* EdU+ Rep1 & *spo11* EdU+ Rep2) plus SPO11-oligos over protein-coding genes, transposable elements and their respective sets of shuffled intervals. Samples colour coding is indicated in the top right corner of the last plot. Each plot corresponds to the intervals of the feature referenced above normalised to the same length (2kb), with the start and end indicated below the plot plus 2kb upstream and downstream.

Lower plots: Heatmaps with the stack of all the normalised intervals used to compute the profile of the plot right above expressed as the colour-coded log2 ratio of CPM-normalised ChIP/input. Heatmap scale is shown to the right. For each profile, a column of five heatmaps is shown below corresponding to each individual sample profiled with their names indicated to the left.

Mean density profiles and heatmaps were generated over SPO11 hotspots as detailed above, as well as for crossovers and the respective shuffled intervals. In the case of crossovers, using the central point of the crossover intervals as reference point to profile the data over 5kb upstream and downstream rather than using start and end coordinates (Figure 28). A higher density of DSB repair-associated DNA synthesis tracks is expected both at DSB hotspots and around crossovers with respect to adjacent regions, signatures that should be lost in the *spo11* mutant. An enrichment with a similar profile and magnitude as the SPO11-oligos themselves was detected over SPO11 hotspots for the two WT EdU+ replicates, but surprisingly also for the *spo11* EdU+

replicates. This enrichment was consistent among the majority of SPO11 hotspots, as can be seen in the heatmaps. For crossovers, there is a slightly higher density of SPO11-oligos at the centre of the intervals that flattens with the distance from the centre that was as well replicated not only in our WT samples, but also in the *spo11* mutant.

In addition to SPO11 hotspots and crossovers, a higher density of SPO11-oligos has been reported at gene promoters and terminators with respect to their upstream and downstream regions and especially with respect to gene bodies, in which there are significantly depleted. A significant higher density of SPO11-oligos has been observed as well at transposable elements [361]. We thus replicated this analysis for our samples together with the reconstructed SPO11-oligos data from the same publication over protein-coding genes, transposable elements and their respective random shuffled intervals sets (Figure 29). Again, a similar profile to that of SPO11-oligos was obtained, not only for the two WT EdU+ samples, but also for two *spo11* samples. Localized enrichments at gene promoters, terminators and transposable elements, with similar shapes and magnitudes to the SPO11 oligo profile, were detected in all samples with respect to adjacent regions. Likewise, the expected depletion at gene bodies was observed in all samples.

Given the possibility of "contamination" from cells that had incorporated EdU during replication, we decided to plot the data over replication initiation regions. Wheeler *et al.* [905] divided these regions into two classes: strong initiation regions (sIRs) and weak initiation regions (sIRs). Analysis of the genomic location of sIRs and wIRs revealed that sIRs are evenly spaced along chromosome arms and depleted in centromeric and pericentromeric regions, while wIRs are predominantly situated at centromeric and pericentromeric regions. These centromeric and pericentromeric regions are believed to be late replicating based on analyses of partially labelled early prophase I cells and replication data. Differences in the two profiles might thus be informative and we chose to plot the profiles over the two classes separately at this step although previous analyses had been done with the merged replication initiation regions (Figure 30). The centres of sIRs and wIRs were used as reference points to plot 6kb regions (3kb downstream and upstream). A localized enrichment at the centre of sIRs was detected at the two WT and *spo11* replicates that faded with distance from the sIRs centre. Interestingly, this similar enrichment profile was detected once again in SPO11-oligos, observation that might reflect a relation between DSB formation and pre-meiotic replication that has been explored in detail in other organisms, but little in Arabidopsis. A light enrichment around the centre of wIRs could be noted for all samples, which show slightly higher mean density than both sIRs and random intervals

along the whole 6kb plotted. That this minor difference is a reflection of the presence of partially replicated cells appears unlikely, but cannot be excluded.

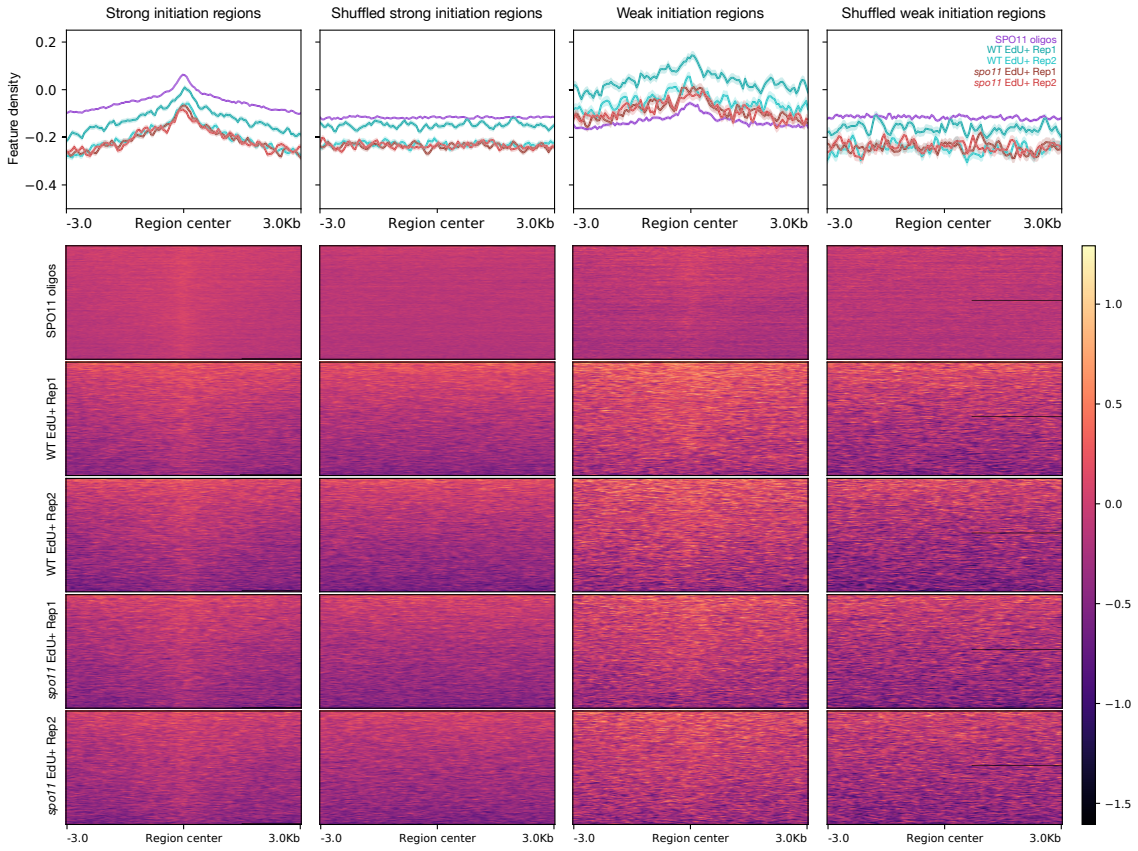

Figure 30. Both WT and *spo11* samples as well as SPO11-oligos show local enrichments over replication initiation regions.

Upper plots: Read density profiles expressed as the mean log2 ratio of CPM-normalised ChIP/input of our two WT samples (WT EdU+ Rep1 & WT EdU+ Rep2) , our two *spo11* samples (*spo11* EdU+ Rep1 & *spo11* EdU+ Rep2) plus SPO11-oligos over strong initiation regions, weak initiation regions and their respective sets of shuffled intervals. Samples colour coding is indicated in the top right corner of the last plot. Each plot corresponds to the intervals of the feature referenced above centred to the middle point of the interval as a reference point plus 3kb upstream and downstream.

Lower plots: Heatmaps with the stack of all the normalised intervals used to compute the profile of the plot right above expressed as the colour-coded log2 ratio of CPM-normalised ChIP/input. Heatmap scale is shown to the right. For each profile, a column of five heatmaps is shown below corresponding to each individual sample profiled with their names indicated to the left.

Finally, coverage files of the WT and *spo11* EdU+ samples and SPO11-oligos were generated, computing the mean log2 ratio of CPM-normalized ChIP/input, dividing the genome in 10kb windows smoothed with a 100-window rolling mean to explore their landscape at genome-wide scale (Figure 31). A similar profile is obtained from the WT and *spo11* samples along chromosome arms. Both WT samples show a

higher density at pericentromeric and centromeric regions than *spo11*, a signature that is observable in all five chromosomes. This does not however correlate with the relative SPO11-oligos in these regions.

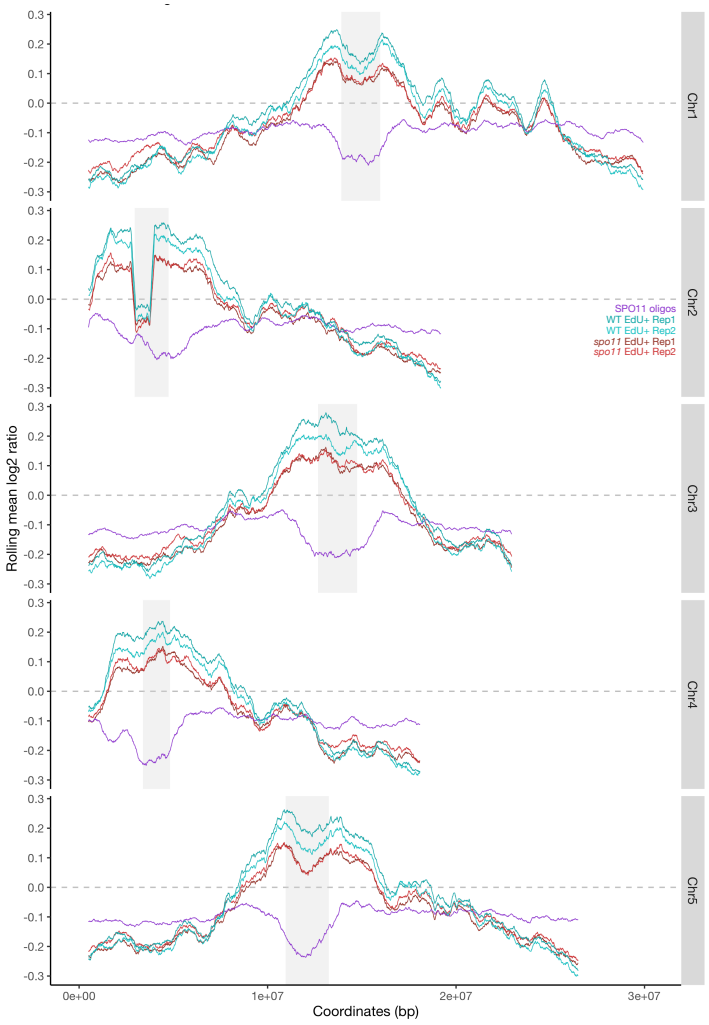

Figure 31. WT and *spo11* samples have similar profiles along the chromosomes that do not correlate at this scale with SPO11-oligos.

Read density profiles expressed as a rolling mean of the log2 ratio of CPM-normalised ChIP/input of our two WT samples (WT EdU+ Rep1 & WT EdU+ Rep2) , our two *spo11* samples (*spo11* EdU+ Rep1 & *spo11* EdU+ Rep2) plus SPO11-oligos along each of the five chromosomes of *Arabidopsis thaliana*. The rolling mean was calculated dividing the genome into 10kb windows and smoothed using 100 windows whose mean is centred to the middle. Chromosome names are indicated to the left and samples colour coding is indicated to the right of Chr2. The coordinates of the centromeres taken from Underwood *et al.* (2018) are indicated with a grey box.

Discussion

Identification of meiotic DNA repair-associated DNA synthesis tracts

In this work, we developed and tested with success a protocol to specifically label DNA synthesis tracts associated to meiotic DSB repair through *in vivo* incorporation of the thymidine analogue EdU. EdU-substituted DNA can be efficiently labelled by chemical cross-linking to a number of ligands (fluorochromes, biotin...) through the "Click-It" reaction.

Adapting available protocols to establish the timeline of meiotic stages in Arabidopsis showed that by incubating inflorescences for 24 hours in EdU solution, we could identify two sub-populations of meiocytes with a different EdU signal.

The first subpopulation consisted on early prophase I cells (leptotene – zygotene) whose chromosomes were either totally or partially labelled, showing a strong fluorescent signal. This pattern is consistent with genomic EdU incorporation during pre-meiotic S-phase replication for a number of reasons:

I) The strong fluorescent signal is similar to that observed in previous reports of EdU/BrdU incorporation during pre-meiotic replication [442,845,887,893].

II) Extrapolating from the meiotic timelines in these published reports, pollen mother cells in pre-meiotic S-phase at the beginning of the pulse are expected to advance to leptotene-zygotene after 24 hours.

III) The signal in partially labelled early prophase I cells is detected principally in DAPI-dense heterochromatic regions, known to be late-replicating regions of the Arabidopsis genome in accordance to what might be expected of cells that were caught in late S-phase at the beginning of the pulse.

IV) The signal is not SPO11-dependent, hence not related to meiotic recombination.

The second subpopulation consisted of cells at meiotic stages from pachytene to the end of meiosis (tetrads) whose chromosomes show a fainter and discrete EdU signal. Resolving into individual foci at the stages in which the chromosomes are less condensed, these foci group into "patches" with further chromosome condensation. This signal has a series of hallmarks that permit its identification with confidence as EdU incorporation at DSB repair-associated DNA synthesis tracts:

I) The discrete EdU foci observed at pachytene and later stages are not only significantly smaller in size than the general leptotene-zygotene signal, but also much

fainter. This is expected given the predicted size of DNA synthesis tracts associated to HR events (few bases to some kilobases of DNA) with respect to replicative labelling (megabases to the full genome).

II) The meiotic stages of the cells showing this signal after 24 hours incubation follow, in terms of meiotic progression (thus time, generally), those with total or partial replicative labelling. This observation, together with the extrapolations from Arabidopsis meiotic timelines, permit us to infer than the cells had completed S-phase at the beginning of the pulse and undergone meiotic prophase I up to, at least, pachytene in presence of EdU. Immunolocalization data of proteins involved in meiotic recombination in Arabidopsis together with molecular data of HR intermediates in other organisms suggest that most DNA synthesis associated to meiotic DSB repair must have occurred during the incubation period in these cells [349,653,845,884,907].

III) The numbers of EdU foci measured at pachytene are in compatible with the estimations of DSBs and HR intermediates reported in Arabidopsis (discussed below in detail).

IV) DAPI-dense heterochromatic regions corresponding with the centromeres have a significantly lower density (almost absence) of EdU foci in pachytene/diplotene and EdU signal even when it condenses with the chromosomes at diakinesis/MI. This is congruent with SPO11-oligo mapping showing that centromeric and pericentromeric regions have a much lower density of DSBs than the rest of the chromosome [11,361].

V) Finally, we have shown that these discrete EdU foci are SPO11-dependent, confirming with high confidence that they result of EdU incorporation at DNA synthesis tracts associated to meiotic DSB repair.

Such differentiation of the two patterns of labelling in meiocytes subjected to a pulse of a detectable nucleotide analogue described here has been previously reported in multiple organisms [875,877–879]. Despite the more limited understanding of the course of DSB repair and meiotic recombination at the time of these reports and the lack of controls such as the *spo11* mutant, they already hypothesised that the DNA synthesis observed during prophase I might be linked with crossover formation.

In a more recent study in budding yeast, Terasawa *et al.* could differentiate cells that incorporated BrdU during pre-meiotic replication from those that had incorporated it during prophase I [884]. In this case, and similarly to our observations, the signal of the subpopulation bearing prophase I labelling was lost in a *spo11* mutant, confirming the dependence of the incorporation on DSB formation. Using molecular techniques they could also detect the incorporation of BrdU at one DSB hotspot. This incorporation

was dependent on DSB formation (Spo11), end resection (Rad50) and homology search/invasion (Dmc1) and correlated with DSB levels when this site was compared with two adjacent sites with intermediate and low DSB levels. BrdU tracts were detected in CO and NCO molecules formed at this hotspot.

Meiotic DSB repair-associated DNA synthesis tracts mirror meiotic recombination features

We counted 409.5 ± 7.96 (mean + SEM; n = 45) DNA repair-associated DNA synthesis foci in WT pachytenes. We chose this stage among the ones labelled because the combination of chromosome condensation and synapsis offers a good resolution of the discrete EdU signals with respect to posterior stages and most recombination events are thought to be resolved or close to resolution at pachytene.

The immunolocalization of early recombination intermediates - RAD51 in most cases - has been traditionally the measure for comparative analysis of DSB formation in Arabidopsis. Nevertheless, despite the use an analogous techniques and genetic background, the consistency between publications of reported numbers of RAD51 foci per cell is low, with reported means of between 90 and 250 foci per cell and equally variable standard deviations [245,275,283,284,385,411,485,689,701,711,730,894,895,908–911]. This variability might have its origin in a number of factors, including the use of different antibodies, incubation times, number of cells counted, microscopes, variations of the protocol and/or the ability of the person performing the experiment. Although yielding exploitable results in a given study by comparing with internal controls, this variability is a problem when discussing absolute numbers of DSBs. On top of this, a recent publication analysing images acquired using a STED superresolution microscope reported more than 1000 RAD51 foci per cell which, if validated with the proper controls, might force upward revision of prior estimations of DSB numbers [912]. For the sake of this comparison, however, we will use a conservative estimation of 150-250 RAD51 foci. This is in agreement with a recent publication in which multiple proteins of the SPO11 complex and co-factors in DSB formation were immunolocalised, most of their averages falling within this 150-250 range. SPO11-1, for example, averages a maximum of 239 ± 30 (mean + SD) foci at the peak of its dynamic along prophase I [282].

Taking an estimation 150-250 DSBs per cell by average as a standard, our 409.5 DNA repair-associated synthesis tracts per cell might seem high at first sight if we just assume the detection of one tract per DSB repair event. However, we believe that this

number may well be within the expected range for Arabidopsis WT meiosis, due to a number of factors:

I) The first feature to point out is that the association of DSB proteins and recombinases with the chromosome is dynamic, including loading onto the chromosomes, to which they remain attached for an undefined time until they disassociate. This dynamic is not perfectly synchronous but there are hour-long windows in which the chromosomes are receiving DSBs and in which these DSBs are being processed and loading recombinases. This obviously has a technical implication when using fixed material for immunohistochemical analysis: any given cell will show the events in which the marker protein was loaded onto the chromosomes at the moment of fixation. We will miss those in which the event has advanced, removing that protein from the chromosomes, or those in which it is still to occur, in which that protein has not yet bound. These approaches thus inherently underestimate the absolute numbers of DSBs. This underestimation would be significant if the turnover of the marker proteins is fast and have lesser impact if the proteins stay on the chromosome for a longer time. The impact of this is seen in the differences in published estimated DSB numbers in different prophase I substages, which show significant differences between cells scored as leptotene, zygotene and pachytene [282–284]. This result thus accords well with this argument of a dynamic process leading to an important underestimation when pooling all cells to give a sole number (which is the most common practice). EdU-substituted DNA synthesis tracts, on the other hand, remain in the DNA from the moment they are synthesised until the end of meiosis (and beyond). This means that if we count at a timepoint in which we expect all or most of them to have been generated, the margin for underestimation due to their dynamics narrows significantly, resulting both in more accurate estimation and higher numbers than those obtained via immunolocalization of marker proteins.

II) Different classes of EdU signals were apparent when visually analysing images of pachytenes:

- single focus located on one of the homologues (one lateral axis)

- pairs of parallel foci in both homologues that are spatially separated (both lateral axes)

- pairs of parallel foci in both homologues that appear to be in contact (both lateral axes)

The mechanistic models of the meiotic recombination pathways predict different configurations of DNA synthesis tracts associated to an HR event. The most obvious

feature is that DNA synthesis may happen prior to resolution in one or both of the two chromatids involved in the HR event, depending on the capture and extension of the second resected end of the DSB and the resolution of the resulting dHJ, as shown in Figure 32. In meiosis for HR events involving interhomologue interactions, this would mean in one chromosome or in both homologous chromosomes.

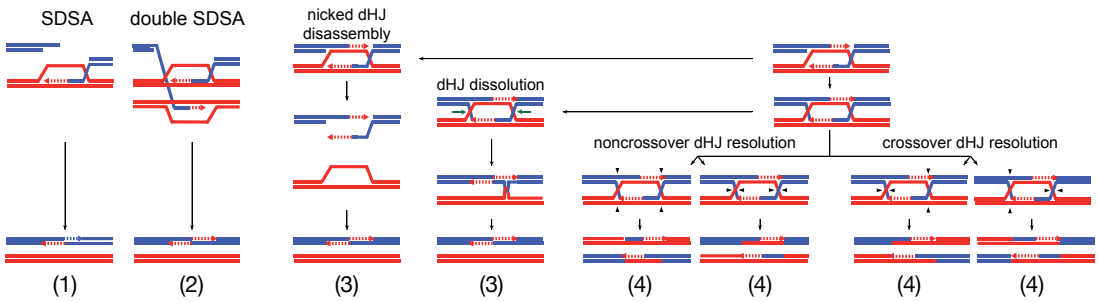

Figure 32. DNA synthesis tracts are mechanistically inherent to all meiotic recombination pathways
Adapted from Marsolier-Kergoat *et al.* (2018)

In SDSA events (Figure 32, 1), the first invading 3' end finds homology, is extended via DNA synthesis and recaptured, followed by gap filling - via DNA synthesis as well - and ligation. Thus only the initially broken chromatid will bear (EdU-substituted) neosynthesized DNA tracts. In double SDSA events (2), both ends of the DSB invade different chromatids to then be recaptured and ligated, but the result in terms of situation of the neosynthesized DNA tracts is the same, both would end up in the chromatid in which the DSB was induced.

If a second end invasion happens and it is captured into the D-loop, extended and stabilised forming a double Holiday junction, multiple resolution scenarios arise. Both dHJ disassembly or topological dissolution of the dHJ (3) would end up, similarly to SDSA, in NCO events with EdU-substituted neosynthesized DNA tracts in the initially broken chromatid. However, nucleolytic resolution of the dHJ (4) would result in one of these tracts in the chromatid of the initial DSB, while the other, after nicking and ligation, would end up in the donor chromatid independently of the cleavage configuration and the nature of the product - NCO or CO (although in meiosis, as previously pointed out, there is a bias towards CO). It is important to remark that these classes are extracted from the canonical models of meiotic recombination pathways but there are events such as class II CO in which the molecular nature of the intermediates is less well understood, as well as different possibilities of more complex events that might alter these final dispositions. Furthermore, the lack of molecular tools

to analyse recombination intermediates and non-crossover outcomes in Arabidopsis has impeded to unveil which of these pathways do happen in its meiosis and in which proportions.

Whether the different EdU focus classes inferred by visual inspection translate into the possible molecular configurations of repair products remains to be tested. Terasawa *et al.* were able to analyse single DNA synthesis tracts' length and positioning with respect to the DSB hotspots using stretched DNA fibres combined with the detection of BrdU plus multiple FISH probes as reference [884]. By doing so they observed two main classes of tracts: tracts that extended from the DSBs towards only one side of the DSB and tracts that extended towards both sides. These two classes corresponds to the tracts expected in single DNA molecules that took part in CO events in the first case and NCO events via SDSA in the second, which were further validated studying their dynamics in recombination mutants (Figure 32). Although this DNA combing plus fibre FISH technique has been employed in Arabidopsis [61], the lack of strong meiotic DSB hotspots with a precisely localised DSB site complicates the replication of this experiment. Creation of strong meiotic DSB-inducing CRISPR/Cas system (Chapter III) might solve this issue in the future. Another solution to differentiate classes of events could be the combination of EdU labelling with immunohistochemical markers of, for example, crossovers (HEI10, MLH1) or earlier recombination intermediates.

If the presence of double foci resulting from a single meiotic recombination event - hence a single DSB – is confirmed, this would result in an overestimation of total events when counting EdU foci with respect to RAD51 or SPO11 countings, in which at the levels of resolution of confocal microscopy yield only one focus per event. This phenomenon combined with the underestimation related to the dynamics of protein loading/disassociation might add to a difference between the mean number of events scored via of both methods.

III) A third feature which, although also present in immunolocalization analyses, seem interesting to point out is that a small fraction of the WT EdU foci were observed in *spo11* cells (39.2 ± 2.83). Whether these foci are predominantly real tracts of DNA synthesis in which EdU was incorporated or background is not clear. The observation of EdU signal in other stages in which chromosomes are more condensed with less background suggests that at least a portion of these foci are real. Multiple origins can be hypothesized for these tracts: SPO11-independent DSBs inherited from S-phase, spontaneous DSBs, DSBs generated by interlocks or other anomalous chromosome structures generated in the defective prophase I of *spo11* and/or residual meiotic DSBs

in this mutant allele. On the other hand, the quantification method considered an EdU focus those signals of a certain intensity that overlapped with the chromosomes excluding the obvious much-brighter organelles that carry DNA. It is thus possible than some background and/or not-that-bright organellar DNA foci might be quantified as well in *spo11* mutant cells.

Insights on the development of a protocol to map meiotic DSB repair-associated DNA synthesis tracts

The labelling of DSB repair-associated DNA synthesis tracts not only is promising as a cytological tool for meiotic studies but we think it may open a window for the molecular characterization of NCO and/or intersister events, so far indetectable in Arabidopsis, while offering further insight of the mechanistic details of CO formation. We thus focused in developing a protocol for their molecular detection, localization and characterization.

In this regard, we manually isolated considerable numbers of a prophase I-enriched populations of meiocytes following their incubation for 24 hours in EdU. We consistently accumulated pools of around 15.000-17.000 cells for NGS library preparation. Considering our measurement of 409.5 mean foci per cell, these numbers of cells have the theoretical potential of yielding up to 6-7 million individual tracts to pull-down, sequence and map to look for regions of enrichment for meiotic HR events. While the method is time consuming, it is easily scalable if needed.

Following gDNA extraction of this subpopulation of meiocytes, we set up a protocol to biotinylate and pull-down EdU-substituted fragments onto streptavidin-coupled magnetic beads within the NGS library preparation workflow. The recovery of adapter-ligated fragments of the expected size after library prep PCR in the samples incubated with EdU and their absence (at the resolution level of the TapeStation) in EdU- controls confirmed functional and specific pull-down and amplification of the EdU-substituted biotinylated fragments.

Our biological negative controls (*spo11*) did however pull down adapter-ligated fragments with similar efficiencies to the wild-type samples, using the pull-down to input ratio as reference. Several sources might contribute for EdU-substituted DNA in *spo11* samples: I) early prophase I meiocytes whose whole genome has incorporated EdU during replication; II) somatic cells that replicated during the EdU pulse; and/or III) mitochondria and chloroplasts' DNA that, as seen in the microscope pictures, incorporate EdU during the pulse. Although the cell collection protocol was optimised for isolation of the desired subpopulation of meiocytes, a single 4C cell that had

replicated during the pulse potentially carry almost 300Mb of EdU-substituted genomic DNA that may have a substantial impact in a pool of DSB repair-associated EdU tracts of tens to some thousand DNA base pairs. Nevertheless, organellar fragments are easily discarded at the mapping step and replicative labelling is expected to result in a rather flat profile present in both samples and controls which we hoped to difference from enrichment regions exclusive to WT samples at data treatment and analysis.

One issue worth noting is that in our WT and *spo11* pull-down replicates from samples incubated with EdU we obtained very high percentages of duplicated sequences (sequences that shared the same starting and ending coordinates). This issue was replicated in different attempts of the experiment. Several sources of duplicated sequences are known in NGS experiments and we tackled this issue by adding adapters bearing Unique Molecule Identifiers (UMIs). These UMIs are random sequences of, in this case, 11nt included in the ligated adapters that permit us to difference identical fragments generated prior to PCR (that will have different UMI) from PCR duplicates (same UMI). This second class is a major potential source of error in quantification and it is standard practice to avoid PCR duplicates by reducing amplification to the minimum needed or/and by removing duplicates at the data processing workflow.

Although their possible impact on quantification was dealt with the UMIs, high percentages of PCR duplicates in our samples reveal a potential problem of library complexity - reducing the final number of sequences to analyse. Whether this issue reflects the need of more starting material, the loss of cells at storage and/or early steps of gDNA extraction, the loss of gDNA at any step of the extraction or library preparation or a not-enough efficient pull-down (or a combination of several sources) remains to be tested and will potentially solve some of the issues related to low sequencing depth and background.

Rather paradoxical enrichments were detected in the pull-down of meiotic DSB repair-associated DNA synthesis tracts

We were able to detect regions of enrichment for EdU-substituted DNA tracts both in our WT samples and *spo11* samples. Unexpectedly, the absolute number of called peaks was similar in our WT and *spo11* samples. No significant overlapping was detected between the two WT replicates or the two *spo11* replicates, nor was a differential enrichment of EdU-substituted tract density found in any of the samples of both backgrounds when profiled over the peaks of the other replicate of the same background.

For further characterization, we decided to select the WT-specific and *spo11*-specific peaks for differential comparison of these regions with data from bibliography of features that might correlate with our data: SPO11-oligos, crossovers and replication initiation regions. All DSB repair-associated DNA synthesis tracts have a DSB of origin, so it seems plausible to hypothesise that SPO11 hotspots might show a relatively strong overlapping with regions of EdU-substituted tract enrichment. Some mechanistic aspects of meiotic recombination downstream DSB formation might differentiate the shape of the regions of enrichment of both features and complicate the analysis, such as resection length, branch migration or the resolution outcome. However, at least differences with the *spo11* samples, in which little or no overlapping with SPO11 hotspots should occur, are expected. The overlapping with mapped crossovers might not be that strong, given that although all crossovers should include DNA synthesis tracts, crossovers only represent around 5% of the total meiotic recombination events and it is not clear whether the events happening at different Arabidopsis DSB hotspots have similar chances of ending up in a CO or there are biases. Finally, we included replication initiation regions as a possible reference for enrichments related to DNA replication instead of meiotic recombination.

No differential overlapping was detected between the regions of enrichment of any of these three features and the called peaks in our WT samples with respect to those called in the *spo11* samples. A size comparison of these regions was performed as well. Although statistically significant differences were detected between the WT peaks and the *spo11* peaks (WT peaks slightly wider by average), both are much shorter than either published SPO11 hotspots or crossovers. The comparison with crossovers is not very informative however, because the methods used for scoring differ significantly. As mentioned above, it is expected that regions of enrichment of DSB repair-associated synthesis tracts should be wider than SPO11 hotspots by average. However, the opposite relation was found. These observations together do not allow us to discern if the called peaks in our samples are biologically relevant or merely artefactual.

We decided to explore our data deeper by computing the profiles of our two WT and two *spo11* samples over multiple features in which SPO11-oligo enrichments have been reported under the hypothesis that via this method we might detect local enrichments even if they were not strong enough or the sequencing depth was not enough to be called as peaks. Strikingly, enrichments over SPO11 hotspots and, although less-so, over mapped crossovers were detected in all WT and *spo11* samples of the same magnitude than SPO11-oligos. Similarly, an enrichment over gene promoters, terminators and transposable elements and a depletion over gene bodies of

similar magnitude than SPO11-oligos was found as well in both the WT samples and the negative controls.

These results are rather paradoxical. The low number of called peaks in WT samples, the absence of differences of these with those called in *spo11* samples, the reduced size of the peaks and the lack of enrichment of SPO11-oligos over the WT peaks may indicate that they are simply artifacts. However, we detected an enrichment of our data over published and validated SPO11 hotspots and, to a lesser degree, mapped crossovers, plus a signature over protein-coding genes and transposable elements mirroring these of SPO11 oligo data not only in shape but also in magnitude. The specific enrichments and signatures in the WT samples do not occur randomly, as validated by replicating the analyses over a shuffled set of intervals of each feature, obtaining flat profiles. They may thus point to successful detection of local enrichments of DSB repair-associated DNA synthesis tracts. Non-detection of individual peaks might be explained by a lack of sequencing depth or the presence of excessive background. Nevertheless, the obtention of similar results in the *spo11* samples in which, due to the absence of DSBs, no meiotic-specific enrichments of any kind are expected, casts doubts over the origin of the enrichments detected on our WT samples, in addition to raising similar questions regarding those reported for the SPO11-oligo mapping.

A fortuitous correlation between the profiles of our samples and those of SPO11-oligos seems unlikely due to the specificity of the regions observed, the flat profiles observed in all sets of shuffled intervals and the complexity of some of the signatures. The profiles over protein-coding genes not only show a peak of enrichment, but a rather complex signature including an enrichment over the promoters, a depletion over gene bodies and an enrichment over terminators that is replicated in all samples – SPO11-oligos and our four independent replicates.

Another possibility is that the correlation is not random but there are different origins for these enrichments that overlap in the genome. Features like SPO11 hotspots and replication initiation regions in Arabidopsis share similar associated genetic and epigenetic features, including low nucleosome occupancy, AT-richness and both SPO11-oligos and replication initiation regions are depleted in gene bodies and enriched in transposable elements, specially Helitrons [361,905]. Among the sets of intervals taken from the bibliography, 781 of them overlap, which represent around 15% of the totals of both SPO11 hotspots and replication initiation regions. A local enrichment of SPO11-oligos could be detected over replication initiation regions when plotting the profile over them. Direct coupling of pre-meiotic replication and DSB formation has been described in multiple organisms as well as DSB enrichments in early replicating regions [338–341,344]. So

it might be hypothesised that, given that we have the same profiles in WT and *spo11* samples, these enrichments could have a replicative origin while still correlating with SPO11-oligo data. If a significant number cells in the pool had partially undergone replication during the pulse and not properly cleaned up from the targeted subpopulation of meiocytes, replication initiation regions might show an enrichment. They are early replicating regions at local level (with respect to adjacent regions) and thus might have higher chances of having incorporated EdU in partially replicated somatic cells and being pulled down if carried along. But the heatmaps plotting the density of our samples over SPO11 hotspots show almost ubiquitous enrichment over all hotspots, not in a subset of hotspots as it might be expected from the 15% overlapping of these with replication initiation regions. So although not possible to exclude without further analysis, this hypothesis does not seem convincing.

A third hypothesis might be that the enrichments observed in both our results and SPO11-oligos are merely a common technical artifact. Due to the specificities of the experimental setup, SPO11 oligo data do not have a "biological" control without DSBs, such as our *spo11* mutant samples, to sequence and compare with. For this experiment, the SPO11-1-Myc fusion protein needed for the pull-down must function to form DSB for these fragments to be generated. However, the SPO11-1-Myc protein was cytologically localised in the chromosomes, was able to rescue the DSB-null phenotype of *spo11* mutants, replicates WT recombination rates in multiple intervals and was proven to be pulled-down efficiently and specifically, confirming its role as a functional SPO11-1 and reinforcing the confidence on the SPO11-oligo-seq data. Regarding possible library preparation-related artefacts, our library preparation workflow starts with naked chromatin, discarding in principle potential chromatin state-related biases. SPO11 hotspots are AT-enriched and preferential cleavage on AT-richer regions have been described in library preparation kits including enzymatic fragmentation [913]. Nevertheless, while our library preparation method includes fragmentation, the SPO11-oligo workflow does not (due to the inherent nature of SPO11-oligos which are already 30-40nt fragments), excluding a shared fragmentation bias. Library preparation methods from that point on are completely different and we have not been able to identify common bias-inducing steps. Finally, in the two workflows we use an "input control" library to normalise the data: in the SPO11-oligo case an independent gDNA library was sequenced and trimmed down to match the fragment length of SPO11-oligos, in ours a subsample of the input to the pull-down step for each replicate. This input control has the function of eliminating potential library preparation or sequencing biases. So, to our eyes, there are not obvious sources

of common biases that might be interpreted as local enrichments over specific features that may support this hypothesis.

We could not get to a satisfying conclusion to explain this correlation between our WT samples, our *spo11* samples and the published SPO11-oligo data. Therefore, we hope that future efforts will help solve this issue and successfully obtain a map of DSB repair-associated DNA synthesis tracts of Arabidopsis meiocytes and, at the same time, go a step further using the characterization of these tracts as a source of mechanistic information of meiotic recombination events yet to be characterised in the model plant.

Conclusions

Revisiting the initial hypothesis and the objectives proposed at the beginning of this project, we may conclude that:

I) We successfully designed and validated an easy and reproducible protocol for the incorporation of EdU at DNA repair-associated DNA synthesis tracts during prophase I. This protocol permits the cytological detection and the differentiation of the subpopulation of meiocytes bearing this labelling from meiocytes that incorporated EdU at pre-meiotic replication.

II) This DNA repair-associated DNA synthesis EdU signal fulfills multiple predictions drawn from Arabidopsis meiotic recombination models and features: it is SPO11-dependent, EdU foci numbers concord with reported numbers of meiotic DSBs, it is noticeably less dense in heterochromatic regions known to receive lower numbers of DSBs and different patterns of foci could be observed that might mirror different classes of meiotic recombination events.

III) A protocol was developed to successfully isolate a subpopulation of meiocytes enriched in the stages known to carry DNA repair-associated DNA synthesis labelling; to extract genomic DNA from these cells, conjugate the EdU-substituted tracts with biotin and pull them down specifically and efficiently for preparation of NGS sequencing libraries.

IV) Regions of enrichment of DNA repair-associated DNA synthesis tracts in the genome were detected, as well as specific enrichments over features known to be enriched in DSBs, including SPO11 hotspots, mapped crossovers, gene promoters and terminators.

V) Surprisingly, these enrichments were replicated to similar levels in samples lacking meiotic DSBs – *spo11* mutant - incubated in EdU as well. The similarity to SPO11-oligo enrichments and the fact that this is seen in *spo11* mutant samples is particularly intriguing. This presumably points to the existence of the influence of underlying genomic and or technical feature(s) on recombination initiation maps from both the EdU and SPO11-oligo pull-downs. At this point, however, the datasets are not sufficiently complete to support drawing of definite conclusions.

The results obtained and their interpretation allows to confidently validate the initial hypothesis: Arabidopsis meiotic cells undergoing prophase I in the presence of EdU will incorporate this nucleotide analogue within meiotic DSB repair-associated DNA synthesis tracts. We were able to cytologically detect this signal following a

protocol that not only is easier to perform and more reproducible that the standard protocols to analyse DSB numbers in Arabidopsis but it arguably offers a better resolution and the facility to score higher numbers of good quality labelled cells. While we could not draw high confidence conclusions from the molecular detection and mapping of these tracts given the similarity of the signal of the negative control, we were able to set up a series of steps in the protocol that we think will be useful to accomplish it in the near future.

Future work

This project is still is in progress and we believe it has the potential to yield relevant information about the repair of DSB during meiosis in Arabidopsis. Among the things that can be done, there may be included:

- As an ongoing project wrapped in this document at the given moment to conclude this thesis, we did not get to include results about the objective V: the analysis of individual DNA repair-associated DNA synthesis tracts. Nanopore DNA sequencing permits the direct detection of multiple nucleotide analogues incorporated into genomic DNA, including EdU and BrdU [914–917]. This approach has been already used in budding yeast for the study of DNA replication [914,916,917]. While transferring this approach to the detection of DSB repair-associated DNA synthesis tracts in Arabidopsis presents a series of challenges that we have already started to address, notably the accumulation of sufficiently high numbers of cells, the considerably shorter length of the tracts (in principle) and the differentiation from replicative "contamination", it also has major advantages. Direct detection avoid issues with PCR duplicates that we have been experimenting throughout this work. It also permits the combination of the analysis of DNA synthesis tracts with the conversion on SNPs in hybrid plants, likely helping to difference events originated at meiotic recombination from replicative incorporation. The co-detection of DNA synthesis tracts and conversion tracts associated to a meiotic recombination event would open a promising door in the detailed molecular characterisation of both crossover and non-crossover events during Arabidopsis meiosis and we hope to carry it out with success in the near future.

- To try different durations of the EdU pulse with the aim of visualising these EdU foci in meiotic cells prior to pachytene. This would offer the possibility of building a timeline of the appearance of DSB repair-associated DNA synthesis tracts and thus of the dynamics of repair along the whole Arabidopsis prophase I.

- To combine the labelling of DSB repair-associated DNA synthesis tracts with the immunolocalization of meiotic proteins. Combination with immunolabelling of proteins of the synaptonemal complex would facilitate the interpretation of the different patterns of EdU foci, as it offers a reference point to identify the position of those with respect to it and to the two homologous chromosomes. Combination with the immunolabelling of crossover markers, such as MLH1 or HEI10, may help identifying a differential pattern of EdU labelling associated to these events. The inclusion of EdU labelling in a time course in combination with proteins associated DSB formation (SPO11 complex proteins i.e.), early recombination intermediates (RAD51, DMC1 i.e.), mid-late intermediates (ZMM proteins i.e.) and resolution of recombination (MLH1 i.e.) as well as structural components of the chromosomal axes and the synaptonemal complex (ASY, ZYP1 i.e.) would help understanding the dynamics of those in relation to precedent and subsequent HR events.

- The analysis of the numbers and the dynamics of DSB repair-associated DNA synthesis foci in mutants of genes associated with meiotic recombination. As pointed out before, the ease and resolution of this technique offers a new tool for the standard cytological characterization of meiotic mutants.

- The transfer of this technique to other species. There are plant species, including some of agronomical interest, in which genetic transformation remains a challenge or involves expensive, time-consuming and technically difficult methods. This hampers the use of fusion proteins for the study of meiotic recombination. The option of labelling meiotic recombination events by doing a pulse of a nucleoside analogue or injecting it into the germinal tissues may thus present a cheaper, much faster and, although it need the proper set-up, probably technically more accessible alternative.

REFERENCES

1. Watson, J. D. & Crick, F. H. C. Molecular structure of nucleic acids: A structure for deoxyribose nucleic acid. *Nature* **171**, 737–738 (1953).
2. Thal, J. *Sylva Hercynia: sive catalogus plantarum sponte nascentium in montibus & locis plerisque Hercyniae Sylvae quae respicit Saxoniam.* (1588).
3. Holl, F. & Heynhold, G. Flora von Sachsen. *Verlag von Justus Nauman* **1**, 948 (1842).
4. Steinitz-Sears, L. M. Chromosome Studies in Arabidopsis Thaliana. *Genetics* **48**, 483–490 (1963).
5. Krämer, U. Planting molecular functions in an ecological context with Arabidopsis thaliana. *Elife* **4**, 1–13 (2015).
6. Provart, N. J. *et al.* 50 years of Arabidopsis research: Highlights and future directions. *New Phytol.* **209**, 921–944 (2016).
7. Woodward, A. W. & Bartel, B. Biology in bloom: A primer on the arabidopsis thaliana model system. *Genetics* **208**, 1337–1349 (2018).
8. Laibach, F. Zur Frage nach der Individualität der Chromosomen im Pflanzenreich. *Beih. Bot. Zentralbl.* **22**, (1907).
9. Reinholz, E. Auslösung von Röntgen-Mutationen bei Arabidopsis thaliana (L.) Heynh. und ihre Bedeutung für die Pflanzenzüchtung und Evolutionstheorie. *FIAT Rep. No. 1006* 1–70 (1945).
10. Wang, B. *et al.* High-quality Arabidopsis thaliana Genome Assembly with Nanopore and HiFi Long Reads. *Genomics. Proteomics Bioinformatics* (2021).
11. Naish, M. *et al.* The genetic and epigenetic landscape of the Arabidopsis centromeres. *Science (80-.).* **374**, 2021.05.30.446350 (2021).
12. Ahmad, M., Jarillo, J.A., and Cashmore, A. R. PHR2: A Novel Arabidopsis Gene Related To The Blue-Light Photoreceptor/Photolyase Family. *Plant Physiol.* **117**, 718 (1998).
13. Nakajima, S. *et al.* Cloning and characterization of a gene (UVR3) required for photorepair of 6-4 photoproducts in Arabidopsis thaliana. *Nucleic Acids Res.* **26**, 638–644 (1998).
14. Tanaka, A. *et al.* An ultraviolet-B-resistant mutant with enhanced DNA repair in arabidopsis. *Plant Physiol.* **129**, 64–71 (2002).
15. Spampinato, C. P. Protecting DNA from errors and damage: an overview of DNA repair mechanisms in plants compared to mammals. *Cell. Mol. Life Sci.* **74**, 1693–1709 (2017).
16. Banaś, A. K. *et al.* All you need is light. Photorepair of uv-induced pyrimidine dimers. *Genes (Basel).* **11**, 1–17 (2020).
17. Roldán-Arjona, T., Ariza, R. R. & Córdoba-Cañero, D. DNA Base Excision Repair in Plants: An Unfolding Story With Familiar and Novel Characters. *Frontiers in Plant Science* **10**, (2019).
18. Jiricny, J. Postreplicative mismatch repair. *Cold Spring Harb. Perspect. Biol.* **5**, 1–23 (2013).
19. Kunkel, T. A. & Erie, D. A. Eukaryotic Mismatch Repair in Relation to DNA Replication. *Annu. Rev. Genet.* **49**, 291–313 (2015).
20. Gómez, R. & Spampinato, C. P. Mismatch recognition function of Arabidopsis thaliana MutSγ. *DNA Repair (Amst).* **12**, 257–264 (2013).
21. De Jager, M. *et al.* Human Rad50/Mre11 is a flexible complex that can tether DNA ends. *Mol. Cell* **8**, 1129–1135 (2001).
22. Käshammer, L. *et al.* Mechanism of DNA End Sensing and Processing by the Mre11-Rad50 Complex. *Mol. Cell* **76**, 382-394.e6 (2019).
23. Hopfner, K. P. *et al.* The Rad50 zinc-hook is a structure joining Mre11 complexes in DNA recombination and repair. *Nature* **418**, 562–566 (2002).
24. Van der linden, E., Sanchez, H., Kinoshita, E., Kanaar, R. & Wyman, C. RAD50 and NBS1 form a stable complex functional in DNA binding and tethering. *Nucleic Acids Res.* **37**, 1580–1588 (2009).
25. Abraham, R. T. PI 3-kinase related kinases: 'Big' players in stress-induced signaling pathways. *DNA Repair (Amst).* **3**, 883–887 (2004).
26. Nakada, D., Matsumoto, K. & Sugimoto, K. ATM-related Tel1 associates with double-strand breaks through an Xrs2-dependent mechanism. *Genes Dev.* **17**, 1957–1962 (2003).
27. You, Z., Chahwan, C., Bailis, J., Hunter, T. & Russell, P. ATM Activation and Its Recruitment to Damaged DNA Require Binding to the C Terminus of Nbs1. *Mol. Cell. Biol.* **25**, 5363–5379 (2005).
28. Lee, J. H. & Paull, T. T. Direct Activation of the ATM Protein Kinase by the Mre11/Rad50/Nbs1 Complex. *Science (80-.).* **304**, 93–96 (2004).
29. Limbo, O., Yamada, Y. & Russell, P. Mre11-Rad50–dependent activity of ATM/Tel1 at DNA breaks and telomeres in the absence of Nbs1. *Mol. Biol. Cell* **29**, 1389–1399 (2018).

30. Cannon, B. *et al.* Visualization of local DNA unwinding by Mre11/Rad50/ Nbs1 using single-molecule FRET. *Proc. Natl. Acad. Sci. U. S. A.* **110**, 18868–18873 (2013).
31. Paull, T. T. Mechanisms of ATM activation. *Annu. Rev. Biochem.* **84**, 711–738 (2015).
32. Wang, Q. *et al.* Rad17 recruits the MRE11-RAD50-NBS1 complex to regulate the cellular response to DNA double-strand breaks. *EMBO J.* **33**, 862–877 (2014).
33. Stucki, M. *et al.* MDC1 directly binds phosphorylated histone H2AX to regulate cellular responses to DNA double-strand breaks. *Cell* **123**, 1213–1226 (2005).
34. Cassani, C. *et al.* Tel1 and Rif2 Regulate MRX Functions in End-Tethering and Repair of DNA Double-Strand Breaks. *PLoS Biol.* **14**, e1002387 (2016).
35. Gobbini, E., Cassani, C., Villa, M., Bonetti, D. & Longhese, M. P. Functions and regulation of the MRX complex at DNA double-strand breaks. *Microb. Cell* **3**, 329–337 (2016).
36. Zou, L. & Elledge, S. J. Sensing DNA damage through ATRIP recognition of RPA-ssDNA complexes. *Science (80-.).* **300**, 1542–1548 (2003).
37. Lee, Y. C., Zhou, Q., Chen, J. & Yuan, J. RPA-Binding Protein ETAA1 Is an ATR Activator Involved in DNA Replication Stress Response. *Curr. Biol.* **26**, 3257–3268 (2016).
38. Biswas, H., Goto, G., Wang, W., Sung, P. & Sugimoto, K. Ddc2ATRIP promotes Mec1ATR activation at RPA-ssDNA tracts. *PLoS Genet.* **15**, (2019).
39. Navadgi-Patil, V. M., Kumar, S. & Burgers, P. M. The unstructured c-terminal tail of yeast Dpb11 (Human TopBP1) protein is dispensable for DNA replication and the S phase checkpoint but required for the G 2/M checkpoint. *J. Biol. Chem.* **286**, 40999–41007 (2011).
40. Navadgi-Patil, V. M. & Burgers, P. M. The Unstructured C-Terminal Tail of the 9-1-1 Clamp Subunit Ddc1 Activates Mec1/ATR via Two Distinct Mechanisms. *Mol. Cell* **36**, 743–753 (2009).
41. Kumar, S. & Burgers, P. M. Lagging strand maturation factor Dna2 is a component of the replication checkpoint initiation machinery. *Genes Dev.* **27**, 313–321 (2013).
42. Kumagai, A., Lee, J., Yoo, H. Y. & Dunphy, W. G. TopBP1 activates the ATR-ATRIP complex. *Cell* **124**, 943–955 (2006).
43. Zhou, C. *et al.* Profiling DNA damage-induced phosphorylation in budding yeast reveals diverse signaling networks. *Proc. Natl. Acad. Sci.* **113**, E3667–E3675 (2016).
44. Schlam-Babayov, S. *et al.* Phosphoproteomics reveals novel modes of function and inter-relationships among PIKKs in response to genotoxic stress. *EMBO J.* **40**, e104400 (2021).
45. Roitinger, E. *et al.* Quantitative Phosphoproteomics of the Ataxia Telangiectasia-Mutated (ATM) and Ataxia Telangiectasia-Mutated and Rad3-related (ATR) Dependent DNA Damage Response in Arabidopsis thaliana. *Mol. Cell. Proteomics* **14**, 556 (2015).
46. Paull, T. T. *et al.* A critical role for histone H2AX in recruitment of repair factors to nuclear foci after DNA damage. *Curr. Biol.* **10**, 886–895 (2000).
47. Nakamura, T. M., Du, L.-L., Redon, C. & Russell, P. Histone H2A Phosphorylation Controls Crb2 Recruitment at DNA Breaks, Maintains Checkpoint Arrest, and Influences DNA Repair in Fission Yeast. *Mol. Cell. Biol.* **24**, 6215–6230 (2004).
48. Hartung, F.; Puchta, H. Isolation of the complete cDNA of the Mre11 homologue of Arabidopsis (Accession No. AJ243822) indicates conservation of DNA recombination mechanisms between plants and other eucaryotes (PGR 99-132). *Plant Physiol.* **121**, 311 (1999).
49. Gallego, M. E. *et al.* Disruption of the Arabidopsis RAD50 gene leads to plant sterility and MMS sensitivity. *Plant Journal* **25**, 31–41 (2001).
50. Waterworth, W. M. *et al.* NBS1 is involved in DNA repair and plays a synergistic role with ATM in mediating meiotic homologous recombination in plants. *Plant J.* **52**, 41–52 (2007).
51. Garcia, V., Salanoubat, M., Choisne, N. & Tissier, A. An ATM homologue from Arabidopsis thaliana: Complete genomic organisation and expression analysis. *Nucleic Acids Res.* **28**, 1692–1699 (2000).
52. Culligan, K., Tissier, A. & Britt, A. ATR regulates a G2-phase cell-cycle checkpoint in Arabidopsis thaliana. *Plant Cell* **16**, 1091–1104 (2004).
53. Aklilu, B. B., Soderquist, R. S. & Culligan, K. M. Genetic analysis of the Replication Protein A large subunit family in Arabidopsis reveals unique and overlapping roles in DNA repair, meiosis and DNA replication. *Nucleic Acids Res.* **42**, 3104–3118 (2014).
54. Aklilu, B. B. *et al.* Functional diversification of replication protein a paralogs and telomere length maintenance in arabidopsis. *Genetics* **215**, 989–1002 (2020).
55. Xiao, Y. & Weaver, D. T. Conditional gene targeted deletion by Cre recombinase demonstrates the requirement for the double-strand break repair Mre11 protein in murine embryonic stem cells. *Nucleic Acids Res.* **25**, 2985–2991 (1997).
56. Luo, G. *et al.* Disruption of mRad50 causes embryonic stem cell lethality, abnormal embryonic development, and sensitivity to ionizing radiation. *Proc. Natl. Acad. Sci. U. S. A.* **96**, 7376–7381 (1999).

57. Zhu, J., Petersen, S., Tessarollo, L. & Nussenzweig, A. Targeted disruption of the Nijmegen breakage syndrome gene NBS1 leads to early embryonic lethality in mice. *Curr. Biol.* **11**, 105–109 (2001).
58. Gallego, M. E. & White, C. I. RAD50 function is essential for telomere maintenance in Arabidopsis. *Proc. Natl. Acad. Sci. U. S. A.* **98**, 1711–1716 (2001).
59. Bundock, P. & Hooykaas, P. Severe developmental defects, hypersensitivity to DNA-damaging agents, and lengthened telomeres in Arabidopsis MRE11 mutants. *Plant Cell* **14**, 2451–2462 (2002).
60. Puizina, J., Siroky, J., Mokros, P., Schweizer, D. & Riha, K. Mre11 deficiency in Arabidopsis is associated with chromosomal instability in somatic cells and Spo11-dependent genome fragmentation during meiosis. *Plant Cell* **16**, 1968–1978 (2004).
61. Vannier, J. B., Depeiges, A., White, C. & Gallego, M. E. Two roles for Rad50 in telomere maintenance. *EMBO J.* **25**, 4577–4585 (2006).
62. Garcia, V. *et al.* AtATM is essential for meiosis and the somatic response to DNA damage in plants. *Plant Cell* **15**, 119–132 (2003).
63. Culligan, K., Tissier, A. & Britt, A. ATR regulates a G2-phase cell-cycle checkpoint in Arabidopsis thaliana. *Plant Cell* **16**, 1091–1104 (2004).
64. Culligan, K. M., Robertson, C. E., Foreman, J., Doerner, P. & Britt, A. B. ATR and ATM play both distinct and additive roles in response to ionizing radiation. *Plant J.* **48**, 947–961 (2006).
65. Sweeney, P. R., Britt, A. B. & Culligan, K. M. The Arabidopsis ATRIP ortholog is required for a programmed response to replication inhibitors. *Plant J.* **60**, 518–526 (2009).
66. Amiard, S. *et al.* Distinct roles of the ATR kinase and the Mre11-Rad50-Nbs1 complex in the maintenance of chromosomal stability in Arabidopsis. *Plant Cell* **22**, 3020–3033 (2010).
67. Ricaud, L. *et al.* ATM-mediated transcriptional and developmental responses to γ-rays in Arabidopsis. *PLoS One* **2**, e430 (2007).
68. Yoshiyama, K., Conklin, P. A., Huefner, N. D. & Britt, A. B. Suppressor of gamma response 1 (SOG1) encodes a putative transcription factor governing multiple responses to DNA damage. *Proc. Natl. Acad. Sci. U. S. A.* **106**, 12843–12848 (2009).
69. Roitinger, E. *et al.* Quantitative phosphoproteomics of the ataxia telangiectasia-mutated (ATM) and ataxia telangiectasia-mutated and Rad3-related (ATR) dependent DNA damage response in arabidopsis thaliana. *Molecular and Cellular Proteomics* **14**, 556–571 (2015).
70. Vespa, L., Couvillion, M., Spangler, E. & Shippen, D. E. ATM and ATR make distinct contributions to chromosome end protection and the maintenance of telomeric DNA in Arabidopsis. *Genes Dev.* **19**, 2111–2115 (2005).
71. Amiard, S., Depeiges, A., Allain, E., White, C. I. & Gallego, M. E. Arabidopsis ATM and ATR kinases prevent propagation of genome damage caused by telomere dysfunction. *Plant Cell* **23**, 4254–4265 (2011).
72. Marini, F., Rawal, C. C., Liberi, G. & Pellicioli, A. Regulation of DNA Double Strand Breaks Processing: Focus on Barriers. *Front. Mol. Biosci.* **6**, 1–8 (2019).
73. Zhao, F., Kim, W., Kloeber, J. A. & Lou, Z. DNA end resection and its role in DNA replication and DSB repair choice in mammalian cells. *Exp. Mol. Med.* **52**, 1705–1714 (2020).
74. Wang, H. *et al.* The Interaction of CtIP and Nbs1 Connects CDK and ATM to Regulate HR-Mediated Double-Strand Break Repair. *PLoS Genet.* **9**, (2013).
75. Liang, J., Suhandynata, R. T. & Zhou, H. Phosphorylation of Sae2 mediates Forkhead-associated (FHA) domain-specific interaction and regulates its DNA repair function. *J. Biol. Chem.* **290**, 10751–10763 (2015).
76. Usui, T. *et al.* Complex formation and functional versatility of Mre11 of budding yeast in recombination. *Cell* **95**, 705–716 (1998).
77. Paull, T. T. & Gellert, M. The 3′ to 5′ exonuclease activity of Mre11 facilitates repair of DNA double-strand breaks. *Mol. Cell* **1**, 969–979 (1998).
78. Majka, J., Alford, B., Ausio, J., Finn, R. M. & McMurray, C. T. ATP hydrolysis by RAD50 protein switches MRE11 enzyme from endonuclease to exonuclease. *J. Biol. Chem.* **287**, 2328–2341 (2012).
79. Tishkoff, D. X. *et al.* Identification and characterization of Saccharomyces cerevisiae EXO1, a gene encoding an exonuclease that interacts with MSH2. *Proc. Natl. Acad. Sci. U. S. A.* **94**, 7487–7492 (1997).
80. Wilson, D. M. *et al.* Hex1: A new human Rad2 nuclease family member with homology to yeast exonuclease 1. *Nucleic Acids Res.* **26**, 3762–3768 (1998).
81. Cannavo, E., Cejka, P. & Kowalczykowski, S. C. Relationship of DNA degradation by Saccharomyces cerevisiae Exonuclease 1 and its stimulation by RPA and Mre11-Rad50-Xrs2 to DNA end resection. *Proc. Natl. Acad. Sci. U. S. A.* **110**, E1661–E1668 (2013).
82. Cejka, P. *et al.* DNA end resection by Dna2-Sgs1-RPA and its stimulation by Top3-Rmi1 and Mre11-Rad50-Xrs2. *Nature* **467**, 112–116 (2010).
83. Nimonkar, A. V. *et al.* BLM-DNA2-RPA-MRN and EXO1-BLM-RPA-MRN constitute two DNA end resection machineries for human DNA break repair. *Genes Dev.* **25**, 350–362 (2011).

84. Sturzenegger, A. *et al.* DNA2 cooperates with the WRN and BLM RecQ helicases to mediate long-range DNA end resection in human cells. *J. Biol. Chem.* **289**, 27314–27326 (2014).
85. Boulton, S. J. & Jackson, S. P. Identification of a Saccharomyces cerevisiae Ku80 homologue: Roles in DNA double strand break rejoining and in telomeric maintenance. *Nucleic Acids Res.* **24**, 4639–4648 (1996).
86. Pierce, A. J., Hu, P., Han, M., Ellis, N. & Jasin, M. Ku DNA end-binding protein modulates homologous repair of double-strand breaks in mammalian cells. *Genes Dev.* **15**, 3237–3242 (2001).
87. Huertas, P., Cortés-Ledesma, F., Sartori, A. A., Aguilera, A. & Jackson, S. P. CDK targets Sae2 to control DNA-end resection and homologous recombination. *Nature* **455**, 689–692 (2008).
88. Cruz-García, A., López-Saavedra, A. & Huertas, P. BRCA1 accelerates CtIP-ediated DNA-end resection. *Cell Rep.* **9**, 451–459 (2014).
89. Langerak, P., Mejia-Ramirez, E., Limbo, O. & Russell, P. Release of Ku and MRN from DNA ends by Mre11 nuclease activity and Ctp1 is required for homologous recombination repair of double-strand breaks. *PLoS Genet.* **7**, e1002271 (2011).
90. Myler, L. R. *et al.* Single-Molecule Imaging Reveals How Mre11-Rad50-Nbs1 Initiates DNA Break Repair. *Mol. Cell* **67**, 891-898.e4 (2017).
91. Lee, K. J. *et al.* Phosphorylation of Ku dictates DNA double-strand break (DSB) repair pathway choice in S phase. *Nucleic Acids Res.* **44**, 1732–1745 (2015).
92. Escribano-Díaz, C. *et al.* A Cell Cycle-Dependent Regulatory Circuit Composed of 53BP1-RIF1 and BRCA1-CtIP Controls DNA Repair Pathway Choice. *Mol. Cell* **49**, 872–883 (2013).
93. Mirman, Z. *et al.* 53BP1–RIF1–shieldin counteracts DSB resection through CST- and Polα-dependent fill-in. *Nature* **560**, 112–116 (2018).
94. Yu, T. Y., Kimble, M. T. & Symington, L. S. Sae2 antagonizes Rad9 accumulation at DNA double-strand breaks to attenuate checkpoint signaling and facilitate end resection. *Proc. Natl. Acad. Sci. U. S. A.* **115**, E11961–E11969 (2018).
95. Uanschou, C. *et al.* A novel plant gene essential for meiosis is related to the human CtIP and the yeast COM1/SAE2 gene. *EMBO J.* **26**, 5061–5070 (2007).
96. Jia, N., Liu, X. & Gao, H. A DNA2 homolog is required for DNA damage repair, cell cycle regulation, and meristem maintenance in plants. *Plant Physiol.* **171**, 318–333 (2016).
97. Hartung, F., Suer, S. & Puchta, H. Two closely related RecQ helicases have antagonistic roles in homologous recombination and DNA repair in Arabidopsis thaliana. *Proc. Natl. Acad. Sci. U. S. A.* **104**, 18836–18841 (2007).
98. Kobbe, D., Blanck, S., Demand, K., Focke, M. & Puchta, H. AtRECQ2, a RecQ helicase homologue from Arabidopsis thaliana, is able to disrupt various recombinogenic DNA structures in vitro. *Plant J.* **55**, 397–405 (2008).
99. Röhrig, S. *et al.* The RecQ-like helicase HRQ1 is involved in DNA crosslink repair in Arabidopsis in a common pathway with the Fanconi anemia-associated nuclease FAN1 and the postreplicative repair ATPase RAD5A. *New Phytol.* **218**, 1478–1490 (2018).
100. Furukawa, T., Imamura, T., Kitamoto, H. K. & Shimada, H. Rice exonuclease-1 homologue, OsEXO1, that interacts with DNA polymerase λ and RPA subunit proteins, is involved in cell proliferation. *Plant Mol. Biol.* **66**, 519–531 (2008).
101. Kwon, Y. I. *et al.* Overexpression of OsRecQl4 and/or OsExo1 enhances DSB-induced homologous recombination in rice. *Plant Cell Physiol.* **53**, 2142–2152 (2012).
102. Sharda, M., Badrinarayanan, A. & Seshasayee, A. S. N. Evolutionary and Comparative Analysis of Bacterial Nonhomologous End Joining Repair. *Genome Biol. Evol.* **12**, 2450–2466 (2020).
103. Bétermier, M., Bertrand, P. & Lopez, B. S. Is Non-Homologous End-Joining Really an Inherently Error-Prone Process? *PLoS Genet.* **10**, e1004086 (2014).
104. Frit, P., Ropars, V., Modesti, M., Charbonnier, J. B. & Calsou, P. Plugged into the Ku-DNA hub: The NHEJ network. *Prog. Biophys. Mol. Biol.* **147**, 62–76 (2019).
105. Gottlieb, T. M. & Jackson, S. P. The DNA-dependent protein kinase: Requirement for DNA ends and association with Ku antigen. *Cell* **72**, 131–142 (1993).
106. Nick McElhinny, S. A., Snowden, C. M., McCarville, J. & Ramsden, D. A. Ku Recruits the XRCC4-Ligase IV Complex to DNA Ends. *Mol. Cell. Biol.* **20**, 2996–3003 (2000).
107. Chen, L., Trujillo, K., Ramos, W., Sung, P. & Tomkinson, A. E. Promotion of Dnl4-Catalyzed DNA end-joining by the Rad50/Mre11/Xrs2 and Hdf1/Hdf2 complexes. *Mol. Cell* **8**, 1105–1115 (2001).
108. Löbrich, M. & Jeggo, P. A Process of Resection-Dependent Nonhomologous End Joining Involving the Goddess Artemis. *Trends Biochem. Sci.* **42**, 690–701 (2017).
109. Chang, H. H. Y., Pannunzio, N. R., Adachi, N. & Lieber, M. R. Non-homologous DNA end joining and alternative pathways to double-strand break repair. *Nat. Rev. Mol. Cell Biol. 2017 188* **18**, 495–506 (2017).
110. Emerson, C. H. & Bertuch, A. A. Consider the workhorse: Nonhomologous end-joining in budding yeast.

Biochem. Cell Biol. **94**, 396–406 (2016).

111. Tamura, K., Adachi, Y., Chiba, K., Oguchi, K. & Takahashi, H. Identification of Ku70 and Ku80 homologues in Arabidopsis thaliana: Evidence for a role in the repair of DNA double-strand breaks. *Plant J.* **29**, 771–781 (2002).
112. West, C. E., Waterworth, W. M., Jiang, Q. & Bray, C. M. Arabidopsis DNA ligase IV is induced by γ-irradiation and interacts with an Arabidopsis homologue of the double strand break repair protein XRCC4. *Plant J.* **24**, 67–78 (2000).
113. García-Díaz, M. *et al.* DNA polymerase lambda (Pol λ), a novel eukaryotic DNA polymerase with a potential role in meiosis. *J. Mol. Biol.* **301**, 851–867 (2000).
114. West, C. E. *et al.* Disruption of the Arabidopsis AtKu80 gene demonstrates an essential role for AtKu80 protein in efficient repair of DNA double-strand breaks in vivo. *Plant J.* **31**, 517–528 (2002).
115. Riha, K., Watson, J. M., Parkey, J. & Shippen, D. E. Telomere length deregulation and enhanced sensitivity to genotoxic stress in Arabidopsis mutants deficient in Ku70. *EMBO J.* **21**, 2819–2826 (2002).
116. Bundock, P., van Attikum, H. & Hooykaas, P. Increased telomere length and hypersensitivity to DNA damaging agents in an Arabidopsis KU70 mutant. *Nucleic Acids Res.* **30**, 3395–3400 (2002).
117. Friesner, J. & Britt, A. B. Ku80- and DNA ligase IV-deficient plants are sensitive to ionizing radiation and defective in T-DNA integration. *Plant J.* **34**, 427–440 (2003).
118. Gallego, M. E., Bleuyard, J. Y., Daoudal-Cotterell, S., Jallut, N. & White, C. I. Ku80 plays a role in non-homologous recombination but is not required for T-DNA integration in Arabidopsis. *Plant J.* **35**, 557–565 (2003).
119. van Attikum, H. *et al.* The Arabidopsis AtLIG4 gene is required for the repair of DNA damage, but not for the integration of Agrobacterium T-DNA. *Nucleic Acids Res.* **31**, 4247–4255 (2003).
120. Roy, S., Choudhury, S. R., Singh, S. K. & Das, K. P. AtPolλ, a homolog of mammalian DNA polymerase λ in arabidopsis thaliana, is involved in the repair of UV-B induced DNA damage through the dark repair pathway. *Plant Cell Physiol.* **52**, 448–467 (2011).
121. Roy, S., Roy Choudhury, S., Sengupta, D. N. & Pada Das, K. Involvement of AtPolλ in the repair of high salt- and DNA cross-linking agent-induced double strand breaks in arabidopsis. *Plant Physiol.* **162**, 1195–1210 (2013).
122. Truong, L. N. *et al.* Microhomology-mediated End Joining and Homologous Recombination share the initial end resection step to repair DNA double-strand breaks in mammalian cells. *Proc. Natl. Acad. Sci. U. S. A.* **110**, 7720–7725 (2013).
123. Decottignies, A. Microhomology-mediated end joining in fission yeast is repressed by Pku70 and relies on genes involved in homologous recombination. *Genetics* **176**, 1403–1415 (2007).
124. Wang, M. *et al.* PARP-1 and Ku compete for repair of DNA double strand breaks by distinct NHEJ pathways. *Nucleic Acids Res.* **34**, 6170–6182 (2006).
125. Ray Chaudhuri, A. & Nussenzweig, A. The multifaceted roles of PARP1 in DNA repair and chromatin remodelling. *Nat. Rev. Mol. Cell Biol.* **18**, 610–621 (2017).
126. Deng, S. K., Gibb, B., De Almeida, M. J., Greene, E. C. & Symington, L. S. RPA antagonizes microhomology-mediated repair of DNA double-strand breaks. *Nat. Struct. Mol. Biol.* **21**, 405–412 (2014).
127. Mcvey, M. RPA puts the brakes on MMEJ. *Nat. Struct. Mol. Biol.* **21**, 348–349 (2014).
128. Ma, J.-L., Kim, E. M., Haber, J. E. & Lee, S. E. Yeast Mre11 and Rad1 Proteins Define a Ku-Independent Mechanism To Repair Double-Strand Breaks Lacking Overlapping End Sequences. *Mol. Cell. Biol.* **23**, 8820–8828 (2003).
129. Ahmad, A. *et al.* ERCC1-XPF Endonuclease Facilitates DNA Double-Strand Break Repair. *Mol. Cell. Biol.* **28**, 5082–5092 (2008).
130. Lee, K. & Sang, E. L. Saccharomyces cerevisiae Sae2- and Tel1-dependent single-strand DNA formation at DNA break promotes microhomology-mediated end joining. *Genetics* **176**, 2003–2014 (2007).
131. Kent, T., Chandramouly, G., Mcdevitt, S. M., Ozdemir, A. Y. & Pomerantz, R. T. Mechanism of microhomology-mediated end-joining promoted by human DNA polymerase θ. *Nat. Struct. Mol. Biol.* **22**, 230–237 (2015).
132. Gorbunova, V. & Levy, A. A. Non-homologous DNA end joining in plant cells is associated with deletions and filler DNA insertions. *Nucleic Acids Res.* **25**, 4650 (1997).
133. Salomon, S. & Puchta, H. Capture of genomic and T-DNA sequences during double-strand break repair in somatic plant cells. *EMBO J.* **17**, 6086–6095 (1998).
134. Wolter, F., Schindele, P., Beying, N., Scheben, A. & Puchta, H. Different DNA repair pathways are involved in single-strand break-induced genomic changes in plants. *Plant Cell* **33**, 3454–3469 (2021).
135. Seol, J. H., Shim, E. Y. & Lee, S. E. Microhomology-mediated end joining: Good, bad and ugly. *Mutat. Res. - Fundam. Mol. Mech. Mutagen.* **809**, 81–87 (2018).
136. Gallego, F., Fleck, O., Li, A., Wyrzykowska, J. & Tinland, B. AtRAD1, a plant homologue of human and

yeast nucleotide excision repair endonucleases, is involved in dark repair of UV damages and recombination. *Plant J.* **21**, 507–518 (2000).

137. Hefner, E., Preuss, S. B. & Britt, A. B. Arabidopsis mutants sensitive to gamma radiation include the homologue of the human repair gene ERCC1. *J. Exp. Bot.* **54**, 669–680 (2003).
138. Inagaki, S. *et al.* Arabidopsis TEBICHI, with helicase and DNA polymerase domains, is required for regulated cell division and differentiation in meristems. *Plant Cell* **18**, 879–892 (2006).
139. Dubest, S., Gallego, M. E. & White, C. I. Role of the AtRad1p endonuclease in homologous recombination in plants. *EMBO Rep.* **3**, 1049–1054 (2002).
140. Dubest, S., Gallego, M. E. & White, C. I. Roles of the AtErcc1 protein in recombination. *Plant J.* **39**, 334–342 (2004).
141. Gallego, M. E., Jalut, N. & White, C. I. Telomerase dependence of telomere lengthening in ku80 mutant arabidopsis. *Plant Cell* **15**, 782–789 (2003).
142. Heacock, M., Spangler, E., Riha, K., Puizina, J. & Shippen, D. E. Molecular analysis of telomere fusions in Arabidopsis: Multiple pathways for chromosome end-joining. *EMBO J.* **23**, 2304–2313 (2004).
143. Vannier, J. B., Depeiges, A., White, C. & Gallego, M. E. ERCC1/XPF protects short telomeres from homologous recombination in Arabidopsis thaliana. *PLoS Genet.* **5**, e1000380 (2009).
144. Van Kregten, M. *et al.* T-DNA integration in plants results from polymerase-θ-mediated DNA repair. *Nat. Plants* **2**, 1–6 (2016).
145. Nishizawa-Yokoi, A. *et al.* Agrobacterium T-DNA integration in somatic cells does not require the activity of DNA polymerase θ. *New Phytol.* **229**, 2859–2872 (2021).
146. Waterworth, W. M. *et al.* DNA ligase 1 deficient plants display severe growth defects and delayed repair of both DNA single and double strand breaks. *BMC Plant Biol.* **9**, (2009).
147. Charbonnel, C., Gallego, M. E. & White, C. I. Xrcc1-dependent and Ku-dependent DNA double-strand break repair kinetics in Arabidopsis plants. *Plant J.* **64**, 280–290 (2010).
148. Charbonnel, C., Allain, E., Gallego, M. E. & White, C. I. Kinetic analysis of DNA double-strand break repair pathways in Arabidopsis. *DNA Repair (Amst).* **10**, 611–619 (2011).
149. Bhargava, R., Onyango, D. O. & Stark, J. M. Regulation of Single-Strand Annealing and its Role in Genome Maintenance. *Trends Genet.* **32**, 566–575 (2016).
150. Yang, Y. G. *et al.* Conditional deletion of Nbs1 in murine cells reveals its role in branching repair pathways of DNA double-strand breaks. *EMBO J.* **25**, 5527–5538 (2006).
151. Muñoz, M. C. *et al.* Ring finger nuclear factor RNF168 is important for defects in homologous recombination caused by loss of the breast cancer susceptibility factor BRCA1. *J. Biol. Chem.* **287**, 40618–40628 (2012).
152. Sturzenegger, A. *et al.* DNA2 cooperates with the WRN and BLM RecQ helicases to mediate long-range DNA end resection in human cells. *J. Biol. Chem.* **289**, 27314–27326 (2014).
153. Ivanov, E. L., Sugawara, N., Fishman-Lobell, J. & Haber, J. E. Genetic requirements for the single-strand annealing pathway of double-strand break repair in Saccharomyces cerevisiae. *Genetics* **142**, 693–704 (1996).
154. Mimitou, E. P. & Symington, L. S. Sae2, Exo1 and Sgs1 collaborate in DNA double-strand break processing. *Nature* **455**, 770–774 (2008).
155. Escribano-Díaz, C. *et al.* A Cell Cycle-Dependent Regulatory Circuit Composed of 53BP1-RIF1 and BRCA1-CtIP Controls DNA Repair Pathway Choice. *Mol. Cell* **49**, 872–883 (2013).
156. Ochs, F. *et al.* 53BP1 fosters fidelity of homology-directed DNA repair. *Nat. Struct. Mol. Biol.* **23**, 714–721 (2016).
157. Lazzaro, F. *et al.* Histone methyltransferase Dot1 and Rad9 inhibit single-stranded DNA accumulation at DSBs and uncapped telomeres. *EMBO J.* **27**, 1502–1512 (2008).
158. Ferrari, M. *et al.* Functional Interplay between the 53BP1-Ortholog Rad9 and the Mre11 Complex Regulates Resection, End-Tethering and Repair of a Double-Strand Break. *PLoS Genet.* **11**, e1004928 (2015).
159. Sugawara, N., Pâques, F., Colaiácovo, M. & Haber, J. E. Role of Saccharomyces cerevisiae Msh2 and Msh3 repair proteins in double-strand break-induced recombination. *Proc. Natl. Acad. Sci. U. S. A.* **94**, 9214–9219 (1997).
160. Van Dyck, E., Stasiak, A. Z., Stasiak, A. & West, S. C. Visualization of recombination intermediates produced by RAD52-mediated single-strand annealing. *EMBO Rep.* **2**, 905–909 (2001).
161. Motycka, T. A., Bessho, T., Post, S. M., Sung, P. & Tomkinson, A. E. Physical and Functional Interaction between the XPF/ERCC1 Endonuclease and hRad52. *J. Biol. Chem.* **279**, 13634–13639 (2004).
162. Bennardo, N., Cheng, A., Huang, N. & Stark, J. M. Alternative-NHEJ is a mechanistically distinct pathway of mammalian chromosome break repair. *PLoS Genet.* **4**, e1000110 (2008).
163. Sugawara, N., Goldfarb, T., Studamire, B., Alani, E. & Haber, J. E. Heteroduplex rejection during single-strand annealing requires Sgs1 helicase and mismatch repair proteins Msh2 and Msh6 but not Pms1. *Proc. Natl. Acad. Sci. U. S. A.* **101**, 9315–9320 (2004).
164. Chakraborty, U., George, C. M., Lyndaker, A. M. & Alani, E. A delicate balance between repair and

replication factors regulates recombination between divergent DNA sequences in Saccharomyces cerevisiae. *Genetics* **202**, 525–540 (2016).

165. Dronkert, M. L. G. *et al.* Mouse RAD54 Affects DNA Double-Strand Break Repair and Sister Chromatid Exchange . *Mol. Cell. Biol.* **20**, 3147–3156 (2000).
166. Tutt, A. *et al.* Mutation in Brca2 stimulates error-prone homology-directed repair of DNA double-strand breaks occurring between repeated sequences. *EMBO J.* **20**, 4704–4716 (2001).
167. Orel, N., Kyryk, A. & Puchta, H. Different pathways of homologous recombination are used for the repair of double-strand breaks within tandemly arranged sequences in the plant genome. *Plant J.* **35**, 604–612 (2003).
168. Roth, N. *et al.* The requirement for recombination factors differs considerably between different pathways of homologous double-strand break repair in somatic plant cells. *Plant J.* **72**, 781–790 (2012).
169. Samach, A., Gurevich, V., Avivi-Ragolsky, N. & Levy, A. A. The effects of AtRad52 over-expression on homologous recombination in Arabidopsis. *Plant J.* **95**, 30–40 (2018).
170. Lafleuriel, J., Degroote, F., Depeiges, A. & Picard, G. Impact of the loss of AtMSH2 on double-strand break-induced recombination between highly diverged homeologous sequences in Arabidopsis thaliana germinal tissues. *Plant Mol. Biol.* **63**, 833–846 (2007).
171. Mannuss, A. *et al.* RAD5A, RECQ4A, AND MUS81 have specific functions in homologous recombination and define different pathways of dna repair in Arabidopsis thaliana. *Plant Cell* **22**, 3318–3330 (2010).
172. Onaka, A. T. *et al.* DNA replication machinery prevents Rad52-dependent single-strand annealing that leads to gross chromosomal rearrangements at centromeres. *Commun. Biol.* **3**, 2–13 (2020).
173. Serra, H., Da Ines, O., Degroote, F., Gallego, M. E. & White, C. I. Roles of XRCC2, RAD51B and RAD51D in RAD51-Independent SSA Recombination. *PLoS Genet.* **9**, e1003971 (2013).
174. Aboussekhra, A., Chanet, R., Adjiri, A. & Fabre, F. Semidominant suppressors of Srs2 helicase mutations of Saccharomyces cerevisiae map in the RAD51 gene, whose sequence predicts a protein with similarities to procaryotic RecA proteins. *Mol. Cell. Biol.* **12**, 3224–3234 (1992).
175. Shinohara, A. *et al.* Cloning of human, mouse and fission yeast recombination genes homologous to RAD51 and recA. *Nat. Genet.* **4**, 239–243 (1993).
176. Sugiyama, T. & Kowalczykowski, S. C. Rad52 Protein Associates with Replication Protein A (RPA)-Single-stranded DNA to Accelerate Rad51-mediated Displacement of RPA and Presynaptic Complex Formation. *J. Biol. Chem.* **277**, 31663–31672 (2002).
177. Liu, J., Doty, T., Gibson, B. & Heyer, W. D. Human BRCA2 protein promotes RAD51 filament formation on RPA-covered single-stranded DNA. *Nat. Struct. Mol. Biol.* **17**, 1260–1262 (2010).
178. Lovett, S. T. Sequence of the RAD55 gene of Saccharomyces cerevisiae: similarity of RAD55 to prokaryotic RecA and other RecA-like proteins. *Gene* **142**, 103–106 (1994).
179. Shor, E., Weinstein, J. & Rothstein, R. A genetic screen for top3 suppressors in Saccharomyces cerevisiae identifies SHU1, SHU2, PSY3 and CSM2: Four genes involved in error-free DNA repair. *Genetics* **169**, 1275–1289 (2005).
180. Zhang, S. *et al.* Structural basis for the functional role of the Shu complex in homologous recombination. *Nucleic Acids Res.* **45**, 13068–13079 (2017).
181. Tebbs, R. S. *et al.* Correction of chromosomal instability and sensitivity to diverse mutagens by a cloned cDNA of the XRCC3 DNA repair gene. *Proc. Natl. Acad. Sci. U. S. A.* **92**, 6354–6358 (1995).
182. Albala, J. S. *et al.* Identification of a novel human RAD51 homolog, RAD51B. *Genomics* **46**, 476–479 (1997).
183. Dosanjh, M. K. *et al.* Isolation and characterization of RAD51C, a new human member of the RAD51 family of related genes. *Nucleic Acids Res.* **26**, 1179–1184 (1998).
184. Pittman, D. L., Weinberg, L. R. & Schimenti, J. C. Identification, characterization, and genetic mapping of Rad51d, a new mouse and human RAD51/RecA-related gene. *Genomics* **49**, 103–111 (1998).
185. Cartwright, R., Tambini, C. E., Simpson, P. J. & Thacker, J. The XRCC2 DNA repair gene from human and mouse encodes a novel member of the recA/RAD51 family. *Nucleic Acids Res.* **26**, 3084–3089 (1998).
186. Liu, T., Wan, L., Wu, Y., Chen, J. & Huang, J. hSWS1 • SWSAP1 is an evolutionarily conserved complex required for efficient homologous recombination repair. *J. Biol. Chem.* **286**, 41758–41766 (2011).
187. Sung, P. Yeast Rad55 and Rad57 proteins form a heterodimer that functions with replication protein A to promote DNA strand exchange by Rad51 recombinase. *Genes Dev.* **11**, 1111–1121 (1997).
188. Sasanuma, H. *et al.* A new protein complex promoting the assembly of Rad51 filaments. *Nat. Commun.* **4**, 1–13 (2013).
189. Roy, U. *et al.* The Rad51 paralog complex Rad55-Rad57 acts as a molecular chaperone during homologous recombination. *Mol. Cell* **81**, 1043-1057.e8 (2021).
190. Masson, J. Y. *et al.* Identification and purification of two distinct complexes containing the five RAD51 paralogs. *Genes Dev.* **15**, 3296–3307 (2001).
191. Garcin, E. B. *et al.* Differential requirements for the RAD51 paralogs in genome repair and maintenance in human cells. *PLoS Genet.* **15**, e1008355 (2019).

192. Mazin, A. V., Alexeev, A. A. & Kowalczykowski, S. C. A novel function of Rad54 protein: Stabilization of the Rad51 nucleoprotein filament. *J. Biol. Chem.* **278**, 14029–14036 (2003).
193. Qi, Z. *et al.* DNA sequence alignment by microhomology sampling during homologous recombination. *Cell* **160**, 856–869 (2015).
194. Xu, J. *et al.* Cryo-EM structures of human RAD51 recombinase filaments during catalysis of DNA-strand exchange. *Nat. Struct. Mol. Biol.* **24**, 40–46 (2017).
195. Greene, E. C. DNA Sequence Alignment during Homologous Recombination. *J. Biol. Chem.* **291**, 11572–11580 (2016).
196. Yang, H., Zhou, C., Dhar, A. & Pavletich, N. P. Mechanism of strand exchange from RecA–DNA synaptic and D-loop structures. *Nature* **586**, 801–806 (2020).
197. Lee, A. J., Endo, M., Hobbs, J. K., Davies, A. G. & Wälti, C. Micro-homology intermediates: RecA's transient sampling revealed at the single molecule level. *Nucleic Acids Res.* **49**, 1426–1435 (2021).
198. Tavares, E. M., Wright, W. D., Heyer, W.-D. D., Le Cam, E. & Dupaigne, P. In vitro role of Rad54 in Rad51-ssDNA filament-dependent homology search and synaptic complexes formation. *Nat. Commun. 2019 101* **10**, 1–12 (2019).
199. Chi, P., San Filippo, J., Sehorn, M. G., Petukhova, G. V. & Sung, P. Bipartite stimulatory action of the Hop2-Mnd1 complex on the Rad51 recombinase. *Genes Dev.* **21**, 1747–1757 (2007).
200. Wiese, C. *et al.* Promotion of Homologous Recombination and Genomic Stability by RAD51AP1 via RAD51 Recombinase Enhancement. *Mol. Cell* **28**, 482–490 (2007).
201. Dray, E. *et al.* Enhancement of RAD51 recombinase activity by the tumor suppressor PALB2. *Nat. Struct. Mol. Biol.* **17**, 1255–1259 (2010).
202. Zhao, W. *et al.* BRCA1-BARD1 promotes RAD51-mediated homologous DNA pairing. *Nature* **550**, 360–365 (2017).
203. Wright, W. D. & Heyer, W. D. Rad54 Functions as a Heteroduplex DNA Pump Modulated by Its DNA Substrates and Rad51 during D Loop Formation. *Mol. Cell* **53**, 420–432 (2014).
204. Liu, J. *et al.* Srs2 promotes synthesis-dependent strand annealing by disrupting DNA polymerase d-extending D-loops. *Elife* **6**, (2017).
205. Kohzaki, M. *et al.* Cooperative Roles of Vertebrate Fbh1 and Blm DNA Helicases in Avoidance of Crossovers during Recombination Initiated by Replication Fork Collapse. *Mol. Cell. Biol.* **27**, 2812–2820 (2007).
206. Prakash, R. *et al.* Yeast Mphl helicase dissociates Rad51-made D-loops: Implications for crossover control in mitotic recombination. *Genes Dev.* **23**, 67–79 (2009).
207. Gari, K., Décaillet, C., Delannoy, M., Wu, L. & Constantinou, A. Remodeling of DNA replication structures by the branch point translocase FANCM. *Proc. Natl. Acad. Sci. U. S. A.* **105**, 16107–16112 (2008).
208. Fasching, C. L., Cejka, P., Kowalczykowski, S. C. & Heyer, W. D. Top3-Rmi1 dissolve Rad51-mediated D loops by a topoisomerase-based mechanism. *Mol. Cell* **57**, 595–606 (2015).
209. Solinger, J. A., Kiianitsa, K. & Heyer, W. D. Rad54, a Swi2/Snf2-like recombinational repair protein, disassembles Rad51:dsDNA filaments. *Mol. Cell* **10**, 1175–1188 (2002).
210. Veaute, X. *et al.* The Srs2 helicase prevents recombination by disrupting Rad51 nucleoprotein filaments. *Nature* **423**, 309–312 (2003).
211. Simandlova, J. *et al.* FBH1 helicase disrupts RAD51 filaments in vitro and modulates homologous recombination in mammalian cells. *J. Biol. Chem.* **288**, 34168–34180 (2013).
212. Corrette-Bennett, S. E., Borgeson, C., Sommer, D., Burgers, P. M. J. & Lahue, R. S. DNA polymerase δ, RFC and PCNA are required for repair synthesis of large looped heteroduplexes in Saccharomyces cerevisiae. *Nucleic Acids Res.* **32**, 6268–6275 (2004).
213. Sebesta, M. *et al.* Role of PCNA and TLS polymerases in D-loop extension during homologous recombination in humans. *DNA Repair (Amst).* **12**, 691–698 (2013).
214. Nimonkar, A. V., Sica, R. A. & Kowalczykowski, S. C. Rad52 promotes second-end DNA capture in double-stranded break repair to form complement-stabilized joint molecules. *Proc. Natl. Acad. Sci. U. S. A.* **106**, 3077–3082 (2009).
215. Szostak, J. W., Orr-Weaver, T. L., Rothstein, R. J. & Stahl, F. W. The double-strand-break repair model for recombination. *Cell* **33**, 25–35 (1983).
216. Schwacha, A. & Kleckner, N. Identification of joint molecules that form frequently between homologs but rarely between sister chromatids during yeast meiosis. *Cell* **76**, 51–63 (1994).
217. Schwacha, A. & Kleckner, N. Identification of double holliday junctions as intermediates in meiotic recombination. *Cell* **83**, 783–791 (1995).
218. Schwacha, A. & Kleckner, N. Interhomolog bias during meiotic recombination: Meiotic functions promote a highly differentiated interhomolog-only pathway. *Cell* **90**, 1123–1135 (1997).
219. Schwartz, E. K. & Heyer, W. D. Processing of joint molecule intermediates by structure-selective endonucleases during homologous recombination in eukaryotes. *Chromosoma* **120**, 109–127 (2011).

220. Machín, F. Implications of metastable nicks and nicked holliday junctions in processing joint molecules in mitosis and meiosis. *Genes (Basel).* **11**, 1–31 (2020).
221. Raynard, S., Bussen, W. & Sung, P. A double holliday junction dissolvasome comprising BLM, topoisomerase IIIα, and BLAP75. *J. Biol. Chem.* **281**, 13861–13864 (2006).
222. Singh, T. R. *et al.* BLAP18/RMI2, a novel OB-fold-containing protein, is an essential component of the Bloom helicase-double Holliday junction dissolvasome. *Genes Dev.* **22**, 2856–2868 (2008).
223. Cejka, P., Plank, J. L., Bachrati, C. Z., Hickson, I. D. & Kowalczykowski, S. C. Rmi1 stimulates decatenation of double Holliday junctions during dissolution by Sgs1-Top3. *Nat. Struct. Mol. Biol.* **17**, 1377–1382 (2010).
224. Kaliraman, V., Mullen, J. R., Fricke, W. M., Bastin-Shanower, S. A. & Brill, S. J. Functional overlap between Sgs1-Top3 and the Mms4-Mus81 endonuclease. *Genes Dev.* **15**, 2730–2740 (2001).
225. Boddy, M. N. *et al.* Mus81-Eme1 are essential components of a Holliday junction resolvase. *Cell* **107**, 537–548 (2001).
226. Fricke, W. M. & Brill, S. J. Slx1 - Slx4 is a second structure-specific endonuclease functionally redundant with Sgs1 - Top3. *Genes Dev.* **17**, 1768–1778 (2003).
227. Ip, S. C. Y. *et al.* Identification of Holliday junction resolvases from humans and yeast. *Nature* **456**, 357–361 (2008).
228. Svendsen, J. M. *et al.* Mammalian BTBD12/SLX4 Assembles A Holliday Junction Resolvase and Is Required for DNA Repair. *Cell* **138**, 63–77 (2009).
229. Doutriaux, M. P., Couteau, F., Bergounioux, C. & White, C. Isolation and characterisation of the RAD51 and DMC1 homologs from Arabidopsis thaliana. *Mol. Gen. Genet.* **257**, 283–291 (1998).
230. Li, W. *et al.* The Arabidopsis AtRAD51 gene is dispensable for vegetative development but required for meiosis. *Proc. Natl. Acad. Sci. U. S. A.* **101**, 10596–10601 (2004).
231. Wang, S., Durrant, W. E., Song, J., Spivey, N. W. & Dong, X. Arabidopsis BRCA2 and RAD51 proteins are specifically involved in defense gene transcription during plant immune responses. *Proc. Natl. Acad. Sci. U. S. A.* **107**, 22716–22721 (2010).
232. Doutriaux, M. P., Couteau, F., Bergounioux, C. & White, C. Isolation and characterisation of the RAD51 and DMC1 homologs from Arabidopsis thaliana. *Mol. Gen. Genet.* **257**, 283–291 (1998).
233. Da Ines, O. *et al.* Effects of XRCC2 and RAD51B mutations on somatic and meiotic recombination in Arabidopsis thaliana. *Plant J.* **74**, 959–970 (2013).
234. Da Ines, O. *et al.* Meiotic Recombination in Arabidopsis Is Catalysed by DMC1, with RAD51 Playing a Supporting Role. *PLoS Genet.* **9**, e1003787 (2013).
235. Bleuyard, J. Y. & White, C. I. The Arabidopsis homologue of Xrcc3 plays an essential role in meiosis. *EMBO J.* **23**, 439–449 (2004).
236. Bleuyard, J. Y., Gallego, M. E., Savigny, F. & White, C. I. Differing requirements for the Arabidopsis Rad51 paralogs in meiosis and DNA repair. *Plant J.* **41**, 533–545 (2005).
237. Osakabe, K. *et al.* Isolation and characterization of the RAD54 gene from Arabidopsis thaliana. *Plant J.* **48**, 827–842 (2006).
238. Seeliger, K., Dukowic-Schulze, S., Wurz-Wildersinn, R., Pacher, M. & Puchta, H. BRCA2 is a mediator of RAD51- and DMC1-facilitated homologous recombination in Arabidopsis thaliana. *New Phytol.* **193**, 364–375 (2012).
239. Wang, Y. *et al.* The Arabidopsis RAD51 paralogs RAD51B, RAD51D and XRCC2 play partially redundant roles in somatic DNA repair and gene regulation. *New Phytol.* **201**, 292–304 (2014).
240. Séguéla-Arnaud, M. *et al.* Multiple mechanisms limit meiotic crossovers: TOP3α and two BLM homologs antagonize crossovers in parallel to FANCM. *Proc. Natl. Acad. Sci. U. S. A.* **112**, 4713–4718 (2015).
241. Hartung, F., Suer, S., Knoll, A., Wurz-Wildersinn, R. & Puchta, H. Topoisomerase 3α and RMI1 suppress somatic crossovers and are essential for resolution of meiotic recombination intermediates in Arabidopsis thaliana. *PLoS Genet.* **4**, e1000285 (2008).
242. Chaganti, R. S. K., Schonberg, S. & German, J. A manyfold increase in sister chromatid exchanges in Bloom's syndrome lymphocytes. *Proc. Natl. Acad. Sci. U. S. A.* **71**, 4508–4512 (1974).
243. Onoda, F., Seki, M., Miyajima, A. & Enomoto, T. Elevation of sister chromatid exchange in Saccharomyces cerevisiae sgs1 disruptants and the relevance of the disruptants as a system to evaluate mutations in Bloom's syndrome gene. *Mutat. Res. - DNA Repair* **459**, 203–209 (2000).
244. Blanck, S. *et al.* A SRS2 homolog from Arabidopsis thaliana disrupts recombinogenic DNA intermediates and facilitates single strand annealing. *Nucleic Acids Res.* **37**, 7163–7176 (2009).
245. Knoll, A. *et al.* The fanconi anemia ortholog FANCM ensures ordered homologous recombination in both somatic and meiotic Cells in Arabidopsis. *Plant Cell* **24**, 1448–1464 (2012).
246. Roth, N. *et al.* The requirement for recombination factors differs considerably between different pathways of homologous double-strand break repair in somatic plant cells. *Plant J.* **72**, 781–790 (2012).
247. Rocha, C. R. R., Silva, M. M., Quinet, A., Cabral-Neto, J. B. & Menck, C. F. M. DNA repair pathways and

cisplatin resistance: An intimate relationship. *Clinics* **73**, (2018).
248. Chen, J., Ghorai, M. K., Kenney, G. & Stubbe, J. A. Mechanistic studies on bleomycin-mediated DNA damage: Multiple binding modes can result in double-stranded DNA cleavage. *Nucleic Acids Res.* **36**, 3781–3790 (2008).
249. Hartung, F., Suer, S., Bergmann, T. & Puchta, H. The role of AtMUS81 in DNA repair and its genetic interaction with the helicase AtRecQ4A. *Nucleic Acids Res.* **34**, 4438–4448 (2006).
250. Bauknecht, M. & Kobbe, D. AtGEN1 and AtSEND1, two paralogs in Arabidopsis, possess holliday junction resolvase activity. *Plant Physiol.* **166**, 202–16 (2014).
251. Olivier, M. *et al.* The structure-specific endonucleases MUS81 and SEND1 are essential for telomere stability in arabidopsis. *Plant Cell* **28**, 74–86 (2016).
252. Geuting, V. *et al.* Two Distinct MUS81-EME1 Complexes from Arabidopsis Process Holliday Junctions. *Plant Physiol.* **150**, 1062–1071 (2009).
253. Fabre, F., Chan, A., Heyer, W. D. & Gangloff, S. Alternate pathways involving Sgs1/Top3, Mus81/ Mms4, and Srs2 prevent formation of toxic recombination intermediates from single-stranded gaps created by DNA replication. *Proc. Natl. Acad. Sci. U. S. A.* **99**, 16887–16892 (2002).
254. Johnson-Schlitz, D. & Engels, W. R. Template disruptions and failure of double Holliday junction dissolution during double-strand break repair in Drosophila BLM mutants. *Proc. Natl. Acad. Sci. U. S. A.* **103**, 16840–16845 (2006).
255. Anand, R. P., Lovett, S. T. & Haber, J. E. Break-induced DNA replication. *Cold Spring Harb. Perspect. Biol.* **5**, (2013).
256. Wu, X. & Malkova, A. Break-induced replication mechanisms in yeast and mammals. *Curr. Opin. Genet. Dev.* **71**, 163–170 (2021).
257. Lydeard, J. R., Jain, S., Yamaguchi, M. & Haber, J. E. Break-induced replication and telomerase-independent telomere maintenance require Pol32. *Nature* **448**, 820–823 (2007).
258. Lydeard, J. R. *et al.* Break-induced replication requires all essential DNA replication factors except those specific for pre-RC assembly. *Genes Dev.* **24**, 1133–1144 (2010).
259. Wilson, M. A. *et al.* Pif1 helicase and Polδ promote recombination-coupled DNA synthesis via bubble migration. *Nature* **502**, 393–396 (2013).
260. Li, S. *et al.* PIF1 helicase promotes break-induced replication in mammalian cells. *EMBO J.* **40**, (2021).
261. Saini, N. *et al.* Migrating bubble during break-induced replication drives conservative DNA synthesis. *Nature* **502**, 389–392 (2013).
262. Olivier, M., Charbonnel, C., Amiard, S., White, C. I. & Gallego, M. E. RAD51 and RTEL1 compensate telomere loss in the absence of telomerase. *Nucleic Acids Res.* **46**, 2432–2445 (2018).
263. Fogg, P. C. M., Colloms, S., Rosser, S., Stark, M. & Smith, M. C. M. New applications for phage integrases. *J. Mol. Biol.* **426**, 2703–2716 (2014).
264. Khan, F. A. & Ali, S. O. Physiological Roles of DNA Double-Strand Breaks. *J. Nucleic Acids* **2017**, (2017).
265. Speijer, D., Lukeš, J. & Eliáš, M. Sex is a ubiquitous, ancient, and inherent attribute of eukaryotic life. *Proc. Natl. Acad. Sci. U. S. A.* **112**, 8827–8834 (2015).
266. Fu, C., Coelho, M. A., David-Palma, M., Priest, S. J. & Heitman, J. Genetic and genomic evolution of sexual reproduction: echoes from LECA to the fungal kingdom. *Curr. Opin. Genet. Dev.* **58–59**, 70–75 (2019).
267. Ross, K. J., Fransz, P. & Jones, G. H. A light microscopic atlas of meiosis in Arabidopsis thaliana. *Chromosom. Res.* **4**, 507–516 (1996).
268. Ross, K. J. *et al.* Cytological characterization of four meiotic mutants of Arabidopsis isolated from T-DNA-transformed lines. *Chromosom. Res.* **5**, 551–559 (1997).
269. Nakajima, K. Be my baby: patterning toward plant germ cells. *Curr. Opin. Plant Biol.* **41**, 110–115 (2018).
270. Oliver, C. *et al.* Loss of function of Arabidopsis microRNA-machinery genes impairs fertility, and has effects on homologous recombination and meiotic chromatin dynamics. *Sci. Rep.* **7**, 1–14 (2017).
271. Cai, X., Dong, F., Edelmann, R. E. & Makaroff, C. A. The Arabidopsis SYN1 cohesin protein is required for sister chromatid arm cohesion and homologous chromosome pairing. *J. Cell Sci.* **116**, 2999–3007 (2003).
272. Hurel, A. *et al.* A cytological approach to studying meiotic recombination and chromosome dynamics in Arabidopsis thaliana male meiocytes in three dimensions. *Plant J.* **95**, 385–396 (2018).
273. Fernández-Jiménez, N. & Pradillo, M. The role of the nuclear envelope in the regulation of chromatin dynamics during cell division. *J. Exp. Bot.* **71**, 5148–5159 (2020).
274. Armstrong, S. J., Caryl, A. P., Jones, G. H. & Franklin, F. C. H. Asy1, a protein required for meiotic chromosome synapsis, localizes to axis-associated chromatin in Arabidopsis and Brassica. *J. Cell Sci.* **115**, 3645–3655 (2002).
275. Ferdous, M. *et al.* Inter-Homolog Crossing-Over and Synapsis in Arabidopsis Meiosis Are Dependent on the Chromosome Axis Protein AtASY3. *PLOS Genet.* **8**, e1002507 (2012).
276. Chambon, A. *et al.* Identification of ASYNAPTIC4, a Component of the Meiotic Chromosome Axis. *Plant*

Physiol. **178**, 233 (2018).
277. López, E., Pradillo, M., Romero, C., Santos, J. L. & Cuñado, N. Pairing and synapsis in wild type Arabidopsis thaliana. *Chromosom. Res.* **16**, 701–708 (2008).
278. Panoli, A. P. *et al.* AtMNDI is required for homologous pairing during meiosis in Arabidopsis. *BMC Mol. Biol.* **7**, 1–12 (2006).
279. Higgins, J. D., Sanchez-Moran, E., Armstrong, S. J., Jones, G. H. & Franklin, F. C. H. The Arabidopsis synaptonemal complex protein ZYP1 is required for chromosome synapsis and normal fidelity of crossing over. *Genes Dev.* **19**, 2488–2500 (2005).
280. France, M. G. *et al.* ZYP1 is required for obligate cross-over formation and cross-over interference in Arabidopsis. *Proc. Natl. Acad. Sci. U. S. A.* **118**, 1539–47 (2021).
281. Capilla-Pérez, L. *et al.* The synaptonemal complex imposes crossover interference and heterochiasmy in Arabidopsis. *Proc. Natl. Acad. Sci. U. S. A.* **118**, 1539–47 (2021).
282. Vrielynck, N. *et al.* Conservation and divergence of meiotic DNA double strand break forming mechanisms in Arabidopsis thaliana . *Nucleic Acids Res.* **49**, 9821–9835 (2021).
283. Kurzbauer, M. T., Uanschou, C., Chen, D. & Schlögelhofer, P. The recombinases DMC1 and RAD51 are functionally and spatially separated during meiosis in Arabidopsis. *Plant Cell* **24**, 2058–2070 (2012).
284. Fernandes, J. B. *et al.* FIGL1 and its novel partner FLIP form a conserved complex that regulates homologous recombination. *PLoS Genet.* **14**, e1007317 (2018).
285. Jackson, N. *et al.* Reduced meiotic crossovers and delayed prophase I progression in AtMLH3-deficient Arabidopsis. *EMBO J.* **25**, 1315–1323 (2006).
286. McKee, B. D., Yan, R. & Tsai, J.-H. Meiosis in male Drosophila. *Spermatogenesis* **2**, 167 (2012).
287. Nokkala, S. & Grozeva, S. Achiasmatic male meiosis in Myrmedobia coleoptrata(Fn.) (Heteroptera, Microphysidae). *Firenze Univ. Press* **53**, 5–8 (2012).
288. Cabral, G., Marques, A., Schubert, V., Pedrosa-Harand, A. & Schlögelhofer, P. Chiasmatic and achiasmatic inverted meiosis of plants with holocentric chromosomes. *Nat. Commun. 2014 51* **5**, 1–11 (2014).
289. Prusicki, M. A. *et al.* Live cell imaging of meiosis in Arabidopsis thaliana. *Elife* **8**, (2019).
290. Xu, R. Y. *et al.* The Arabidopsis anaphase-promoting complex/cyclosome subunit 8 is required for male meiosis. *New Phytol.* **224**, 229–241 (2019).
291. Xue, Z. *et al.* OsMTOPVIB is required for meiotic bipolar spindle assembly. *Proc. Natl. Acad. Sci. U. S. A.* **116**, 15967–15972 (2019).
292. Fransz, P. *et al.* Cytogenetics for the model system Arabidopsis thaliana. *Plant J.* **13**, 867–876 (1998).
293. Moran, E. S., Armstrong, S. J., Santos, J. L., Franklin, F. C. H. & Jones, G. H. Chiasma formation in Arabidopsis thaliana accession Wassileskija and in two meiotic mutants. *Chromosom. Res.* **9**, 121–128 (2001).
294. Liu, Z. & Makaroff, C. A. Arabidopsis separase AESP is essential for embryo development and the release of cohesin during meiosis. *Plant Cell* **18**, 1213–1225 (2006).
295. Cromer, L. *et al.* Patronus is the elusive plant securin, preventing chromosome separation by antagonizing separase. *Proc. Natl. Acad. Sci. U. S. A.* **116**, 16018–16027 (2019).
296. Zamariola, L. *et al.* SHUGOSHINs and PATRONUS protect meiotic centromere cohesion in Arabidopsis thaliana. *Plant J.* **77**, 782–794 (2014).
297. Yuan, G. *et al.* PROTEIN PHOSHATASE 2A B'α and β maintain centromeric sister chromatid cohesion during meiosis in Arabidopsis. *Plant Physiol.* **178**, 317–328 (2018).
298. Zamariola, L., Tiang, C. L., De Storme, N., Pawlowski, W. & Geelen, D. Chromosome segregation in plant meiosis. *Front. Plant Sci.* **5**, 279 (2014).
299. De Storme, N. & Geelen, D. Cytokinesis in plant male meiosis. *Plant Signal. Behav.* **8**, (2013).
300. Wilson, Z. A. & Zhang, D. B. From arabidopsis to rice: Pathways in pollen development. *J. Exp. Bot.* **60**, 1479–1492 (2009).
301. Keeney, S. Spo11 and the formation of DNA double-strand breaks in meiosis. *Genome Dyn. Stab.* **2**, 81–123 (2008).
302. Jing, J. L., Zhang, T., Wang, Y. Z. & He, Y. Advances towards how meiotic recombination is initiated: A comparative view and perspectives for plant meiosis research. *Int. J. Mol. Sci.* **20**, (2019).
303. Vrielynck, N. *et al.* A DNA topoisomerase VI-like complex initiates meiotic recombination. *Science (80-.).* **351**, 939–943 (2016).
304. Robert, T. *et al.* The Topo VIB-Like protein family is required for meiotic DNA double-strand break formation. *Science (80-.).* **351**, 943–949 (2016).
305. Hartung, F. & Puchta, H. Molecular characterisation of two paralogous SPO11 homologues in Arabidopsis thaliana. *Nucleic Acids Res.* **28**, 1548–1554 (2000).
306. Hartung, F. & Puchta, H. Molecular characterization of homologues of both subunits A (SPO11) and B of the archaebacterial topoisomerase 6 in plants. *Gene* **271**, 81–86 (2001).
307. Grelon, M., Vezon, D., Gendrot, G. & Pelletier, G. AtSPO11-1 is necessary for efficient meiotic recombination

in plants. *EMBO J.* **20**, 589–600 (2001).
308. Stacey, N. J. *et al.* Arabidopsis SPO11-2 functions with SPO11-1 in meiotic recombination. *Plant J.* **48**, 206–216 (2006).
309. Hartung, F. *et al.* The catalytically active tyrosine residues of both SPO11-1 and SPO11-2 are required for meiotic double-strand break induction in Arabidopsis. *Plant Cell* **19**, 3090–3099 (2007).
310. Yadav, V. K. & Claeys Bouuaert, C. Mechanism and Control of Meiotic DNA Double-Strand Break Formation in S. cerevisiae. *Front. Cell Dev. Biol.* **9**, 1–20 (2021).
311. Arora, C., Kee, K., Maleki, S. & Keeney, S. Antiviral protein Ski8 is a direct partner of Spo11 in meiotic DNA break formation, independent of its cytoplasmic role in RNA metabolism. *Mol. Cell* **13**, 549–559 (2004).
312. Kee, K., Protacio, R. U., Arora, C. & Keeney, S. Spatial organization and dynamics of the association of Rec102 and Rec104 with meiotic chromosomes. *EMBO J.* **23**, 1815–1824 (2004).
313. Claeys Bouuaert, C. *et al.* Structural and functional characterization of the Spo11 core complex. *Nat. Struct. Mol. Biol. 2021 281* **28**, 92–102 (2021).
314. GM, C. & AM, V. C. elegans mre-11 is required for meiotic recombination and DNA repair but is dispensable for the meiotic G(2) DNA damage checkpoint. *Genes Dev.* **15**, 522–534 (2001).
315. Keeney, S. Mechanism and control of meiotic recombination initiation. *Curr. Top. Dev. Biol.* **52**, 1–53 (2001).
316. Borde, V. *et al.* Association of Mre11p with Double-Strand Break Sites during Yeast Meiosis. *Mol. Cell* **13**, 389–401 (2004).
317. Claeys Bouuaert, C. *et al.* DNA-driven condensation assembles the meiotic DNA break machinery. *Nature* **592**, 144–149 (2021).
318. Li, J., Hooker, G. W. & Roeder, G. S. Saccharomyces cerevisiae Mer2, Mei4 and Rec114 form a complex required for meiotic double-strand break formation. *Genetics* **173**, 1969–1981 (2006).
319. Claeys Bouuaert, C. *et al.* DNA-driven condensation assembles the meiotic DNA break machinery. *Nature* **592**, 144–149 (2021).
320. Romanienko, P. J. & Camerini-Otero, R. D. The mouse Spo11 gene is required for meiotic chromosome synapsis. *Mol. Cell* **6**, 975–987 (2000).
321. Kumar, R. *et al.* Mouse REC114 is essential for meiotic DNA double-strand break formation and forms a complex with MEI4. *Life Sci. Alliance* **1**, (2018).
322. Kumar, R., Bourbon, H. M. & De Massy, B. Functional conservation of Mei4 for meiotic DNA double-strand break formation from yeasts to mice. *Genes Dev.* **24**, 1266–1280 (2010).
323. Stanzione, M. *et al.* Meiotic DNA break formation requires the unsynapsed chromosome axis-binding protein IHO1 (CCDC36) in mice. *Nat. Cell Biol.* **18**, 1208–1220 (2016).
324. Libby, B. J., Reinholdt, L. G. & Schimenti, J. C. Positional cloning and characterization of Mei1, a vertebrate-specific gene required for normal meiotic chromosome synapsis in mice. *Proc. Natl. Acad. Sci. U. S. A.* **100**, 15706–15711 (2003).
325. Kumar, R. *et al.* MEI4 - a central player in the regulation of meiotic DNA double-strand break formation in the mouse. *J. Cell Sci.* **128**, 1800–1811 (2015).
326. Kumar, R. & de Massy, B. Initiation of meiotic recombination in mammals. *Genes (Basel).* **1**, 521–549 (2010).
327. De Muyt, A. *et al.* AtPRD1 is required for meiotic double strand break formation in Arabidopsis thaliana. *EMBO J.* **26**, 4126–4137 (2007).
328. De Muyt, A. *et al.* A high throughput genetic screen identifies new early meiotic recombination functions in Arabidopsis thaliana. *PLoS Genet.* **5**, e1000654 (2009).
329. Zhang, C. *et al.* The Arabidopsis thaliana DSB formation (AtDFO) gene is required for meiotic double-strand break formation. *Plant J.* **72**, 271–281 (2012).
330. Bleuyard, J.-Y., Gallego, M. E. & White, C. I. Meiotic defects in the Arabidopsis rad50 mutant point to conservation of the MRX complex function in early stages of meiotic recombination. *Chromosom. 2004 1134* **113**, 197–203 (2004).
331. Jolivet, S., Vezon, D., Froger, N. & Mercier, R. Non conservation of the meiotic function of the Ski8/Rec103 homolog in Arabidopsis. *Genes to Cells* **11**, 615–622 (2006).
332. Pawlowski, W. P. *et al.* Coordination of Meiotic Recombination, Pairing, and Synapsis by PHS1. *Science (80-.).* **303**, 89–92 (2004).
333. Wu, Z. *et al.* OsSDS is essential for DSB formation in rice meiosis. *Front. Plant Sci.* **6**, (2015).
334. Liu, J., Wu, T. C. & Lichten, M. The location and structure of double-strand DNA breaks induced during yeast meiosis: Evidence for a covalently linked DNA-protein intermediate. *EMBO J.* **14**, 4599–4608 (1995).
335. Keeney, S. & Kleckner, N. Covalent protein-DNA complexes at the 5′ strand termini of meiosis-specific double-strand breaks in yeast. *Proc. Natl. Acad. Sci. U. S. A.* **92**, 11274–11278 (1995).
336. Johnson, D. *et al.* Concerted cutting by Spo11 illuminates meiotic DNA break mechanics. *Nature* **594**, 572–576 (2021).
337. Prieler, S. *et al.* Spo11 generates gaps through concerted cuts at sites of topological stress. *Nature* **594**, 577–

582 (2021).
338. Borde, V., Goldman, A. S. H. & Lichten, M. Direct coupling between meiotic DNA replication and recombination initiation. *Science (80-.).* **290**, 806–809 (2000).
339. Wu, P.-Y. J. & Nurse, P. Replication Origin Selection Regulates the Distribution of Meiotic Recombination. *Mol. Cell* **53**, 655 (2014).
340. Pratto, F. *et al.* Meiotic recombination mirrors patterns of germline replication in mice and humans. *Cell* **184**, 4251-4267.e20 (2021).
341. Higgins, J. D. *et al.* Spatiotemporal asymmetry of the meiotic program underlies the predominantly distal distribution of meiotic crossovers in barley. *Plant Cell* **24**, 4096–4109 (2012).
342. Henderson, K. A., Kee, K., Maleki, S., Santini, P. A. & Keeney, S. Cyclin-Dependent Kinase Directly Regulates Initiation of Meiotic Recombination. *Cell* **125**, 1321–1332 (2006).
343. Wan, L. *et al.* Cdc28-Clb5 (CDK-S) and Cdc7-Dbf4 (DDK) collaborate to initiate meiotic recombination in yeast. *Genes Dev.* **22**, 386–397 (2008).
344. Murakami, H. & Keeney, S. Temporospatial coordination of meiotic dna replication and recombination via DDK recruitment to replisomes. *Cell* **158**, 861–873 (2014).
345. Blitzblau, H. G. & Hochwagen, A. ATR/Mec1 prevents lethal meiotic recombination initiation on partially replicated chromosomes in budding yeast. *Elife* **2**, (2013).
346. Gray, S., Allison, R. M., Garcia, V., Goldman, A. S. H. & Neale, M. J. Positive regulation of meiotic DNA double-strand break formation by activation of the DNA damage checkpoint kinase Mec1(ATR). *Open Biol.* **3**, (2013).
347. Chen, X. *et al.* Mek1 coordinates meiotic progression with DNA break repair by directly phosphorylating and inhibiting the yeast pachytene exit regulator Ndt80. *PLoS Genet.* **14**, e1007832 (2018).
348. Thacker, D., Mohibullah, N., Zhu, X. & Keeney, S. Homologue engagement controls meiotic DNA break number and distribution. *Nat. 2014 5107504* **510**, 241–246 (2014).
349. T, A. & M, L. Differential timing and control of noncrossover and crossover recombination during meiosis. *Cell* **106**, 47–57 (2001).
350. Stamper, E. L. *et al.* Identification of DSB-1, a Protein Required for Initiation of Meiotic Recombination in Caenorhabditis elegans, Illuminates a Crossover Assurance Checkpoint. *PLoS Genet.* **9**, e1003679 (2013).
351. Mu, X., Murakami, H., Mohibullah, N. & Keeney, S. Chromosome-autonomous feedback down-regulates meiotic DNA break competence upon synaptonemal complex formation. *Genes Dev.* **34**, 1605–1618 (2020).
352. Subramanian, V. V. *et al.* Persistent DNA-break potential near telomeres increases initiation of meiotic recombination on short chromosomes. *Nat. Commun.* **10**, (2019).
353. Murakami, H. *et al.* Multilayered mechanisms ensure that short chromosomes recombine in meiosis. *Nature* **582**, 124–128 (2020).
354. Kauppi, L. *et al.* Numerical constraints and feedback control of double-strand breaks in mouse meiosis. *Genes Dev.* **27**, 873–886 (2013).
355. Dereli, I. *et al.* Four-pronged negative feedback of DSB machinery in meiotic DNA-break control in mice. *Nucleic Acids Res.* **49**, 2609–2628 (2021).
356. Wojtasz, L. *et al.* Mouse HORMAD1 and HORMAD2, two conserved meiotic chromosomal proteins, are depleted from synapsed chromosome axes with the help of TRIP13 AAA-ATPase. *PLoS Genet.* **5**, (2009).
357. Pan, J. *et al.* A hierarchical combination of factors shapes the genome-wide topography of yeast meiotic recombination initiation. *Cell* **144**, 719–731 (2011).
358. Smagulova, F. *et al.* Genome-wide analysis reveals novel molecular features of mouse recombination hotspots. *Nature* **472**, 375–378 (2011).
359. Pratto, F. *et al.* Recombination initiation maps of individual human genomes. *Science (80-.).* **346**, 1256442–1256442 (2014).
360. He, Y. *et al.* Genomic features shaping the landscape of meiotic double-strand-break hotspots in maize. *Proc. Natl. Acad. Sci. U. S. A.* **114**, 12231–12236 (2017).
361. Choi, K. *et al.* Nucleosomes and DNA methylation shape meiotic DSB frequency in Arabidopsis thaliana transposons and gene regulatory regions. *Genome Res.* **28**, 532–546 (2018).
362. Auton, A. *et al.* Genetic Recombination Is Targeted towards Gene Promoter Regions in Dogs. *PLOS Genet.* **9**, e1003984 (2013).
363. Singhal, S. *et al.* Stable recombination hotspots in birds. *Science (80-.).* **350**, 928–932 (2015).
364. Baudat, F. *et al.* PRDM9 is a major determinant of meiotic recombination hotspots in humans and mice. *Science (80-.).* **327**, 836–840 (2010).
365. Grey, C. *et al.* Mouse Prdm9 DNA-binding specificity determines sites of histone H3 lysine 4 trimethylation for initiation of meiotic recombination. *PLoS Biol.* **9**, e1001176 (2011).
366. Diagouraga, B. *et al.* PRDM9 Methyltransferase Activity Is Essential for Meiotic DNA Double-Strand Break Formation at Its Binding Sites. *Mol. Cell* **69**, 853-865.e6 (2018).

367. Borde, V. *et al.* Histone H3 lysine 4 trimethylation marks meiotic recombination initiation sites. *EMBO J.* **28**, 99–111 (2009).
368. Brick, K., Smagulova, F., Khil, P., Camerini-Otero, R. D. & Petukhova, G. V. Genetic recombination is directed away from functional genomic elements in mice. *Nature* **485**, 642–645 (2012).
369. Baker, C. L., Walker, M., Kajita, S., Petkov, P. M. & Paigen, K. PRDM9 binding organizes hotspot nucleosomes and limits Holliday junction migration. *Genome Res.* **24**, 724–732 (2014).
370. Yamada, S. *et al.* Molecular structures and mechanisms of DNA break processing in mouse meiosis. *Genes Dev.* **34**, 806–818 (2020).
371. Blat, Y., Protacio, R. U., Hunter, N. & Kleckner, N. Physical and functional interactions among basic chromosome organizational features govern early steps of meiotic chiasma formation. *Cell* **111**, 791–802 (2002).
372. Glynn, E. F. *et al.* Genome-wide mapping of the cohesin complex in the yeast Saccharomyces cerevisiae. *PLoS Biol.* **2**, e259 (2004).
373. Panizza, S. *et al.* Spo11-accessory proteins link double-strand break sites to the chromosome axis in early meiotic recombination. *Cell* **146**, 372–383 (2011).
374. Kumar, R. *et al.* Mouse REC114 is essential for meiotic DNA double-strand break formation and forms a complex with MEI4. *Life Sci. Alliance* **1**, (2018).
375. Kleckner, N. Chiasma formation: Chromatin/axis interplay and the role(s) of the synaptonemal complex. *Chromosoma* **115**, 175–194 (2006).
376. Acquaviva, L. *et al.* The COMPASS subunit Spp1 links histone methylation to initiation of meiotic recombination. *Science (80-.).* **339**, 215–218 (2013).
377. Sommermeyer, V., Béneut, C., Chaplais, E., Serrentino, M. E. & Borde, V. Spp1, a Member of the Set1 Complex, Promotes Meiotic DSB Formation in Promoters by Tethering Histone H3K4 Methylation Sites to Chromosome Axes. *Mol. Cell* **49**, 43–54 (2013).
378. Adam, C. *et al.* The PHD finger protein Spp1 has distinct functions in the Set1 and the meiotic DSB formation complexes. *PLoS Genet.* **14**, e1007223 (2018).
379. Tischfield, S. E. & Keeney, S. Scale matters the spatial correlation of yeast meiotic DNA breaks with histone H3 trimethylation is driven largely by independent colocalization at promoters. *Cell Cycle* **11**, 1496–1503 (2012).
380. Jiang, Y. *et al.* CXXC finger protein 1-mediated histone H3 lysine-4 trimethylation is essential for proper meiotic crossover formation in mice. *Dev.* **147**, (2020).
381. Imai, Y. *et al.* The PRDM9 KRAB domain is required for meiosis and involved in protein interactions. *Chromosoma* **126**, 681–695 (2017).
382. Wells, D. *et al.* ZCWPW1 is recruited to recombination hotspots by PRDM9, and is essential for meiotic double strand break repair. *Elife* **9**, 1–38 (2020).
383. Huang, T. *et al.* The histone modification reader zcwpw1 links histone methylation to prdm9-induced double strand break repair. *Elife* **9**, 1–48 (2020).
384. Choi, K. *et al.* Arabidopsis meiotic crossover hot spots overlap with H2A.Z nucleosomes at gene promoters. *Nat. Genet.* **45**, 1327–1338 (2013).
385. Lambing, C. *et al.* Interacting Genomic Landscapes of REC8-Cohesin, Chromatin, and Meiotic Recombination in Arabidopsis. *Plant Cell* **32**, 1218–1239 (2020).
386. Garcia, V., Gray, S., Allison, R. M., Cooper, T. J. & Neale, M. J. Tel1ATM-mediated interference suppresses clustered meiotic double-strand-break formation. *Nature* **520**, 114–118 (2015).
387. Mohibullah, N. & Keeney, S. Numerical and spatial patterning of yeast meiotic DNA breaks by Tel1. *Genome Res.* **27**, 278–288 (2017).
388. Zhang, L., Kleckner, N. E., Storlazzi, A. & Kim, K. P. Meiotic double-strand breaks occur once per pair of (sister) chromatids and, via Mec1/ATR and Tel1/ATM, once per quartet of chromatids. *Proc. Natl. Acad. Sci. U. S. A.* **108**, 20036–20041 (2011).
389. Lange, J. *et al.* The Landscape of Mouse Meiotic Double-Strand Break Formation, Processing, and Repair. *Cell* **167**, 695-708.e16 (2016).
390. Sun, X. *et al.* Transcription dynamically patterns the meiotic chromosome-axis interface. *Elife* **4**, (2015).
391. Xue, M. *et al.* The Number of Meiotic Double-Strand Breaks Influences Crossover Distribution in Arabidopsis. *Plant Cell* **30**, 2628–2638 (2018).
392. Lange, J. *et al.* ATM controls meiotic double-strand-break formation. *Nature* **479**, 237–240 (2011).
393. Joyce, E. F. *et al.* Drosophila ATM and ATR have distinct activities in the regulation of meiotic DNA damage and repair. *J. Cell Biol.* **195**, 359–367 (2011).
394. Carballo, J. A. *et al.* Budding Yeast ATM/ATR Control Meiotic Double-Strand Break (DSB) Levels by Down-Regulating Rec114, an Essential Component of the DSB-machinery. *PLoS Genet.* **9**, (2013).
395. Argunhan, B. *et al.* Direct and Indirect Control of the Initiation of Meiotic Recombination by DNA Damage

Checkpoint Mechanisms in Budding Yeast. *PLoS One* **8**, e65875 (2013).
396. Lukaszewicz, A., Lange, J., Keeney, S. & Jasin, M. Control of meiotic double-strand-break formation by ATM: local and global views. *Cell Cycle* **17**, 1155–1172 (2018).
397. Kurzbauer, M.-T. *et al.* ATM controls meiotic DNA double-strand break formation and recombination and affects synaptonemal complex organization in plants. *Plant Cell* **33**, 1633–1656 (2021).
398. Yun, H. & Kim, K. Ku complex suppresses recombination in the absence of MRX activity during budding yeast meiosis. *BMB Rep.* **52**, 607–612 (2019).
399. Ouyang, H. *et al.* Ku70 is required for DNA repair but not for T cell antigen receptor gene recombination in vivo. *J. Exp. Med.* **186**, 921–929 (1997).
400. Nussenzweig, A. *et al.* Requirement for Ku80 in growth and immunoglobulin V(D)J recombination. *Nature* **382**, 551–555 (1996).
401. Goedecke, W., Eijpe, M., Offenberg, H. H., Van Aalderen, M. & Heyting, C. Mre11 and Ku70 interact in somatic cells, but are differentially expressed in early meiosis. *Nat. Genet.* **23**, 194–198 (1999).
402. Ahmed, E. A., Philippens, M. E. P., Kal, H. B., de Rooij, D. G. & de Boer, P. Genetic probing of homologous recombination and non-homologous end joining during meiotic prophase in irradiated mouse spermatocytes. *Mutat. Res. - Fundam. Mol. Mech. Mutagen.* **688**, 12–18 (2010).
403. Enguita-Marruedo, A. *et al.* Transition from a meiotic to a somatic-like DNA damage response during the pachytene stage in mouse meiosis. *PLoS Genet.* **15**, (2019).
404. Yin, Y. & Smolikove, S. Impaired Resection of Meiotic Double-Strand Breaks Channels Repair to Nonhomologous End Joining in Caenorhabditis elegans. *Mol. Cell. Biol.* **33**, 2732–2747 (2013).
405. Lemmens, B. B. L. G., Johnson, N. M. & Tijsterman, M. COM-1 Promotes Homologous Recombination during Caenorhabditis elegans Meiosis by Antagonizing Ku-Mediated Non-Homologous End Joining. *PLoS Genet.* **9**, 1003276 (2013).
406. Girard, C., Roelens, B., Zawadzki, K. A. & Villeneuve, A. M. Interdependent and separable functions of Caenorhabditis elegans MRN-C complex members couple formation and repair of meiotic DSBs. *Proc. Natl. Acad. Sci. U. S. A.* **115**, E4443–E4452 (2018).
407. Yun, H. & Kim, K. Ku complex suppresses recombination in the absence of MRX activity during budding yeast meiosis. *BMB Rep.* **52**, 607–612 (2019).
408. Joyce, E. F. & McKim, K. S. Drosophila PCH2 is required for a pachytene checkpoint that monitors double-strand-break-independent events leading to meiotic crossover formation. *Genetics* **181**, 39–51 (2009).
409. Joyce, E. F., Paul, A., Chen, K. E., Tanneti, N. & McKim, K. S. Multiple barriers to nonhomologous DNA end joining during meiosis in Drosophila. *Genetics* **191**, 739–746 (2012).
410. Hatkevich, T., Miller, D. E., Turcotte, C. A., Miller, M. C. & Sekelsky, J. A pathway for error-free non-homologous end joining of resected meiotic double-strand breaks. *Nucleic Acids Res.* **49**, 879–890 (2021).
411. Sims, J., Copenhaver, G. P. & Schlögelhofer, P. Meiotic DNA repair in the nucleolus employs a nonhomologous end-joining mechanism. *Plant Cell* **31**, 2259–2275 (2019).
412. Mimitou, E. P., Yamada, S. & Keeney, S. A global view of meiotic double-strand break end resection. *Science (80-.).* **355**, 40–45 (2017).
413. Waterworth, W. M. *et al.* NBS1 is involved in DNA repair and plays a synergistic role with ATM in mediating meiotic homologous recombination in plants. *Plant J.* **52**, 41–52 (2007).
414. Williams, B. R. *et al.* A murine model of Nijmegen breakage syndrome. *Curr. Biol.* **12**, 648–653 (2002).
415. Kang, J., Bronson, R. T. & Xu, Y. Targeted disruption of NBS1 reveals its roles in mouse development and DNA repair. *EMBO J.* **21**, 1447–1455 (2002).
416. Difilippantonio, S. *et al.* Role of Nbs1 in the activation of the Atm kinase revealed in humanized mouse models. *Nat. Cell Biol.* **7**, 675–685 (2005).
417. Aklilu, B. B. & Culligan, K. M. Molecular Evolution and Functional Diversification of Replication Protein A1 in Plants. *Front. Plant Sci.* **0**, 33 (2016).
418. Lin, Z., Kong, H., Nei, M. & Ma, H. Origins and evolution of the recA/RAD51 gene family: Evidence for ancient gene duplication and endosymbiotic gene transfer. *Proc. Natl. Acad. Sci. U. S. A.* **103**, 10328–10333 (2006).
419. Bonilla, B., Hengel, S. R., Grundy, M. K. & Bernstein, K. A. RAD51 Gene Family Structure and Function. *Annu. Rev. Genet.* **54**, 25–46 (2020).
420. Klimyuk, V. I. & Jones, J. D. G. AtDMC1, the Arabidopsis homologue of the yeast DMC1 gene: Characterization, transposon-induced allelic variation and meiosis-associated expression. *Plant J.* **11**, 1–14 (1997).
421. Kobayashi, W. *et al.* Homologous pairing activities of Arabidopsis thaliana RAD51 and DMC1. *J. Biochem.* **165**, 289–295 (2019).
422. Crickard, J. B. & Greene, E. C. The biochemistry of early meiotic recombination intermediates. *Cell Cycle* **17**, 2520–2530 (2018).

423. Chang, H. Y. *et al.* Functional relationship of ATP hydrolysis, presynaptic filament stability, and homologous DNA pairing activity of the human meiotic recombinase DMC1. *J. Biol. Chem.* **290**, 19863–19873 (2015).
424. Bugreev, D. V. & Mazin, A. V. Ca2+ activates human homologous recombination protein Rad51 by modulating its ATPase activity. *Proc. Natl. Acad. Sci. U. S. A.* **101**, 9988–9993 (2004).
425. Bugreev, D. V., Golub, E. I., Stasiak, A. Z., Stasiak, A. & Mazin, A. V. Activation of human meiosis-specific recombinase Dmc1 by Ca2+. *J. Biol. Chem.* **280**, 26886–26895 (2005).
426. Lee, M. H. *et al.* Calcium ion promotes yeast Dmc1 activity via formation of long and fine helical filaments with single-stranded DNA. *J. Biol. Chem.* **280**, 40980–40984 (2005).
427. Lee, J. Y. *et al.* Base triplet stepping by the Rad51/RecA family of recombinases. *Science (80-.).* **349**, 977–981 (2015).
428. Lee, J. Y. *et al.* Sequence imperfections and base triplet recognition by the Rad51/RecA family of recombinases. *J. Biol. Chem.* **292**, 11125–11135 (2017).
429. Danilowicz, C., Yang, D., Kelley, C., Prévost, C. & Prentiss, M. The poor homology stringency in the heteroduplex allows strand exchange to incorporate desirable mismatches without sacrificing recognition in vivo. *Nucleic Acids Res.* **43**, 6473–6485 (2015).
430. Anand, R., Beach, A., Li, K. & Haber, J. Rad51-mediated double-strand break repair and mismatch correction of divergent substrates. *Nature* **544**, 377–380 (2017).
431. Bishop, D. K. RecA homologs Dmc1 and Rad51 interact to form multiple nuclear complexes prior to meiotic chromosome synapsis. *Cell* **79**, 1081–1092 (1994).
432. Brown, M. S., Grubb, J., Zhang, A., Rust, M. J. & Bishop, D. K. Small Rad51 and Dmc1 Complexes Often Co-occupy Both Ends of a Meiotic DNA Double Strand Break. *PLoS Genet.* **11**, e1005653 (2015).
433. Hinch, A. G. *et al.* The Configuration of RPA, RAD51, and DMC1 Binding in Meiosis Reveals the Nature of Critical Recombination Intermediates. *Mol. Cell* **79**, 689-701.e10 (2020).
434. Slotman, J. A. *et al.* Super-resolution imaging of RAD51 and DMC1 in DNA repair foci reveals dynamic distribution patterns in meiotic prophase. *PLoS Genet.* **16**, e1008595 (2020).
435. Murayama, Y., Tsutsui, Y. & Iwasaki, H. The fission yeast meiosis-specific Dmc1 recombinase mediates formation and branch migration of Holliday junctions by preferentially promoting strand exchange in a direction opposite to that of Rad51. *Genes Dev.* **25**, 516–527 (2011).
436. Brown, M. S. & Bishop, D. K. DNA strand exchange and RecA homologs in meiosis. *Cold Spring Harb. Perspect. Biol.* **7**, 16659–16660 (2015).
437. Brooks Crickard, J., Kaniecki, K., Kwon, Y., Sung, P. & Greene, E. C. Spontaneous self-segregation of Rad51 and Dmc1 DNA recombinases within mixed recombinase filaments. *J. Biol. Chem.* **293**, 4191–4200 (2018).
438. Lan, W. H. *et al.* Rad51 facilitates filament assembly of meiosis-specific Dmc1 recombinase. *Proc. Natl. Acad. Sci. U. S. A.* **117**, 11257–11264 (2020).
439. Cloud, V., Chan, Y. L., Grubb, J., Budke, B. & Bishop, D. K. Rad51 is an accessory factor for Dmc1-mediated joint molecule formation during meiosis. *Science (80-.).* **337**, 1222–1225 (2012).
440. Bishop, D. K. Rad51, the lead in mitotic recombinational DNA repair, plays a supporting role in budding yeast meiosis. *Cell Cycle* **11**, 4105–4106 (2012).
441. Kobayashi, W., Sekine, S., Machida, S. & Kurumizaka, H. Green fluorescent protein fused to the C terminus ofRAD51 specifically interferes with secondary DNAbinding by the RAD51-ssDNA complex. *Genes Genet. Syst.* **89**, 169–179 (2014).
442. Singh, G., Da Ines, O., Gallego, M. E. & White, C. I. Analysis of the impact of the absence of RAD51 strand exchange activity in Arabidopsis meiosis. *PLoS One* **12**, e0183006 (2017).
443. Gasior, S. L., Wong, A. K., Kora, Y., Shinohara, A. & Bishop, D. K. Rad52 associates with RPA and functions with Rad55 and Rad57 to assemble meiotic recombination complexes. *Genes Dev.* **12**, 2208–2221 (1998).
444. Waterman, D. P. *et al.* Live cell monitoring of double strand breaks in S. Cerevisiae. *PLoS Genet.* **15**, (2019).
445. Ma, C. J., Kwon, Y., Sung, P. & Greene, E. C. Human RAD52 interactions with replication protein A and the RAD51 presynaptic complex. *J. Biol. Chem.* **292**, 11702–11713 (2017).
446. Crickard, J. B. & Greene, E. C. Biochemical attributes of mitotic and meiotic presynaptic complexes. *DNA Repair (Amst).* **71**, 148–157 (2018).
447. Hayase, A. *et al.* A protein complex containing Mei5 and Sae3 promotes the assembly of the meiosis-specific RecA homolog Dmc1. *Cell* **119**, 927–940 (2004).
448. Ferrari, S. R., Grubb, J. & Bishop, D. K. The Mei5-Sae3 protein complex mediates Dmc1 activity in Saccharomyces cerevisiae. *J. Biol. Chem.* **284**, 11766–11770 (2009).
449. Lao, J. P., Oh, S. D., Shinohara, M., Shinohara, A. & Hunter, N. Rad52 Promotes Postinvasion Steps of Meiotic Double-Strand-Break Repair. *Mol. Cell* **29**, 517–524 (2008).
450. Resnick, M. A., Nitiss, J., Edwards, C. & Malone, R. E. Meiosis can induce recombination in rad52 mutants of Saccharomyces cerevisiae. *Genetics* **113**, 531–550 (1986).
451. Say, A. F. *et al.* The budding yeast Mei5–Sae3 complex interacts with Rad51 and preferentially binds a DNA

fork structure. *DNA Repair (Amst).* **10**, 586–594 (2011).
452. Gottifredi, V. & Wiesmüller, L. Current Understanding of RAD52 Functions : *Cancers (Basel).* **12**, 1–8 (2020).
453. Yuan, J. & Chen, J. The role of the human SWI5-MEI5 complex in homologous recombination repair. *J. Biol. Chem.* **286**, 9888–9893 (2011).
454. Haruta, N. *et al.* The Swi5-Sfr1 complex stimulates Rhp51/Rad51 - and Dmc1-mediated DNA strand exchange in vitro. *Nat. Struct. Mol. Biol.* **13**, 823–830 (2006).
455. Argunhan, B., Murayama, Y. & Iwasaki, H. The differentiated and conserved roles of Swi5-Sfr1 in homologous recombination. *FEBS Lett.* **591**, 2035–2047 (2017).
456. Sharan, S. K. *et al.* Embryonic lethality and radiation hypersensitivity mediated by Rad51 in mice lacking Brca2. *Nature* **386**, 804–810 (1997).
457. Sharan, S. K. *et al.* BRCA2 deficiency in mice leads to meiotic impairment and infertility. *Development* **131**, 131–142 (2004).
458. Tarsounas, M., Davies, D. & West, S. C. BRCA2-dependent and independent formation of RAD51 nuclear foci. *Oncogene* **22**, 1115–1123 (2003).
459. Siaud, N. *et al.* Brca2 is involved in meiosis in Arabidopsis thaliana as suggested by its interaction with Dmc1. *EMBO J.* **23**, 1392–1401 (2004).
460. Dray, E., Siaud, N., Dubois, E. & Doutriaux, M. P. Interaction between Arabidopsis Brca2 and its partners Rad51, Dmc1, and Dss1. *Plant Physiol.* **140**, 1059–1069 (2006).
461. Thorslund, T., Esashi, F. & West, S. C. Interactions between human BRCA2 protein and the meiosis-specific recombinase DMC1. *EMBO J.* **26**, 2915–2922 (2007).
462. Jensen, R. B., Carreira, A. & Kowalczykowski, S. C. Purified human BRCA2 stimulates RAD51-mediated recombination. *Nature* **467**, 678–683 (2010).
463. Martinez, J. S. *et al.* BRCA2 regulates DMC1-mediated recombination through the BRC repeats. *Proc. Natl. Acad. Sci. U. S. A.* **113**, 3515–3520 (2016).
464. Tarsounas, M., Davies, A. A. & West, S. C. RAD51 localization and activation following DNA damage. *Philos. Trans. R. Soc. B Biol. Sci.* **359**, 87–93 (2004).
465. Zhao, W. *et al.* Promotion of BRCA2-Dependent Homologous Recombination by DSS1 via RPA Targeting and DNA Mimicry. *Mol. Cell* **59**, 176–187 (2015).
466. Zhang, J., Fujiwara, Y., Yamamoto, S. & Shibuya, H. A meiosis-specific BRCA2 binding protein recruits recombinases to DNA double-strand breaks to ensure homologous recombination. *Nat. Commun.* **10**, (2019).
467. Takemoto, K. *et al.* Meiosis-Specific C19orf57/4930432K21Rik/BRME1 Modulates Localization of RAD51 and DMC1 to DSBs in Mouse Meiotic Recombination. *Cell Rep.* **31**, (2020).
468. Ma, E. *et al.* Rad52-Rad51 association is essential to protect Rad51 filaments against Srs2, but facultative for filament formation. *Elife* **7**, (2018).
469. Ma, E., Maloisel, L., Le Falher, L., Guérois, R. & Coïc, E. Rad52 oligomeric n-terminal domain stabilizes rad51 nucleoprotein filaments and contributes to their protection against srs2. *Cells* **10**, (2021).
470. Leu, J. Y., Chua, P. R. & Roeder, G. S. The meiosis-specific Hop2 protein of S. cerevisiae ensures synapsis between homologous chromosomes. *Cell* **94**, 375–386 (1998).
471. Tsubouchi, H. & Roeder, G. S. The Mnd1 Protein Forms a Complex with Hop2 To Promote Homologous Chromosome Pairing and Meiotic Double-Strand Break Repair. *Mol. Cell. Biol.* **22**, 3078–3088 (2002).
472. Henry, J. M. *et al.* Mnd1/Hop2 Facilitates Dmc1-Dependent Interhomolog Crossover Formation in Meiosis of Budding Yeast. *Mol. Cell. Biol.* **26**, 2913–2923 (2006).
473. Chan, Y. L., Brown, M. S., Qin, D., Handa, N. & Bishop, D. K. The third exon of the budding yeast meiotic recombination gene HOP2 is required for calcium-dependent and recombinase Dmc1-specific stimulation of homologous strand assimilation. *J. Biol. Chem.* **289**, 18076–18086 (2014).
474. Brooks Crickard, J., Kwon, Y., Sung, P. & Greene, E. C. Dynamic interactions of the homologous pairing 2 (Hop2)–meiotic nuclear divisions 1 (Mnd1) protein complex with meiotic presynaptic filaments in budding yeast. *J. Biol. Chem.* **294**, 490–501 (2019).
475. Petukhova, G. V *et al.* The Hop2 and Mnd1 proteins act in concert with Rad51 and Dmc1 in meiotic recombination. *Nat. Struct. Mol. Biol. 2005 125* **12**, 449–453 (2005).
476. Pezza, R. J., Petukhova, G. V., Ghirlando, R. & Camerini-Otero, R. D. Molecular Activities of Meiosis-specific Proteins Hop2, Mnd1, and the Hop2-Mnd1 Complex. *J. Biol. Chem.* **281**, 18426–18434 (2006).
477. Pezza, R. J., Voloshin, O. N., Vanevski, F. & Camerini-Otero, R. D. Hop2/Mnd1 acts on two critical steps in Dmc1-promoted homologous pairing. *Genes Dev.* **21**, 1758–1766 (2007).
478. Chi, P., Filippo, J. S., Sehorn, M. G., Petukhova, G. V. & Sung, P. Bipartite stimulatory action of the Hop2–Mnd1 complex on the Rad51 recombinase. *Genes Dev.* **21**, 1747–1757 (2007).
479. Cho, N. W., Dilley, R. L., Lampson, M. A. & Greenberg, R. A. Interchromosomal homology searches drive directional ALT telomere movement and synapsis. *Cell* **159**, 108–121 (2014).

480. Zhao, W. & Sung, P. Significance of ligand interactions involving Hop2-Mnd1 and the RAD51 and DMC1 recombinases in homologous DNA repair and XX ovarian dysgenesis. *Nucleic Acids Res.* **43**, 4055–4066 (2015).
481. Peng, M. *et al.* GT198 Splice Variants Display Dominant-Negative Activities and Are Induced by Inactivating Mutations. *Genes and Cancer* **4**, 26–38 (2013).
482. Pezza, R. J. *et al.* The dual role of HOP2 in mammalian meiotic homologous recombination. *Nucleic Acids Res.* **42**, 2346–2357 (2014).
483. Schommer, C., Beven, A., Lawrenson, T., Shaw, P. & Sablowski, R. AHP2 is required for bivalent formation and for segregation of homologous chromosomes in Arabidopsis meiosis. *Plant J.* **36**, 1–11 (2003).
484. Vignard, J. *et al.* The interplay of RecA-related proteins and the MND1-HOP2 complex during meiosis in Arabidopsis thaliana. *PLoS Genet.* **3**, 1894–1906 (2007).
485. Uanschou, C. *et al.* Sufficient amounts of functional HOP2/MND1 complex promote interhomolog DNA repair but are dispensable for intersister DNA repair during meiosis in Arabidopsis. *Plant Cell* **25**, 4924–4940 (2013).
486. Farahani-Tafreshi, Y. *et al.* The Arabidopsis HOP2 gene has a role in preventing illegitimate connections between nonhomologous chromosome regions. *Chromosom. Res.* **30**, 59–75 (2022).
487. Lovett, S. T. & Mortimer, R. K. Characterization of null mutants of the RAD55 gene of Saccharomyces cerevisiae: effects of temperature, osmotic strength and mating type. *Genetics* **116**, 547–553 (1987).
488. Johnson, R. D. & Symington, L. S. Functional differences and interactions among the putative RecA homologs Rad51, Rad55, and Rad57. *Mol. Cell. Biol.* **15**, 4843–4850 (1995).
489. Gasior, S. L., Wong, A. K., Kora, Y., Shinohara, A. & Bishop, D. K. Rad52 associates with RPA and functions with Rad55 and Rad57 to assemble meiotic recombination complexes. *Genes Dev.* **12**, 2208–2221 (1998).
490. Fung, C. W., Mozlin, A. M. & Symington, L. S. Suppression of the double-strand-break-repair defect of the Saccharomyces cerevisiae rad57 mutant. *Genetics* **181**, 1195–1206 (2009).
491. Sung, P. Yeast Rad55 and Rad57 proteins form a heterodimer that functions with replication protein A to promote DNA strand exchange by Rad51 recombinase. *Genes Dev.* **11**, 1111–1121 (1997).
492. Liu, J. *et al.* Rad51 paralogues Rad55-Rad57 balance the antirecombinase Srs2 in Rad51 filament formation. *Nature* **479**, 245–248 (2011).
493. Gaines, W. A. *et al.* Promotion of presynaptic filament assembly by the ensemble of S. cerevisiae Rad51 paralogues with Rad52. *Nat. Commun.* **6**, 1–7 (2015).
494. Martino, J. & Bernstein, K. A. The Shu complex is a conserved regulator of homologous recombination. *FEMS Yeast Res.* **16**, 73 (2016).
495. Sasanuma, H. *et al.* A new protein complex promoting the assembly of Rad51 filaments. *Nat. Commun. 2013 41* **4**, 1–13 (2013).
496. Sullivan, M. R. & Bernstein, K. A. RAD-ical new insights into RAD51 regulation. *Genes* **9**, 629 (2018).
497. Abreu, C. M. *et al.* Shu complex SWS1-SWSAP1 promotes early steps in mouse meiotic recombination. *Nat. Commun.* **9**, (2018).
498. Kurumizaka, H. *et al.* Homologous-pairing activity of the human DNA-repair proteins Xrcc3 · Rad51C. *Proc. Natl. Acad. Sci. U. S. A.* **98**, 5538–5543 (2001).
499. Kurumizaka, H. *et al.* Homologous pairing and ring and filament structure formation activities of the human Xrcc2 · Rad51D complex. *J. Biol. Chem.* **277**, 14315–14320 (2002).
500. Masson, J. Y., Stasiak, A. Z., Stasiak, A., Benson, F. E. & West, S. C. Complex formation by the human RAD51C and XRCC3 recombination repair proteins. *Proc. Natl. Acad. Sci. U. S. A.* **98**, 8440–8446 (2001).
501. Pittman, D. L. & Schimenti, J. C. Midgestation lethality in mice deficient for the RecA-related gene, Rad51d/Rad51l3. *Genesis* **26**, 167–173 (2000).
502. Deans, B., Griffin, C. S., O'Regan, P., Jasin, M. & Thacker, J. Homologous Recombination Deficiency Leads to Profound Genetic Instability in Cells Derived from Xrcc2-Knockout Mice. *Cancer Res.* **63**, 8181–8187 (2003).
503. Kuznetsov, S. G., Haines, D. C., Martin, B. K. & Sharan, S. K. Loss of Rad51c leads to embryonic lethality and modulation of Trp53-dependent tumorigenesis in mice. *Cancer Res.* **69**, 863–872 (2009).
504. Shu, Z., Smith, S., Wang, L., Rice, M. C. & Kmiec, E. B. Disruption of muREC2/RAD51L1 in Mice Results in Early Embryonic Lethality Which Can Be Partially Rescued in a p53 −/− Background . *Mol. Cell. Biol.* **19**, 8686–8693 (1999).
505. Smiraldo, P. G., Gruver, A. M., Osborn, J. C. & Pittman, D. L. Extensive chromosomal instability in Rad51d-deficient mouse cells. *Cancer Res.* **65**, 2089–2096 (2005).
506. Adam, J., Deans, B. & Thacker, J. A role for Xrcc2 in the early stages of mouse development. *DNA Repair (Amst).* **6**, 224–234 (2007).
507. Tumiati, M. *et al.* Loss of Rad51c accelerates tumourigenesis in sebaceous glands of Trp53-mutant mice. *J. Pathol.* **235**, 136–146 (2015).
508. Jones, N. J., Cox, R. & Thacker, J. Isolation and cross-sensitivity of X-ray-sensitive mutants of V79-4 hamster

cells. *Mutat. Res. DNA Repair Reports* **183**, 279–286 (1987).
509. Fuller, L. F. & Painter, R. B. A Chinese hamster ovary cell line hypersensitive to ionizing radiation and deficient in repair replication. *Mutat. Res. DNA Repair Reports* **193**, 109–121 (1988).
510. Bishop, D. K. *et al.* Xrcc3 is required for assembly of Rad51 complexes in Vivo. *J. Biol. Chem.* **273**, 21482–21488 (1998).
511. Takata, M. *et al.* The Rad51 Paralog Rad51B Promotes Homologous Recombinational Repair. *Mol. Cell. Biol.* **20**, 6476–6482 (2000).
512. Takata, M. *et al.* Chromosome Instability and Defective Recombinational Repair in Knockout Mutants of the Five Rad51 Paralogs. *Mol. Cell. Biol.* **21**, 2858–2866 (2001).
513. Jensen, R. B., Ozes, A., Kim, T., Estep, A. & Kowalczykowski, S. C. BRCA2 is epistatic to the RAD51 paralogs in response to DNA damage. *DNA Repair (Amst).* **12**, 306–311 (2013).
514. Chun, J., Buechelmaier, E. S. & Powell, S. N. Rad51 Paralog Complexes BCDX2 and CX3 Act at Different Stages in the BRCA1-BRCA2-Dependent Homologous Recombination Pathway. *Mol. Cell. Biol.* **33**, 387–395 (2013).
515. Kuznetsov, S. *et al.* RAD51C deficiency in mice results in early prophase I arrest in males and sister chromatid separation at metaphase II in females. *J. Cell Biol.* **176**, 581–592 (2007).
516. Liu, Y., Tarsounas, M., O'Regan, P. & West, S. C. Role of RAD51C and XRCC3 in genetic recombination and DNA repair. *J. Biol. Chem.* **282**, 1973–1979 (2007).
517. Yang, Y. *et al.* XRCC2 mutation causes meiotic arrest, azoospermia and infertility. *J. Med. Genet.* **55**, 628–636 (2018).
518. Martín, V. *et al.* Sws1 is a conserved regulator of homologous recombination in eukaryotic cells. *EMBO J.* **25**, 2564–2574 (2006).
519. Liu, T., Wan, L., Wu, Y., Chen, J. & Huang, J. hSWS1•SWSAP1 is an evolutionarily conserved complex required for efficient homologous recombination repair. *J. Biol. Chem.* **286**, 41758–41766 (2011).
520. Osakabe, K., Yoshioka, T., Ichikawa, H. & Toki, S. Molecular cloning and characterization of RAD51-like genes from Arabidopsis thaliana. *Plant Mol. Biol.* **50**, 71–81 (2002).
521. Osakabe, K. *et al.* Arabidopsis Rad51B is important for double-strand DNA breaks repair in somatic cells. *Plant Mol. Biol.* **57**, 819–833 (2005).
522. Li, W. *et al.* The AtRAD51C gene is required for normal meiotic chromosome synapsis and double-stranded break repair in Arabidopsis. *Plant Physiol.* **138**, 965–976 (2005).
523. Su, H. *et al.* Arabidopsis RAD51, RAD51C and XRCC3 proteins form a complex and facilitate RAD51 localization on chromosomes for meiotic recombination. *PLoS Genet.* **13**, e1006827 (2017).
524. Abe, K. *et al.* Arabidopsis RAD51C gene is important for homologous recombination in meiosis and mitosis. *Plant Physiol.* **139**, 896–908 (2005).
525. Durrant, W. E., Wang, S. & Dong, X. Arabidopsis SNI1 and RAD51D regulate both gene transcription and DNA recombination during the defense response. *Proc. Natl. Acad. Sci. U. S. A.* **104**, 4223–4227 (2007).
526. Da Ines, O. *et al.* Effects of XRCC2 and RAD51B mutations on somatic and meiotic recombination in Arabidopsis thaliana. *Plant J.* **74**, 959–970 (2013).
527. Bleuyard, J. Y., Gallego, M. E. & White, C. I. The atspo11-1 mutation rescues atxrcc3 meiotic chromosome fragmentation. *Plant Mol. Biol.* **56**, 217–224 (2004).
528. Raz, A., Dahan-Meir, T., Melamed-Bessudo, C., Leshkowitz, D. & Levy, A. A. Redistribution of Meiotic Crossovers Along Wheat Chromosomes by Virus-Induced Gene Silencing. *Front. Plant Sci.* **11**, 2332 (2021).
529. Charlot, F. *et al.* RAD51B plays an essential role during somatic and meiotic recombination in Physcomitrella. *Nucleic Acids Res.* **42**, 11965–11978 (2014).
530. Tang, D. *et al.* OsRAD51C is essential for double-strand break repair in rice meiosis. *Front. Plant Sci.* **5**, 167 (2014).
531. Byun, M. Y. & Kim, W. T. Suppression of OsRAD51D results in defects in reproductive development in rice (Oryza sativa L.). *Plant J.* **79**, 256–269 (2014).
532. Zhang, B. *et al.* XRCC3 is essential for proper double-strand break repair and homologous recombination in rice meiosis. *J. Exp. Bot.* **66**, 5713–5725 (2015).
533. Zhang, F. *et al.* OsRAD51D promotes homologous pairing and recombination by preventing nonhomologous interactions in rice meiosis. *New Phytol.* **227**, 824–839 (2020).
534. Petukhova, G., Stratton, S. & Sung, P. Catalysis of homologous DNA pairing by yeast Rad51 and Rad54 proteins. *Nature* **393**, 91–94 (1998).
535. Petukhova, G., Sung, P. & Klein, H. Promotion of Rad51-dependent D-loop formation by yeast recombination factor Rdh54/Tid1. *Genes Dev.* **14**, 2206–2215 (2000).
536. Nimonkar, A. V., Amitani, I., Baskin, R. J. & Kowalczykowski, S. C. Single molecule imaging of Tid1/Rdh54, a Rad54 homolog that translocates on duplex DNA and can disrupt joint molecules. *J. Biol. Chem.* **282**, 30776–30784 (2007).

537. Raschle, M., Van Komen, S., Chi, P., Ellenberger, T. & Sung, P. Multiple interactions with the rad51 recombinase govern the homologous recombination function of Rad54. *J. Biol. Chem.* **279**, 51973–51980 (2004).
538. Nimonkar, A. V. *et al.* Saccharomyces cerevisiae Dmc1 and Rad51 proteins preferentially function with Tid1 and Rad54 proteins, respectively, to promote DNA strand invasion during genetic recombination. *J. Biol. Chem.* **287**, 28727–28737 (2012).
539. Solinger, J. A., Kiianitsa, K. & Heyer, W. D. Rad54, a Swi2/Snf2-like recombinational repair protein, disassembles Rad51:dsDNA filaments. *Mol. Cell* **10**, 1175–1188 (2002).
540. Li, X. *et al.* Rad51 and Rad54 ATPase activities are both required to modulate Rad51-dsDNA filament dynamics. *Nucleic Acids Res.* **35**, 4124–4140 (2007).
541. Alexeev, A., Mazin, A. & Kowalczykowski, S. C. Rad54 protein possesses chromatin-remodeling activity stimulated by the Rad51-ssDNA nucleoprotein filament. *Nat. Struct. Biol.* **10**, 182–186 (2003).
542. Kwon, Y. H. *et al.* ATP-dependent chromatin remodeling by the Saccharomyces cerevisiae homologous recombination factor Rdh54. *J. Biol. Chem.* **283**, 10445–10452 (2008).
543. Lisby, M., Barlow, J. H., Burgess, R. C. & Rothstein, R. Choreography of the DNA damage response: Spatiotemporal relationships among checkpoint and repair proteins. *Cell* **118**, 699–713 (2004).
544. Klein, H. L. RDH54, a RAD54 homologue in Saccharomyces cerevisiae, is required for mitotic diploid-specific recombination and repair and for meiosis. *Genetics* **147**, 1533–1543 (1997).
545. Shinohara, M. *et al.* Characterization of the roles of the Saccharomyces cerevisiae RAD54 gene and a homologue of RAD54, RDH54/TID1, in mitosis and meiosis. *Genetics* **147**, 1545–1556 (1997).
546. Crickard, J. B., Moevus, C. J., Kwon, Y., Sung, P. & Greene, E. C. Rad54 Drives ATP Hydrolysis-Dependent DNA Sequence Alignment during Homologous Recombination. *Cell* **181**, 1380-1394.e18 (2020).
547. Crickard, J. B., Greene, E. C. & Rothstein, R. J. Discrete roles for Rad54 and Rdh54 during homologous recombination This review comes from a themed issue on Homologous recombi-nation in meiosis and repair. *Curr. Opin. Genet. Dev.* **71**, 48–54 (2021).
548. Tsubouchi, H. & Roeder, G. S. Budding yeast Hed1 down-regulates the mitotic recombination machinery when meiotic recombination is impaired. *Genes Dev.* **20**, 1766–1775 (2006).
549. Busygina, V. *et al.* Hed1 regulates Rad51-mediated recombination via a novel mechanism. *Genes Dev.* **22**, 786–795 (2008).
550. Busygina, V. *et al.* Novel attributes of hed1 affect dynamics and activity of the rad51 presynaptic filament during meiotic recombination. *J. Biol. Chem.* **287**, 1566–1575 (2012).
551. Crickard, J. B. *et al.* Regulation of Hed1 and Rad54 binding during maturation of the meiosis-specific presynaptic complex. *EMBO J.* **37**, (2018).
552. Callender, T. L. *et al.* Mek1 Down Regulates Rad51 Activity during Yeast Meiosis by Phosphorylation of Hed1. *PLoS Genet.* **12**, e1006226 (2016).
553. Niu, H. *et al.* Regulation of Meiotic Recombination via Mek1-Mediated Rad54 Phosphorylation. *Mol. Cell* **36**, 393–404 (2009).
554. Liu, Y. *et al.* Down-Regulation of Rad51 Activity during Meiosis in Yeast Prevents Competition with Dmc1 for Repair of Double-Strand Breaks. *PLoS Genet.* **10**, 1004005 (2014).
555. Swagemakers, S. M. A., Essers, J., De Wit, J., Hoeijmakers, J. H. J. & Kanaar, R. The human Rad54 recombinational DNA repair protein is a double-stranded DNA-dependent ATPase. *J. Biol. Chem.* **273**, 28292–28297 (1998).
556. Tanaka, K., Kagawa, W., Kinebuchi, T., Kurumizaka, H. & Miyagawa, K. Human Rad54B is a double-stranded DNA-dependent ATPase and has biochemical properties different from its structural homolog in yeast, Tid1/Rdh54. *Nucleic Acids Res.* **30**, 1346–1353 (2002).
557. Wesoly, J. *et al.* Differential Contributions of Mammalian Rad54 Paralogs to Recombination, DNA Damage Repair, and Meiosis. *Mol. Cell. Biol.* **26**, 976–989 (2006).
558. Zhang, Z., Fan, H. Y., Goldman, J. A. & Kingston, R. E. Homology-driven chromatin remodeling by human RAD54. *Nat. Struct. Mol. Biol.* **14**, 397–405 (2007).
559. Tan, T. L. R. *et al.* Mouse Rad54 affects DNA conformation and DNA-damage-induced Rad51 foci formation. *Curr. Biol.* **9**, 325–328 (1999).
560. Murzik, U. *et al.* Rad54B targeting to DNA double-strand break repair sites requires complex formation with S100A11. *Mol. Biol. Cell* **19**, 2926–2935 (2008).
561. Essers, J. *et al.* Disruption of mouse RAD54 reduces ionizing radiation resistance and homologous recombination. *Cell* **89**, 195–204 (1997).
562. Messiaen, S. *et al.* Rad54 is required for the normal development of male and female germ cells and contributes to the maintainance of their genome integrity after genotoxic stress. *Cell Death Dis. 2013 48* **4**, e774–e774 (2013).
563. Russo, A., Cordelli, E., Salvitti, T., Palumbo, E. & Pacchierotti, F. Rad54/Rad54B deficiency is associated

to increased chromosome breakage in mouse spermatocytes. *Mutagenesis* **33**, 323–332 (2018).
564. Sehorn, M. G., Sigurdsson, S., Bussen, W., Unger, V. M. & Sung, P. Human meiotic recombinase Dmc1 promotes ATP-dependent homologous DNA strand exchange. *Nature* **429**, 433–437 (2004).
565. Sarai, N. *et al.* Stimulation of Dmc1-mediated DNA strand exchange by the human Rad54B protein. *Nucleic Acids Res.* **34**, 4429–4437 (2006).
566. Shaked, H., Avivi-Ragolsky, N. & Levy, A. A. Involvement of the arabidopsis SWI2/SNF2 chromatin remodeling gene family in DNA damage response and recombination. *Genetics* **173**, 985–994 (2006).
567. Klutstein, M. *et al.* Functional conservation of the yeast and Arabidopsis RAD54-like genes. *Genetics* **178**, 2389–2397 (2008).
568. Hirakawa, T., Katagiri, Y., Ando, T. & Matsunaga, S. DNA double-strand breaks alter the spatial arrangement of homologous loci in plant cells. *Sci. Rep.* **5**, 1–8 (2015).
569. Hirakawa, T., Hasegawa, J., White, C. I. & Matsunaga, S. RAD54 forms DNA repair foci in response to DNA damage in living plant cells. *Plant J.* **90**, 372–382 (2017).
570. Janssens, F. A. La Theorie de la Chiasmatypie nouvelle interprétation des cinèses de maturation. *Cellule* **25**, 389–411 (1909).
571. Creighton, H. B. & McClintock, B. A Correlation of Cytological and Genetical Crossing-Over in Zea Mays. *Proc. Natl. Acad. Sci.* **17**, 492–497 (1931).
572. Morgan, L. V. A Closed X Chromosome in Drosophila Melanogaster. *Genetics* **18**, 250–283 (1933).
573. Novitski, E. Genetic measures of centromere activity in Drosophila melanogaster. *J. Cell. Physiol. Suppl.* **45**, 151–169 (1955).
574. Haber, J. E., Thorburn, P. C. & Rogers, D. Meiotic and mitotic behavior of dicentric chromosomes in Saccharomyces cerevisiae. *Genetics* **106**, 185–205 (1984).
575. Schwartz, D. Evidence for Sister-Strand Crossing over in Maize. *Genetics* **38**, 251 (1953).
576. Oh, S. D. *et al.* BLM Ortholog, Sgs1, Prevents Aberrant Crossing-over by Suppressing Formation of Multichromatid Joint Molecules. *Cell* **130**, 259–272 (2007).
577. Jessop, L. & Lichten, M. Mus81/Mms4 Endonuclease and Sgs1 Helicase Collaborate to Ensure Proper Recombination Intermediate Metabolism during Meiosis. *Mol. Cell* **31**, 313–323 (2008).
578. Goldfarb, T. & Lichten, M. Frequent and efficient use of the sister chromatid for DNA double-strand break repair during budding yeast meiosis. *PLoS Biol.* **8**, e1000520 (2010).
579. Hyppa, R. W. & Smith, G. R. Crossover Invariance Determined by Partner Choice for Meiotic DNA Break Repair. *Cell* **142**, 243–255 (2010).
580. Taylor, J. H. Distribution of tritium-labeled dna among chromosomes during meiosis I. Spermatogenesis in the grasshopper. *J. Cell Biol.* **25**, 41–55 (1965).
581. Craig-Cameron, T. & Jones, G. H. The analysis of exchanges in tritium-labelled meiotic chromosomes 1. Schistocerca gregaria. *Heredity (Edinb).* **25**, 223–232 (1970).
582. Jones, G. H. The analysis of exchanges in tritium-labelled meiotic chromosomes - II. Stethophyma grossum. *Chromosoma* **34**, 367–382 (1971).
583. Jones, G. H. & Tease, C. Analysis of exchanges in differentially stained meiotic chromosomes of Locusta migratoria after BrdU-substitution and FPG staining - IV. The nature of 'terminal' associations. *Chromosoma* **89**, 33–36 (1984).
584. Allen, J. W. & Latt, S. A. An in vivo 5 bromodeoxyuridine 33258 Hoechst method for analysis of replication kinetics and sister chromatid exchange formation in mouse spermatogonia and bone marrow. *J. Cell Biol.* **70**, 325–340 (1976).
585. Allen, J. W. BrdU-dye characterization of late replication and meiotic recombination in Armenian hamster germ cells. *Chromosoma* **74**, 189–207 (1979).
586. Almanzar, D. E., Gordon, S. G. & Rog, O. Meiotic sister chromatid exchanges are rare in C. elegans. *Curr. Biol.* **31**, 1499-1507.e3 (2021).
587. Ahuja, J. S., Harvey, C. S., Wheeler, D. L. & Lichten, M. Repeated strand invasion and extensive branch migration are hallmarks of meiotic recombination. *Mol. Cell* **81**, 4258-4270.e4 (2021).
588. Hunter, N. & Kleckner, N. The single-end invasion: An asymmetric intermediate at the double-strand break to double-holliday junction transition of meiotic recombination. *Cell* **106**, 59–70 (2001).
589. Bzymek, M., Thayer, N. H., Oh, S. D., Kleckner, N. & Hunter, N. Double holliday junctions are intermediates of DNA break repair. *Nature* **464**, 937–941 (2010).
590. Hunter, N. Meiotic recombination: The essence of heredity. *Cold Spring Harb. Perspect. Biol.* **7**, (2015).
591. Pyatnitskaya, A., Borde, V. & De Muyt, A. Crossing and zipping: molecular duties of the ZMM proteins in meiosis. *Chromosoma* **128**, 181–198 (2019).
592. Higgins, J. D., Armstrong, S. J., Franklin, F. C. H. & Jones, G. H. The Arabidopsis MutS homolog AtMSH4 functions at an early step in recombination: Evidence for two classes of recombination in Arabidopsis. *Genes Dev.* **18**, 2557–2570 (2004).

593. Chen, C., Zhang, W., Timofejeva, L., Gerardin, Y. & Ma, H. The Arabidopsis ROCK-N-ROLLERS gene encodes a homolog of the yeast ATP-dependent DNA helicase MER3 and is required for normal meiotic crossover formation. *Plant J.* **43**, 321–334 (2005).
594. Mercier, R. *et al.* Two meiotic crossover classes cohabit in Arabidopsis: One is dependent on MER3, whereas the other one is not. *Curr. Biol.* **15**, 692–701 (2005).
595. Wijeratne, A. J., Chen, C., Zhang, W., Timofejeva, L. & Ma, H. The Arabidopsis thaliana PARTING DANCERS gene encoding a novel protein is required for normal meiotic homologous recombination. *Mol. Biol. Cell* **17**, 1331–1343 (2006).
596. Macaisne, N., Vignard, J. & Mercier, R. SHOC1 and PTD form an XPF-ERCC1-like complex that is required for formation of class I crossovers. *J. Cell Sci.* **124**, 2687–2691 (2011).
597. Chelysheva, L. *et al.* Zip4/Spo22 is required for class I CO formation but not for synapsis completion in Arabidopsis thaliana. *PLoS Genet.* **3**, 802–813 (2007).
598. Lu, X. *et al.* The Arabidopsis MutS homolog AtMSH5 is required for normal meiosis. *Cell Res.* **18**, 589–599 (2008).
599. Macaisne, N. *et al.* SHOC1, an XPF Endonuclease-Related Protein, Is Essential for the Formation of Class I Meiotic Crossovers. *Curr. Biol.* **18**, 1432–1437 (2008).
600. Chelysheva, L. *et al.* The Arabidopsis HEI10 is a new ZMM protein related to Zip3. *PLoS Genet.* **8**, 1539–47 (2012).
601. Higgins, J. D., Buckling, E. F., Franklin, F. C. H. & Jones, G. H. Expression and functional analysis of AtMUS81 in Arabidopsis meiosis reveals a role in the second pathway of crossing-over. *Plant J.* **54**, 152–162 (2008).
602. Börner, G. V., Kleckner, N. & Hunter, N. Crossover/noncrossover differentiation, synaptonemal complex formation, and regulatory surveillance at the leptotene/zygotene transition of meiosis. *Cell* **117**, 29–45 (2004).
603. Mancera, E., Bourgon, R., Brozzi, A., Huber, W. & Steinmetz, L. M. High-resolution mapping of meiotic crossovers and non-crossovers in yeast. *Nature* **454**, 479–485 (2008).
604. Chen, S. Y. *et al.* Global Analysis of the Meiotic Crossover Landscape. *Dev. Cell* **15**, 401–415 (2008).
605. Oke, A., Anderson, C. M., Yam, P. & Fung, J. C. Controlling Meiotic Recombinational Repair – Specifying the Roles of ZMMs, Sgs1 and Mus81/Mms4 in Crossover Formation. *PLoS Genet.* **10**, 1539–47 (2014).
606. Argueso, J. L., Wanat, J., Gemici, Z. & Alani, E. Competing crossover pathways act during meiosis in Saccharomyces cerevisiae. *Genetics* **168**, 1805–1816 (2004).
607. De los Santos, T. *et al.* The MUS81/MMS4 endonuclease acts independently of double-holliday junction resolution to promote a distinct subset of crossovers during meiosis in budding yeast. *Genetics* **164**, 81–94 (2003).
608. Nakagawa, T., Flores-Rozas, H. & Kolodner, R. D. The MER3 Helicase Involved in Meiotic Crossing Over Is Stimulated by Single-stranded DNA-binding Proteins and Unwinds DNA in the 3′ to 5′ Direction. *J. Biol. Chem.* **276**, 31487–31493 (2001).
609. Nakagawa, T. & Kolodner, R. D. The MER3 DNA helicase catalyzes the unwinding of Holliday junctions. *J. Biol. Chem.* **277**, 28019–28024 (2002).
610. Mazina, O. M., Mazin, A. V., Nakagawa, T., Kolodner, R. D. & Kowalczykowski, S. C. Saccharomyces cerevisiae Mer3 helicase stimulates 3′-5′ heteroduplex extension by Rad51: Implications for crossover control in meiotic recombination. *Cell* **117**, 47–56 (2004).
611. Duroc, Y. *et al.* Concerted action of the MutLβ heterodimer and Mer3 helicase regulates the global extent of meiotic gene conversion. *Elife* **6**, 1539–47 (2017).
612. De Muyt, A. *et al.* A meiotic XPF–ERCC1-like complex recognizes joint molecule recombination intermediates to promote crossover formation. *Genes Dev.* **32**, 283–296 (2018).
613. Arora, K. & Corbett, K. D. The conserved XPF:ERCC1-like Zip2:Spo16 complex controls meiotic crossover formation through structure-specific DNA binding. *Nucleic Acids Res.* **47**, 2365–2376 (2019).
614. Cheng, C. H. *et al.* SUMO modifications control assembly of synaptonemal complex and polycomplex in meiosis of Saccharomyces cerevisiae. *Genes Dev.* **20**, 2067–2081 (2006).
615. Qiao, H. *et al.* Antagonistic roles of ubiquitin ligase HEI10 and SUMO ligase RNF212 regulate meiotic recombination. *Nat. Genet.* **46**, 194–199 (2014).
616. De Muyt, A. *et al.* E3 ligase Hei10: A multifaceted structure-based signaling molecule with roles within and beyond meiosis. *Genes Dev.* **28**, 1111–1123 (2014).
617. Gray, S. & Cohen, P. E. Control of Meiotic Crossovers: From Double-Strand Break Formation to Designation. *Annu. Rev. Genet.* **50**, 175–210 (2016).
618. Chelysheva, L. *et al.* The Arabidopsis HEI10 is a new ZMM protein related to Zip3. *PLoS Genet.* **8**, 1539–47 (2012).
619. Nguyen, H., Labella, S., Silva, N., Jantsch, V. & Zetka, M. C. elegans ZHP-4 is required at multiple distinct steps in the formation of crossovers and their transition to segregation competent chiasmata. *PLoS Genet.*

14, e1007776 (2018).
620. Zhang, L., Köhler, S., Rillo-Bohn, R. & Dernburg, A. F. A compartmentalized signaling network mediates crossover control in meiosis. *Elife* **7**, (2018).
621. Ross-Macdonald, P. & Roeder, G. S. Mutation of a meiosis-specific MutS homolog decreases crossing over but not mismatch correction. *Cell* **79**, 1069–1080 (1994).
622. Hollingsworth, N. M., Ponte, L. & Halsey, C. MSH5, a novel MutS homolog, facilitates meiotic reciprocal recombination between homologs in Saccharomyces cerevisiae but not mismatch repair. *Genes Dev.* **9**, 1728–1739 (1995).
623. Manhart, C. M. & Alani, E. Roles for mismatch repair family proteins in promoting meiotic crossing over. *DNA Repair (Amst).* **38**, 84–93 (2016).
624. Santucci-Darmanin, S. *et al.* MSH4 acts in conjunction with MLH1 during mammalian meiosis. *FASEB J.* **14**, 1539–1547 (2000).
625. Santucci-Darmanin, S. *et al.* The DNA mismatch-repair MLH3 protein interacts with MSH4 in meiotic cells, supporting a role for this MutL homolog in mammalian meiotic recombination. *Hum. Mol. Genet.* **11**, 1697–1706 (2002).
626. Sym, M., Engebrecht, J. A. & Roeder, G. S. ZIP1 is a synaptonemal complex protein required for meiotic chromosome synapsis. *Cell* **72**, 365–378 (1993).
627. Tung, K. S. & Roeder, G. S. Meiotic chromosome morphology and behavior in zip1 mutants of Saccharomyces cerevisiae. *Genetics* **149**, 817–832 (1998).
628. De Vries, F. A. T. *et al.* Mouse Sycp1 functions in synaptonemal complex assembly, meiotic recombination, and XY body formation. *Genes Dev.* **19**, 1376–1389 (2005).
629. Serrentino, M. E., Chaplais, E., Sommermeyer, V. & Borde, V. Differential Association of the Conserved SUMO Ligase Zip3 with Meiotic Double-Strand Break Sites Reveals Regional Variations in the Outcome of Meiotic Recombination. *PLoS Genet.* **9**, e1003416 (2013).
630. Chen, X. *et al.* Phosphorylation of the Synaptonemal Complex Protein Zip1 Regulates the Crossover/Noncrossover Decision during Yeast Meiosis. *PLoS Biol.* **13**, (2015).
631. Voelkel-Meiman, K., Cheng, S. Y., Morehouse, S. J. & Macqueen, A. J. Synaptonemal complex proteins of budding yeast define reciprocal roles in MutSγ-mediated crossover formation. *Genetics* **203**, 1091–1103 (2016).
632. Otto, S. P. & Payseur, B. A. Crossover Interference: Shedding Light on the Evolution of Recombination. *Annu. Rev. Genet.* **53**, 19–44 (2019).
633. Kan, R. *et al.* Comparative analysis of meiotic progression in female mice bearing mutations in genes of the DNA mismatch repair pathway. *Biol. Reprod.* **78**, 462–471 (2008).
634. Dion, É., Li, L., Jean, M. & Belzile, F. An Arabidopsis MLH1 mutant exhibits reproductive defects and reveals a dual role for this gene in mitotic recombination. *Plant J.* **51**, 431–440 (2007).
635. Rogacheva, M. V. *et al.* Mlh1-Mlh3, a meiotic crossover and DNA mismatch repair factor,is a Msh2-Msh3-stimulated endonuclease. *J. Biol. Chem.* **289**, 5664–5673 (2014).
636. Ranjha, L., Anand, R. & Cejka, P. The Saccharomyces cerevisiae Mlh1-Mlh3 heterodimer is an endonuclease that preferentially binds to holliday junctions. *J. Biol. Chem.* **289**, 5674–5686 (2014).
637. Manhart, C. M. *et al.* The mismatch repair and meiotic recombination endonuclease Mlh1-Mlh3 is activated by polymer formation and can cleave DNA substrates in trans. *PLoS Biol.* **15**, e2001164 (2017).
638. Schaetzlein, S. *et al.* Mammalian Exo1 encodes both structural and catalytic functions that play distinct roles in essential biological processes. *Proc. Natl. Acad. Sci. U. S. A.* **110**, E2470–E2479 (2013).
639. Kulkarni, D. S. *et al.* PCNA activates the MutLγ endonuclease to promote meiotic crossing over. *Nature* **586**, 623–627 (2020).
640. Cannavo, E. *et al.* Regulation of the MLH1–MLH3 endonuclease in meiosis. *Nature* **586**, 618–622 (2020).
641. Sanchez, A. *et al.* Exo1 recruits Cdc5 polo kinase to MutLγ to ensure efficient meiotic crossover formation. *Proc. Natl. Acad. Sci. U. S. A.* **117**, 30577–30588 (2020).
642. Santucci-Darmanin, S. *et al.* The DNA mismatch-repair MLH3 protein interacts with MSH4 in meiotic cells, supporting a role for this MutL homolog in mammalian meiotic recombination. *Hum. Mol. Genet.* **11**, 1697–1706 (2002).
643. Pluciennik, A. *et al.* PCNA function in the activation and strand direction of MutLα endonuclease in mismatch repair. *Proc. Natl. Acad. Sci. U. S. A.* **107**, 16066–16071 (2010).
644. Al-Sweel, N. *et al.* Mlh3 Mutations in Baker'S Yeast Alter Meiotic Recombination Outcomes By Increasing Noncrossover Events Genome-Wide. *PLoS Genet.* **13**, e1006974 (2017).
645. Franklin, F. C. H. *et al.* Control of meiotic recombination in Arabidopsis: Role of the MutL and MutS homologues. *Biochem. Soc. Trans.* **34**, 542–544 (2006).
646. Osman, F., Dixon, J., Doe, C. L. & Whitby, M. C. Generating crossovers by resolution of nicked Holliday junctions: A role for Mus81-Eme1 in meiosis. *Mol. Cell* **12**, 761–774 (2003).

647. Mercier, R. *et al.* Two meiotic crossover classes cohabit in Arabidopsis: One is dependent on MER3, whereas the other one is not. *Curr. Biol.* **15**, 692–701 (2005).
648. Falquet, B. & Rass, U. Structure-specific endonucleases and the resolution of chromosome underreplication. *Genes (Basel).* **10**, (2019).
649. Matos, J., Blanco, M. G., Maslen, S., Skehel, J. M. & West, S. C. Regulatory control of the resolution of DNA recombination intermediates during meiosis and mitosis. *Cell* **147**, 158–172 (2011).
650. De Muyt, A. *et al.* BLM Helicase Ortholog Sgs1 Is a Central Regulator of Meiotic Recombination Intermediate Metabolism. *Mol. Cell* **46**, 43–53 (2012).
651. Zakharyevich, K., Tang, S., Ma, Y. & Hunter, N. Delineation of joint molecule resolution pathways in meiosis identifies a crossover-specific resolvase. *Cell* **149**, 334–347 (2012).
652. Arter, M. *et al.* Regulated Crossing-Over Requires Inactivation of Yen1/GEN1 Resolvase during Meiotic Prophase I. *Dev. Cell* **45**, 785-800.e6 (2018).
653. Alonso-Ramos, P. *et al.* The cdc14 phosphatase controls resolution of recombination intermediates and crossover formation during meiosis. *Int. J. Mol. Sci.* **22**, (2021).
654. Bauknecht, M. & Kobbe, D. AtGEN1 and AtSEND1, Two Paralogs in Arabidopsis, Possess Holliday Junction Resolvase Activity. *Plant Physiol.* **166**, 202–216 (2014).
655. Mullen, J. R., Kaliraman, V., Ibrahim, S. S. & Brill, S. J. Requirement for three novel protein complexes in the absence of the Sgs1 DNA helicase in Saccharomyces cerevisiae. *Genetics* **157**, 103–118 (2001).
656. Ciccia, A., Constantinou, A. & West, S. C. Identification and Characterization of the Human Mus81-Emel Endonuclease. *J. Biol. Chem.* **278**, 25172–25178 (2003).
657. Gaskell, L. J., Osman, F., Gilbert, R. J. C. & Whitby, M. C. Mus81 cleavage of Holliday junctions: A failsafe for processing meiotic recombination intermediates? *EMBO J.* **26**, 1891–1901 (2007).
658. Hollingsworth, N. M. & Brill, S. J. The Mus81 solution to resolution: Generating meiotic crossovers without Holliday junctions. *Genes Dev.* **18**, 117–125 (2004).
659. Boddy, M. N. *et al.* Mus81-Eme1 are essential components of a Holliday junction resolvase. *Cell* **107**, 537–548 (2001).
660. Smith, G. R., Boddy, M. N., Shanahan, P. & Russell, P. Fission Yeast Mus81 · Eme1 Holliday Junction Resolvase Is Required for Meiotic Crossing over but Not for Gene Conversion. *Genetics* **165**, 2289–2293 (2003).
661. Cromie, G. A. *et al.* Single Holliday Junctions Are Intermediates of Meiotic Recombination. *Cell* **127**, 1167–1178 (2006).
662. Trowbridge, K., McKim, K., Brill, S. J. & Sekelsky, J. Synthetic lethality of drosophila in the absence of the MUS81 endonuclease and the DmBlm helicase is associated with elevated apoptosis. *Genetics* **176**, 1993–2001 (2007).
663. Berchowitz, L. E., Francis, K. E., Bey, A. L. & Copenhaver, G. P. The Role of AtMUS81 in Interference-Insensitive Crossovers in Arabidopsis thailana. *PLoS Genet.* e132 (2005).
664. Higgins, J. D., Buckling, E. F., Franklin, F. C. H. & Jones, G. H. Expression and functional analysis of AtMUS81 in Arabidopsis meiosis reveals a role in the second pathway of crossing-over. *Plant J.* **54**, 152–162 (2008).
665. Holloway, J. K., Booth, J., Edelmann, W., McGowan, C. H. & Cohen, P. E. MUS81 generates a subset of MLH1-MLH3-independent crossovers in mammalian meiosis. *PLoS Genet.* **4**, e1000186 (2008).
666. Castor, D. *et al.* Cooperative control of holliday junction resolution and DNA Repair by the SLX1 and MUS81-EME1 nucleases. *Mol. Cell* **52**, 221–233 (2013).
667. Holloway, J. K. *et al.* Mammalian BTBD12 (SLX4) protects against genomic instability during mammalian spermatogenesis. *PLoS Genet.* **7**, e1002094 (2011).
668. Higashide, M. & Shinohara, M. Budding yeast SLX4 contributes to the appropriate distribution of crossovers and meiotic double-strand break formation on bivalents during meiosis. *G3 Genes, Genomes, Genet.* **6**, 2033–2042 (2016).
669. Guervilly, J. H. & Gaillard, P. H. SLX4: multitasking to maintain genome stability. *Crit. Rev. Biochem. Mol. Biol.* **53**, 475–514 (2018).
670. Saito, T. T., Youds, J. L., Boulton, S. J. & Colaiácovo, M. P. Caenorhabditis elegans HIM-18/SLX-4 interacts with SLX-1 and XPF-1 and maintains genomic integrity in the germline by processing recombination intermediates. *PLoS Genet.* **5**, 1000735 (2009).
671. Saito, T. T., Lui, D. Y., Kim, H. M., Meyer, K. & Colaiácovo, M. P. Interplay between Structure-Specific Endonucleases for Crossover Control during Caenorhabditis elegans Meiosis. *PLoS Genet.* **9**, 1003586 (2013).
672. Agostinho, A. *et al.* Combinatorial Regulation of Meiotic Holliday Junction Resolution in C. elegans by HIM-6 (BLM) Helicase, SLX-4, and the SLX-1, MUS-81 and XPF-1 Nucleases. *PLoS Genet.* **9**, 1003591 (2013).
673. Van Brabant, A. J. *et al.* Binding and melting of D-loops by the Bloom syndrome helicase. *Biochemistry* **39**, 14617–14625 (2000).

674. Karow, J. K., Constantinou, A., Li, J. L., West, S. C. & Hickson, I. D. The Bloom's syndrome gene product promotes branch migration of Holliday junctions. *Proc. Natl. Acad. Sci. U. S. A.* **97**, 6504–6508 (2000).
675. Bachrati, C. Z., Borts, R. H. & Hickson, I. D. Mobile D-loops are a preferred substrate for the Bloom's syndrome helicase. *Nucleic Acids Res.* **34**, 2269–2279 (2006).
676. Ira, G., Malkova, A., Liberi, G., Foiani, M. & Haber, J. E. Srs2 and Sgs1-Top3 Suppress Crossovers during Double-Strand Break Repair in Yeast. *Cell* **115**, 401–411 (2003).
677. Wu, L. & Hickson, I. O. The Bloom's syndrome helicase suppresses crossing over during homologous recombination. *Nature* **426**, 870–874 (2003).
678. Wu, L. *et al.* BLAP75/RMI1 promotes the BLM-dependent dissolution of homologous recombination intermediates. *Proc. Natl. Acad. Sci. U. S. A.* **103**, 4068–4073 (2006).
679. Bussen, W., Raynard, S., Busygina, V., Singh, A. K. & Sung, P. Holliday junction processing activity of the BLM-Topo IIIα-BLAP75 complex. *J. Biol. Chem.* **282**, 31484–31492 (2007).
680. Xu, D. *et al.* RMI, a new OB-fold complex essential for Bloom syndrome protein to maintain genome stability. *Genes Dev.* **22**, 2843–2855 (2008).
681. Singh, T. R. *et al.* BLAP18/RMI2, a novel OB-fold-containing protein, is an essential component of the Bloom helicase-double Holliday junction dissolvasome. *Genes Dev.* **22**, 2856–2868 (2008).
682. Bocquet, N. *et al.* Structural and mechanistic insight into Holliday-junction dissolution by Topoisomerase IIIα and RMI1. *Nat. Struct. Mol. Biol.* **21**, 261–268 (2014).
683. Jessop, L., Rockmill, B., Roeder, G. S. & Lichten, M. Meiotic chromosome synapsis-promoting proteins antagonize the anti-crossover activity of sgs1. *PLoS Genet.* **2**, 1402–1412 (2006).
684. Holloway, J. K., Morelli, M. A., Borst, P. L. & Cohen, P. E. Mammalian BLM helicase is critical for integrating multiple pathways of meiotic recombination. *J. Cell Biol.* **188**, 779–789 (2010).
685. Tang, S., Wu, M. K. Y., Zhang, R. & Hunter, N. Pervasive and essential roles of the top3-rmi1 decatenase orchestrate recombination and facilitate chromosome segregation in meiosis. *Mol. Cell* **57**, 607–621 (2015).
686. Kaur, H., DeMuyt, A. & Lichten, M. Top3-Rmi1 DNA single-strand decatenase is integral to the formation and resolution of meiotic recombination intermediates. *Mol. Cell* **57**, 583–594 (2015).
687. Grigaitis, R. *et al.* Phosphorylation of the RecQ Helicase Sgs1/BLM Controls Its DNA Unwinding Activity during Meiosis and Mitosis. *Dev. Cell* **53**, 706-723.e5 (2020).
688. Higgins, J. D., Ferdous, M., Osman, K. & Franklin, F. C. H. The RecQ helicase AtRECQ4A is required to remove inter-chromosomal telomeric connections that arise during meiotic recombination in Arabidopsis. *Plant J.* **65**, 492–502 (2011).
689. Serra, H. *et al.* Massive crossover elevation via combination of HEI10 and recq4a recq4b during Arabidopsis meiosis. *Proc. Natl. Acad. Sci. U. S. A.* **115**, 2437–2442 (2018).
690. Chelysheva, L., Vezon, D., Belcram, K., Gendrot, G. & Grelon, M. The Arabidopsis BLAP75/Rmi1 homologue plays crucial roles in meiotic double-strand break repair. *PLoS Genet.* **4**, e1000309 (2008).
691. Dorn, A. *et al.* The topoisomerase 3α zinc-finger domain T1 of Arabidopsis thaliana is required for targeting the enzyme activity to Holliday junction-like DNA repair intermediates. *PLoS Genet.* **14**, e1007674 (2018).
692. Gari, K., Décaillet, C., Delannoy, M., Wu, L. & Constantinou, A. Remodeling of DNA replication structures by the branch point translocase FANCM. *Proc. Natl. Acad. Sci. U. S. A.* **105**, 16107–16112 (2008).
693. Prakash, R. *et al.* Yeast Mphl helicase dissociates Rad51-made D-loops: Implications for crossover control in mitotic recombination. *Genes Dev.* **23**, 67–79 (2009).
694. Crismani, W. *et al.* FANCM limits meiotic crossovers. *Science (80-.).* **336**, 1588–1590 (2012).
695. Fernandes, J. B., Séguéla-Arnaud, M., Larchevêque, C., Lloyd, A. H. & Mercier, R. Unleashing meiotic crossovers in hybrid plants. *Proc. Natl. Acad. Sci. U. S. A.* **115**, 2431–2436 (2018).
696. Dangel, N. J., Knoll, A. & Puchta, H. MHF1 plays Fanconi anaemia complementation group M protein (FANCM)-dependent and FANCM-independent roles in DNA repair and homologous recombination in plants. *Plant J.* **78**, 822–833 (2014).
697. Girard, C. *et al.* FANCM-associated proteins MHF1 and MHF2, but not the other Fanconi anemia factors, limit meiotic crossovers. *Nucleic Acids Res.* **42**, 9087–9095 (2014).
698. Blary, A. & Jenczewski, E. Manipulation of crossover frequency and distribution for plant breeding. *Theor. Appl. Genet.* **132**, 575–592 (2019).
699. Lorenz, A. *et al.* The fission yeast FANCM ortholog directs non-crossover recombination during meiosis. *Science (80-.).* **336**, 1585–1588 (2012).
700. Sandhu, R. *et al.* DNA Helicase Mph1FANCM Ensures Meiotic Recombination between Parental Chromosomes by Dissociating Precocious Displacement Loops. *Dev. Cell* **53**, 458-472.e5 (2020).
701. Girard, C. *et al.* AAA-ATPase FIDGETIN-LIKE 1 and Helicase FANCM Antagonize Meiotic Crossovers by Distinct Mechanisms. *PLoS Genet.* **11**, e1005369 (2015).
702. Kumar, R., Duhamel, M., Coutant, E., Ben-Nahia, E. & Mercier, R. Antagonism between BRCA2 and FIGL1 regulates homologous recombination. *Nucleic Acids Res.* **47**, 5170–5180 (2019).

703. Yuan, J. & Chen, J. FIGNL1-containing protein complex is required for efficient homologous recombination repair. *Proc. Natl. Acad. Sci. U. S. A.* **110**, 10640–10645 (2013).
704. Matsuzaki, K., Kondo, S., Ishikawa, T. & Shinohara, A. Human RAD51 paralogue SWSAP1 fosters RAD51 filament by regulating the anti-recombinase FIGNL1 AAA+ ATPase. *Nat. Commun.* **10**, 1–15 (2019).
705. Martini, E., Diaz, R. L., Hunter, N. & Keeney, S. Crossover Homeostasis in Yeast Meiosis. *Cell* **126**, 285–295 (2006).
706. Cole, F. *et al.* Homeostatic control of recombination is implemented progressively in mouse meiosis. *Nat. Cell Biol.* **14**, 424–430 (2012).
707. Rosu, S., Libuda, D. E. & Villeneuve, A. M. Robust crossover assurance and regulated interhomolog access maintain meiotic crossover number. *Science (80-.).* **334**, 1286–1289 (2011).
708. Sidhu, G. K. *et al.* Recombination patterns in maize reveal limits to crossover homeostasis. *Proc. Natl. Acad. Sci. U. S. A.* **112**, 15982–15987 (2015).
709. Anderson, C. M., Oke, A., Yam, P., Zhuge, T. & Fung, J. C. Reduced Crossover Interference and Increased ZMM-Independent Recombination in the Absence of Tel1/ATM. *PLoS Genet.* **11**, (2015).
710. Barchi, M. *et al.* ATM promotes the obligate XY crossover and both crossover control and chromosome axis integrity on autosomes. *PLoS Genet.* **4**, 1000076 (2008).
711. Varas, J., Sánchez-Morán, E., Copenhaver, G. P., Santos, J. L. & Pradillo, M. Analysis of the Relationships between DNA Double-Strand Breaks, Synaptonemal Complex and Crossovers Using the Atfas1-4 Mutant. *PLoS Genet.* **11**, (2015).
712. Brandvain, Y. & Coop, G. Scrambling eggs: Meiotic drive and the evolution of female recombination rates. *Genetics* **190**, 709–723 (2012).
713. Popa, A., Samollow, P., Gautier, C. & Mouchiroud, D. The sex-specific impact of meiotic recombination on nucleotide composition. *Genome Biol. Evol.* **4**, 412–422 (2012).
714. Bherer, C., Campbell, C. L. & Auton, A. Refined genetic maps reveal sexual dimorphism in human meiotic recombination at multiple scales. *Nat. Commun.* **8**, (2017).
715. Paigen, K. *et al.* The recombinational anatomy of a mouse chromosome. *PLoS Genet.* **4**, e1000119 (2008).
716. Brick, K. *et al.* Extensive sex differences at the initiation of genetic recombination. *Nature* **561**, 338–342 (2018).
717. Vizir, I. & Korol, A. B. Sex difference in recombination frequency in arabidopsis. *Heredity (Edinb).* **65**, 379–383 (1990).
718. Giraut, L. *et al.* Genome-wide crossover distribution in Arabidopsis thaliana meiosis reveals sex-specific patterns along chromosomes. *PLoS Genet.* **7**, 1002354 (2011).
719. Lynn, A. *et al.* Covariation of synaptonemal complex length and mammalian meiotic exchange rates. *Science (80-.).* **296**, 2222–2225 (2002).
720. Tease, C. & Hultén, M. A. Inter-sex variation in synaptonemal complex lengths largely determine the different recombination rates in male and female germ cells. *Cytogenet. Genome Res.* **107**, 208–215 (2004).
721. Wang, R. J., Dumont, B. L., Jing, P. & Payseur, B. A. A first genetic portrait of synaptonemal complex variatino. *PLoS Genet.* **15**, e1008337 (2019).
722. Madison, B. S., Nath, S., Flanagan, M. K. & Dorsey, B. A. Sexual dimorphism of synaptonemal complex length among populations of threespine stickleback fish. *bioRxiv* 2020.07.30.228825 (2021).
723. Morgan, C. *et al.* Diffusion-mediated HEI10 coarsening can explain meiotic crossover positioning in Arabidopsis. *Nat. Commun.* **12**, 1–11 (2021).
724. Drouaud, J. *et al.* Sex-specific crossover distributions and variations in interference level along Arabidopsis thaliana chromosome 4. *PLoS Genet.* **3**, 1096–1107 (2007).
725. Zickler, D. & Kleckner, N. A few of our favorite things: Pairing, the bouquet, crossover interference and evolution of meiosis. *Semin. Cell Dev. Biol.* **54**, 135–148 (2016).
726. Sturtevant, A. H. The linear arrangement of six sex-linked factors in Drosophila, as shown by their mode of association. *J. Exp. Zool.* **14**, 43–59 (1913).
727. Plough, H. H. The effect of temperature on crossingover in Drosophila. *J. Exp. Zool.* **24**, 147–209 (1917).
728. Francis, K. E. *et al.* Pollen tetrad-based visual assay for meiotic recombination in Arabidopsis. *Proc. Natl. Acad. Sci. U. S. A.* **104**, 3913–3918 (2007).
729. Lloyd, A., Morgan, C., Franklin, F. C. H. & Bomblies, K. Plasticity of meiotic recombination rates in response to temperature in arabidopsis. *Genetics* **208**, 1409–1420 (2018).
730. Modliszewski, J. L. *et al.* Elevated temperature increases meiotic crossover frequency via the interfering (Type I) pathway in Arabidopsis thaliana. *PLoS Genet.* **14**, e1007384 (2018).
731. Weitz, A. P., Dukic, M., Zeitler, L. & Bomblies, K. Male meiotic recombination rate varies with seasonal temperature fluctuations in wild populations of autotetraploid Arabidopsis arenosa. *Mol. Ecol.* **30**, 4630–4641 (2021).
732. De Storme, N. & Geelen, D. High temperatures alter cross-over distribution and induce male meiotic

restitution in Arabidopsis thaliana. *Commun. Biol.* **3**, (2020).
733. Lei, X. *et al.* Heat stress interferes with chromosome segregation and cytokinesis during male meiosis in Arabidopsis thaliana. *Plant Signal. Behav.* **15**, (2020).
734. Si, W. *et al.* Widely distributed hot and cold spots in meiotic recombination as shown by the sequencing of rice F2 plants. *New Phytol.* **206**, 1491–1502 (2015).
735. Prasad, P. V. V. & Djanaguiraman, M. Response of floret fertility and individual grain weight of wheat to high temperature stress: Sensitive stages and thresholds for temperature and duration. *Funct. Plant Biol.* **41**, 1261–1269 (2014).
736. Prasad, P. V. V., Djanaguiraman, M., Perumal, R. & Ciampitti, I. A. Impact of high temperature stress on floret fertility and individual grain weight of grain sorghum: Sensitive stages and thresholds for temperature and duration. *Front. Plant Sci.* **6**, (2015).
737. Phillips, D. *et al.* The effect of temperature on the male and female recombination landscape of barley. *New Phytol.* **208**, 421–429 (2015).
738. Dreissig, S., Mascher, M., Heckmann, S. & Purugganan, M. Variation in Recombination Rate Is Shaped by Domestication and Environmental Conditions in Barley. *Mol. Biol. Evol.* **36**, 2029–2039 (2019).
739. Satomura, K., Osada, N. & Endo, T. Achiasmy and sex chromosome evolution. *Ecol. Genet. Genomics* **13**, (2019).
740. Darlington, C. D. & Dark, S. O. S. The Origin and Behaviour of Chiasmata, II Stenobothrus parallelus. *Cytologia (Tokyo).* **3**, 169–185 (1932).
741. Mather, K. The Determination of Position in Crossing-over. II. *Cytologia (Tokyo).* 514–526 (1937).
742. Murakami, H., Mu, X. & Keeney, S. How do small chromosomes know they are small? Maximizing meiotic break formation on the shortest yeast chromosomes. *Curr. Genet.* **67**, 431–437 (2021).
743. Rosu, S. *et al.* The C. elegans DSB-2 Protein Reveals a Regulatory Network that Controls Competence for Meiotic DSB Formation and Promotes Crossover Assurance. *PLoS Genet.* **9**, e1003674 (2013).
744. Yu, Z., Kim, Y. & Dernburg, A. F. Meiotic recombination and the crossover assurance checkpoint in Caenorhabditis elegans. *Semin. Cell Dev. Biol.* **54**, 106–116 (2016).
745. Duroc, Y. *et al.* The Kinesin AtPSS1 Promotes Synapsis and is Required for Proper Crossover Distribution in Meiosis. *PLoS Genet.* **10**, e1004674 (2014).
746. Morgan, T. H. An attempt to analyze the constitution of the chromosomes on the basis of sex-limited inheritance in Drosophila. *J. Exp. Zool.* **11**, 365–413 (1911).
747. Morgan, T. H. Random segregation versus coupling in Mendelian inheritance. *Science (80-.).* **34**, 384 (1911).
748. Sturtevant, A. H. The behavior of the chromosomes as studied through linkage. *Z. Indukt. Abstamm. Vererbungsl.* **13**, 234–287 (1915).
749. Muller, H. J. The Mechanism of Crossing-Over. *Am. Nat.* **50**, 193–221 (1916).
750. Weinstein, A. Coincidence of Crossing Over in Drosophila Melanogaster (Ampelophila) . *Genetics* **3**, 135–172 (1918).
751. Muller, H. J. The Mechanism of Crossing-Over II. *Am. Nat.* **50**, 284–305 (1916).
752. Pazhayam, N. M., Turcotte, C. A. & Sekelsky, J. Meiotic Crossover Patterning. *Front. Cell Dev. Biol.* **9**, 1–20 (2021).
753. Zickler, D. & Kleckner, N. Recombination, pairing, and synapsis of homologs during meiosis. *Cold Spring Harb. Perspect. Biol.* **7**, 1–28 (2015).
754. King, J. S. & Mortimer, R. K. A polymerization model of chiasma interference and corresponding computer simulation. *Genetics* **126**, 1127–1138 (1990).
755. Kleckner, N. *et al.* A mechanical basis for chromosome function. *Proc. Natl. Acad. Sci. U. S. A.* **101**, 12592–12597 (2004).
756. Lande, R. & Stahl, F. W. Chiasma interference and the distribution of exchanges in Drosophila melanogaster. *Cold Spring Harb. Symp. Quant. Biol.* **58**, 543–552 (1993).
757. Haenel, Q., Laurentino, T. G., Roesti, M. & Berner, D. Meta-analysis of chromosome-scale crossover rate variation in eukaryotes and its significance to evolutionary genomics. *Mol. Ecol.* **27**, 2477–2497 (2018).
758. Zhang, L. *et al.* Topoisomerase II mediates meiotic crossover interference. *Nature* **511**, 551–556 (2014).
759. Talbert, P. B. & Henikoff, S. What makes a centromere? *Exp. Cell Res.* **389**, 111895 (2020).
760. Underwood, C. J. *et al.* Epigenetic activation of meiotic recombination near Arabidopsis thaliana centromeres via loss of H3K9me2 and non-CG DNA methylation. *Genome Res.* **28**, 519–531 (2018).
761. Colomé-Tatché, M. *et al.* Features of the Arabidopsis recombination landscape resulting from the combined loss of sequence variation and DNA methylation. *Proc. Natl. Acad. Sci.* **109**, 16240–16245 (2012).
762. Melamed-Bessudo, C. & Levy, A. A. Deficiency in DNA methylation increases meiotic crossover rates in euchromatic but not in heterochromatic regions in Arabidopsis. *Proc. Natl. Acad. Sci. U. S. A.* **109**, E981–E988 (2012).
763. Mirouze, M. *et al.* Loss of DNA methylation affects the recombination landscape in Arabidopsis. *Proc. Natl.*

Acad. Sci. U. S. A. **109**, 5880–5885 (2012).
764. Yelina, N. E., Choi, K., Chelysheva, L., Macaulay, M. & De Snoo, B. Epigenetic Remodeling of Meiotic Crossover Frequency in Arabidopsis thaliana DNA Methyltransferase Mutants. *PLoS Genet* **8**, 1002844 (2012).
765. Yelina, N. E. *et al.* DNA methylation epigenetically silences crossover hot spots and controls chromosomal domains of meiotic recombination in Arabidopsis. *Genes Dev.* **29**, 2183–2202 (2015).
766. Kianian, P. M. A. *et al.* High-resolution crossover mapping reveals similarities and differences of male and female recombination in maize. *Nat. Commun.* **9**, 1–10 (2018).
767. Gutierrez-Gonzalez, J. J., Mascher, M., Poland, J. & Muehlbauer, G. J. Dense genotyping-by-sequencing linkage maps of two Synthetic W7984×Opata reference populations provide insights into wheat structural diversity. *Sci. Rep.* **9**, 1–15 (2019).
768. Rommel Fuentes, R. *et al.* Meiotic recombination profiling of interspecific hybrid F1 tomato pollen by linked read sequencing. *Plant J.* **102**, 480–492 (2020).
769. Dreissig, S. *et al.* Natural variation in meiotic recombination rate shapes introgression patterns in intraspecific hybrids between wild and domesticated barley. *New Phytol.* **228**, 1852–1863 (2020).
770. Tock, A. J. *et al.* Crossover-active regions of the wheat genome are distinguished by DMC1, the chromosome axis, H3K27me3, and signatures of adaptation. *Genome Res.* **31**, 1614–1628 (2021).
771. Hartmann, M., Umbanhowar, J. & Sekelsky, J. Centromere-proximal meiotic crossovers in drosophila melanogaster are suppressed by both highly repetitive heterochromatin and proximity to the centromere. *Genetics* **213**, 113–125 (2019).
772. Zeng, X. *et al.* Nuclear envelope-associated chromosome dynamics during meiotic prophase I. *Front. Cell Dev. Biol.* **5**, 121 (2018).
773. Pratto, F. *et al.* Recombination initiation maps of individual human genomes. *Science (80-.).* **346**, 1256442 (2014).
774. Liu, H., Maclean, C. J. & Zhang, J. Evolution of the yeast recombination landscape. *Mol. Biol. Evol.* **36**, 412–422 (2019).
775. Li, R. *et al.* A high-resolution map of non-crossover events reveals impacts of genetic diversity on mammalian meiotic recombination. *Nat. Commun.* **10**, 1–15 (2019).
776. Osman, K. *et al.* Distal Bias of Meiotic Crossovers in Hexaploid Bread Wheat Reflects Spatio-Temporal Asymmetry of the Meiotic Program. *Front. Plant Sci.* **12**, 120 (2021).
777. Lambing, C., Kuo, P. C., Tock, A. J., Topp, S. D. & Henderson, I. R. ASY1 acts as a dosage-dependent antagonist of telomere-led recombination and mediates crossover interference in Arabidopsis. *Proc. Natl. Acad. Sci. U. S. A.* **117**, 13647–13658 (2020).
778. Parvanov, E. D., Petkov, P. M. & Paigen, K. Prdm9 controls activation of mammalian recombination hotspots. *Science (80-.).* **327**, 835 (2010).
779. Schwartz, J. J., Roach, D. J., Thomas, J. H. & Shendure, J. Primate evolution of the recombination regulator PRDM9. *Nat. Commun.* **5**, 1–7 (2014).
780. Ahlawat, S. *et al.* Evidence of positive selection and concerted evolution in the rapidly evolving PRDM9 zinc finger domain in goats and sheep. *Anim. Genet.* **47**, 740–751 (2016).
781. Alleva, B., Brick, K., Pratto, F., Huang, M. & Camerini-Otero, R. D. Cataloging Human PRDM9 Allelic Variation Using Long-Read Sequencing Reveals PRDM9 Population Specificity and Two Distinct Groupings of Related Alleles. *Front. Cell Dev. Biol.* **9**, 3058 (2021).
782. Berg, I. L. *et al.* PRDM9 variation strongly influences recombination hot-spot activity and meiotic instability in humans. *Nat. Genet.* **42**, 859–863 (2010).
783. Gerton, J. L. *et al.* Global mapping of meiotic recombination hotspots and coldspots in the yeast Saccharomyces cerevisiae. *Proc. Natl. Acad. Sci. U. S. A.* **97**, 11383–11390 (2000).
784. Smeds, L., Mugal, C. F., Qvarnström, A. & Ellegren, H. High-Resolution Mapping of Crossover and Non-crossover Recombination Events by Whole-Genome Re-sequencing of an Avian Pedigree. *PLoS Genet.* **12**, e1006044 (2016).
785. He, Y. *et al.* Genomic features shaping the landscape of meiotic double-strand-break hotspots in maize. *Proc. Natl. Acad. Sci. U. S. A.* **114**, 12231–12236 (2017).
786. Petes, T. D. Meiotic recombination hot spots and cold spots. *Nat. Rev. Genet.* **2**, 360–369 (2001).
787. Dluzewska, J., Szymanska, M. & Ziolkowski, P. A. Where to Cross Over? Defining Crossover Sites in Plants. *Front. Genet.* **9**, 1–20 (2018).
788. de Boer, E., Jasin, M. & Keeney, S. Local and sex-specific biases in crossover vs. noncrossover outcomes at meiotic recombination hot spots in mice. *Genes Dev.* **29**, 1721–1733 (2015).
789. Duret, L. & Galtier, N. Biased gene conversion and the evolution of mammalian genomic landscapes. *Annu. Rev. Genomics Hum. Genet.* **10**, 285–311 (2009).
790. Giraut, L. *et al.* Genome-wide crossover distribution in Arabidopsis thaliana meiosis reveals sex-specific

patterns along chromosomes. *PLoS Genet.* **7**, 1002354 (2011).
791. Rowan, B. A. *et al.* An ultra high-density arabidopsis thaliana crossover map that refines the influences of structural variation and epigenetic features. *Genetics* **213**, 771–787 (2019).
792. Borts, R. H. & Haber, J. E. Meiotic recombination in yeast: Alteration by multiple heterozygosities. *Science (80-.).* **237**, 1459–1465 (1987).
793. Datta, A., Hendrix, M., Lipsitch, M. & Jinks-Robertson, S. Dual roles for DNA sequence identity and the mismatch repair system in the regulation of mitotic crossing-over in yeast. *Proc. Natl. Acad. Sci. U. S. A.* **94**, 9757–9762 (1997).
794. Chen, W. & Jinks-Robertson, S. The role of the mismatch repair machinery in regulating mitotic and meiotic recombination between diverged sequences in yeast. *Genetics* **151**, 1299–1313 (1999).
795. Spies, M. & Fishel, R. Mismatch repair during homologous and homeologous recombination. *Cold Spring Harb. Perspect. Biol.* **7**, a022657 (2015).
796. Elliott, B. & Jasin, M. Repair of Double-Strand Breaks by Homologous Recombination in Mismatch Repair-Defective Mammalian Cells. *Mol. Cell. Biol.* **21**, 2671–2682 (2001).
797. Li, L., Jean, M. & Belzile, F. The impact of sequence divergence and DNA mismatch repair on homeologous recombination in Arabidopsis. *Plant J.* **45**, 908–916 (2006).
798. Serra, H. *et al.* Interhomolog polymorphism shapes meiotic crossover within the Arabidopsis RAC1 and RPP13 disease resistance genes. *PLoS Genet.* **14**, (2018).
799. Peterson, S. E., Keeney, S. & Jasin, M. Mechanistic Insight into Crossing over during Mouse Meiosis. *Mol. Cell* **78**, 1252-1263.e3 (2020).
800. Ziolkowski, P. A. *et al.* Juxtaposition of heterozygous and homozygous regions causes reciprocal crossover remodelling via interference during Arabidopsis meiosis. *Elife* **4**, (2015).
801. Blackwell, A. R. *et al.* MSH 2 shapes the meiotic crossover landscape in relation to interhomolog polymorphism in Arabidopsis . *EMBO J.* **39**, (2020).
802. Begun, D. J. & Aquadro, C. F. Levels of naturally occurring DNA polymorphism correlate with recombination rates in D. melanogaster. *Nature* **356**, 519–520 (1992).
803. Spencer, C. C. A. *et al.* The influence of recombination on human genetic diversity. *PLoS Genet.* **2**, 1375–1385 (2006).
804. Gore, M. A. *et al.* A first-generation haplotype map of maize. *Science (80-.).* **326**, 1115–1117 (2009).
805. Paape, T. *et al.* Fine-scale population recombination rates, hotspots, and correlates of recombination in the Medicago truncatula genome. *Genome Biol. Evol.* **4**, 726–737 (2012).
806. Cutter, A. D. & Payseur, B. A. Genomic signatures of selection at linked sites: Unifying the disparity among species. *Nat. Rev. Genet.* **14**, 262–274 (2013).
807. Martini, E. *et al.* Genome-wide analysis of heteroduplex DNA in mismatch repair-deficient yeast cells reveals novel properties of meiotic recombination pathways. *PLoS Genet.* **7**, e1002305 (2011).
808. Cooper, T. J. *et al.* Mismatch repair impedes meiotic crossover interference. *bioRxiv* 480418 (2018).
809. Getun, I. V., Wu, Z. K., Khalil, A. M. & Bois, P. R. J. Nucleosome occupancy landscape and dynamics at mouse recombination hotspots. *EMBO Rep.* **11**, 555–560 (2010).
810. Székvölgyi, L., Ohta, K. & Nicolas, A. Initiation of meiotic homologous recombination: Flexibility, impact of histone modifications, and chromatin remodeling. *Cold Spring Harb. Perspect. Biol.* **7**, 1–18 (2015).
811. Storey, A. J. *et al.* Chromatin-mediated regulators of meiotic recombination revealed by proteomics of a recombination hotspot. *Epigenetics and Chromatin* **11**, 1–15 (2018).
812. Luo, Y. *et al.* A plant-specific SWR1 chromatin-remodeling complex couples histone H2A.Z deposition with nucleosome sliding. *EMBO J.* **39**, e102008 (2020).
813. Yamada, S. *et al.* The histone variant H2A.Z promotes initiation of meiotic recombination in fission yeast. *Nucleic Acids Res.* **46**, 609–620 (2018).
814. González-Arranz, S. *et al.* Functional impact of the H2A.Z histone variant during meiosis in Saccharomyces cerevisiae. *Genetics* **209**, 997–1015 (2018).
815. González-Arranz, S. *et al.* SWR1-Independent Association of H2A.Z to the LINC Complex Promotes Meiotic Chromosome Motion. *Front. Cell Dev. Biol.* **8**, 1051 (2020).
816. Malkova, A., Klein, F., Leung, W. Y. & Haber, J. E. HO endonuclease-induced recombination in yeast meiosis resembles Spo11-induced events. *Proc. Natl. Acad. Sci. U. S. A.* **97**, 14500–14505 (2000).
817. Yisehak, L. & MacQueen, A. J. HO endonuclease-initiated recombination in yeast meiosis fails to promote homologous centromere pairing and is not constrained to utilize the Dmc1 recombinase. *G3 Genes, Genomes, Genet.* **8**, 3637–3659 (2018).
818. Neale, M. J., Ramachandran, M., Trelles-Sticken, E., Scherthan, H. & Goldman, A. S. H. Wild-type levels of Spo11-induced DSBs are required for normal single-strand resection during meiosis. *Mol. Cell* **9**, 835–846 (2002).
819. Shodhan, A., Medhi, D. & Lichten, M. Noncanonical contributions of MutLγ to VDE-Initiated crossovers

during Saccharomyces cerevisiae meiosis. *G3 Genes, Genomes, Genet.* **9**, 1647–1654 (2019).
820. Farah, J. A., Cromie, G. A. & Smith, G. R. Ctp1 and Exonuclease 1, alternative nucleases regulated by the MRN complex, are required for efficient meiotic recombination. *Proc. Natl. Acad. Sci.* **106**, 9356–9361 (2009).
821. Ishino, Y., Krupovic, M. & Forterre, P. History of CRISPR-Cas from encounter with a mysterious repeated sequence to genome editing technology. *J. Bacteriol.* **200**, (2018).
822. Kozovska, Z., Rajcaniova, S., Munteanu, P., Dzacovska, S. & Demkova, L. CRISPR: History and perspectives to the future. *Biomed. Pharmacother.* **141**, 111917 (2021).
823. Alonso, J. M. *et al.* Genome-wide insertional mutagenesis of Arabidopsis thaliana. *Science (80-.).* **301**, 653–657 (2003).
824. Pradillo, M. *et al.* Together yes, but not coupled: New insights into the roles of RAD51 and DMC1 in plant meiotic recombination. *Plant J.* **69**, 921–933 (2012).
825. Li, W. *et al.* The Arabidopsis AtRAD51 gene is dispensable for vegetative development but required for meiosis. *Proc. Natl. Acad. Sci. U. S. A.* **101**, 10596–10601 (2004).
826. Berchowitz, L. E. & Copenhaver, G. P. Fluorescent Arabidopsis tetrads: A visual assay for quickly developing large crossover and crossover interference data sets. *Nat. Protoc.* **3**, 41–50 (2008).
827. Mali, P. *et al.* RNA-guided human genome engineering via Cas9. *Science (80-.).* **339**, 823–826 (2013).
828. Curtis, M. D. & Grossniklaus, U. A Gateway Cloning Vector Set for High-Throughput Functional Analysis of Genes in Planta. *Plant Physiol.* **133**, 462–469 (2003).
829. Choi, K., Yelina, N. E., Serra, H. & Henderson, I. R. Quantification and sequencing of crossover recombinant molecules from Arabidopsis pollen DNA. in *Methods in Molecular Biology* **1551**, 23–57 (2017).
830. Lian, Q. *et al.* The megabase-scale crossover landscape is independent of sequence divergence. *bioRxiv* 2022.01.10.474936 (2022).
831. Bourguet, P. *et al.* The histone variant H2A.W and linker histone H1 co-regulate heterochromatin accessibility and DNA methylation. *Nat. Commun.* **12**, 1–12 (2021).
832. Yu, X. *et al.* The BORDER family of negative transcription elongation factors regulates flowering time in Arabidopsis. *Curr. Biol.* **31**, 5377-5384.e5 (2021).
833. Eid, A., Ali, Z. & Mahfouz, M. M. High efficiency of targeted mutagenesis in arabidopsis via meiotic promoter-driven expression of Cas9 endonuclease. *Plant Cell Rep.* **35**, 1555–1558 (2016).
834. Xu, P., Su, H., Chen, W. & Lu, P. The application of a meiocyte-specific CRISPR/Cas9 (MSC) system and a suicide-MSC system in generating inheritable and stable mutations in arabidopsis. *Front. Plant Sci.* **9**, 1007 (2018).
835. Filler-Hayut, S., Kniazev, K., Melamed-Bessudo, C. & Levy, A. A. Targeted inter-homologs recombination in arabidopsis euchromatin and heterochromatin. *Int. J. Mol. Sci.* **22**, 12096 (2021).
836. van Overbeek, M. *et al.* DNA Repair Profiling Reveals Nonrandom Outcomes at Cas9-Mediated Breaks. *Mol. Cell* **63**, 633–646 (2016).
837. Liu, M. *et al.* Global detection of DNA repair outcomes induced by CRISPR-Cas9. *Nucleic Acids Res.* **49**, 8732–8742 (2021).
838. Feng, Z. *et al.* A highly efficient cell division-specific CRISPR/Cas9 system generates homozygous mutants for multiple genes in arabidopsis. *Int. J. Mol. Sci.* **19**, (2018).
839. Desfeux, C., Clough, S. J. & Bent, A. F. Female reproductive tissues are the primary target of Agrobacterium-mediated transformation by the Arabidopsis floral-dip method. *Plant Physiol.* **123**, 895–904 (2000).
840. Klepikova, A. V., Logacheva, M. D., Dmitriev, S. E. & Penin, A. A. RNA-seq analysis of an apical meristem time series reveals a critical point in Arabidopsis thaliana flower initiation. *BMC Genomics* **16**, 1–16 (2015).
841. Klepikova, A. V., Kasianov, A. S., Gerasimov, E. S., Logacheva, M. D. & Penin, A. A. A high resolution map of the Arabidopsis thaliana developmental transcriptome based on RNA-seq profiling. *Plant J.* **88**, 1058–1070 (2016).
842. Qin, Y. *et al.* ACTIN-RELATED PROTEIN6 regulates female meiosis by modulating meiotic gene expression in Arabidopsis. *Plant Cell* **26**, 1612–1628 (2014).
843. Hayashi, M., Chin, G. M. & Villeneuve, A. M. C. elegans germ cells switch between distinct modes of double-strand break repair during meiotic prophase progression. *PLoS Genet.* **3**, 2068–2084 (2007).
844. Stamper, E. L. *et al.* Identification of DSB-1, a Protein Required for Initiation of Meiotic Recombination in Caenorhabditis elegans, Illuminates a Crossover Assurance Checkpoint. *PLoS Genet.* **9**, e1003679 (2013).
845. Sanchez-Moran, E., Santos, J. L., Jones, G. H. & Franklin, F. C. H. ASY1 mediates AtDMC1-dependent interhomolog recombination during meiosis in Arabidopsis. *Genes Dev.* **21**, 2220–2233 (2007).
846. Fowler, K. R., Hyppa, R. W., Cromie, G. A. & Smith, G. R. Physical basis for long-distance communication along meiotic chromosomes. *Proc. Natl. Acad. Sci. U. S. A.* **115**, E9333–E9342 (2018).
847. Mu, X., Murakami, H., Mohibullah, N. & Keeney, S. Chromosome-autonomous feedback down-regulates meiotic DNA break competence upon synaptonemal complex formation. *Genes Dev.* **34**, 1605–1618 (2020).
848. Fukuda, T., Kugou, K., Sasanuma, H., Shibata, T. & Ohta, K. Targeted induction of meiotic double-strand

breaks reveals chromosomal domain-dependent regulation of Spo11 and interactions among potential sites of meiotic recombination. *Nucleic Acids Res.* **36**, 984–997 (2008).
849. Pecia, A. *et al.* Targeted Stimulation of Meiotic Recombination. *Cell* **111**, 173–184 (2002).
850. Murakami, H. & Nicolas, A. Locally, Meiotic Double-Strand Breaks Targeted by Gal4BD-Spo11 Occur at Discrete Sites with a Sequence Preference. *Mol. Cell. Biol.* **29**, 3500–3516 (2009).
851. Sarno, R. *et al.* Programming sites of meiotic crossovers using Spo11 fusion proteins. *Nucleic Acids Res.* **45**, e164–e164 (2017).
852. Yelina, N. E., Gonzalez-Jorge, S., Hirsz, D., Yang, Z. & Henderson, I. R. CRISPR targeting of MEIOTIC-TOPOISOMERASE VIB-dCas9 to a recombination hotspot is insufficient to increase crossover frequency in Arabidopsis. *bioRxiv* 2021.02.01.429210 (2021).
853. Sarno, R. *et al.* Programming sites of meiotic crossovers using Spo11 fusion proteins. *Nucleic Acids Res.* **45**, 1–14 (2017).
854. Hayut, S. F., Bessudo, C. M. & Levy, A. A. Targeted recombination between homologous chromosomes for precise breeding in tomato. *Nat. Commun.* **8**, 1–9 (2017).
855. Kouranov, A. *et al.* Demonstration of targeted crossovers in hybrid maize using CRISPR technology. *Commun. Biol.* **5**, (2022).
856. Beying, N., Schmidt, C., Pacher, M., Houben, A. & Puchta, H. CRISPR–Cas9-mediated induction of heritable chromosomal translocations in Arabidopsis. *Nat. Plants* **6**, 638–645 (2020).
857. Schmidt, C. *et al.* Changing local recombination patterns in Arabidopsis by CRISPR/Cas mediated chromosome engineering. *Nat. Commun.* **11**, 1–8 (2020).
858. Rönspies, M. *et al.* Massive Crossover Suppression by CRISPR-Cas-mediated Plant Chromosome Engineering. *Res. Sq.* 1–13 (2022).
859. Zheng, N. *et al.* CRISPR/Cas9-Based Gene Editing Using Egg Cell-Specific Promoters in Arabidopsis and Soybean. *Front. Plant Sci.* **11**, 800 (2020).
860. Kirkpatrick, D. T., Dominska, M. & Petes, T. D. Conversion-type and restoration-type repair of DNA mismatches formed during meiotic recombination in Saccharomyces cerevisiae. *Genetics* **149**, 1693–1705 (1998).
861. Martini, E. *et al.* Genome-Wide Analysis of Heteroduplex DNA in Mismatch Repair–Deficient Yeast Cells Reveals Novel Properties of Meiotic Recombination Pathways. *PLOS Genet.* **7**, e1002305 (2011).
862. Wijnker, E. *et al.* The genomic landscape of meiotic crossovers and gene conversions in Arabidopsis thaliana. *Elife* **2013**, (2013).
863. Marsolier-Kergoat, M. C., Khan, M. M., Schott, J., Zhu, X. & Llorente, B. Mechanistic View and Genetic Control of DNA Recombination during Meiosis. *Mol. Cell* **70**, 9-20.e6 (2018).
864. Serra, H. *et al.* Interhomolog polymorphism shapes meiotic crossover within the Arabidopsis RAC1 and RPP13 disease resistance genes. *PLoS Genet.* **14**, (2018).
865. Lu, P. *et al.* Analysis of Arabidopsis genome-wide variations before and after meiosis and meiotic recombination by resequencing Landsberg erecta and all four products of a single meiosis. *Genome Res.* **22**, 508–518 (2012).
866. Nidhi, S. *et al.* Novel CRISPR–Cas Systems: An Updated Review of the Current Achievements, Applications, and Future Research Perspectives. *Int. J. Mol. Sci.* **22**, 3327 (2021).
867. Di Stazio, M., Foschi, N., Athanasakis, E., Gasparini, P. & d'Adamo, A. P. Systematic analysis of factors that improve homologous direct repair (HDR) efficiency in CRISPR/Cas9 technique. *PLoS One* **16**, 1–15 (2021).
868. Capdeville, N., Merker, L., Schindele, P. & Puchta, H. Sophisticated CRISPR/Cas tools for fine-tuning plant performance. *J. Plant Physiol.* **257**, 153332 (2021).
869. Hassan, M. M. *et al.* Construct design for CRISPR/Cas-based genome editing in plants. *Trends Plant Sci.* **26**, 1133–1152 (2021).
870. Malik, A. *et al.* Evaluating the cleavage efficacy of CRISPR-Cas9 sgRNAs targeting ineffective regions of Arabidopsis thaliana genome. *PeerJ* **9**, e11409 (2021).
871. Hiranniramol, K., Chen, Y. & Wang, X. CRISPR/Cas9 Guide RNA Design Rules for Predicting Activity. *Methods Mol. Biol.* **2115**, 351–364 (2020).
872. Grützner, R. *et al.* High-efficiency genome editing in plants mediated by a Cas9 gene containing multiple introns. *Plant Commun.* **2**, 100135 (2021).
873. Malzahn, A. A. *et al.* Application of CRISPR-Cas12a temperature sensitivity for improved genome editing in rice, maize, and Arabidopsis. *BMC Biol.* **17**, (2019).
874. LeBlanc, C. *et al.* Increased efficiency of targeted mutagenesis by CRISPR/Cas9 in plants using heat stress. *Plant J.* **93**, 377–386 (2018).
875. Hotta, Y. & Stern, H. Transient phosphorylation of deoxyribosides and regulation of deoxyribonucleic acid synthesis. *J. Biophys. Biochem. Cytol.* **11**, 311–9 (1961).

876. Prensky, W. Uptake of thymine-methyl-H" by pachytene chromosomes of Lilium longiflorum. *Genetics* **47**, 937–997 (1962).
877. Wimber, D. E. & Prensky, W. Autoradiography with meiotic chromosomes of the male newdt (Triturus viridescens) using H3-thymidine. *Genetics* **48**, 1731–8 (1963).
878. Lima-de-Faria, A., German, J., Ghatnekar, M., Mcogovern, J. & Anderson, L. in Vitro Labelling of Human Meiotic Chromosomes With H3-Thymidine. *Hereditas* **60**, 249–261 (1968).
879. Mukherjee, A. B. & Cohen, M. M. DNA synthesis during meiotic prophase in male mice. *Nature* **219**, 489–490 (1968).
880. Holliday, R. A mechanism for gene conversion in fungi. *Genet. Res.* **5**, 282–304 (1964).
881. Meselson, M. S. & Radding, C. M. A general model for genetic recombination. *Proc. Natl. Acad. Sci. U. S. A.* **72**, 358–361 (1975).
882. Carpenter, A. T. C. EM autoradiographic evidence that DNA synthesis occurs at recombination nodules during meiosis in Drosophila melanogaster females. *Chromosoma* **83**, 59–80 (1981).
883. Moses, M. J., Dresser, M. E. & Poorman, P. A. Composition and role of the synaptonemal complex. *Symp. Soc. Exp. Biol.* **38**, 245–70 (1984).
884. Terasawa, M. *et al.* Meiotic recombination-related DNA synthesis and its implications for cross-over and non-cross-over recombinant formation. *Proc. Natl. Acad. Sci. U. S. A.* **104**, 5965–5970 (2007).
885. Loidl, J., Lukaszewicz, A., Howard-Till, R. A. & Koestler, T. The Tetrahymena meiotic chromosome bouquet is organized by centromeres and promotes interhomolog recombination. *J. Cell Sci.* **125**, 5873–5880 (2012).
886. Armstrong, S. J. & Jones, G. H. Meiotic cytology and chromosome behaviour in wild-type Arabidopsis thaliana. *J. Exp. Bot.* **54**, 1–10 (2003).
887. Stronghill, P. E., Azimi, W. & Hasenkampf, C. A. A novel method to follow meiotic progression in Arabidopsis using confocal microscopy and 5-ethynyl-2′-deoxyuridine labeling. *Plant Methods* **10**, 33 (2014).
888. Chen, C. & Retzel, E. F. Analyzing the meiotic transcriptome using isolated meiocytes of arabidopsis thalianaanalyzing the meiotic transcriptome using isolated meiocytes of arabidopsis thaliana. *Methods Mol. Biol.* **990**, 203–213 (2013).
889. Sims, J., Chen, C., Schlögelhofer, P. & Kurzbauer, M. T. Targeted Analysis of Chromatin Events (TACE). *Methods Mol. Biol.* **2061**, 47–58 (2020).
890. Kit Leng Lui, S. *et al.* Monitoring genome-wide replication fork directionality by Okazaki fragment sequencing in mammalian cells. *Nat. Protoc.* **16**, 1193–1218 (2021).
891. Valuchova, S. *et al.* Imaging plant germline differentiation within arabidopsis flowers by light sheet microscopy. *Elife* **9**, (2020).
892. Rossig, C., Le Lievre, L., Pilkington, S. M. & Brownfield, L. A simple and rapid method for imaging male meiotic cells in anthers of model and non-model plant species. *Plant Reprod.* **34**, 37–46 (2021).
893. Armstrong, S. J., Franklin, F. C. H. & Jones, G. H. A meiotic time-course for Arabidopsis thaliana. *Sex. Plant Reprod.* **16**, 141–149 (2003).
894. Varas, J. *et al.* Absence of SUN1 and SUN2 proteins in Arabidopsis thaliana leads to a delay in meiotic progression and defects in synapsis and recombination. *Plant J.* **81**, 329–346 (2015).
895. Lambing, C. *et al.* Arabidopsis PCH2 Mediates Meiotic Chromosome Remodeling and Maturation of Crossovers. *PLoS Genet.* **11**, e1005372 (2015).
896. Dvořáčkova, M. *et al.* Replication of ribosomal DNA in Arabidopsis occurs both inside and outside the nucleolus during S phase progression. *J. Cell Sci.* **131**, (2018).
897. Cavanagh, B. L., Walker, T., Norazit, A. & Meedeniya, A. C. B. Thymidine analogues for tracking DNA synthesis. *Molecules* **16**, 7980–7993 (2011).
898. Ligasová, A. & Koberna, K. DNA replication: From radioisotopes to click chemistry. *Molecules* **23**, (2018).
899. Concia, L. *et al.* Genome-wide analysis of the arabidopsis replication timing program. *Plant Physiol.* **176**, 2166–2185 (2018).
900. Da Ines, O. & White, C. I. Centromere Associations in Meiotic Chromosome Pairing. *Annu. Rev. Genet.* **49**, 95–114 (2015).
901. Koornneef, M., Fransz, P. & De Jong, H. Cytogenetic tools for Arabidopsis thaliana. *Chromosom. Res.* **11**, 183–194 (2003).
902. Singh, A. & Xu, Y. J. The cell killing mechanisms of hydroxyurea. *Genes (Basel).* **7**, (2016).
903. Fuchs, J., Cheblal, A. & Gasser, S. M. Underappreciated Roles of DNA Polymerase δ in Replication Stress Survival. *Trends Genet.* **37**, 476–487 (2021).
904. Costas, C. *et al.* Genome-wide mapping of Arabidopsis thaliana origins of DNA replication and their associated epigenetic marks. *Nat. Struct. Mol. Biol.* **18**, 395–400 (2011).
905. Wheeler, E. *et al.* Arabidopsis DNA replication initiates in intergenic, AT-rich open chromatin. *Plant Physiol.* **183**, 206–220 (2020).
906. Kliszczak, A. E., Rainey, M. D., Harhen, B., Boisvert, F. M. & Santocanale, C. DNA mediated chromatin

pull-down for the study of chromatin replication. *Sci. Rep.* **1**, 1–7 (2011).

907. Chelysheva, L. *et al.* An Easy Protocol for Studying Chromatin and Recombination Protein Dynamics during *Arabidopsisthaliana* Meiosis: Immunodetection of Cohesins, Histones and MLH1. *Cytogenet. Genome Res.* **129**, 143–153 (2010).
908. Sanchez-Rebato, M. H., Bouatta, A. M., Gallego, M. E., White, C. I. & Ines, O. Da. RAD54 is essential for RAD51-mediated repair of meiotic DSB in Arabidopsis. *PLoS Genet.* **17**, (2021).
909. Kurzbauer, M. T. *et al.* Arabidopsis thaliana FANCD2 promotes meiotic crossover formation. *Plant Cell* **30**, 415–428 (2018).
910. Xue, M. *et al.* The Number of Meiotic Double-Strand Breaks Influences Crossover Distribution in Arabidopsis. *Plant Cell* **30**, 2628–2638 (2018).
911. Su, H. *et al.* Arabidopsis RAD51, RAD51C and XRCC3 proteins form a complex and facilitate RAD51 localization on chromosomes for meiotic recombination. *PLoS Genet.* **13**, 1–27 (2017).
912. Sims, J., Schlögelhofer, P. & Kurzbauer, M.-T. From Microscopy to Nanoscopy: Defining an Arabidopsis thaliana Meiotic Atlas at the Nanometer Scale. *Front. Plant Sci.* **0**, 954 (2021).
913. Ribarska, T., Bjørnstad, P. M., Sundaram, A. Y. M. & Gilfillan, G. D. Optimization of enzymatic fragmentation is crucial to maximize genome coverage: a comparison of library preparation methods for Illumina sequencing. *BMC Genomics* **23**, 1–11 (2022).
914. Müller, C. A. *et al.* Capturing the dynamics of genome replication on individual ultra-long nanopore sequence reads. *Nat. Methods* **16**, 429–436 (2019).
915. Georgieva, D., Liu, Q., Wang, K. & Egli, D. Detection of base analogs incorporated during DNA replication by nanopore sequencing. *Nucleic Acids Res.* **48**, E88 (2020).
916. Hennion, M. *et al.* FORK-seq: Replication landscape of the Saccharomyces cerevisiae genome by nanopore sequencing. *Genome Biol.* **21**, 1–25 (2020).
917. Boemo, M. A. DNAscent v2: detecting replication forks in nanopore sequencing data with deep learning. *BMC Genomics* **22**, 1–8 (2021).

SUPPLEMENTARY MATERIAL

Supplementary table 1. Raw numbers of pollen countings in pDMC1::Cas9 lines.

Interval	Target site	Genotype	T1 line	No colour pollen (Parental 1)	Red + Yellow pollen (Parental 2)	Red pollen (Recombinant 1)	Yellow pollen (Recombinant 2)	Genetic distance (cM)
I1b		Cas9- gRNA-		331	304	34	29	9.03
				283	272	32	31	10.19
				574	509	61	57	9.07
				495	445	41	31	7.11
				453	400	56	42	10.30
				731	739	71	69	8.70
		Cas+ gRNA-		463	460	35	39	7.42
				722	711	55	58	7.31
	Site 1	Cas9+ gRNA+	1	502`	492	41	42	7.70
				563	531	55	63	9.73
			2	500	459	37	42	7.61
				391	406	36	42	8.91
			3	775	755	31	37	4.25
	Site 2	Cas9+ gRNA+	1	548	550	47	57	8.65
				392	356	33	25	7.19
				497	495	43	41	7.80
			2	457	469	76	54	12.31
				462	420	81	74	14.94
				467	466	74	71	13.45
			3	284	292	24	19	6.94
				434	413	92	99	18.40
				469	415	64	60	12.30
CEN3		Cas9- gRNA-		653	662	97	123	14.33
				526	593	89	88	13.66
				495	555	84	86	13.93
	Site 1	Cas9+ gRNA+	1	431	430	77	73	14.84
				450	441	57	69	12.39
			2	511	473	72	88	13.99
				449	477	89	77	15.20
				503	505	78	75	13.18
	Site 2	Cas9+ gRNA+	1	469	484	87	90	15.66
			2	514	503	107	106	17.32
				531	524	76	86	13.31
			3	584	588	82	93	13.35
				460	454	87	67	14.42
				461	462	85	69	14.30

Supplementary table 2. Raw numbers of FTL pollen countings in pRAD51::Cas9 lines.

Interval	Target site	Genotype	T1 line	No colour pollen (Parental 1)	Red + Yellow pollen (Parental 2)	Red pollen (Recombinant 1)	Yellow pollen (Recombinant 2)	Genetic distance (cM)
I1b		Cas9- gRNA-		331	304	34	29	9.03
				283	272	32	31	10.19
				574	509	61	57	9.07
				495	445	41	31	7.11
				453	400	56	42	10.30
				731	739	71	69	8.70
		Cas+ gRNA-		463	460	35	39	7.42
				722	711	55	58	7.31
	Site 1	Cas9+ gRNA+	1	476	488	50	49	9.31
				776	792	84	70	8.94
			2	554	546	58	58	9.54
				446	473	73	72	13.63
				465	515	64	61	11.31
			3	1037	1029	78	75	6.90
	Site 2	Cas9+ gRNA+	1	448	465	45	36	8.15
				576	556	50	47	7.89
			2	807	814	77	88	9.24
				427	421	36	31	7.32
				586	549	60	46	8.54
			3	260	287	28	45	11.77
				359	330	31	35	8.47
CEN3		Cas9- gRNA-		653	662	97	123	14.33
				526	593	89	88	13.66
				495	555	84	86	13.93
	Site 1	Cas9+ gRNA+	1	468	455	63	88	14.06
				477	487	90	104	16.75
			2	585	530	97	103	15.21
				485	456	53	58	10.55
				444	459	97	123	19.59
			3	469	473	90	103	17.00
				484	464	74	90	14.75
	Site 2	Cas9+ gRNA+	1	451	420	69	80	14.61
				529	542	138	111	18.86
				457	447	102	106	18.71
			2	498	532	75	73	12.56
				408	416	89	88	17.68
				437	408	84	83	16.50
			3	475	504	84	82	14.50
				436	401	86	97	17.94
				517	485	88	79	14.29

Supplementary table 3. Raw numbers of Illumina reads analysed for I1b - Site 2.

Interval	Target site	PCR	Genotype	Total reads	Col-0 reads (Parental 1)	Ler-0 reads (Parental 2)	Recombinant reads	Recombination rate (%)	Target site-mutated reads	Mutation rate (%)
I1b	Site 2	1	pRAD51::Cas9+ gRNA-	12742	5538	7008	3	0.023	21	0.165
				14386	6286	7850	8	0.056	29	0.202
				14069	5844	7987	13	0.092	32	0.227
				13581	6032	7301	16	0.118	37	0.272
				11914	5151	6576	8	0.067	33	0.276
			pRAD51::Cas+ gRNA+	11537	5053	6280	8	0.069	33	0.286
				9632	4197	5255	5	0.052	24	0.249
				8696	3774	4786	7	0.080	15	0.172
				10351	4283	5892	9	0.087	26	0.251
				13020	5559	7226	7	0.054	30	0.230
				9455	4091	5181	9	0.095	30	0.317
				11326	4756	6397	7	0.062	19	0.168
				8818	3885	4746	8	0.091	22	0.249
		2	pRAD51::Cas9+ gRNA-	12145	5082	6420	56	0.461	54	0.445
				8304	3708	4210	27	0.325	30	0.361
				7337	3669	3323	26	0.354	38	0.517
				14674	5888	8204	46	0.313	50	0.340
				11092	4741	5921	32	0.288	39	0.352
			pRAD51::Cas9+ gRNA+	9961	5285	4142	29	0.291	63	0.621
				10005	4335	5143	46	0.460	42	0.410
				8721	3687	4626	25	0.287	39	0.447
				6292	2757	3275	21	0.334	23	0.366
				7183	3124	3745	19	0.265	36	0.500
				10583	4338	5764	32	0.302	51	0.482
				7121	2982	3810	17	0.239	20	0.281
				11584	5010	6068	39	0.337	48	0.414

Supplementary table 4. Raw numbers of Illumina reads analysed for I1b - Site 2.

Interval	Target site	Genotype	Total reads	Col-0 reads (Parental 1)	Ler-0 reads (Parental 2)	Recombinant reads	Recombination rate (%)	Target site-mutated reads	Mutation rate (%)
CEN3	Site 1	pDMC1:: Cas9+ gRNA-	10194	5033	4948	39	0.383	18	0.176
			7365	3788	3423	31	0.421	12	0.163
			5906	3198	2594	23	0.389	8	0.135
			16022	8591	7159	56	0.349	28	0.175
			17850	8947	8556	68	0.381	47	0.263
		pDMC1:: Cas+ gRNA+	13178	12621	381	18	0.136	53	0.402
			16811	8579	7932	55	0.327	35	0.208
			12095	6138	5694	47	0.388	27	0.223
			9636	9325	177	22	0.228	42	0.436
			16405	8291	7749	74	0.451	28	0.171
			15090	7842	6980	52	0.344	24	0.159
		pRAD51:: Cas9+ gRNA+	17878	9064	8498	54	0.302	32	0.179
			14163	7026	6817	64	0.452	34	0.240
			16480	9936	6213	49	0.297	59	0.358
			14032	6924	6823	61	0.435	42	0.299
			12212	6769	5206	50	0.409	30	0.246
			11765	6028	5518	52	0.442	20	0.170

Supplementary table 5. Number of reads and percentage identified of the different parental and recombinant classes for I1b - Site 2 and CEN3 - Site 1.

Interval	Target site	PCR	Genotype	Total reads	Col-0 reads (Parental 1)	Ler-0 reads (Parental 2)	CO reads	C->L NCO reads	L->C NCO reads
I1b	Site 2	1	pRAD51:: Cas9+ gRNA-	66611	44.02 %	55.87 %	0.043 %	0.012 %	0.048 %
			pRAD51:: Cas9+ gRNA+	83693	43.80 %	56.08 %	0.039 %	0.016 %	0.059 %
		2	pRAD51:: Cas9+ gRNA-	53283	45.42 %	54.11 %	0.206 %	0.058 %	0.198 %
			pRAD51:: Cas9+ gRNA+	71133	46.61 %	52.89 %	0.245 %	0.074 %	0.177 %
CEN3	Site 1		pDMC1:: Cas9+ gRNA-	57224	52.11 %	47.27 %	0.307 %	0.115 %	0.190 %
			pDMC1:: Cas+ gRNA+	60310	51.69 %	47.68 %	0.278 %	0.134 %	0.218 %
			pRAD51:: Cas9+ gRNA+	86386	53.51 %	45.83 %	0.322 %	0.113 %	0.226 %

Supplementary table 6. EdU foci countings per cell.

	Wild-type		*spo11*
	Confocal	SIM	Confocal
	454	403	96
	263	355	51
	340	329	45
	392	423	77
	369	427	37
	348	480	42
	465	341	27
	474	414	42
	470	434	13
	447	400	15
	492		30
	510		33
	402		46
	437		29
	405		24
	379		55
	458		40
	462		32
	450		26
	404		28
	443		24
	420		21
	436		44
	387		61
	361		47
	419		50
	323		43
	489		37
	369		32
	389		56
	344		50
	370		28
	364		28
	477		26
	410		37
No. of cells	35	10	35
Mean	412.10	400.60	39.20
Std. Deviation	55.51	16.73	46.62
Std. Error of mean	9.38	2.83	14.74
No. of cells	45		
Mean	409.50		
Std. Deviation	53.37		
Std. Error of mean	7.96		

RÉSUMÉ EN FRANÇAIS

Chapitre I. Introduction générale.

L'acide désoxyribonucléique (ADN) est la molécule qui code l'information génétique et fonctionne comme l'unité primaire d'héritage dans la plupart des organismes vivants. Les molécules d'ADN sont un hétéropolymère de quatre désoxyribonucléotides, comprenant l'une des quatre bases azotées différentes : cytosine (C), guanine (G), adénine (A) et thymidine (T) ; elles sont liées de manière covalente en une chaîne par le squelette désoxyribose-sucre-phosphate. Chez les organismes eucaryotes, les molécules d'ADN se présentent généralement sous la forme d'une structure en double hélice composée de deux chaînes d'ADN polynucléotidiques enroulées l'une autour de l'autre. L'information génétique est codée physiquement par la séquence de nucléotides des molécules d'ADN, mais son interprétation repose également sur la manière dont cette séquence est modifiée, transcrite, traduite et dont tous ces processus sont régulés par la machinerie cellulaire et l'environnement dans lequel la cellule existe. Ainsi, les modifications physiques, chimiques et enzymatiques des molécules d'ADN peuvent introduire des changements dans la séquence d'ADN et/ou dans la façon dont elle est interprétée et, par conséquent, dans la structure et la fonction de la cellule et de l'organisme. L'étude de la façon dont l'ADN est modifié et réparé est un domaine de recherche majeur depuis que sa structure a été déterminée dans les années 1950.

Les sources de dommages de l'ADN peuvent être regroupées en deux grandes catégories selon leur origine endogène et exogène. Les dommages endogènes de l'ADN proviennent principalement d'erreurs lors de la réplication de l'ADN, d'interactions de l'ADN avec des sous-produits réactifs du métabolisme cellulaire et de modifications spontanées. Les dommages exogènes impliquent des agents physico-chimiques environnementaux qui modifient l'ADN, tels que les rayonnements ionisants et UV et les mutagènes chimiques tels que les agents réticulants ou les agents alkylants. La nature chimique des modifications est diverse et détermine la manière dont elles sont signalées et réparées. Les lésions vont des modifications réversibles, qui peuvent être facilement réparées sans erreur, aux modifications qui peuvent aboutir à la perte définitive d'une partie du matériel génétique ou sa réorganisation, entraînant un dysfonctionnement cellulaire, la mort cellulaire et un large éventail de pathologies chez les êtres vivants. Néanmoins, les modifications de l'ADN sont également l'un des principaux moteurs de l'évolution, car elles peuvent produire des mutations héréditaires dans un organisme qui sont potentiellement bénéfiques en termes de fitness. Dans

l'étude des dommages à l'ADN et de leur réparation, l'utilisation d'organismes modèles classiques a été prédominante, comme dans de nombreux autres domaines. Depuis les années 1970/80, *Arabidopsis thaliana est* devenu l'organisme modèle pour les plantes supérieures.

Les rayonnements ionisants, les espèces réactives de l'oxygène, les composés chimiques (agents alkylants, agents de réticulation, composés radiomimétiques, inhibiteurs de l'ADN polymérase et inhibiteurs de la topoisomérase) ou les erreurs de réplication (collisions entre les machineries de transcription et de réplication et réplication sur une cassure simple brin) peuvent entraîner la rupture simultanée du squelette phosphate des deux brins d'ADN, ce qui donne une cassure double-brin (CDB). Les cassures double-brin sont l'une des lésions de l'ADN les plus cytotoxiques et leur réparation fait intervenir plusieurs mécanismes de réparation. La discontinuité générée dans l'hélice d'ADN peut entraîner la perte du fragment complet de l'extrémité terminale de la cassure si elle n'est pas réparée, ce qui, selon la position de la cassure, le contenu génétique et l'état du cycle cellulaire, entre autres facteurs, peut potentiellement conduire à un arrêt du cycle cellulaire, à la mort cellulaire ou à des altérations génétiques majeures. De plus, une réparation erronée des CDB peut entraîner des délétions, des insertions et des translocations avec des conséquences potentielles similaires pour l'intégrité du génome. La nature hautement délétère des CDBs a donc conduit à l'émergence et à l'évolution de mécanismes de détection, de signalisation et de réparation des CDBs omniprésents dans le monde vivant.

La détection des cassures double-brin est la première étape de la réponse aux lésions de l'ADN (DDR) déclenchée par les cassures. Un élément clé de cette réponse est le complexe MRX/MRN. Ce complexe joue un rôle prépondérant dans l'activation de Tel1/ATM. Mec1/ATR est activé par un ADN monocaténaire persistant recouvert de RPA. Une fois Tel1/ATM et Mec1/ATR activés et recrutés sur les sites de CDB, ils phosphorylent un grand nombre de cibles coordonnant le remodelage de la chromatine, la réparation des CDBs, la régulation du cycle cellulaire et l'expression génique associée au stress génotoxique. H2A/H2AX est une cible clé pour les événements en aval de la réparation des CDBs. La variante phosphorylée de cette histone par les PIKK de la DDR, appelée γH2AX, joue un rôle clé dans le recrutement et l'accumulation des protéines de réparation de l'ADN aux sites de CDB. Après la détection et la signalisation d'une cassure double brin (**CDB**), les extrémités de la CDB peuvent être reliées si elles présentent des extrémités compatibles et ne nécessitent pas de traitement supplémentaire. Les extrémités franches ont une forte affinité pour le complexe KU70-KU80 (**protection de l'extrémité de l'ADN**) qui, si il n'est pas retiré des extrémités de la cassure double brin, canalise la réparation vers *non-homologous end*

joining (**NHEJ**). Ce processus peut cependant être perturbé par le complexe MRX/MRN, dont l'activité endonucléase et exonucléase est capable de libérer KU70-KU80 des extrémités de la CDB et d'initier la résection de ces extrémités, générant ainsi des extrémités d'ADN simple brin 3' sortantes (**libération de KU et résection des extrémités de l'ADN**) qui peuvent être étendues par d'autres exonucléases. Ces extrémités réséquées sont des substrats pour la recherche d'homologie et l'appariement des bases de l'ADN. Si de courtes régions homologues sont exposées, elles peuvent s'hybrider (**hybridation des microhomologies**) et la CDB est résolue par clivage des queues non homologues, comblement des lacunes par synthèse d'ADN et ligature des extrémités de l'ADN (**clivage des *flaps*, *gap filling* et ligature**) selon la voie de jonction des extrémités médiée par les microhomologies (**MMEJ)**. Les régions homologues plus longues situées de part et d'autre d'une CDB peuvent être prises en charge de façon similaire par la voie du *single strand annealing* (**SSA**) avec différents facteurs impliqués. Le chargement de RAD51 et la formation du nucléofilament RAD51-ADNsb (**Formation du filament RAD51**) canalisent la réparation vers les voies de recombinaison homologue (RH) via la recherche d'homologie médiée par RAD51 et l'échange de brins (**Invasion and DNA *strand exchange***). Dans les tissus somatiques, la chromatide sœur est le modèle préféré au chromosome homologue. Après l'échange de brins, le brin invahisseur peut être étendu par synthèse d'ADN en stabilisant l'intermédiaire *D-loop* (**synthèse d'ADN**). À ce stade, le brin envahisseur peut être dissocié de la *D-loop* et recapturé sur sa chromatide d'origine, en utilisant l'extrémité étendue pour combler l'espace de la CDB, s'hybrider avec l'autre côté de la CDB et se résoudre par remplissage de l'espace et ligature (**recapture, *gap filling* et ligature**) dans ce qui est connu comme la voie de *synthesis-dependent strand annealing* (**SDSA**). Si la seconde extrémité est capturée dans la *D-loop*, la double jonction de Holliday ou dHJ qui en résulte (**capture de la seconde extrémité et formation de la dHJ**) peut ensuite être résolue par dissolution topologique ou résolution nucléolytique de la dHJ (**résolution ou dissolution de la dHJ**). Tous les résultats de la voie SDSA, de la dissolution de la dHJ et d'une partie de la résolution nucléolytique de la dHJ donneront lieu à des produits de conversion génique non associés à un crossing-over entre les chromatides impliquées. La résolution nucléolytique de l'intermédiaire dHJ aboutit à une conversion génique associée (CO) ou non (NCO) à un échange réciproque des segments terminaux des chromatides impliquées, selon les plans de clivage des deux HJ. Dans le cas où la seconde extrémité de la chromatide cassée n'est pas présente, comme dans le cas de télomères déprotégés ou de fourches de réplication effondrées (**perte de la seconde extrémité**), la *D-loop* peut se transformer en une bulle migratrice capable de régénérer le segment perdu de la chromatide via un

mécanisme similaire à la réplication (**migration de la bulle et synthèse du brin traînant**) connu sous le nom de *break-induced replication* ou **BIR**.

La réparation des cassures double-brin par des mécanismes de jonction des extrémités ou de recombinaison homologue est un processus essentiel pour faire face à l'apparition spontanée de ces lésions dans le génome, afin de préserver l'intégrité de celui-ci. Les dommages spontanés de l'ADN ne sont cependant pas la seule source de CDBs. Une induction physiologique et programmée de cassures double-brin est également une caractéristique conservée chez les eucaryotes à reproduction sexuée, qui se produit au début de la méiose et qui est réparée par recombinaison homologue comme voie principale de manière hautement régulée. La méiose est une division cellulaire spécialisée des cellules germinales qui consiste en un cycle de réplication de l'ADN suivi de deux cycles de ségrégation (ou division) des chromosomes, contrairement à la mitose, au cours de laquelle une seule étape de ségrégation des chromosomes a lieu. La méiose produit quatre gamètes contenant la moitié du nombre de chromosomes de la cellule germinale parentale. Au cours de la première division méiotique, un processus induit et hautement régulé de dommages et de réparation de l'ADN est essentiel, dans la plupart des cas, pour un alignement et une ségrégation corrects des chromosomes. Les principaux mécanismes de réparation de l'ADN mis en jeu entraînent une recombinaison génétique importante, mélangeant les génomes parentaux et générant de nouvelles combinaisons alléliques.

Au début de la méiose, un ensemble de **cassures double-brin** est introduit par le complexe SPO11. Après la formation de la cassure double brin, les **extrémités de la cassure double brin sont résectées** et les recombinases DMC1 et RAD51 sont chargées sur les extrémités 3'-ADNsb recouvertes de RPA, formant ainsi les filaments présynaptiques. Les filaments présynaptiques envahissent le chromosome homologue en catalysant la **recherche d'homologie et l'échange de brins**. Bien que chez Arabidopsis il n'y ait actuellement aucune preuve concrète de l'invasion et de la résolution des intermédiaires de recombinaison avec la **chromatide sœur**, cela a été rapporté dans d'autres organismes. Une fois l'homologie trouvée, l'intermédiaire d'invasion précoce est stabilisé dans la ***D-loop* adaptée à l'extension de l'extrémité d'invasion via la synthèse d'ADN**. Cette *D-loop* étendue peut alors être transformée en : I) l'extrémité envahissante étendue est dissociée par des hélicases et recapturée vers sa chromatide d'origine, favorisant à partir du segment étendu le pontage des deux extrémités de la rupture, le remplissage et la ligature pour compléter la réparation produisant un événement de conversion génique NCO **(SDSA)**; ou II) la seconde extrémité de la CDB est capturée dans la *D-loop* étendue, générant une **double jonction de Holiday (dHJ)**. La dHJ peut aussi bien être résolue par plusieurs voies:

I) par la dissolution topologique médiée par STR/RTR, produisant un événement de conversion de gène NCO **(dissolution de la dHJ)**; II) par la résolution médiée par MLH1-MLH3 introduisant des coupures simple brin dans le même plan de clivage, produisant un événement de conversion de gène NCO **(résolution NCO - dHJ)**; ou III) par la résolution médiée par MLH1-MLH3 introduisant des coupures simple brin dans différents plans de clivage, produisant un événement CO de classe I avec sa conversion de gène associée **(résolution CO de classe I - dHJ)**. La résolution médiée par MLH1-MLH3 est biaisée vers la production d'événements CO de classe I en méiose. Une deuxième classe de CO **(Classe II CO)** résulte de la résolution d'un ensemble mal compris d'intermédiaires de recombinaison via l'action de nucléases spécifiques à la structure. La formation d'événements NCO par cette voie a également été suggérée dans des organismes tels que la levure bourgeonnante.

Chapitre II. RAD54 est essentiel pour la réparation des CDB dépendante de RAD51 chez Arabidopsis.

In vivo, l'assemblage et l'activité du filament d'ADN liée à la recombinase nécessitent l'aide d'un nombre variable de cofacteurs. L'activité du nucléofilament RAD51 est en outre soutenue par la protéine hautement conservée RAD54, qui appartient à la famille des ADN hélicases SWI2/SNF2. Il s'agit d'une ATPase dépendante de l'ADNdb qui utilise l'énergie de l'hydrolyse de l'ATP pour se déplacer le long de l'ADNdb. Il s'agit donc d'une protéine motrice qui remplit de multiples fonctions dans la recombinaison homologue. En particulier, RAD54 est un cofacteur essentiel stimulant l'activité de RAD51. Il a été démontré qu'il stabilise le nucléofilament de RAD51, remodèle les nucléosomes, stimule la recherche d'homologie et l'activité d'invasion de brins de RAD51, dissocie RAD51 lié après l'achèvement de l'échange de brins et catalyse même la migration des branches. En conséquence, la délétion de RAD54 a des conséquences dramatiques sur la réparation des dommages à l'ADN dans les cellules mitotiques. Le rôle de RAD54 dans la recombinaison méiotique est moins clair. Chez la drosophile et *C. elegans*, qui dépendent exclusivement de RAD51 (et non de DMC1), RAD54 est essentiel pour la recombinaison méiotique. Pourtant, chez la plupart des eucaryotes, la RH méiotique est médiée par RAD51 et DMC1 spécifique à la méiose. Il est toutefois intéressant de noter que si RAD51 est essentiel pour la recherche d'homologie et l'invasion des brins dans les cellules mitotiques, il ne joue qu'un rôle accessoire pour DMC1 en méiose. Ainsi, DMC1 est la recombinase méiotique active mais a besoin du soutien de RAD51 pour fonctionner.

Des données provenant de la levure bourgeonnante ont démontré que l'activité de Rad51 est régulée à la baisse au cours de la méiose pour favoriser Dmc1 qui catalyse l'échange de brins d'ADN en utilisant le chromosome homologue comme matrice.

Les paralogues de RAD51 sont également importants pour la recombinaison homologue et la réparation de l'ADN dans les cellules somatiques. La levure bourgeonnante possède deux paralogues de Rad51, Rad55 et Rad57, qui forment un hétérodimère et sont essentiels à la recombinaison méiotique, ainsi que quatre protéines Shu (Psy3, Csm2, Shu1 et Shu3) formant le complexe Shu/PCSS qui est également requis pour l'assemblage des filaments de Rad51 et la recombinaison méiotique. *Arabidopsis thaliana*, comme les vertébrés, possède cinq paralogues de RAD51 (en plus de DMC1) : RAD51B, RAD51C, RAD51D, XRCC2 et XRCC3 qui forment des complexes différents. Les mutants vertébrés pour l'un des paralogues de RAD51 sont létaux à l'état embryonnaire, ce qui a entravé l'étude de leurs phénotypes méiotiques. Néanmoins, un certain nombre d'études ont démontré que RAD51C et XRCC3 sont essentiels pour la recombinaison méiotique tant chez les vertébrés que chez les plantes. En revanche, les rôles méiotiques possibles de RAD51B, RAD51D et XRCC2 sont moins clairement compris. Ces trois gènes sont fortement exprimés dans les tissus méiotiques des animaux et des plantes. Chez l'homme, la mutation de XRCC2 a été liée à l'arrêt méiotique, l'azoospermie et l'infertilité, et l'absence de RAD51B ou RAD51D entraîne des défauts méiotiques chez la mousse *Physcomitrella patens* et le riz, respectivement. Le mutant *xrcc2* d'Arabidopsis et, dans une moindre mesure, *rad51b*, ont été associés à une augmentation des taux de recombinaison méiotique, mais les trois mutants sont entièrement fertiles et ne présentent aucun défaut méiotique détectable.

Le comportement méiotique de RAD54 concorde avec son rôle de partenaire essentiel pour la fonction des filaments de RAD51. Des données biochimiques, moléculaires et cytologiques antérieures chez Arabidopsis, la levure et la souris suggèrent que DMC1 est responsable de la catalyse de la réaction d'échange de brins des filaments présynaptiques, RAD51 jouant un rôle de soutien essentiel dans la réparation de la plupart, sinon de la totalité, des cassures double brin méiotiques. En l'absence de DMC1, RAD51 répare efficacement les cassures double brin méiotiques, mais sans produire de crossover interhomologues. En dépit de son rôle clé dans la recombinaison dépendante de RAD51 dans les cellules somatiques, la fertilité des plantes mutantes *rad54* a été interprétée comme montrant que RAD54 ne fonctionne pas dans la méiose. Nous avons émis l'hypothèse que ce manque apparent de rôle méiotique de RAD54 pourrait simplement être une conséquence du rôle non catalytique de RAD51 dans le soutien de la fonction de DMC1 en méiose. Si tel est le cas et étant donné que RAD51 catalyse la recombinaison méiotique en l'absence de DMC1, RAD54

devrait être nécessaire pour réparer les CDB induites par SPO11 dans la méiose des mutants *dmc1*. Nous avons également appliqué cet argument aux paralogues de RAD51, RAD51B, RAD51D et XRCC2, cofacteurs clés de la formation et/ou de l'activité des nucléofilaments de RAD51 dans les cellules somatiques mais non requis pendant la méiose.

Deux allèles mutants du RAD54 d'Arabidopsis - *rad54-1* et *rad54-2* - ont été utilisés pour confirmer le rôle du RAD54 dans la réparation des CDB et la recombinaison homologue dans les cellules somatiques en testant la sensibilité des mutants à l'agent mutagène d'ADN Mitomycine C (MMC). La MMC est connue pour former des adduits de liaisons transversales entre brins d'ADN, qui produisent des cassures de brins d'ADN *in vivo*. L'importance de la recombinaison homologue dans la réparation des liaisons transversales de l'ADN a conduit à l'utilisation de l'hypersensibilité à la MMC comme test de l'efficacité de la RH dans un certain nombre d'organismes. Chez Arabidopsis, cela se voit dans l'hypersensibilité MMC de nombreux mutants déficients en recombinaison homologue. Comme il a été montré précédemment, les plantes *rad54-1* présentent une hypersensibilité claire à la MMC. L'hypersensibilité à la MMC est également observée chez les plantes *rad54-2*, confirmant l'importance de RAD54 dans la recombinaison homologue dans les cellules somatiques.

Les défauts méiotiques se traduisent généralement par une baisse de la fertilité et donc par une réduction du nombre de graines chez Arabidopsis. Nous avons donc contrôlé le nombre de graines par silique dans nos deux lignées mutantes *rad54* et n'avons trouvé, comme prévu, aucun défaut de fertilité chez *rad54-1* ou *rad54-2.* En accord avec les résultats précédents, ceci confirme que RAD54 n'est pas nécessaire pour la méiose chez les plantes, malgré son importance dans la recombinaison somatique. Cette conclusion a été confirmée par des analyses cytogénétiques de chromosomes marqués au 4',6-diamidino-2-phénylindole (DAPI) au cours de la méiose mâle. Pendant la prophase I, les chromosomes méiotiques se condensent, s'apparient, se recombinent et leur synapse commence. La synapse complète des homologues est observée au pachytène. Les chromosomes se condensent encore et cinq bivalents (deux chromosomes homologues attachés par la cohésion des chromatides sœurs et les chiasmas) sont visibles en métaphase I. Chaque chromosome se sépare ensuite de son homologue, ce qui conduit à la formation de deux groupes de cinq chromosomes facilement visualisables en métaphase II. La méiose II se poursuit et donne naissance à 4 noyaux haploïdes équilibrés. Chez les mutants *rad54*, les étapes méiotiques sont similaires à celles du type sauvage, donnant lieu aux 4 produits méiotiques haploïdes attendus. Ainsi, la progression méiotique n'est pas affectée par l'absence de RAD54.

Nous avons ensuite cherché à analyser plus précisément l'impact de RAD54 sur la recombinaison méiotique en mesurant les taux de CO méiotiques dans des intervalles génétiques marqués par des transgènes codant pour des protéines marqueurs fluorescentes exprimées dans le pollen (FTL). Ces lignes FTL permettent de mesurer directement la recombinaison entre les marqueurs fluorescents liés en évaluant la fluorescence du pollen en tétrade. Nous avons déterminé les taux de CO dans deux intervalles adjacents sur les chromosomes 1 (I1b et I1c) et 2 (I2f et I2g) dans des plantes de type sauvage et des plantes mutantes *rad54-2*. Dans les plantes de type sauvage, I1b (1,8 Mb) s'étend sur 10,3 cM et I1c (4,1 Mb) sur 22,2 cM. Aucune différence dans la fréquence de recombinaison n'a été observée pour l'un ou l'autre intervalle chez les mutants *rad54-2* avec 9 cM et 22,7 cM pour I1b et I1c, respectivement. Les analyses de deux intervalles supplémentaires, I2f (0,7 Mb) et I2g (0,4 Mb), sur le chromosome 2 ont confirmé ce résultat, aucune différence significative de fréquence de recombinaison n'ayant été observée entre le type sauvage et les mutants *rad54-2* (6,8 cM à 6,9 cM pour I2f et 4,3 cM à 4,9 cM pour I2g). Nous avons obtenu des résultats similaires pour les plantes mutantes *rad54-1*. Conformément à ces résultats, nous avons trouvé un rapport d'interférence (IR) similaire dans les plantes de type sauvage et les mutants *rad54* pour les deux intervalles (IR I1bc : 0,35 dans le type sauvage et 0,36 dans le *rad54-2* ; IR I2fg : 0,09 dans le type sauvage, 0,1 dans le *rad54-1* et 0,1 dans le *rad54-2* ; $p > 0,05$, z-test).

Ainsi, l'absence de RAD54 n'affecte pas les taux de CO méiotiques dans au moins 4 intervalles différents sur 2 chromosomes. Ces résultats ont été confirmés à l'échelle du génome en comptant le nombre de chiasmas en métaphase I des méiocytes mâles de type sauvage, *rad54-1* et *rad54-2*, qui montrent des moyennes de 9,6 (ET = 1,3 ; n = 19), 9,6 (ET = 1,5 ; n = 25) et 9,1 (ET = 1 ; n = 19) chiasmas par méiose, respectivement ($p > 0,05$, tests t non appariés à deux extrémités).

La méiose chez les mutants *dmc1* d'Arabidopsis a été bien décrite. L'absence de DMC1 entraîne l'asynapsie et l'absence de CO inter-homologue. Cependant, des univalents intacts sont observés en métaphase I en raison de la réparation des CDB par RAD51 très probablement en utilisant la chromatide sœur comme donneur. En revanche, les analyses des doubles mutants *dmc1 rad54* montrent une absence de synapse et une fragmentation massive des chromosomes, un phénotype méiotique analogue à celui observé chez les mutants *rad51*. L'absence de synapse chez les doubles mutants *dmc1 rad54* a été confirmée par l'immunolocalisation de la protéine ASY1 de l'élément axial du complexe synaptonémal (SC) et de la protéine ZYP1 du filament transversal du SC. Ainsi, en l'absence de DMC1, la réparation méiotique RH-dépendante de RAD51 dépend effectivement de la présence de RAD54. Cet effet est

confirmé par la réduction significative de la fertilité causée par l'absence de RAD54 dans les plantes mutantes *dmc1*. Ainsi, au-delà du soutien de DMC1, soit RAD51 ne joue pas un rôle actif (ou ne joue qu'un rôle mineur) dans la recombinaison méiotique chez les plantes WT, soit son rôle est capable d'être compensé par DMC1 sans produire de modification détectable de la progression ou des produits méiotiques.

Nous avons quantifié la formation de foyers méiotiques de RAD51 comme un indicateur de la formation de nucléofilaments de RAD51 dans ces plantes. Nous avons effectué une co-immunolocalisation de RAD51 et de la protéine d'axe, ASY1, dans des méiocytes de type sauvage, *rad54*, *dmc1*, et *dmc1 rad54* et compté le nombre de foyers RAD51 tout au long de la prophase I précoce. Dans les méiocytes de type sauvage, nous avons observé une moyenne de 91 ± 29 foyers RAD51 (± ET, n = 35). Des nombres similaires de foyers RAD51 ont été observés dans les plantes de mutants simples *rad54* (89 ± 18, n = 22) et *dmc1* (97 ± 26, n = 50) et, fait important, le nombre de foyers RAD51 était également inchangé dans les mutants doubles *dmc1 rad54* (94 ± 16, n = 56). Conformément au rôle connu de RAD54 dans le soutien de l'activité du nucléofilament mitotique RAD51, ce rôle méiotique consiste vraisemblablement à faciliter l'invasion dépendante de RAD51 du duplex d'ADN donneur.

Compte tenu de ces résultats, il semble possible, par analogie avec RAD54, que l'absence de phénotype méiotique visible chez les mutants *rad51b*, *rad51d* ou *xrcc2* soit simplement une conséquence de l'activité d'invasion de brin de RAD51 qui n'est pas requise pour la recombinaison méiotique en présence de DMC1. Nous avons donc cherché à tester l'impact des paralogues de RAD51 dans la réparation méiotique des CDB dépendante de RAD51 en analysant la progression méiotique en leur absence dans un fond mutant *dmc1*. Comme décrit ci-dessus, les mutants *dmc1* sont caractérisés par de forts défauts synaptiques et une absence de CO. Cependant, les CDB méiotiques sont encore réparées, comme le montre la présence d'univalents achiasmatiques intacts en métaphase I, qui se séparent de façon aléatoire en anaphase I. Ces analyses n'ont pas montré d'effet détectable de l'absence de RAD51B, RAD51D ou XRCC2 dans le fond mutant *dmc1*. En revanche, la fragmentation chromosomique attendue est observée dans la méiose des mutants *xrcc3* et ceci n'est pas affecté par l'absence supplémentaire de DMC1. Ainsi, bien qu'ils soient exprimés dans les cellules méiotiques et qu'ils jouent des rôles clés dans l'activité de RAD51 dans les cellules somatiques, RAD51B, RAD51D et XRCC2 ne sont pas nécessaires pour la réparation des CDB méiotiques dépendante de RAD51 chez Arabidopsis.

Nous apportons ici la preuve que RAD54 chez Arabidopsis est essentiel à la réparation des cassures double-brin méiotiques médiée par le RAD51. Cette exigence

pour RAD54 n'est pas observée en présence de DMC1, car la plupart (toutes?) des CDB méiotiques sont réparées par DMC1, RAD51 jouant un rôle de soutien à DMC1 dans ce processus. Cependant, en l'absence de DMC1, RAD51 catalyse la réparation des CDB méiotiques, ce qui conduit à la ségrégation de chromosomes univalents intacts lors de l'anaphase méiotique I. Ainsi, l'absence de RAD54 d'Arabidopsis n'a aucun effet détectable sur la recombinaison méiotique chez les plantes de type sauvage, mais devient essentielle pour la réparation des CDB méiotiques dépendante de RAD51 en l'absence de DMC1 (comme on l'observe chez les mutants *dmc1* et *sds*). Les résultats d'analyses équivalentes avec trois protéines paralogues de RAD51, XRCC2, RAD51B et RAD51D, régulateurs positifs essentiels de la recombinaison homologue dans les cellules somatiques, montrent que cet effet n'est pas simplement le reflet d'un contexte de recombinaison RAD51-dépendant de la mitose dans la méiose de *dmc1*. Les mutants de ces protéines médiatrices clés de RAD51 ne présentent aucun phénotype méiotique détectable, au-delà d'un léger phénotype d'hyper-recombinaison méiotique rapporté pour les plantes *xrcc2* et *rad51b*. Nous rapportons ici que, contrairement à RAD54, les paralogues de RAD51, RAD51B, RAD51D et XRCC2, ne sont pas nécessaires à la réparation des CDB méiotiques dépendante de RAD51 chez Arabidopsis, bien qu'ils soient exprimés dans les cellules méiotiques et jouent des rôles clés dans l'activité somatique de RAD51.

Une autre conclusion déduite de nos données est que RAD54 d'Arabidopsis n'est pas nécessaire à l'activité de DMC1, que ce soit seul ou en tant que cofacteur de RAD51. Le fait que l'absence de RAD54 n'ait aucun effet détectable sur la recombinaison méiotique en présence de DMC1 nous indique que la fonction de RAD51 en tant que facteur accessoire essentiel pour DMC1 est indépendante de RAD54. Cette conclusion concorde avec l'absence rapportée d'interaction entre RAD54 et DMC1 chez Arabidopsis. Pourtant, le nucléofilament de DMC1 doit effectuer une recherche d'homologie et une invasion de brins, ce qui nécessite des translocases d'ADN dépendantes de l'ATP. Nous émettons donc l'hypothèse qu'il existe un second homologue de RAD54 spécifique de DMC1, encore inconnu, chez les plantes. RAD54 est un facteur de remodelage SWI2/SNF2 qui appartient à la famille des hélicases SF2, dont un certain nombre sont codées par le génome d'Arabidopsis, mais à ce jour, seul RAD54 (ce travail) a été identifié comme impliqué dans la méiose.

Chapitre III. Introduction ciblée de cassures double-brin au début de la méiose chez Arabidopsis en utilisant CRISPR/Cas9

Le ciblage des CDB et l'utilisation des *hotspots* des CDB méiotiques pour les études moléculaires des mécanismes et de la régulation de la recombinaison méiotique restent un défi chez *Arabidopsis thaliana* et d'autres espèces végétales. S'il est disponible, le ciblage à petite échelle des points d'initiation des événements de recombinaison méiotique offrirait:

I) une fenêtre prédéterminée comprenant un aperçu détaillé du paysage génétique et épigénétique du site pour l'observation et l'analyse des événements d'intérêt;

II) le point d'initiation connu de ces événements faciliterait l'analyse des intermédiaires et/ou des produits de recombinaison en aval, et offrirait la possibilité de contrôler la directionnalité des événements RH en induisant le site de clivage dans l'un des deux chromosomes homologues;

III) un outil d'analyse et de comparaison reproductible de la recombinaison méiotique chez des individus ayant des fonds génétiques différents, des paysages locaux ou soumis à des traitements ou des conditions différentes.

La cartographie récemment publiée des oligonucléotides SPO11 chez Arabidopsis a révélé des milliers de *hotspots* de CDB méiotiques endogènes, répartis sur l'ensemble du génome. Cependant, aucun motif de séquence d'ADN commun (tel que le motif PRDM9 chez la plupart des vertébrés) ou toute autre signature pouvant servir à centrer dans une certaine mesure l'initiation des événements de recombinaison n'a été identifié. Les *hotspots* de CDB d'Arabidopsis sont des régions assez larges d'enrichissement en CDB par rapport aux autres organismes (≈900bp en moyenne contre ≈150bp chez la souris ou ≈250bp chez la levure bourgeonnante). A notre connaissance, aucune étude approfondie cartographiant les événements de recombinaison individuels aux *hotspots* de CDB n'a été publiée chez Arabidopsis, comme cela a été fait chez la souris par exemple. Une approche inverse a été explorée, en cartographiant la densité de SPO11-oligo le long des *hotspots* de recombinaison connus chez Arabidopsis. De manière surprenante, bien que le taux de recombinaison et la densité SPO11-oligo soient positivement corrélés à l'échelle chromosomique, aucune corrélation positive n'est trouvée à des échelles plus fines dans ces régions. Afin d'interpréter ce résultat apparemment contradictoire, il est important de rappeler que le *crossover* marque le site de résolution d'un événement de recombinaison et que la proximité des sites d'initiation et de résolution peut être influencée par un certain nombre de facteurs. Ceux-ci incluent la variabilité de la longueur de la résection et la symétrie par rapport

au site de la CDB, l'occurrence de multiples cycles d'invasion et de dissolution des extrémités, la migration des jonctions de Holliday et la présence et la densité des polymorphismes inter-homologues. En dépit de ces considérations, la non-corrélation entre la densité des CDB et le taux de recombinaison au *hotspot* de croisement suggère une grande variabilité dans le positionnement des CDB et complique donc l'analyse des résultats de la recombinaison méiotique et de leurs détails mécanistiques sur la base de l'utilisation des *hotspots* des CDB endogènes.

Une alternative intéressante à l'étude des *hotspots* des CDB endogènes a été l'introduction ciblée de cassures de l'ADN à des endroits souhaités. Parmi les systèmes utilisés pour induire des CDB méiotiques, ceux introduits par des nucléases telles que HO, I-SceI ou VDE se sont avérés capables d'être réparés via les voies de recombinaison méiotiques canoniques suivies par les CDB catalysées par SPO11. Ces nucléases sont cependant spécifiques d'un site, ce qui signifie qu'elles ciblent une séquence de reconnaissance définie, ce qui, chez des espèces comme Arabidopsis, impliquerait l'intégration de ces séquences via une transformation d'ADN-T. Cette approche présente donc deux inconvénients principaux : I) la limitation de l'étude de la réparation d'une séquence d'ADN-T transgénique, et non d'une séquence génomique endogène d'Arabidopsis ; et II) la nature aléatoire de l'intégration de l'ADN-T, empêchant le contrôle du contexte génomique, génétique et épigénétique du site.

L'émergence de CRISPR/Cas en tant qu'outil polyvalent, efficace et facile à concevoir pour cibler et cliver n'importe quelle séquence endogène adjacente à un motif PAM de la version Cas choisie ouvre la porte à l'induction de CDBs localisées pendant la méiose pour ce type d'études. Parmi les différents systèmes CRISPR/Cas, ceux incluant Cas9 sont capables d'induire des CDBs à extrémités franches, vraisemblablement un substrat approprié pour la réparation via les voies de recombinaison méiotique.

Compte tenu du potentiel de la technologie CRISPR/Cas9 pour induire des CDBs à haute efficacité et à des emplacements génomiques souhaités avec un contrôle au niveau d'une seule base du site de clivage, nous avons émis l'hypothèse que les CDBs induites par CRISPR/Cas9 au début de la méiose chez Arabidopsis seront réparés via les voies de recombinaison méiotique canoniques, y compris la formation de crossovers inter-homologues. Comme indiqué ci-dessus, l'application réussie d'un tel outil permettant de cibler la recombinaison méiotique serait d'une grande importance pour l'application et l'étude de la recombinaison méiotique chez la plante modèle.

Nous avons cloné le gène humain codon-optimisé *Streptococcus pyogenes* Cas9 (SpCas9) dans des vecteurs d'expression codant soit pour le promoteur *DMC1*

d'*Arabidopsis thaliana* (pDMC1), soit pour le promoteur *RAD51* (pRAD51) afin de piloter son expression *in planta.* Les ARN CRISPR ont été commandés pour être synthétisés sous forme de molécules d'ADN codant pour les sgRNA complets (tracrRNA fusionné individuellement à chacun des crRNA), précédés d'un promoteur U6 d'*Arabidopsis thaliana* (pU6) et suivis d'un terminateur poly(A) pour l'expression *in planta.* Chaque cassette pU6::sgRNA a également été clonée dans des vecteurs d'expression. Pour cibler l'activité de SpCas9 aux endroits désirés, les crRNA ont été conçus de manière à ce que: I) ils ciblent des positions uniques dans le génome; II) ils se situent en dehors des gènes codant pour des protéines afin d'éviter des effets indirects dans la biologie de la plante en perturbant un gène; et III) ils incluent des polymorphismes de séquence d'ADN cartographiés dans la séquence cible entre Col-0 (Col) et Ler-0 (Ler), de sorte qu'ils devraient être actifs sur le chromosome Col et non sur le chromosome Ler dans les plantes hybrides Col/Ler. Ce dernier point a été inclus pour avoir des informations sur la directionnalité des événements potentiels de recombinaison méiotique entre chromosomes homologues dans les hybrides Col x Ler. En exploitant les lignées de marqueurs polliniques fluorescents FTL développées à l'origine par le laboratoire Copenhaver, nous avons choisi quatre cibles différentes dans deux intervalles génétiques marqués (I1b et CEN3) qui permettent d'évaluer le taux de recombinaison de l'intervalle en identifiant et en comptant les différentes classes parentales et recombinantes des gamètes (pollen).

La validation des constructions contre deux sites cibles a été effectuée dans des cellules somatiques (plus abondantes et plus faciles à collecter que les méiocytes) par séquençage de nouvelle génération afin de mesurer leur expression et leur capacité à cliver les cibles chromosomiques. Bien qu'il soit limité à la détection de la réparation mutagène des CDB induites, ce test fournit une image plus complète que le simple test de la présence du transcrit ou de la protéine. Nous avons pu détecter des délétions de sites cibles dans environ 2 à 5% des séquences dans la plupart des *pools* de plantes (4/5) portant la construction pestradiol::Cas9 et cultivées dans un milieu supplémenté en estradiol pour les deux cibles testées. Ces séquences présentaient des profils de délétion attendus du clivage de Cas9 : principalement des délétions courtes (quelques paires de bases jusqu'à 100 pb environ) couvrant le site de coupure ainsi que des insertions de 1 pb centrées autour de celui-ci. Une augmentation de l'efficacité de coupure a également été détectée dans un des *pools* de plantes exprimant pDMC1:Cas9 et le gRNA pour CEN3 - Site 1 (1/6 pools total) avec un profil similaire de courtes délétions autour du site de coupure. Aucune différence avec les contrôles n'a été observée dans les 5 pools portant les constructions pRAD51::Cas9.

Dans notre plan expérimental pour induire des CDB méiotiques, comme mentionné ci-dessus, nos sites cibles ont été placés dans deux intervalles marqués FTL qui nous permettent de mesurer le taux de recombinaison sous l'hypothèse qu'un système CRISPR/Cas9 efficace clivant ces sites devrait générer un excès de crossovers dans ces intervalles (donc une augmentation de la distance génétique), comme cela a été rapporté dans des études avec des stratégies analogues chez d'autres espèces. Dans l'ensemble, nous n'avons pas obtenu d'augmentation statistiquement significative des taux de recombinaison moyens entre les lignées portant pDMC1::Cas9 ou pRAD51::Cas9 plus le gRNA pour l'un des quatre sites cibles par rapport aux témoins. Nous avons cependant détecté des augmentations du taux de recombinaison dans les plantes individuelles allant de 3 à 8 cM environ par rapport à la distribution dans le contrôle pour au moins trois des sites cibles: I1b - Site 2 dans les plantes portant pDMC1::Cas9 et les deux sites CEN3 dans les plantes portant pRAD51::Cas9. Plus précisément, le ciblage CRISPR/Cas9 a entraîné une distribution élargie des taux de recombinaison méiotique entre les individus, certaines plantes présentant des augmentations de taux de recombinaison méiotique de près de 2 fois par rapport à la moyenne du contrôle.

Les plantes F2 analysées pour chacune de ces combinaisons promoteur-plus-cible proviennent du croisement de différentes plantes transformées T1, chacune avec des intégrations indépendantes des ADN-Ts du système CRISPR/Cas9. Ainsi, le sous-ensemble de plantes avec un taux de recombinaison accru pour chaque combinaison pourrait provenir soit I) de lignées T1 particulières dans lesquelles le système CRISPR/Cas9 est efficacement exprimé et initie des événements RH produisant des *crossovers* alors qu'il ne le fait pas dans d'autres (variabilité inter-lignée) ; ou II) de plantes individuelles provenant de plusieurs lignées T1 avec un taux de recombinaison accru alors que d'autres appartenant à la même lignée maintiennent des taux similaires à ceux du contrôle (variabilité intra-lignée). Pour vérifier cela, nous les avons divisés en sous-pools par lignée T1 parentale et avons répété les analyses. Lorsqu'on les divise par lignée T1 parentale, on remarque pour les plantes pRAD51::Cas9 ciblant les sites CEN3 que les augmentations de recombinaison ne sont pas limitées à la descendance de plantes T1 parentales particulières, mais que les plantes avec des taux de recombinaison accrus et contrôlés coexistent dans la plupart des lignées. Dans le cas de pDMC1::Cas9 I1b - Site 2, les deux phénomènes ont pu être observés: l'une des lignées semble présenter une augmentation cohérente du taux de recombinaison dans le score de trois plantes, bien que probablement plus de plantes soient nécessaires pour une plus grande confiance dans l'observation, tandis que la deuxième lignée montre une forte

variabilité intra-lignée, y compris une plante avec une augmentation de 2 fois par rapport au taux de recombinaison moyen contrôle.

À la lumière des observations utilisant des systèmes à base de rapporteurs pour analyser les crossovers, nous avons opté pour une approche NGS sur l'ADN de pollen de plantes hybrides Col x Ler F1. Cela nous a permis d'analyser les résultats de la recombinaison méiotique au niveau de la molécule unique : les tracts de conversion, les événements de *crossover* et de *non-crossover* et leurs proportions. Malheureusement, ces analyses de séquençage d'ADN n'ont pas fourni de preuves de l'induction de crossovers méiotiques sur l'un ou l'autre des deux sites cibles analysés (I1b - Site 2 & CEN3 - Site 1) dans les plantes portant CRISPR/Cas9 plus le gRNA correspondant par rapport aux plantes dépourvues du gRNA.

En réexaminant l'hypothèse initiale et les objectifs proposés au début de ce projet, nous concluons que:

I) Nous avons conçu et transformé dans des plantes d'Arabidopsis des constructions CRISPR/Cas9 contrôlées par des promoteurs connus pour s'exprimer au début de la méiose et capables d'induire des cassures double-brin aux sites cibles choisis avec une efficacité modérée.

II) Les plantes individuelles portant ces systèmes CRISPR/Cas9 ont subi des augmentations de la distance génétique des intervalles couvrant certains des sites cibles par rapport aux plantes témoins, ce qui suggère une induction de crossovers inter-homologues sur ces sites. Néanmoins, une grande variabilité au sein et entre les lignées de transformants a été observée pour ces systèmes.

III) L'analyse de deux des sites cibles par séquençage de nouvelle génération de l'ADN génomique du pollen n'a montré aucune augmentation des crossovers inter-homologues, des non crossovers ou des mutations au niveau du site cible dans les plantes portant les systèmes CRISPR/Cas9 par rapport aux témoins.

L'augmentation observée des distances génétiques des intervalles couvrant les sites cibles de CRISPR/Cas9 n'est donc pas confirmée par le séquençage des amplicons Illumina des produits. Il semble probable que cela puisse être expliqué par les limitations que le séquençage NGS de courte longueur a pu avoir pour la détection de ces événements (voir discussion), mais dans tous les cas, cela empêche toute conclusion ferme concernant les résultats génétiques prometteurs.

Chapitre IV. Analyse des segments de synthèse d'ADN associés à la réparation des CDB méiotiques chez Arabidopsis.

La synthèse d'ADN est inhérente à de multiples mécanismes de réparation de l'ADN et, notamment, à la réparation des CDB par recombinaison homologue. Étant donné l'occurrence de CDB programmées au début de la méiose qui sont réparées en utilisant la RH comme mécanisme de réparation primaire, on peut s'attendre à ce que si une impulsion d'un analogue nucléosidique est synchronisée avec la réparation méiotique des CDB, des segments d'analogue nucléotidique incorporé puissent être localisées tant que leur taille et leur luminosité sont suffisantes pour être visibles à la résolution du microscope. L'incorporation en milieu de phase I de H^3-thymidine ou de C^{14}-thymidine a déjà été observée dans les années 1960 dans des autoradiographies de cellules méiotiques des plantes *Lilium longiflorum* et *Trillium erectum*, de l'amphibien *Triturum viridescens*, de la souris ou de l'homme. Bien qu'à cette époque le mécanisme moléculaire réel de la recombinaison homologue n'ait pas encore été décrit (Holliday a publié son modèle en 1964 et il n'a pas inclus la synthèse de l'ADN jusqu'à la mise à jour de Meselson et Radding en 1975), Wimber et Prensky ont déjà proposé, concernant leur observation chez *T. viridescens,* une relation entre la synthèse de l'ADN en prophase I méiotique et le croisement génétique, ajoutant : "*nous ne pouvons pas exclure la possibilité que la synthèse d'ADN observée pendant la prophase résulte de la rupture et de la réparation des chromatides*". Après que la synthèse de l'ADN ait été incluse comme processus inhérent dans les modèles moléculaires RH, l'incorporation de H^3-thymidine pendant le pachytène a également été décrite dans les méiocytes femelles de la drosophile associés aux nodules de recombinaison et dans les spermatocytes de la souris associés au complexe synaptonémique, offrant une preuve directe de la relation entre la synthèse de l'ADN et la recombinaison.

Une caractérisation plus poussée de l'incorporation d'analogues de nucléotides au cours de la prophase I méiotique a ensuite été réalisée en utilisant la 5-Bromo-2´-Déoxyuridine (BrdU) chez la levure bourgeonnante, dans laquelle le marquage s'est avéré dépendant de SPO11 et sa présence a été confirmée au niveau des *hotspots* de recombinaison et dans les molécules d'ADN recombinant, caractérisant également les segments de BrdU à une seule molécule au niveau des *hotspots* et le moment de leur apparition par rapport aux autres caractéristiques méiotiques. Ce travail a offert une preuve directe de la synthèse d'ADN associée à la réparation des CDB méiotiques prédite par les modèles RH en détail, confirmant certaines des signatures mécanistiques attendues et révélant le potentiel de cette technique dans l'étude de la recombinaison méiotique. L'observation d'un schéma similaire de marquage BrdU dépendant de SPO11

a été décrit chez Tetrahymena mais, à notre connaissance, aucune autre donnée n'a été publiée chez d'autres organismes. D'où l'intérêt de cette étude qui consiste à essayer cette approche pour localiser les événements de réparation des CDB lors de la prophase méiotique I d'Arabidopsis via l'incorporation d'analogues nucléotidiques pouvant être détectés cytologiquement.

Des études sur Arabidopsis ont utilisé l'incorporation de BrdU ou de 5-éthynyl-2'-désoxyuridine (EdU) pendant la phase S pré-méiotique dans le but d'analyser la chronologie de la méiose. Pour ce faire, des impulsions de 2 heures ont été appliquées aux inflorescences, après quoi elles ont été rincées avec de l'eau pour arrêter l'incorporation de l'EdU/BrdU et laissées en incubation pendant un nombre variable d'heures pour ensuite suivre les étapes marquées avec BrdU/EdU à chaque point temporel. Ce dispositif expérimental permet l'incorporation des analogues nucléotidiques pendant la phase S pré-méiotique, marquant de vastes régions du génome facilement détectables dans les préparations chromosomiques au microscope sous la forme d'un signal fluorescent particulièrement brillant, soit de grandes taches dans les chromosomes, soit directement le génome entier, en fonction de la synchronisation entre l'impulsion et la phase S.

Malgré cette application de l'incorporation de BrdU/EdU aux cellules mères du pollen d'Arabidopsis avant la méiose, il n'existe aucun rapport sur son incorporation à la synthèse d'ADN associée à la réparation des CDB pendant la méiose. L'incorporation et la détection réussies de ces analogues nucléotidiques pourraient s'avérer un outil puissant pour la localisation et l'analyse de la plupart des événements de recombinaison méiotique se produisant au cours de la méiose d'Arabidopsis, y compris ceux qui sont indétectables avec les outils moléculaires actuels.

Nous avons donc émis l'hypothèse que les cellules méiotiques d'Arabidopsis subissant la prophase I en présence d'EdU incorporeraient l'analogue nucléotidique dans les segments de synthèse d'ADN associés à la réparation méiotique des CDB qui deviendraient détectables à l'aide de techniques cytologiques et moléculaires. De tels segments contenant l'EdU dans le génome seraient les "empreintes" de la recombinaison méiotique et auraient un grand potentiel pour l'étude de la réparation méiotique des CDB.

Dans ce travail, nous avons développé et testé avec succès un protocole pour marquer spécifiquement les segments de synthèse de l'ADN associées à la réparation méiotique des CDB par incorporation *in vivo* de l'analogue de la thymidine EdU. L'ADN contenant l'EdU peut être efficacement marqué par réticulation chimique à un certain nombre de ligands (fluorochromes, biotine...) par la réaction "Click-It".

L'adaptation des protocoles disponibles pour établir la chronologie des étapes méiotiques chez Arabidopsis a montré qu'en incubant des inflorescences pendant 24 heures dans une solution d'EdU, nous pouvions identifier deux sous-populations de méiocytes avec un signal EdU différent.

La première sous-population était constituée de cellules en début de prophase I (leptotène - zygotène) dont les chromosomes étaient soit totalement soit partiellement marqués, montrant un fort signal fluorescent. Ce schéma est cohérent avec l'incorporation d'EdU dans l'ensemble du génome pendant la réplication en phase S pré-méiotique, et ce pour plusieurs raisons :

I) Le fort signal fluorescent est similaire à celui observé dans les rapports précédents sur l'incorporation d'EdU/BrdU pendant la réplication pré-méiotique.

II) En extrapolant à partir des chronologies méiotiques dans ces rapports publiés, les cellules mères de pollen en phase S pré-méiotique au début de l'incubation devraient passer au leptotène-zygotène après 24 heures.

III) Le signal dans les cellules en début de prophase I partiellement marquées est détecté principalement dans les régions hétérochromatiques denses en DAPI, connues pour être des régions à réplication tardive du génome d'Arabidopsis, conformément à ce que l'on pourrait attendre des cellules qui ont été prises en fin de phase S au début de l'incubation.

IV) Le signal n'est pas dépendant de SPO11, donc non lié à la recombinaison méiotique.

La deuxième sous-population est constituée de cellules aux stades méiotiques allant du pachytène à la fin de la méiose (tétrades) dont les chromosomes présentent un signal EdU plus faible et discret. Présents en foyers individuels aux stades où les chromosomes sont moins condensés, ces foyers se regroupent en "taches" quand les chromosomes se condensent. Ce signal présente une série de caractéristiques qui permettent de l'identifier avec certitude comme étant l'incorporation d'EdU au niveau des chaînes de synthèse d'ADN associées à la réparation des CDB :

I) Les foyers EdU discrets observés au pachytène et aux stades ultérieurs sont non seulement de taille nettement inférieure au signal général du leptotène-zygotène, mais aussi beaucoup plus faibles. Ceci est attendu étant donné la taille prévue des segments de synthèse d'ADN associés aux événements RH (quelques bases à quelques kilobases d'ADN) par rapport à l'étiquetage réplicatif (mégabases au génome complet).

II) Les stades méiotiques des cellules présentant ce signal après 24 heures d'incubation suivent, en terme de progression méiotique (donc de temps, en général),

ceux présentant un marquage réplicatif total ou partiel. Cette observation, ainsi que les extrapolations à partir des chronologies méiotiques d'Arabidopsis, nous permettent de déduire que les cellules ont terminé la phase S au début de l'incubation et ont subi la prophase méiotique I jusqu'à, au moins, le pachytène en présence d'EdU. Les données d'immunolocalisation des protéines impliquées dans la recombinaison méiotique chez Arabidopsis ainsi que les données moléculaires des intermédiaires RH chez d'autres organismes suggèrent que la plupart des synthèses d'ADN associées à la réparation méiotique des CDB doivent avoir eu lieu pendant la période d'incubation dans ces cellules.

III) Les nombres de foyers EdU mesurés au pachytène sont compatibles avec les estimations de CDBs et d'intermédiaires RH rapportées chez Arabidopsis (discutées en détail ci-dessous).

IV) Les régions hétérochromatiques denses en DAPI correspondant aux centromères ont une densité significativement plus faible (quasi absence) de foyers EdU en pachytène/diplotène et un signal EdU même lorsqu'elles se condensent avec les chromosomes en diakinèse/MI. Ceci est congruent avec la cartographie SPO11-oligo montrant que les régions centromériques et péricentromériques ont une densité de CDBs beaucoup plus faible que le reste du chromosome.

V) Enfin, nous avons montré que ces foyers discrets d'EdU sont dépendants de SPO11, confirmant avec une grande confiance qu'ils résultent de l'incorporation d'EdU dans les segments de synthèse d'ADN associés à la réparation méiotique des CDB.

Nous avons compté 409,5 ± 7,96 (moyenne + SEM ; n = 45) foyers de synthèse d'ADN associés à la réparation de l'ADN dans les pachytènes WT. Nous avons choisi ce stade parmi ceux marqués car la combinaison de la condensation des chromosomes et de la synapse offre une bonne résolution des signaux EdU discrets par rapport aux stades postérieurs et on pense que la plupart des événements de recombinaison sont résolus ou proches de la résolution au pachytène. Dans les plantes *spo11*, 39,2 ± 2,83 foyers EdU par cellule ont été notés. Ces nombres sont conformes aux estimations de CDB chez Arabidopsis méiose, ainsi qu'à la baisse significative attendue chez un mutant - *spo11* - dépourvu de CDB méiotiques.

Les modèles de recombinaison méiotique prédisent différents modèles de synthèse de l'ADN selon la façon dont les intermédiaires de recombinaison sont formés et résolus. Les événements non croisés générés par la dissolution de la SDSA ou de la dHJ produisent des segments de synthèse d'ADN dans une seule des deux chromatides impliquées (et donc dans un des chromosomes homologues dans la recombinaison interhomologue). D'autre part, la résolution nucléolytique de la double jonction de

Holiday, qui donne lieu à des produits de *crossover* ou de *non-crossover*, génère des segments de synthèse d'ADN dans les deux chromatides impliquées, et donc dans les deux chromosomes dans les événements inter-homologues. Dans les cellules pachytènes WT bien étalées, bien que la synapse maintienne les deux chromosomes homologues ensemble, il existe des segments dans lesquels ils peuvent être visuellement différenciés car les deux signaux DAPI sont séparés par un espace de plus faible intensité DAPI. Des modèles différents de foyers d'EdU peuvent donc être observés lorsqu'on les examine en détail.

Lorsque les foyers EdU individuels sont analysés visuellement par rapport aux chromosomes, aucun biais évident dans leur disposition n'est observé. Des foyers EdU situés à la fois sur les côtés internes (face au chromosome homologue) et externes des chromosomes ont été observés, ainsi qu'au milieu du chromosome. Lorsque les foyers EdU sont analysés par rapport aux foyers adjacents, différentes classes ont pu être détectées visuellement : des foyers uniques sur l'un des homologues sans aucun foyer en parallèle sur l'autre homologue ; des paires de foyers en parallèle (à un emplacement similaire) sur les deux homologues qui sont séparés dans l'espace ; et des paires de foyers en parallèle (à un emplacement similaire) sur les deux homologues dont les signaux sont en contact dans une certaine mesure. Il reste à déterminer si la différenciation de ces deux dernières classes est biologiquement pertinente ou résulte d'un artefact de résolution ou de perspective d'imagerie. Une quantification des proportions de chaque classe reste à faire dans un futur proche.

Le marquage des segments de synthèse d'ADN associés à la réparation des CDB est non seulement prometteur en tant qu'outil cytologique pour les études méiotiques, mais nous pensons qu'il peut ouvrir la voie à la caractérisation moléculaire des événements NCO et/ou intersister, jusqu'à présent indétectables chez Arabidopsis, tout en offrant une meilleure compréhension des mécanismes mécanistiques de la formation de CO. Nous nous sommes donc concentrés sur le développement d'un protocole pour leur détection, localisation et caractérisation moléculaires.

À cet égard, nous avons isolé manuellement un nombre considérable de populations de méiocytes en prophase I après leur incubation pendant 24 heures dans l'EdU. Nous avons accumulé des pools d'environ 15.000-17.000 cellules pour la préparation de la bibliothèque NGS. Compte tenu de notre mesure de 409,5 foyers moyens par cellule, ces nombres de cellules ont le potentiel théorique de produire jusqu'à 6-7 millions de segments individuels à precipiter, séquencer et cartographier pour rechercher des régions d'enrichissement pour les événements RH méiotiques. Bien que la méthode prenne du temps, elle est facilement extensible si nécessaire.

Après l'extraction de l'ADNg de cette sous-population de méiocytes, nous avons mis en place un protocole de biotinylation et de *pull-down* des fragments ayant incorporé l'EdU sur des billes magnétiques couplées à la streptavidine dans le cadre de la préparation des bibliothèques NGS. La récupération de fragments liés à l'adaptateur de la taille attendue après la préparation de la bibliothèque par PCR dans les échantillons incubés avec EdU et leur absence (au niveau de résolution de la TapeStation) dans les contrôles EdU ont confirmé l'extraction et l'amplification fonctionnelles et spécifiques des fragments biotinylés contenant l'EdU. Ces bibliothèques NGS ont été séquencées et les données ont été traitées pour l'analyse des régions putatives des segments d'ADN contenant l'EdU.

Nous avons pu détecter des régions d'enrichissement pour les segments d'ADN contenant l'EdU à la fois dans nos échantillons WT et dans nos échantillons *spo11*. De manière inattendue, le nombre absolu de pics était similaire dans nos échantillons WT et *spo11*. Aucun chevauchement significatif n'a été détecté entre les deux réplicats WT ou les deux réplicats *spo11*, et aucun enrichissement différentiel de la densité de régions contenant l'EdU n'a été trouvé dans aucun des échantillons des deux génotype lorsqu'ils sont profilés par rapport aux pics de l'autre réplicat du même génotype.

Pour une caractérisation plus poussée, nous avons décidé de sélectionner les pics spécifiques de WT et de *spo11* pour une comparaison différentielle de ces régions avec les données de la bibliographie des caractéristiques qui pourraient être en corrélation avec nos données: SPO11-oligos, *crossovers* et régions d'initiation de la réplication. Toutes les régions de synthèse d'ADN associées à la réparation des CDB ont une CDB d'origine, il semble donc plausible de supposer que les *hotspots* de SPO11 pourraient présenter un chevauchement relativement fort avec les régions contenant l'EdU. Certains aspects mécanistiques de la recombinaison méiotique en aval de la formation des CDB pourraient différencier la forme des régions d'enrichissement des deux caractéristiques et compliquer l'analyse, comme la longueur de la résection, la migration des branches ou le résultat de la résolution. Cependant, on s'attend au moins à des différences avec les échantillons *spo11*, dans lesquels il devrait y avoir peu ou pas de chevauchement avec les *hotspots* de SPO11. Le chevauchement avec les *crossovers* cartographiés n'est peut-être pas si fort, étant donné que, bien que tous les *crossovers* devraient inclure des tracts de synthèse d'ADN, les *crossovers* ne représentent qu'environ 5 % du total des événements de recombinaison méiotique et qu'il n'est pas clair si les événements qui se produisent à différents *hotspots* de CDB d'Arabidopsis ont des chances similaires d'aboutir à un CO ou s'il existe des biais. Enfin, nous avons inclus les régions d'initiation de la réplication comme référence possible pour les enrichissements liés à la réplication de l'ADN plutôt qu'à la recombinaison méiotique.

Aucun chevauchement différentiel n'a été détecté entre les régions d'enrichissement de l'une de ces trois caractéristiques et les pics détectés dans nos échantillons WT par rapport à ceux détectés dans les échantillons *spo11*. Une comparaison de la taille de ces régions a également été effectuée. Bien que des différences statistiquement significatives aient été détectées entre les pics WT et les pics *spo11* (pics WT légèrement plus larges en moyenne), les deux sont beaucoup plus courts que les *hotspots* SPO11 ou les *crossovers* publiés. La comparaison avec les *crossovers* n'est cependant pas très informative, car les méthodes utilisées pour la notation diffèrent considérablement. Comme mentionné ci-dessus, on s'attend à ce que les régions d'enrichissement en ségments de synthèse associés à la réparation des CDB soient en moyenne plus larges que les *hotspots* SPO11. Cependant, la relation inverse a été trouvée. L'ensemble de ces observations ne nous permet pas de discerner si les pics dans nos échantillons sont biologiquement pertinents ou simplement artéfactuels.

Nous avons décidé d'explorer nos données plus en profondeur en calculant les profils de nos deux échantillons WT et de nos deux échantillons *spo11* sur de multiples caractéristiques dans lesquelles des enrichissements SPO11-oligo ont été signalés, dans l'hypothèse où, grâce à cette méthode, nous pourrions détecter des enrichissements locaux même s'ils ne sont pas assez forts ou si la profondeur de séquençage n'est pas suffisante pour être qualifiés de pics. Il est frappant de constater que des enrichissements sur les *hotspots* de SPO11 et, dans une moindre mesure, sur les crossovers cartographiés ont été détectés dans tous les échantillons WT et *spo11*, de la même ampleur que les SPO11-oligos. De même, un enrichissement sur les promoteurs de gènes, les terminateurs et les éléments transposables et un appauvrissement sur les corps de gènes d'une ampleur similaire à celle de SPO11-oligos ont été trouvés aussi bien dans les échantillons WT que dans les contrôles négatifs.

Ces résultats sont plutôt paradoxaux. Le faible nombre de pics dans les échantillons WT, l'absence de différence entre ceux-ci et ceux dans les échantillons *spo11*, la taille réduite des pics et l'absence d'enrichissement de SPO11-oligos par rapport aux pics WT peuvent indiquer qu'il s'agit simplement d'artefacts. Cependant, nous avons détecté un enrichissement de nos données sur les *hotspots* SPO11 publiés et validés et, à un moindre degré, sur les crossovers cartographiés, ainsi qu'une signature sur les gènes codant pour les protéines et les éléments transposables reflétant celles des données des SPO11-oligos non seulement dans leur forme mais aussi dans leur ampleur. Les enrichissements et les signatures spécifiques dans les échantillons WT ne se produisent pas de manière aléatoire, comme cela a été validé en répétant les analyses sur un ensemble mélangé d'intervalles de chaque caractéristique, obtenant ainsi des profils plats. Ils peuvent donc indiquer une détection réussie d'enrichissements locaux

de segments de synthèse d'ADN associés à la réparation des CDB. La non-détection de pics individuels pourrait s'expliquer par un manque de profondeur de séquençage ou par la présence d'un fond excessif. Néanmoins, l'obtention de résultats similaires dans les échantillons *spo11* dans lesquels, en raison de l'absence de CDBs, aucun enrichissement spécifique à la méiotique n'est attendu, jette des doutes sur l'origine des enrichissements détectés sur nos échantillons WT, en plus de soulever des questions similaires à celles rapportées pour la cartographie SPO11-oligo.

Une corrélation fortuite entre les profils de nos échantillons et ceux de SPO11-oligos semble peu probable en raison de la spécificité des régions observées, des profils plats observés dans tous les ensembles d'intervalles mélangés et de la complexité de certaines des signatures. Les profils sur les gènes codant pour des protéines ne montrent pas seulement un pic d'enrichissement, mais une signature assez complexe comprenant un enrichissement sur les promoteurs, un appauvrissement sur les corps des gènes et un enrichissement sur les terminateurs qui est répliqué dans tous les échantillons - SPO11-oligos et nos quatre réplicats indépendants.

Une autre possibilité est que la corrélation n'est pas aléatoire mais qu'il existe différentes origines pour ces enrichissements qui se chevauchent dans le génome. Des caractéristiques telles que les *hotspots* SPO11 et les régions d'initiation de la réplication chez Arabidopsis partagent des caractéristiques génétiques et épigénétiques associées similaires, notamment une faible occupation des nucléosomes, une richesse en AT, et tant les *hotspots* SPO11 que les régions d'initiation de la réplication sont appauvris en corps de gènes et enrichis en éléments transposables, notamment en Hélitrons. Parmi les ensembles d'intervalles tirés de la bibliographie, 781 d'entre eux se chevauchent, ce qui représente environ 15 % des totaux des *hotspots* SPO11 et des régions d'initiation de la réplication. Un enrichissement local de SPO11-oligos a pu être détecté sur les régions d'initiation de la réplication en traçant le profil sur celles-ci. Le couplage direct de la réplication pré-méiotique et de la formation de CDB a été décrit dans de nombreux organismes ainsi que des enrichissements en CDB dans les régions de réplication précoce. On pourrait donc émettre l'hypothèse que, étant donné que nous avons les mêmes profils dans les échantillons WT et *spo11*, ces enrichissements pourraient avoir une origine réplicative tout en restant en corrélation avec les données SPO11-oligo. Si un nombre significatif de cellules dans le pool avait partiellement subi une réplication pendant l'incubation et n'avait pas été correctement nettoyé de la sous-population ciblée de méiocytes, les régions d'initiation de réplication pourraient présenter un enrichissement. Il s'agit de régions à réplication précoce au niveau local (par rapport aux régions adjacentes) et elles ont donc plus de chances d'avoir incorporé l'EdU dans des cellules somatiques partiellement répliquées et d'être entraînées vers le bas si elles

sont transportées. Mais les cartes thermiques représentant la densité de nos échantillons sur les *hotspots* de SPO11 montrent un enrichissement presque omniprésent sur tous les *hotspots*, et non dans un sous-ensemble de *hotspots* comme on pourrait s'y attendre en raison du chevauchement de 15 % de ceux-ci avec les régions d'initiation de la réplication. Ainsi, bien qu'il ne soit pas possible de l'exclure sans une analyse plus approfondie, cette hypothèse ne semble pas convaincante.

Une troisième hypothèse pourrait être que les enrichissements observés à la fois dans nos résultats et dans les SPO11-oligos sont simplement un artefact technique commun. En raison des spécificités de la configuration expérimentale, les données de SPO11-oligos ne disposent pas d'un contrôle "biologique" sans CDBs, comme nos échantillons de mutants *spo11*, à séquencer et à comparer. Pour cette expérience, la protéine de fusion SPO11-1-Myc nécessaire pour le *pull-down* doit fonctionner pour former des CDB pour que ces fragments soient générés. Cependant, la protéine SPO11-1-Myc, cytologiquement localisée dans les chromosomes, était capable de sauver le phénotype CDB-nul des mutants *spo11*, reproduit les taux de recombinaison WT dans de multiples intervalles et s'est avérée être tirée vers le bas efficacement et spécifiquement, confirmant son rôle en tant que SPO11-1 fonctionnelle et renforçant la confiance dans les données SPO11-oligo-seq. En ce qui concerne les artefacts possibles liés à la préparation des librairies, notre processus de préparation des librairies commence avec de la chromatine nue, éliminant en principe les biais potentiels liés à l'état de la chromatine. Les *hotspots* de SPO11 sont enrichis en AT et un clivage préférentiel sur les régions riches en AT a été décrit dans les kits de préparation de librairies comprenant une fragmentation enzymatique. Néanmoins, alors que notre méthode de préparation de bibliothèque inclut la fragmentation, le protocole de SPO11-oligo ne le fait pas (en raison de la nature inhérente des SPO11-oligos qui sont déjà des fragments de 30-40nt), ce qui exclut un biais de fragmentation partagé. Les méthodes de préparation des bibliothèques à partir de ce point sont complètement différentes et nous n'avons pas été en mesure d'identifier les étapes communes induisant un biais. Enfin, dans les deux protocoles, nous utilisons une bibliothèque de "contrôle d'entrée" pour normaliser les données : dans le cas de SPO11-oligo, une bibliothèque d'ADNg indépendante a été séquencée et réduite pour correspondre à la longueur de fragment de SPO11-oligos, dans le nôtre, un sous-échantillon de l'entrée de l'étape de *pull-down* pour chaque réplicat. Ce contrôle de l'entrée a pour fonction d'éliminer les biais potentiels de préparation de la bibliothèque ou de séquençage. Ainsi, à nos yeux, il n'y a pas de sources évidentes de biais communs qui pourraient être interprétés comme des enrichissements locaux sur des caractéristiques spécifiques qui pourraient soutenir cette hypothèse.

Nous n'avons pas pu arriver à une conclusion satisfaisante pour expliquer cette corrélation entre nos échantillons WT, nos échantillons *spo11* et les données SPO11-oligo publiées. Par conséquent, nous espérons que les efforts futurs permettront de résoudre ce problème et d'obtenir avec succès une carte des segments de synthèse d'ADN associés à la réparation des CDB dans les méiocytes d'Arabidopsis et, en même temps, d'aller plus loin en utilisant la caractérisation de ces segments comme source d'informations mécanistiques des événements de recombinaison méiotique qui doivent encore être caractérisés dans la plante modèle.

En réexaminant l'hypothèse initiale et les objectifs proposés au début de ce projet, nous pouvons conclure que :

I) Nous avons conçu et validé avec succès un protocole facile et reproductible pour l'incorporation de l'EdU dans les segments de synthèse d'ADN associés à la réparation de l'ADN pendant la prophase I. Ce protocole permet la détection cytologique et la différenciation de la sous-population de méiocytes portant ce marquage des méiocytes qui ont incorporé l'EdU lors de la réplication pré-méiotique.

II) Ce signal EdU de synthèse de l'ADN associé à la réparation de l'ADN répond à de multiples prédictions tirées des modèles et des caractéristiques de la recombinaison méiotique d'Arabidopsis : il est dépendant de SPO11, le nombre de foyers EdU concorde avec le nombre de CDB méiotiques rapportés, il est nettement moins dense dans les régions hétérochromatiques connues pour recevoir un nombre plus faible de CDB et différents modèles de foyers peuvent être observés qui pourraient refléter différentes classes d'événements de recombinaison méiotique.

III) Un protocole a été mis au point pour isoler avec succès une sous-population de méiocytes enrichie dans les stades connus pour porter un marquage de synthèse d'ADN associé à la réparation de l'ADN ; pour extraire l'ADN génomique de ces cellules, conjuguer les segments contenant l'EdU avec de la biotine et les précipiter spécifiquement et efficacement pour la préparation de bibliothèques de séquençage NGS.

IV) Des régions d'enrichissement des segments de synthèse de l'ADN associés à la réparation de l'ADN dans le génome ont été détectées, ainsi que des enrichissements spécifiques sur des caractéristiques connues pour être enrichies en CDB, notamment les *hotspots* SPO11, les crossovers cartographiés, les promoteurs de gènes et les terminateurs.

V) De manière surprenante, ces enrichissements ont été reproduits à des niveaux similaires dans des échantillons dépourvus de CDB méiotiques - mutants *spo11* - incubés

dans l'EdU également. La similitude avec les enrichissements par SPO11-oligo et le fait que cela soit observé dans les échantillons de mutants *spo11* est particulièrement intriguant. Cela indique vraisemblablement l'existence d'une influence des caractéristiques génomiques et/ou techniques sous-jacentes sur les cartes d'initiation de la recombinaison provenant à la fois des *pull-downs* EdU et SPO11-oligo. À ce stade, cependant, les ensembles de données ne sont pas suffisamment complets pour permettre de tirer des conclusions définitives.

Les résultats obtenus et leur interprétation permettent de valider avec confiance l'hypothèse initiale : les cellules méiotiques d'Arabidopsis subissant la prophase I en présence d'EdU incorporeront cet analogue nucléotidique dans les voies de synthèse d'ADN associées à la réparation des CDB méiotiques. Nous avons pu détecter ce signal par cytologie en suivant un protocole qui est non seulement plus facile à réaliser et plus reproductible que les protocoles standard d'analyse du nombre de CDB chez Arabidopsis, mais qui offre également une meilleure résolution et la possibilité d'obtenir un plus grand nombre de cellules marquées de bonne qualité. Bien que nous n'ayons pas pu tirer de conclusion très fiable de la détection et de la cartographie moléculaires de ces segments étant donné la similitude du signal avec le contrôle négatif, nous avons pu mettre en place une série d'étapes dans le protocole qui, selon nous, sera utile pour l'accomplir dans un avenir proche.